A forward genetic screen to identify factors that control meiotic recombination in *Arabidopsis thaliana*

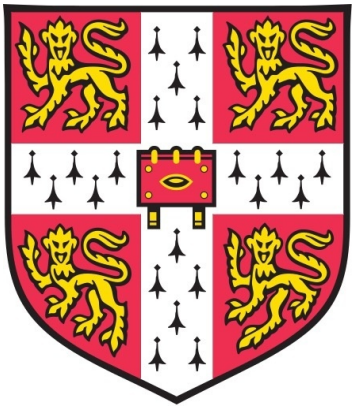

Divyashree Coimbatore Nageswaran

Department of Plant Sciences
University of Cambridge

This dissertation is submitted for the degree of
Doctor of Philosophy

Darwin College September 2018

For my dear husband and parents

Declaration

This dissertation is the result of my own work and includes nothing which is the outcome of work done in collaboration except as declared in the Preface and specified in the text. It is not substantially the same as any that I have submitted, or, is being concurrently submitted for a degree or diploma or other qualification at the University of Cambridge or any other University or similar institution except as declared in the Preface and specified in the text. I further state that no substantial part of my dissertation has already been submitted, or, is being concurrently submitted for any such degree, diploma or other qualification at the University of Cambridge or any other University or similar institution except as declared in the Preface and specified in the text. It does not exceed the prescribed word limit for the relevant Degree Committee.

Divyashree C Nageswaran

Acknowledgements

First, I thank my PhD supervisor, Dr Ian Henderson for providing this great platform to be a part of COMREC Marie Curie ITN, his constant guidance and exceptional support. I thank all the PIs of the network for their constructive feedbacks on my work. I take this opportunity to thank Department of Plant Sciences, University of Cambridge for the PhD admission offer that fulfilled my dreams. I thank the EU funding body for their generosity to support young people taking the science path.

I sincerely thank Dr Kyuha Choi, who initiated this project and for being an amazing mentor, especially during my initial stages of research. I specially thank Dr Christophe Lambing, who taught me cytology and made great contributions to this project. I thank Dr Heidi Serra for the opportunity to collaborate on her publication. I express my gratitude to Dr Bruno Santos, Dr Xiaohui Zhao and Dr Andy Tock for bioinformatics support. I wholeheartedly thank Dr Pawel Bastor, Mel, Liliana and James for all the help and support that helped me achieve good research outcomes.

I thank Dr Monica Pradillo and Pablo Parra (Complutense University, Madrid) for teaching me immunocytology. I thank Dr Steve Barnes and Dr Glenda Willems (SesVanderHave, Belgium) for their guidance on the internship project. I express my esteem and profound sense of gratitude to Professor Sir David Baulcombe, Dr Alex Webb and Dr Uta Paszkowski for their valuable feedbacks on my talks/posters.

I express my heartfelt gratitude to all my PhD, post-doc and some faculty friends- Charlie, Patrick, Luke, Alex, Sasha, Claire, Catherine, Emma, Heidi, Quentin Badolle, Daniel, Claudia, Antonia, Artemis, Sara Lopez, Francisco, Zhengming, Sebastian A, Gita, Joiselle, Natasha and Sabrina for their guidance and motivation. I shall always remember the fun-filled moments spent with them all these 4 years. I also thank all my COMREC friends for their motivational support and the wonderful times during meiosis meetings shall be memorable forever.

I express my love in loads to my husband, parents, brother, in-laws and grandparents for their eternal love, moral support and sacrifices to relish the moment of my achievement in life. Last of all, I thank God behind every single action.

A forward genetic screen to identify factors that control meiotic recombination in *Arabidopsis thaliana*

Divyashree C Nageswaran

Department of Plant Sciences, University of Cambridge, UK.

Meiotic recombination promotes genetic variation by reciprocal exchange of genetic material producing novel allelic combinations that influence important agronomic traits in crop plants. Therefore, harnessing meiotic recombination has the potential to accelerate crop improvement via classical breeding. Numerous genes involved in crossover formation have been identified in model systems. For example, SPO11 mediates generation of meiotic DNA double-strand breaks (DSBs) across all eukaryotes, which may be repaired as crossovers. However, downstream regulators of recombination remain to be identified, including those with species-specific roles. To isolate crossover frequency modifiers I performed a high-throughput forward genetic screen using EMS mutagenesis of Arabidopsis carrying a fluorescent crossover reporter line called *420*. The primary screen isolated nine mutants from ~3,000 scored individuals that showed significantly higher (*high crossover rate*, *hcr*) or lower (*low crossover rate*, *lcr*) crossover frequency, including a new *fancm* allele. Four mutants (*hcr1*, *hcr2*, *hcr3* and *lcr1*) were mapped by sequencing and candidate genes identified. The *hcr1* mutation was confirmed as being located within the *PROTEIN PHOSPHATASE X-1* (*PPX-1*) gene, using isolation of an independent allele and complementation studies. Similarly, the *lcr1* mutation was confirmed to be within the gene *TBP-ASSOCIATED FACTOR 4B* (*TAF4B*). Using immunocytological staining I observed that *hcr1* did not show changes in DSB-associated foci (RAD51), but it did show a significant increase in crossover-associated MLH1 foci. The *hcr1* mutation increases crossovers mainly in the sub-telomeric chromosome regions, which remain sensitive to crossover interference. Also the genetic interaction between the *hcr1* and *fancm* mutations is additive. These results support a model where PPX-1 acts to limit recombination via the Class I interfering CO pathway, downstream of DSB formation. In summary, this genetic screen has led to discovery of novel genes that regulate meiotic recombination and their functional characterization may find utility in crop breeding programs.

List of contents

1. General Introduction

2. General Methods

List of Figures

List of Tables

Abbreviations

ATP	- Adenosine-tri-phosphate
ATPase	- enzyme capable to hydrolyze ATP
BF	- Beam-film
bp	- basepair
BC	- backcross
CTL	- Columbia traffic lines
CCD	- Charge-coupled device
CO	- Crossover
Col or Col-0	- Columbia ecotype
CoC	- Coefficient of Coincidence
cM	- centimorgan
CFP	- Cyan fluorescent protein
cDNA	- complementary DNA
DNA	- Deoxyribonucleic acid
dsDNA	- double stranded DNA
DAPI	- 4′,6-Diamidine-2′-phenylindole dihydrochloride
DSBs	- Double-stranded breaks
DSBR	- DSB repair model
dHJ	- double-Holliday Junction
D-loop	- Displacement loop
dCAPS	- derived cleaved amplified polymorphic sequence
DCO	- Double crossover
EMS	- Ethyl-methyl sulfonate
FTL	- Fluorescent tagged lines
GLM	- Generalized linear model
GFP	- Green fluorescent protein
hcr	- high crossover rate
HR	- Homologous recombination
H3K4me3	- Histone 3 lysine 4 tri methylation
HJ	- Holliday junction
IS	- Inter-sister
IH	- Inter-homolog

JM	- Joint molecules
kb	- kilobase
Ler-0	- *Landsberg erecta* ecotype
LE	- Lateral elements
LND	- Low nucleosome density
lcr	- low crossover rate
Mb	- megabase
mRNA	- messenger RNA
MDS	- Multi-dimensional scaling
NCO	- Non-crossover
NHEJ	- Non-homologous end joining
PCR	- Polymerase chain reaction
PTC	- Premature termination codon
P	- Probability value
PCA	- Principle component analysis
PMC	- Pollen mother cells
QTL	- Quantitative trait loci
RFP	- Red fluorescent protein
RT-PCR	- Reverse transcription PCR
RNA	- Ribonucleic acid
rlog	- regularized logarithm
SC	- Synaptonemal complex
SCO	- Single crossover
SDSA	- Synthesis-dependent strand annealing
ssDNA	- Single-stranded DNA
SEI	- Single-end invasion
SEC	- Second end capture
SNP	- Single nucleotide polymorphisms
SHORE	- Short read analysis pipeline
SHOREmap	- visual extension of SHORE
TLAC	- Tethered loop axis chromosome model
T-DNA	- Transfer DNA
WT	- Wild type

Chapter 1- General Introduction

1.1. Meiosis and mitosis

Meiosis is a specialized eukaryotic cell division, during which gametes are produced and which is fundamental for propagation of sexually reproducing organisms (Harrison et al. 2010; Osman et al. 2011). During meiosis, diploid (2n) cells are reduced to half the chromosome number producing haploid progeny cells (n), by a single round of DNA replication followed by two rounds of chromosome segregation (Villeneuve and Hillers 2001; Osman et al. 2011; Mercier et al. 2015; Gray and Cohen 2016). Haploid gametes may then fuse together to form a diploid cell upon fertilization (Harrison et al. 2010; Osman et al. 2011; Mercier et al. 2015; Lambing and Heckmann 2018). Proper chromosome segregation during meiosis and restoration of the original ploidy level (2n) is required for fertility (Villeneuve and Hillers 2001; Zamariola et al. 2014a; Mercier et al. 2015; Lambing and Heckmann 2018). Different to meiosis, mitosis produces identical daughter cells (2n) by a single round of chromosome segregation during which sister chromatids are separated to opposite poles, preceded by a single round of DNA replication (Gray and Cohen 2016).

1.2. The first and second meiotic divisions

During meiotic S-phase, homologous chromosomes undergo DNA replication in a diploid cell (2n) (Figure 1.1). Cohesion is established between the duplicated sister chromatids by loading of the cohesin complex (Uhlmann and Nasmyth 1998; Nasmyth and Haering 2005; Osman et al. 2011; Makrantoni and Marston 2018). Like in mitosis, meiosis I and II are divided into prophase, metaphase, anaphase and telophase, however with no interphase between the two rounds of nuclear division (Figure 1.2) (Osman et al. 2011; Mercier et al. 2015; Wang and Copenhaver 2018). The major events of meiotic prophase I include chromosome pairing, synapsis and homologous recombination (Keeney and Neale 2006; Osman et al. 2011; Mercier et al. 2015; Ziolkowski and Henderson 2017) (Figure 1.1, 1.2). At prophase I during leptotene, meiotic recombination is initiated with formation of DNA double stranded breaks (DSBs) mediated by SPO11 topoisomerase-like complexes (Keeney 1997; Keeney and Neale 2006; de Massy 2013).

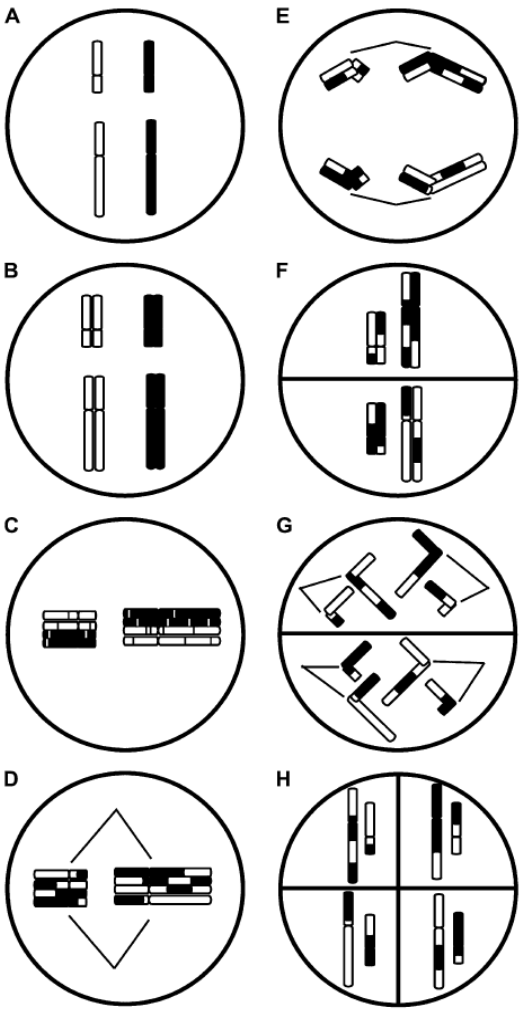

Figure 1.1. Major steps during meiosis. A) Two chromosome pairs from maternal (white) and paternal (black) individuals in a diploid cell. **B)** Each chromosome undergoes replication during meiotic S-phase **C)** Homologous chromosomes form bivalents, pair and synapse during meiosis I. Paired chromosomes undergo DNA double stranded breaks during meiotic prophase I. **D)** Spindles attached to the paired bivalents with completed recombination events **E)** Paired homologous chromosomes move to opposite poles. **F)** At the end of meiosis I, each of the two daughter nuclei contain one pair of replicated and recombined homologous chromosomes **G)** In meiosis II, sister chromatids are separated and move to opposite poles **H)** At the end of meiosis II, four haploid recombined gametes are formed that are subjected to fertilization (reproduced from Harrison et al. 2010).

A subset of these DSBs are repaired as crossovers between the homologous chromosomes, which creates genetic diversity between the gametes. Both DSB formation and recombination are closely integrated with meiotic chromosome structure (Lam and Keeney 2015) (Figure 1.1, 1.2, 1.3). At zygotene, sister chromatids of the paired homologs are linearly organised into chromatin loop arrays, anchored at their bases by proteinaceous axial elements (Kleckner 1996; Zickler and

Kleckner 1999; Lam and Keeney 2015). The paired homologs initiate synapsis between the loop-axis configuration, forming two lateral elements (LEs) (Nancy Kleckner 1996; Zickler and Kleckner 1999; Page and Hawley 2004; Lam and Keeney 2015). For example, in Arabidopsis the chromosome axis protein ASY1 localizes to the axial and lateral elements (Armstrong et al. 2002). The LEs are connected by transverse filaments that include the central element protein (ZYP1) that assemble the synaptonemal complex (SC) (Zickler and Kleckner 1999; Page and Hawley 2004; Higgins et al. 2005; Lam and Keeney 2015) (Figure 1.3). At pachytene, synapsis is complete and paired homologs are held together by the SC. In addition at least one reciprocal exchange of DNA between non-sister chromatids called a crossover (CO) forms at this stage, which are cytologically evident as chiasma (Page and Hawley 2004; Mercier et al. 2015; Lambing and Heckmann 2018) (Figure 1.2). At diplotene and diakinesis stages the SC begins to dis-assemble and the chromosomes undergo de-synapsis and gradual condensation occurs to form bivalent structures connected with chiasmata (Figure 1.2) (Kleckner 1996; Armstrong and Jones 2003).

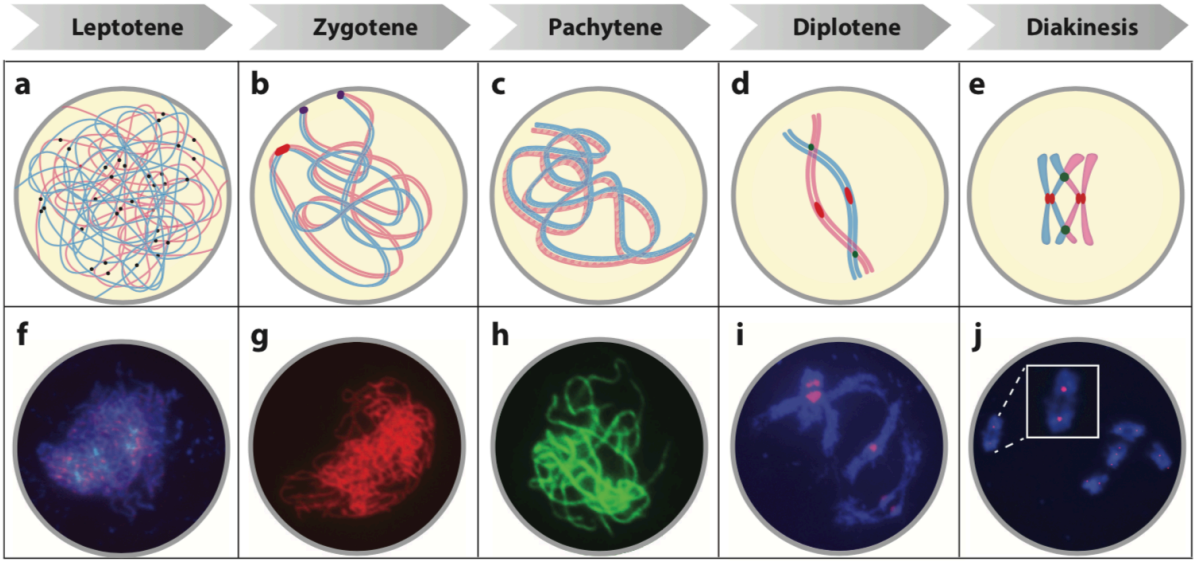

Figure 1.2. Schematic representation of Meiotic prophase I events. Prophase I consists of 5 stages. At leptotene **(a,f)**, meiotic recombination begins with DSB formation (black dots). **f)** The DSBs are marked by γH2A.X (pink spots) on immunolocalization. **(b,g)** During stage zygotene, homologs physically pair forming bivalents and synapsis is initiated (purple spots are telomeres and red spots are centromeres). **g)** Immunolocalization of ASY1 (red) marks the meiotic axis. **(c-h)** At pachytene stage, homologs are fully synapsed and appear condensed followed by chiasma (crossover) formation from repaired DSBs. **h)** ZYP1 (green) a synaptonemal complex (SC) central element protein on immunolocalization. **(d-i)** During diplotene, homologs separate except where the crossovers formed and disappearance of SC assembly**. i)** Labelling of spreads by chromosome fluorescence

in situ hybridization (CEN-FISH) represented by pink spots. **(e-j)** At diakinesis stage, the homologs are found further condensed and are linked by chiasma (blue dots) and sister chromatids are preserved by cohesion (red spots are centromeres). **j)** MLH1 (pink spots), a Class I CO marker on immunolocalization (reproduced from Wang and Copenhaver 2018).

The physical links established by crossovers assure correct alignment of homologs on the metaphase I plate and at least one CO per bivalent is required for proper chromosome segregation from the metaphase I plate to opposite poles (Keeney and Neale 2006; Mercier et al. 2015; Lambing and Heckmann 2018) (Figure 1.1). Additionally, the orientation of sister kinetochores attached to microtubules towards the same spindle pole (mono-orientation) is an important feature of meiosis required for balanced segregation (Keeney and Neale 2006; Mercier et al. 2015; Lambing and Heckmann 2018). Furthermore, chromosome cohesion is regulated by cohesin complexes containing the REC8 kleisin subunit, which is cleaved by Separase to allow segregation. Protection of centromeric cohesion is mediated by SHUGOSHIN (SGO1), which recruits a phosphatase that protects REC8 from cleavage, which assures balanced segregation of homologs to opposite spindle poles at anaphase I (Kleckner 1996; Watanabe and Nurse 1999; Kitajima et al. 2003; Hauf and Watanabe 2004; Kitajima, Kawashima, and Watanabe 2004; Gregan et al. 2005; Kitajima et al. 2006; Marston 2014; Zamariola et al. 2014b). At the end of meiosis I, two daughter cells are produced, with each carrying one replicated homologous chromosome, which is thus termed a “reductional division” (Kleckner 1996; Zamariola et al. 2014a) (Figure 1.1). The second meiotic division, also called a “mitotic equational division” during which the centromeric cohesion is lost via REC8 cleavage after anaphase II and bi-orientation of kinetochores allows separation of sister chromatids to opposite poles producing four haploid gametes (Kleckner 1996; Kitajima et al. 2003; Nasmyth 2005; Tanaka 2005; Mercier et al. 2015) (Figure 1.1). Hence, chromosome segregation during meiosis I and II differ by both altered forms kinetochore orientation and cohesion release.

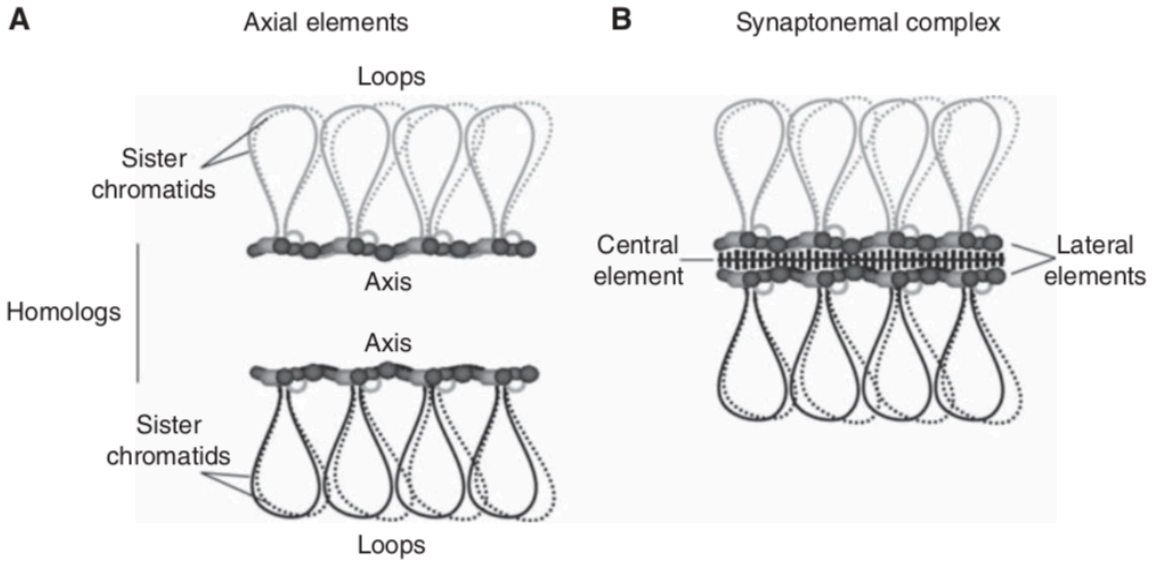

Figure 1.3. Meiotic chromosome structure during prophase I. A) Pairs of sister chromatids are arranged into linear chromatin loop arrays along the structure axis, called axial elements. **B)** During zygotene, paired homologs start to synapse and the axial elements are brought together to form lateral elements/LEs. The two LEs are bridged by transverse filaments which combines with the central element to form the tripartite structure, called synaptonemal complex (SC). At pachytene, SC extend to entire length and completes formation (reproduced from Lam and Keeney 2015).

1.3. Meiotic recombination

Accurate chromosome segregation during the first round of meiotic division requires meiotic recombination, which is initiated by a large number of DNA double stranded breaks that are repaired as crossovers (COs) or non-crossovers (NCOs) (Villeneuve and Hillers 2001; Harrison et al. 2010; Mercier et al. 2015; Lambing et al. 2017) (Figure 1.4). Chromosome mis-segregation occurs due to reduced or absent recombination, kinetochore bi-orientation, defective spindle assembly checkpoint (SAC) or deterioration of sister chromatid cohesion during meiosis I, which may cause gamete or foetal aneuploidy due to loss or gain of chromosomes (Lister et al. 2010; Watanabe 2012; Chiang et al. 2012; Jessberger 2012; Cole et al. 2012; Herbert et al. 2015; Wang et al. 2017). In humans aneuploidy increases with the maternal age (>26 years) causing higher infertility rates and errors in pregnancy causing miscarriage or birth defects like Down syndrome (trisomy 21) (Lister et al. 2010; Nagaoka et al. 2012; Cole et al. 2012; Franasiak et al. 2014; Herbert et al. 2015). Inefficiency in crossover maturation leads to chiasma patterns that promote mis-segregation and elevates aneuploidy risk (Cole et al. 2012; Wang et al. 2017).

In plants, mutation of genes required for DSB formation, such as *SPO11-1*, show an absence of chromosome pairing and synapsis (Grelon et al. 2001). As a result univalents randomly segregate at the end of meiosis-I and as a consequence the resulting gametes exhibit aneuploidy and *spo11-1* shows a sterile phenotype (Grelon et al. 2001). Additionally, crossovers generate genetic variation by reshuffling homologous chromosomes, which can accelerate the efficiency of natural selection and adaptation (Schuermann et al. 2005; Harrison et al. 2010; Mercier et al. 2015; Lambing, 2017). Importantly, the number and distribution of crossover events is a constraint to allelic variation that can limit breeding efficiency (Lambing et al. 2017; Lambing and Heckmann 2018). This may potentially be altered by genetic engineering and traditional breeding methods that can accelerate crop improvement and provide food security (Lambing and Heckmann 2018). For example, disruption of multiple anti-CO factors, including *FANCM*, *RECQ4A* and *RECQ4B*, can increase crossover frequency up to nine-fold without affecting chromosome segregation and thus may improve the efficiency of crop breeding programs (Séguéla-Arnaud et al. 2015).

1.4. Molecular events within meiotic recombination

Meiotic recombination pathways involve various steps from DNA double-strand break (DSB) formation to interhomolog CO and NCO formation,. NCOs, which may be detected as gene conversions, are also formed from DSBs being repaired via synthesis-dependent strand annealing (SDSA) pathway or other mechanisms (Lam and Keeney 2015; Mercier et al. 2015; Lambing et al. 2017) (Figure 1.4).

1.4.1. DSB formation

Meiotic recombination is initiated by DNA double stranded breaks (DSBs) catalysed by SPO11, a member of a well conserved protein family across eukaryotes (Keeney 1997; Keeney and Neale 2006; de Massy 2013) (Figure 1.4). SPO11 exhibits sequence similarities to the A subunit of the DNA topoisomerase from Archaea, called topoisomerase VI (TOPOVIA) (Bergerat et al., 1997). SPO11 forms an intermediate by remaining covalently linked to the 5’ ends of single-stranded DNA (ssDNA) through conserved tyrosine residues (Bergerat et al.,1997; Malik et al. 2007; Edlinger and Schlögelhofer 2011; de Massy 2013; Lam and Keeney 2015).

Unlike many other eukaryotes, *Arabidopsis thaliana* encodes three SPO11 homologs, termed *SPO11-1*, *SPO11-2* and *SPO11-3* (Hartung 2000; Hartung and Puchta 2001; Hartung et al. 2002; Stacey et al. 2006). SPO11-1 and SPO11-2 are both A subunits with active tyrosine residues and were found to share a phenotypically similar effect in mutants (Stacey et al. 2006). Both single mutants are sterile and show univalent segregation and the *spo11-1 spo11-2* double mutants did not differ from single mutants, which together implies they act together during induction of meiotic DSBs, potentially forming an obligate heterodimer (Hartung et al. 2007). SPO11-3 encodes a TOPOVIA subunit and interacts with TOPOVIB (Hartung and Puchta 2001; Hartung et al. 2002; Stacey et al. 2006; Malik et al. 2007). While SPO11-1 is necessary for efficient meiotic recombination (Grelon et al. 2001), SPO11-3 is involved in somatic endo-reduplication and has no known meiotic roles (Hartung and Puchta 2001; Hartung et al. 2002; Stacey et al. 2006). Recently, a structural homolog of the archaea TOPOVIB subunit called *meiotic topoisomerase VIB-like* (*mTOPOVIB*) was shown to form a heterotrimeric complex with SPO11-1 and SPO11-2 during meiotic recombination initiation and is also required for maintaining the heterodimeric state of SPO11-1 and SPO11-2 (Vrielynck et al. 2016).

There are nine other proteins (Mei4, Mer2, Mre11, Rad50, Rec102, Rec104, Rec114 and Ski8) that interact directly or indirectly with SPO11 in *Saccharomyces cerevisiae* (budding yeast) to promote DSBs (Lam and Keeney 2015). Unlike SPO11, these proteins are less conserved across species. For instance, the Mre11-Rad50-Xrs2 (MRX) complex in budding yeast and *Caenorhabditis elegans* is important for DSB formation, whereas their orthologs are important for meiotic DSB processing in *Arabidopsis thaliana*, *Saccharomyces pombe* (fission yeast), *Drosophila melanogaster* and *Coprinus cinereus* (Lam and Keeney 2015; Mercier et al. 2015). Similarly, Ski8 is essential for DSB formation in *S.cerevisiae*, *S.pombe* and *Sordaria macrospora*, however it has no meiotic recombination role in Arabidopsis (Jolivet et al. 2006; Lam and Keeney 2015). In Arabidopsis, several genes were identified through classical genetic screens as being involved in DSB formation, including *PRD1*, *PRD2*, *PRD3*, and *DFO* (De Muyt et al. 2007, 2009; Zhang et al. 2012). PRD1 shows similarities to the mouse protein MEI1 (De Muyt et al. 2007). PRD2 shows some similarities to Mei4 in mouse (De Muyt et al. 2009; Kumar et al. 2010).

PRD3 and DFO do not show conserved domains outside of the plant kingdom, indicating these proteins may be plant-specific (De Muyt et al. 2009; Zhang et al. 2012). Therefore, the formation of DSB machinery is variable among eukaryotes, potentially due to functional divergence (Mercier et al. 2015).

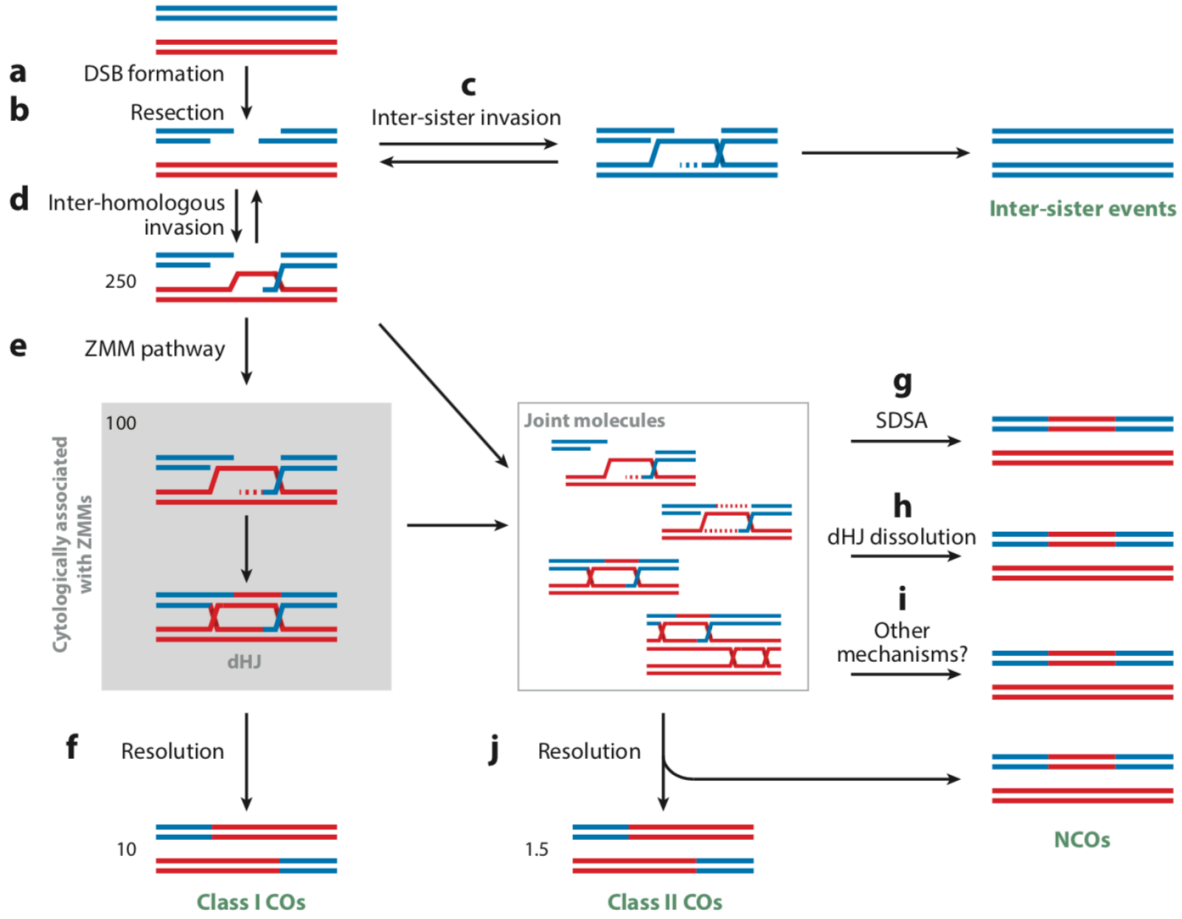

Figure 1.4. Meiotic recombination machinery. a) Recombination is initiated by DNA double stranded breaks (DSBs) are **b)** processed to produce into 3'OH ended single stranded DNA (ssDNA). This ssDNA invades into either **c)** sister chromatids or **d)** non-sister chromatids of the two homologous chromosomes to form a displacement loop (D-loop) **e)** the inter-homologous intermediates proceed to form double-Holliday junctions (dHjs) and **f)** Class I COs are matured from the dHJ intermediates repaired by the ZMM pathway. NCOs are formed from joint molecule (JM) intermediates through different mechanisms such as **g)** synthesis-dependent strand annealing (SDSA) **h)** dHj dissolution, and **i)** other mechanisms. **j)** Class II COs are produced from JM intermediates independent of Class I pathway. The proteins involved in every step are mentioned in the text. From 250 DSBs estimated in *Arabidopsis thaliana*, only 10 COs are resolved by the ZMM proteins which amount to nearly 85% of the total COs (reproduced from Mercier et al. 2015).

1.4.2. The tethered loop-axis chromosome (TLAC) model

Meiotic DSBs mediated by SPO11 and its accessory proteins are thought to preferentially form in the chromatin loops, whereas recombination occurs between chromatin loop sequences that become spatially tethered to the chromosome axis (Blat et al. 2002; Panizza et al. 2011) (Figure 1.5). In budding yeast and mouse, DSBs occur at clusters of recombination initiation sites extending to a few kilobases (~1-2 kb), called “DSB hotspots” (Baudat and Nicolas 1997; Smagulova et al. 2011; Baudat et al. 2013). The DSB hotspots in budding yeast are predominantly located within nucleosome-depleted regions in gene promoters enriched and in proximity to the euchromatic mark H3K4me3 (Pan et al. 2011; Lam and Keeney 2015; Lambing et al. 2017). DSB hotspots in Arabidopsis also showed elevations at gene promoters, in addition to terminators and introns, which were nucleosome-depleted (Choi et al. 2018). In many cases nucleosome depletion was associated with A-T sequence richness, which thereby allow SPO11 access to form DSBs (Choi et al. 2018).

Tethering of chromatin loops to the axis may happen before or after DSB formation (Kleckner 2006; Panizza et al. 2011; Lam and Keeney 2015). However, the DSB proteins are stably bound to sites of chromosome axes rather than the loops containing DSB hotspots, suggesting a pre-DSB tethering loop-axis chromosome (TLAC) model (Panizza et al. 2011; Lam and Keeney 2015). In yeast, this tethering is mediated by Spp1 (COMPASS subunit, SET1 complex), which physically interacts with Mer2 and H3K4me3 close to gene promoters. Together this promotes DSB formation by tethering chromatin to the chromosome axes and activating SPO11 access to nucleosome depleted regions (Acquaviva et al. 2013; Sommermeyer et al. 2013). In mouse, the PRDM9 protein binds to create the H3K4me3 modification and directly recruits the DSB machinery (Lam and Keeney 2015). In addition, the PRDM9 KRAB domain and its interacting proteins may bridge between hotspot DNA and chromosome axes, suggesting a conserved chromatin tethering mechanism (Imai et al. 2017; Parvanov et al. 2017). In plants, chromatin loop-tethering could also involve axial elements during DSB formation (Lambing et al. 2017).

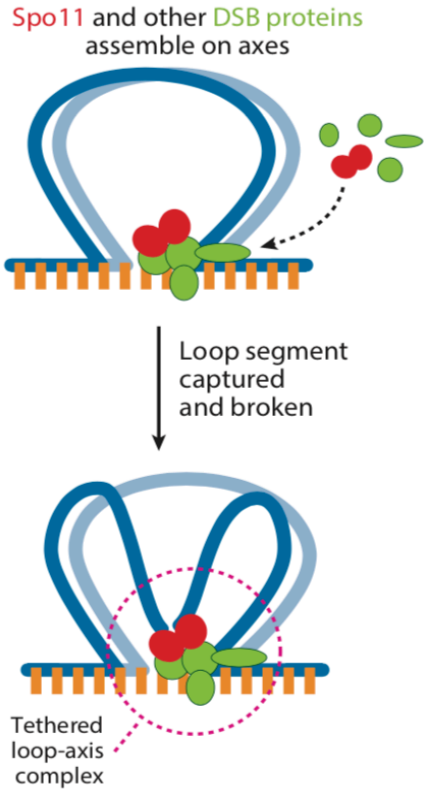

Figure 1.5. Tethered Loop-Axis Chromosome (TLAC) model integrated with DSB formation. DSBs are usually formed in the chromatin loops (blue) of DNA and recombination arises in spatial juxtaposition to underlying chromosome axes. The proposed model is the DSB machinery with SPO11 (red) and its accessory proteins (green) assembles on the chromosome axes, captures a nearby DNA loop segment and creates a break, thus forming a tethered loop-axis complex (reproduced from Keeney et al. 2014).

1.4.3. Meiotic DSB regulation

Programmed DSBs are dangerous lesions with the potential to cause genomic damage, however it is also important for meiotic cells to initiate recombination in order to create genetic diversity and balance chromosome segregation. To avoid the risk of mutations, aneuploidy or meiotic arrest, SPO11 activity needs to be tightly regulated at the right time, location and levels (Murakami and Keeney 2008; Keeney et al. 2014; Lambing et al. 2017). According to yeast models, the coordinated activities of CDK (cyclin-dependent kinase) and DDK (Dbf4-dependent Cdc7 kinase) assures DSB formation (Murakami and Keeney 2008; Keeney et al. 2014; Lam and Keeney 2015) (Figure 1.6). DDK recruitment to replisomes phosphorylates Mer2 at the beginning of replication fork, which coordinates replication with DSB formation and meiotic recombination (Murakami and Keeney 2008; Murakami and Keeney 2014a, 2014b). The number of DSBs to be formed per meiosis is constrained by a

process called “DSB homeostasis”. Hence DSBs undergo regulatory process by activation of cell cycle checkpoint kinases/CDKs (Cooper et al. 2014; Keeney, et al. 2014) (Figure 1.6). In mouse, DSB number is also regulated by Tel1/ATM, which restricts SPO11 activity in which a negative feedback loop represses further DSB formation upon ATM activation (Lange et al. 2011). Similarly, Tel1/Mec1 (ATM/ATR homologue) in budding yeast down-regulates Rec114 (a component of DSB machinery) activity via phosphorylation, which subsequently reduces or delays DSB formation (Carballo et al. 2013). Tel1/ATM activation controls DSB distribution, which results in DSB interference in adjacent chromosome regions (Cooper et al. 2014; Garcia et al. 2015; Mohibullah and Keeney 2017). Also, DSBs occur only once per four chromatids, which is locally regulated by Mec1/ATR and Tel1/ATM (Zhang et al. 2011) (Figure 1.6). DSB number and distribution are also controlled via a feedback mechanism involving homolog engagement, in which DSB formation ceases once pairing and synapsis of homologs occurs (Figure 1.6) (Kauppi et al. 2013; Thacker et al. 2014; Keeney et al. 2014; Lam and Keeney 2015).

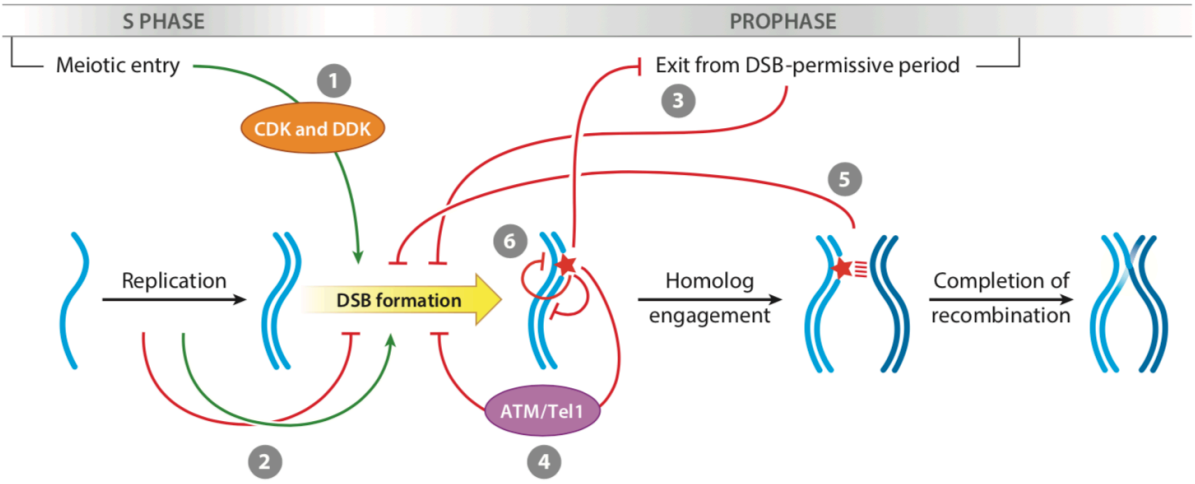

Figure 1.6. Regulatory circuits controlling DSB timing, number and distribution. 1) Cell cycle regulatory kinases (CDK and DDK) link to DSB formation on replicated chromatids. **2)** DNA replication influences temporospatial DSB patterns (green arrows) which is inhibited by replication stress (red arrow). **3)** DSB formation terminates while progression through prophase occurs. **4)** Tel1/ATM is activated which limits activity of SPO11 via negative feedback mechanism which prevents further DSB formation **5)** Homolog engagement changes chromosome structure that further restrains DSB formation **6)** Local DSB patterns regulated by ATM/ATR which limits DSBs at potential sites in *cis* (along the same DNA molecule) and in *trans* (between sister chromatids or homologous chromosomes) (reproduced from Keeney et al. 2014).

1.4.4. Meiotic DSB processing

After DSB formation, SPO11 remains covalently bonded at the 5' termini of the DSBs, which requires removal (Edlinger and Schlögelhofer 2011). Therefore, the DNA ends are nicked and resected to produce 3'-OH single stranded DNAs (ssDNAs) which is required for further steps in the recombination pathway (Neale et al. 2005; Lambing et al. 2017) (Figure 1.4). The evolutionary conserved MRX/MRN complex (Mre11-Rad50-Xrs2/Nbs1) in eukaryotes protects the genome integrity via DSB repair, DNA damage checkpoint, meiosis and telomere maintenance (Borde 2007; Šamanić et al. 2013). In budding yeast, the MRX/MRN complex (Mre11-3'-5' exonuclease) together with Sae2/Com1 initiates 3'-ended resection by endonucleolytic cleavage to release short oligonucleotides (20-40 nt) that are bound to SPO11 (Neale et al. 2005; Symington et al. 2014; Mercier et al. 2015). The short 3'-ssDNAs are then resected by Exo1/Sgs1-Dna2 (5'-3' exonuclease) which may extend 100 bp to tens of kilobases (Zakharyevich et al. 2010; Garcia et al. 2011; Symington et al. 2014; Mercier et al. 2015). In *C.elegans*, an EXO-1-dependent homologous recombination (HR) repair exists in the absence of non-homologous end joining pathway (NHEJ) and MRX/MRN (Yin and Smolikove 2013). However, the Com1/Sae2/CtIP protein function in *C.elegans* plays a conserved role in the generation of 3'-ssDNA tails (Penkner et al. 2007). In plants, the genes *MRE11*, *RAD50* and *COM1* and *NBS1*/*XRS2* are essential in the early stages of DSB repair (Puizina et al. 2004; Bleuyard et al. 2004; Uanschou et al. 2007; Waterworth et al. 2007).

1.4.5. ATM-ATR checkpoint activation during DSB processing

ATM (ataxia-telangiectasia-mutated) and ATR (ATM- and Rad3-Related) are master regulators of DNA damage signalling and belongs to a superfamily of large protein kinases, which hold a phosphatidylinositol 3-kinase (PI3K) signature at the carboxyl-terminus (Shiloh 2001; Cimprich and Cortez 2008). ATM is recruited to DSB sites through an interaction with NBS1/XRS2, which is a component of MRN complex (Jazayeri et al. 2006), however this recruitment mechanism is not well understood in plants (Roitinger et al. 2015). The endonucleolytic activity of MRN complex (Mre11-Rad50-Nbs1) is vital for ATM activation (Jazayeri et al. 2008). ATM and NBS1 are important for generating RPA (replication factor) coated 3'-ssDNAs which further

facilitates recruitment of ATR and activation of CHK1 (checkpoint kinase1) by phosphorylation (Jazayeri et al. 2006). These 3'-ssDNAs are required for loading of the strand exchange proteins RAD51 and DMC1 (Neale and Keeney 2006; Mercier et al. 2015). Once ATR is recruited, it binds to a regulatory protein ATRIP (ATR-interacting protein) and recognises the RPA coated 3'-ssDNA filaments from DSB processing and also from stalled replication forks (Matsuoka et al. 2007). Both ATM and ATR phosphorylate many substrates, including CHK1 and CHK2 (checkpoint kinases) which further phosphorylates proteins downstream of the signalling cascade called the "DNA damage response" (DDR) (Matsuoka et al. 1998, 2007).

The Arabidopsis *atm* mutants are partially sterile which is attributed to chromosome fragmentation during meiosis (Garcia et al. 2003). The Arabidopsis *mre11* mutant exhibits ATM-deficiency during meiosis causing complete sterility in *mre11-2 atm-2* double mutants, indicating a role in DNA damage signalling (Šamanić et al. 2013). In contrast to *atm*, *atr* mutants are viable and fully fertile (Culligan et al. 2004). Whereas the *atm atr* double mutants are completely sterile with ectopic chromosomal interactions being eliminated by defective *spo11*, suggesting that ATM and ATR promote timely processing of DSBs (Culligan and Britt 2008).

1.4.6. Interhomolog strand invasion during meiosis

Following DSB processing and resection, the 3'-ssDNAs bound by RPA proteins are replaced by the evolutionarily conserved RecA-related recombinases RAD51 and DMC1 (Bishop et al. 1992; Shinohara et al. 1992; Neale and Keeney 2006; Brown and Bishop 2015). RAD51 and DMC1 form pre-synaptic nucleofilaments on ssDNA tails flanking the DSB sites (Neale and Keeney 2006; Cloud et al. 2012; Pradillo et al. 2014; Brown and Bishop 2015). These filaments mediate the invasion of either intact sister chromatids or one of the two non-sister homologous chromatids to form joint molecules (JMs) or an intermediate displacement loop (D-loop) (Neale and Keeney 2006; Brown and Bishop 2015; Mercier et al. 2015) (Figure 1.4). Although inter-sister (IS) invasion can lead to DSB repair, chiasmata are formed only between homologs and inter-homolog (IH) invasion is preferred (IH bias) during meiosis (Schwacha and Kleckner 1997; Villeneuve and Hillers 2001; Brown and Bishop 2015).

The majority of eukaryotes have two structural and functional homologs of the bacterial related strand exchange proteins such as RecA, RAD51 and DMC1 (Ramesh et al. 2005; Brown and Bishop 2015). The genes *RAD51* and *DMC1* diverged following a gene duplication event which occurred during early divergence of prokaryotes and eukaryotes (Ramesh et al. 2005; Brown and Bishop 2015). Most organisms like plants, mammals and yeast possess both RAD51 and DMC1 that are required in meiotic recombination, homolog pairing and synapsis (Villeneuve and Hillers 2001; Ramesh et al. 2005; Brown and Bishop 2015). Organisms like *Drosophila*, *Sordaria* and *C.elegans* belong to "RAD51-only" group are efficient in pairing and synapsis independent of recombination (Villeneuve and Hillers 2001; Pradillo et al. 2014; Brown and Bishop 2015). Interestingly, the species which lost *MND1* and *HOP2* genes also lost *DMC1*, implying an interdependence of the three proteins (Villeneuve and Hillers 2001; Ramesh et al. 2005; Brown and Bishop 2015). Arabidopsis requires SPO11 proteins (SPO11-1 and SPO11-2) to achieve synapsis, hence is grouped with organisms having DMC1 homologs such as yeast, mouse, grasshopper and *Coprinus* (Grelon et al. 2001; Stacey et al. 2006; Pradillo et al. 2014).

RAD51 is involved in both mitotic and meiotic DSB repair, whereas DMC1 is specific to meiosis (Bishop et al. 1992; Shinohara et al. 1992; Villeneuve and Hillers 2001). In budding yeast, *dmc1* mutants accumulate processed DSBs at high levels and undergo meiotic arrest upon checkpoint activation (Bishop et al. 1992; Schwacha and Kleckner 1997). Similarly, *rad51* mutants accumulate DSBs at higher levels than *dmc1* mutants. A subset of *rad51* cells undergo meiosis and form spores with severe viability defects (Shinohara et al. 1992, 1997), and do not form DMC1 foci (Bishop 1994). In addition, *dmc1* mutants accumulate IH intermediates, show altered SC formation and arrest in late prophase I (Bishop 1994). However, recombination is completely absent in *rad51 dmc1* double mutants (Bishop 1994). In contrast to yeast, RAD51 is only involved in efficient DSB repair whereas DMC1 is dispensable in Arabidopsis (Couteau et al. 1999; Li et al. 2004). In Arabidopsis *dmc1* mutants, DSBs are efficiently repaired from intact sister chromatid duplexes, however plants have reduced fertility as COs are eliminated (Couteau et al. 1999). In Arabidopsis *rad51* mutants, defects in pairing and synapsis and SPO11-dependent chromosome fragmentation suggest that RAD51 efficiently repairs DSBs, whereas DMC1 is

essential for efficient IH repair during meiosis (Couteau et al. 1999). Like in yeast, Arabidopsis RAD51 is dispensable for CO formation during meiosis, demonstrating that RAD51 acts as an accessory factor for DMC1-mediated joint molecule formation (Cloud et al. 2012; Da Ines et al. 2013).

The recombinases RAD51 and DMC1 have similar biochemical properties and both proteins are capable of homology search and strand invasion forming a D-loop structure (Brown and Bishop 2015). However, DMC1 promotes exchange in the 5'-3' direction, whereas RAD51 promotes exchange in the 3'-5' direction towards 3'-ended ssDNA (Murayama et al. 2011). Indeed, several factors are important for proper loading, stabilization and activation of these strand exchange proteins. Accessory factors such as ASY1, MND1, HOP2, MEI5, SAE3, SDS, MCM8, ATM, ATR, BRCA2, XRCC2, XRCC3, FIGL1 and FLIP1 co-associate with RAD51 and DMC1 during DSB repair and regulate inter-homolog bias (Mercier et al. 2015; Brown and Bishop 2015; Wang and Copenhaver 2018). For example, MCM8 is involved in a RAD51 backup pathway, which repairs DSBs independent of DMC1 (Crismani et al. 2013). ASY1 is an axial element protein that coordinates the strand exchange activity of RecA homologs to favour inter-homolog recombination that is DMC1-dependent (Sanchez-Moran et al. 2007). The MND1-HOP2 complex is required to assist DMC1-dependent activities (Vignard et al. 2007). In yeast HOP1 (ASY1 ortholog) phosphorylation mediated by Tel1/Mec1 (ATM/ATR) checkpoint kinases assures DMC1-dependent interhomolog recombination (Carballo et al. 2008). The ATR kinase negatively regulates DMC1 loading at meiotic DSB sites, and its removal promotes DMC1-mediated meiotic inter-homolog DSB repair governed by ASY1 (Kurzbauer et al. 2012; Sanchez-Moran et al. 2007). Recently, the anti-crossover factors FIGL1 and FLIP1 have also been found to regulate dynamics of RAD51 and DMC1 (Girard et al. 2015; Fernandes et al. 2018).

Models have been proposed recently with RAD51 and DMC1 loading onto processed DSBs. In the proposed asymmetric loading model in Arabidopsis (Kurzbauer et al. 2012), SPO11-mediated DSBs activates ATM kinase that phosphorylates ASY1, thereby producing a signal that is locally restricted in the area of the DSB site. The processed DSBs produced with 3'ssDNAs are bound by the RPA trimeric complex which activates ATR via ATRIP (interacting partner). ATR

blocks loading of DMC1, but not RAD51. Hence, RAD51 replaces RPA by loading onto one end of the DSB. Subsequent loading of DMC1 to another end of the DSBs takes place once ATR signalling is attenuated. The recombinases on both ends of the DSBs thus search for homologous sequences. ATR, on the other hand, impedes access to IS chromatids for efficient IH recombination. Hence, RAD51 loading may weaken ATR signalling activity to allow loading of DMC1 (Kurzbauer et al. 2012) (Figure 1.7). However, it is also possible that pairs of RAD51 filaments loaded onto both the ends of DSBs stimulate the assembly of DMC1 filaments in the presence of mediating accessory factors (Figure 1.7) (Brown and Bishop 2015).

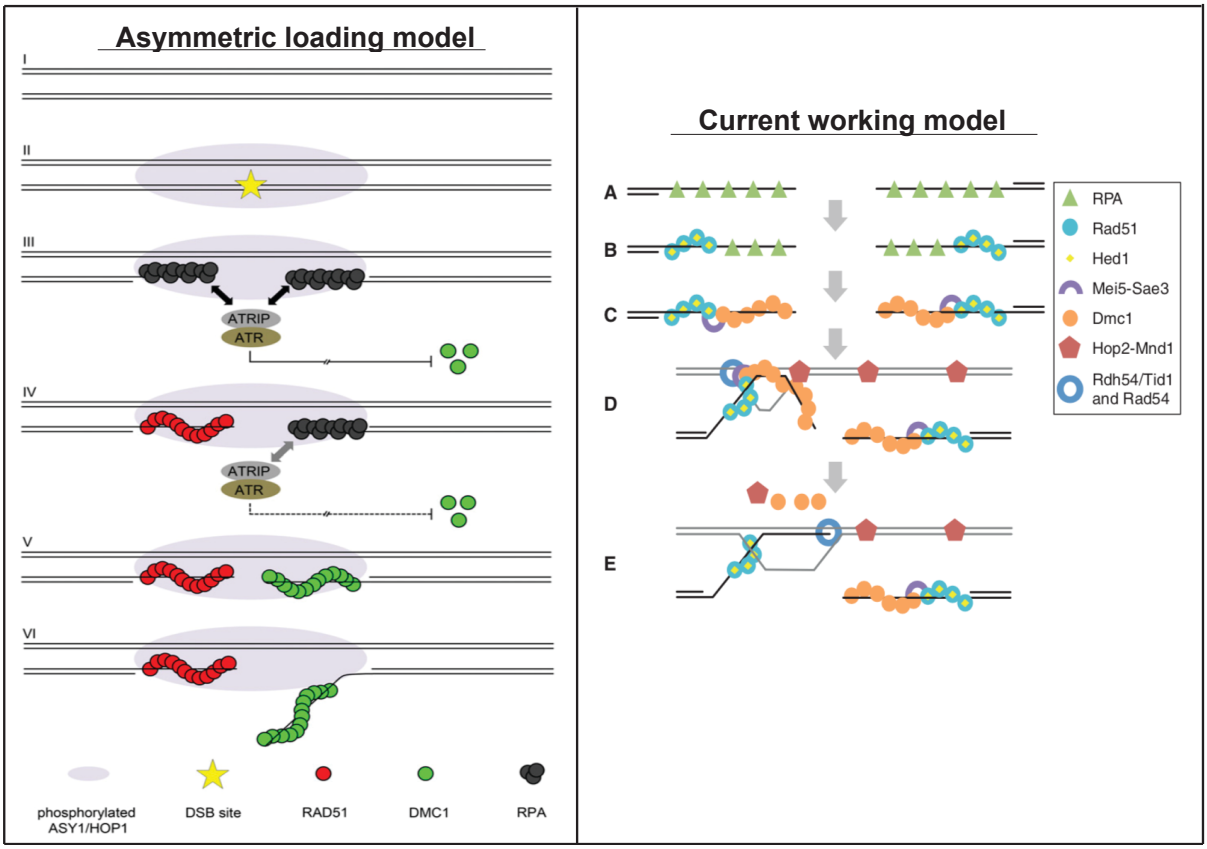

Figure 1.7. Proposed models of RAD51 and DMC1 loading during inter-homolog strand invasion. Asymmetric loading model (reproduced from Kurzbauer et al. 2012)**: I)** DSBs occur in one of the sister chromatids. **II)** DSBs lead to ATM kinase activation and ASY1 (Hop1) phosphorylation that produces a signal confined to the break site. **III)** DSB processing produces RPA coated 3'-OH ssDNAs which activates ATR via ATRIP. Recruitment of ATR-ATRIP blocks only DMC1 loading. **IV)** RAD51 is loaded onto one end of DSBs replacing RPA and ATR signalling is attenuated. **V)** Following ATR attenuation, DMC1 is loaded on to another end of the DSBs. **VI)** RAD51 end is retained whereas DMC1 is released for homology search. Current working model (reproduced from Brown and Bishop 2015): **A)** RPA is deposited on both ends of 3-ssDNAs. **B)** RAD51 (with set of mediators) replaces RPA and loaded on to both ends. Hed1 (RAD51 regulator) prevents RAD51 to form D-loops **C)** Mei5-Sae3 promotes loading initiation of DMC1 at the end of RAD51.

D) DMC1 elongates on DNA and search for homologous sequences and completes the formation of heteroduplex DNA from one end. Efficient homology search requires Hop2-Mnd1 complex which is bound to dsDNA. **E)** The Rad54 then binds to RAD51 by replacing DMC1 and translocates along the heteroduplex extending to the 3' prime end.

1.4.7. Crossover and non-crossover formation

The nascent D-loop formed from strand invasion at early zygotene has two possible repair fates, that is termed crossover/non-crossover (CO/NCO) differentiation. First, after D-loop extension, it can be dismantled leading to repair of DSBs by synthesis-dependent strand annealing mechanism (SDSA) and the resultant recombination event is termed a NCO that lacks reciprocal exchange, but may cause a gene conversion (Hunter and Kleckner 2001; Börner et al. 2004; Mercier et al. 2015; Brown and Bishop 2015; Lambing et al. 2017) (Figure 1.4). The second fate is that this nascent D-loop stabilizes to form an asymmetric intermediate called the single-end invasion (SEI), which may undergo second end-capture (SEC) of the DNA from the same DSBs either by single strand annealing or an independent strand invasion (Hunter and Kleckner 2001; Brown and Bishop 2015; Lambing et al. 2017). These SEC intermediates stabilize to form joint molecules (JM) which may then resolve into Class II COs or be dissolved by other mechanisms to form NCOs (Mercier et al. 2015; Lambing et al. 2017). However, if the SEC happens from the opposite DSB end, it forms a stable double-Holliday junction (dHJs) intermediate (Brown and Bishop 2015; Lambing et al. 2017). The dHJ intermediates may then be resolved as a Class I CO or dissolved into a NCO (Figure 1.4) (Brown and Bishop 2015; Mercier et al. 2015; Lambing et al. 2017).

In most eukaryotes, CO formation is bifurcated into Class I interfering (dHJ-dependent/ZMM) and Class II non-interfering CO pathways (Figure 1.4). Class I COs resolved by the ZMM pathway are subject to interference, where one crossover inhibits the formation of adjacent crossovers, thus the COs are tightly regulated and evenly spaced per chromosome pair (Jones and Franklin 2006; Wang et al. 2015). The Class I pathway is mediated by a set of proteins identified in budding yeast, called the ZMM proteins (Börner et al. 2004; Lynn et al. 2007). This ZMM group includes Zip1, Zip2, Zip3, Zip4, Msh4, Msh5 and Mer3 in budding yeast (Börner et al. 2004; Lynn et al. 2007). Other ZMM proteins have been identified which include

Spo16 in budding yeast, COSA-1 (CO-associated site 1) in *C.elegans* and HEI10 in mammals (Shinohara et al. 2008; Yokoo et al. 2012; Qiao et al. 2014). In budding yeast, *zmm* mutants exhibit normal NCOs while COs are reduced. Additionally, these mutants show defects in formation of SC, SEIs and dHJ molecules (Börner et al. 2004; Shinohara et al. 2008). In Arabidopsis, mutations in *MER3*, *MSH4*, *MSH5*, *SHOC1*, *PTD*, *HEI10* and *ZIP4* genes result in a significant reduction in CO numbers by nearly 80-90% (Higgins et al. 2004, 2008a; Macaisne et al. 2008, 2011; Chelysheva et al. 2007, 2012). In *mer3* mutants, COs are slightly reduced to 71-76 %, and its combination with *shoc1* further reduced crossovers by 85 %. Similarly, *msh4 and msh5* single mutants showed reduced chiasma frequency to ~87 % of wild type (Higgins et al. 2004; Higgins et al. 2008a). Hence, it is clear that ZMM pathway accounts for majority of the COs in wild type Arabidopsis (Mercier et al. 2015).

The ZMM proteins are critical for stabilization of dHJ intermediates and co-ordinately promote SC polymerization which is required for Class I CO formation. (Mazina et al. 2004; Snowden et al. 2004; Lynn et al. 2007; Hunter 2015; Zickler and Kleckner 2015). The MSH4-MSH5 heterodimer (MutS family-related) recognize dHJ early intermediates, forms a sliding clamp in the presence of ATP and stabilizes and preserves the DSB repair (DSBR) intermediates for dHJ formation (Snowden et al. 2004; Lynn et al. 2007). The MER3 helicase unwinds the heteroduplex DNA in the 3'-5' direction using ATP *in vitro* stimulated by RAD51 activity and prevents duplex extension in the 5'-3' direction, indicating it promotes stabilization of nascent JMs to permit SEC for dHJ-dependent CO formation (Nakagawa et al. 2001; Nakagawa and Kolodner 2002; Mazina et al. 2004; Chen et al. 2005; Mercier et al. 2005). In addition, the ZMMs appears to block the dissociation of JMs by opposing anti-CO activities of the STR (Sgs1-Top3-Rmi1) complex (Jessop et al. 2006; Oh et al. 2007; Kaur et al. 2015; Tang et al. 2015; Séguéla-Arnaud et al. 2015). For example, Zip2-Spo16 in budding yeast forms a XPF-ERCC1-like complex as well as stably forms a complex with Zip4 (De Muyt et al. 2018). Zip4 acts to link axis components and the CO machinery, whereas the XPF-ERCC1-like complex recognises the JM intermediates protecting them from being dismantled by the anti-CO STR complex and thereby promotes CO formation (De Muyt et al. 2018). Southern blot analysis via 2-D gels detected SEIs, JMs and dHJ molecules at yeast recombination hotspot and

IH CO/NCO differentiation events during SEI-dHJ transition, which is modulated by REC8 cohesin-axis components (Hunter and Kleckner 2001; Lynn et al. 2007; Kim et al. 2010).

A large number of precursors are repaired into a small number of interfering COs (Börner et al. 2004; Lynn et al. 2007; Mercier et al. 2015; Hunter 2015). For example, Arabidopsis MSH4-MSH5 foci at leptotene-zygotene stage are high in number and then gradually reduce at mid-zygotene and do not persist later in pachytene (Higgins et al. 2004; Higgins, Vignard, et al. 2008). Also, Arabidopsis HEI10 (related to Zip3) appears as numerous foci at early prophase and disappears during pachytene where it becomes restricted to a limited number of bright foci that colocalize with MLH1 (ZMM CO marker) and Class I chiasmata from late pachytene to diakinesis (Lynn et al. 2007; Chelysheva et al. 2012). Thus from numerous early recombination intermediates processed by ZMMs, only a few mature into COs marked by late HEI10 and MLH1 foci (Figure 1.4) (Mercier et al. 2015).

Budding yeast Zip3 is a RING domain E3 ligase that catalyses SUMO conjugation and is required for normal localization of other ZMMs (Agarwal and Roeder 2000; Cheng et al. 2006; Shinohara et al. 2008). Unlike Arabidopsis HEI10, mouse possesses HEI10 (ubiquitin E3 ligase) as well as RNF212 (SUMO ligase) (Chelysheva et al. 2012; Reynolds et al. 2013; Qiao et al. 2014). RNF212 selectively localizes to pre-crossover sites to stabilize the MutSγ complex, MSH4-MSH5 and HEI10 limits cross-over by ubiquitylation and displacing the RNF212 and MutSγ complex, suggesting antagonistic roles during meiotic recombination. Interestingly, RNF212 and HEI10 have been identified to show dosage sensitivity, that is the heterozygous mutants (*rnf212/+* and *hei10/+)* showed reduced COs (Reynolds et al. 2013; Qiao et al. 2014). RNF212 variants show association with variation in the genome-wide recombination rate (Kong et al. 2008). In Arabidopsis, *HEI10* was also identified as a natural crossover modifier whose additional copies on transformation doubled the recombination rate, indicating its function as a dosage-sensitive CO regulator (Ziolkowski et al. 2017). Another ZMM protein is Zip4/Spo22 which is required for class I interfering COs, however is not important for SC (Zip1) polymerization as synapsis completes in Arabidopsis *zip4* mutants (Chelysheva et al.

2007). SHOC1 promotes Class I interfering COs along with PTD, MSH4, MSH5, MER3, MLH3 through a meiosis-specific XPF-ERCC1-like heterodimeric complex (Macaisne et al. 2008, 2011).

The two conserved mismatch-repair factors or MutLγ homologs comprising MLH1 and MLH3 act in the ZMM pathway, although they are not classified as ZMMs (Mercier et al. 2015; Hunter 2015). The ZMM stabilized dHJs are subjected to the MutLγ homologs (MLH1-MLH3) combined with EXO1 resolves the JMs into COs (Zakharyevich et al. 2010, 2012; Ranjha et al. 2014; Rogacheva et al. 2014). In budding yeast *exo1* and *mlh1/3* mutants, joint molecule formation occurs normally whereas crossing-over is diminished, indicating EXO1 and MLH1/3 are important for CO-specific resolution (Zakharyevich et al. 2010, 2012). Although EXO1 nuclease activity is not required for CO functions, its interaction with MutLγ factors are important (Zakharyevich et al. 2012). The MLH1-MLH3 heterodimeric complex preferentially binds to Holliday junctions *in vitro* and its endonuclease activity indicates a direct role in dHJ resolution, therefore is important for pro-CO formation (Ranjha et al. 2014; Rogacheva et al. 2014). In the majority of organisms, MutLγ proteins specifically mark Class I COs (ZMM-dependent) at late prophase and is used as a cytological marker of crossovers (Lhuissier et al. 2007; Chelysheva et al. 2010; Mercier et al. 2015; Hunter 2015). In Arabidopsis, CO frequency was reduced to ~50 % of the wild type level in *mlh1* and *mlh3* mutants (Jackson et al. 2006; Chelysheva et al. 2012).

A minority of COs (5 to 25 %) are resolved into Class II COs by MUS81-EME1/MMS4, SLX1-SLX4 and YEN1/GEN1 structure specific endonucleases which efficiently process the JMs (Hunter 2015). Genetic and microscopic imaging analyses show that Class II COs account for 10 to 20 % of the total COs and exhibit no interference (Berchowitz et al. 2007; Anderson et al. 2014) (Figure 1.4). Most eukaryotes possess two pathways to resolve dHJs into COs, however some organisms are dependent on one pathway or the other (Matos et al. 2011; Mercier et al. 2015). For example, fission yeast is dependent on MUS81-EME1 only for CO formation (Boddy et al. 2001; Osman et al. 2003), whereas Class II COs do not form

in *C.elegans*. However, budding yeast and Arabidopsis perform both Class I and II COs (Gray and Cohen 2016; Mercier et al. 2015).

MUS81 interacts with the non-catalytic subunit EME1 (in mammals and fission yeast) or MMS4 in budding yeast for biochemical activity (Hunter 2015; Gray and Cohen 2016). Arabidopsis consists of two EME1 homologs, EME1A and EME1B which form a complex with MUS81 (MUS81-EME1A/B). These MUS81-EME1A/B complexes cleave 3'-flaps, nicked HJs and intact HJs with reduced efficiency *in vitro* (Geuting et al. 2009). MUS81-EME1/MMS4 is an XPF endonuclease which is capable of cleaving branched DNA structures such as D-loop, nicked HJs and 3'-flaps *in vitro* (Schwartz and Heyer 2011; Mukherjee et al. 2014). In budding yeast, *mus81* and *msh4* mutants show a slight reduction in CO formation but form spores efficiently with reduced viability to 50%, indicating that a few unresolved HJs affects meiosis significantly (de los Santos et al. 2001, 2003; Boddy et al. 2001; Haber and Heyer 2001). Although, MUS81-MMS4 and Sgs1 helicase collaborate to eliminate aberrant JMs, it has a minor role in resolution in the absence of Sgs1, hence functions as a backup mechanism (Kaliraman et al. 2001; Oh et al. 2008). In mouse, *mus81* mutants showed significant meiotic defects during its progression such as smaller testis size, upregulated MLH1 accumulation in an interference-independent manner, and a subset of DSBs unrepaired. This indicates that in the absence of Class II COs, the Class I may be elevated (Holloway et al. 2008). In fission yeast, MUS81 is exclusively essential for meiotic crossovers and not gene conversions. In the absence of MUS81 or EME1, meiosis is deficient with reduced spore viability and unresolved HJs (Smith et al. 2003). In Arabidopsis, *mus81-2* mutants show normal meiosis with fully fertile plants (Higgins et al. 2008b), whereas they show deficiency in homologous recombination in somatic cells after induction by genotoxic stress (Hartung et al. 2006). However, CO frequency was measured using pollen tetrad visual assay at chromosome 1 and 3 intervals showed a moderate reduction of ~9% to 12% in *mus81-2* mutants compared to *msh4* mutants (~75 %) and the *mus81 msh4* double showed a 80% reduction compared to wild type (Berchowitz et al. 2007). This is consistent with the reduced chiasma frequency (0.85 per cell) compared to *msh4* (1.25 per cell), concluding that MUS81 accounts for a subset of COs (~10%) that are interference-insensitive (Higgins et al. 2004, 2008b; Berchowitz et al. 2007).

SLX1 nuclease activity depends on its interaction with the scaffold protein SLX4 and the SLX1-SLX4 complex cleaves the branched structures, 5'-flaps and HJs (Fricke and Brill 2003; Svendsen et al. 2009; Gaur et al. 2015). SLX4 also interacts with the structurally related flap endonucleases such as ERCC4, XPF-ERCC1 and MUS81-EME1 (Svendsen et al. 2009; Kim 2014). *In vitro* studies revealed the endonuclease activity of GEN1 (Yen1 in yeast) in HJ resolution (Ip et al. 2008). In budding yeast, *yen1*, *slx1* and *slx4* single mutants show no defects in meiotic recombination although the resolution activities of Yen1 and Slx1/4 are robust in *sgs1 mms4* double mutant background (Zakharyevich et al. 2012). In *yen1*, the JMs disappear with a delay in parallel to delayed appearance of COs and meiotic divisions, indicating Yen1 facilitates timely resolution of JMs in wild type cells (Zakharyevich et al. 2012; Matos et al. 2011). Similarly, time course experiments in *slx1* and *slx4* suggested a slightly delayed turnover of some JM intermediates (Zakharyevich et al. 2012). SLX1/SLX4 nucleases are essential to resolve a subset of JMs in the absence of Sgs1 (Zakharyevich et al. 2012; De Muyt et al. 2012). Similar to *mus81*, mutation in mouse *Slx4/Btbd12* delays meiotic DSB repair while normal CO numbers formed, however a subset of COs that are resolved by MLH1 showed a Class I foci increase (Holloway et al. 2011). There are plant homologs of these recombination factors however their functions are unknown.

Yen1, on the other hand, acts as a resolvase specifically in the absence of Mus81-Mms4, although it is non-essential for meiotic recombination (Matos et al. 2011; De Muyt et al. 2012; Zakharyevich et al. 2012). Also, Mus81-Mms4 and Yen1 resolve JMs formed in the absence of Top3 and Rmi1 (anti-CO factors) similar to their activities in the absence of Sgs1 (Oh et al. 2008; De Muyt et al. 2012; Zakharyevich et al. 2012; Kaur et al. 2015). Both Mus81-MMs4 and Yen1 are tightly regulated by Cdc5-mediated phosphorylation that extend to sequential activation. First, Mus81-Mms4 is activated during meiosis I which produces COs required for chromosome segregation. Later, Yen1 is activated in meiosis II to resolve the persistent HJs (Matos et al. 2011; Matos and West 2014). Two paralogs such as GEN1 and SEND1 are known to possess HJ resolvase activity, however its functions are yet to be characterized (Bauknecht and Kobbe 2014). In budding yeast, absence of all three HJ resolvases (Mus81-Mms4, Slx1-Slx4 and Yen1) showed a moderate reduction in

JM resolution and CO formation, indicating their role in JM resolution to majorly Class II COs and a small fraction is repaired by Class I CO factors (Zakharyevich et al. 2012; De Muyt et al. 2012).

In addition to the two CO pathways, there are other mechanisms that significantly contribute to DSB repair by dissolution of 3'-ssDNA invasion intermediates via synthesis-dependent strand annealing (SDSA) pathway forming NCOs (Mercier et al. 2015; Brown and Bishop 2015; Lambing et al. 2017) (Figure 1.4). A suppressor screen in Arabidopsis using *zmm* mutant (*zip4*) identified three major groups of anti-CO factors that promote NCO formation. The first group forms the FANCM (Fanconi anemia of complementation group M) and its direct DNA binding co-factors MHF1 and MHF2 are capable of unwinding the D-loop during SDSA and promote NCOs (Crismani and Mercier 2012; Girard et al. 2014). *In vitro* studies in fission yeast also demonstrated the FANCM activity (Lorenz et al. 2012). The Arabidopsis *FANCM* mutation restores CO formation in the absence of ZIP4 and showed an increase in CO frequency to 3-fold (Crismani et al. 2012). Second, STR/BTR/RTR complex is also involved in the active disassembly of the extended D-loops via SDSA to promote NCOs (Kaur et al. 2015; Séguéla-Arnaud et al. 2015; Tang et al. 2015). TOPOISOMERASE3α (TOP3α) is a member of the human BLM-TOP3α-RMI1-RMI2 (or *S.cerevisiae* Sgs1-Top3-Rmi1) complex is essential for mitotic and meiotic DNA repair (Kohl and Sekelsky 2013; Hunter 2015). This STR/BTR complex exhibits a strong anti-CO activity *in vivo* and act to prevent aberrant recombination intermediates during meiosis I (Jessop et al. 2006; Oh et al. 2007, 2008; Séguéla-Arnaud et al. 2015; Kaur et al. 2015; Tang et al. 2015). The Top3-Rmi1 heterodimer alone has a decatenase activity, which dissolves dHJs forming a complex with Sgs1/BLM. Later, it resolves some molecules produced by Sgs1 activity (Kaur, et al. 2015). Like Sgs1, Top3-Rmi1 is essential for all meiotic recombination functions (CO and NCO roles) defined for Sgs1/STR complex (Kaur, DeMuyt, and Lichten 2015; Tang et al. 2015). Notably, Top3-Rmi1 performs Sgs1-independent functions in resolving JMs to remove recombination-dependent chromosome entanglements at anaphase. Hence, a late of Top3-Rmi1 is essential for accurate chromosome segregation during meiosis (Kaur et al. 2015; Tang et al. 2015).

An absence of the STR complex leads to aberrant multi-chromatid structures which form the recombination intermediates and JM resolution to COs and NCOs becomes relaxed that is highly dependent on Class II nucleases (Mus81-Mms4, Slx1/4 and Yen1) and *Ndt80* and independent of Class I MutLγ (MLH1/3) factors (Jessop et al. 2006; Oh et al. 2007, 2008; De Muyt et al. 2012; Zakharyevich et al. 2012; Kaur et al. 2015; Tang et al. 2015). Consistently, in budding yeast, absence of all three nucleases showed high levels of COs which are dependent on both Sgs1 and MLH1/3 (De Muyt et al. 2012; Zakharyevich et al. 2012). Thus, STR complex exhibits dual functions in pro-CO (facilitate Class I CO) and NCO formation (via SDSA) (Jessop et al. 2006; Oh et al. 2007, 2008; De Muyt et al. 2012; Zakharyevich et al. 2012; Kaur et al. 2015; Tang et al. 2015). The Arabidopsis TOP3α forms a complex *in vivo* with RMI, RMI2, and the RECQ4A proteins (Séguéla-Arnaud et al. 2015). RecQ helicases (3'-5' DNA helicase) are conserved throughout all kingdoms with respect to structure and function (Hartung and Puchta 2006; Hartung et al. 2007). RECQ4A is related to Sgs1/BLM helicase and RECQ4B is a close paralog evolved from a duplication event specific to Brassicaceae family (Hartung and Puchta 2006; Hartung et al. 2007). These RECQ4 helicases have biochemical activities in disassembly of D-loops and dHJ decatenation (Bernstein et al. 2010). The *recq4a* and *recq4b* single mutants show no effect in CO frequency, whereas a ~1.5-fold increase in *top3α-R640X* (premature STOP codon at position 640) and *top3α-R640X recq4b* mutants, and an ~6-fold increase in CO frequency in the *top3α-R640X recq4a/b* double mutants (Séguéla-Arnaud et al. 2015). Genetic analyses of *top3α-R640X recq4a/b* with *fancm* shows a cumulative crossover increase of up to 9-fold, indicating they act independently to repress CO formation, which may presumably reflect differing the processing of intermediates. Despite the significant CO increase in *fancm top3α-R640X recq4a/b* mutants these plants are fertile (Séguéla-Arnaud et al. 2015).

Third, the conserved AAA-ATPase FIDGETIN-LIKE-1 (FIGL1) is an anti-CO factor that limits COs by controlling the dynamics of RAD51 and DMC1 during strand invasion (Fernandes et al. 2018). This was validated by the persistence of RAD51 and DMC1 foci (DSB markers) in the *figl* mutant. Unlike *fancm*, mutation in FIGL increases COs in both inbred and hybrid contexts. FIGL also acts independently of

FANCM similar to BLM helicases, as *fancm figl* double exhibits a synergistic increase in crossovers (Fernandes et al. 2018). As FIGL1 limits strand invasion, FANCM unwinds D-loop via SDSA suggesting their individual mechanisms to promote NCOs (Girard et al. 2015). Recently, a new partner of FIGL1 has been identified called FLIP1, which together limits meiotic recombination (Fernandes et al. 2018). Interestingly, the observed extra COs arise in the Arabidopsis anti-CO mutants are likely to involve in Class II/non-interfering pathway that is MUS81-dependent (Crismani et al. 2012; Girard et al. 2014, 2015; Séguéla-Arnaud et al. 2015; Fernandes et al. 2018). Combining the mutations in anti-CO helicases *RECQ4* and *FIGL1* increases COs to 7.8-fold (Fernandes et al. 2017). Also, the combination of pro-crossover factor *HEI10* and mutations in *RECQ4A* and *RECQ4B* shows a massive CO increase specially in the euchromatic regions (Serra et al. 2018). These combinations were validated in Arabidopsis Col/Ler hybrids, suggesting its significant impact in crop breeding programs (Fernandes et al. 2017; Serra et al. 2018).

1.5. Crossover number and location regulation

In many species, CO distribution is not homogeneous along chromosomes. In species like Arabidopsis, budding yeast, humans and wheat, > 80% of recombination events occur in less than a quarter of the genome (Mercier et al. 2015; Mézard, Tagliaro Jahns, and Grelon 2015). In many plants, the distribution is skewed towards the distal end of the chromosomes and also the centromeric regions are devoid of COs (Mercier et al. 2015). Moreover, CO distribution varies between sexes within the same species (Giraut et al. 2011). The COs are derived from DSB events, however not every DSB has a chance to give rise to a CO and rather is repaired to form NCOs (Mercier et al. 2015; Mézard et al. 2015; Lambing et al. 2017). At the fine scale, COs and NCOs exist in clusters of small regions of a few kilobases (1-2 kb) called hotspots and their localization reflects the position of DSBs (Choi et al. 2013; Drouaud et al. 2013; Mercier et al. 2015). In mammals, hotspots are targeted to DNA sequence motifs by the zinc finger domain protein PRDM9 (Baudat et al. 2010; Baudat et al. 2013; Parvanov et al. 2010). The PRDM9-dependent COs occur mainly in the intergenic regions and introns (Myers 2005; Kong et al. 2010). PRDM9 has a SET domain with histone H3 lysine 4 tri-methyltransferase activity that targets the modification of hotspot chromatin during meiotic prophase and promotes

recombination initiation (Hayashi, Yoshida, and Matsui 2005; Smagulova et al. 2011; Grey et al. 2011; Brick et al. 2012). In contrast, hotspots in budding yeast are not sequence-dependent and occur largely in the chromatin accessible regions of low nucleosome density (LND) in gene promoters (Pan et al. 2011). Moreover, budding yeast hotspots are closely associated with H3K4me3 (Acquaviva et al. 2013; Sommermeyer et al. 2013). In Arabidopsis, which lacks PRDM9, COs are increased towards gene promoters and terminators, and hotspots were associated with active chromatin modifications, including H2A.Z, H3K4me3, LND and low DNA methylation (Choi et al. 2013). Hotspot A-rich and CTT DNA motifs found in the upstream and downstream of transcriptional start sites (TSS) may contribute to chromatin reorganisation which is important for DSB formation (Choi et al. 2013).

Other than genetic and epigenetic factors that promote recombination, heterochromatic marks suppress COs. Loss of DNA methylation (CG context) in the *methyltransferase1* (*met1*) in Arabidopsis show epigenetic remodelling of CO frequencies with increases in centromeric regions which is compensated by the decrease in peri-centromeric regions and increase in the euchromatic distal chromosome regions. However, the total CO number between wild type and *met1* remains the same (Yelina et al. 2012). Further, using RNA-dependent DNA methylation (RdDM) of hotspots located in the euchromatic regions recombination could be silenced (Yelina et al. 2015). This triggered dense DNA methylation in the targeted regions, with methylation in both CG and non-CG sequence contexts, suggesting that de novo DNA methylation causes a localized silencing of meiotic recombination (Yelina et al. 2015). Similarly, loss of heterochromatic mark H3K9me2 and non-CG methylation in the *chromomethylase3* (*cmt3*) show elevated meiotic DSBs and COs in the pericentromeric regions (Underwood et al. 2018). At megabase scale, juxtaposition of homozygous and heterozygous regions in Arabidopsis hybrids (e.g. Col/Ler F_1) generated from natural accessions favour COs in the heterozygous regions at the expense of homozygous regions due to CO interference (Ziolkowski et al. 2015). Hence, heterozygosity may promote Class I CO dependent pathways, whereas it inhibits Class II non-interfering CO pathway (Ziolkowski et al. 2015). Other *cis* factors include single nucleotide polymorphisms (SNPs) and indels that locally inhibit COs at the hotspot scale (~1-2 kb), structural polymorphisms, including inversions and translocations, and *trans* modifiers on the

same or different chromosomes (e.g. *HEI10*) (Ziolkowski and Henderson 2017; Ziolkowski et al. 2017).

In most eukaryotes, COs are relatively few in number. Typically, there are 1-3 COs per bivalent per meiosis and it does not increase in proportion with their physical genome size (Mb) (Mercier et al. 2015; Fernandes et al. 2017). Nearly 80% of the chromosomes have 3 COs or fewer with few exceptions (Mercier et al. 2015; Fernandes et al. 2017). For example, wheat chromosome 3B has a physical size 900 Mb and has an average of ~3 CO/meiosis, which is comparable to the longest chromosome in Arabidopsis (31 Mb) and the smallest one in budding yeast (0.3 Mb) (Mercier et al. 2015; Fernandes et al. 2017). In contrast, fission yeast have three chromosomes with more than 9 COs/chromosome, likely due to loss of CO interference (Berchowitz and Copenhaver 2010; Mercier et al. 2015; Fernandes et al. 2017) (Figure 1.8). However, the CO limitation observed in species like wheat is not due to shortage of DSBs. In fact, the estimated DSBs in many species greatly exceed the final CO number. For example, in Arabidopsis, ~250 DSBs (counting RAD51/DMC1 foci) are produced which mature into ~10 COs with ~2 COs per chromosome (Girard et al. 2015; Mercier et al. 2015). In mouse spermatocytes, ~200 DSBs are produced with high cell-cell variability and the final COs marked by MLH1 are ~22-24 in number with little variation (Cole et al. 2012).

Hence, CO numbers are tightly regulated by three related mechanisms such as CO assurance, interference and homeostasis. To better understand these mechanisms, a beam-film (BF) model was proposed (Kleckner et al. 2004; Wang et al. 2015). Each homolog pair obtains at least one CO which is required for accurate chromosome segregation, defining a regulatory pattern termed CO assurance (Hunter 2015; Wang et al. 2015). According to Beam-film (BF) model, obligatory COs are assured by the level of accumulated mechanical stress for CO designation along the chromosome axes (Kleckner et al. 2004; Wang et al. 2015). In addition, occurrence of the obligatory COs requires that the CO-designated interactions must efficiently produce the final CO products, or else the effect of efficient designation will be lost (Wang et al. 2015). For example, inefficient maturation into COs at the designated sites increased aneuploidy during human female meiosis (Wang et al. 2017).

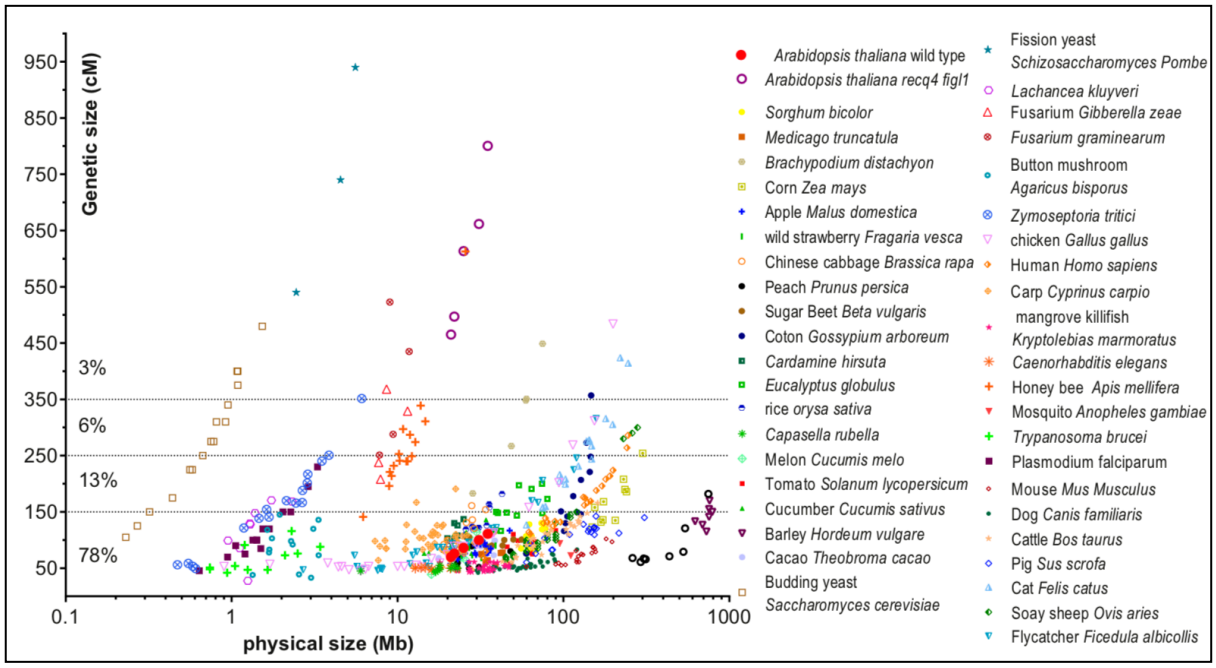

Figure 1.8. Crossovers are limited in eukaryotes. A plot with representation of more species in number (reproduced from Fernandes et al. 2017) compared to the previously published (Mercier et al. 2015). Chromosomes from a range of eukaryotic species (right side of the plot) are plotted according to their physical size (x-axis Mb, log scale) and genetic size (y-axis centimorgan/cM, linear scale). Sex chromosomes have been excluded for plotting. The physical size is based on genome sequence assembly and the genetic size is based on F2 or male/female average. This dataset is provided in this article. At the lower limit, chromosomes measure 50 cM which correspond to at least one CO/ bivalent. In contrast to wild type *Arabidopsis thaliana,* COs/chromosome increased in *recq4 figl1* hybrid (Col/Ler) background.

One could speculate how the obligatory COs are achieved in different organisms. For example, in *C.elegans*, COSA-1 foci (Class I CO marker) localizes to crossover sites with one per chromosome pair and Class II COs do not exist (Yokoo et al. 2012). In mouse, MLH1 foci (Class I CO marker) with at least one per chromosome pair are seen (Cole et al. 2012). In Arabidopsis *zip4* mutants no chiasma are formed in majority of the chromosomes, whereas in *fancm* and *fancm zip4* chiasma frequency is mostly increased with the majority of chromosomes having at least one on each arm. However, extra COs formed are repaired by the Class II/non-interfering pathway. The absence of bivalents during metaphase I in *fancm zip4 mus81* triple indicates that obligatory COs cannot be assured by the Class II pathway, hence is likely to be Class I-dependent (Crismani et al. 2012).

Crossover interference is another mechanism which limits COs. A phenomenon whereby adjacent crossovers are observed less frequently than expected by chance, which acts over megabase physical scales, leading to COs that are evenly spaced along the chromosomes (Berchowitz and Copenhaver 2010; Wang et al. 2015). This was originally identified in the genetic map of *Drosophila* constructed by Sturtevant in which the sex-linked factors are arranged in linear series on the chromosomes and the expected probability of double crossovers (DCO) acts as an interference index (Sturtevant 1913). Genetic analysis and cytology methods have been established to measure COs and interference in model organisms. Measuring CO interference is generally based on two kinds of analysis namely, the Gamma-distribution model and Coefficient of Coincidence (CoC) (Mcpeek and Speed 1995; Zhang et al. 2014a). The Gamma-distribution model measures the inter-crossover distances (Mcpeek and Speed 1995), whereas CoC curves analyse the inter-interval distance at which the interference is affected (Zhang et al. 2014a). For CoC analysis, the chromosome of interest is divided into number of intervals and for every interval the CO frequency is measured. Then, the intervals are considered as pairs. For each pair of intervals, CoC is measured as the ratio between the observed and expected frequency of DCOs (Figure 1.9) (Zhang et al. 2014a; Ziolkowski and Henderson 2017).

The third mechanism of CO control is homeostasis. CO assurance and interference together prescribe the upper and lower limits of CO numbers and support the CO homeostasis mechanism (Hunter 2015). Despite high variations in the DSB numbers, CO numbers per meiosis are formed with low variation (Yokoo et al. 2012; Cole et al. 2012). In mice, RAD51 and DMC1 foci (DSB markers) showed high variability whereas MLH1 foci (Class I CO marker) showed less variation between cells, suggesting a homeostatic control (Cole et al. 2012). Obligatory COs do not necessarily require robust CO interference, however it is possible that CO interference establishes a link to homeostasis. For example, Topoisomerase II mutants that reduced interference also showed reduced homeostasis (Zhang et al. 2014b). In contrast, CO interference was completely lost in the *zip2* and *zip4/spo22* mutants, however reduction in CO homeostasis was modest, indicating their interaction is complex (Chen et al. 2008).

1.6. Measurement of Crossovers and Interference in Arabidopsis

In Arabidopsis, COs and interference may be measured using seed or pollen visual assaying tools (Melamed-Bessudo et al. 2005; Francis et al. 2007). A seed-based fluorescent assay was developed based on transformation of T-DNAs expressing GFP and RFP markers expressed under a seed-specific promoter, *NapA*. Fluorescent tagged lines (FTLs) with two markers linked in *cis*, constitute a genetic interval (Melamed-Bessudo et al. 2005; Wu et al. 2015; Ziolkowski et al. 2015). Plants that are hemizygous for the T-DNAs generate progenies with segregating patterns of red and green fluorescence which are then used to measure CO frequency between the transgenes under a fluorescence microscope (Melamed-Bessudo et al. 2005; Wu et al. 2015; Ziolkowski et al. 2015). However, seed-based FTLs do not have an additional marker to measure CO interference in a pair of intervals. A pollen visual assay was developed to measure male recombination in the haploid gametes (Francis et al. 2007; Berchowitz and Copenhaver 2008). This system utilizes transformation of three fluorescent markers (YFP, DsRed and CFP) into *quartet1* plants expressed under a pollen-specific promoter, *LAT52* (Francis et al. 2007; Berchowitz and Copenhaver 2008). The *quartet1* mutations causes the four sister gametes produced during male meiosis to remain physically attached as a meiotic quartet (Francis et al. 2007; Berchowitz and Copenhaver 2008). Mapped single marker insertions are crossed to generate a single genetic interval with two markers linked in *cis* or an adjacent interval with a third marker. Tetrad analysis of fluorescent pollen is a robust method to measure COs and interference (Francis et al. 2007; Berchowitz and Copenhaver 2008), however is a time-consuming. Therefore, the *qrt1* mutation in the FTL lines was removed in later works to analyse single pollen grains via flow cytometry (Yelina et al. 2013; Ziolkowski et al. 2015) .

Quantitative assays thus measure regional CO rates. Classical genetic mapping using Arabidopsis natural populations (e.g. Col x Ler) can be used to map COs genome-wide with the help of single nucleotide polymorphic markers (Drouaud et al. 2007; Giraut et al. 2011; Salomé et al. 2012). Recently, whole-genome sequencing of meiotic tetrads mapped genome-wide meiotic COs to a fine-scale (Wijnker et al. 2013). Backcross populations are more powerful for quantitative analysis of interference strength compared to segregating F_2 populations (Drouaud et al. 2007;

Giraut et al. 2011). Various cytological methods are also used to measure COs and interference. Measurement of Class I CO marker foci (e.g. MLH1) are used to estimate crossover number (Lhuissier et al. 2007; Chelysheva et al. 2010; Cole et al. 2012). Crossover patterning is forced to occur on recombination-mediated bridges that connect homolog axes in parallel to SC installation, hence SC length is used as a substitute for chromosome length during meiotic prophase (Zhang et al. 2014a; Wang et al. 2015). The physical position of COs is determined by Class I CO markers (Zip3 or MLH1) along the synapsed chromosomes and the distribution of physical distance (μm) between the COs are used to measure interference (Lhuissier et al. 2007; Zhang et al. 2014a; Wang et al. 2015). Hence, genetic approaches have allowed us to characterize mutants according to CO frequency and interference levels, which can estimate the CO pathway they are involved in.

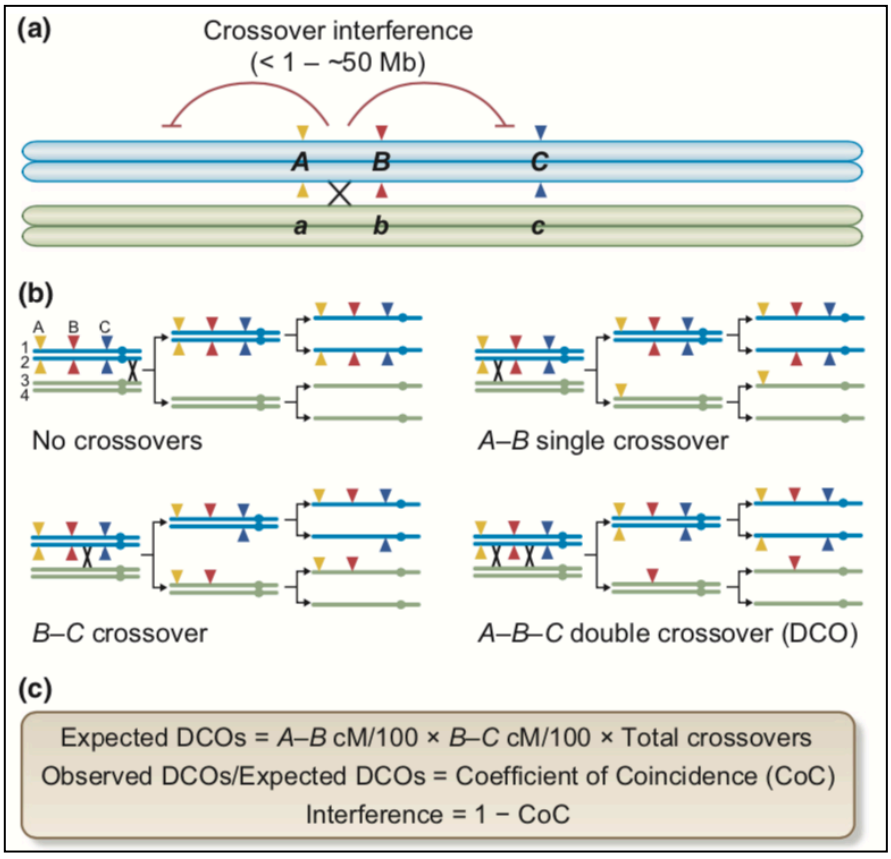

Figure 1.9. CO interference during recombination. (a) Paired and replicated homologous chromosomes (Blue and green) on which CO interference is shown on megabase (Mb) scales. Three loci A,B and C (in coloured triangles) and their allelic forms a, b and c are shown. 'X' (in black) denotes a CO between two non-sister homologous chromatids, and is between A and B loci. The occurrence of CO between A and B lowers the probability of CO occurrence in the adjacent regions.**(b)** Homologous chromosome segregation through meiosis I and II with different CO patterns between the three loci (A,B,C). **(c)** Interference is measured by comparing

observed DCOs with those of expected from the CO frequency (cM) measured for A-B and B-C intervals. CoC is calculated as the ratio of observed to expected DCOs and Interference is shown as 1-CoC (reproduced from Ziolkowski and Henderson 2017).

According to the BF model, interference establishes an inhibitory zone around the CO designated sites. Assuming this, a true interference mutant should show a hyper-recombination phenotype (Zhang et al. 2014a, 2014b; Wang et al. 2015; Hunter 2015). However this phenotype is seen in anti-crossover mutants due to increase in Class II CO events at the expense of NCOs (Crismani et al. 2012; Séguéla-Arnaud et al. 2015; Hunter 2015).

1.7. Project Objectives

As discussed, numerous proteins have been identified that are involved in meiotic recombination. To identify further recombination factors, Dr. Kyuha Choi initiated a forward genetic screen via EMS mutagenesis of Col-*420* reporter line. The objectives of my project were I) to screen for mutants that significantly altered CO frequency (cM), II) map the candidate mutations by sequencing and III) to characterize the candidate gene function in the context of meiotic recombination.

Chapter 2 - General Methods

2.1. Plant materials and growth conditions

The Arabidopsis Columbia (Col-0) accession was used as a wild type control for all experiments. Fluorescent tagged lines (FTL) and traffic lines (TLs) generated in Col-0 background are shown in Figure 2.1 (Melamed-Bessudo et al. 2005; Francis et al. 2007; Wu et al. 2015). T-DNA insertion lines in the Col-0 accession (Table S2) were provided by the Salk Institute Genome Analysis Laboratory (SIGnAL, http://signal.salk.edu/cgi-bin/tdnaexpress) via the Nottingham Arabidopsis Stock Centre (NASC, http://nasc.nott.ac.uk/). The mutant alleles used for genetic analysis were: *ppx-1* (GK_651B07); *ppx-2* (GK-488H09), *pp4r2* (SALK_093051), *zip4-2* (SALK_068052; Chelysheva et al. 2007) and *fancm-1* (Crismani et al. 2012).

Seeds were sown in plastic square pots (~9 seeds/pot) filled with soil-based compost and grown in controlled growth conditions at 22°C, 50-60% humidity and a 16 hour light and 8 hours dark cycle. Seeds sown in trays were covered with domed lids and incubated at 4°C dark for 3-4 days before its transfer to normal growth conditions in order to stratify germination. Water conditions were constantly checked to avoid drying of plants at critical growth stages. Pesticidal sprays were carried out by PGF technicians to maintain plant health throughout my experiments. During flowering and the transition to seed development, plants were staked and well contained so as to maintain the stem bearing siliques upright and to avoid contamination between different genetic backgrounds. Seeds were harvested either per individual, or bulked based on experimental design. Seeds were cleaned using a sieve and stored in small bags or microcentrifuge tubes in the long term.

2.2. Crossing *Arabidopsis thaliana*

As Arabidopsis self-fertilizes lines must be specifically crossed to combine genotypes. To do this plants 5-6 weeks old were selected for crossing. Crosses were performed using sharp forceps by gently emasculating anthers from unopened buds of the female parent plant and then dusted with pollen from 3-4 flowers of the male parent until the yellow pollen visibly coated the stigma. To avoid contamination self-fertilized siliques and open flowers were removed from the female parent plant prior

to crossing and emasculation. Crosses were labelled and plants watered to counter the stresses created out of emasculation. Crosses were collected after 2-3 weeks, once the siliques were mature, elongated and brown and most importantly before shattering of the siliques.

2.3. Seed sterilization

Arabidopsis seeds were surface sterilized using ethanol and then grown *in vitro* for the preparation of DNA libraries and antibiotic selection of plant transformants. Approximately 0.5 g of seeds were placed in 1.5 ml microcentrifuge tubes and washed twice each for 10 minutes with 1 ml of 70% (v/v) ethanol + 0.01% TritonX-100 (Sigma-Aldrich). The tubes were shaken for 10 minutes and then spun in a low-speed rotator and the supernatant discarded. 1 ml of absolute ethanol was then added and washed for 10 min, twice. After the second wash, seeds were dried on a filter paper (Fisher scientific) under a laminar flow workstation for 30 minutes. Dried seeds were then sprinkled onto ½ MS (Murashige and Skoog 1962; Sigma-Aldrich) agar media plates with no sucrose added (see, “Appendix 3”). The plates were sealed with 3M micropore tape, covered with aluminium foil, kept at 4°C dark for 2-4 days and then moved to 22°C growth cabinets.

2.4. EMS mutagenesis of Arabidopsis seeds

The protocol was adapted from a published article (Weigel and Glazebrook 2006) and was performed by Dr Kyuha Choi. Approximately 10,000 dried seeds were sterilized and soaked in 5 ml volume of 100 mM phosphate buffer (pH 7.5). The tubes were allowed to stand upright for the seeds to settle and excess phosphate buffer was removed. Then a fresh volume (5 ml) of 100 mM phosphate buffer was added. Seeds were treated with 0.3% Ethyl-Methyl Sulfonate (EMS; v/v) and incubated for 12 hours at room temperature. M_0 seeds were washed thoroughly 15-20 times with water (5 ml per wash) and were planted immediately in soil after mutagenesis.

2.5. Two-colour analysis of FTL seed and crossover measurement

Seed based fluorescent tagged lines (FTLs) and Columbia traffic lines (CTLs), where fluorescent proteins are driven by the *NapA* promoter, were used to measure

crossovers within specific genetic interval defined by GFP and RFP transgenes that are linked in *cis* (Melamed-Bessudo et al. 2005; Emmanuel et al. 2006; Wu et al. 2015; Ziolkowski et al. 2015) (Figure 2.1). These reporter lines were introduced into various genetic backgrounds and seed analysed using a fluorescence microscope (Leica DFC310FX 1.4, Leica Microsystems, UK). The method of seed-scoring and calculation of genetic distance (cM) was followed as previously described (Ziolkowski et al. 2015). Images of ~1,000-2,000 seeds were captured using charge-coupled device (CCD) camera and appropriate filters (Brightfield, UV-DsRed, UV-GFP3) at x0.72 magnification. The captured images were then loaded into the image analysis software Cellprofiler v2.1.1 (Carpenter et al. 2006). I used a manual scoring pipeline to generate all the data as shown in the results chapters. The pipeline output provides counts for the total seed and histograms that classify fluorescent vs. non-fluorescent seeds for green and red colours. Crossover frequency, or the genetic distance (cM), of a self-fertilized plant was calculated based on colour segregation ratios using the formula: $cM = 100*\{1-[1-2(N_G + N_R)/N_T]^{1/2}\}$, where N_G is the number of green-alone seeds, N_R is the number of red-alone fluorescent seeds and N_T is the total number seeds counted (Ziolkowski et al. 2015).

2.6. Analysis of crossover frequency and interference using three-colour pollen FTL lines

Fluorescent reporter lines expressing in the pollen from the *LAT52* promoter were used to measure crossovers within a genetic interval constituted by two *cis*-linked transgenes (e.g. *I3b*). Additionally, three-colour pollen FTLs were used to measure crossover interference between adjacent intervals (e.g. *I3c*) that comprise three transgenes in *cis*, including e-YFP, DsRed and e-CFP (e.g. *I3bc*). Measurement of crossover frequency or interference was carried out either by tetrad analysis of *quartet1* (*qrt1*) pollen (Francis et al. 2007; Berchowitz and Copenhaver 2008) or flow cytometry of single *QRT1* pollen grain (Yelina et al. 2013). The *I3bc* interval was used for measuring crossover interference by flow cytometry (Figure 2.1).

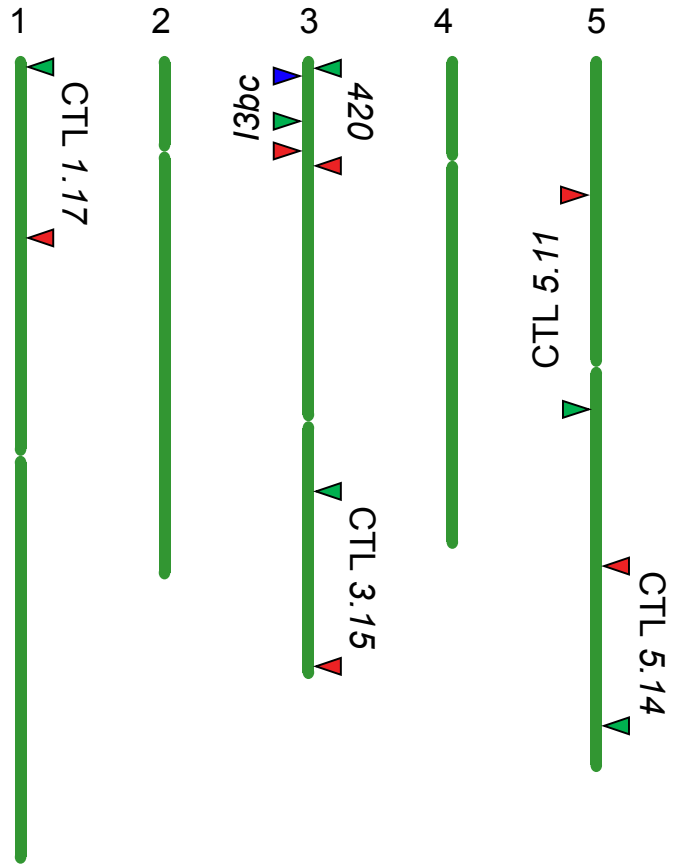

Figure 2.1. Arabidopsis fluorescent reporter lines used. Seed FTL *420*, CTLs *1.17*, *3.15*, *5.11* and three-colour pollen FTL *l3bc* located along the 5 chromosomes. Triangles indicate the fluorescent transgenes e-GFP (in green), RFP or DsRed (in red) and e-CFP (in blue). This figure was developed using Chromosome map tool from TAIR (www.arabidopsis.org).

The procedure for FTL pollen analysis was followed as previously described with minor modifications (Ziolkowski et al. 2015). Each biological replicate comprised inflorescences from 3-5 individual plants as previously mentioned (Yelina et al. 2013). I collected inflorescences from 8-16 individual plants that are 6-7 weeks old in 50 ml polypropylene tubes and concentrated more pollen per biological replicate to obtain sufficient number of double crossover counts. Pollen was extracted with 25-30 ml of freshly prepared pollen sorting buffer (PSB) with 0.01% Triton X-100 (see, “Appendix 1”). The contents were vortexed vigorously for 5-10 minutes. The pollen suspension was then filtered through a 70 μm cell strainer to a fresh 50 ml polypropylene tube and centrifuged at 450 x g for 2-4 minutes. The supernatant was then removed from the yellow pollen pellet. The pellet was washed twice with 15-20 ml of PSB without Triton X-100 and the pollen suspension was centrifuged at 450 x g

for 2-4 minutes. Finally, the supernatant was discarded and the pellet was resuspended with 400-800 μl of PSB without Triton X-100 (Ziolkowski et al. 2015).

In general I used Generalised Linear Model (GLM) to test whether the recombinant and the non-recombinant seed counts were significantly different between genotypes with its biological replicates, assuming a binomial distribution, as previously described (Ziolkowski et al. 2015). In this model, both replicates and genotypes are considered as independent variables. A probability (*P*) value less than 0.05 was taken as indicating a significant difference (Ziolkowski et al. 2015).

2.7. Flow cytometry analysis of FTL pollen

A Cyan ADP Analyser (Beckman Coulter) equipped with 405 nm, 488 nm and 633 nm solid-state lasers and emitter filters 530/40, 613/20 and 450/50 nm were used for sample analysis. The in-built "Summit" software was used to run samples and I retrieved the output as .fcs files. I used "FlowJo" software for the purpose of data analysis using .fcs output files. Polygon gating of pollen populations under appropriate filters obtained eight pollen class counts for each sample or biological replicate with *I3bc*. The FTL T-DNAs were maintained in a hemizygous *cis*-linked states in order to measure single (SCO) and double (DCO) crossovers (Ziolkowski et al. 2015; Serra et al. 2018).

I3b and *I3c* genetic distances (cM) and crossover interference were calculated as described (Ziolkowski et al. 2015; Serra et al. 2018), using the following formulas:

$$N_{total} = (N_{bYr} + N_{ByR} + N_{bYR} + N_{Byr} + N_{BYr} + N_{byR} + N_{BYR} + N_{byr})$$

$$I3b \text{ cM} = (N_{bYr} + N_{ByR} + N_{bYR} + N_{Byr}) / N_{total}$$

$$I3c \text{ cM} = (N_{bYr} + N_{ByR} + N_{BYr} + N_{byR}) / N_{total}$$

Where N_{total} includes all eight possible classes of counts from single grain fluorescent pollen. N_{BYR}, for example is the number of pollen that expressed blue, yellow and red fluorescence, whereas N_{byr} is the number of non-fluorescent pollen.

$$\text{Observed DCOs} = (N_{bYr} + N_{ByR})$$

$$\text{Expected DCOs} = (I3b \text{ cM}/100) \times (I3c \text{ cM}/100) \times N_{total}$$

Coefficient of Coincidence (CoC) = Observed DCOs/ Expected DCOs

Crossover Interference = 1 – CoC

Statistical tests for *I3b* and *I3c* genetic distances was carried out using GLM as previously described (Ziolkowski et al. 2015). Significant differences in CO interference was tested using Pearson's χ^2 test with Yates' continuity correction by comparing observed and expected crossovers between genotypes (Serra et al. 2018).

2.8. DNA extraction for high throughput sequencing

I selected ~30-80 individuals from a *hcr* and *lcr* backcross mapping populations (James et al. 2013) and weighed an equal amount of seed (between 5-10 mg) from an individual, which were then combined into a bulked mutant seed pool. Seed pools were sterilized and sprinkled onto ½ MS (no sucrose) agar plates (see, "Appendix 3"). Approximately, 7-10 day old seedlings from each *hcr* or *lcr* mutant seed pool were harvested for DNA extraction. This procedure was slightly modified from harvesting leaf tissues from a single *hcr* or *lcr* mutant individual in order to bulk into a single genomic DNA (Hartwig et al. 2012; Allen et al. 2013).

For genomic DNA isolation a protocol was followed as provided by Dr. Kyuha Choi for enriching nuclear DNA. Approximately 3 grams of leaf tissues were ground three times in liquid nitrogen (N_2) using a mortar-pestle, or until the material was a fine-powder. The ground leaf powder was transferred into a pre-chilled new mortar containing 40 ml of freshly prepared nuclear isolation buffer (See, Appendix 1) + 400 µl of 100mM PMSF + 40 µl of 1mM pepstatin + 4 mini EDTA Complete tablets and the contents were homogenized well in solution. The tissue lysate was transferred to a fresh 50 ml polypropylene tube kept on ice and incubated at 4°C for 30 minutes on a rocker. The contents were filtered through a layer of miracloth into a fresh 50 ml polypropylene tube, kept on ice for ~30 minutes and centrifuged at 4°C, 3000 x g for 25 minutes. The supernatants were discarded and 2 ml of Cetyl Trimethyl Ammonium Bromide (CTAB; see, "Appendix 1") buffer added to the pellet, which was gently pipetted until dissolved. The sample aliquots in 0.5-1.5 ml microcentrifuge tubes were incubated at 65°C for 30 minutes in a thermomixer and an equal volume

of phenol-chloroform (1:1) added, vortexed for 1 minute and then centrifuged at maximum speed (16,000 x g) for 20 minutes. The maximum volume of supernatant was transferred to a fresh 1.5 ml microcentrifuge tube without disturbing the organic interface. Then an equal volume of isopropanol and 3M NaOAC (1/10th the supernatant volume) were added and incubated at -20°C for 2 hours or 4°C overnight. The samples were centrifuged at 15,000 x g, 4°C for 30 minutes and the pellets were retained. The pellets were washed with 70% ethanol and centrifuged at 16,000 x g for 10 minutes. The pellets were then dried for 5 minutes at room temperature, re-suspended in 100-200 μl of TE buffer + 2 μl of RNase (10 μg/μl) and incubated at 37°C for 30 minutes. DNA was purified by precipitating with 95% ethanol (2.5 times the DNA volume) + 3M NaOAC (1/10th the DNA volume) and kept at -20°C for 30 minutes and then centrifuged at 15,000 x g, 4°C for 15 minutes. The pellets were washed with 70% ethanol, air dried and re-suspended in 100-200 μl of TE buffer. DNA concentration per μl were estimated using a Qubit fluorometric assay (Invitrogen).

The extracted DNA was mechanically sheared to a size range between ~200-500 bp using a Bioruptor sonicator (Diagenode, UK). 1 μg of input DNA diluted in 150 μl of TE buffer was sonicated for 22 minutes at high voltage with 30 second cycles of ON-OFF conditions. The sonicated DNA (150 μl) was cleaned (PCR purification kit, Qiagen), concentrated to a 60 μl volume and then loaded onto a agarose gel and size separated by electrophoresis. I excised the desired DNA size (~300-400 bp) from a 2% agarose gel stained with 1X SYBR gold (120 Volts, 30 minutes run) using a UV transilluminator. DNA concentration was measured using a Qubit fluorimeter (Invitrogen) after gel extraction (Qiagen).

2.9. Sequencing library construction

50 ng concentration of sheared DNA (~300-400 bp) in 60 μl volume was used as an input for library construction. The steps involved in library preparation were performed according to the Illumina Truseq Nano DNA LT library prep kit. The Truseq universal adaptor (120 bp) includes an adaptor index (6 bp) that was ligated to the input DNA followed by an additional PCR enrichment (Illumina). Adaptor-indexed libraries of ~300 bp size were checked using a bioanalyser (BioRad). The

DNA library was also measured by Qubit and diluted to a 4 nmol concentration prior to sequencing.

Before sequencing the DNA library (insert) was cloned into the pGEM-T Easy vector (Promega) (Table S1) using the quick protocol. A ligation reaction was set up with reaction components such as 2X rapid ligation buffer (5 μl), 50 ng vector (1 μl), 3U/μl T4 DNA ligase (1 μl) and DNA insert (1 μl). The insert concentration (ng) needed for a 1:1 (vector: insert) molar ratio was calculated using the formula: [bp of insert / bp of vector] x ng of vector. The amount of insert DNA (1 μl) was then added and adjusted to a reaction volume to 10 μl. The reaction was incubated at 4°C overnight. I used *Escherichia coli* (*E.coli*) DH5α competent cells for transformation of the ligated products. A 50 μl volume of cells were added with 2 μl of the ligation products and mixed gently by flicking the reaction tube. The cells were incubated on ice for 20 minutes followed by a heat shock for 45-50 seconds in a water bath at 42°C and then immediately returned to ice for 2 minutes. 950 μl of LB or SOC medium (see, "Appendix 3) were then added and incubated at 37°C for 1.5 hours with ~150 rpm shaking. The cells was centrifuged at maximum speed for 1 minute and re-suspended in 200 μl of LB. 50-100 μl of cell resuspension was then plated onto a LB agar plates containing antibiotics and blue/white selection markers (see, "Appendix 3"). The plates were incubated at 37°C overnight. *E.coli* overnight cultures (see, "Appendix 3") were prepared from selected white colonies from the insert DNA library transformation and plasmid DNA extracted using a Qiagen protocol (Qiaquick Spin Miniprep kit, # 27104). The plasmid DNA was Sanger sequenced to confirm DNA library insert size, the presence of adaptors and the expected sequence homology to the Arabidopsis genome.

The sample libraries were sequenced on an Illumina Genome Analyser in a 75 bp paired end run using a NextSeq 500/550 Mid Output v2 kit 150 cycles (2 x 75 cycles) (Illumina, FC-404-2001). The short read analysis pipeline (SHORE) was applied to individually align the paired sequencing reads to the Col-0 reference genome (The Arabidopsis Information Resource 10/ TAIR10) using an alignment tool called GenomeMapper (Ossowski et al. 2008; Schneeberger 2009; Hartwig et al. 2012). The command lines shown in "Appendix 6" were used according to the SHOREmap

v3.0 manual (Alonso and Stepanova 2015). Raw reads were trimmed based on quality values with a cut-off Phred score of +33 or +64 using the function SHORE *import*. The paired end alignments were corrected to an expected insert size of ~300 basepairs (bp). The SHORE command *consensus* was used to detect sequence variations between the mutant or control libraries and the TAIR10 reference assembly. Background SNPs from the mutant and control libraries were discarded by cross-comparison and filtering. The EMS-filtered SNPs with high quality marker scores (SHORE score = >40) and supported by at least 10 unique reads were used in SHOREmap *backcross* for allele frequency analysis. Allele frequency estimates were calculated as the ratio of mutant allele reads divided by the total reads at a specific locus (Hartwig et al. 2012). Using the function SHOREmap *annotate* we then utilized the TAIR10 gene annotation to produce chromosomal lists of EMS changes that include predicted effects on gene function and expression.

2.10. Manual genotyping analysis of Arabidopsis

A smaller scale method of DNA extraction was used for genotyping large populations for which a cruder extraction was sufficient. Small leaves (1-2) from young rosettes were collected onto a 96-well collection tubes together a 3 mm glass bead. 200 μl of extraction buffer without SDS (see, “Appendix 1”), were added to each well and disrupted using a Tissuelyser (Qiagen). The samples were ground for 2 minutes twice at 30 Hz frequency. The plates were given a pulse spin on a Beckman coulter high speed centrifuge to remove the liquid from the lids. A further 200 μl of extraction buffer with SDS added (see, “Appendix 1”) were added to the lysed samples and centrifuged at 3000 x g for 7 minutes. Whilst spinning, 200 μl of isopropanol was added to each well of 0.8 ml 96 well storage plates. Then, 200 μl of supernatant per sample was dispensed into this plates, mixed well and incubated at room temperature for 10 minutes, followed by centrifugation at 3000 x g for 35 minutes at 4°C. The supernatant was then poured off and the DNA pellets were retained. These pellets were washed with 150 μl of 70% Ethanol (v/v), which was discarded immediately. The plates were placed upside down on a paper towel and given a pulse spin at ~100 x g for 1 minute to remove excess ethanol. The pellets were air dried for 30-45 minutes and finally re-suspended in 150 μl of nuclease-free water

(ThermoFisher). The plates were stored at 4°C for temporary use and -20°C for longer term storage.

For PCR analysis lyophilized primer oligos (Sigma-Aldrich) were re-suspended in nuclease-free water to a final stock concentration of 100 μM. The working concentration of primers were diluted to 10 μM for PCR. The primers used for genotyping are listed in Appendix 5 (Tables S3-S6). T-DNA insertion lines (Alonso et al. 2003) were identified using a Seqviewer tool from TAIR (https://seqviewer.arabidopsis.org). The Arabidopsis T-DNA Express Gene Mapping Tool (http://signal.salk.edu/cgi-bin/tdnaexpress) was also used to identify the T-DNA position and orientation relative to gene annotation. The left (LP) and right (RP) primers were designed such that oligo length was between 18-25 bp, melting temperature (T_m) was between 55-63°C and GC content was between 40-60 %.The T-DNA border (BP) primers include LBb1.3, LB1/LB3 and GK for the corresponding insertions such as SALK, SAIL and GABI-KAT, respectively (http://signal.salk.edu/tdnaprimers.2.html). Leaf DNA samples were amplified with all three primers (BP+LP+RP) for genotyping (Table 2.1, 2.2). The T-DNA insertion lines obtained from NASC can be either homozygous or heterozygous for the insertion. Therefore, I verified the genotypes according to the amplicon size and number of DNA bands. I designed primers such that wild type genotypes (no T-DNA insertion) amplified approximately 1 kb genomic region of the candidate gene using LP+RP primers. Homozygous T-DNA insertion genotypes showed two bands of ~400 and 700 bp resulting from amplification using RP (sequence from candidate gene) and T-DNA border (LB) primers. Whereas hemizygous T-DNA genotypes (with insertion in one of the chromosome pairs) displayed three bands (one WT and two T-DNA bands). These PCR products were separated by electrophoresis using on a 2.5% agarose gel and ethidium bromide (EtBr) staining.

I used the derived Cleaved Amplified Polymorphic Sequence (dCAPS) markers to identify EMS induced single nucleotide polymorphisms (SNP) by restriction digestion of PCR products (Neff et al. 1998). Using dCAPS finder (helix.wustl.edu/dcaps/), a 50 bp gene sequence that is identical to both wild type and mutant alleles except for the EMS-SNP was selected. The dCAPS primers contain mismatches (up to 3) that

create a new restriction site dependent on the genomic sequence. A forward or reverse primer (21-25 bp) with the recognition sequence for the restriction enzyme (e.g. *Fok*I, *Mbo*II, *Aat*II) was designed to preferentially cleave wild type or mutant PCR amplicons. The other primer (forward or reverse) was designed from the gene sequence and the primer pair was designed to amplify a product size ~100-200 bp (Table 2.1, 2.2). Following restriction enzyme digestion (Table 2.3), the wild type and mutant products varied by at least 20-30 bp when visualized on a 3.5 % agarose gel and EtBr staining.

Reaction mix	1X (T-DNA)	1X (others)
DNA (from 150 μl)	2 μl	2 μl
dNTPs (2.5 mM each)	1 μl	1 μl
10X Dream-Taq Buffer (25 mM $MgCl_2$)	1 μl	1 μl
Forward or LP (10 μM)	1 μl	1 μl
Reverse or RP (10 μM)	1 μl	1 μl
T-DNA Border or BP (10 μM)	1 μl	---
Dream-Taq polymerase (1.25 U/μl)	0.08 μl	0.08 μl
Water (nuclease-free)	up to 10 μl	up to 10 μl

Table 2.1. PCR components for genotyping. The reaction mixture was prepared up to a volume of 10 μl /reaction using T-DNA and other (dCAPS, transgene-specific and RT-PCR specific) primers.

Step	Temperature (°C)	Time	Number of cycles
Initial Denaturation	95	5 min	1
Denaturation	94	30 s	28-37
Annealing	Primer Tm-5	30 s	
Extension	72	1 min/kb	
Final Extension	72	5-10 min	1

Table 2.2. PCR steps for genotyping. A simple PCR program with the critical steps such as optimal annealing temperature and extension time were modified based on Tm of primers used and amplicon size.

Digestion mix	1X
PCR product	10 μl
10X Buffer	1.5 μl
Enzyme (20,000 units/ml)	0.2 μl
Water (nuclease-free)	up to 15 μl

Table 2.3. Restriction enzyme digestion of PCR amplicon. The restriction enzyme cutters and buffers, temperature and time for digestion was followed as provided by the manufacturer (NEB). A 5 μl reaction mix was added to the 10 μl dCAPS PCR product and digested at 37°C for 1-2 hours.

2.11. Gel electrophoresis of DNA, staining and image capture

The percentage of agarose gels were calculated and prepared according to PCR amplicon size. An adequate quantity of agarose (Sigma-Aldrich) was weighed and dissolved in 1X Tris-borate-EDTA (TBE; see, "Appendix 1") using a microwave. The melted gel had Ethidium bromide (10 μl / 100 ml gel) or Midori green (4-6 μl / 100 ml gel) added to it and was then poured into a gel casting unit. DNA (7-8 μl) mixed with loading dye (NEB or 10X PCR buffer inclusive) was loaded into gel wells, while the gel was in an electrophoresis tank (BioRad) filled with 1X TBE. A 100 bp or 1 kb DNA ladder was also loaded alongside to verify the expected amplicon size. High percentage (2.5-3.5%) agarose gels were run at a specific voltage (180-240 V) for 30-45 minutes, whereas low percentage gels (1-2%) were run at 90-130 V for 15-30 minutes. Gel images were captured using a G:Box (Syngene), and the UV exposure adjusted using the Genesnap software (Syngene).

2.12. Cloning *HCR1* genomic DNA for complementation experiments

For the purposes of cloning, genomic DNA was first extracted by CTAB method (see, "under 2.8"). Gene-specific primers were designed manually against the nucleotide sequence of interest. Oligo properties including %GC, primer Tm, secondary structure and primer dimer were checked using Sigma-Aldrich oligo tool (https://www.sigma aldrich.com). A *HCR1* (*PPX-1*) containing genomic fragment (4.5 kb) was amplified using specific primers (Table 2.4, 2.5) bordered by restriction sites chosen from the multiple cloning site (MCS) region of the binary vector pGREEN0029 (Table S1). The insert DNA was ligated into the vector as described above (see, "under 2.8"). The cloned construct was transformed into *E.coli* DH5α

cells (see, “under 2.8”) and the kanamycin selected colonies were Sanger sequenced using middle primers within the insert (Table S5).

Reaction mix	1X (gene-specific)
DNA (from 150 μl)	2-2.5 μl
dNTPs (2.5 mM each)	2 μl
5X Phusion HF buffer	10 μl
Forward primer (10 μM)	2 μl
Reverse primer (10 μM)	2 μl
Phusion (2 U/μl)	0.8 μl
Water (nuclease-free)	up to 50 μl

Table 2.4. Reaction components of a gene-specific PCR. A high quality DNA was amplified using gene-specific primers (Sigma-Aldrich) and Phusion High-Fidelity DNA polymerase (ThermoFisher). The PCR reaction mix was made up to a 50 μl volume per reaction as provided by the manufacturer (NEB).

Step	Temperature (°C)	Time	Number of cycles
Initial Denaturation	95	5 min	1
Denaturation	94	30 s	35-37
Annealing	Primer Tm-5	30 s	
Extension	72	15-30 s /kb	
Final Extension	72	5-10 min	1

Table 2.5. Thermocycling conditions using Phusion polymerase. Annealing temperature and extension time were modified based on Primer Tm and PCR product size.

2.13. Agrobacterium transformation by electroporation method

DNA constructs can be transformed into the *Agrobacterium tumefaciens* (*A.tumefaciens*) strain GV3101 by electroporation. The Agrobacterium cells were mixed with pSOUP, which is a helper plasmid used for replication of pGREEN plasmids (Hellens et al. 2000). A 40 μl aliquot of electrocompetent cells were added to 1-2 μl (~50-100 ng) of DNA construct and mixed by gentle flicking. The cells were kept on ice for a minute and transferred into pre-cooled GenePulser electroporation cuvettes (0.1 cm gap, BioRad, #1652089). Air bubbles were gently removed by

tapping the cuvettes. The cuvettes were inserted in the correct orientation into a Gene Pulser Xcell™ instrument (BioRad, #1652662) and the electroporation programme used: 25 μF capacitance, 200 Ω resistance and 2400 V voltage. Electroporation was performed for 2 seconds followed by immediate addition of 500 μl pre-cooled SOC medium (see, "Appendix 3"). The electroporated cells were kept at room temperature for 5-10 minutes and incubated at 28 °C in a shaker for 2.5-3.0 hours. The cell cultures were plated onto solid LB medium with antibiotics (see, "Appendix 3") and incubated at 28°C for 2 days. Glycerol stocks were also prepared for long term storage of Agrobacterium constructs.

2.14. Agrobacterium-mediated transformation of Arabidopsis by floral dipping

A published protocol was followed with minor modifications, as previously described (Zhang et al. 2006). Inflorescences of Arabidopsis plants 5-6 weeks old were cut back 6-10 days before dipping. A single colony of Agrobacterium GV3101 strain with the DNA binary vector of choice was inoculated into 5 ml of liquid LB medium with appropriate antibiotics (see, "Appendix 3") and incubated at 28°C for 2 days. This 5 ml feeder culture was inoculated into 400 ml of liquid LB medium and grown for 16-24 hours until the cells reached ~1.5 -2.0 OD using a UV spectrophotometer (Biowave DNA life Sciences Spectrophotometer, #5300-15). The Agrobacterium cells were centrifuged at 4000 x g for 8 minutes at room temperature and the cells gently resuspended in 500 ml of 5% (w/v) sucrose solution. For efficient transformation, the OD was adjusted to 1.0. The cell suspension was supplemented with 0.02 % Silwet L-77 (v/v) and immediately mixed well before dipping. The T_0 plants were inverted and dipped into the Agrobacterium cell suspension for 10-30 seconds with gentle agitation. The excess liquid from the dipped plants was removed and the plants wrapped with a plastic film to maintain humidity for 16 to 24 hours. The treated plants were also covered with a black polythene sheet for 16 to 24 hours to limit light exposure.

2.15. Selection of Arabidopsis T_1 transformants

Harvested T_1 seeds were dried and surface sterilized (see, “under 2.2”) and then sprinkled onto ½ MS (no sucrose) agar plates (see, “Appendix 3”) with kanamycin (50 mg/ml) for the selection of transformants. Once transformants had been transferred to soil the plants were genotyped for the presence of the transgene using PCR (Table 2.1, 2.2). Primers were designed from both left and right borders of the transgene are shown in Table S5.

2.16. RNA extraction, cDNA synthesis and RT-PCR analysis of gene expression

Flower samples were collected in 2 ml microcentrifuge tubes and immediately placed into liquid nitrogen and samples stored at -80°C. The tissue was ground using a tissuelyser (Qiagen) for 2 minutes at 30 Hz frequency for three times. 1.5 mL Trizol (Invitrogen) was added to the ground samples and mixed by vortexing in a fume hood. The samples were centrifuged for 10 minutes at 10 000 rpm at 4°C, and the supernatant transferred to a new tube and incubated for 5 minutes at room temperature. 300 μl of chloroform was added to the samples and mixed by vortexing under a fume hood. The samples were again centrifuged for 15 minutes at 10 000 rpm at 4°C. Only the aqueous upper phase per sample was transferred to a new tube and 750 μl of isopropanol added. The samples were mixed by gentle flicking and incubated at -20°C overnight. The supernatant was discarded and the pellet was retained after centrifuge for 10 minutes at 10 000 rpm at 4°C. The pellet was washed twice with 1 mL 75% EtOH and incubated for 20 minutes at -20°C. The supernatant was again discarded after centrifuging for 10 minutes at 10 000 rpm at 4°C. Ethanol surrounding the pellet was removed using a 10 μl pipette and the pellet was air dried for 5 minutes. Finally, the RNA pellet was resuspended in 30-50 μl nuclease-free water (ThermoFisher). RNA concentrations (ng/μl) were measured using a Nanodrop spectrophotometer (ThermoFisher, # ND-2000). The absorbance at 260/280 nm was measured and values of ~1.9-2.0 taken as indicating high quality RNA free from DNA contamination.

0.5-1.0 μg RNA per sample were used for DNaseI treatment. 3 μl 10X Turbo DNase Buffer and 1 μl TURBO DNAse (Invitrogen, # 18068015) were added to the RNA per flower sample in a 1.5 ml microcentrifuge tube and made up the volume to 30 μl using nuclease free water. The samples were gently mixed and incubated at 37°C for 30 minutes. 2 μl of DNase inactivation reagent (Invitrogen) were added to terminate the reaction followed by incubation at room temperature for 5 minutes and then stored at -20°C or -80°C. The DNaseI-treated RNA concentration was checked using a Nanodrop spectrophotometer (ThermoFisher, # ND-2000) prior to cDNA synthesis.

The first strand of cDNA synthesis was performed using SuperScript III Reverse transcriptase (Invitrogen, #18080093). 0.5-1.0 μg DNase-treated RNA per sample was added with 1 μl oligo$(dT)_{18}$ (500 ng/μl), 1 μl 10 mM dNTP mix (Invitrogen) and were made up to 14.6 μl with sterile distilled water. The reaction mixture was heated to 65°C for 5 minutes and incubated on ice for 1 minute. A proportional amount of 5X First strand buffer (4 μl), 0.1 M DTT (1 μl), RNase OUT (0.2 μl) and SuperScript III RT (0.2 μl) were added to the heated mixture and mixed well by pipetting. The mixture was incubated at 50°C for 30-60 minutes and the reaction was inactivated at 70°C for 15 minutes. The synthesized cDNA was diluted to 50 μl and 1-2 μl cDNA was used as a template for RT-PCR. The PCR components (Table 2.1) and thermocycling conditions (Table 2.2) were used similar to genotyping reactions. Primers (18-24 bp) were designed using NCBI Primer-Blast for the coding sequence (CDS) and are listed (Table S6).

2.17. RNA-seq data analysis

RNA-seq data from published work (Walker et al. 2018) were analysed to identify differentially expressed genes in Col-0 meiocytes compared to Col-0 leaf tissues using three biological replicates for each type of tissue. The data analysis was entirely carried out by Dr. Andy Tock. Transcript abundances were quantified for each stranded single-end RNA-seq library derived from Col-0 meiocytes or Col-0 leaf tissue by mapping reads to the Arabidopsis TAIR10 reference transcriptome using Salmon version 0.9.1 in “quasi-mapping-based mode” with default parameters (Patro et al. 2017). Transcript-level estimates were added to provide a single expression

estimate for every parent gene identifier (Soneson et al. 2016). The regularised logarithm (rlog) transformation was applied to enable exploration of relationships between samples. This yielded approximately equal variances across mean expression estimates. Using the rlog-transformed data, Euclidian distances between samples were calculated and visualised as a heatmap (Love et al. 2016). Also, sample-to-sample distances were visualised with principal component analysis (PCA) and multi-dimensional scaling (MDS) plots (Love et al. 2016). The sample distances obtained from different tissues were found to be greater than those between biological replicates of the same tissue type.

Differentially expressed genes in Col-0 meiocytes compared to Col leaf tissue were identified using DESeq2 version 1.16.1 in R version 3.4.0 (Love et al. 2014). For analysis, untransformed gene expression values were used agreeing to DESeq2 model-fitting assumptions. Within the given contrast, genes with more than one read across all samples were retained. Also, more stringent and independent filtering of genes with low mean read counts was applied once the differentially expressed genes had been extracted. Independent filtering enables identification of more differentially expressed genes at the specified significance threshold by improving the performance of the multiple testing correction (Love et al. 2014). Differentially expressed genes were identified with Benjamini-Hochberg-adjusted *P*-values < 0.1, < 0.05 or < 0.01 (Benjamini and Hochberg 1995; Love et al. 2014). To moderate the $\log_2$ fold changes obtained for genes with low or highly variable expression levels, a Bayesian method applied in DESeq2 was used. The moderated $\log_2$ fold changes were plotted against the mean of normalised counts for each gene in MA-plots (Love et al. 2014). Then, the read counts normalised by library size and log-transformed for each differentially expressed gene were plotted (Love et al. 2016) .

2.18. Meiotic cytological techniques

The recipes for reagents (see, “Appendix 1”) and the protocols for various cytology techniques were provided by Dr. Christophe Lambing (postdoc) and Dr. Monica Pradillo. Super frost microscopic slides (Fisher Scientific) and coverslips (22 x 22 mm and 24 x 40 mm ; Fisher Scientific) were used for all sample preparations.

For Alexander staining of pollen I collected mature anthers from different genotypes and kept them in water until used for slide preparation. To the centre of the slide, I added 15-20 μl of Alexander's stain solution (see, " Appendix 1") and squashed anthers using the edge of forceps to release the pollen grains. Then a coverslip was applied and viewed under a Leitz Dialux 22 binocular microscope. I scored ~1,000 pollen grains and calculated the proportion of viable and inviable pollen grains. Viable grains stained purple, whereas inviable grains stained green. Pairwise t-tests with correction for multiple testing was performed to test for significant differences between genotypes.

Chromosome spreads of Arabidopsis pollen mother cells (PMCs) were prepared using fixed buds as previously described (Chelysheva et al. 2010), with minor modifications. I collected inflorescences from 5-6 weeks old plants that were fixed in a fixative solution (3:1, ethanol: acetic acid, v/v) and kept for 3-4 hours on ice. Fresh fixative solution was added to the inflorescences multiple times until they turned white. Once the buds are fixed, they can be stored at 4°C for longer periods. Fixed buds ~0.2-0.7 mm length, linked to the floral stages 8-10 (Smyth et al.1990) and meiotic stages (Armstrong and Jones 2003) were immersed in a fresh fixative solution on a black tile and dissected using a pair of needles under a Nikon SMZ 800 stereomicroscope. The dissected buds were washed three times with 1ml of citrate buffer (see, "Appendix 1") and 500 μl of an enzyme solution added, followed by incubation at 37°C for 1.5 hours in a moist box. After incubation, the reaction was terminated by replacing the enzyme solution with 800 μl citrate buffer. Depending on the bud size, I transferred one or two buds to a drop of sterile distilled water on a slide and gently tapped with a brass rod. Then I added 5 μl of 60 % acetic acid twice to the mixture containing meiocytes and mixed well with a needle or 20 μl pipette tip. The slides were placed on a heated block at 48 °C for 1 minute and 120-140 μl of ice-cold fixative solution added on the slide and then immediately dried after slide inversion using a hairdryer. The slides were stained with 7-10 μl of DAPI (Sigma-Aldrich, # 28718-90-3) in Vectashield (Vectorlabs, # H-1200-10) solution (see, "Appendix 1").

Immunostaining of ASY1, ZYP1 and MLH1 were prepared from chromosome spreads using fixed buds (Chelysheva et al. 2010), whereas immunostaining of

ASY1 and RAD51 were prepared from fresh buds (Armstrong et al. 2002). The following primary antibodies were used: α-ASY1 (rat, 1:200 or 1:500 dilution) (Armstrong et al. 2002), α-ZYP1 (rabbit, 1:200 dilution) (Higgins et al. 2005), α-MLH1 (rabbit, 1:200 dilution) (Chelysheva et al. 2010) and α-RAD51 (rabbit, 1:300 dilution) (Sanchez-Moran et al. 2007). The slides prepared from fixed buds were microwaved in 10 mM citrate buffer (pH 6.0) for 30 seconds and immediately transferred to 1 X PBST (Sigma-Aldrich; see, "Appendix 1"), as previously described (Chelysheva et al. 2010). The immunocytological protocol was followed as previously described (Armstrong et al. 2002), with minor modifications. The slides were washed in 1 X PBST for three times, each for 5 minutes and then incubated in primary antibodies (ASY1 1:200 +ZYP1 1:200 or ASY1 1:200 + MLH1 1:200) diluted in 1% BSA PBST for 48 hours at 4°C in a moist box. After 2 days, the slides were washed in 1 X PBST for three times for 15 minutes and incubated in secondary antibodies (anti-rabbit FITC, 1:50 ; anti-rat Cy3,1:200; Sigma-Aldrich) in 1% BSA PBST at 37°C for 30 minutes in a moist box. The slides were finally washed in 1 X PBS-T three times for 15 minutes and stained with 7-10 μl of DAPI (Sigma-Aldrich, # 28718-90-3) in Vectashield (Vectorlabs, # H-1200-10) solution (see, "Appendix 1").

Immunostaining of ASY1 and RAD51 were prepared from fresh buds containing immature anthers as described (Armstrong et al. 2002), with minor modifications. Fresh buds ~0.2-0.5 mm length linked to the floral stages 8-9 (Smyth et al.1990) and meiotic stages (Armstrong and Jones 2003) were dissected on a wet filter paper (Fisher Scientific) using a forcep and a needle, under a Nikon SMZ 800 stereomicroscope. I dissected immature anthers from 5-10 buds ranging in size for each slide and added 10 μl of EM digestion mix (see, "Appendix 1"). The slides were incubated in a moist box on a heated block at 37°C for 5 minutes. To release meiocytes, the anthers were gently tapped using a brass rod and 10 μl of EM digestion mix was added. The slides were again incubated in a moist box on a heated block at 37°C for 7 minutes. To separate the meiocytes from tissue clusters, I added 20 μl of 1 % lipsol (v/v; see, "Appendix 1") to each slide and gently mixed for 2 minutes with a needle and incubated for 4 minutes at room temperature. Then I added 35-40 μl of 4 % paraformaldehyde (w/v; pH 8.0; see, "Appendix 1") on each slide and air-dried for 2 to 4 hours. The slides were washed in 1 X PBS-T solution

three times for 15 minutes each and then incubated in primary antibodies (ASY1 1:500 +RAD51 1:300) diluted in 3% BSA PBST for 16-24 hours at 4°C in a moist box. Following incubation, the slides were washed in 1 X PBS-T three times for 15 minutes each and incubated in secondary antibodies (anti-rabbit FITC, 1:50, Sigma-Aldrich ; anti-rat Alexa red 555,1:500; Invitrogen) in 1% BSA PBST at 37°C for 1 hour in a moist box. The slides were finally washed in 1 X PBS-T three times for 15 minutes and counterstained with 15-20 μl of DAPI (Sigma-Aldrich, # 28718-90-3) in Vectashield (Vectorlabs, # H-1200-10) solution (see, “Appendix 1”) and used 24 x 40 mm coverslips (Fisher Scientific) only for the ASY1-RAD51 immunostained slides.

Microscopy was performed using a DeltaVision Personal DV microscope (Applied precision/GE Healthcare) equipped with a CDD Coolsnap HQ2 camera (Photometrics). Image capture was performed using SoftWoRx software version 5.5 (Applied precision/GE Healthcare). Individual cells immunostained with ASY1-RAD51 were acquired as Z stacks of 10 optical sections of 0.2 μM each. The maximum intensity projection for each cell was decided using ImageJ, and MLH1 or RAD51 foci associated with the meiotic chromosome axis protein ASY1 were counted manually. I used Mann-Whitney Wilcoxon tests to investigate significant differences between genotypes based on MLH1 or RAD51 foci counts.

Acknowledgements

I thank the Plant Growth Facility (PGF) for providing growth space and maintenance. I thank Dr Avraham Levy, Dr Scott Poethig and Dr Gregory Copenhaver for the seed FTLs, traffic lines and pollen FTLs. I thank Dr Kim Osman and Dr Chris Franklin (University of Birmingham, UK) for the ASY1 and ZYP1 antibodies, Dr Mathilde Grelon (INRA, France) for the MLH1 antibody, Dr Monica Pradillo (Complutense University, Madrid, Spain) for the RAD51 antibody and the Gurdon Institute Imaging Facility for microscope access. I thank the Stem Cell Institute Facility for access to Cyan ADP Analyser. I also thank Dr Christophe Lambing for Cytology, Dr Kyuha Choi for supervision and Dr Bruno Santos, Dr Xiaohui Zhao and Dr Andy Tock for bioinformatics support.

Chapter 3 - A forward genetic screen for modifiers of meiotic crossover frequency in *Arabidopsis thaliana*

3.1. Summary

This chapter describes a high-throughput forward genetic screen performed in Arabidopsis via EMS mutagenesis of a fluorescent crossover reporter line *420.* The aim of the screen was to identify factors that modify *420* meiotic crossover frequency relative to wild type. The *420* line allows high throughput visual scoring of recombination rate using a fluorescent dissecting microscope. We initiated this screen by growing ~10,000 EMS-treated M_0 seeds, which produced M_1 and were self-fertilized to generate large M_2 populations. From an initial screen of 21 M_2 mutant pools, 5 *high crossover rate* (*hcr*) and 4 *low crossover rate* (*lcr*) mutants were identified and confirmed to be heritable in the M_3 generation. This included identification of the known anti-crossover factor *fancm*. Mapping populations were developed to identify the causal mutations using mapping-by-sequencing approaches. Four *hcr1*, *hcr2*, *hcr3* and *lcr1* mutant populations were mapped in this way and I identified candidate mutations using the SHOREmap pipeline.

3.2. Introduction

Although forward genetic screens are time-consuming, they are a powerful method to identify novel genes and can be easily applied in model species like *Arabidopsis thaliana.* Forward and reverse genetic approaches allow us to identify gene functions associated with a specialized biological process by scoring for phenotypes of interest. Mutagenesis is typically performed via ethyl methyl sulfonate (EMS), fast neutrons, γ-radiations, T-DNA (transferred-DNA) or transposon insertions. These different methods lead to varying spectrums of point mutations, insertions, deletions and rearrangements in the Arabidopsis genome (Page and Grossniklaus 2002; Alonso and Ecker 2006; Zuryn and Jarriault 2013). Chemical mutagenesis via EMS generate a greater diversity of mutations compared to T-DNA insertional mutagenesis. As unlike insertional mutations that tend to produce complete gene knock-outs, EMS can generate dominant mutations, mutations in the promoter or in the coding region that result in knock-down of gene expression or protein function. EMS screens produce a range of alleles can be isolated caused by single nucleotide transitions (G>A or C>T).

These changes can include premature stop codons, splice site mutations and amino acid substitutions, which can cause both loss (null and hypomorphic) and gain of function changes. Hence, a wide range of EMS-induced alleles are typically obtained that are powerful tool for gene characterization (Page and Grossniklaus 2002; Alonso and Ecker 2006; Zuryn and Jarriault 2013). In addition, EMS introduces dozens of random mutations in each individual, whereas T-DNA insertions form typically between one to three per plant line (Georg Jander et al. 2002; Henikoff and Comai 2003).

Classical map-based cloning approach have been extensively applied in Arabidopsis forward genetic screens to identify causal mutations (Georg Jander et al. 2002; Page and Grossniklaus 2002). Genome sequences from Arabidopsis ecotypes have provided databases of molecular markers that are used to detect linkage between genomic regions and causal mutations (Alonso-Blanco and Koornneef 2000; Jander et al. 2002; Lister et al. 2009). More recently, deep sequencing strategies (e.g. SHORE) aid in the *de novo* detection of spontaneous and EMS-induced mutations in Arabidopsis (Ossowski et al. 2008, 2010; Schneeberger 2009). Short read sequencing pipelines simultaneously map a large pool of recombinants from outcrossed or isogenic backcross populations to aid direct identification (SHOREmap) of EMS point mutations, non-EMS mutations and small deletions via whole genome sequencing (Ossowski et al. 2008, 2010; Schneeberger 2009). In addition, these approaches can be applied to map Quantitative Trait loci (QTLs), large deletions and dominant mutations, (Guo et al. 2012; Hartwig et al., 2012; Lister et al., 2009; Ossowski et al., 2008; Schneeberger 2009, 2014). Overall, next generation sequencing platforms have significantly accelerated genetic mapping projects to identify candidate genes.

With respect to meiosis, a large forward genetic screen for reduced fertility, with a secondary cytological screen for meiotic defects, has identified genes that act during meiosis, including *SPO11-1*, *SPO11-2*, *PRD1*, *PRD2*, *PRD3* and *MTOPV1B* (Grelon et al. 2001; Stacey et al. 2006; De Muyt et al. 2007, 2009; Vrielynck et al. 2016). Subsequently, a suppressor screen using sterile *zmm* mutants, for example *zip4*, has identified the major anti-crossover pathways in Arabidopsis that include *FANCM*, *RECQ4a RECQ4b*, *TOP3-*α, *FIGL1* and *FLIP1*, whose loss of function promote

Class II crossovers (Crismani et al. 2012; Séguéla-Arnaud et al. 2015; Girard et al. 2015; Fernandes et al. 2018). However, it is also possible that mutations may exist that could quantitatively modify recombination rate without causing dramatic changes to fertility. Fluorescent tagged lines (FTLs) are an effective tool for quantitatively measuring meiotic recombination. FTLs use linked T-DNAs that are kept in a hemizygous state that express different colours of fluorescent protein from promoters that show specific expression in the seed (*NapA*) or pollen (*LAT52*) (Melamed-Bessudo et al. 2005; Francis et al. 2007). FTLs are a powerful means to measure crossover frequency and have previously been crossed to natural accessions of Arabidopsis in order to identify *cis* and *trans* modifiers of crossover frequency (Ziolkowski et al. 2015, 2017). For example, Col x Ler recombinant populations have identified polymorphisms in *HEI10*, a major QTL controlling Class I crossovers (Chelysheva et al. 2012; Ziolkowski et al. 2017). Importantly, it was also shown that elevated *HEI10* dosage can increase crossovers several fold (Ziolkowski et al. 2017). In order to identify novel regulators of meiotic crossover frequency, I have performed an EMS forward genetic screen using the seed based fluorescent crossover reporter *420* (Melamed-Bessudo et al. 2005). This screen is based on visual scoring of crossover frequency, which allows quantitative modifiers of recombination to be identified that may not have an effect on fertility.

3.3. Results

3.3.1. A genetic screen for modifiers of meiotic crossover frequency

The *420* genetic interval consists of two T-DNAs encoding different colours of fluorescent protein (GFP and RFP) markers, which define a 5.1 megabase (Mb) region located in the sub-telomeric region of chromosome 3 (Melamed-Bessudo et al. 2005). In wild type, *420* measures a crossover frequency of ~20 cM (20.89 $\pm$ 1.40 cM) in an otherwise Col/Col inbred background (Table S7). The expression of the fluorescent transgenes are driven by the *NapA* promoter, which is expressed in the seed (Stuitje et al. 2003; Melamed-Bessudo et al. 2005; Wu et al. 2015). *420/*++ hemizygotes can be self-fertilized or backcrossed in order to measure crossover frequency in the progeny seed of different genetic backgrounds using fluorescence microscopy (Melamed-Bessudo et al. 2005; Emmanuel et al. 2006; Ziolkowski et al. 2015).

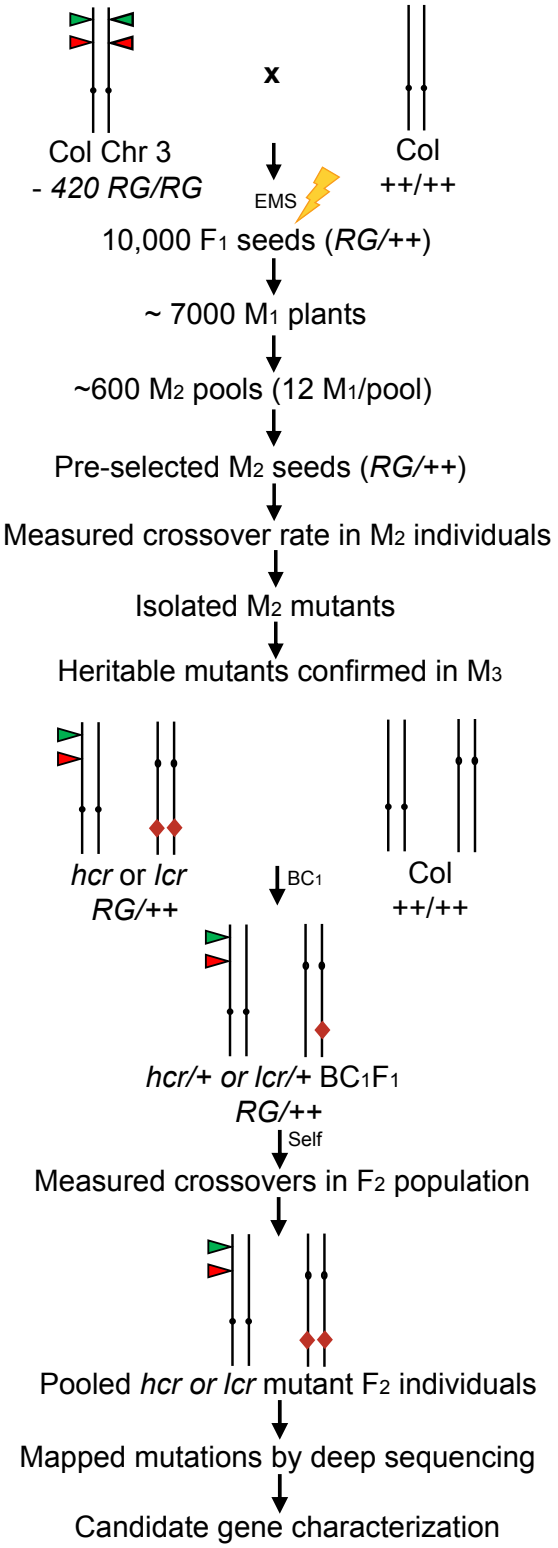

Figure 3.1. A genetic screen to isolate mutants that display higher or lower recombination rate. The pipeline of EMS mutagenesis screen is shown starting with generation of *420* hemizygous *RG/++* fluorescent crossover reporter lines in the Col/Col background. Chromosome 3 is shown with the *420* FTL transgenes represented as red and green triangles. A putative recombination rate mutation is shown (orange square) on the second chromosome.

We have extensively used this *420* interval to detect the effects of natural variation (Ziolkowski et al. 2017), polymorphism patterns influencing recombination rates (Ziolkowski et al. 2015) and epigenetic effects on crossover frequency (Yelina et al. 2012; Underwood et al. 2018). Hence, we proceeded to use *420* in a forward genetic screen using EMS mutagenesis.

A modified procedure for EMS mutagenesis (Weigel and Glazebrook 2006) was carried out prior to my Ph.D by Dr Kyuha Choi to generate the screening material. It is possible to obtain at least one allele per locus from <5,000 M_1 plants, which depends on EMS dosage, mutation frequency per locus, and the structure and size of the target locus (Page and Grossniklaus 2002; Georg Jander et al. 2003). A large number of *420/420* plants were crossed to wild type Col-0 to generate ~10,000 *420/*++ F_1 seeds, which were treated with 0.3% EMS for 12 hours at room temperature (see, "General Methods 2.4"). Hence, ~7000 M_1 plants were generated and seeds from 12 independent M_1 plants were combined to generate ~600 small M_2 pools. Seed representatives within these pools were pre-selected under a fluorescence dissecting microscope for the linked RFP and GFP transgenes to be hemizygous (i.e. non-fluorescent seeds and seeds with brightest red and green fluorescence were discarded). From each M_2 pool, ~150 seeds were grown and self-fertilized to produce individual M_2 plants for measuring *420* crossover rates. In this way, Kyuha and I generated <10% of the screen that amounted to 38 M_2 pools. Approximately 6,000 plants were then screened for altered *420* recombination rates (Figure 3.1).

Seeds from M_2 individuals from each pool were harvested and scored based on the segregation of *420* genetic markers. As these individuals were progenies of pre-selected M_2 seeds (*RG/*++), ~3,000 plants were scorable. The remaining individuals were not scorable due to weak fluorescence intensity of red and green from certain mutant pools which resulted in poor pre-selection efficiency of *RG/*++ seeds (Figure 3.1). Images captured under fluorescence microscopy were analysed using Cell profiler software and crossover frequency per individual was calculated from the seed fluorescent patterns (see "General Methods 2.5"). We selected M_2 individuals that showed an altered *420* crossover rate (Table 3.1) compared to an

external control, which was wild type non-EMS treated Col-*420 RG/*++, whose mean crossover rate is 20.89 ± 1.40 cM (Table S7).

Isolates	Green	Red	Both	None	Total	None/Total	CO rate (cM)	G/non G	R/non R	G/T	R/T	G/R
1b-43	221	236	1289	313	2059	0.22	25.43	2.75	2.86	0.11	0.11	0.94
7a-38	289	255	1546	352	2442	0.22	25.54	3.02	2.81	0.12	0.10	1.13
6d-35	244	234	1333	291	2102	0.23	26.16	3.00	2.93	0.12	0.11	1.04
3a-35	181	191	1027	229	1628	0.23	26.31	2.88	2.97	0.11	0.12	0.95
586b-14	270	238	1358	310	2176	0.23	26.99	2.97	2.75	0.12	0.11	1.13
1a-21	241	296	1406	311	2254	0.24	27.65	2.71	3.08	0.11	0.13	0.81
14a-8	264	250	1350	274	2138	0.24	27.95	3.08	2.97	0.12	0.12	1.06
581a-39	181	175	923	192	1471	0.24	28.17	3.01	2.94	0.12	0.12	1.03
16a-10	206	215	1080	231	1732	0.24	28.32	2.88	2.96	0.12	0.12	0.96
8a-23	290	284	1340	263	2177	0.26	31.25	2.98	2.94	0.13	0.13	1.02
11c-4	273	273	1140	199	1885	0.29	35.14	2.99	2.99	0.14	0.14	1.00
6d-9	218	210	869	168	1465	0.29	35.53	2.88	2.80	0.15	0.14	1.04
8c-2	254	246	1013	191	1704	0.29	35.72	2.90	2.83	0.15	0.14	1.03
15a-23	36	29	1329	470	1864	0.03	3.55	2.74	2.68	0.02	0.02	1.24
5a-23	58	64	1200	356	1678	0.07	7.56	3.00	3.05	0.03	0.04	0.91
593a-9	177	182	1834	499	2692	0.13	14.37	2.95	2.98	0.07	0.07	0.97
7b-9	100	102	986	255	1443	0.14	15.15	3.04	3.06	0.07	0.07	0.98
593a-26	182	183	1681	436	2482	0.15	15.98	3.01	3.02	0.07	0.07	0.99
5a-9	148	143	1338	335	1964	0.15	16.12	3.11	3.07	0.08	0.07	1.03
598a-18	119	121	1085	274	1599	0.15	16.35	3.05	3.07	0.07	0.08	0.98
8c-20	136	166	1348	358	2008	0.15	16.38	2.83	3.06	0.07	0.08	0.82

Table 3.1. *420* crossover rate (cM) of putative mutants isolated from M_2 pools. Isolates highlighted in orange show >24 cM and in blue <17 cM within *420*. Columns 2, 3, 4 and 5 displays the number of green alone, red alone, both green and red and non-fluorescent seeds. Column 6 shows the total number of seeds and Column 7 with the calculation of non-coloured seeds divided by total seed number. Columns 9 and 10 shows the segregation ratio of green versus non-green and red versus non-red. Columns 11, 12 and 13 displays the calculation of green/total, red/total and green/red. Column 8 shows the crossover rate (CO) in centimorgans (cM), which is calculated by the formula, $cM = 100*\{1-[1-2(Green + Red)/Total]^{1/2}\}$ (Ziolkowski et al. 2015).

Additionally, putative mutants were compared to the remaining wild type-like individuals (~18-22 cM) within their mutant pools (Figure 3.2; Table S8). Scorable M_2 individuals from numerous other mutant pools showed wild type-like (~20 cM) or mild phenotypes (e.g. ~17-24 cM). The stability of the background *420* recombination rate in the EMS population was in the range of ~17-24 cM (21.08 ± 1.77 cM; Table S9). The entire genetic screen was performed in controlled environment conditions (see "General Methods 2.1"). Putative mutants were also filtered using additional parameters including, (i) colour segregation ratios of fluorescent versus non-fluorescent seeds were determined to be close to 3:1 (Figure 3.3; Table 3.2), (ii) the total number of seeds per individual were selected to be ~1,000-2,000 in order to

obtain reasonable counts from all four fluorescent classes (red alone, green alone, both colours and neither colour) (Table 3.2), (iii) seed quality was selected to be high (% of live and dead seeds; Figure 3.4), (iv) red-green fluorescence intensity was selected not to be weak, which can indicate transgene silencing (Figure 3.5) and (v) FTL transgenes linked in *cis* only were selected (Individuals showing >50 cM with transgenes in *trans* configuration were discarded (Table 3.2) and (vi) individuals within the same M_2 pool with similar recombination rates were assumed to be allelic, therefore only one of the two was selected for further study (Table 3.3). Initially we selected individuals outside of these parameters and their M_3 progeny were found to revert to wild type phenotype. Based on the above filters, 21 M_2 mutants were selected (Table 3.1), allowed to self-fertilize and their progenies were scored for heritability of *420* recombination phenotypes in the M_3 generation (Figure 3.1).

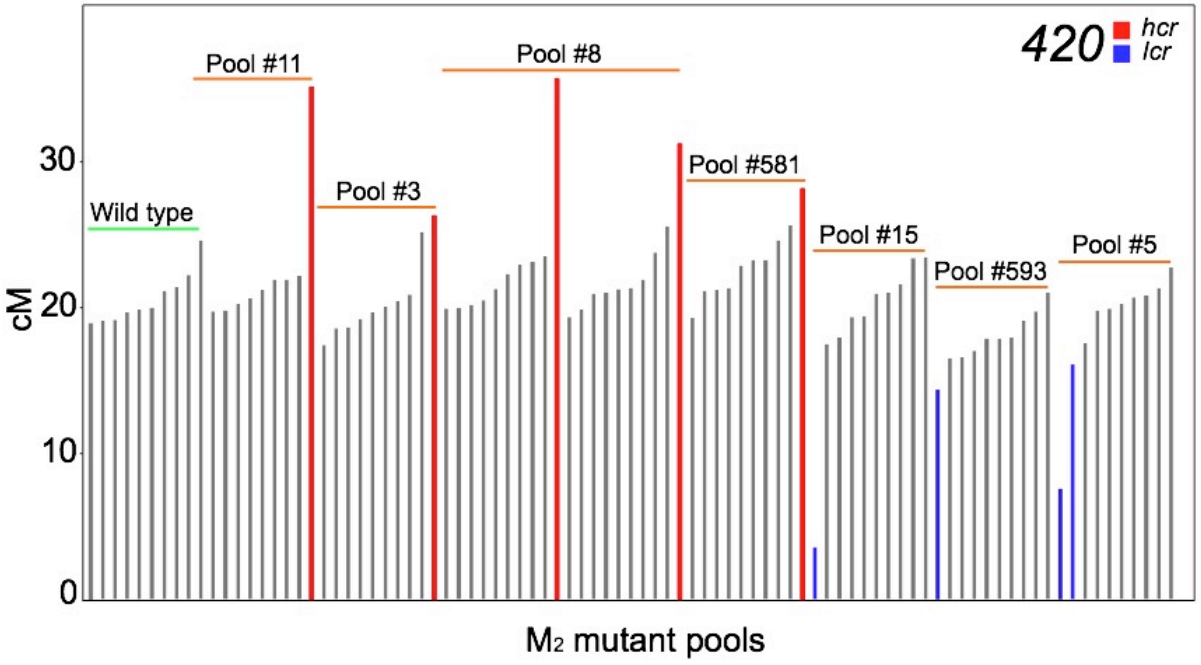

Figure 3.2. Selected M_2 isolates compared with wild type unmutagenized and wild type-like individuals within mutant pools. *420* genetic distance (cM) is plotted for a subset of M_2 pools which were found to contain high (*hcr,* red) or low recombination (*lcr,* blue) mutants.

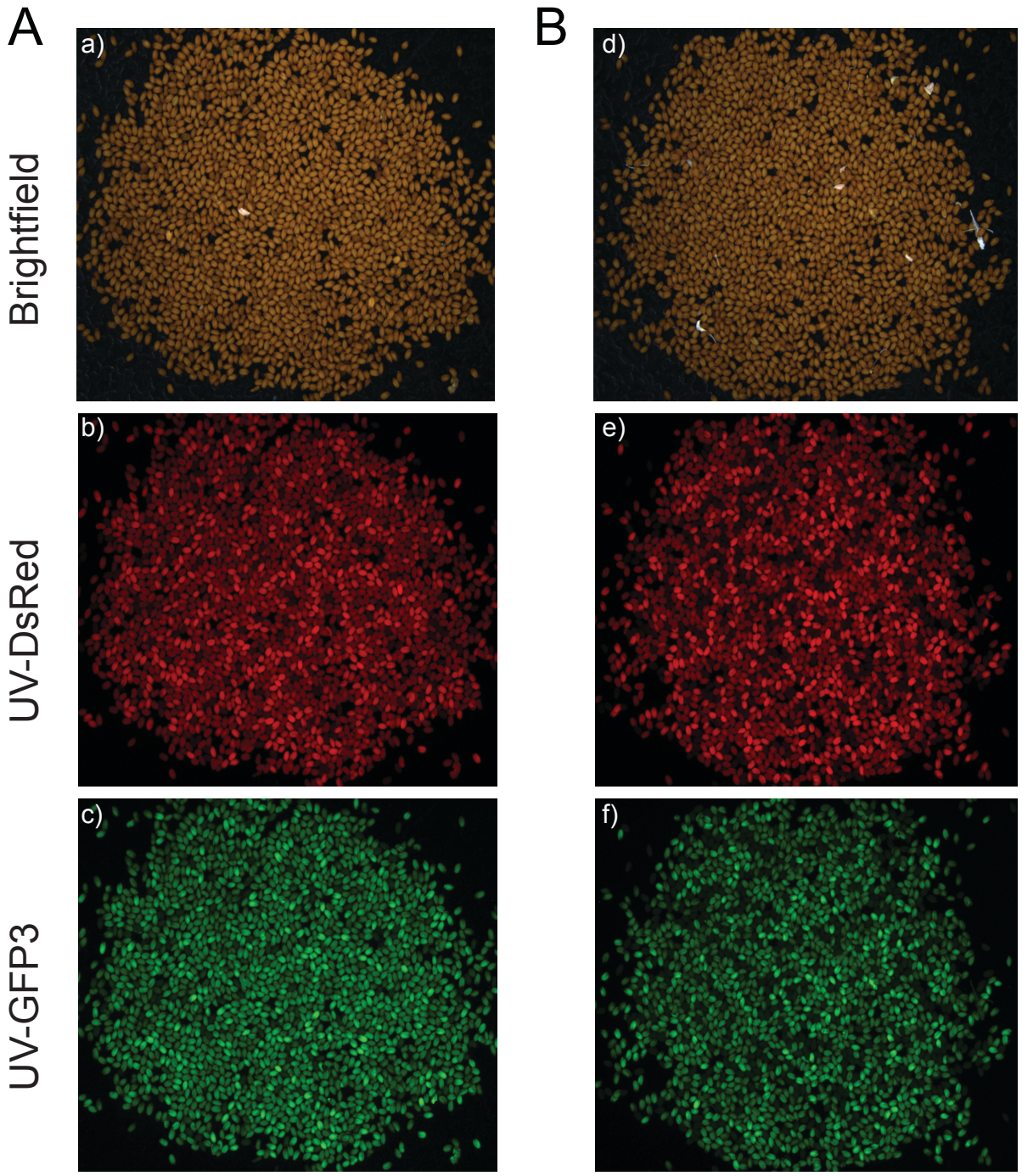

Figure 3.3. Red-green segregation ratio of fluorescent versus non-fluorescent seeds in M_2 isolates. Images (A, B) were captured using a fluorescent dissecting microscope under appropriate filters, (a, d) Brightfield; (b, e) UV-DsRed and (c, f) UV-GFP3. Visual observation of **A)** a seed individual with improper segregation of red (RR, R/r, rr) and green (GG, G/g, gg) and **B)** an example of a scorable line with proper segregation.

Bad lines	Green	Red	Both	None	Total	None/Total	CO rate (cM)	G/non G	R/non R	G/T	R/T	G/R
5a-5	31	22	291	87	431	0.12	13.16	2.95	2.65	0.07	0.05	1.41
12c-22	121	125	1886	219	2351	0.10	11.08	5.83	5.91	0.05	0.05	0.97
11a-25	5	23	141	27	196	0.14	15.48	2.92	5.13	0.03	0.12	0.22
3c-19	67	65	332	98	562	0.23	27.18	2.45	2.41	0.12	0.12	1.03
6c-19	37	129	387	101	654	0.25	29.83	1.84	3.74	0.06	0.20	0.29
8a-27	353	256	1289	572	2470	0.25	28.80	1.98	1.67	0.14	0.10	1.38
3b-32	566	566	1177	17	2326	0.49	83.67	2.99	2.99	0.24	0.24	1.00
586b-31	555	555	1104	20	2234	0.50	92.08	2.89	2.89	0.25	0.25	1.00

Table 3.2. Unsuitable individuals in M_2 based on selection parameters. Representative lines shown have low seed number (in green, <1000), poor colour segregation ratio (in yellow, not ~3:1) and a *trans* crossover phenotype (in brown, ≥ 50 cM).

Isolates	Green	Red	Both	None	Total	None/Total	CO rate (cM)	G/non G	R/non R	G/T	R/T	G/R
5a-9	148	143	1338	335	1964	0.15	16.12	3.11	3.07	0.08	0.07	1.03
5b-14	163	168	1569	413	2313	0.14	15.51	2.98	3.02	0.07	0.07	0.97
598a-18	119	121	1085	274	1599	0.15	16.35	3.05	3.07	0.07	0.08	0.98
598b-7	153	151	1377	348	2029	0.15	16.31	3.07	3.05	0.08	0.07	1.01
1b-43	221	236	1289	313	2059	0.22	25.43	2.75	2.86	0.11	0.11	0.94
1a-10	228	214	1291	286	2019	0.22	25.02	3.04	2.93	0.11	0.11	1.07
581a-39	181	175	923	192	1471	0.24	28.17	3.01	2.94	0.12	0.12	1.03
581a-10	215	236	1171	272	1894	0.24	27.63	2.73	2.89	0.11	0.12	0.91

Table 3.3. Putative allelic mutants identified in the same M_2 pool with similar *420* crossover frequency (cM). Examples of selected *hcr* (in orange) and *lcr* (in blue) M_2 individuals are provided.

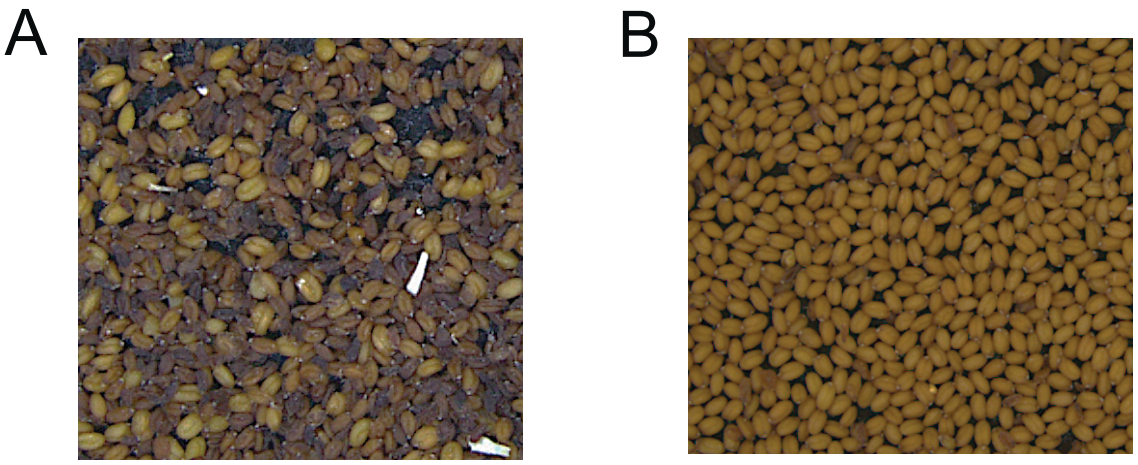

Figure 3.4. Selection of M_2 isolates based on seed quality. Brightfield (UV) images were captured using fluorescence microscopy. **A)** A seed line with majority of dead seeds and **B)** a healthy line with the majority of live seeds.

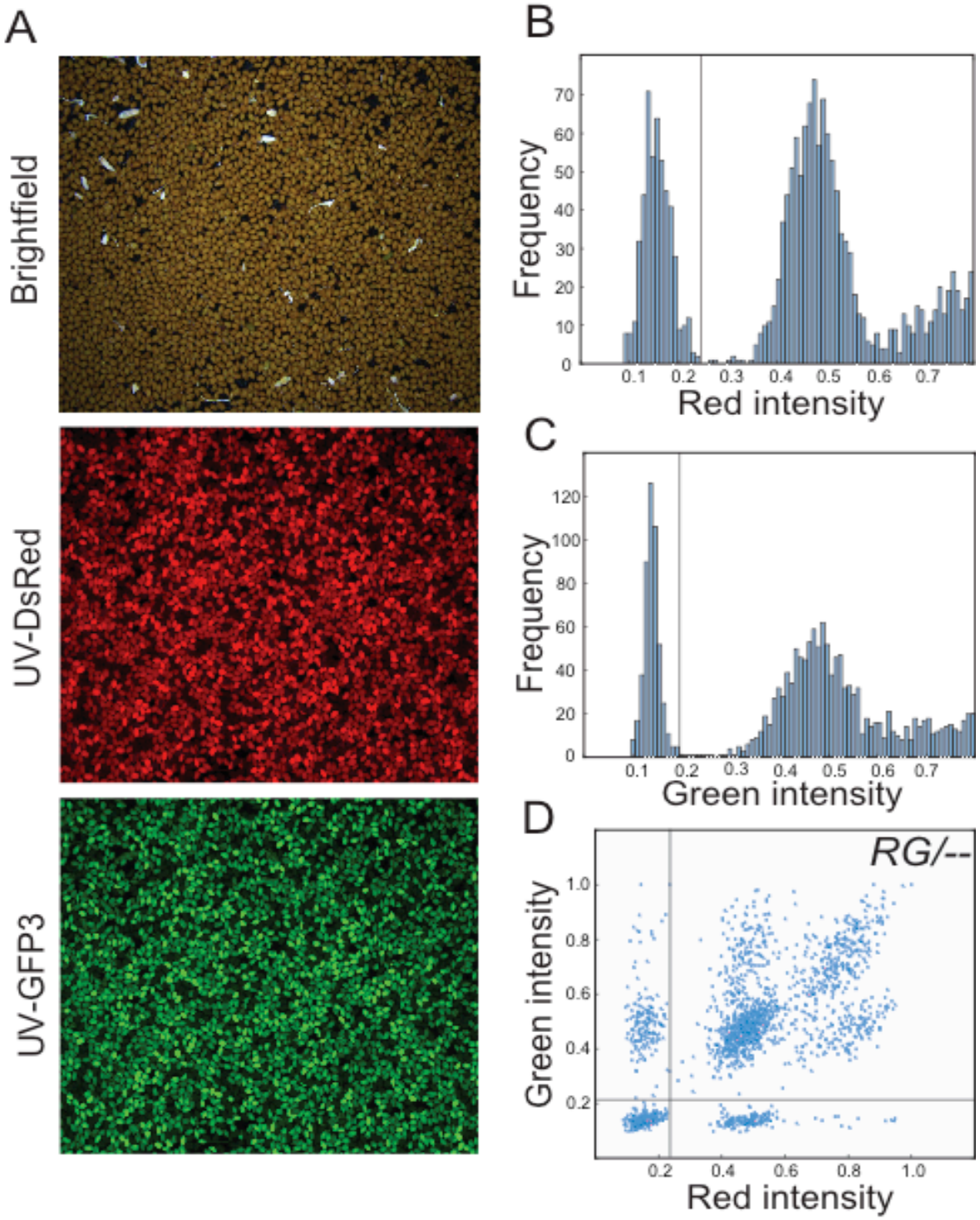

Figure 3.5. Red-green fluorescence intensity in M_2 lines. A) Bright field and intense images of a representative good seed line using (i) Brightfield, (ii) UV-DsRed and (iii) UV-GFP3 filters. **B-C)** Cellprofiler output showing histograms of seed expressed fluorescence intensities, with non-coloured and coloured seed separated by vertical lines. **D)** A plot of red vs green intensities of the seeds, with each dot indicating an individual seed.

Following this screening protocol, we confirmed 5 *high crossover rate* (*hcr*) and 4 *low crossover rate* (*lcr)* M_2 mutants (Table S10, S11) with significantly altered *420* crossover frequency compared to control lines in M_3 (Table 3.1). To test for significant differences between recombinant and non-recombinant *420* seed counts of wild type (Col-0) and mutant replicates, a generalised linear model (GLM) assuming binomial count distribution was used (Figure 3.6, $P < 2.0 \times 10^{-16}$). The M_3 progeny of the remaining isolates showed wild type-like or weak phenotypes compared to M_2 (Table S12).

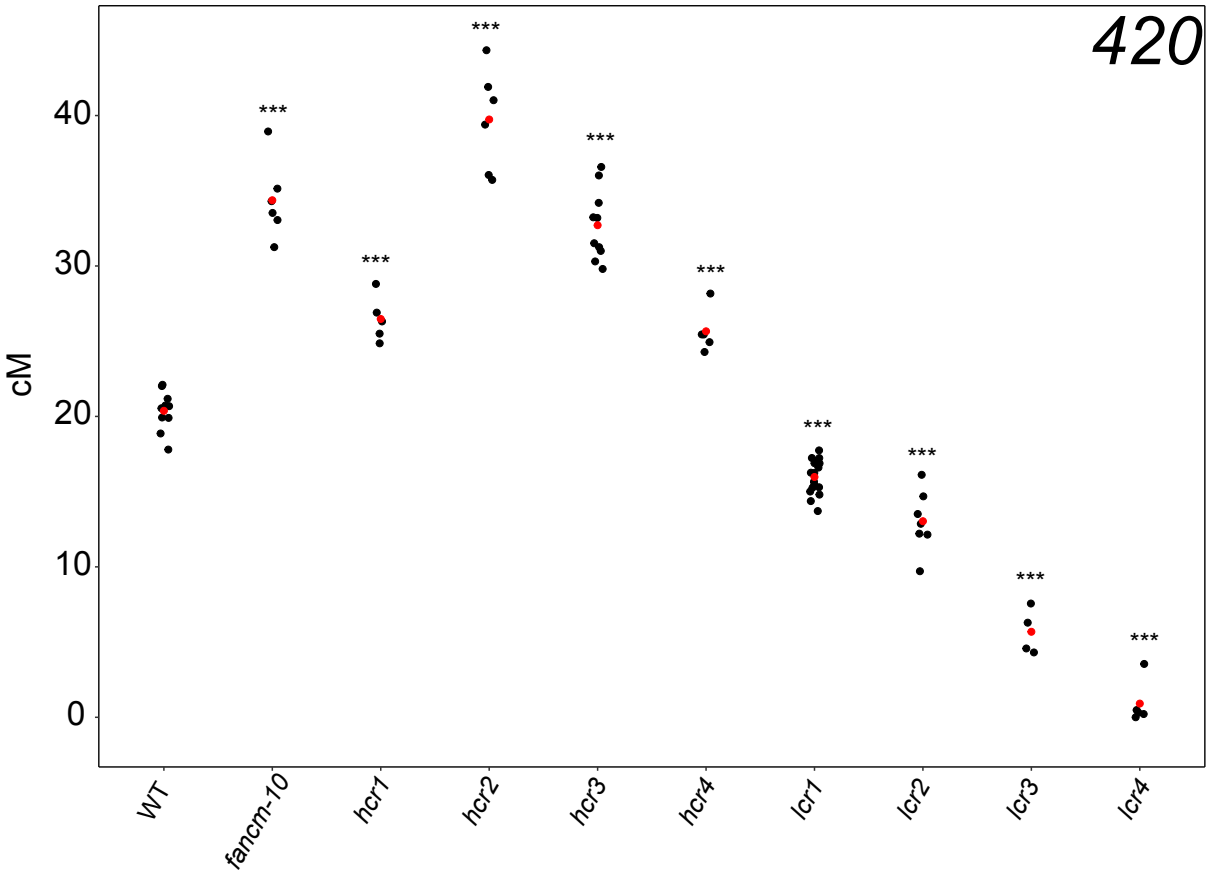

Figure 3.6. *420* crossover frequency (cM) of *hcr* and *lcr* M_2 mutants that were heritable in M_3. Mean values are indicated by red dots. To test for significance between wild type (Col-0) and each *hcr* (*fancm-10*, *hcr1*, *hcr2*, *hcr3* and *hcr4*) and *lcr* (*lcr1*, *lcr2*, *lcr3* and *lcr4*) mutants, a Generalised linear model (GLM) was used assuming binomial distribution of count values (*** = $P < 0.001$).

We identified a new *fancm* allele (*fancm-10*), in addition to *hcr1*, *hcr2*, *hcr3* and *hcr4*. The *fancm-1* recombination rate at *420* interval has been reported to be ~35 cM (Ziolkowski et al. 2015). The M_2 isolate 11c-4 (35.14 cM) was predicted to be an alternative allele of the known gene *FANCM*-At1g35530 (Crismani et al. 2012), which was validated by Sanger sequencing using several primers, particularly flanking the SF2 helicase domain (see, "Appendix 5") . An EMS change in nucleotide from G to A at 13,092,874 position in the Col-0 genomic sequence (Figure S1) leads to a non-synonymous substitution of Glycine to Serine at the 540th amino acid position (G540S), which is in the conserved motif of SF2 helicase domain (Figure 3.7). Excluding *fancm*, *hcr2* (35.72 cM) displayed a strong recombination phenotype (40.54 $\pm$ 3.08 cM) in M_3 progeny (Figure 3.6; Table S10), however we consistently observed a colour segregation distortion ratio (<3:1 or ~2:1) of fluorescent (red-green) versus non-fluorescent seeds (non-red/green) seeds (Table S10). We also observed that mutant *hcr3* (31.25 cM) is late flowering compared to wild type, in addition to showing a high crossover rate (32.87 $\pm$ 2.43 cM) in M_3 progeny (Figure 3.6; Table S10). The *hcr1* (26.31 cM) mutant displayed high recombination rate (26.51 $\pm$ 1.75 cM) as in the M_2 generation, whereas *hcr4* (28.17 cM) exhibited a weaker phenotype (25.03 $\pm$ 0.55 cM) in the M_3 generation, but significantly showed higher crossover frequency to wild type (Figure 3.6; Table S10).

We also found four heritable low recombination mutants, including *lcr1*, *lcr2*, *lcr3* and *lcr4*. Interestingly, *lcr4* (3.55 cM in M_2) showed close to zero recombination rate (0.25 $\pm$ 0.20 cM) in the M_3 generation (Figure 3.6; Table S11). Further, *lcr4 420 RG/*++ was backcrossed to wild type Col-0 which resulted in wild type level of recombination (~20 cM) in the F_1, whereas the *lcr4* cross with wild type Col *420 RG/*++ showed no recombination (data not shown). Therefore, we predicted *lcr4* to be caused by a local structural rearrangement that suppresses *420* crossover frequency, whereas it is likely to be similar to wild type elsewhere in the genome. The *lcr1* mutant (14.37 cM) in the M_3 generation showed a relatively weaker phenotype (16.08 $\pm$ 1.10 cM) but was significantly different from wild type (Figure 3.6; Table S11). Mutants *lcr2* and *lcr3* also displayed low crossover rates in their M_3 progenies, however the colour segregation ratio appeared non-Mendelian (>3:1), probably influenced by multiple genes (Figure 3.6; Table S11).

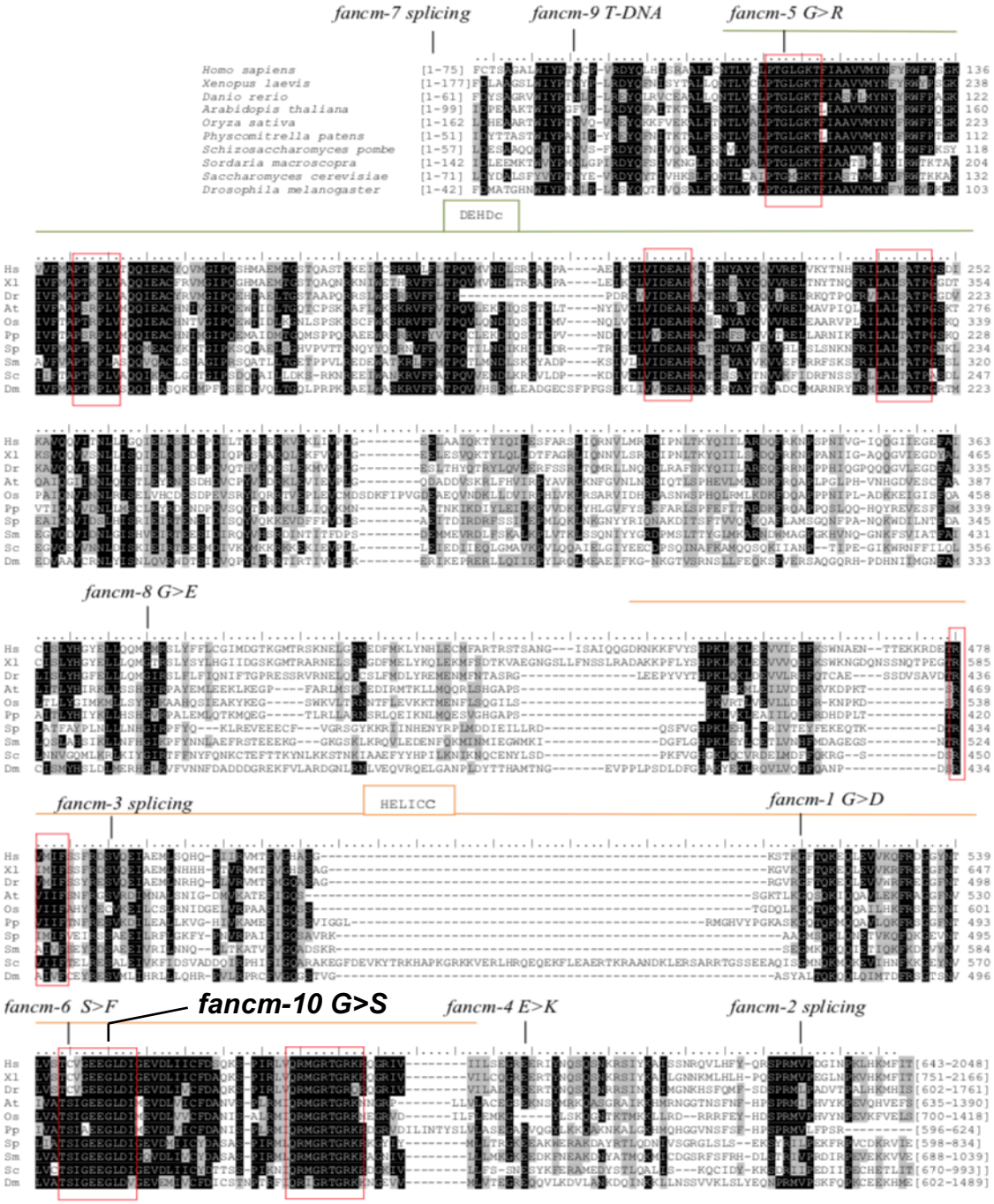

Figure 3.7. Identification of a new *fancm-10* allele from the EMS screen. Multiple sequence alignment of DEHDc and HELICC domains of FANCM in different model species. Previously identified *fancm-1* to *fancm-9* alleles, along with the new *fancm-10* (in bold) and their mutation positions are indicated. *fancm-10* is located in the conserved motif of the SF2 helicase domain (red-box). All other descriptions are mentioned in the original article (Crismani et al. 2012).

3.3.2. An isogenic mapping population for mapping-by-sequencing

EMS-induced mutations can be identified robustly using the SHORE mapping pipeline (Schneeberger 2009; Lister et al. 2009; Hartwig et al. 2012; Allen et al. 2013). This approach can use polymorphic natural accessions (e.g. Col x Ler) to generate F_1 progenies and subsequently to produce F_2 populations. Within such F_2 populations, a quarter of plants should show the mutant phenotype (if recessive). DNA from bulk segregants can then be isolated and pooled for sequencing library construction. Also, a large number F_2 recombinants can be pooled to extract a single genomic DNA for simultaneous mapping and candidate gene sequencing. The allele frequency of the candidate sites can be used to assess linkage between genomic regions and derived mutations (Schneeberger 2009; Lister et al. 2009; Hartwig et al. 2012; Allen et al. 2013). However, *420* crossover frequency is extensively modified in F_1 and F_2 generations by natural genetic variation acting in both *cis* and *trans* (Ziolkowski et al. 2015, 2017). Although mapping-by-sequencing is a simple and rapid approach compared to conventional mapping, its utilization is impeded by the use of inter-accession crosses that would confound our mapping due to quantitative traits that would modify crossover frequency. Therefore, we adopted a different strategy which was to backcross a mutant line with *420/*++ to a non-mutagenized progenitor (Col-0) and repeat this screen, unaided by natural polymorphisms (Col/Ler), but still testing for allele frequency biases in novel EMS-derived mutations observed in the background.

Heritable mutant lines including *hcr1*, *hcr2*, *hcr3*, *lcr1*, *lcr2* and *lcr3* were backcrossed to wild-type Col-0, which produced F_1 individuals with hemizygous *420* FTL transgenes and heterozygous candidate mutations (Figure 3.1). The F_1 progeny of these crosses were scored for *420* crossover frequency. This demonstrated that mutants *hcr1*, *lcr1* and *lcr2* demonstrated were recessive, whereas *hcr2* and *hcr3* revealed semi-dominant phenotypes (Table 3.4). Additionally, we crossed *hcr* mutants to *fancm* and *fancm zip4* double mutants (Crismani et al. 2012) to investigate the semi-dominant phenotype in the mutants *hcr2* and *hcr3*, respectively. The double mutant *fancm zip4* exhibits a similar high recombination phenotype as *fancm* (~35 cM) within the *420* interval (Ziolkowski et al. 2015). F_1 progeny of *hcr1* crossed to *fancm zip4* validated a wild type level of recombination. In contrast to the

BC_1F_1 phenotype, F_1 lines of *hcr2* showed wild type crossover rate from reciprocal crosses with *fancm* and *fancm zip4*, whereas *hcr3* continued to display a semi-dominant phenotype (Table 3.5).

BC_1F_1 progeny	Green	Red	Both	None	Total	CO rate (cM)	G/non G	R/non R	G/R	Mean cM	SD
hcr1 420 x Col-0-1	178	167	1108	269	1722	22.59	2.95	2.85	1.07	21.32	0.86
hcr1 420 x Col-0-2	209	208	1436	352	2205	21.15	2.94	2.93	1.00		
hcr1 420 x Col-0-3	203	215	1473	351	2242	20.81	2.96	3.05	0.94		
hcr1 420 x Col-0-4	231	211	1548	388	2378	20.74	2.97	2.84	1.09		
hcr2 420 x Col-0-1	219	210	1098	346	1873	26.39	2.37	2.32	1.04	26.01	0.52
hcr2 420 x Col-0-2	250	230	1239	387	2106	26.23	2.41	2.31	1.09		
hcr2 420 x Col-0-3	228	239	1254	384	2105	25.41	2.38	2.44	0.95		
hcr3 x Col *420*-1	244	255	1609	346	2454	22.97	3.08	3.16	0.96	25.27	1.79
hcr3 x Col *420*-2	230	255	1515	327	2327	23.64	3.00	3.18	0.90		
hcr3 x Col *420*-3	225	264	1517	356	2362	23.45	2.81	3.07	0.85		
hcr3 x Col *420*-4	239	248	1401	319	2207	25.26	2.89	2.96	0.96		
hcr3 x Col *420*-5	250	233	1282	282	2047	27.33	2.97	2.85	1.07		
hcr3 x Col *420*-6	245	251	1512	349	2357	23.90	2.93	2.97	0.98		
hcr3 x Col *420*-7	259	275	1479	329	2342	26.25	2.88	2.98	0.94		
hcr3 x Col *420*-8	218	244	1353	311	2126	24.81	2.83	3.02	0.89		
hcr3 x Col *420*-9	247	232	1322	274	2075	26.63	3.10	2.98	1.06		
hcr3 x Col *420*-10	218	224	1316	261	2019	25.02	3.16	3.22	0.97		
hcr3 x Col *420*-11	189	221	1021	237	1668	28.70	2.64	2.92	0.86		
lcr1 420 x Col-0-1	173	175	1391	368	2107	18.17	2.88	2.89	0.99	19.07	0.78
lcr1 420 x Col-0-2	207	208	1530	414	2359	19.49	2.79	2.80	1.00		
lcr1 420 x Col-0-3	229	198	1601	392	2420	19.56	3.10	2.90	1.16		
lcr2 420 x Col-0-1	209	203	1511	383	2306	19.83	2.94	2.90	1.03	18.93	0.90
lcr2 420 x Col-0-2	212	179	1530	362	2283	18.92	3.22	2.98	1.18		
lcr2 420 x Col-0-3	172	195	1490	380	2237	18.03	2.89	3.05	0.88		

Table 3.4. *420* crossover rate (cM) of BC_1F_1 progenies of *hcr* and *lcr* mutants. Mean crossover (CO) rate and standard deviation (SD) were calculated. Segregation distortion ratio observed in *hcr2* F_1 progenies (in yellow).

From one BC_1F_1 line, ~300-600 (*RG/*++) seeds were pre-selected to produce a population of F_2 individuals, termed BC_1F_2. SHOREmapping approach involves phenotyping of the mapping populations (Hartwig et al. 2012). Therefore, all the individuals (~300-600) of *hcr* or *lcr* BC_1F_2 populations were scored for *420* crossover frequency. We then used these data to select individuals in order to prepare sequencing libraries for *hcr1*, *hcr2*, *hcr3* and *lcr1* mapping populations. The *hcr3* population was generated and sequenced by Dr. Kyuha Choi (data not shown). Within isogenic mapping populations, EMS-induced mutations segregate except for the causal or closely linked mutations that should be fixed in the mutant F_2 pool showing the phenotype (James et al. 2013; Allen et al. 2013).

Hence, a quarter of *hcr* or *lcr* BC_1F_2 progenies should show the mutant phenotype (if recessive) and carry homozygous candidate mutations (Figure 3.1, 3.8). Note that a greater proportion of individuals from *hcr* and *lcr* mapping populations showed higher crossover frequency than wild type, which could be due to EMS polymorphisms per se affecting recombination (Ziolkowski et al. 2015; Figure 3.8; Table S13, S14, S15). Consistent with this, subsequent rounds of backcrossing (BC_2 or BC_3) reduced this variation in recombination rate between the F_2 progenies (shown in Chapter 4 and 5; Zuryn et al. 2010). While *lcr2* and *lcr3* were heritable in the M_3 generation, their BC_1F_2 progenies failed to recover the mutant phenotype and hence were discarded from further analysis.

F_1 progeny	Green	Red	Both	None	Total	CO rate (cM)	G/non G	R/non R	G/R	Mean cM	SD
hcr1 420 x *fancm zip4*-1	217	243	1600	392	2452	20.96	2.86	3.03	0.89	21.05	0.96
hcr1 420 x *fancm zip4*-2	211	248	1596	405	2460	20.83	2.77	2.99	0.85		
hcr1 420 x *fancm zip4*-3	241	241	1546	399	2427	22.36	2.79	2.79	1.00		
hcr1 420 x *fancm zip4*-4	101	120	817	187	1225	20.05	2.99	3.25	0.84		
hcr2 420 x *fancm zip4*-1	267	233	1480	364	2344	24.28	2.93	2.71	1.15	22.23	2.89
hcr2 420 x *fancm zip4*-2	221	236	1656	405	2518	20.19	2.93	3.02	0.94		
fancm 420 x *hcr2*-1	245	232	1619	396	2492	21.44	2.97	2.89	1.06	21.67	0.18
fancm 420 x *hcr2*-2	215	219	1478	333	2245	21.68	3.07	3.10	0.98		
fancm 420 x *hcr2*-3	248	250	1675	403	2576	21.68	2.94	2.96	0.99		
fancm 420 x *hcr2*-4	226	266	1624	409	2525	21.88	2.74	2.98	0.85		
hcr3 420 x *fancm zip4* -1	262	271	1475	321	2329	26.36	2.93	2.99	0.97	26.22	1.26
hcr3 420 x *fancm zip4* -2	228	264	1308	309	2109	26.96	2.68	2.93	0.86		
hcr3 420 x *fancm zip4* -3	276	258	1608	351	2493	24.40	3.09	2.98	1.07		
hcr3 420 x *fancm zip4* -4	165	185	936	206	1492	27.14	2.82	3.02	0.89		
hcr3 x *fancm 420*-1	229	274	1459	353	2315	24.80	2.69	2.98	0.84	25.22	1.31
hcr3 x *fancm 420*-2	270	253	1437	312	2272	26.54	3.02	2.90	1.07		
hcr3 x *fancm 420*-3	232	234	1322	275	2063	25.96	3.05	3.07	0.99		
hcr3 x *fancm 420*-4	239	248	1517	337	2341	23.58	3.00	3.06	0.96		

Table 3.5. *420* crossover frequency (cM) of F_1 progenies of *hcr* mutants crossed to *fancm* and *fancm zip4*. Mean CO rate (cM) and standard deviation (SD) were calculated.

3.3.3. SHOREmap identification of candidate mutations

Unlike outcrossed populations, mapping-by-sequencing of backcross populations requires high sequence coverage and pool size due to limited marker density. An optimal sequencing coverage of ~50x from ~50 pooled individuals showing the mutant phenotype from each BC_1F_2 population is recommended for predicting homozygous mutations (James et al. 2013; Schneeberger 2014). Depending on the population size, seeds of ~30-80 *hcr* or *lcr* F_2 individuals representing homozygous mutant phenotypes (Table S16, S17, S18) were pooled and bulk DNA isolated for

sequencing libraries (see “General Methods 2.8”). The nuclear isolated DNA was mechanically sheared to a fragment size in the range of 200 to 500 bp. Low (<250 bp) and high (>400 bp) DNA fragments were excised followed by ligation of universal adaptors that including adaptor indexes (see, “General Methods 2.9”). These Adaptor-indexed DNA libraries with ~300 bp size were sequenced on a single lane of an Illumina Genome Analyser in a 75 bp paired end run. We sequenced our lab strain Col-*420* (external control) along with mutant libraries as a control. Additionally, a wild type-like individual from EMS mutagenesis (internal control) was backcrossed once to parental Col-0 and its F_2 progenies were pooled and sequenced in the same manner. However, I did not prioritize detection of fixed and non-fixed EMS mutations between external and internal control data sets. Using SHORE, the adaptor-trimmed wild type (EMS/Non-EMS) and mutant reads were aligned to the Col-0 reference genome (TAIR10) respectively, and used to call for novel variant SNPs (Ossowski et al. 2008; Hartwig et al. 2012; James et al. 2013; see "General Methods 2.9").

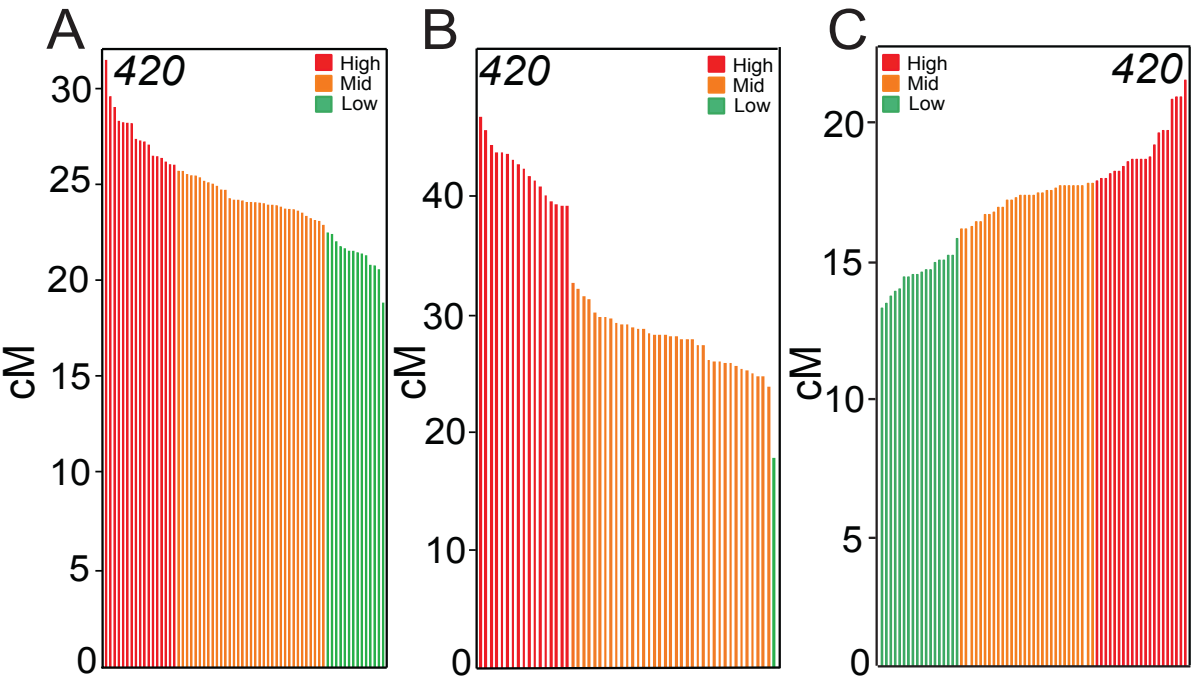

Figure 3.8. Backcross mapping population for deep sequencing. *420* genetic distance (cM) is plotted from (A,B,C) *hcr1*, *hcr2* and *lcr1* BC_1F_2 population used for mapping-by-sequencing. The samples are colour-coded according to high (red), mid (orange) and low (green) recombination rate. These samples were assigned to the three classes based on isolated M_2 mutant and wild type range of phenotypes. The ‘high’ samples from *hcr1* (~26-32 cM) and *hcr2* (~38-47 cM) populations, and the ‘low’ samples (~13-15 cM) from *lcr1* were selected for library construction.

SHOREmap, a visual extension of SHORE (Schneeberger 2009) identified candidate mutations for *hcr1*, *hcr2*, *hcr3* and *lcr1* sequences. Both wild type references provided a similar candidate SNP list for all of the mapped mutants after SHOREmap analysis. Hence, we filtered all the SNP variants using Col-*420* (external control) as shown. From *hcr1* SHOREmap, four mutations with nucleotide transitions (G>A or C>T) and a biased allele frequency were observed on chromosome 4 (Figure 3.9). Mutations were screened for those, (i) with greater than 80% allele frequency, and (ii) non-synonymous, splice site or premature stop codon changes in predicted genes (Hartwig et al. 2012; Lindner et al. 2012). Additional filters were taken into consideration when examining candidates including, (i) predicted or known function relevant to the biological process of meiosis, (ii) candidate protein location in the nucleus, and (iii) known molecular functions provided in the TAIR database. According to these criteria, a splice site donor mutation with a C>T transition in intron 3 of At4g26720 at 13,471,378 bp position of the TAIR10 assembly, which encodes PROTEIN PHOSPHATASE X-1 (PPX-1;Table S19) was identified. Similarly, we identified a plausible *hcr2* candidate mutation in *DOF4.2* (At4g21030), a transcription factor with a nonsynonymous G>A change in the coding sequence region (CDS) at 11,231,903 bp position on chromosome 4, encodes a DNA-binding with one finger protein (Figure 3.10; Table S20).

Interestingly, several SNPs with >0.5 allele frequency on chromosome 3 of *hcr3* and chromosome 1 of *lcr1* SHOREmaps were observed (Figure 3.11, 3.12), which may be due to low pool size (James et al. 2013). In this context, filtering strategies could help to narrow down the potential causative SNPs despite low genome coverage or mapping quality of reads (Lindner et al. 2012). Thus, two putative *hcr3* C>T candidate mutations were shortlisted from chromosome 3. The first candidate is a splice site acceptor mutation in intron 1 of At3g45580 at 16,731,099 bp position, which encodes a RING/U-box zinc finger protein. The other *hcr3* mutation is in gene *J3* (At3g44110) with a non-synonymous change in the coding sequence at 15,870,106 bp position on chromosome 3, encodes a DNAJ homologue 3 (Figure 3.11; Table S21). Similarly, two probable *lcr1* candidates located in chromosome 1 were identified. One of the *lcr1* candidates is a non-synonymous G>A transition found in the *TBP-associated factor 4B* (*TAF4B*; At1g27720) at 9,646,825 bp position. This mutation is located within exon 3 and is predicted to cause a

premature stop codon and hence to produce a truncated protein. The other change is a non-synonymous C>T mutation with an allele frequency ~80%, in the exon 2 of the At1g48360 at 17,868,922 bp position, encodes a FAN1 or FANCONI/FANCD2 associated NUCLEASE I (Figure 3.12; Table S22).

3.4. Discussion

A forward genetic screen via EMS mutagenesis identified putative candidate genes that may regulate meiotic recombination in *Arabidopsis thaliana*. Previous meiotic screens isolated mutants based on fertility defects, which were further validated through cytogenetic studies (De Muyt et al. 2009; Crismani et al. 2012). We introduced seed based reporter systems (Melamed-Bessudo et al. 2005) in our genetic screen to identify mutants with quantitatively different crossover frequency from wild type. This has increased the potential of finding novel genes that are less studied in meiosis context (see, “Results 3.3.”).

Few previously characterized meiotic genes in Arabidopsis, including *SPO11-1*, *SPO11-2*, *PRD1*, *AHP2*, *DMC1*, *ASY1* and *SDS* were recognized again through screening for fertility (De Muyt et al. 2009). Likewise, we identified an alternative allele of the anti-crossover factor, *FANCM* (Crismani et al. 2012), which validated the success of our reporter based screen. In addition to that, *hcr* and *lcr* mutants displayed a non-*fancm* (i.e. unlike *fancm* CO rate) recombination from the F_1 progenies of the cross with *fancm* and *fancm zip4* (Table 3.5), which proved that they are not alleles of *fancm*. The heritability of *hcr* and *lcr* phenotypes (Figure 3.6) and recovery of homozygotes in BC_1F_2 progenies (Figure 3.8) allowed mapping candidate mutations by deep sequencing approach (Schneeberger 2009).

Mapping-by-sequencing approaches using isogenic mapping populations can be applied to map recessive, dominant, semi-dominant, lethal, poorly transmitted mutations, hard-to-score phenotypes and second-site modifiers even from complex genetic or transgenic backgrounds (Hartwig et al. 2012; Lindner et al. 2012; Schneeberger 2014). Using SHOREmap, we were able to map both recessive (*hcr1*, *lcr1*; Figure 3.9, 3.12*)* and semi-dominant (*hcr2, hcr3)* mutations (Figure 3.10, 3.11). However, causative SNPs obtained for *hcr3* and *lcr1* mutations showed an allele

frequency of ~80% and not close to 1 as expected (Allen et al. 2013). Mis-scoring of F_2 progenies with greater variation in phenotype owing to putative *cis* effects from one round of backcross makes it challenging to clearly demarcate homozygous mutant individuals from the rest of the population (Figure 3.8). Hence, this can weaken the allele frequency by introducing wild type alleles at the causative locus (James et al. 2013; Ziolkowski et al. 2015). Low sequence coverage (<50x) of *hcr3* and *lcr1* may also have caused ambiguity in determining the plausible candidate from the chromosomes observed with allele frequency distortion (James et al. 2013). Excluding all discrepancies, I next narrowed down the candidate genes obtained from mapping mutants based on functional relevance.

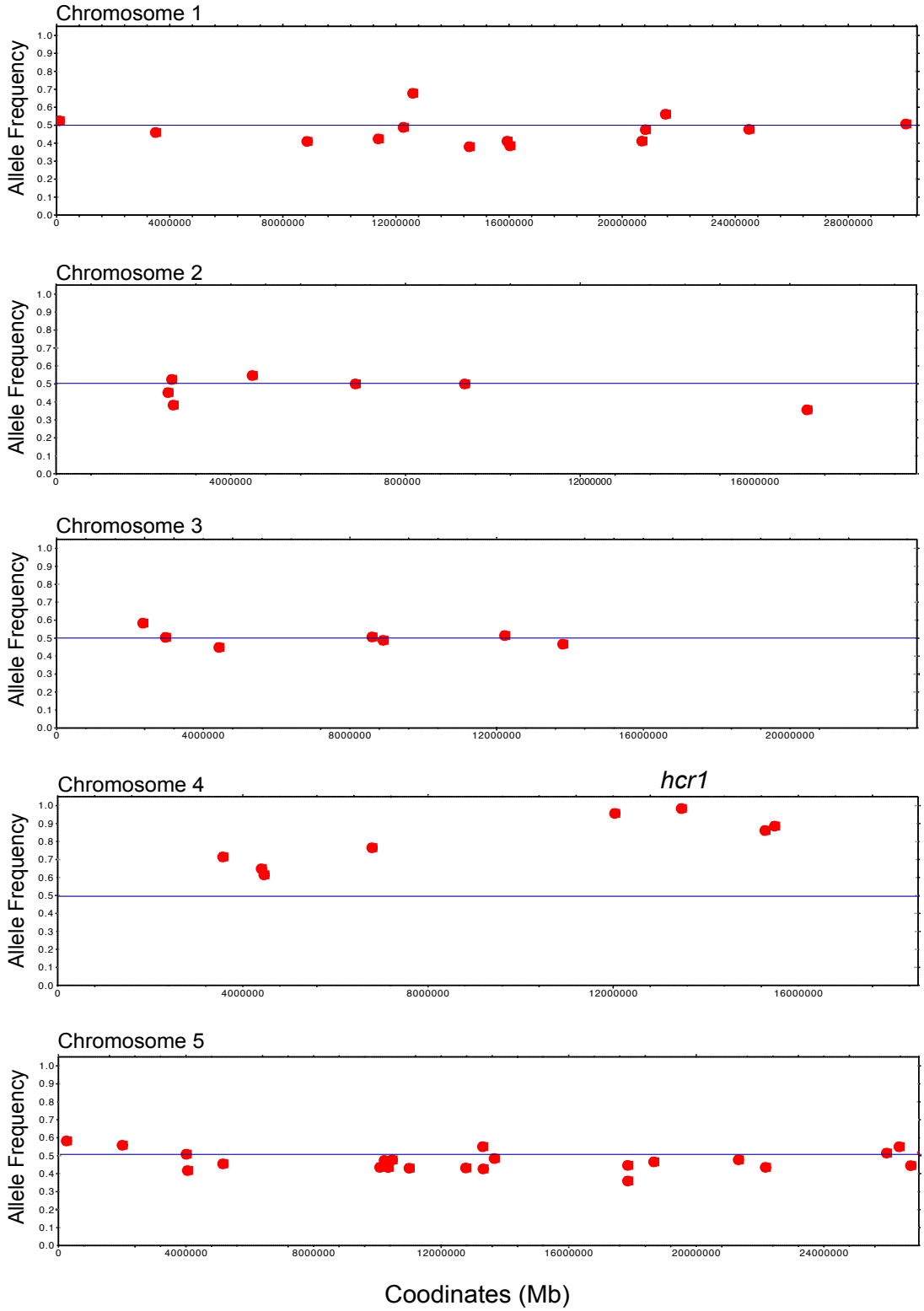

Figure 3.9. *hcr1* candidate mutations identified using SHOREmap. The allele frequency of EMS derived mutations in the *hcr1* BC_1F_2 DNA library are plotted along the 5 Arabidopsis chromosomes as shown. The horizontal line (in blue) indicates the 0.5 allele frequency, which is expected to show non-association with crossover frequency. According to selection criteria described in text, the position of the *hcr1* mutation is indicated in chromosome 4.

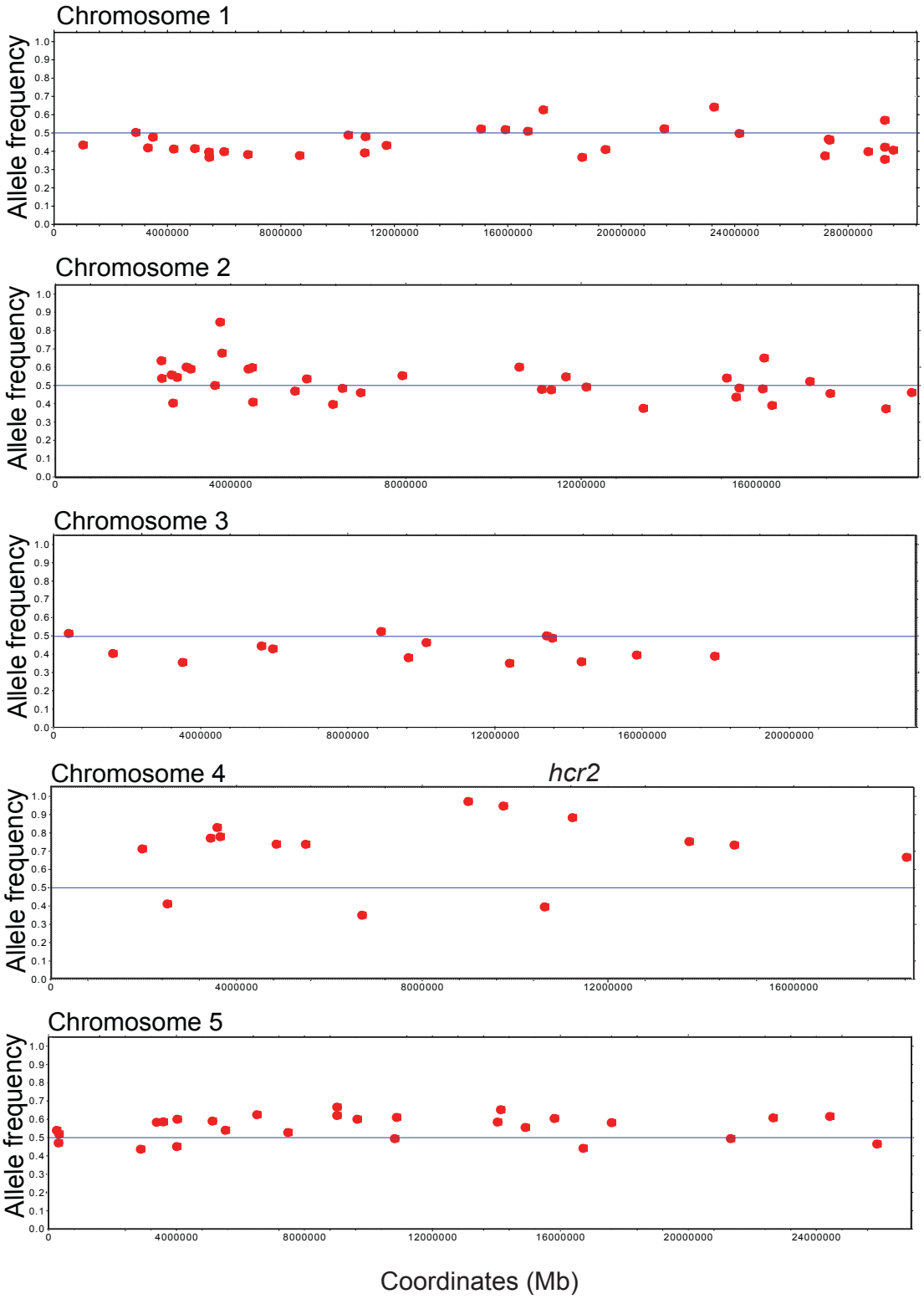

Figure 3.10. *hcr2* plausible candidates identified from SHOREmap. The allele frequency of EMS derived mutations in the *hcr2* BC_1F_2 DNA library are plotted along the 5 Arabidopsis chromosomes as shown. The horizontal line (in blue) indicates the 0.5 allele frequency, which is expected to show non-association with the crossover frequency. The position of *hcr2* mutation is indicated in chromosome 4 based on selection parameters described in text.

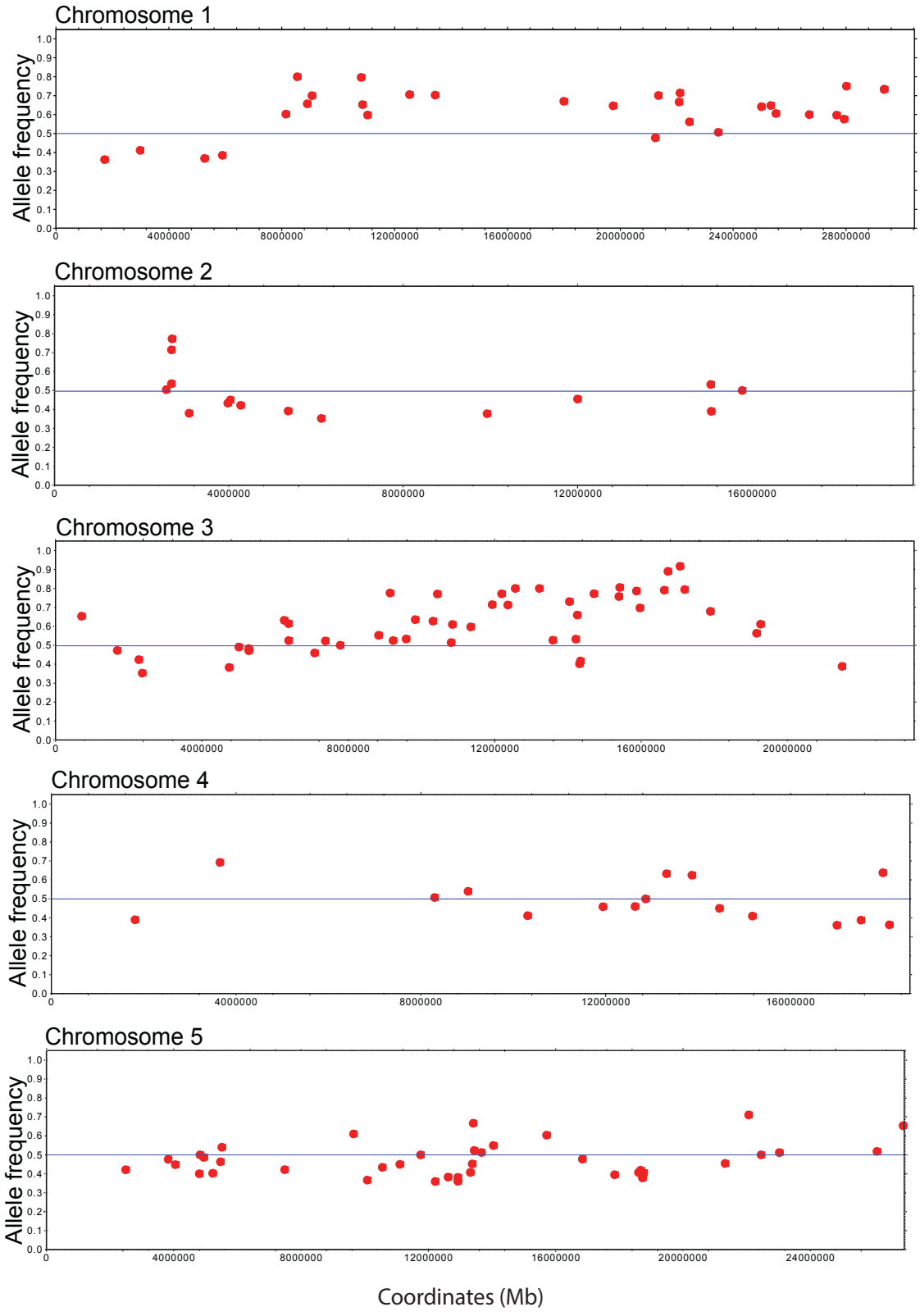

Figure 3.11. *hcr3* putative candidates identified using SHOREmap. The allele frequency of EMS derived mutations in the *hcr3* BC_1F_2 DNA library are plotted along the 5 Arabidopsis chromosomes as shown. The horizontal line (in blue) indicates 50% allele frequency, which is expected to show non-association with crossover frequency. Allele frequency with distortion observed in chromosome 3.

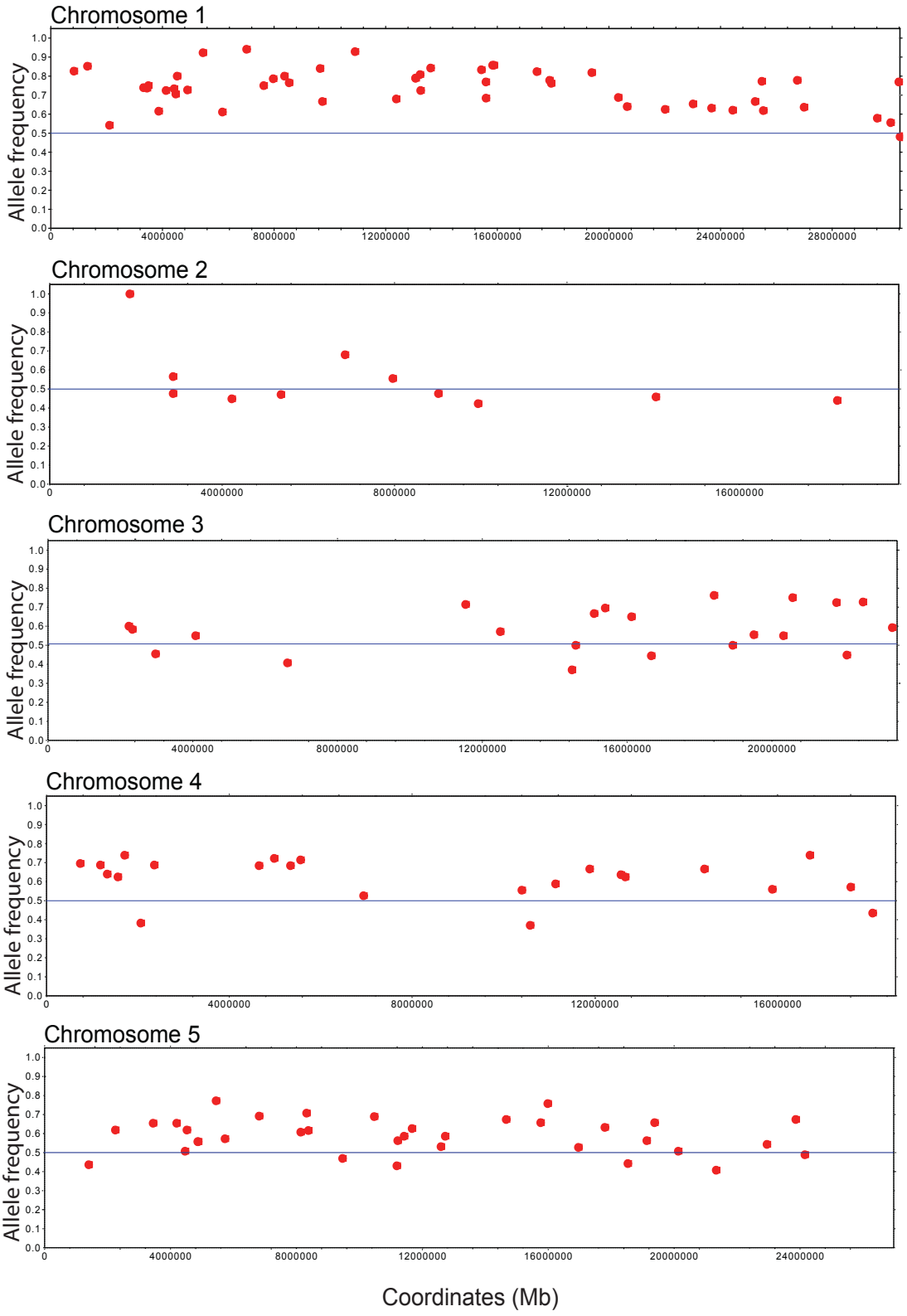

Figure 3.12. *Icr1* causal mutations identified using SHOREmap. The allele frequency of EMS derived mutations in the *Icr1* BC_1F_2 DNA library are plotted along the 5 Arabidopsis chromosomes as shown. The horizontal line (in blue) indicates the 0.5 allele frequency, which is expected to show non-association with crossover frequency. Allele frequency with bias found in chromosome 1.

Chapter 4 - HIGH CROSSOVER RATE 1 / PROTEIN PHOSPHATASE X-1 represses meiotic crossover in *Arabidopsis thaliana*

4.1. Summary

The test of *PPX-1* as a candidate for *hcr1* lead me to perform further experiments to prove this, in addition to investigating the function of this protein in the meiotic recombination pathway.

4.2. Introduction

PPX-1 belongs to the Arabidopsis PP4/PPX family (Moorhead et al. 2009). Once *PPX-1* was identified as a candidate gene for the *hcr1* mutation I performed a literature survey of the role of PP4 in *Arabidopsis thaliana*. Both PPX-1 (At4g26720) and PPX-2 (At5g55260) encode catalytic subunits of PPX complexes (Moorhead et al. 2009). The *PPX-1* and *PPX-2* genes are composed of eight exons and seven introns and are expressed at low levels in flowers, leaves, stems and roots (Pérez-Callejón et al. 1993). The intron-exon organization of *PP4*/*PPX* is entirely different from its close relative PP2A, although they encode structurally-related proteins (Pujol et al. 2000). Arabidopsis PP4/PPX complexes also consist of two regulatory subunits, including PP4R2 (At5g17070) and PP4R3 (At3g06670) (Lillo et al. 2014). PP4R3 has been identified as SMEK1 (Suppressor of MEK1), which is a conserved protein acts as a suppressor in the MAPK (Mitogen-activated protein kinase) cascade (Mendoza et al. 2005). The two PP4 catalytic subunits (PPX1 and PPX-2) together with the regulatory subunit PP4R3/SMEK1 form a complex to dephosphorylate HYL1 (HYPONASTIC LEAVES 1), a core co-factor which promotes miRNA biogenesis by antagonizing the MAPK signalling cascade (Su et al. 2017). However, prior to this genetic screen there was no evidence of *Arabidopsis* PP4 to involve in meiosis-related processes. In this chapter, I show that *PPX-1* is *HCR1* by allelism testing and genomic complementation. I also characterize the function of *HCR1/PPX-1* as a repressor of interfering meiotic crossover formation in *Arabidopsis thaliana*.

4.3. Results

4.3.1. The *hcr1* mutation is within *PROTEIN PHOSPHATASE X-1*

The *hcr1* candidate gene *PPX-1* (At4g26720) is composed of 8 exons and 7 introns with a nucleotide length of 2,457 bp (Pujol et al. 2000) (Figure 4.1). The putative *hcr1* mutation (C>T) caused by EMS was found at the intron 3 splice donor site (Figure 4.1). The *hcr1-1* EMS allele causes a ~78 bp increase in amplicon size following RT-PCR using primers that spanned the intron-exon junction and the mutation, when *hcr1* was compared to wild type and *hcr1-2* allele (T-DNA insertion) Figure 4.1). This is due to the intron retention between exons 3 and 4, that was validated by Sanger sequencing from both WT and *hcr1-1* RT-PCR products amplified from floral cDNA (Figure 4.1). The retained intron sequence results from the point mutation at the splicing site and which leads to introduction of a premature termination codon (PTC) (Jacob and Smith 2017) at 1,109 bp within the genomic sequence. This PTC is predicted to produce a non-functional protein following mRNA translation. The truncated PPX-1 protein is predicted to be 116 amino acid residues in length compared to the wild type protein of 305 residues (Pérez-Callejón et al. 1993). Amino acid residues starting at the 112th position are annotated to form the catalytic active site (https://www.uniprot.org/ uniprot/P48529# P48529-1).

To confirm that the predicted mutation is responsible for *hcr1* phenotype, one of the 'high' recombination individuals used to generate the genotyping-by-sequencing DNA library (Table S16) was backcrossed for a second time (BC_2) with the *420* parental line to produce F_1 and then selfed to generate F_2 progeny (Table S23). Genotyping of 50 *hcr1* BC_2F_2 individuals using a dCAPS marker (Table S4) designed against the *ppx-1* mutation (see, "General Methods 2.10"), showed a segregation ratio close to 1:2:1 (15 WT: 23 *hcr1* heterozygote: 12 *hcr1* homozygote). Twelve BC_2F_2 plants showed the *hcr1-1/hcr1-1* genotype and a mean *420* crossover frequency of 25.27 ± 1.78 cM, similar to the M_2 isolate (26.31 cM), which was significantly different to wild type (GLM, $P < 2.0 \times 10^{-16}$; Figure 4.2; Table S23). The fifteen wild type genotype individuals displayed a wild type crossover phenotype (19.16 ± 1.03 cM) (Figure 4.2; Table S23) which was not significantly different to other wild types. The remaining BC_2F_2 progeny that were of heterozygous *hcr1-1/+* genotype exhibited a mean crossover frequency 21.42 ± 1.89 cM that was

significantly different from both wild type (GLM, $P = 1.24 \times 10^{-8}$) and *hcr1-1/hcr1-1* (GLM, $P < 2.0 \times 10^{-16}$) recombination rates (Figure 4.2; Table S23). As the *hcr1-1/+* genotypes exhibited a phenotype intermediate to wild type and *hcr1-1*, this indicates that *hcr1* is not completely recessive in this population. In conclusion, segregation analysis of the *hcr1/ppx1* mutation in the BC_2F_2 population is consistent with this mutation causing the higher recombination phenotype at *420*.

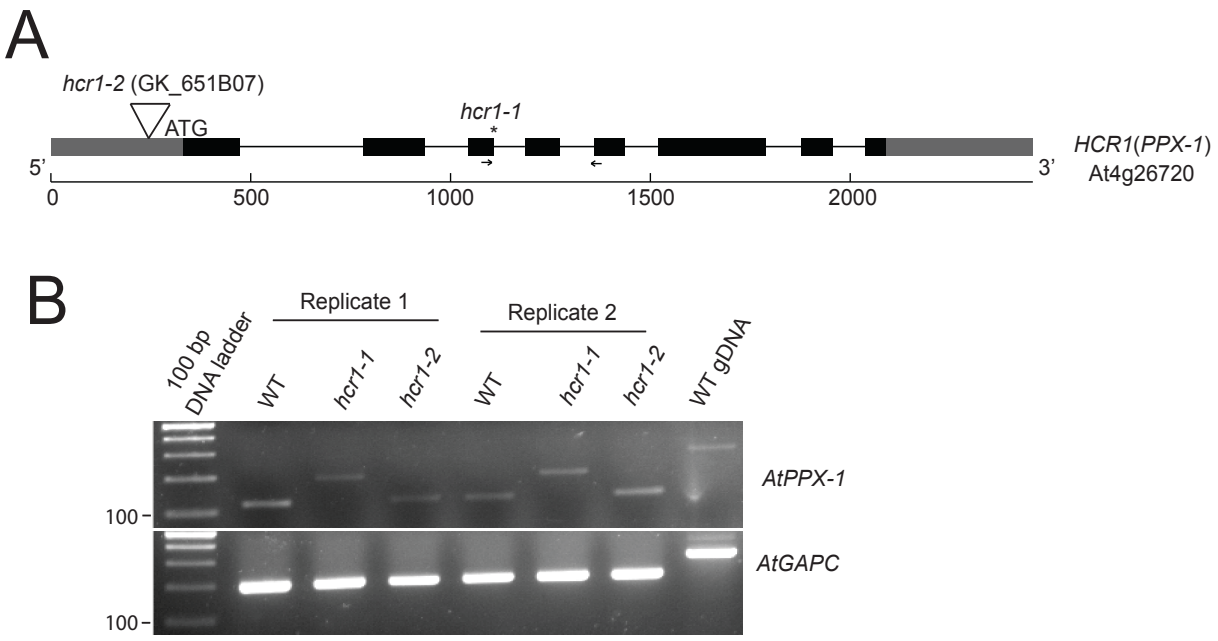

C

3'-GACATTTGAAGAGCCATATTTACGCAAACACTCATCATAAAATCCATAAACCT ACTAAAAGCAGACTTTATGAATAGTCTGAATATATACATACACAAAAGCAAAATT TTCAAATGAGACTGCATTCATCTGTGTGATTTGCCTGC**-5'**

Figure 4.1. Arabidopsis *PPX-1* and the location of *hcr1-1* and *hcr1-2* mutations. A) A map of the At4g26720 locus (GenBank ID: NM_118806) with intron-exon organization of *PPX-1* drawn using Gene structure display server 2.0 tool (https//:gsds.cbi.pku.edu.cn). The exons are drawn as boxes (black=CDS, grey=UTR). Scale bar indicates bp. The EMS allele *hcr1-1* mutation position is located at the splice donor site of intron 3 (1,109th bp) as indicated by the star. The arrows spanning the *hcr1-1* mutation indicate the position of primers used for RT-PCR. The *hcr1-2* corresponds to GK_651B07, where the T-DNA insertion is in the 5'UTR as indicated by a triangle. **B)** Wild type Col, *hcr1-1* and *hcr1-2* floral cDNA was generated for two biological replicates and used for RT-PCR amplification with *PPX-1* (indicated in **A**) and *GAPC* control primers. RT-PCR amplicon size for wild type, *hcr1-1*, *hcr1-2* and genomic DNA (positive control) are shown. **C)** Sanger sequencing of *hcr1-1* (~200 bp) amplicons using the reverse primer (indicated in **A**) confirmed retention of ~78 bp of intron (shown in yellow) in *hcr1-1* between the exons (underlined) with the point mutation "T" (in red) at intron 3 splice donor site shown.

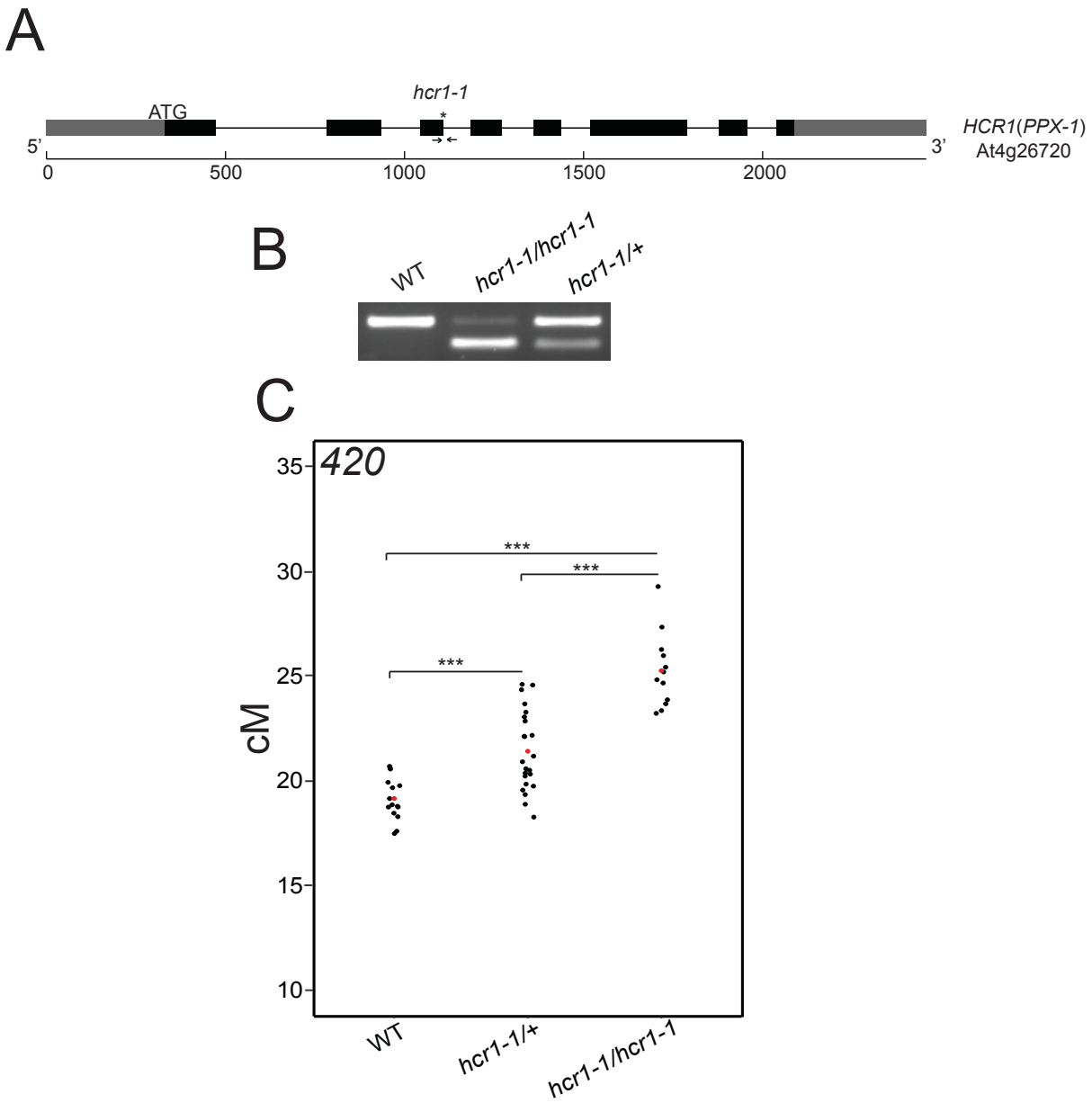

Figure 4.2. The *hcr1-1* dCAPs marker shows co-segregation with *420* phenotype in a BC_2F_2 population. A) Genotyping of a *hcr1-1* BC_2F_2 population was performed using a dCAPs marker for the *hcr1* mutation, which is indicated as arrows in the *HCR1* (*PPX-1*) gene map. **B)** Restriction digestion of PCR amplified products using *Fok*I followed by gel electrophoresis and ethidium bromide staining is shown. The higher molecular weight uncut band represents the wild type genotype and the lower band indicates the *hcr1-1* genotype. The *hcr1-1/+* genotype is represented by bright wild type and weak *hcr1-1/hcr1-1* bands. **C)** *420* crossover rate (cM) of BC_2F_2 individuals with respective genotypes, including wild type Col (19.16 ± 1.03 cM), *hcr1-1/+* heterozygotes (21.42 ± 1.89 cM) and *hcr1-1* homozygotes (25.27 ± 1.78 cM) are plotted. Mean values are indicated by red dots. Significance tests between (i) wild type and *hcr1-1*, (ii) wild type and *hcr1-1/+* and (iii) *hcr1-1/+* and *hcr1-1* using a GLM are indicated as ***, which equals $P < 0.001$.

The identity of *HCR1* as *PPX-1* was further validated by a genomic complementation experiment (Figure 4.3). A 4.5 kb genomic fragment containing ~2 kb of promoter sequence and the *HCR1* (*PPX-1*) gene open reading frame including introns and UTRs was PCR amplified using gene specific primers flanked by *Pst*I and *Sma*I restriction sites (see, "Appendix 5"). This genomic *HCR1* fragment was then cloned into the pGREEN0029 binary vector (see, "Appendix 2"). This binary vector was used for Agrobacterium-mediated transformation of a *hcr1-1 420 RG/*++ BC_2F_2 line and T_1 lines selected from the transformed seed. Additionally, an empty vector (pGREEN0029) was transformed into wild type Col *420 RG/*++ (WT-empty) and *hcr1-1 420 RG/*++ (*hcr1-1/hcr1-1* empty) lines, which generated control T_1 lines. Transformants were identified following kanamycin selection and I confirmed the presence of the *PPX-1* transgene using PCR. Eight independent *hcr1-1/HCR1* T_1 and 33 control (WT-empty + *hcr1-1/hcr1-1* empty) T_1 lines, with segregating *420* were obtained (Table S24). *420* genetic distance (cM) of the complementing T_1 lines (*hcr1-1/*HCR1) showed no significant difference from the wild type empty vector control T_1 (GLM, P=0.306; Figure 4.3; Table S24) and the untransformed wild type (GLM, P=0.309; Figure 4.3). *420* genetic distance of the complementing *hcr1-1/HCR1* T_1 lines were significantly different from the *hcr1-1/hcr1-1* empty vector control T_1 (GLM, $P < 2.0 \times 10^{-16}$; Figure 4.3; Table S24) and the untransformed *hcr1-1* (GLM, $P < 2.0 \times 10^{-16}$; Figure 4.3). These experiments provide further genetic proof that the causal mutation in the *hcr1* mutant is within *PPX-1*.

As an additional genetic test of the identity of *HCR1* as *PPX-1* I obtained an independent T-DNA allele (GK_651B07) in this gene, which I named *hcr1-2* (Figure 4.1). I confirmed the T-DNA location in this line in the 5' untranslated region (UTR) using PCR amplification and Sanger sequencing (Figure S2). I crossed *hcr1-1* and *hcr1-2* together and measured *420* crossover frequency in the F_1 progeny (Figure 4.4; Table S25). I used wild type Col *420*, *hcr1-2 420* F_3 and *hcr1-1 420* BC_2F_2 control lines to compare with *hcr1-1/hcr1-2* test cross F_1 progenies (Figure 4.4; Table S25). The *hcr1-1/hcr1-2* F_1 individuals (24.17 $\pm$ 1.71 cM) were non-significant in *420* crossover frequency compared to *hcr1-1* (25.01 $\pm$ 2.15 cM; GLM, P = 0.101), and were significantly different from wild type (19.87 $\pm$ 1.45 cM; GLM, $P < 2.0 \times 10^{-16}$; Figure 4.4; Table S25).

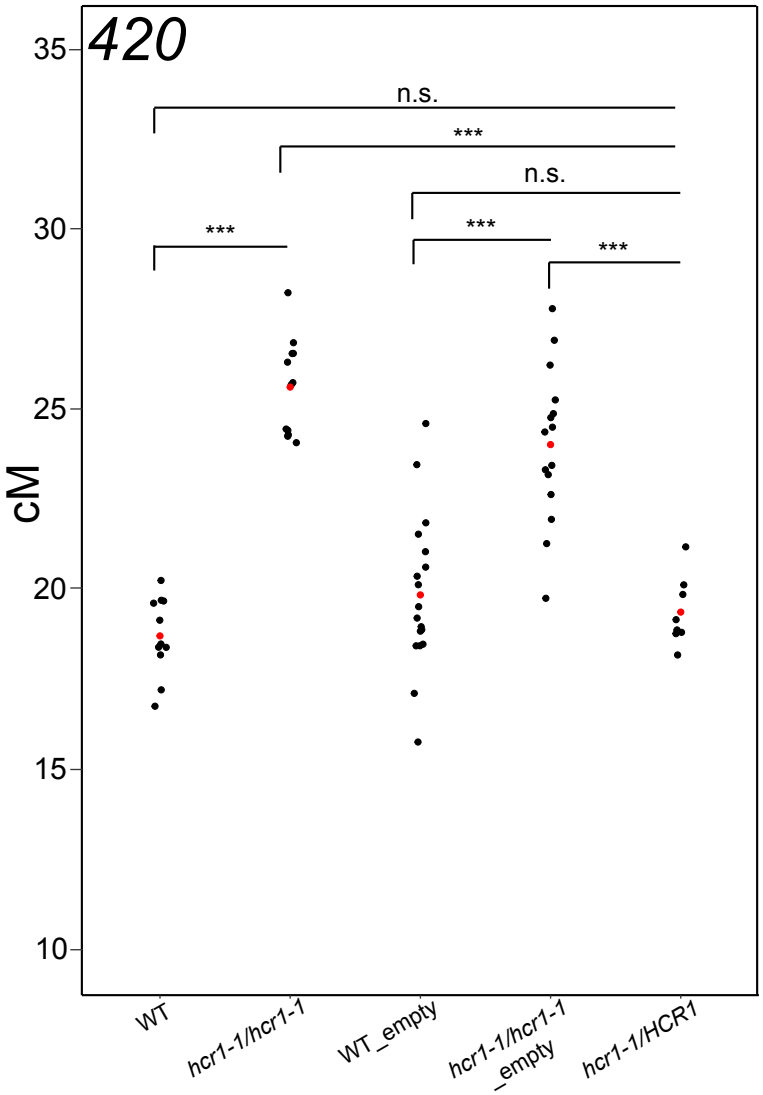

Figure 4.3. Genomic complementation of *hcr1* using a *HCR1*/*PPX-1* (At4g26720) transgene. *420* genetic distance (cM) measured for wild type Col and *hcr1-1* transformed with empty vectors and compared with *hcr1-1* transformed with *HCR1*. The data from untransformed wild type Col and *hcr1-1* plotted were not grown at the same time as the transformants. Mean values are indicated by red dots. Significance tests using a GLM between, (i) wild type empty transformants and *hcr1-1* empty transformants, (ii) wild type empty transformants and *hcr1-1* transformed with *HCR1* and (iii) *hcr1-1* empty transformants and *hcr1-1* transformed with *HCR1*, (iv) Untransformed wild type and *hcr1-1,* (v) Untransformed wild type and *hcr1-1* transformed with *HCR1*, and (vi) Untransformed *hcr1-1* and *hcr1-1* transformed with *HCR1* are indicated (*** = $P < 0.001$; n.s.= non-significant, where $P > 0.05$).

Interestingly, *hcr1-1/hcr1-2* F_1 individuals (24.17 ± 1.71 cM) were significantly different from *hcr1-2* homozygotes (22.98 ± 1.5 cM; GLM, $P = 0.008$; Figure 4.4; Table S25). Also, *hcr1-2* (22.98 ± 1.5 cM) showed significant differences in crossover frequency from *hcr1-1* (25.01 ± 2.15 cM; GLM, $P = 3.44 \times 10^{-5}$; Figure 4.4;

Table S25). Due to the insertion position of the *hcr1-2* T-DNA before the start codon, it is possible that this allele does not represent a complete null, although this allele showed a significant increase in *420* crossover frequency compared to wild type (19.87 ± 1.45 cM; GLM, $P < 2.0 \times 10^{-16}$; Figure 4.4; Table S25). Together these analyses provide further genetic evidence that *HCR1* is *PPX-1*.

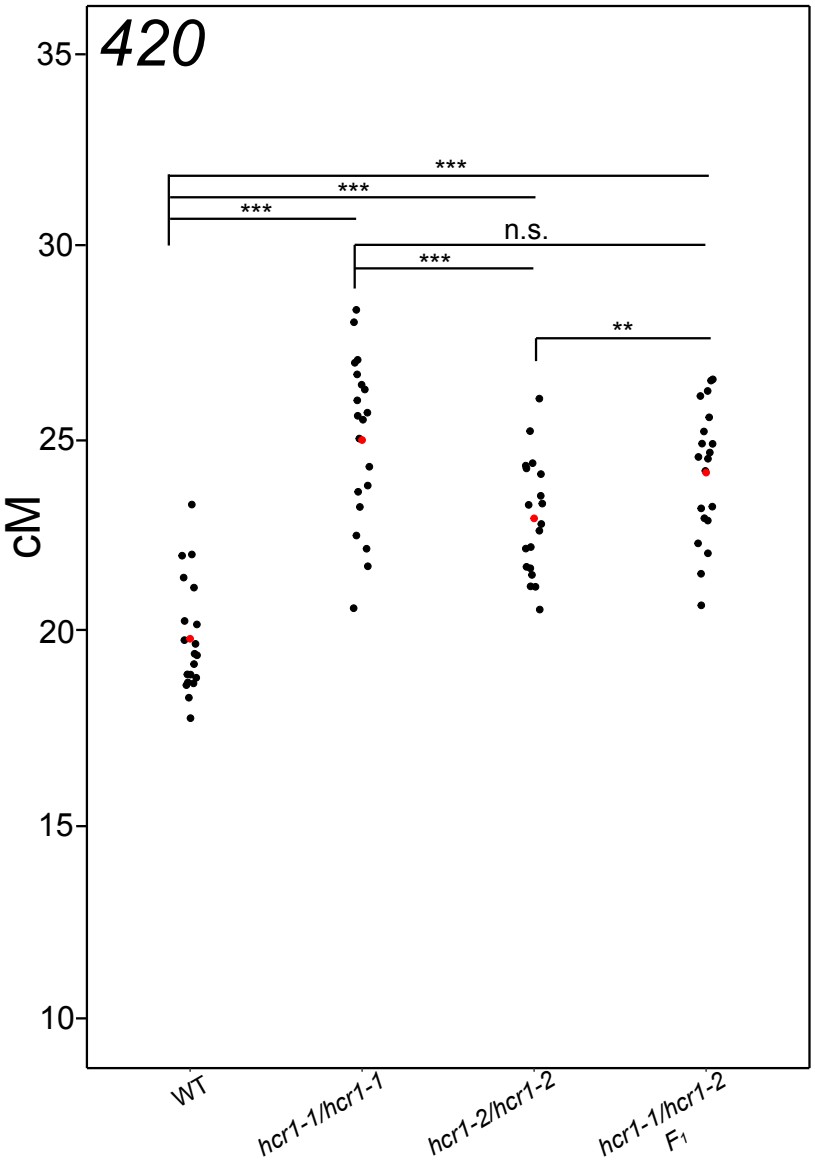

Figure 4.4. Allelism testing between *hcr1-1* and *hcr1-2* mutations. *420* genetic distance (cM) measured in F_1 progeny of a cross between *hcr1-1* and *hcr1-2* alleles and controls, including, wild type Col, *hcr1-1/hcr1-1* and *hcr1-2/hcr1-2* lines. Mean values are indicated by red dots. Significance tests by GLM between, (i) control lines, (ii) each control and *hcr1-1/hcr1-2* F_1 lines are indicated (*** = P<0.001; ** = $P < 0.01$; n.s.= non-significant, where $P > 0.05$).

4.3.2. Genetic analysis of the Arabidopsis PP4/PPX complex

The PPX-1 (At4g26720) phosphatase catalytic subunit is highly similar (93% amino acid identity) to PPX-2 (At5g55260), which encodes an alternative catalytic subunit of PP4 (Pérez-Callejón et al. 1993; Moorhead et al. 2009). The Arabidopsis catalytic isoform PPX-1 is known to interact with the regulatory subunit PP4R3 (At3g06670) (Su et al. 2017). However, we do not know whether PPX-1 binds to PP4R2 (At5g17070), or to PPX-2, or to PP4R3, as different complexes that may also function in meiotic recombination. Therefore, it is important to assess whether these subunits exhibit a crossover phenotype similar to *hcr1/ppx1* or not. Therefore, I obtained T-DNA insertion lines within the genes encoding subunits of the PP4 complex (see, "Appendix 4"), which were crossed to *420* in order to assess their crossover phenotypes. *PPX-2* and *PP4R2* are composed of 8 exons and 7 introns, as seen for *HCR1*/*PPX-1* (Figure 4.5), whereas *PP4R3* consists of 25 exons and 24 introns (not shown). Since, *PP4R3* was found to be located within the *420* interval, it was necessary to cross these mutants to another FTL interval. However, homozygous T-DNA lines (*pp4r3/pp4r3*) could not be isolated from the segregating line (*pp4r3/*+) provided by NASC (not shown), hence was not utilized for this study.

T-DNA insertions into gene exons and introns may have more severe effects on gene function, compared to insertions within promoters or 5' prime or 3' prime UTRs (Wang 2008). The location of T-DNAs inserted into *ppx-2* (GK-488H09) and *pp4r2* (SALK_093051) (Figure 4.5) were confirmed in the 3' prime end of intron 3 and exon 7 regions, respectively using PCR amplification (Figure S2). In addition, RT-PCR was used to show an absence of mRNA transcripts in *ppx-2* and *pp4r2* T-DNA alleles compared to wild type, using primers that spanned the T-DNA insertions (Figure 4.5). However, *hcr1-2* produced wild type transcripts as expected for the primers close to *hcr1-1* mutation (Figure 4.1). *420* crossover frequency in *hcr1-2* (24.04 $\pm$ 1.09 cM) was significantly different to wild type (18.58 $\pm$ 1.82 cM; GLM, $P < 2.0\text{x}10^{-16}$) and *hcr1-2/*+ heterozygotes (20.24 $\pm$ 1.49 cM; GLM, $P < 2.0 \text{ x } 10^{-16}$), which were identified in an F_2 population (Figure 4.6; Table S26). Similarly, *pp4r2* (24.30 $\pm$ 3.52 cM) displayed a significant increase in *420* crossover frequency compared to wild type (20.46 $\pm$ 2.96 cM; GLM, $P = 1.33\text{x}10^{-10}$) and *pp4r2/*+ heterozygotes (20.55 $\pm$ 2.65 cM; GLM, $P < 2.0 \text{ x } 10^{-16}$; Figure 4.6; Table S28).

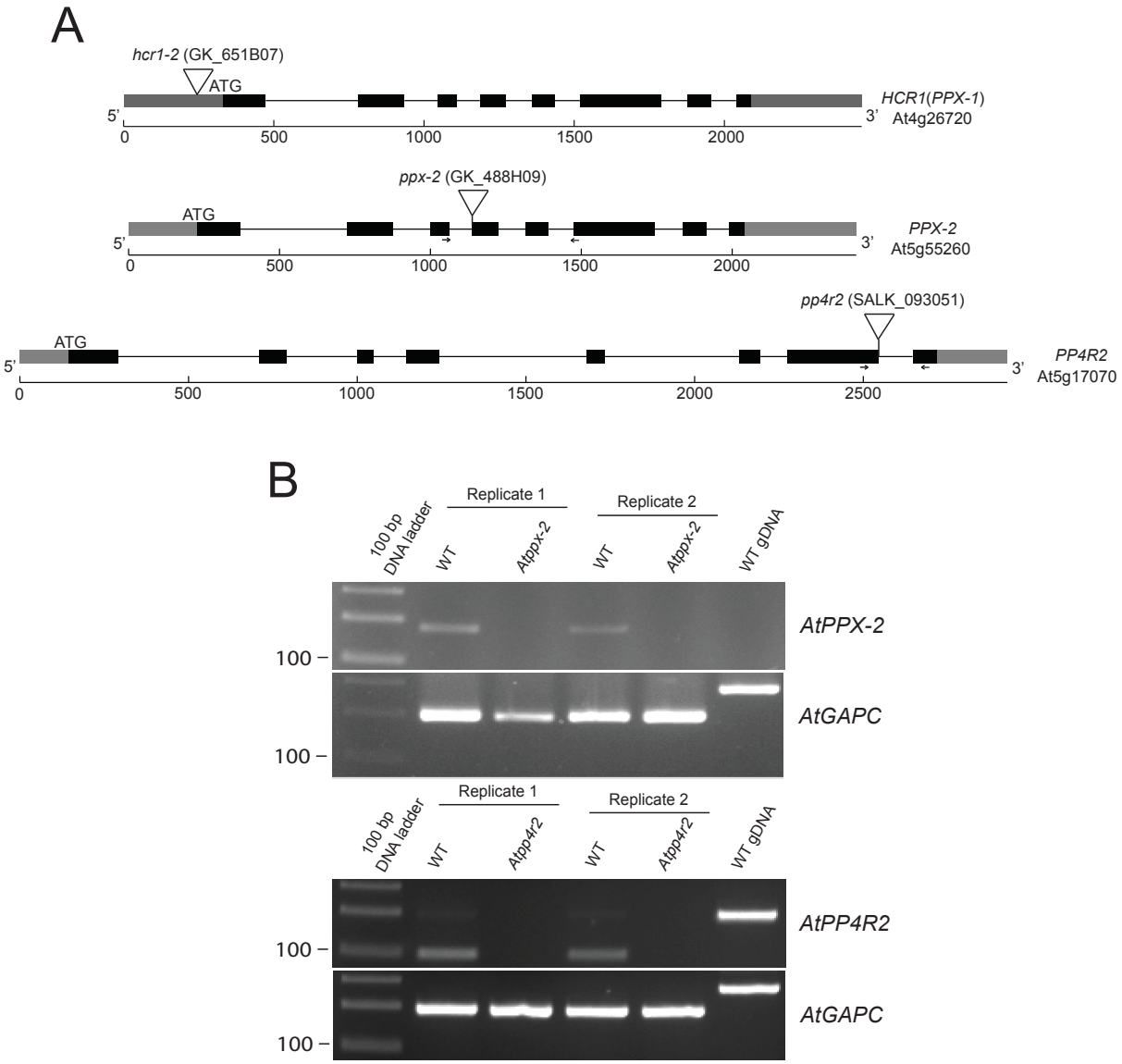

Figure 4.5. T-DNA insertions in the Arabidopsis PP4/PPX subunits. A) A map of At4g26720 (GenBank ID: NM_118806), At5g55260 (GenBank ID: NM_124908) and At5g17070 (GenBank ID: NM_121713) locus with intron-exon organization of *HCR1*/*PPX-1*, *PPX-2* and *PP4R3* drawn using Gene structure display server 2.0 tool. The exons are drawn as boxes (black=CDS, grey=UTR). Scale bars indicate bp. The *hcr1-2* T-DNA corresponds to GK_651B07 line and the insertion is in the 5' UTR as indicated by a triangle. Similarly, *ppx-2* and *pp4r2* correspond to GK_488H09 and SALK_093051 insertion lines, where the T-DNAs are inserted in intron 3 and exon 7, respectively. The arrows spanning *ppx-2* and *pp4r2* T-DNA insertions indicate the position of primers used for RT-PCR. **B)** Wild type Col, *ppx-2* and *pp4r2* floral cDNA with two biological replicates each were analysed by RT-PCR amplification for *PPX-2*, *PP4R2* (indicated in "**A**") and *GAPC* (housekeeping gene) control primers. RT-PCR amplicon sizes for wild type, *ppx-2*, *pp4r2* cDNAs and wild type genomic DNA (positive/negative control) are shown.

In contrast, *ppx-2* (19.40 ± 0.68 cM) mutants were not significantly different to wild type (19.89 ± 1.66 cM; GLM, *P*=0.366) and *ppx-2/+* heterozygotes (19.53 ± 1.44 cM; GLM, *P*=0.795) (Figure 4.6; Table S27). It was interesting to observe no significant difference between *ppx-1* and *pp4r2* phenotypes (Figure 4.6; GLM, *P*=0.869), which may imply a functional relationship between these proteins. However *ppx-1* and *pp4r2* were significantly different in crossover frequency compared to *ppx-2* (Figure 4.6; GLM, $P = 2.85 \times 10^{-15}$ and 7.69×10^{-15}, respectively). Hence, *ppx-2* does not show a crossover phenotype, in contrast to the *ppx-1* and *pp4r2* single mutants.

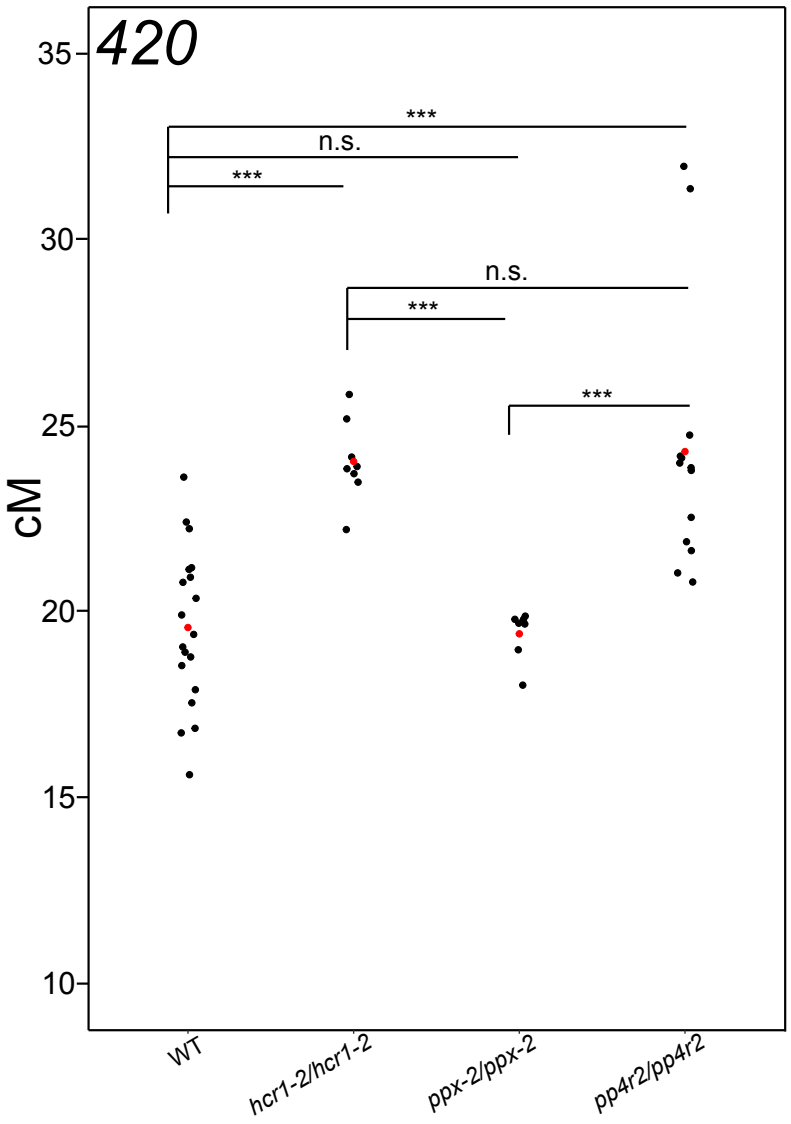

Figure 4.6. Subunits of the Arabidopsis PP4/PPX complex and regulation of crossover frequency. T-DNA lines *hcr1-2* (GK_651B07), *ppx-2* (GK_488H09) and *pp4r2* (SALK_093051) that are inserted within the *HCR1/PPX-1* (At4g26720), *PPX-2* (At5g55260) and *PP4R2* (At5g17070) genes respectively were crossed to the *420 RG/++* line and crossover frequency (cM) measured in segregating F_2 genotypes

(WT, *ppx/+* and *ppx/ppx*). Wild type Col genotypes from all three F_2 populations were combined for plotting. Mean values are indicated by red dots. Significance tests by GLM between (i) wild type and a) *hcr1-2*, b) *ppx-2* and c) *pp4r2*, (ii) between *hcr1-2* and a) *ppx-2* and b) *pp4r2*, and (iii) between *ppx-2* and *pp4r2* are indicated (*** = $P < 0.001$; n.s.= non-significant, where $P > 0.05$).

To assess meiotic expression of the *PP4* genes, I queried RNA-seq recently generated from Arabidopsis male meiocytes (Walker et al. 2018). *PPX-1*, *PP4R2* and *PP4R3* genes showed significantly upregulated expression in the wild type (Col-0) male meiocytes compared to somatic leaf tissues (Figure 4.7), as analysed by DESeq2 (Love et al. 2014). However, *PPX-2* showed no expression and hence was not plotted. The DESeq2 analysis was performed by Dr. Andy Tock. To test for significant differences, a Wald test was applied with an adjusted $P < 0.01$ for each *PP4/PPX* gene using Benjamini-Hochberg approach to multiple testing corrections (Benjamini and Hochberg 1995; Love et al. 2014). Meiocyte expression correlated with the crossover phenotypes characterized for *PPX-1*, *PPX-2*, *PP4R2* genes (Figure 4.6, 4.7). I speculate that based on expression analysis, that *PP4R3* is also involved in meiosis-related functions, although due to a lack of T-DNA insertion alleles I was not able to test this (Figure 4.7).

To verify whether the increase in crossover frequency caused by *hcr1-1* was related to changes in fertility, I performed Alexander staining of pollen (see, “General Methods 2.18”) and scored the percentage of viable and inviable grains. Additionally, I scored *hcr1-2*, *ppx-2* and *pp4r2* genotypes (Figure 4.8; Table S29). The *hcr1-1*, *hcr1-2*, *ppx-2* and *pp4r2* mutants showed no significant difference in pollen viability compared to wild type Col-0 using pairwise t-tests with corrections for multiple testing (Figure 4.8; Table S29). I also measured seed set by scoring the number of seeds per silique (total = 5 siliques) from 5 plants per genotype (total = 25 siliques) and calculated the average number of seed set per plant in wild type Col-0, *hcr1-1*, *hcr1-2*, *ppx-2* and *pp4r2* mutants (Figure 4.9; Table S30). The observed mean seed set in *hcr1-1*, *ppx-2* and *pp4r2* mutants showed no significant differences compared to wild type Col-0 using pairwise t-tests with corrections for multiple testing (Figure 4.9; Table S30). However, the average number of seeds in *hcr1-2* showed a significant increase compared to wild type Col-0 (pairwise t-tests with corrections for

multiple testing; P = 0.01) (Figure 4.9; Table S30). Together this analysis suggests that these genotypes have no defects in fertility.

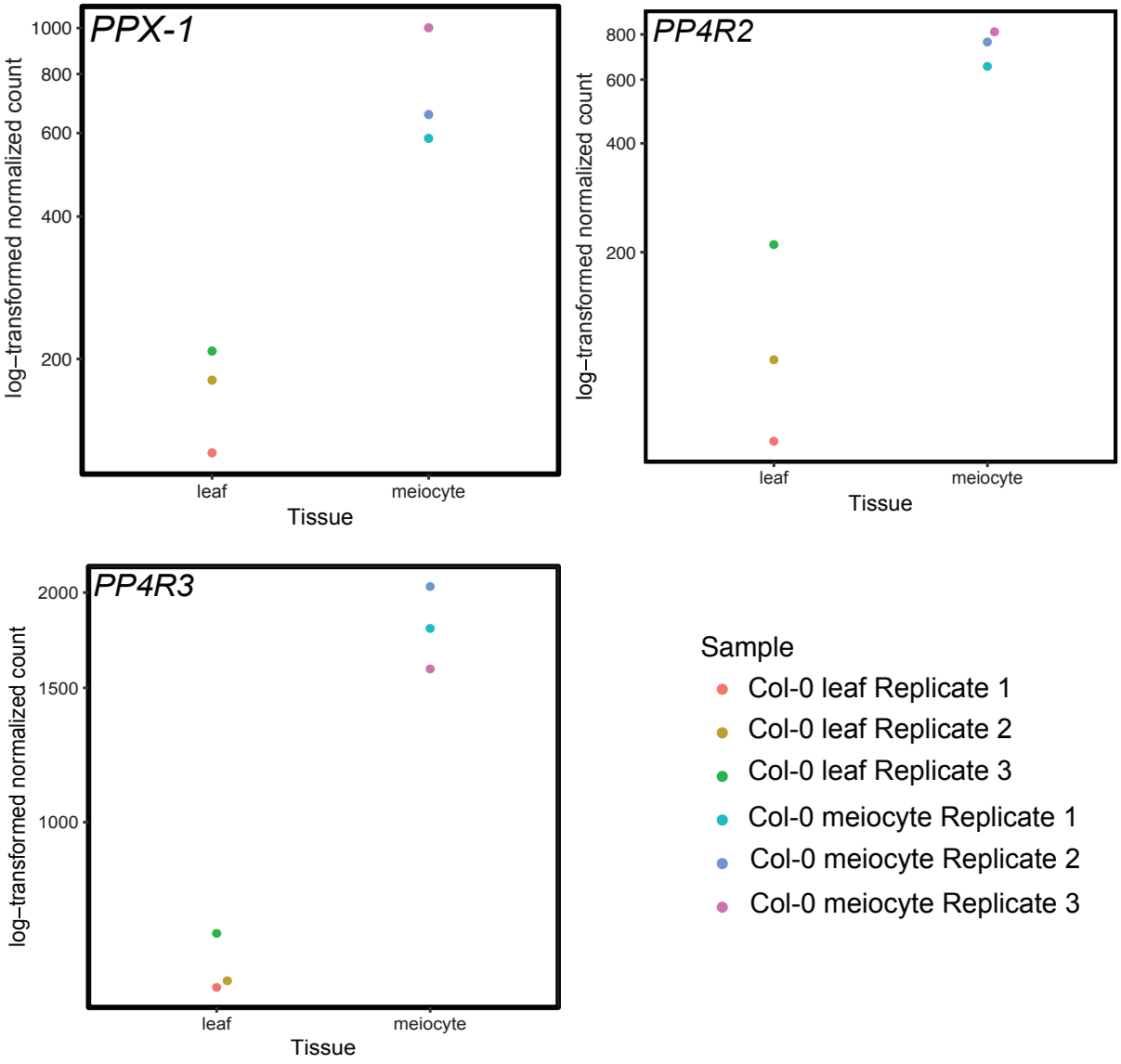

Figure 4.7. Meiotic RNA-seq analysis of Arabidopsis *PP4/PPX* genes differentially expressed in wild type Col-0 leaf and male meiocytes. Three biological replicates of Col-0 leaf and meiocyte RNA samples (colour-coded) were sequenced in published work (Walker et al. 2018). The plots were generated using DESeq2-derived normalized expression value for *PPX-1*, *PP4R2* and *PP4R3* genes in meiocytes and leaves (Love et al. 2014, 2016). Normalized and log-transformed read counts were plotted against the tissue types for all three genes (Love et al. 2016).

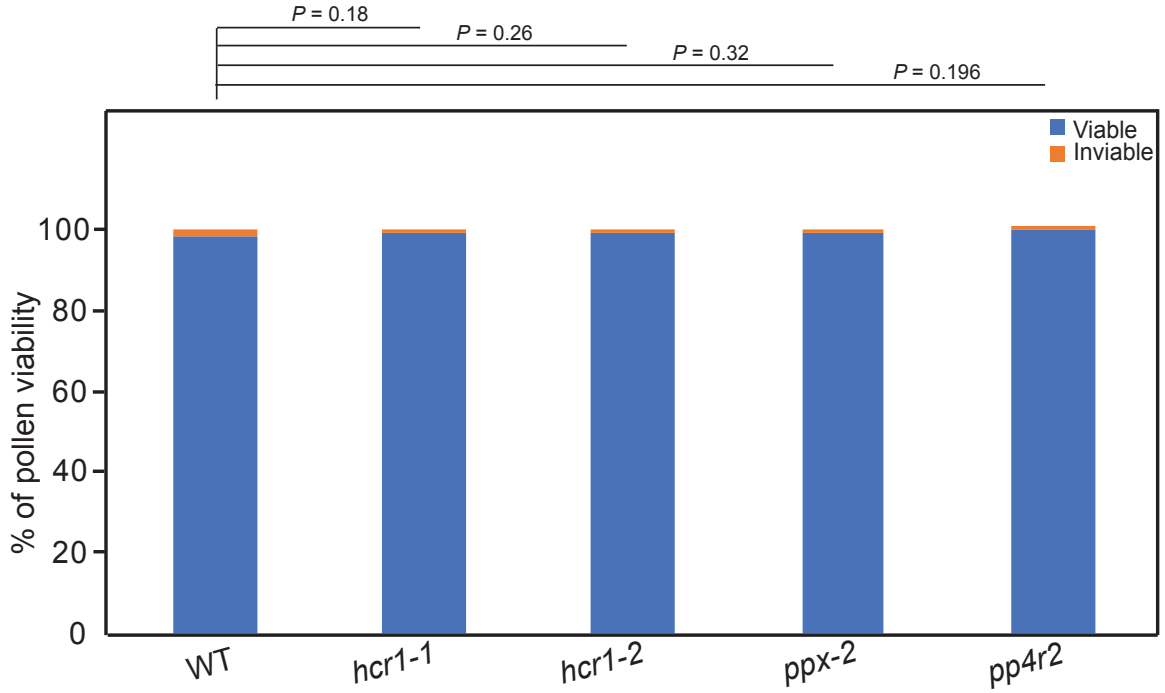

Figure 4.8. Pollen viability in wild type Col-0, *hcr1-1*, *hcr1-2*, *ppx-2* and *pp4r2*. A bar plot showing the proportion of viable (blue) and inviable (orange) pollen grains using Alexander staining. I assessed pollen viability from 6 plants per genotype using Alexander staining of ~1,000 pollen grains from mature open flowers. Viable grains turn purple to staining, whereas inviable pollen stain green. Pairwise t-tests with corrections for multiple testing were performed between wild type and genotypes are indicated by *P*-values ($P > 0.05$=non-significant).

4.3.3. Meiotic chromosome behaviour in *hcr1* mutants

I next used chromosome spreads and DAPI staining of DNA to investigate defects in male meiosis in the *hcr1-1* mutant and the major meiotic stages are shown (Figure 4.10). I prepared the chromosome spreads for all the cytological experiments and Christophe Lambing analysed the slides. From this section onwards, I refer to the *hcr1-1* EMS allele *as hcr1*. The wild type meiosis stages are previously described (Ross, Fransz, and Jones 1996). At leptotene, the chromosome threads appear as thin threads and unpaired (Figure 4.10a). During pachytene, the chromosomes complete synapsis (Figure 4.10b) that begins at zygotene. The thick stained bivalent chromosomes at pachytene also display condensed heterochromatic regions (Figure 4.10b). During late prophase I the diplotene and diakinesis stages occur, where chromosomes desynapse and condensation of five bivalents are seen aligned on the metaphase I plate (Figure 4.10c). At anaphase I, homologous chromosomes separate and migrate to poles (Figure 4.10d). Following telophase I is the dyad stage where two groups of partially decondensed chromosomes are evident

(Figure 4.10e). At the end of second meiotic division tetrads of four haploid microspores are seen (Figure 4.10f). In *hcr1*, all the meiotic stages (Figure 4.10 g-l) appeared similar to wild type and appeared to progress normally through meiosis.

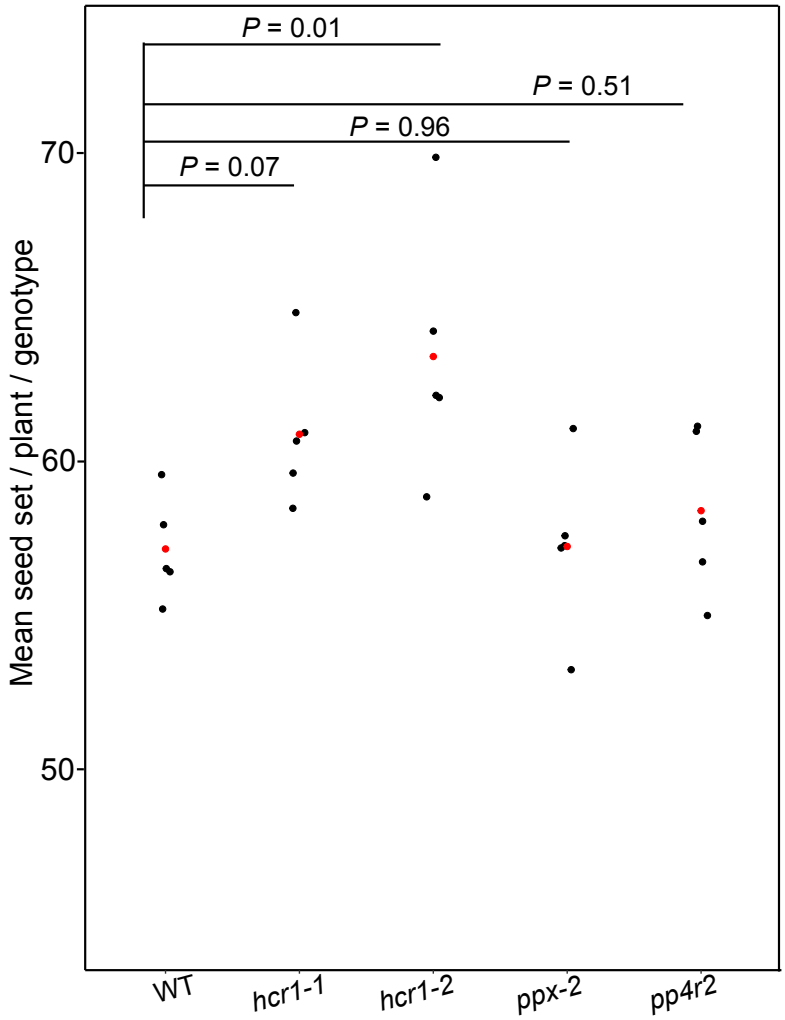

Figure 4.9. Seed set in wild type Col-0, *hcr1-1*, *hcr1-2*, *ppx-2* and *pp4r2*. A plot showing the mean seed set per plant (total = 5 siliques/plant) per genotype (total = 25 siliques from 5 plants). Pairwise t-tests with corrections for multiple testing were performed between wild type and genotypes are indicated by *P*-values (*P* > 0.05=non-significant).

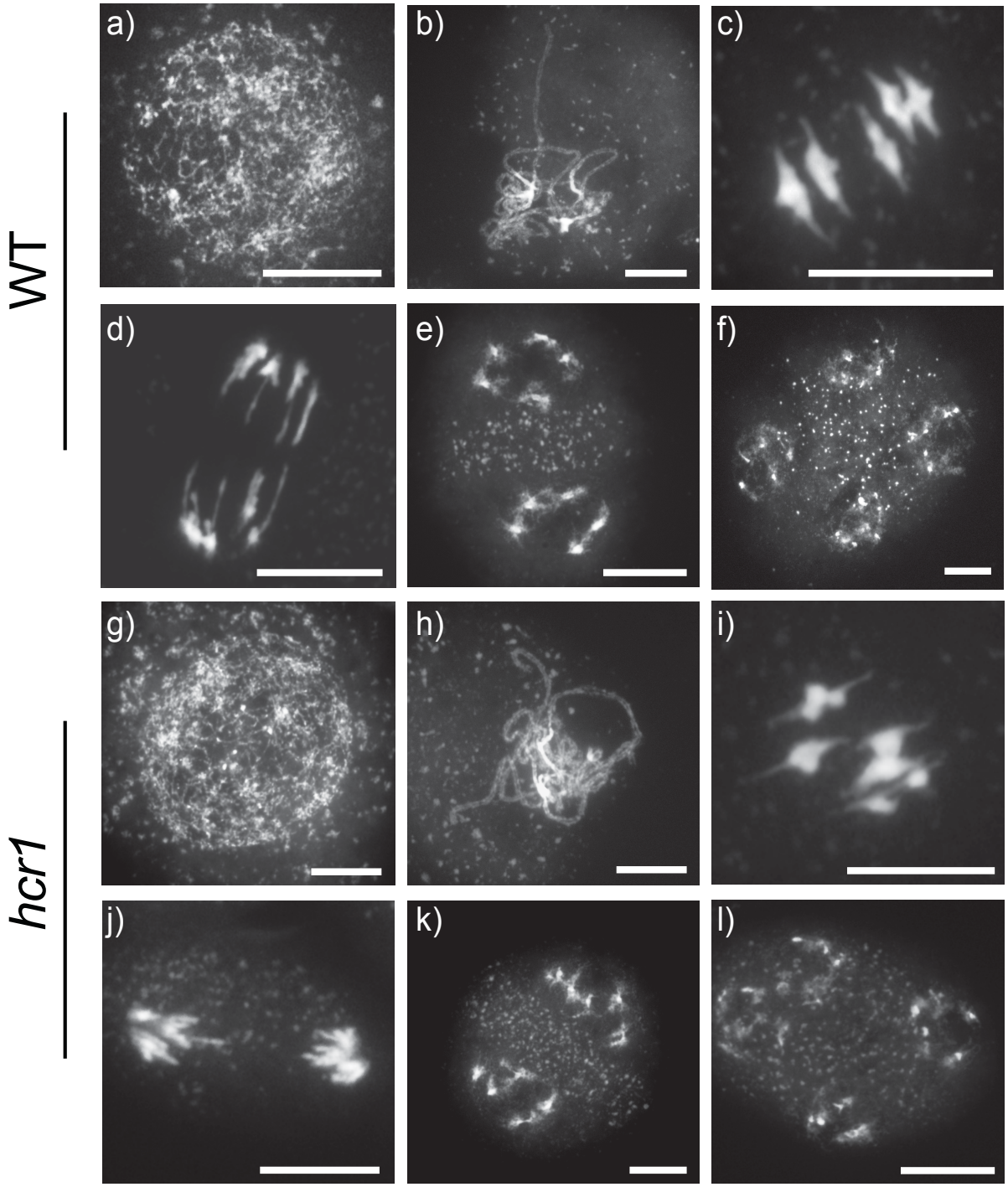

Figure 4.10. Meiotic atlas from Arabidopsis wildtype Col-0 and mutant *hcr1* pollen mother cells. DAPI-stained chromosome spreads from wild type **(a-f)** and *hcr1* **(g-l)** pollen mother cells (PMCs). The meiotic stages, including **(a,g)** Leptotene; **(b,h)** Pachytene; **(c,i)** Metaphase I; **(d,j)** Anaphase I; **(e,k)** dyad and **(f,l)** tetrad are shown. Scale Bars = 10 μm.

Following this, I examined synapsis in *hcr1* mutant by immunolocalization of ASY1 (a meiotic chromosome axis protein) (Armstrong et al. 2002) and ZYP1 (a SC central element protein) (Higgins et al. 2005) at pachytene stage (Figure 4.11). In both wild

type and mutant *hcr1*, the pachytene cells (n=50) showed nearly complete synapsis with most of the ASY1 axis (green) covered with ZYP1 signal (red; Figure 4.11), suggesting synapsis is unaffected in *hcr1*.

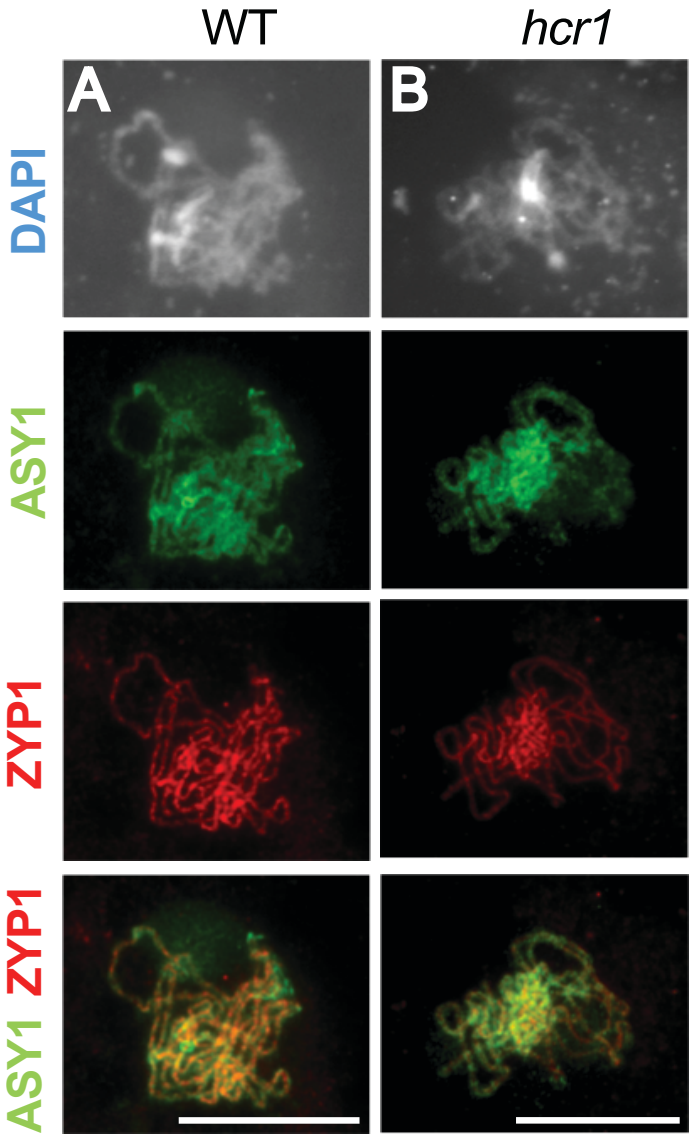

Figure 4.11. Immunolocalization of ASY1 and ZYP1 in wild type Col-0 and *hcr1* at pachytene stage. (A-B) Dual localization of ASY1 (green), ZYP1 (red) and merged images (red-green). DAPI-stained DNA from wild type and *hcr1* are also shown. Scale bars = 10 μm.

4.3.4. The *hcr1* mutation mainly affects Class I interfering crossovers

MLH1 is a putative double Holliday junction (dHJ) resolvase that acts in the Class I interfering crossover (CO) pathway (Lhuissier et al. 2007; Chelysheva et al. 2010; Mercier et al. 2015). Immunostaining of MLH1 meiotic recombination detects foci that corresponds to Class I CO sites in Arabidopsis (Lhuissier et al. 2007; Chelysheva et

al. 2010). MLH1 co-localizes with chiasmata at diakinesis where a maximum number of foci per cell is reached (Lhuissier et al. 2007; Chelysheva et al. 2010). Previously the mean number of MLH1 foci per meiotic cell at diakinesis was reported to be 9.95 ± 1.4 in wild type Col-0 (Chelysheva et al. 2010). MLH1 immunostaining showed the total number of MLH1 foci per cell at diakinesis in *hcr1* (12.1 ± 1.6; n=50) was significantly different to wild type (10.4 ± 1.3; n=51) (Mann-Whitney Wilcoxon test, P= 5.26 x 10^{-7}) (Figure 4.12; Table S31). The MLH1 foci in *hcr1* were observed to be concentrated in the chromosome arm regions (Figure 4.12). However, the MLH1 foci on DAPI dense heterochromatin in wild type (1.7 ± 1.1) and *hcr1* (1.6 ± 0.9) was similar and not significantly different (Mann-Whitney Wilcoxon test, P=0.53) (Table S31). This suggests that *hcr1* increases Class I crossovers largely in the chromosome arms. In wild type, ~12% of the chromosome pairs had 1 MLH1 foci, ~65% of the bivalents had two foci, ~18% had three and < 3% had four and five foci respectively. In *hcr1*, nearly 30% had three foci and ~7% had four foci (Figure 4.12). This suggests *hcr1* crossovers may have altered spacing along the chromosomes and therefore measuring CO interference could test this.

To further investigate crossover frequency in *hcr1* I used six genetic FTL intervals where fluorescent proteins are expressed in the seed (*5.14*, *1.17*, *3.15*, *5.11*) (Wu et al. 2015) or the pollen (*I3bc*) (Francis et al. 2007; Berchowitz and Copenhaver 2008). These FTL intervals are located on the sub-telomeric (CTL *5.14*, *1.17*, *3.15* and FTL *I3bc*) and centromeric (CTL *5.11*) regions of the chromosomes (Figure 4.13). This allowed me to investigate whether *hcr1* crossover increased particularly in the arms or the centromeric regions. I compared crossover frequency between wild type and *hcr1* homozygotes in FTL/CTL F_2 populations or its siblings. The *hcr1* mutant showed a 9.4 cM significant increase in crossover frequency in FTL interval *1.17* (*hcr1* - 32.23 ± 3.09 cM; WT - 22.83 ± 1.73 cM; GLM, P < 2.0 x 10^{-16}) and a 5.83 cM increase in FTL interval *3.15* (*hcr1* - 29.29 ± 1.6 cM; WT - 23.46 ± 2.15 cM; GLM, P < 2.0 x 10^{-16}) (Figure 4.13; Table S32). The *I3bc* interval overlaps the seed reporter line *420* on chromosome 3 (Figure 4.13). *hcr1* showed a 3.57 cM increase in the pollen FTL *I3b* (15.52 ± 0.5 cM; GLM, P = 6.63 x 10^{-4}) and 1.33 cM in *I3c* (5.19 ± 0.39 cM; P = 2.71 x 10^{-3}) compared to wild type (*I3b*, 11.95 ± 0.71 cM; *I3c*, 3.86 ± 0.13 cM) crossover phenotype (Figure 4.13; Table S36). Also, *hcr1* displayed a

1.9 cM increase (11.64 ± 1.66 cM) in the FTL *5.14* that was significantly different to wild type crossover phenotype (9.73 ± 1.84 cM; GLM, P = 6.61 x 10^{-10}). However, crossover rates between wild type and *hcr1* in the centromeric interval *5.11* showed no significant difference (GLM, P = 0.51) (Figure 4.13; Table S32). From these data, I conclude that *hcr1* increases crossovers most strongly in the sub-telomeric and interstitial regions of the chromosome arms.

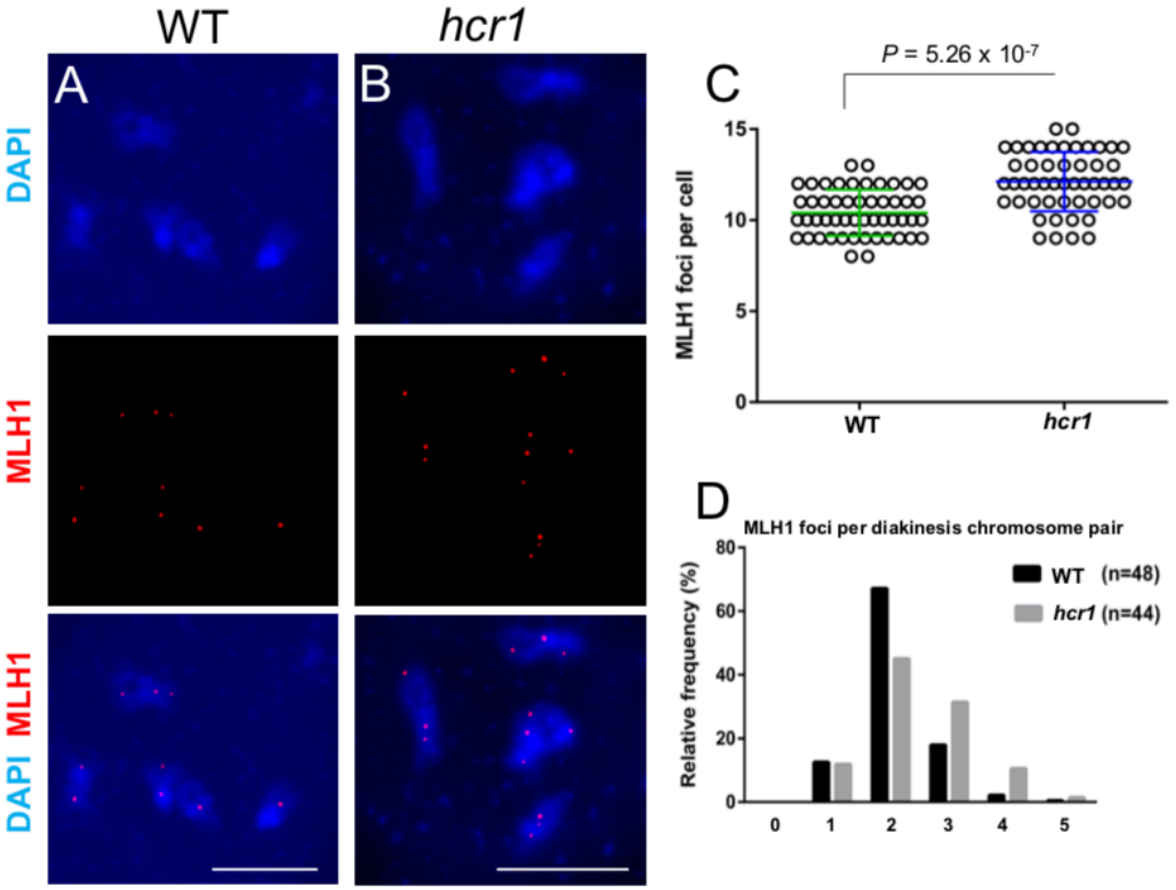

Figure 4.12. MLH1 immunolocalization in wild type Col-0 and *hcr1*. A-B) MLH1 immunostaining in pollen mother cells at diakinesis stage in wild type and *hcr1*. Images represent DAPI-stained (blue) meiotic cells immunostained for MLH1 is visualized as foci (red) at diakinesis. Scale bar = 10 μm. **C)** Scatter plot of MLH1 foci number per cell quantified at diakinesis in wild type and *hcr1*. A Mann-Whitney Wilcoxon test was performed to test the significance difference in foci number between wild type and *hcr1* indicated by a *P*-value (*P*<0.05=significant). **D)** A column plot showing the MLH1 foci number distribution among chromosome pairs at diakinesis.

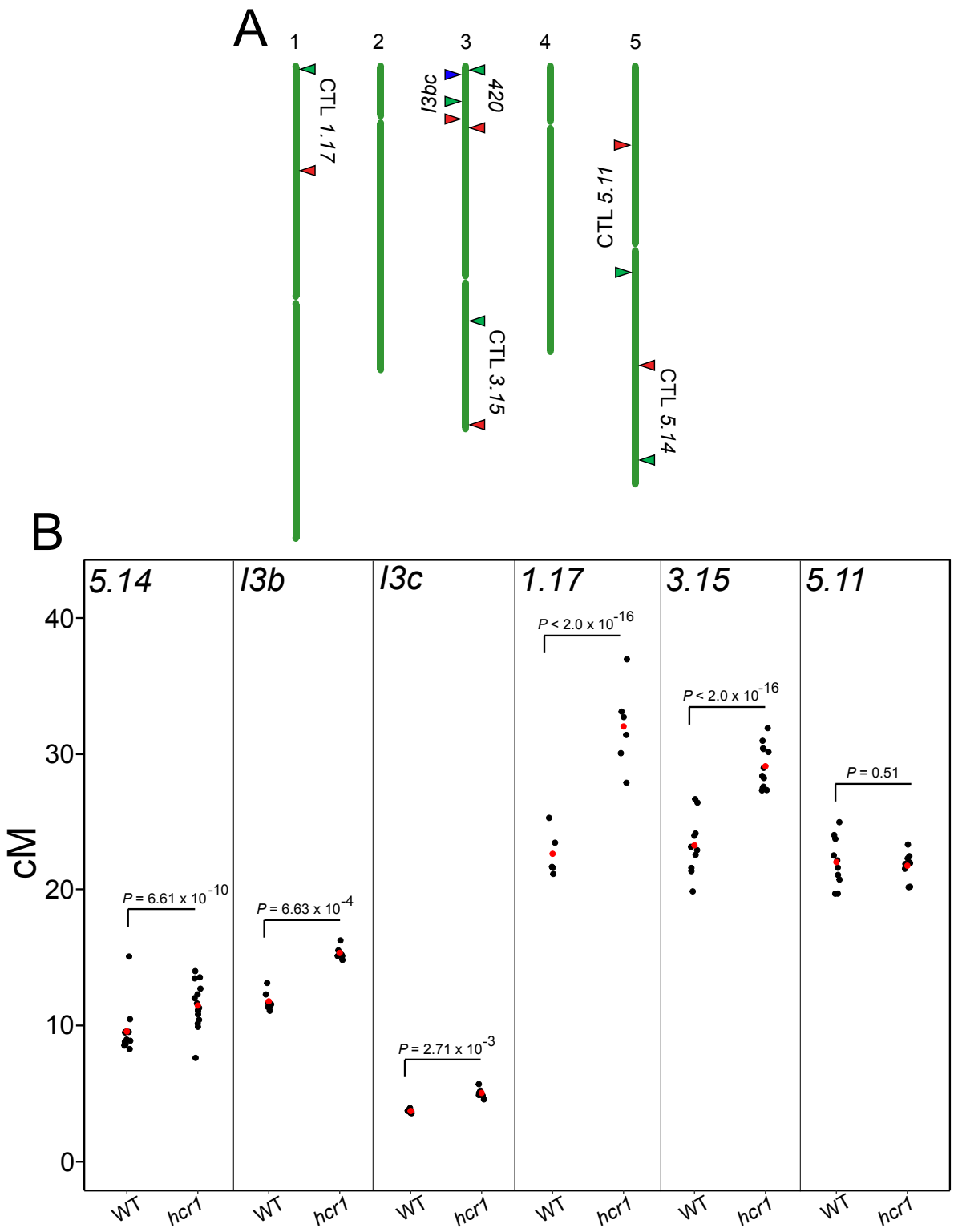

Figure 4.13. Measurement of crossover rates using multiple FTL/CTL intervals in wild type Col and mutant *hcr1*. (A-B) Genetic distances (cM) in six genetic intervals using fluorescence microscopy or flow cytometry analysis with fluorescent tagged lines (FTL) and Columbia traffic lines (CTL) (Figure 2.1 is repeated in **A**) were calculated. *I3b* and *I3c* are adjacent intervals located on chromosome 3. Mean values are indicated by red dots. A generalised linear model (GLM) was performed to test for significant differences in the count data between wild type and *hcr1* indicated by a *P*-value ($P > 0.05$ = non-significant).

To further investigate the nature of crossovers affected by *hcr1*, I performed a genetic interaction study using *zip4* (where Class I COs are defective) and *fancm* (where Class II COs are increased) mutants. I crossed *hcr1* with *fancm zip4* double produced double (*hcr1 fancm*, *hcr1 zip4*) and triple (*hcr1 fancm zip4*) mutants (Figure 4.14,4.15) that were confirmed by PCR genotyping (see, "General Methods 2.10") and measured *420* crossover frequency. The *hcr1 zip4* double plants were observed to have partial sterility, similar to *zip4* and produced few seeds (Figure 4.14). This indicates that mutation of *HCR1* does not suppress fertility in the absence of *ZIP4* in contrast to *fancm* (Crismani et al. 2012). The *hcr1 fancm* double mutant (40.32 ± 1.56 cM) showed a significant increase of ~5 cM compared to *fancm* (34.52 ± 1.92 cM; GLM P =1.6 x 10^{-9}) and *fancm zip4* double mutants (35 ± 1.77 cM; GLM P=2.31x10^{-10}) (Figure 4.15; Table S33). Note that *fancm* and *fancm zip4* double exhibit the same crossover phenotype at *420* interval as in published work (Ziolkowski et al. 2015). The *hcr1 fancm* double mutant (40.32 ± 1.56 cM) showed a 15.8 cM significant increase compared to *hcr1* (24.48 ± 0.87 cM; GLM, P < 2.0x10^{-16}) (Figure 4.15; Table S33). Hence, this additive increase indicates that *hcr1* affects Class I interfering crossovers. However, contrary to the above finding, the *hcr1 fancm zip4* (37.47 ± 1.79 cM) triple mutant exhibited a ~2 cM significant increase compared to *fancm zip4* double (35 ± 1.77 cM; GLM, P=1.28 x 10^{-4}) and *fancm* (34.52 ± 1.92 cM; GLM, P=1.79 x 10^{-4}) (Figure 4.15; Table S33). In addition to that, *hcr1 fancm* double (40.32 ± 1.56 cM) and *hcr1 fancm zip4* triple mutants (37.47 ± 1.79 cM) were significantly different in crossover frequency (Figure 4.15; Table S33). This also suggests a role of *hcr1* in promoting non-interfering crossovers. However, comparing the proportion of viable and inviable pollen grains showed no significant difference in *zip4* and *hcr1 zip4* double mutants (pairwise t-test with correction for multiple testing, P = 0.37) (Figure 4.14; Table S34).

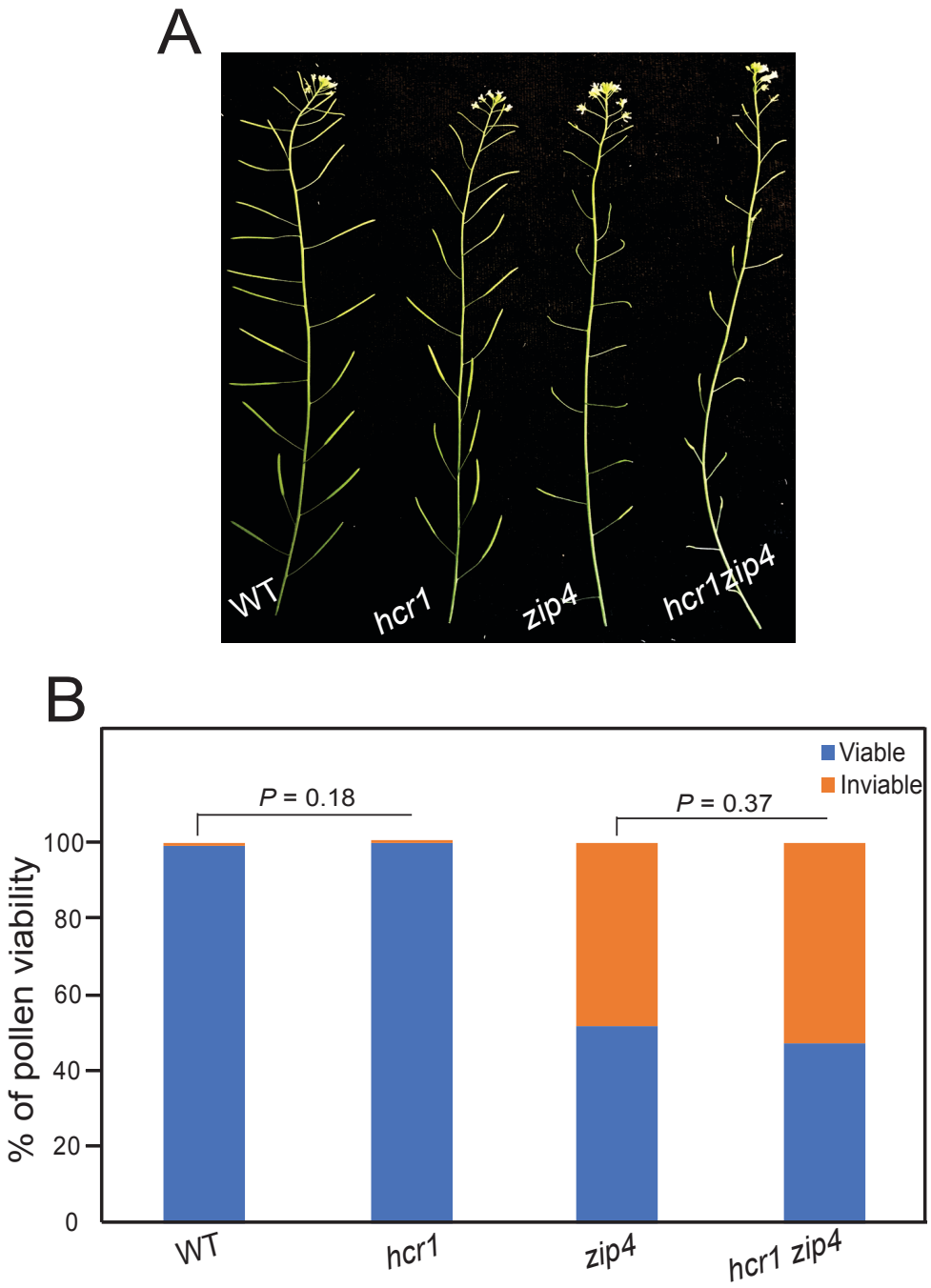

Figure 4.14. Pollen viability of *zip4* and *hcr1 zip4* double mutants. A) Images showing *zip4* and *hcr1 zip4* double mutants with short siliques compared to wild type Col-0 and *hcr1*. **B)** A bar plot showing the proportion of viable (blue) and inviable (orange) pollen grains using Alexander staining. I assessed pollen viability from 6 plants per genotype in wild type Col-0, *hcr1*, *zip4* and *hcr1 zip4* double mutants. Pairwise t-tests with corrections for multiple testing was performed between wild type and genotypes and are indicated by *P*-values ($P > 0.05$=non-significant).

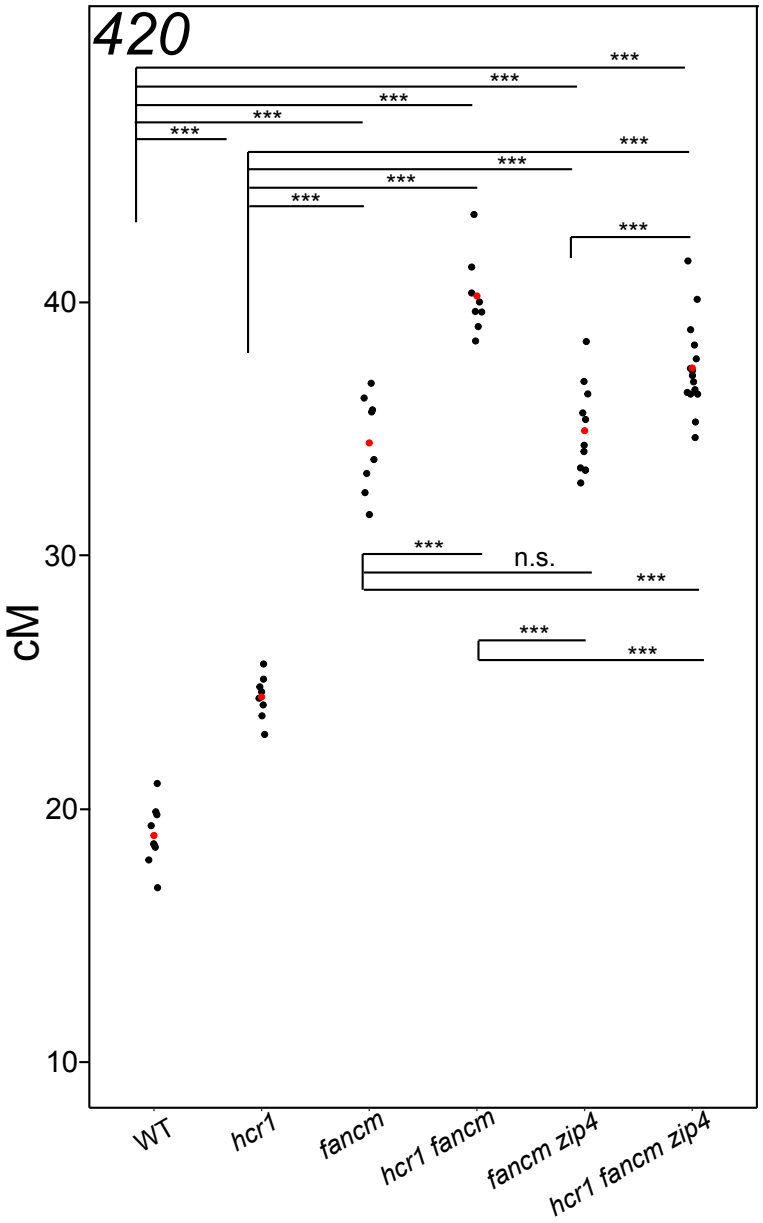

Figure 4.15. Genetic interactions between *hcr1*, *fancm zip4* mutations. *420* recombination (cM) measured in wild type Col, *hcr1*, *fancm*, *fancm zip4 double*, *hcr1 fancm* double and *hcr1 fancm zip4* triple mutants. Mean values are indicated by red dots. Significant tests between genotypes using GLM are indicated (*** = P<0.001; n.s.= non-significant, where P > 0.05).

Combining my MLH1 CO distribution data and the above FTL genetic analysis, I speculated whether *hcr1* may exhibit changes to CO interference due an influence on the balance of Class I and Class I COs. Therefore, I next used flow cytometry analysis to measure double crossovers (DCOs) and crossover interference using the three colour (Blue/B, Yellow/Y, Red/R) *I3bc* interval (Table S35, S36).

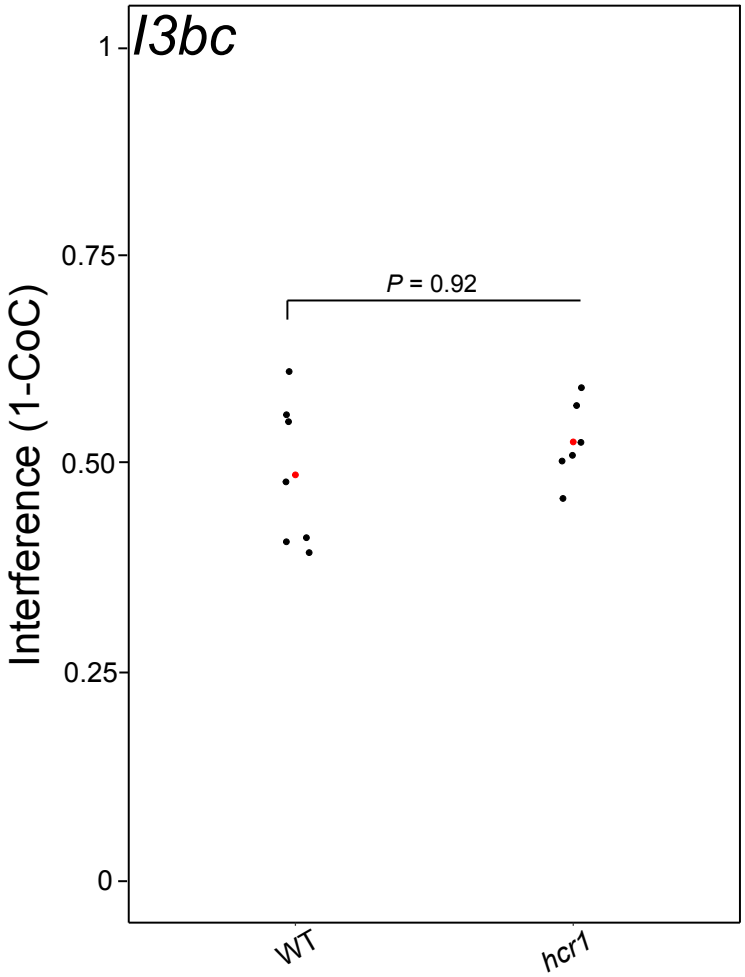

Figure 4.16. Crossover interference measurement between *I3b* and *I3c* intervals in wild type Col and mutant *hcr1*. Interference (1-CoC) was calculated using the [1- (Observed DCOs/Expected DCOs)]. Mean values are indicated by red dots and black dots represent replicates. To test for significant differences between wild type and *hcr1* interference, Pearson's χ^2 test with Yates' continuity correction was performed which is indicated by a *P*-value (*P*>0.05 = non-significant).

Eight fluorescent pollen classes such as N_{BYR}, N_{byr}, N_{bYr}, N_{ByR}, N_{bYR}, N_{BYr}, N_{byR} and N_{Byr} were obtained from biological replicates of wild type and *hcr1* (Table S35). For example, N_{BYR} indicates the number of pollen fluorescent for all three colours, whereas N_{Byr} is only blue fluorescent. The non-crossover (NCO) pollen classes are N_{BYR} and N_{byr} (non-fluorescent), whereas the single crossover (SCO) classes are N_{bYR}, N_{BYr}, N_{byR} and N_{Byr}. The observed double crossover (DCO) classes are N_{bYr} and N_{ByR} (Table S35). *I3b* [(N_{bYr} + N_{ByR} + N_{bYR} + N_{Byr}) / N_{Total}] and *I3c* [(N_{bYr} + N_{ByR} + N_{BYr} + N_{byR}) / N_{total}] genetic distances (cM) for wild type and *hcr1* were calculated as shown above (Figure 4.13; Table S36). To calculate CO interference, the observed DCOs (N_{bYr} + N_{ByR}) are compared to the expected number without interference,

which is (*I3b* cM/100) x (*I3c* cM/100) x N_{Total} (Table S36). The Coefficient of Coincidence (CoC) is calculated by dividing observed DCOs by expected DCOs, and the strength of interference is calculated as 1-CoC (Table S36) (Ziolkowski et al. 2015; Serra et al. 2018). Using this analysis *hcr1* showed no significant difference in crossover interference level compared to wild type (Pearson's χ^2 test with Yates' continuity correction, *P*=0.92) (Figure 4.16; Table S36). Hence, although chromosome arm regions show an increase in crossover frequency in *hcr1*, which is mainly due to increased Class I COs, there does not appear to be a significant change in interference, at least in *I3bc*.

4.3.5. Cytological markers of DSBs are unchanged in *hcr1*

As crossovers are formed from repair of DNA double-strand breaks, I measured meiotic DSB levels in *hcr1* by immunostaining of ASY1 and RAD51 (Figure 4.17). The ASY1 HORMA domain protein marks the chromosome axis (Armstrong et al. 2002) and RAD51 is a RecA homologue that marks the DSB foci (Vignard et al. 2007). Arabidopsis DSBs are estimated to number between ~100-200 per meiotic cell from cytological measurement of DSB-associated γH2A.X, RAD51 and DMC1 foci (Choi et al. 2013; Fernandes et al. 2018). At leptotene, the average number of RAD51 foci per cell in *hcr1* (145 ± 21.4; n=14) was not significantly different from wild type (151 ± 18.5; n=14) (Mann-Whitney Wilcoxon test, *P* = 0.32) (Figure 4.17; Table S37). This indicates that the crossover increase observed in *hcr1* did not result from extra DSBs or slower turnover during repair. Also this indicates that *hcr1* acts downstream of DSB formation in the meiotic recombination pathway.

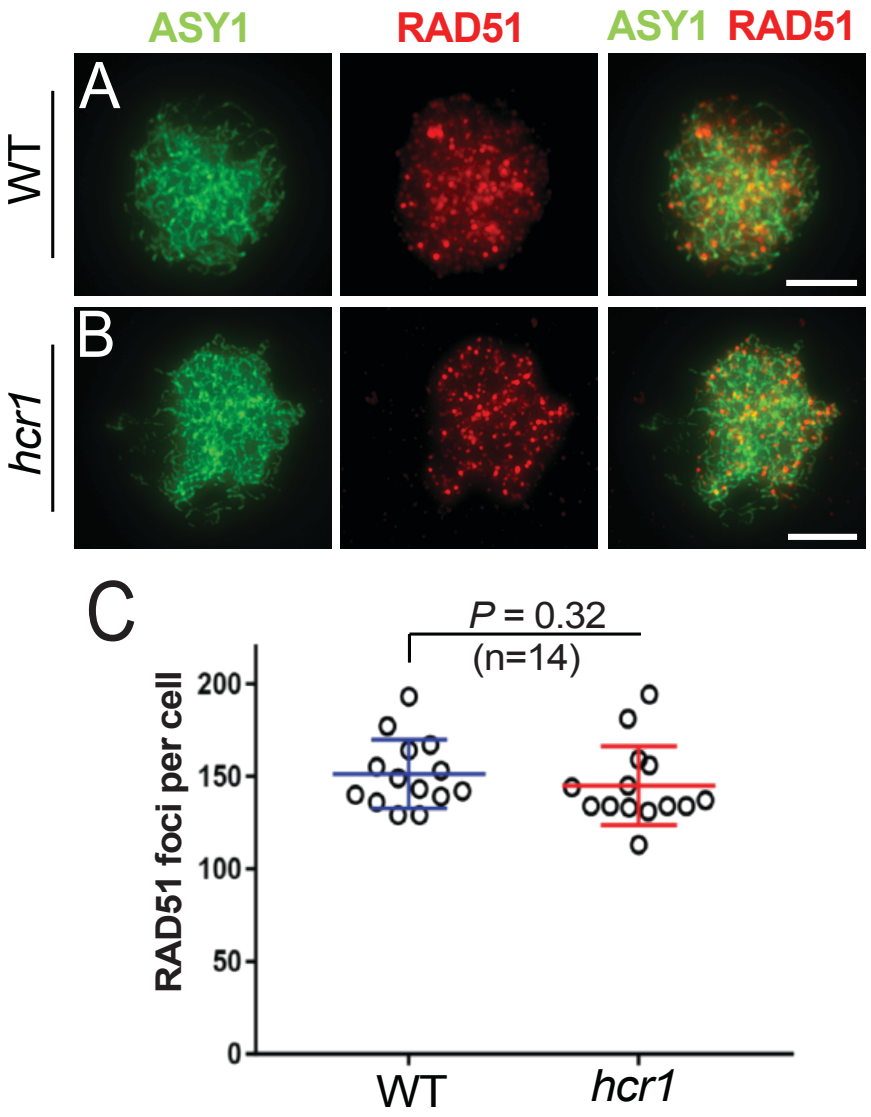

Figure 4.17. RAD51 immunolocalization in wild type Col-0 and *hcr1*. (A-B) Meiotic axis (ASY1, green) associated RAD51 immunostaining visualized as foci (red) in pollen mother cells at leptotene stage in wild type and *hcr1*. Scale bar = 10 μm. **C)** Scatter plot of RAD51 foci number per cell quantified at leptotene stage in wild type and *hcr1*. A Mann-Whitney Wilcoxon test was performed to test for significant differences in RAD51 foci number between wild type and *hcr1* indicated by a *P*-value (*P* > 0.05 = non-significant).

4.4. Discussion

In this chapter I have shown by genetic complementation and allelism testing that the candidate gene responsible for the *hcr1* mutation is *PROTEIN PHOSPHATASE X-1* (*PPX-1*, At4g26720) located on chromosome 4. PP4/PPX is known to play a central role in regulation of DSB initiation, pairing, synapsis and CO formation in model organisms including *C.elegans* and budding yeast (Sumiyoshi et al. 2002; Falk et al. 2010; Sato-Carlton et al. 2014). For example, absence of chiasmata formed between

homologous chromosomes during prophase I in *C.elegans* oocytes resulted from lack of *pph-4.1* activity, indicating the role of PPH-4.1 (PPX-1 homolog) during female meiosis (Sumiyoshi et al. 2002). Also, defects in DSB initiation and CO formation become worse with the increasing maternal age *C.elegans*, demonstrating an increased dependence on PPH-4.1 (Sato-Carlton et al. 2014). In budding yeast, Mec1(ATR-like) and PP4 coordinates meiotic prophase events in response to DSB initiation and checkpoint control of homology-independent centromeric pairing (Falk et al. 2010). Hence, the identification of PPX-1 from this recombination screen and its functional characterization provides an interesting parallel in plants. Genetic analysis of the *PP4/PPX* genes characterized their phenotypes and was connected to their meiocyte-enriched expression (Figures 4.6 & 4.7). Arabidopsis PP4 catalytic subunits (PPX1, PPX-2) partner with regulatory subunits (PP4R2, PP4R3) to perform specific functions (Su et al. 2017). I observed that mutations in *PPX-1* and *PP4R2* were phenotypically similar for *420* crossover frequency (Figure 4.6), and therefore would be predicted to function together as a complex during meiotic recombination. Also, *PPX-2* shows no crossover phenotype nor is it expressed in meiocytes, implying the gene has no meiotic function. It is unknown whether *PP4R3* has a meiotic phenotype and interacts with *PPX1* and *PP4R2* during recombination.

In *C.elegans*, COSA-1 (CO site marker) and RAD51 (DSB marker) foci was reduced in *pph-4.1* mutants, indicating that PPH-4.1 is required for maintaining wild type level of COs and DSBs (Sato-Carlton et al. 2014). By combining genetic and cytological analysis, *hcr1* mutant increases crossovers mainly in the chromosome arm regions which is interference-dependent (Figure 4.12 to 4.16). However, the DSB foci (RAD51) number in *hcr1* were observed unchanged compared to wild type (Figure 4.17). Hence, I propose a model where HCR1/PP4/PPX-1 represses COs mainly via the Class I interfering CO pathway by acting downstream of DSB formation. Yet, we cannot exclude the fact that as *hcr1 fancm zip4* triple mutants shows a further increase that *hcr1* may also have a minor effect on the Class II crossover pathway. However, the fertility of *zip4* and *hcr1 zip4* showed no significant changes. Moreover, detection and quantification of the difference is very difficult due to the level of sterility shown by the homozygous *zip4* and *hcr1 zip4* mutants.

Chapter 5 - Genetic and cytogenetic characterization of *hcr2*, *hcr3*, and *lcr1*

5.1. Introduction

In the last two chapters I identified putative candidate genes for *hcr1*, *hcr2*, *hcr3* and *lcr1* mutants by deep sequencing and functionally characterized the *hcr1* mutant. Further characterization of *hcr2* (*420* 35.72 cM) and *hcr3* (*420* 31.25 cM) mutants are currently in progress and I present preliminary work towards these ends in this chapter. Specifically, I performed MLH1 immunolocalization in the *hcr2* and *hcr3* mutants. Additionally, via allelism testing, I confirmed the *lcr1* mutation to be an allele of the *TAF4B* gene.

5.2. Results

5.2.1. Inheritance of the *hcr2* crossover phenotype is evident in a BC_2F_2 population

In Chapter 3, I presented isolation of the *hcr2* mutant (*420* 35.72 cM; Table 3.1), which displayed a strong *420* phenotype that was inherited in the M_3 generation (40.54 $\pm$ 3.08 cM; Figure 3.6; Table S10). The *hcr2* 'high' recombination phenotype was also evident in F_2 individuals derived from the first round of backcross (BC_1) that were bulked for deep sequencing (Figure 3.8; Table S17). However, we also noticed a colour segregation distortion ratio (<3:1 or ~2:1) in *hcr2* M_2 (Table 3.1) and subsequently in the M_3 (Table S10), BC_1F_1 (Table 3.4) and BC_1F_2 progenies (Table S15). To further investigate I selected a *hcr2* BC_1F_2 individual (42.81 cM) from the library pool (Table S17) and backcrossed for the second time (BC_2) to Col *420 RG/*++ to produce an F_1 generation (Table 5.1), and then selfed to produce an F_2 population (Table S38). Unlike *hcr2* BC_1F_1 (*hcr2 420 RG/*++ x Col-0) that displayed a semi-dominant phenotype (26.01 $\pm$ 0.52 cM; Table 3.4), the BC_2F_1 progenies (*hcr2* x *Col 420 RG/*++) showed a wild type phenotype (21.32 $\pm$ 1.10 cM) with ~3:1 colour segregation ratio (Table 5.1). In contrast to BC_1F_2, *hcr2* BC_2F_2 individuals showed a normal colour segregation (Table S38). This suggests the *hcr2* semi-dominant recombination phenotype may be due to EMS polymorphisms that has been minimized in the second round of backcross.

BC_2F_1 progeny	Green	Red	Both	None	Total	CO rate (cM)	G/non G	R/non R	G/R	Mean cM	SD
hcr2 x Col *420* - #1	121	148	877	203	1349	22.46	2.84	3.16	0.82	21.32	1.10
hcr2 x Col *420* - #2	164	138	1043	213	1558	21.75	3.44	3.13	1.19		
hcr2 x Col *420* - #3	145	122	1054	232	1553	19.00	3.39	3.12	1.19		
hcr2 x Col *420* - #4	160	186	1203	295	1844	20.96	2.83	3.05	0.86		
hcr2 x Col *420* - #5	159	175	1179	255	1768	21.12	3.11	3.27	0.91		
hcr2 x Col *420* - #6	167	173	1218	273	1831	20.71	3.11	3.16	0.97		
hcr2 x Col *420* - #7	167	168	1128	275	1738	21.61	2.92	2.93	0.99		
hcr2 x Col *420* - #8	175	167	1211	290	1843	20.70	3.03	2.96	1.05		
hcr2 x Col *420* - #9	176	178	1173	286	1813	21.93	2.91	2.92	0.99		
hcr2 x Col *420* - #10	166	195	1153	263	1777	22.95	2.88	3.14	0.85		

Table 5.1. *420* genetic distance (cM) measured in *hcr2* BC_2F_1 progenies. One F_1 progeny was selected and crossed to Col *420 RG/++* to generate a BC_2F_2 population. Mean CO rate (cM) and standard deviation (SD) were calculated.

From a population of 55 BC_2F_2 individuals, approximately a quarter of plants (14 in number) showed 'high' recombination in the range of ~29-39 cM and mean 34.21 ± 1.68 cM (Figure 5.1; Table S38), which I considered as displaying the *hcr2* phenotype (35.72 cM; Table 3.1). The remaining 3/4 of the population showed a range of 'low' recombination phenotypes (~15-23 cM) and a mean of 18.41 ± 1.92 cM (Figure 5.1; Table S38). However, BC_1F_2 individuals were classified into three groups (high, mid and low; Figure 5.1) according to that observed for *hcr2* (Figure 3.6; Table 3.1, S10) and wild type range of phenotypes (Table S7). From 55 BC_1F_2 individuals, 17 individuals showed a 'high' recombination in the range of ~38-47 cM (Figure 5.1; Table S15) and a mean 42.22 ± 2.32 cM. The remaining individuals displayed 'mid' or intermediate (~24-32 cM) recombination phenotypes or were in the 'low' range (~18-22 cM) showing a wild type level recombination (Figure 5.1; Table S15). The mean crossover rate (27.64 ± 2.72 cM) of the intermediate individuals were similar to the semi-dominant BC_1F_1 phenotype (26.01 ± 0.52 cM; Table 3.4). In addition to segregation distortion, the intermediate BC_1F_2 phenotype (~24-32 cM) may be influenced by background polymorphisms (Ziolkowski et al. 2015), that may have been reduced in the second round of backcross. Hence, after backcrossing *hcr2* shows a more consistent high recombination phenotype (Figure 5.1).

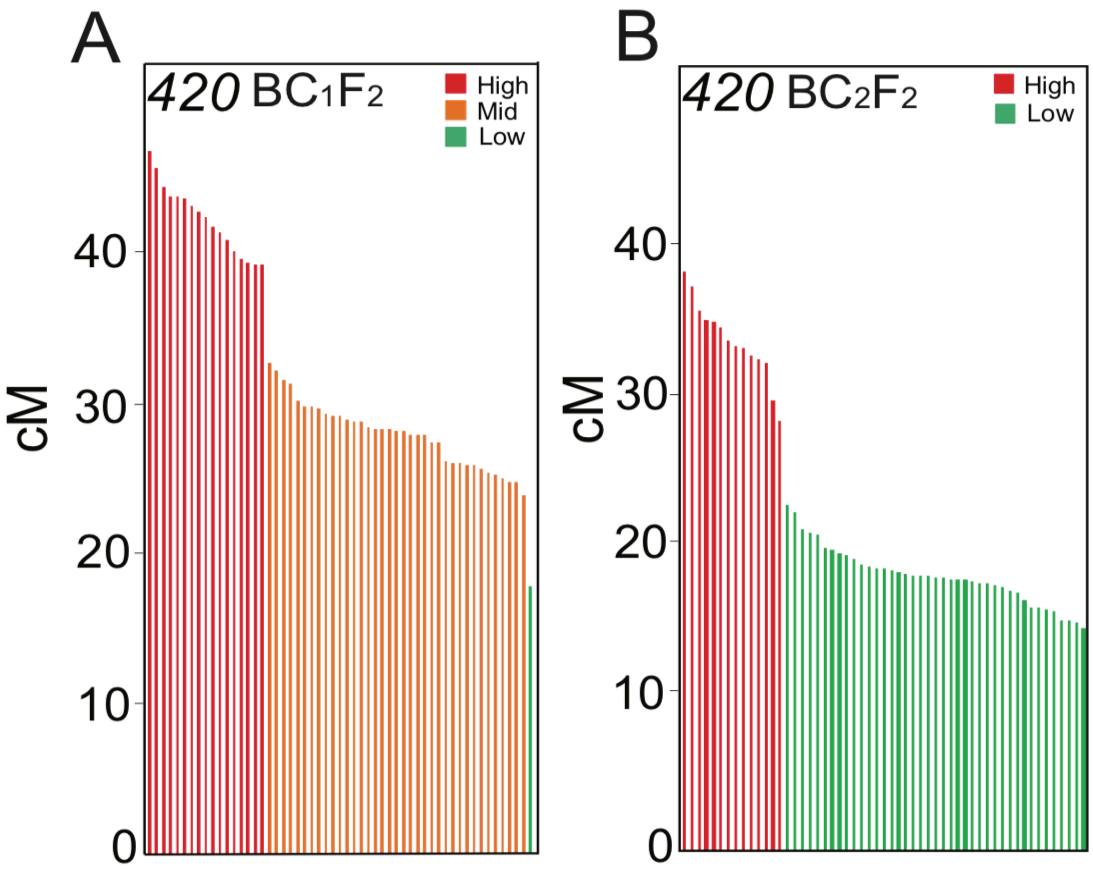

Figure 5.1. Comparison between *hcr2* BC_1 and BC_2 populations. *420* genetic distance (cM) from (**A-B**) *hcr2* BC_1F_2 and BC_2F_2 population is plotted. According to the recombination rate (cM), the individuals are colour-coded as high (red), mid (orange) and low (green). The plot **B** shows 'high' (~29-39 cM) and 'Low' (~15-23 cM) range of phenotypes with no intermediate phenotypes (~24-32 cM) as observed in **A** (Figure 3.8 is repeated in **A**).

5.2.2. *HCR2* and *HCR3* limit Class II and Class I COs respectively

To cytologically test whether *hcr2* and *hcr3* influence the Class I crossover pathway, Christophe Lambing and I performed MLH1 immunostaining, which is a Class I CO associated marker (Chelysheva et al. 2010). Quantification of MLH1 foci (counted by Christophe Lambing) in *hcr2* showed an average number of 11.9 ± 1.4 (n=22; Figure 5.2; Table S39) that was slightly but significantly higher compared to wild type (10.7 ± 1.7; n=24) (Mann–Whitney Wilcoxon test, *P*=0.018). This indicates that *HCR2* likely acts to suppress Class II crossovers (Figure 5.2; Table S39). In contrast to *hcr2*, MLH1 foci numbers increased significantly in *hcr3* (15.6 ± 2.3, n=28), compared to wild type (Mann–Whitney Wilcoxon test, $P=1.59 \times 10^{-8}$), suggesting *HCR3* acts to limit Class I interference-sensitive crossovers (Figure 5.3; Table S39).

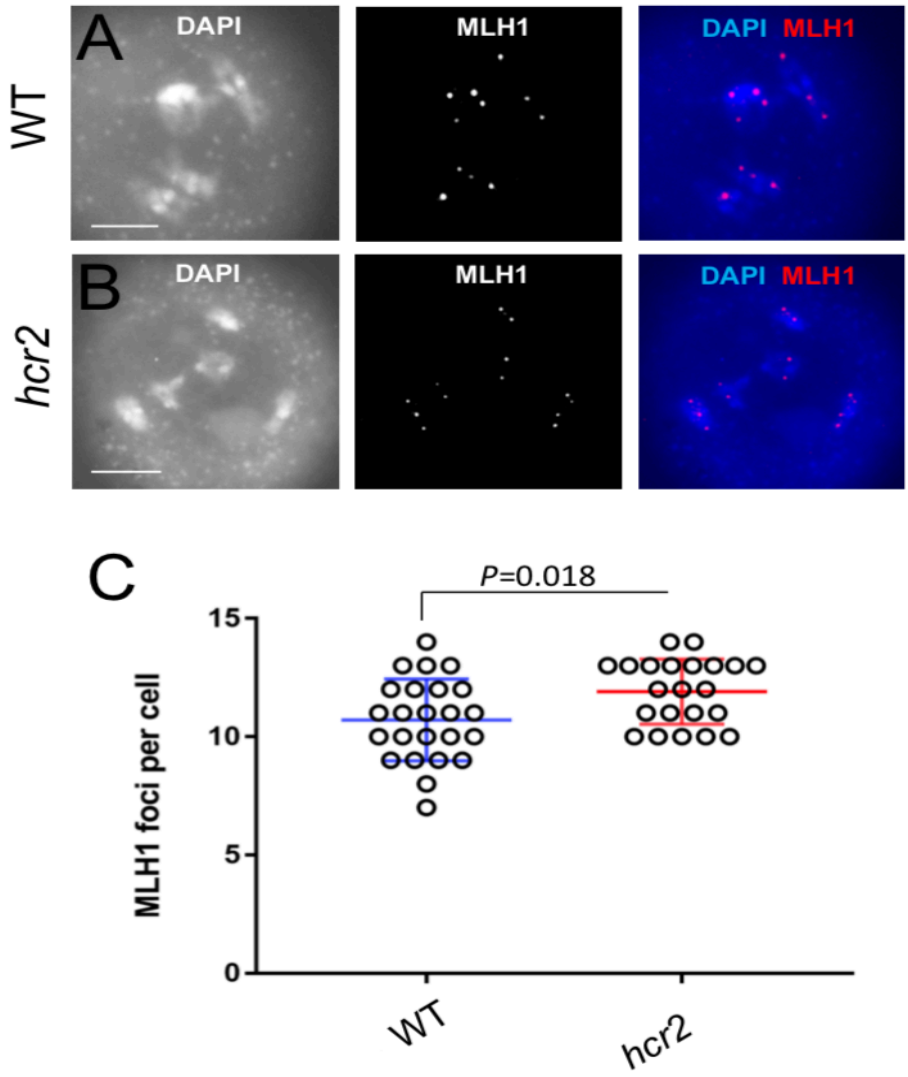

Figure 5.2. MLH1 immunolocalization in wild type Col-0 and *hcr2*. (A-B) MLH1 immunostaining in pollen mother cells at diakinesis stage in wild type and *hcr2*. Images represent DAPI-stained (blue, or white) meiotic cells immunostained for MLH1 is visualized as foci (red) at diakinesis. Scale bar = 10 μm. **C)** Scatter plot of MLH1 foci number per cell quantified at diakinesis in wild type and *hcr2*. A Mann-Whitney Wilcoxon test was performed to test the significance difference in foci number between wild type and *hcr2* indicated by a *P*-value ($P < 0.05$=significant).

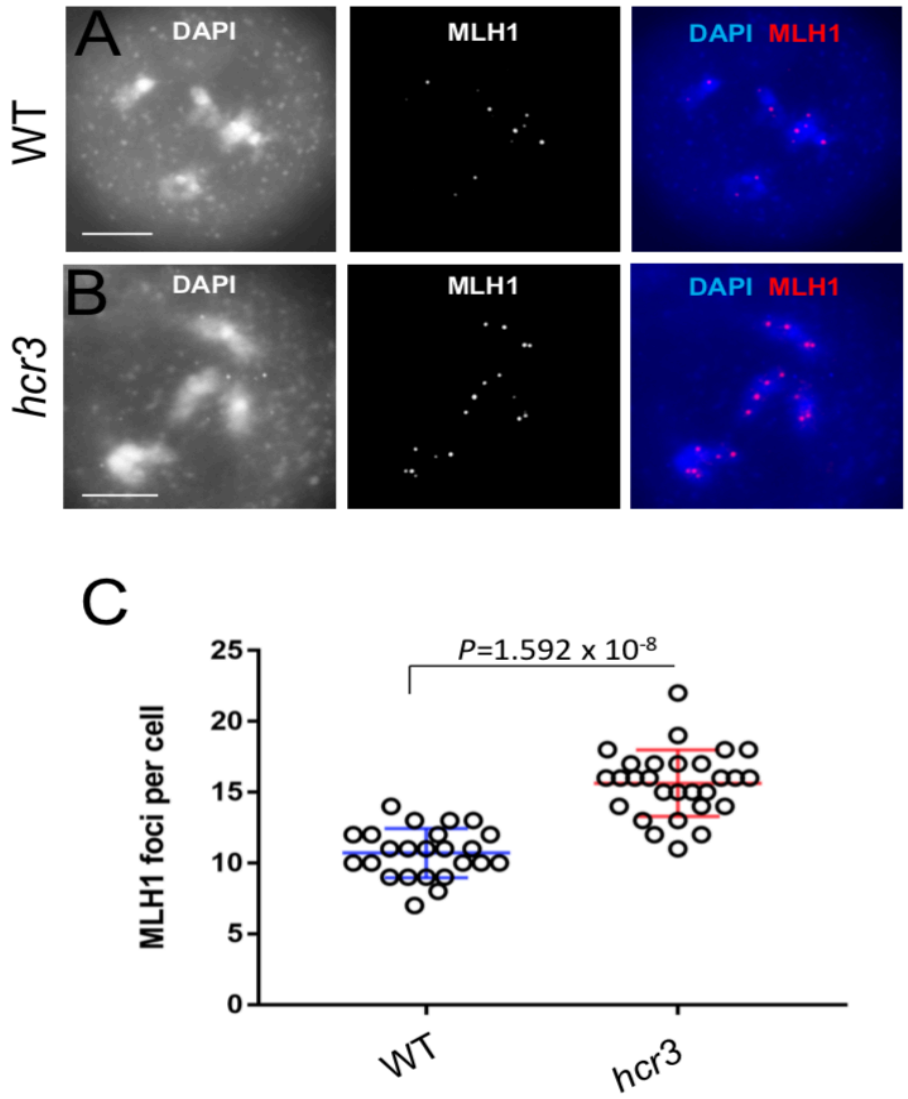

Figure 5.3. MLH1 immunolocalization in wild type Col-0 and *hcr3*. (A-B) MLH1 immunostaining in pollen mother cells at diakinesis stage in wild type and *hcr3*. Images represent DAPI-stained (blue, or white) meiotic cells immunostained for MLH1 is visualized as foci (red, or white) at diakinesis. Scale bars = 10 μm. **C)** Scatter plot of MLH1 foci number per cell quantified at diakinesis in wild type and *hcr3*. A Mann-Whitney Wilcoxon test was performed to test the significance difference in foci number between wild type and *hcr3* indicated by a *P*-value ($P < 0.05$ = significant).

5.2.3. The *lcr1* mutation is within *TBP-associated factor 4B* (*TAF4B)*

I identified a low crossover rate mutant (*lcr1*) from the genetic screen (14.37 cM; Figure 3.2; Table 3.1), which showed a heritable phenotype in the M_3 generation with an average of 16.08 ± 1.10 cM (Figure 3.6; Table S11). An M_3 individual with *420 RG/*++ was backcrossed to Col-0 and a BC_1F_2 population generated (n=~300; Figure 3.8; Table S14). Twenty seven individuals with phenotypes ranging from 13.71 to 14.47 cM were selected for DNA library preparation and subjected to deep sequencing (Table S18). SHOREmapping analysis of the *lcr1* data provided a list of EMS derived SNPs that was filtered for those with allele frequency >80% and identified two putative candidate genes on chromosome 1, including *TBP-associated factor 4B* (*TAF4B*; At1g27720) and *FANCONI/FANCD2 associated NUCLEASE I* (*FANI*; At1g48360) (Figure 3.12; Table S22; see, "Chapter 3"). The *TAF4B* gene is composed of 15 exons and 14 introns and the mutation identified (C>T in 5'-3' direction) introduces a premature stop codon (CAA>TAA) in exon 3 (549 bp of the genomic sequence), which is predicted to produce a truncated protein (Q55X) (Figure 5.4). The other candidate *FAN1* is composed of 15 exons and 14 introns where the mutation (C>T in 5'-3' direction) was identified in the exon 2 and 401 bp position of the genomic sequence and leads to a non-synonymous amino acid change (S>F) (Figure 5.4).

Contemporaneously, Emma Lawrence from our group performed a QTL scan for natural recombination modifiers using a Col-*420* x Bur-0 F_2 population and identified a strong *rQTL1a*^{Bur} on chromosome 1, that acted recessively to reduce crossover frequency. Emma fine-mapped this locus and narrowed down the *rQTL1a*^{Bur} plausible candidate region to ~30 kb containing five genes. Of these genes, she also identified *TAF4B* as the potential candidate for *rQTL1a*^{Bur} which carries a premature stop codon in the Bur accession. This *taf4b-1* (Bur-0) mutation introduces a termination codon (TTA>TAA) in exon 9 at 2,763 bp position of the genomic sequence, which is predicted to knock-out the histone fold domain (Figure 5.4).

Based on the similar phenotype of *lcr1* reducing crossovers I speculated that the *lcr1* mutation to be within *TAF4B.* For example, a Bur-0 introgression containing *taf4b-1* mutation in Col-0 background caused a ~6-8 cM decrease in *420*, whereas *lcr1*

causes a similar ~4-6 cM decrease, compared to wild type. To confirm the candidate mutation responsible for *lcr1* phenotype, I performed a segregation analysis using dCAPS markers (Table S4) for the mutations in the *TAF4B* and *FAN1* genes in the *lcr1* BC_1F_2 population and compared genotypes to *420* recombination (Figure 5.4; Table S40). From genotyping 62 BC_1F_2 plants, I observed a segregation of the genotypes in ratios close to 1:2:1 for both mutations (Figure 5.4; Table S40). In this population, the *lcr1-taf4b* homozygotes (16.13 ± 0.94 cM) showed significantly reduced recombination to their wild type (19.16 ± 1.24 cM; GLM $P = 4.07x10^{-9}$) and *lcr1* heterozygotes (17.39 ± 1.48 cM; GLM $P = 9.45 \times 10^{-3}$) siblings. I used double heterozygotes (*taf4b/+ fan1/+*) to compare with *lcr1-taf4b* and *fan1* homozygotes, hence referred as *lcr1/+* or *lcr1* heterozygotes. In addition, the *lcr1-taf4b* homozygotes showed lower recombination than the *fan1* homozygotes (18.11 ± 1.82 cM, GLM $P = 1.41 \times 10^{-5}$) (Figure 5.4; Table S40). The *fan1* homozygotes (18.11 ± 1.82 cM) displayed a slight but significant reduction in crossovers compared to wild type (19.16 ± 1.24 cM; GLM, P=0.02), but were not-significantly different to *lcr1/+* (17.39 ± 1.48 cM; GLM P=0.05) (Figure 5.4; Table S40). Notably, the *lcr1* allele showed a weaker phenotype (16.13 ± 0.94 cM) compared to *taf4b-1* (14.32 ± 0.98 cM), due to which they exhibited a significant difference (GLM, $P = 5.28 \times 10^{-5}$). The *lcr1* mutation is located at the 549th bp position (exon 3) and is 11 bp upstream of an annotated alternative start codon in some *TAF4B* transcriptional models. Hence, we postulate that some functional transcript is still being produced from the alternative start codon that could be the cause for the weaker *lcr1* phenotype. It is also possible that residual EMS polymorphisms remaining in the BC_1F_2 population could affect recombination frequency.

Emma and I conducted an allelism test between *taf4b-1* and *lcr1* to determine whether the *lcr1* phenotype was caused by mutation in *TAF4B*. The *lcr1*/*taf4b-1* F_1 individuals produced from crossing *taf4b-1* and *lcr1* displayed the mutant phenotype with an average 13.11 ± 0.66 cM that was significantly different to wild type (18.33 ± 1.14 cM; GLM, $P < 2.0 \times 10^{-16}$) and *taf4b-1* heterozygotes (16.77 ± 0.69 cM; GLM, $P < 2.0 \times 10^{-16}$), respectively (Figure 5.5; Table S41). This indicated that the causal mutations are in the same gene due to non-complementation. Although, the premature stop codon in *lcr1* occurs at an earlier position (exon 3) in the gene

sequence than the *taf4b-1* mutation (exon 9), the *lcr1* allele showed a weaker crossover phenotype compared to the Bur-0 *taf4b-1* allele. Nevertheless, *TAF4B* was identified as a recombination modifier from two independent approaches which suggests that this protein plays an important role to maintain wild type recombination levels.

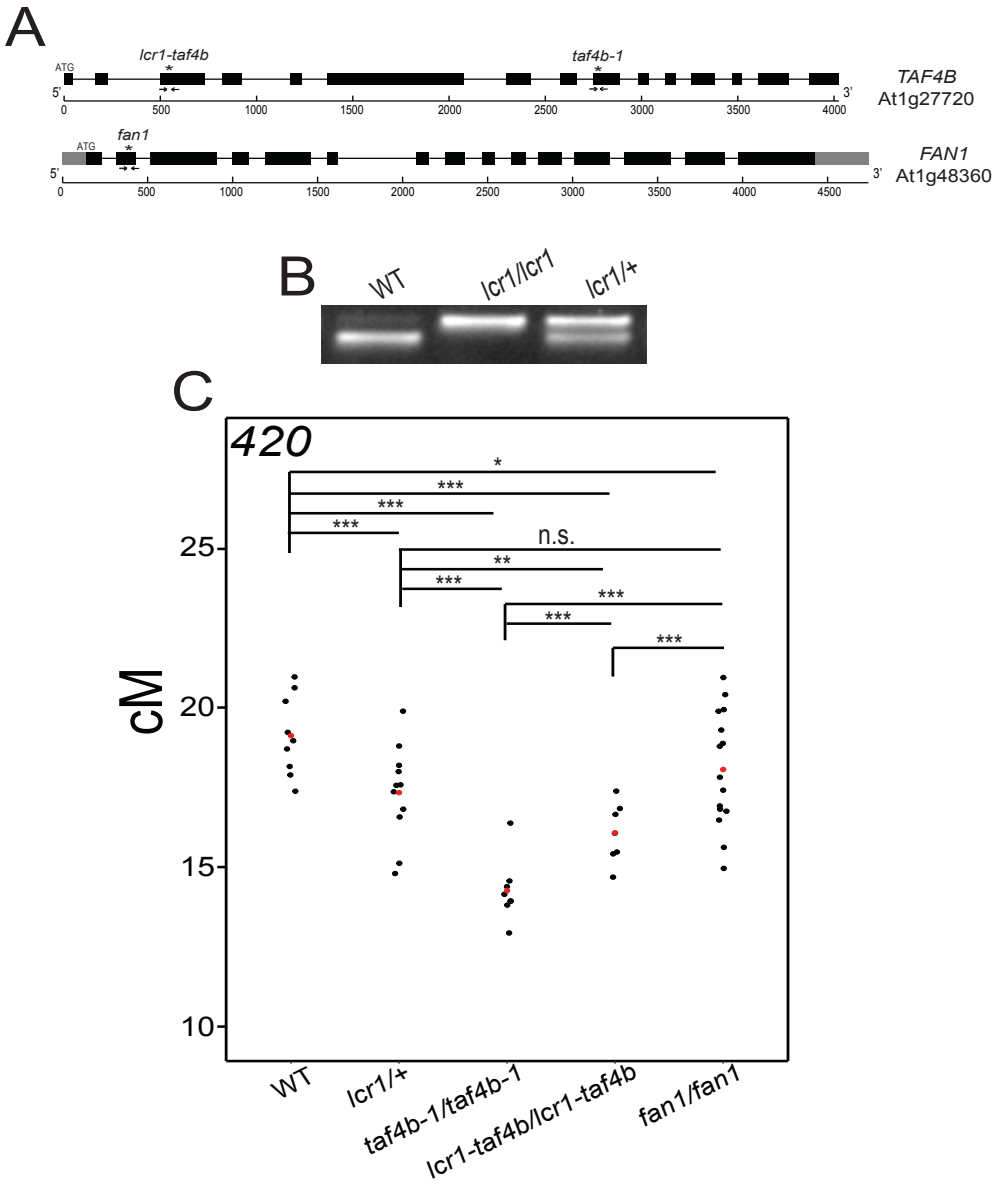

Figure 5.4. The *lcr1* dCAPs marker shows co-segregation with *420* phenotype in a BC_1F_2 population. A) A map of At1g27720 (GenBank ID: NM_102537) and At1g48360 (GenBank ID: NM_001123975) loci with intron-exon organization of *TAF4B* and *FAN1* drawn using Gene structure display server 2.0 tool (http://gsds.cbi.pku.edu.cn). The exons are drawn as boxes (black=CDS, grey=UTR). Scale bars indicate bp. Genotyping of a *lcr1* BC_2F_2 population was performed using a dCAPs marker spanning *lcr1-taf4b* and *fan1* mutations are indicated as arrows in the respective gene maps. **B)** Restriction digestion of PCR amplified products using *Fok*I

cleavage followed by gel electrophoresis and ethidium bromide staining is shown. The higher molecular weight uncut band represents the *lcr1* homozygous genotype and the lower band indicating the presence of the wild type (Col) genotype. The *lcr1/+* genotype is represented by bright *lcr1* and weak wild type bands. **C)** *420* crossover rate (cM) of BC_1F_2 individuals with respective genotypes, including wild type Col, *lcr1/+*, *taf4b-1/taf4b-1*, *lcr1-taf4b/lcr1-taf4b* and *fan1/fan1* are plotted. Mean values are indicated by red dots. Significance tests between genotypes using a GLM are indicated (*** = $P < 0.001$; ** = $P < 0.01$; * = $P < 0.05$; n.s.= non-significant with $P > 0.05$).

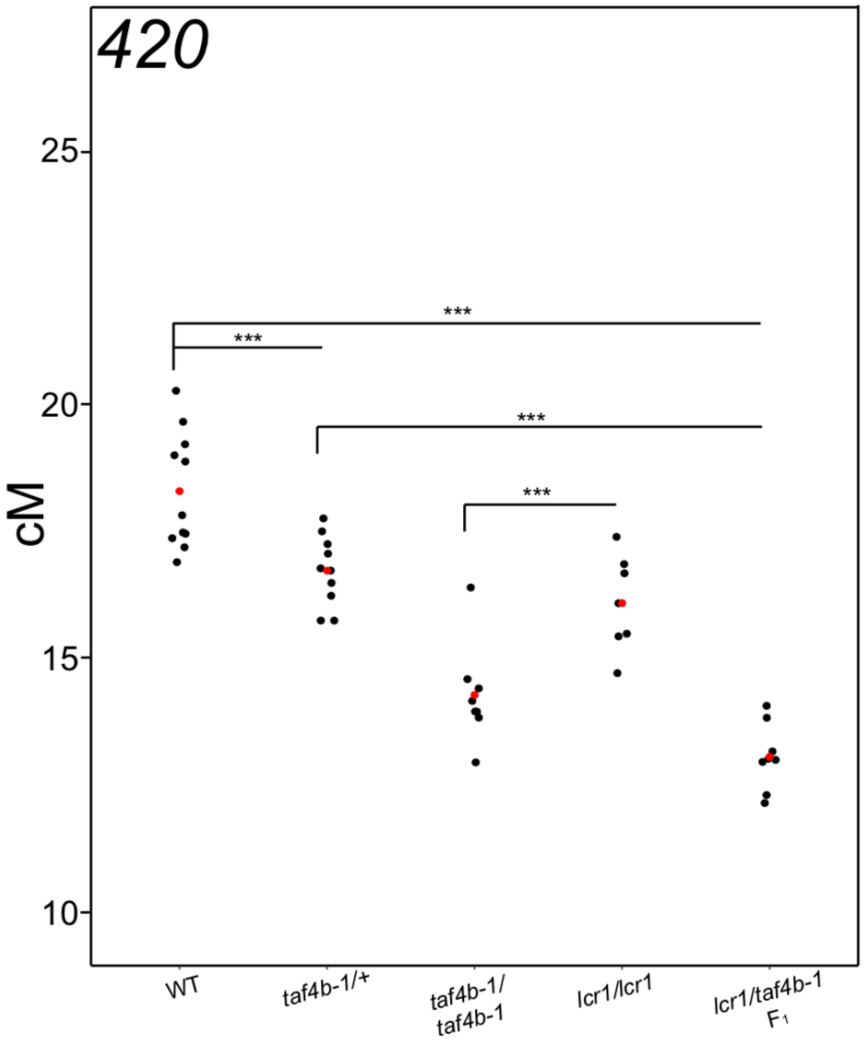

Figure 5.5. Allelism testing between the *lcr1* and *taf4b-1* mutations. *420* genetic distance (cM) measured in F_1 progeny of a cross between *lcr1* and *taf4b-1* alleles and controls, including, wild type Col and *taf4b-1/+* lines are plotted. Additionally, *taf4b-1* and *lcr1* homozygotes were not grown at the same time are plotted to compare its phenotypes with the F_1 progeny. Mean values are indicated by red dots. Significance tests by GLM between, (i) wild type and *taf4b-1/+* (ii) wild type and *lcr1/taf4b-1* F_1 lines and (iii) *taf4b-1/+* and *lcr1/taf4b-1* F_1 lines, and (iv) *lcr1* and *taf4b-1* homozygotes are indicated (***, which equals $P < 0.001$).

Chapter 6 - General Discussion

6.1. Genetic screens for genes involved in meiotic recombination

Forward genetic strategies have provided a strong foundation to identify novel genes, which may involve screening natural variation or mutations derived from chemical mutagenesis (Peters et al. 2003; Schneeberger 2014). Chemical mutagenesis screens are performed in model species using well-defined genetic backgrounds and benefit from the availability of genomic tools to map mutations to specific genes. Next generation technologies have revolutionized the speed of identifying mutations corresponding to mutants from genetic screens (Page and Grossniklaus 2002; Schneeberger 2014). Arabidopsis genes involved in meiotic recombination have been identified successfully with forward genetic approaches using a combination of EMS or T-DNA mutagenesis (De Muyt et al. 2009; Crismani et al. 2012). A primary mode of screening for mutants involved in meiosis has been according to defects in fertility with secondary cytology-based screening for meiotic phenotypes (De Muyt et al. 2009; Crismani et al. 2012). Previously, mutants were subjected to classical map-based cloning to identify the chromosomal region carrying the mutation, or by isolation of T-DNA insertion positions (Georg Jander et al. 2002; De Muyt et al. 2009). For example, a large T-DNA mutant collection (~55,000 lines) was screened for mutants involved in early recombination functions, which identified mutations in *SPO11-1*, *SPO11-2*, *PRD1, PRD2*, *PRD3* and *MTOPVIB* (Grelon et al. 2001; Stacey et al. 2006; De Muyt et al. 2007, 2009; Vrielynck et al. 2016). Similarly, a meiotic suppressor screen performed via EMS mutagenesis isolated genes that increase CO frequency by fertility restoration of Class I CO-defective *zmm* mutants, for example *zip4* (Crismani et al. 2012; Chelysheva et al. 2007). The suppressor mutants were mapped via whole-genome sequencing, which identified mutations in anti-CO factors, including *FANCM*, *MHF1*, *MHF2*, *TOP3α*, *RECQ4A*, *RECQ4B*, *FIGL1* and *FLIP1* (Crismani et al. 2012; Girard et al. 2014; Séguéla-Arnaud et al. 2015; Girard et al. 2015; Fernandes et al. 2018).

Screens based on fertility are relatively non-specific as they can be influenced by mutations in many processes and in addition environmental factors may modify this phenotype. Therefore, in this work we performed a screen that did not rely on fertility

phenotypes, and instead identified mutants that quantitatively alter meiotic crossover frequency in Arabidopsis. To this end, we performed EMS mutagenesis in the seed-expressed Columbia (Col) FTL *420* line hemizygous for both GFP and RFP markers located in *cis* on the sub-telomeric region of chromosome 3 (Melamed-Bessudo et al. 2005). In general, the observed frequency of EMS mutations has been estimated to be 700 per M_1 line and <50,000 M_1 lines are sufficient to have a 95% probability of identifying a given, single nucleotide change (G>A or C>T) in the Arabidopsis genome (Jander et al. 2003). Dr Kyuha Choi generated a population of ~7,000 M_1 plants that were further divided into ~600 small M_2 mutant pools (Figure 3.1, see, "Chapter 3"). Screening of <10% of the mutant pools and *420* scoring of ~3,000 M_2 plants gave rise to 5 *high crossover rate* (*hcr*) and 4 *low crossover rate* (*lcr*) mutants (Figure 3.6, see, "Chapter 3"), including an new allele of the known anti-CO factor, *FANCM* (*fancm-10*, Figure 3.7, see, "Chapter 3") (Crismani et al. 2012). Mapping-by-deep sequencing of *hcr1*, *hcr2*, *hcr3* and *lcr1* mutants identified plausible gene candidates (Figure 3.9 to 3.12, see, "Chapter 3") that have not previously been characterized for recombination functions in Arabidopsis. However, nearly 90% of the screen's genetic material has yet to be scored for recombination, meaning there is a great potential to identify further novel modifiers of recombination.

Since, this screen has been developed using the sub-telomeric interval, the identified candidates will most likely affect CO frequency in the chromosome arm regions. For example, this was evident in the mutant *hcr1*, which increases crossover frequency mainly in the chromosome arms (Figure 4.13, see, "Chapter 4"). It may be interesting for future genetic screens to be designed to identify peri-centromeric or centromeric recombination modifiers via EMS mutagenesis using centromere-spanning FTL intervals. For example, a commonly used pollen-expressed FTL line located on chromosome 3 spans the centromere called *CEN3* (5.405 Mb), is known to show modified crossover frequency by mutations in epigenetic pathways, for example maintenance of DNA methylation (Yelina et al. 2012, 2013; Ziolkowski et al. 2015). However, as *CEN3* is a pollen-based FTL this may be difficult to implement in a forward genetic screen, where seed-based FTLs have major advantages.

The main advantage is that scoring crossovers in progeny seeds is non-destructive, whereas once hydrated for flow cytometric analysis FTL pollen cannot afterwards be

used to pollinate. In contrast, FTL seed with specific fluorescent patterns, and therefore specific recombination patterns, can be pre-selected before growth in the next generation. Seeds can also be stored and analysed for long periods, which is advantageous when working with large mutagenesis populations. Although, some available seed-based centromeric FTLs could be useful (e.g. CTL *5.10*, *5.11*) (Wu et al. 2015), the intervals do not tightly span the centromeres as seen for *CEN3* (Yelina et al. 2012, 2013; Ziolkowski et al. 2015). Therefore, new centromeric FTLs should be developed for forward genetic screening purposes.

6.2. The role of HCR1/PPX-1 in meiotic recombination

I characterized the function of the gene *PROTEIN PHOSPHATASE X-1* (*PPX-1*) or *HIGH CROSSOVER RATE 1* (*HCR1*), which I identified from the *hcr1* mutation (Figure 4.3, 4.4 - see, "Chapter 4"). Phosphorylation is an universal means of reversibly regulating protein activity and is controlled by the antagonistic activities of kinases and phosphatases (Manning et al. 2002; Farkas et al. 2007; Moorhead et al. 2009; Shi 2009; Brautigan 2013; Uhrig et al. 2013). Protein kinases and phosphatases typically constitute between 2-4% of the genes in eukaryotic genomes (Manning et al. 2002; Moorhead et al. 2009). Proteins are phosphorylated on nine amino acids, including, tyrosine, serine, threonine, cysteine, arginine, lysine, aspartate, glutamate and histidine (Moorhead et al. 2009). However, serine, threonine and tyrosine phosphorylation occur most frequently in eukaryotes (Moorhead et al. 2009). Enzymes that dephosphorylate the major phosphorylated amino acid residues (Serine, Threonine and Tyrosine) are classified into four major groups according to catalytic mechanism, domain structure and substrate specificity (Moorhead et al. 2009; Shi 2009). Serine/Threonine phosphatases form a large phosphoprotein phosphatase (PPP) family consisting of 7 sub-groups: PP1, PP2A, PP2B/PPKL, PP4/X, PP5, PP6 and PP7 (Moorhead et al. 2009; Uhrig et al. 2013). The PPP family consists of 26 genes in *Arabidopsis thaliana* (Kerk et al. 2008; Moorhead et al. 2009).

HCR1/PPX-1 belongs to the PP4 subfamily of protein phosphatases. The Arabidopsis PP4/X consists of two catalytic subunits namely PPX-1 and PPX-2 (Pujol et al. 2000). The PP4/X catalytic subunits are structurally closely related to

PP2A and both PP2A and PP4/X catalytic domains are conserved across eukaryotes (Brewis and Cohen 1992; Farkas et al. 2007; Moorhead et al. 2007; Uhrig et al. 2013). These catalytic domains undergo reversible methylation, a covalent post-translational modification at their C-terminus, which controls their interactions with regulatory subunits (Cohen et al. 2005; Shi 2009). Their catalytic subunits are indirectly associated with regulatory subunits using scaffold domains (Brautigan 2013). Arabidopsis PP4 has two regulatory subunits namely, PP4R2 and PP4R3 (Lillo et al. 2014) whose sub-cellular localization is unknown. HCR1/PPX-1 is predicted to be nuclear-localized as it has been identified to repress meiotic crossovers, which is a nuclear-related process (Figure 4.12, 4.13 - see, “Chapter 4”).

PP4/PPX has been identified as playing a role in DSB repair in both mitosis and meiosis in other eukaryotes. In yeast and humans, the PP4/X complex (PP4/X-PP4R2/R3) is involved in γH2A.X dephosphorylation at DSB sites and terminates the activated checkpoint by a signalling cascade of protein kinases (ATM/ATR) to recover cells from G2/M arrest prior to mitosis (Keogh et al. 2006; Nakada et al. 2008; Chowdhury et al. 2008; Kim et al. 2011). During meiotic prophase I, disruption of PP4 in budding yeast causes accumulation of phosphorylated Mec1/ATR targets and the active checkpoint blocks the stabilization of strand invasion intermediates, suggesting a coordinated role of Mec1/ATR and PP4 in response to meiotic recombination initiation and checkpoint control (Falk et al. 2010). Hence I hypothesize that Arabidopsis HCR1/PPX1 and ATM/ATR kinases (Culligan and Britt 2008) may have antagonistic roles in regulating checkpoint targets for efficient DSB repair and recombination (Figure 6.1). However, *hcr1* mutant (loss of PPX-1 activity) does not accumulate meiotic DSBs (RAD51 foci) in early prophase I compared to wild type, indicating the role of HCR1/PPX1 in likely downstream of DSB repair (Figure 4.17). Mass spectrometry-based phospho-proteomic study of ATM and ATR identified several targets including the DNA repair factor, MRE11 (Roitinger et al. 2015). Therefore, phospho-proteome profiling of *hcr1* mutant could reveal the phosphorylated substrate targets and whether they overlap with ATM/ATR targets (e.g. H2A.X), which would indicate their coordinated roles in response to DNA damage. My analysis indicates that HCR1/PPX-1 majorly limits Class I interfering crossovers in Arabidopsis. For example, using MLH1 immunostaining and genetic analysis with *fancm* and *zip4* mutants, I showed that *hcr1* hyper-recombination is

mainly interference-dependent. The additive effect I observed on crossovers in *hcr1 fancm* double mutants further suggests an effect on Class I crossovers (Figure 4.12 to 4.16, see, “Chapter 4”). However, evidence also indicated that *hcr1* has a minor effect on Class II COs (Figure 4.14, 4.15 - see, “Chapter 4”). Together from my observations, I propose a model where the major role of is HCR1/PPX1 is to limit ZMM-dependent crossovers downstream of DSB formation (Figure 6.1).

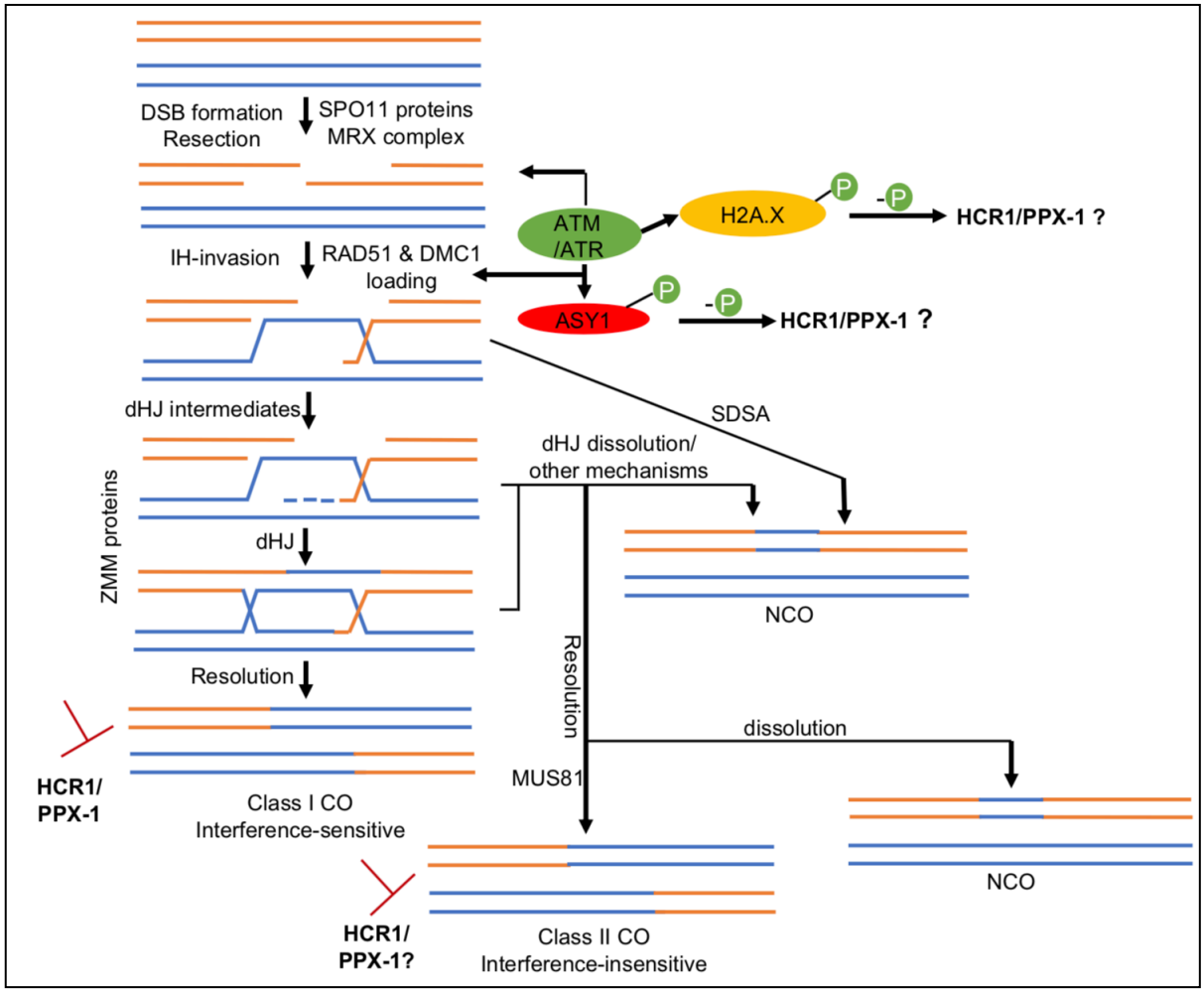

Figure 6.1. A model of Arabidopsis HCR1/PPX-1 role in meiotic recombination. Replicated chromatids of two homologous DNA duplexes in orange and blue. Meiotic recombination is initiated by DSBs mediated by SPO11 proteins on the orange chromosome, resection takes place via the MRX complex to form the 3’-ended RPA coated ssDNAs. This ssDNA undergoes strand invasion mediated via DMC1 and RAD51 recombinases to form a Displacement-loop (D-loop). H2A.X (in yellow circle) and ASY1 (in red circle) are phosphorylated by ATM/ATR kinases (in green circle) in response to DSBs undergoing repair and IH-recombination. Phosphorylated ASY1 allows efficient deposition of DMC1 and RAD51 recombinases to promote IH-repair and impede IS-repair. The IH-recombination intermediates are directed to the ZMM-dependent pathway to produce Class I COs which is interference-sensitive. Increased ASY1 phosphorylated signal is predicted in the absence of HCR1/PPX-1. HCR1 dephosphorylates ASY1 and attenuation of ASY1 signal may limit Class I COs and Class II COs to some extent and may promote IS-repair and NCOs.

Several studies indicate that chromosome axis/SC proteins are important for regulation of CO frequency and interference and chromosome morphogenesis (Hillers and Villeneuve 2003; Nabeshima, Villeneuve, and Hillers 2004; Storlazzi et al. 2008; Zhang, Wang, et al. 2014; Couteau et al. 1999; Grelon et al. 2001; Armstrong et al. 2002; Higgins et al. 2005). For example, the HORMA domain protein ASY1 and its orthologs are widely studied axis proteins in diverse organisms. For example, Arabidopsis *asy1* mutants fail to synapse and CO formation is severely reduced (Ross et al. 1997). ASY1 is detected in male meiotic cells as numerous punctate foci distributed over chromatin which matures into a linear signal as meiosis progresses during leptotene stage (Armstrong et al. 2002). ASY1 signal remains throughout prophase I, however the conserved PCH2 (AAA+ ATPase) localizes to the axis remodelling sites on the chromatin loops and depletes ASY1 during zygotene in parallel to SC formation and patterned CO formation at designated sites (Lambing et al. 2015). In *asy1* mutants localization of DMC1 declines abruptly during meiotic progression due to which DMC1-mediated inter-homolog recombination is severely compromised (Sanchez-Moran et al. 2007). In addition, ASY1 phosphorylation (ATM-mediated) is essential for loading of DMC1 to promote IH-repair and impediment of IS-repair (Kurzbauer et al. 2012). Hence, ASY1 acts an interface between the chromosome axis and IH-recombination bias followed by patterned maturation of crossover designated recombination intermediates (Sanchez-Moran et al. 2007; Kurzbauer et al. 2012; Lambing et al. 2015).

Therefore, I propose that hyper-recombination in *hcr1* could be due to increased phosphorylation of ASY1 mediated by ATM/ATR which subsequently promotes efficient deposition of DMC1 and RAD51 recombinases and maximum IH-recombination intermediates are repaired predominantly by the ZMM-dependent Class I CO pathway. Inactivation or reduced ASY1 signal loses its efficiency to promote IH-repair, therefore may promote more inter-sister repair and NCO formation. To summarize HCR1/PPX-1 may limit ZMM-dependent IH-recombination by dephosphorylation of ASY1 during prophase I (Figure 6.1). To test this hypothesis, future experiments could be based on phosphoproteomic studies, that is *hcr1* mutant can be co-immunoprecipitated (Co-IP) and subjected to affinity proteomic or mass spectrometry analysis to identify the potential phosphorylated targets or associated proteins during prophase I events, especially IH-recombination.

This has been recently demonstrated in Brassica ASY1 (BoASY1) and a protein-protein interaction (PPI) network of co-associated proteins of ASY1 using affinity phosphoproteomics was identified (Osman et al. 2018). As a proof-of-principle, they identified recently characterized axis-associated proteins such as ASY3 and ASY4 (Osman et al. 2018; Ferdous et al. 2012; Chambon et al. 2018). Further analysis using yeast-two-hybrid assays could validate the interaction between the major protein and its targets (e.g. HCR1/PPX-1 and ASY1). Hence, these experiments could explore the mechanistic role of HCR1/PPX-1 in Arabidopsis.

Bibliography

Acquaviva, Laurent, Lóránt Székvölgyi, Bernhard Dichtl, Beatriz Solange Dichtl, Christophe De La, Roche Saint, Alain Nicolas, and Vincent Géli. 2013. “The COMPASS Subunit Spp1 Links Histone Methylation to Initiation of Meiotic Recombination.” *Science* 339 (6116): 215–18.

Agarwal, Seema, and G. Shirleen Roeder. 2000. “Zip3 Provides a Link between Recombination Enzymes and Synaptonemal Complex Proteins.” *Cell* 102 (2): 245–55.

Allen, Robert S., Kenlee Nakasugi, Rachel L. Doran, Anthony A. Millar, and Peter M. Waterhouse. 2013. “Facile Mutant Identification via a Single Parental Backcross Method and Application of Whole Genome Sequencing Based Mapping Pipelines.” *Frontiers in Plant Science* 4: 1–8.

Alonso-Blanco, C, and M Koornneef. 2000. “Natural Variation, an Underexploited Resource of Genetic Variation for Plant Genetics.” *Trends in Plant Science* 5 (99): 22–29.

Alonso, Jose M., and Joseph R. Ecker. 2006. “Moving Forward in Reverse: Genetic Technologies to Enable Genome-Wide Phenomic Screens in Arabidopsis.” *Nature Reviews. Genetics* 7 (7): 524–36.

Alonso, José M, and Anna N Stepanova. 2015. “SHOREmap v3.0: Fast and Accurate Identification of Causal Mutations from Forward Genetic Screens.” *Plant Functional Genomics: Methods and Protocols, Methods in Molecular Biology* 1284: 381–95.

Alonso, José M, Anna N Stepanova, Thomas J Leisse, Christopher J Kim, Huaming Chen, Paul Shinn, Denise K Stevenson, et al. 2003. “Genome-Wide Insertional Mutagenesis of Arabidopsis Thaliana.” *Science* 301 (5633): 653–57.

Anderson, Lorinda K., Leslie D. Lohmiller, Xiaomin Tang, D. Boyd Hammond, Lauren Javernick, Lindsay Shearer, Sayantani Basu-Roy, Olivier C. Martin, and

Matthieu Falque. 2014. “Combined Fluorescent and Electron Microscopic Imaging Unveils the Specific Properties of Two Classes of Meiotic Crossovers.” *Proceedings of the National Academy of Sciences* 111 (37): 13415–20.

Armstrong, S. J., Anthony P. Caryl, Gareth H. Jones, and F. Christopher H. Franklin. 2002. “Asy1, a Protein Required for Meiotic Chromosome Synapsis, Localizes to Axis-Associated Chromatin in Arabidopsis and Brassica.” *Journal of Cell Science* 115 (18): 3645–55.

Armstrong, Susan J., and Gareth H. Jones. 2003. “Meiotic Cytology and Chromosome Behaviour in Wild-Type Arabidopsis Thaliana.” *Journal of Experimental Botany* 54 (380): 1–10.

Baudat, F, J Buard, C Grey, Adi Fledel-Alon, C Ober, Molly Przeworski, G Coop, and B de Massy. 2010. “PRDM9 Is a Major Determinant of Meiotic Recombination Hotspots in Humans and Mice.” *Science* 327 (5967): 836–40.

Baudat, Frédéric, Yukiko Imai, and Bernard De Massy. 2013. “Meiotic Recombination in Mammals: Localization and Regulation.” *Nature Reviews Genetics* 14 (11). Nature Publishing Group: 794–806.

Baudat, Frédéric, and Alain Nicolas. 1997. “Clustering of Meiotic Double-Strand Breaks on Yeast Chromosome III.” *Proceedings of the National Academy of Sciences of the United States of America* 94 (10): 5213–18.

Bauknecht, Markus, and Daniela Kobbe. 2014. “AtGEN1 and AtSEND1, Two Paralogs in Arabidopsis, Possess Holliday Junction Resolvase Activity.” *Plant Physiology* 166 (1): 202–16.

Benjamini, Yoav, and Yosef Hochberg. 1995. “Controlling the False Discovery Rate: A Practical and Powerful Approach to Multiple Testing.” *Journal of Royal Statistical Society* 57 (1): 289–300.

Berchowitz, Luke, and Gregory Copenhaver. 2010. “Genetic Interference: Dont Stand So Close to Me.” *Current Genomics* 11 (2): 91–102.

Berchowitz, Luke E., and Gregory P. Copenhaver. 2008. “Fluorescent Arabidopsis Tetrads: A Visual Assay for Quickly Developing Large Crossover and Crossover Interference Data Sets.” *Nature Protocols* 3 (1): 41–50.

Berchowitz, Luke E., Kirk E. Francis, Alexandra L. Bey, and Gregory P. Copenhaver. 2007. “The Role of AtMUS81 in Interference-Insensitive Crossovers in A. Thaliana.” *PLoS Genetics* 3 (8): 1355–64.

Bergerat, Agnes, Bernard de Massy, Danielle Gadelle, Paul-Christophe Varoutas, Alain Nicolas, and Patrick Forterre. 1997. “An Atypical Topoisomerase II from Archaea with Implications for Meiotic Recombination.” *Nature* 386(6623):414-17.

Bernstein, Kara A., Serge Gangloff, and Rodney Rothstein. 2010. “The RecQ DNA Helicases in DNA Repair.” *Annual Review of Genetics* 44 (1): 393–417.

Bishop, D K, D Park, L Z Xu, and N Kleckner. 1992. “DMC1 - A Meiosis-Specific Yeast Homolog of E-Coli RecA Required for Recombination, Synaptonemal Complex Formation, and Cell Cycle Progression.” *Cell* 69 (3): 439–56.

Bishop, K. 1994. “RecA Homologs Dmcl and Rad51 Interact to Form Multiple Nuclear Complexes Prior to Meiotic Chromosome Synapsis.” *Cell* 79: 1081–92.

Blat, Yuval, Reine U. Protacio, Neil Hunter, and Nancy Kleckner. 2002. “Physical and Functional Interactions among Basic Chromosome Organizational Features Govern Early Steps of Meiotic Chiasma Formation.” *Cell* 111 (6): 791–802.

Bleuyard, Jean-Yves, Maria E. Gallego, and Charles I. White. 2004. “Meiotic Defects in the Arabidopsis Rad50 Mutant Point to Conservation of the MRX Complex Function in Early Stages of Meiotic Recombination.” *Chromosoma* 113 (4): 197–203.

Boddy, Michael N., Pierre Henri L. Gaillard, W. Hayes McDonald, Paul Shanahan, John R. Yates, and Paul Russell. 2001. “Mus81-Eme1 Are Essential Components of a Holliday Junction Resolvase.” *Cell* 107 (4): 537–48.

Borde, Valérie. 2007. “The Multiple Roles of the Mre11 Complex for Meiotic Recombination.” *Chromosome Research* 15 (5): 551–63.

Börner, Valentin G., Nancy Kleckner, and Neil Hunter. 2004. “Crossover / Noncrossover Differentiation , Synaptonemal Complex Formation , and Regulatory Surveillance at the Leptotene / Zygotene Transition of Meiosis.” *Cell* 117: 29–45.

Brautigan, David L. 2013. “Protein Ser/ Thr Phosphatases - The Ugly Ducklings of Cell Signalling.” *FEBS Journal* 280 (2): 324–45.

Brewis, Neil D, and Patricia T W Cohen. 1992. “Protein Phosphatase X Has Been Highly Conserved during Mammalian Evolution.” *Biochimica et Biophysica Acta* 1171: 231–33.

Brick, Kevin, Fatima Smagulova, Pavel Khil, R. Daniel Camerini-Otero, and Galina V. Petukhova. 2012. “Genetic Recombination Is Directed Away from Functional Genomic Elements in Mice.” *Nature* 485 (7400): 642–45.

Brown, M Scott, and Douglas K Bishop. 2015. “DNA Strand Exchange and RecA Homologs.” *Cold Spring Harbor Perspectives in Biology* 7: a016659.

Carballo, Jesús A., Anthony L. Johnson, Steven G. Sedgwick, and Rita S. Cha. 2008. “Phosphorylation of the Axial Element Protein Hop1 by Mec1/Tel1 Ensures Meiotic Interhomolog Recombination.” *Cell* 132 (5): 758–70.

Carballo, Jesús A., Silvia Panizza, Maria Elisabetta Serrentino, Anthony L. Johnson, Marco Geymonat, Valérie Borde, Franz Klein, and Rita S. Cha. 2013. “Budding Yeast ATM/ATR Control Meiotic Double-Strand Break (DSB) Levels by Down-

Regulating Rec114, an Essential Component of the DSB-Machinery." *PLoS Genetics* 9 (6): e1003545.

Carpenter, Anne E, Thouis R Jones, Michael R Lamprecht, Colin Clarke, In Han Kang, Ola Friman, David A Guertin, et al. 2006. "CellProfiler: Image Analysis Software for Identifying and Quantifying Cell Phenotypes." *Genome Biology* 7: R100.

Chambon, Aurélie, Allan West, Daniel Vezon, Christine Horlow, Arnaud De Muyt, Liudmila Chelysheva, Arnaud Ronceret, et al. 2018. "Identification of ASYNAPTIC4, a Component of the Meiotic Chromosome Axis." *Plant Physiology* 178: 233–46.

Chelysheva, Liudmila, Ghislaine Gendrot, Daniel Vezon, Marie Pascale Doutriaux, Raphaël Mercier, and Mathilde Grelon. 2007. "Zip4/Spo22 Is Required for Class I CO Formation but Not for Synapsis Completion in *Arabidopsis thaliana*." *PLoS Genetics* 3 (5): 802–13.

Chelysheva, Liudmila, L. Grandont, N. Vrielynck, S. Le Guin, R. Mercier, and M. Grelon. 2010. "An Easy Protocol for Studying Chromatin and Recombination Protein Dynamics during Arabidopsisthaliana Meiosis: Immunodetection of Cohesins, Histones and MLH1." *Cytogenetic and Genome Research* 129: 143–53.

Chelysheva, Liudmila, Daniel Vezon, Aurélie Chambon, Ghislaine Gendrot, Lucie Pereira, Afef Lemhemdi, Nathalie Vrielynck, Sylvia Le Guin, Maria Novatchkova, and Mathilde Grelon. 2012. "The Arabidopsis HEI10 Is a New ZMM Protein Related to Zip3." *PLoS Genetics* 8 (7): e1002799.

Chen, Changbin, Wei Zhang, Ljudmilla Timofejeva, Ylaine Gerardin, and Hong Ma. 2005. "The Arabidopsis ROCK-N-ROLLERS Gene Encodes a Homolog of the Yeast ATP-Dependent DNA Helicase MER3 and Is Required for Normal Meiotic Crossover Formation." *Plant Journal* 43 (3): 321–34.

Chen, Stacy Y., Tomomi Tsubouchi, Beth Rockmill, Jay S. Sandler, Daniel R. Richards, Gerben Vader, Andreas Hochwagen, G. Shirleen Roeder, and Jennifer C. Fung. 2008. “Global Analysis of the Meiotic Crossover Landscape.” *Developmental Cell* 15 (3): 401–15.

Cheng, Chung Hsu, Yu Hui Lo, Shu Shan Liang, Shih Chieh Ti, Feng Ming Lin, Chia Hui Yeh, Han Yi Huang, and Ting Fang Wang. 2006. “SUMO Modifications Control Assembly of Synaptonemal Complex and Polycomplex in Meiosis of Saccharomyces Cerevisiae.” *Genes and Development* 20 (15): 2067–81.

Chiang, Teresa, Richard M. Schultz, and Michael A. Lampson. 2012. “Meiotic Origins of Maternal Age-Related Aneuploidy1.” *Biology of Reproduction* 86 (1): 1–7. doi:10.1095/biolreprod.111.094367.

Choi, Kyuha, Xiaohui Zhao, Krystyna A. Kelly, Oliver Venn, James D. Higgins, Nataliya E. Yelina, Thomas J. Hardcastle, et al. 2013. “Arabidopsis Meiotic Crossover Hot Spots Overlap with H2A.Z Nucleosomes at Gene Promoters.” *Nature Genetics* 45 (11): 1327–38.

Choi, Kyuha, Xiaohui Zhao, Andrew J Tock, Christophe Lambing, Charles J Underwood, Thomas J Hardcastle, Heïdi Serra, et al. 2018. “Nucleosomes and DNA Methylation Shape Meiotic DSB Frequency in Arabidopsis Thaliana Transposons and Gene Regulatory Regions.” *Genome Research*, 1–16.

Chowdhury, Dipanjan, Xingzhi Xu, Xueyan Zhong, Fariyal Ahmed, Jianing Zhong, Ji Liao, Derek M. Dykxhoorn, David M. Weinstock, Gerd P. Pfeifer, and Judy Lieberman. 2008. “A PP4-Phosphatase Complex Dephosphorylates γ-H2AX Generated during DNA Replication.” *Molecular Cell* 31 (1): 33–46.

Cimprich, Karlene A., and David Cortez. 2008. “ATR: An Essential Regulator of Genome Integrity.” *Nature Reviews Molecular Cell Biology* 9 (8): 616–27.

Cloud, Veronica, Yuen-Ling Chan, Jennifer Grubb, Brian Budke, and Douglas K. Bishop. 2012. “Rad51 Is an Accessory Factor for Dmc1-Mediated Joint Molecule Formation During Meiosis.” *Science* 337 (6099): 1222–25

.

Cohen, Patricia T.W., Amanda Philp, and Cristina Vázquez-Martin. 2005. “Protein Phosphatase 4 - From Obscurity to Vital Functions.” *FEBS Letters* 579 (15): 3278–86.

Cole, Francesca, Liisa Kauppi, Julian Lange, Ignasi Roig, Raymond Wang, Scott Keeney, and Maria Jasin. 2012. “Homeostatic Control of Recombination Is Implemented Progressively in Mouse Meiosis.” *Nature Cell Biology* 14 (4): 424–30.

Cooper, Tim J., Kayleigh Wardell, Valerie Garcia, and Matthew J. Neale. 2014. “Homeostatic Regulation of Meiotic DSB Formation by ATM/ATR.” *Experimental Cell Research* 329 (1): 124–31.

Couteau, Florence, Francois Belzile, Christine Horlow, Olivier Grandjean, Daniel Vezon, and Marie-Pascale Doutriaux. 1999. “Random Chromosome Segregation without Meiotic Arrest in Both Male and Female Meiocytes of a Dmc1 Mutant of Arabidopsis.” *The Plant Cell* 11 (9): 1623.

Crismani, Wayne, Chloé Girard, Nicole Froger, Mónica Pradillo, Juan Luis Santos, Liudmila Chelysheva, Gregory P. Copenhaver, Christine Horlow, and Raphaël Mercier. 2012. “FANCM Limits Meiotic Crossovers.” *Science* 336 (6088): 1588–90.

Crismani, Wayne, Virginie Portemer, Nicole Froger, Liudmila Chelysheva, Christine Horlow, Nathalie Vrielynck, and Raphaël Mercier. 2013. “MCM8 Is Required for a Pathway of Meiotic Double-Strand Break Repair Independent of DMC1 in *Arabidopsis thaliana*.” *PLoS Genetics* 9 (1): e1003165.

Culligan, Kevin M., and Anne B. Britt. 2008. “Both ATM and ATR Promote the Efficient and Accurate Processing of Programmed Meiotic Double-Strand Breaks.” *Plant Journal* 55 (4): 629–38.

Culligan, Kevin, Alain Tissier, and Anne Britt. 2004. “ATR Regulates a G2-Phase Cell-Cycle Checkpoint in *Arabidopsis Thaliana*.” *The Plant Cell* 16 (5): 1091–1104.

Drouaud, Jan, Hossein Khademian, Laurène Giraut, Vanessa Zanni, Sarah Bellalou, Ian R. Henderson, Matthieu Falque, and Christine Mézard. 2013. “Contrasted Patterns of Crossover and Non-Crossover at Arabidopsis Thaliana Meiotic Recombination Hotspots.” *PLoS Genetics* 9 (11): e1003922.

Drouaud, Jan, Raphaël Mercier, Liudmila Chelysheva, Aurélie Bérard, Matthieu Falque, Olivier Martin, Vanessa Zanni, Dominique Brunel, and Christine Mézard. 2007. “Sex-Specific Crossover Distributions and Variations in Interference Level along Arabidopsis Thaliana Chromosome 4.” *PLoS Genetics* 3 (6): 1096–1107.

Edlinger, Bernd, and Peter Schlögelhofer. 2011. “Have a Break: Determinants of Meiotic DNA Double Strand Break (DSB) Formation and Processing in Plants.” *Journal of Experimental Botany* 62 (5): 1545–63.

Emmanuel, Eyal, Elizabeth Yehuda, Cathy Melamed-Bessudo, Naomi Avivi-Ragolsky, and Avraham A. Levy. 2006. “The Role of AtMSH2 in Homologous Recombination in Arabidopsis Thaliana.” *EMBO Reports* 7 (1): 100–105.

Falk, Jill E., Andrew Chi ho Chan, Eva Hoffmann, and Andreas Hochwagen. 2010. “A Mec1- and PP4-Dependent Checkpoint Couples Centromere Pairing to Meiotic Recombination.” *Developmental Cell* 19 (4): 599–611.

Farkas, Ilona, Viktor Dombrádi, Márton Miskei, László Szabados, and Csaba Koncz. 2007. “Arabidopsis PPP Family of Serine/Threonine Phosphatases.” *Trends in Plant Science* 12 (4): 169–76.

Ferdous, Maheen, James D. Higgins, Kim Osman, Christophe Lambing, Elisabeth Roitinger, Karl Mechtler, Susan J. Armstrong, et al. 2012. “Inter-Homolog Crossing-over and Synapsis in Arabidopsis Meiosis Are Dependent on the Chromosome Axis Protein Atasy3.” *PLoS Genetics* 8 (2) e1002507.

Fernandes, Joiselle Blanche, Marine Duhamel, Mathilde Seguéla-Arnaud, Nicole Froger, Chloé Girard, Sandrine Choinard, Victor Solier, et al. 2018. “FIGL1 and Its Novel Partner FLIP Form a Conserved Complex That Regulates Homologous Recombination.” *PLoS Genetics* 14 (4): e1007317.

Fernandes, Joiselle Blanche, Mathilde Seguéla-Arnaud, Cécile Larchevêque, Andrew H. Lloyd, and Raphael Mercier. 2017. “Unleashing Meiotic Crossovers in Hybrid Plants.” *Proceedings of the National Academy of Sciences* 115 (10): 2431-36.

Franasiak, Jason M., Eric J. Forman, Kathleen H. Hong, Marie D. Werner, Kathleen M. Upham, Nathan R. Treff, and Richard T. Scott. 2014. “The Nature of Aneuploidy with Increasing Age of the Female Partner: A Review of 15,169 Consecutive Trophectoderm Biopsies Evaluated with Comprehensive Chromosomal Screening.” *Fertility and Sterility* 101(3): 656-663.

Francis, K. E., S. Y. Lam, B. D. Harrison, A. L. Bey, L. E. Berchowitz, and G. P. Copenhaver. 2007. “Pollen Tetrad-Based Visual Assay for Meiotic Recombination in Arabidopsis.” *Proceedings of the National Academy of Sciences* 104 (10): 3913–18.

Fricke, William M., and Steven J. Brill. 2003. “Slx1 - Slx4 Is a Second Structure-Specific Endonuclease Functionally Redundant with Sgs1 - Top3.” *Genes and Development* 17 (14): 1768–78.

Garcia, V., H. Bruchet, D. Camescasse, F. Granier, D. Bouchez, and A. Tissier. 2003. “AtATM Is Essential for Meiosis and the Somatic Response to DNA Damage in plants.” *The Plant Cell* 15 (1): 119–32.

Garcia, Valerie, Stephen Gray, Rachal M. Allison, Tim J. Cooper, and Matthew J. Neale. 2015. “Tel1ATM-Mediated Interference Suppresses Clustered Meiotic Double-Strand-Break Formation.” *Nature* 520 (7545): 114–18.

Garcia, Valerie, Sarah E L Phelps, Stephen Gray, and Matthew J. Neale. 2011. “Bidirectional Resection of DNA Double-Strand Breaks by Mre11 and Exo1.” *Nature* 479 (7372): 241–44.

Gaur, Vineet, Haley D.M. Wyatt, Stephen C. West, and Marcin Nowotny. 2015. “Structural and Mechanistic Analysis of the Slx1- Report Structural and Mechanistic Analysis of the Slx1-Slx4 Endonuclease.” *Cell Reports* 10: 1467–76.

Geuting, V., D. Kobbe, F. Hartung, J. Durr, M. Focke, and H. Puchta. 2009. “Two Distinct MUS81-EME1 Complexes from Arabidopsis Process Holliday Junctions.” *Plant Physiology* 150 (2): 1062–71. doi:10.1104/pp.109.136846.

Girard, Chloe, Liudmila Chelysheva, Sandrine Choinard, Nicole Froger, Nicolas Macaisne, Afef Lehmemdi, Julien Mazel, Wayne Crismani, and Raphael Mercier. 2015. “AAA-ATPase FIDGETIN-LIKE 1 and Helicase FANCM Antagonize Meiotic Crossovers by Distinct Mechanisms.” *PLoS Genetics* 11 (7): e1005369.

Girard, Chloe, Wayne Crismani, Nicole Froger, Julien Mazel, Afef Lemhemdi, Christine Horlow, and Raphael Mercier. 2014. “FANCM-Associated Proteins MHF1 and MHF2, but Not the Other Fanconi Anemia Factors, Limit Meiotic Crossovers.” *Nucleic Acids Research* 42 (14): 9087–95.

Giraut, Laurène, Matthieu Falque, Jan Drouaud, Lucie Pereira, Olivier C. Martin, and Christine Mézard. 2011. “Genome-Wide Crossover Distribution in Arabidopsis Thaliana Meiosis Reveals Sex-Specific Patterns along Chromosomes.” *PLoS Genetics* 7 (11): e1002354.

Gray, Stephen, and Paula E. Cohen. 2016. “Control of Meiotic Crossovers: From Double-Strand Break Formation to Designation.” *Annual Review of Genetics* 50 (1): 175–210.

Gregan, Juraj, Peter K. Rabitsch, Benjamin Sakem, Ortansa Csutak, Vitaly Latypov, Elisabeth Lehmann, Juerg Kohli, and Kim Nasmyth. 2005. “Novel Genes Required for Meiotic Chromosome Segregation Are Identified by a High-Throughput Knockout Screen in Fission Yeast.” *Current Biology* 15 (18): 1663–69.

Grelon, Mathilde, Daniel Vezon, Ghislaine Gendrot, and Georges Pelletier. 2001. “AtSPO11-1 Is Necessary for Ef®cient Meiotic Recombination in Plants.” *EMBO Journal* 20 (3): 589–600.

Grey, Corinne, Pauline Barthès, Gaëlle Friec, Francina Langa, Frédéric Baudat, and Bernard de Massy. 2011. “Mouse Prdm9 DNA-Binding Specificity Determines Sites of Histone H3 Lysine 4 Trimethylation for Initiation of Meiotic Recombination.” *PLoS Biology* 9 (10): 1–9.

Guo, Ya-Long, Marco Todesco, Jörg Hagmann, Sandip Das, and Detlef Weigel. 2012. “Independent FLC Mutations as Causes and Capsella Rubella.” *Genetics* 192 (October): 729–39.

Haber, James E., and Wolf Dietrich Heyer. 2001. “The Fuss about Mus81.” *Cell* 107 (5): 551–54.

Harrison, C. Jill, Elizabeth Alvey, and Ian R. Henderson. 2010. “Meiosis in Flowering Plants and Other Green Organisms.” *Journal of Experimental Botany* 61 (11): 2863–75.

Hartung, F., S. Suer, T. Bergmann, and Holger Puchta. 2006. “The Role of AtMUS81 in DNA Repair and Its Genetic Interaction with the Helicase AtRecQ4A.” *Nucleic Acids Research* 34 (16): 4438–48.

Hartung, F., S. Suer, and H. Puchta. 2007. “Two Closely Related RecQ Helicases Have Antagonistic Roles in Homologous Recombination and DNA Repair in Arabidopsis Thaliana.” *Proceedings of the National Academy of Sciences* 104 (47): 18836–41.

Hartung, F. 2000. “Molecular Characterisation of Two Paralogous SPO11 Homologues in Arabidopsis Thaliana.” *Nucleic Acids Research* 28 (7): 1548–54.

Hartung, Frank, Karel J Angelis, Armin Meister, Ingo Schubert, Michael Melzer, and Holger Puchta. 2002. “An Archaebacterial Topoisomerase Homolog Not Present in Other Eukaryotes Is Indispensable for Cell Proliferation of Plants” 12 (20): 1787–91.

Hartung, Frank, and Holger Puchta. 2001. “Molecular Characterization of Homologues of Both Subunits A (SPO11) and B of the Archaebacterial Topoisomerase 6 in Plants.” *Gene* 271 (1): 81–86.

Hartung, Frank, and Holger Puchta. 2006. “The RecQ Gene Family in Plants.” *Journal of Plant Physiology* 163 (3): 287–96.

Hartung, Frank, Rebecca Wurz-Wildersinn, Jörg Fuchs, Ingo Schubert, Stefanie Suer, and Holger Puchta. 2007. “The Catalytically Active Tyrosine Residues of Both SPO11-1 and SPO11-2 Are Required for Meiotic Double-Strand Break Induction in *Arabidopsis*.” *The Plant Cell* 19 (10): 3090–99.

Hartwig, B., G. V. James, K. Konrad, K. Schneeberger, and F. Turck. 2012. “Fast Isogenic Mapping-by-Sequencing of Ethyl Methanesulfonate-Induced Mutant Bulks.” *Plant Physiology* 160 (2): 591–600.

Hauf, Silke, and Yoshinori Watanabe. 2004. “Kinetochore Orientation in Mitosis and Meiosis.” *Cell* 119: 317–27.

Hayashi, Katsuhiko, Kayo Yoshida, and Yasuhisa Matsui. 2005. “A Histone H3 Methyltransferase Controls Epigenetic Events Required for Meiotic Prophase.” *Nature* 438 (7066): 374–78.

Hellens, Roger P., E. Anne Edwards, Nicola R. Leyland, Samantha Bean, and Philip M. Mullineaux. 2000. “PGreen: A Versatile and Flexible Binary Ti Vector for Agrobacterium-Mediated Plant Transformation.” *Plant Molecular Biology* 42 (6): 819–32.

Henikoff, Steven, and Luca Comai. 2003. “Single-Nucleotide Mutations for Plant Functional Genomics.” *Annual Review of Plant Biology* 54 (1): 375–401.

Herbert, Mary, Dimitrios Kalleas, Daniel Cooney, Mahdi Lamb, and Lisa Lister. 2015. “Meiosis and Maternal Aging: Insights from Aneuploid Oocytes and Trisomy Births.” *Cold Spring Harbor Perspectives in Biology* 7 (4): a017970.

Higgins, James D, Susan J Armstrong, F Christopher H Franklin, and Gareth H Jones. 2004. “The *Arabidopsis MutS* Homolog *AtMSH4* Functions at an Early Step in Recombination: Evidence for Two Classes of Recombination in *Arabidopsis*.” *Genes & Development* 18 (20): 2557–70.

Higgins, James D., Eugenio Sanchez-Moran, Susan J. Armstrong, Gareth H. Jones, and F. Chris H Franklin. 2005. “The Arabidopsis Synaptonemal Complex Protein ZYP1 Is Required for Chromosome Synapsis and Normal Fidelity of Crossing Over.” *Genes and Development* 19 (20): 2488–2500.

Higgins, James D., Julien Vignard, Raphael Mercier, Alice G. Pugh, F. Chris H. Franklin, and Gareth H. Jones. 2008a. “AtMSH5 Partners AtMSH4 in the Class I Meiotic Crossover Pathway in *Arabidopsis thaliana*, but Is Not Required for Synapsis.” *Plant Journal* 55 (1): 28–39.

Higgins, James D., Ewen F. Buckling, F. Chris H Franklin, and Gareth H. Jones. 2008b. “Expression and Functional Analysis of AtMUS81 in Arabidopsis Meiosis Reveals a Role in the Second Pathway of Crossing-Over.” *Plant Journal* 54 (1): 152–62.

Hillers, Kenneth J., and Anne M. Villeneuve. 2003. “Chromosome-Wide Control of Meiotic Crossing over in C.Elegans.” *Current Biology* 13 (18): 1641–47.

Holloway, J. Kim, James Booth, Winfried Edelmann, Clare H. McGowan, and Paula E. Cohen. 2008. “MUS81 Generates a Subset of MLH1-MLH3-Independent Crossovers in Mammalian Meiosis.” *PLoS Genetics* 4 (9): e1000186.

Holloway, J. Kim, Swapna Mohan, Gabriel Balmus, Xianfei Sun, Andrew Modzelewski, Peter L. Borst, Raimundo Freire, Robert S. Weiss, and Paula E. Cohen. 2011. “Mammalian BTBD12 (SLX4) Protects against Genomic Instability during Mammalian Spermatogenesis.” *PLoS Genetics* 7 (6): e1002094.

Hunter, N, and N Kleckner. 2001. “The Single End Invasion: An Asymetric Intermediate at the Double-Strand-Break to Double-Holiday Junction Transition of Meiotic Recombination.” *Cell* 106 (1): 59–70.

Hunter, Neil. 2015. “Meiotic Recombination : The Essence of Heredity.” *Cold Spring Harbor Perspectives in Biology* 7 (12): 1–36.

Imai, Yukiko, Frédéric Baudat, Miguel Taillepierre, Marcello Stanzione, Attila Toth, and Bernard de Massy. 2017. “The PRDM9 KRAB Domain Is Required for Meiosis and Involved in Protein Interactions.” *Chromosoma* 126 (6): 681–95.

Ines, Olivier Da, Fabienne Degroote, Chantal Goubely, Simon Amiard, Maria E. Gallego, and Charles I. White. 2013. “Meiotic Recombination in Arabidopsis Is Catalysed by DMC1, with RAD51 Playing a Supporting Role.” *PLoS Genetics* 9 (9): e1003787.

Ip, Stephen C.Y., Ulrich Rass, Miguel G. Blanco, Helen R. Flynn, J. Mark Skehel, and Stephen C. West. 2008. “Identification of Holliday Junction Resolvases from Humans and Yeast.” *Nature* 456 (7220): 357–61.

Jackson, Neil, Eugenio Sanchez-Moran, Ewen Buckling, Susan J. Armstrong, Gareth H. Jones, and Frederick Christopher Hugh Franklin. 2006. “Reduced Meiotic Crossovers and Delayed Prophase I Progression in AtMLH3-Deficient Arabidopsis.” *EMBO Journal* 25 (6): 1315–23.

Jacob, Aishwarya G., and Christopher W.J. Smith. 2017. “Intron Retention as a Component of Regulated Gene Expression Programs.” *Human Genetics* 136 (9): 1043–57.

James, Geo Velikkakam, Vipul Patel, Karl J.V. Nordström, Jonas R. Klasen, Patrice A. Salomé, Detlef Weigel, and Korbinian Schneeberger. 2013. “User Guide for Mapping-by-Sequencing in Arabidopsis.” *Genome Biology* 14 (6): R61.

Jander, G., Scott R. Baerson, Jebecka A. Hudak, Kathleen A. Gonzalez, Kenneth J. Gruys, and Robert L Last. 2003. “Ethylmethanesulfonate Saturation Mutagenesis in Arabidopsis to Determine Frequency of Herbicide Resistance.” *Plant Physiology* 131 (1): 139–46.

Jander, Georg, Susan R Norris, Steven D Rounsley, David F Bush, Irena M Levin, Robert L Last. 2002. “Arabidopsis Map-Based Cloning in the post-genome era.” *Plant Physiology* 129(2):440-50.

Jazayeri, Ali, Alessia Balestrini, Elizabeth Garner, James E. Haber, and Vincenzo Costanzo. 2008. “Mre11-Rad50-Nbs1-Dependent Processing of DNA Breaks Generates Oligonucleotides That Stimulate ATM Activity.” *EMBO Journal* 27 (14): 1953–62.

Jazayeri, Ali, Jacob Falck, Claudia Lukas, Jiri Bartek, Graeme C.M. Smith, Jiri Lukas, and Stephen P. Jackson. 2006. “ATM- and Cell Cycle-Dependent Regulation of ATR in Response to DNA Double-Strand Breaks.” *Nature Cell Biology* 8 (1): 37–45.

Jessberger, Rolf. 2012. “Age-Related Aneuploidy through Cohesion Exhaustion.” *EMBO Reports* 13 (6): 539–46.

Jessop, Lea, Beth Rockmill, G. Shirleen Roeder, and Michael Lichten. 2006. “Meiotic Chromosome Synapsis-Promoting Proteins Antagonize the Anti-Crossover Activity of Sgs1.” *PLoS Genetics* 2 (9): e155.

Jolivet, Sylvie, Daniel Vezon, Nicole Froger, and Raphäl Mercier. 2006. “Non Conservation of the Meiotic Function of the Ski8/Rec103 Homolog in Arabidopsis.” *Genes to Cells* 11 (6): 615–22.

Jones, Gareth H., and F. Chris H Franklin. 2006. “Meiotic Crossing-over: Obligation and Interference.” *Cell* 126 (2): 246–48.

Kaliraman, Vivek, Janet R Mullen, William M Fricke, Suzanne a Bastin-shanower, and Steven J Brill. 2001. “Functional Overlap between Sgs1 – Top3 and the Mms4 – Mus81 Endonuclease.” *Genes & Development* 15: 2730–40.

Kauppi, Liisa, Marco Barchi, Julian Lange, Frédéric Baudat, Maria Jasin, and Scott Keeney. 2013. “Numerical Constraints and Feedback Control of Double-Strand Breaks in Mouse Meiosis.” *Genes and Development* 27 (8): 873–86.

Kaur, Hardeep, Arnaud DeMuyt, and Michael Lichten. 2015. “Top3-Rmi1 DNA Single-Strand Decatenase Is Integral to the Formation and Resolution of Meiotic Recombination Intermediates.” *Molecular Cell* 57 (4): 583–94.

Keeney. 1997. “Meiosis-Specific DNA Double-Strand Breaks Are Catalyzed by Spo11, a Member of a Widely Conserved Protein Family.” *Cell* 88 (3): 375–84.

Keeney, S, and M J Neale. 2006. “Initiation of Meiotic Recombination by Formation of DNA Double-Strand Breaks: Mechanism and Regulation.” *Biochemical Society Transactions* 34 (Pt 4): 523–25.

Keeney, Scott, Julian Lange, and Neeman Mohibullah. 2014. “Self-Organization of Meiotic Recombination Initiation: General Principles and Molecular Pathways.” *Annual Review of Genetics* 48 (1): 187–214.

Keogh, Michael Christopher, Jung Ae Kim, Michael Downey, Jeffrey Fillingham, Dipanjan Chowdhury, Jacob C. Harrison, Megumi Onishi, et al. 2006. “A Phosphatase Complex That Dephosphorylates ΓH2AX Regulates DNA Damage Checkpoint Recovery.” *Nature* 439 (7075): 497–501.

Kerk, D., G. Templeton, and G. B.G. Moorhead. 2008. “Evolutionary Radiation Pattern of Novel Protein Phosphatases Revealed by Analysis of Protein Data from the Completely Sequenced Genomes of Humans, Green Algae, and Higher Plants.” *Plant Physiology* 146 (2): 351–67.

Kim, J.-A., W. M. Hicks, J. Li, S. Y. Tay, and J. E. Haber. 2011. “Protein Phosphatases Pph3, Ptc2, and Ptc3 Play Redundant Roles in DNA Double-Strand Break Repair by Homologous Recombination.” *Molecular and Cellular Biology* 31 (3): 507–16.

Kim, Keun P., Beth M. Weiner, Liangran Zhang, Amy Jordan, Job Dekker, and Nancy Kleckner. 2010. “Sister Cohesion and Structural Axis Components Mediate Homolog Bias of Meiotic Recombination.” *Cell* 143 (6): 924–37.

Kim, Yonghwan. 2014. “Nuclease Delivery: Versatile Functions of SLX4/FANCP in Genome Maintenance.” *Molecules and Cells* 37 (8): 569–74.

Kitajima, Tomoya S., Shigehiro A. Kawashima, and Yoshinori Watanabe. 2004. “The Conserved Kinetochore Protein Shugoshin Protects Centromeric Cohesion during Meiosis.” *Nature* 427 (6974): 510–17.

Kitajima, Tomoya S., Yousuke Miyazaki, Masayuki Yamamoto, and Yoshinori Watanabe. 2003. “Rec8 Cleavage by Separase Is Required for Meiotic Nuclear Divisions in Fission Yeast.” *EMBO Journal* 22 (20): 5643–53.

Kitajima, Tomoya S., Takeshi Sakuno, Kei Ichiro Ishiguro, Shun Ichiro Iemura, Tohru Natsume, Shigehiro A. Kawashima, and Yoshinori Watanabe. 2006. “Shugoshin Collaborates with Protein Phosphatase 2A to Protect Cohesin.” *Nature* 441 (1): 46–52.

Kleckner, N., D. Zickler, G. H. Jones, J. Dekker, R. Padmore, J. Henle, and J. Hutchinson. 2004. “A Mechanical Basis for Chromosome Function.” *Proceedings of the National Academy of Sciences* 101 (34): 12592–97.

Kleckner, Nancy. 1996. “Meiosis : How Could It Work ?” *Proceedings of the National Academy of Sciences* 93 (16): 8167–74.

Kleckner, Nancy. 2006. “Chiasma Formation: Chromatin/Axis Interplay and the Role(s) of the Synaptonemal Complex.” *Chromosoma* 115 (3): 175–94.

Kohl, Kathryn P., and Jeff Sekelsky. 2013. “Meiotic and Mitotic Recombination in Meiosis.” *Genetics* 194 (2): 327–34.

Kong, Augustine, Gudmar Thorleifsson, Daniel F. Gudbjartsson, Gisli Masson, Asgeir Sigurdsson, Aslaug Jonasdottir, G. Bragi Walters, et al. 2010. “Fine-Scale Recombination Rate Differences between Sexes, Populations and Individuals.” *Nature* 467 (7319): 1099–1103.

Kong, Augustine, Gudmar Thorleifsson, Hreinn Stefansson, Gisli Masson, Agnar Helgason, Daniel F. Gudbjartsson, Gudrun M. Jonsdottir, et al. 2008. “Sequence Variants in the RNF212 Gene Associate with Genome-Wide Recombination Rate.” *Science* 319 (5868): 1398–1401.

Kumar, Rajeev, Henri Marc Bourbon, and Bernard De Massy. 2010. “Functional Conservation of Mei4 for Meiotic DNA Double-Strand Break Formation from Yeasts to Mice.” *Genes and Development* 24 (12): 1266–80.

Kurzbauer, M.-T., C. Uanschou, D. Chen, and P. Schlogelhofer. 2012. “The Recombinases DMC1 and RAD51 Are Functionally and Spatially Separated during Meiosis in Arabidopsis.” *The Plant Cell* 24 (5): 2058–70.

Lam, Isabel, and Scott Keeney. 2015. “Mechanism and Control of Meiotic Recombination Initiation.” *Cold Spring Harb Perspet Biol* 52: 1–53.

Lambing, Christophe, F. Chris H. Franklin, and Chung-Ju Rachel Wang. 2017. “Understanding and Manipulating Meiotic Recombination in Plants.” *Plant Physiology* 173 (3): 1530–42.

Lambing, Christophe, and Stefan Heckmann. 2018. “Tackling Plant Meiosis: From Model Research to Crop Improvement.” *Frontiers in Plant Science* 9 (829): 1–15.

Lambing, Christophe, Kim Osman, Komsun Nuntasoontorn, Allan West, James D. Higgins, Gregory P. Copenhaver, Jianhua Yang, et al. 2015. “Arabidopsis PCH2 Mediates Meiotic Chromosome Remodeling and Maturation of Crossovers.” *PLoS Genetics* 11 (7): 1–27.

Lange, Julian, Jing Pan, Francesca Cole, Michael P. Thelen, Maria Jasin, and Scott Keeney. 2011. “ATM Controls Meiotic Double-Strand-Break Formation.” *Nature* 479 (7372): 237–40.

Lhuissier, F. G.P., H. H. Offenberg, P. E. Wittich, N. O.E. Vischer, and C. Heyting. 2007. “The Mismatch Repair Protein MLH1 Marks a Subset of Strongly Interfering Crossovers in Tomato.” *The Plant Cell Online* 19 (3): 862–76.

Li, Wuxing, Changbin Chen, Ullrich Markmann-Mulisch, Ljudmilla Timofejeva, Elmon Schmelzer, Hong Ma, and Bernd Reiss. 2004. “The Arabidopsis AtRAD51 Gene Is Dispensable for Vegetative Development but Required for Meiosis.” *Proceedings of the National Academy of Sciences* 101 (29): 10596–601.

Lillo, Cathrine, Amr R.A. Kataya, Behzad Heidari, Maria T. Creighton, Dugassa Nemie-Feyissa, Zekarias Ginbot, and Else M. Jonassen. 2014. “Protein Phosphatases PP2A, PP4 and PP6: Mediators and Regulators in Development and Responses to Environmental Cues.” *Plant Cell and Environment* 37 (12): 2631–48.

Lindner, Heike, Michael T. Raissig, Christian Sailer, Hiroko Shimosato-Asano, Rémy Bruggmann, and Ueli Grossniklaus. 2012. “SNP-Ratio Mapping (SRM): Identifying Lethal Alleles and Mutations in Complex Genetic Backgrounds by next-Generation Sequencing.” *Genetics* 191 (4): 1381–86.

Lister, Lisa Martine, Anna Kouznetsova, Louise Ann Hyslop, Dimitrios Kalleas, Sarah Louise Pace, Jaclyn Catharina Barel, Abinaya Nathan, et al. 2010. “Age-Related Meiotic Segregation Errors in Mammalian Oocytes Are Preceded by Depletion of Cohesin and Sgo2.” *Current Biology* 20 (17): 1511–21.

Lister, Ryan, Brian D. Gregory, and Joseph R. Ecker. 2009. “Next Is Now: New Technologies for Sequencing of Genomes, Transcriptomes, and Beyond.” *Current Opinion in Plant Biology* 12 (2): 107–18.

Lorenz, Alexander, Fekret Osman, Weili Sun, Saikat Nandi, Roland Steinacher, and Matthew C. Whitby. 2012. “The Fission Yeast FANCM Ortholog Directs Non-Crossover Recombination during Meiosis.” *Science* 336 (6088): 1585–88.

los Santos, Teresa De, Neil Hunter, Cindy Lee, Brittany Larkin, Josef Loidl, and Nancy M. Hollingsworth. 2003. “The MUS81/MMS4 Endonuclease Acts Independently of Double-Holliday Junction Resolution to Promote a Distinct Subset of Crossovers during Meiosis in Budding Yeast.” *Genetics* 164 (1): 81–94.

Los Santos, Teresa De, Josef Loidl, Brittany Larkin, and Nancy M. Hollingsworth. 2001. “A Role for MMS4 in the Processing of Recombination Intermediates during Meiosis in Saccharomyces Cerevisiae.” *Genetics* 159 (4): 1511–25.

Love, Michael I., Simon Anders, Vladislav Kim, and Wolfgang Huber. 2016. “RNA-Seq Workflow: Gene-Level Exploratory Analysis and Differential Expression.” *F1000Research* 4: 1070.

Love, Michael I., Wolfgang Huber, and Simon Anders. 2014. “Moderated Estimation of Fold Change and Dispersion for RNA-Seq Data with DESeq2.” *Genome Biology* 15 (12): 1–21.

Lynn, Audrey, Rachel Soucek, and G. Valentin Börner. 2007. “ZMM Proteins during Meiosis: Crossover Artists at Work.” *Chromosome Research* 15 (5): 591–605.

Macaisne, N., J. Vignard, and R. Mercier. 2011. “SHOC1 and PTD Form an XPF-ERCC1-like Complex That Is Required for Formation of Class I Crossovers.” *Journal of Cell Science* 124 (16): 2687–91.

Macaisne, Nicolas, Maria Novatchkova, Lucie Peirera, Daniel Vezon, Sylvie Jolivet, Nicole Froger, Liudmila Chelysheva, Mathilde Grelon, and Raphaël Mercier. 2008. “SHOC1, an XPF Endonuclease-Related Protein, Is Essential for the Formation of Class I Meiotic Crossovers.” *Current Biology* 18 (18): 1432–37.

Makrantoni, Vasso, and Adèle L. Marston. 2018. “Cohesin and Chromosome Segregation.” *Current Biology* 28 (12): R688–R693.

Malik, Shehre Banoo, Marilee A. Ramesh, Alissa M. Hulstrand, and John M. Logsdon. 2007. “Protist Homologs of the Meiotic Spo11 Gene and Topoisomerase VI Reveal an Evolutionary History of Gene Duplication and Lineage-Specific Loss.” *Molecular Biology and Evolution* 24 (12): 2827–41.

Manning, G, G D Plowman, T Hunter, and S Sudarsanam. 2002. “Evolution of Protein Kinase Signaling from Yeast to Man.” *Trends in Biochemical Sciences* 27 (10): 514–20.

Marston, Adele L. 2014. “Chromosome Segregation in Budding Yeast: Sister Chromatid Cohesion and Related Mechanisms.” *Genetics* 196 (1): 31–63.

Massy, Bernard de. 2013. “Initiation of Meiotic Recombination: How and Where? Conservation and Specificities Among Eukaryotes.” *Annual Review of Genetics* 47 (1): 563–99.

Matos, Joao, Miguel G. Blanco, Sarah Maslen, J. Mark Skehel, and Stephen C. West. 2011. “Regulatory Control of the Resolution of DNA Recombination Intermediates during Meiosis and Mitosis.” *Cell* 147 (1): 158–72.

Matos, Joao, and Stephen C. West. 2014. “Holliday Junction Resolution: Regulation in Space and Time.” *DNA Repair* 19: 176–81.

Matsuoka, Shuhei, Bryan A Ballif, Agata Smogorzewska, E Robert Mcdonald iii, Kristen E Hurov, Ji Luo, Corey E Bakalarski, et al. 2007. “ATM and ATR Substrate Analysis Reveals Extensive Protein Network Responsive to DNA Damage.” *Science* 316 (May): 1160–67.

Matsuoka, Shuhei, Mingxia Huang, and Stephen J. Elledge. 1998. “Linkage of ATM to Cell Cycle Regulation by the Chk2 Protein Kinase.” *Science* 282 (5395): 1893–97.

Mazina, Olga M., Alexander V. Mazin, Takuro Nakagawa, Richard D. Kolodner, and Stephen C. Kowalczykowski. 2004. “Saccharomyces Cerevisiae Mer3 Helicase Stimulates 3′-5′ Heteroduplex Extension by Rad51: Implications for Crossover Control in Meiotic Recombination.” *Cell* 117 (1): 47–56.

Mcpeek, Mary Sara, and Terence P Speed. 1995. “Modeling Interference in Genetic Recombination” 1044: 1031–44.

Melamed-Bessudo, Cathy, Elizabeth Yehuda, Antoine R. Stuitje, and Avraham A. Levy. 2005. “A New Seed-Based Assay for Meiotic Recombination in Arabidopsis Thaliana.” *Plant Journal* 43 (3): 458–66.

Mendoza, Michelle C, Fei Du, Negin Iranfar, Nan Tang, Hui Ma, William F Loomis, and Richard A Firtel. 2005. “Loss of SMEK , a Novel , Conserved Protein , Suppresses Mek1 Null Cell Polarity , Chemotaxis , and Gene Expression Defects.” *Molecular and Cellular Biology* 25 (17): 7839–53.

Mercier, Raphaël, Sylvie Jolivet, Daniel Vezon, Emelyne Huppe, Liudmila Chelysheva, Maité Giovanni, Fabien Nogué, et al. 2005. “Two Meiotic Crossover Classes Cohabit in Arabidopsis: One Is Dependent on MER3, Whereas the Other One Is Not.” *Current Biology* 15 (8): 692–701.

Mercier, Raphaël, Christine Mézard, Eric Jenczewski, Nicolas Macaisne, and Mathilde Grelon. 2015. “The Molecular Biology of Meiosis in Plants.” *Annual Review of Plant Biology* 66 (1): 297–327.

Mézard, Christine, Marina Tagliaro Jahns, and Mathilde Grelon. 2015. “Where to Cross? New Insights into the Location of Meiotic Crossovers.” *Trends in Genetics* 31 (7): 393–401.

Mohibullah, Neeman, and Scott Keeney. 2017. “Numerical and Spatial Patterning of Yeast Meiotic DNA Breaks by Tel1.” *Genome Research* 27 (2): 278–88.

Moorhead, Greg B. G., Veerle De Wever, George Templeton, and David Kerk. 2009. “Evolution of Protein Phosphatases in Plants and Animals.” *Biochemical Journal* 417 (2): 401–9.

Moorhead, Greg B. G., Laura Trinkle-Mulcahy, and Annegret Ulke-Lemée. 2007. “Emerging Roles of Nuclear Protein Phosphatases.” *Nature Reviews Molecular Cell Biology* 8 (3): 234–44.

Mukherjee, Sucheta, William Douglass Wright, Kirk Tevebaugh Ehmsen, and Wolf Dietrich Heyer. 2014. “The Mus81-Mms4 Structure-Selective Endonuclease Requires Nicked DNA Junctions to Undergo Conformational Changes and Bend Its DNA Substrates for Cleavage.” *Nucleic Acids Research* 42 (10): 6511–22.

Murakami, H., and S. Keeney. 2008. “Regulating the Formation of DNA Double-Strand Breaks in Meiosis.” *Genes & Development* 22 (3): 286–92.

Murakami, Hajime, and Scott Keeney. 2014a. “DDK Links Replication and Recombination in Meiosis.” *Cell Cycle* 13 (23): 3621–22.

Murakami, Hajime, and Scott Keeney. 2014b. “Temporospatial Coordination of Meiotic Dna Replication and Recombination via DDK Recruitment to Replisomes.” *Cell* 158 (4): 861–73.

Murashige, T and F. Skoog. 1962. “A revised medium for rapid growth and bioassays with tobacco tissue cultures.” *Plant Physiology* 15: 473-97.

Murayama, Yasuto, Yasuhiro Tsutsui, and Hiroshi Iwasaki. 2011. “The Fission Yeast Meiosis-Specific Dmc1 Recombinase Mediates Formation and Branch Migration of Holliday Junctions by Preferentially Promoting Strand Exchange in a Direction Opposite to That of Rad51.” *Genes and Development* 25 (5): 516–27.

Muyt, Arnaud De, Lea Jessop, Elizabeth Kolar, Anuradha Sourirajan, Jianhong Chen, Yaron Dayani, and Michael Lichten. 2012. “BLM Helicase Ortholog Sgs1 Is a Central Regulator of Meiotic Recombination Intermediate Metabolism.” *Molecular Cell* 46 (1): 43–53.

Muyt, Arnaud De, Lucie Pereira, Daniel Vezon, Liudmila Chelysheva, Ghislaine Gendrot, Aurélie Chambon, Sandrine Lainé-Choinard, et al. 2009. “A High Throughput Genetic Screen Identifies New Early Meiotic Recombination Functions in *Arabidopsis thaliana*.” *PLoS Genetics* 5 (9): e1000654.

Muyt, Arnaud De, Alexandra Pyatnitskaya, Jessica Andréani, Lepakshi Ranjha, Claire Ramus, Raphaëlle Laureau, Ambra Fernandez-Vega, et al. 2018. “A Meiotic XPF–ERCC1-like Complex Recognizes Joint Molecule Recombination Intermediates to Promote Crossover Formation.” *Genes and Development* 32 (3–4): 283–96.

Muyt, Arnaud De, Daniel Vezon, Ghislaine Gendrot, Jean Luc Gallois, Rebecca Stevens, and Mathilde Grelon. 2007. “AtPRD1 Is Required for Meiotic Double Strand Break Formation in *Arabidopsis thaliana*.” *EMBO Journal* 26 (18): 4126–37.

Myers, S. 2005. “A Fine-Scale Map of Recombination Rates and Hotspots Across the Human Genome.” *Science* 310 (5746): 321–24.

Nabeshima, Kentaro, Anne M. Villeneuve, and Kenneth J. Hillers. 2004. “Chromosome-Wide Regulation of Meiotic Crossover Formation in *Caenorhabditis elegans* Requires Properly Assembled Chromosome Axes.” *Genetics* 168 (3): 1275–92.

Nagaoka, So I., Terry J. Hassold, and Patricia A. Hunt. 2012. “Human Aneuploidy: Mechanisms and New Insights into an Age-Old Problem.” *Nature Reviews Genetics* 13 (7): 493–504.

Nakada, Shinichiro, Ginny I. Chen, Anne Claude Gingras, and Daniel Durocher. 2008. “PP4 Is a ΓH2AX Phosphatase Required for Recovery from the DNA Damage Checkpoint.” *EMBO Reports* 9 (10): 1019–26.

Nakagawa, Takuro, Hernan Flores-Rozas, and Richard D. Kolodner. 2001. “The MER3 Helicase Involved in Meiotic Crossing Over Is Stimulated by Single-Stranded DNA-Binding Proteins and Unwinds DNA in the 3′ to 5′ Direction.” *Journal of Biological Chemistry* 276 (34): 31487–93.

Nakagawa, Takuro, and Richard D Kolodner. 2002. “Saccharomyces Cerevisiae Mer3 Is a DNA Helicase Involved in Meiotic Crossing Over Saccharomyces Cerevisiae Mer3 Is a DNA Helicase Involved in Meiotic Crossing Over.” *Molecular and Cellular Biology* 22 (10): 3281–91.

Nasmyth, Kim. 2005. “How Do so Few Control so Many?” *Cell* 120 (6): 739–46.

Nasmyth, Kim, and Christian H. Haering. 2005. “The Structure and Function of Smc and Kleisin Complexes.” *Annual Review of Biochemistry* 74 (1): 595–648.

Neale, Matthew J., and Scott Keeney. 2006. “Clarifying the Mechanics of DNA Strand Exchange in Meiotic Recombination.” *Nature* 442 (7099): 153–58.

Neale, Matthew J., Jing Pan, and Scott Keeney. 2005. “Endonucleolytic Processing of Covalent Protein-Linked DNA Double-Strand Breaks.” *Nature* 436 (7053): 1053–57.

Neff, M M, J D Neff, J Chory, and A E Pepper. 1998. “DCAPS, a Simple Technique for the Genetic Analysis of Single Nucleotide Polymorphisms: Experimental Applications in Arabidopsis Thalianagenetics.” *Plant J* 14 (February): 387–92.

Oh, Steve D., Jessica P. Lao, Patty Yi Hwa Hwang, Andrew F. Taylor, Gerald R. Smith, and Neil Hunter. 2007. “BLM Ortholog, Sgs1, Prevents Aberrant Crossing-over by Suppressing Formation of Multichromatid Joint Molecules.” *Cell* 130 (2): 259–72.

Oh, Steve D., Jessica P. Lao, Andrew F. Taylor, Gerald R. Smith, and Neil Hunter. 2008. “RecQ Helicase, Sgs1, and XPF Family Endonuclease, Mus81-Mms4, Resolve Aberrant Joint Molecules during Meiotic Recombination.” *Molecular Cell* 31 (3): 324–36.

Osman, Fekret, Julie Dixon, Claudette L. Doe, and Matthew C. Whitby. 2003. “Generating Crossovers by Resolution of Nicked Holliday Junctions: A Role for Mus81-Eme1 in Meiosis.” *Molecular Cell* 12 (3): 761–74.

Osman, Kim, James D Higgins, Eugenio Sanchez-Moran, Susan J Armstrong, and F Chris H Franklin. 2011. “Pathways to Meiotic Recombination in *Arabidopsis thaliana*.” *New Phytologist* 190 (3): 523–44.

Osman, Kim, Jianhua Yang, Elisabeth Roitinger, Christophe Lambing, Stefan Heckmann, Elaine Howell, Maria Cuacos, et al. 2018. “Affinity Proteomics Reveals Extensive Phosphorylation of the Brassica Chromosome Axis Protein ASY1 and a Network of Associated Proteins at Prophase I of Meiosis.” *Plant Journal* 93 (1): 17–33.

Ossowski, Stephan, Korbinian Schneeberger, Richard M Clark, Christa Lanz, Norman Warthmann, and Detlef Weigel. 2008. “Sequencing of Natural Strains of *Arabidopsis Thaliana* with Short Reads.” *Genome Res.* 18: 2024–33.

Ossowski, Stephan, Korbinian Schneeberger, José Ignacio Lucas-lledó, Richard M Clark, Ruth G Shaw, Detlef Weigel, Michael Lynch, and Norman Warthmann. 2010. “The Rate and Molecular Spectrum of Spontaneous Mutations in *Arabidopsis thaliana*.” *Science* 327 (5961): 92–94.

Page, Damian R., and Ueli Grossniklaus. 2002. “The Art and Design of Genetic

Screens: *Arabidopsis thaliana*." *Nature Reviews Genetics* 3 (2): 124–36.

Page, Scott L., and R. Scott Hawley. 2004. "The Genetics and Molecular Biology of the Synaptonemal Complex." *Annual Review of Cell and Developmental Biology* 20 (1): 525–58.

Pan, Jing, Mariko Sasaki, Ryan Kniewel, Hajime Murakami, Hannah G. Blitzblau, Sam E. Tischfield, Xuan Zhu, et al. 2011. "A Hierarchical Combination of Factors Shapes the Genome-Wide Topography of Yeast Meiotic Recombination Initiation." *Cell* 144 (5): 719–31.

Panizza, Silvia, Marco A. Mendoza, Marc Berlinger, Lingzhi Huang, Alain Nicolas, Katsuhiko Shirahige, and Franz Klein. 2011. "Spo11-Accessory Proteins Link Double-Strand Break Sites to the Chromosome Axis in Early Meiotic Recombination." *Cell* 146 (3): 372–83.

Parvanov, Emil D., Petko M. Petkov, and Kenneth Paigen. 2010. "Prdm9 Controls Activation of Mammalian Recombination Hotspots." *Science* 327 (5967): 835.

Parvanov, Emil D., Hui Tian, Timothy Billings, Ruth L. Saxl, Catrina Spruce, Rakesh Aithal, Lumir Krejci, Kenneth Paigen, and Petko M. Petkov. 2017. "PRDM9 Interactions with Other Proteins Provide a Link between Recombination Hotspots and the Chromosomal Axis in Meiosis." *Molecular Biology of the Cell* 28 (3): 488–99.

Patro, Rob, Geet Duggal, Michael I. Love, Rafael A. Irizarry, and Carl Kingsford. 2017. "Salmon Provides Fast and Bias-Aware Quantification of Transcript Expression." *Nature Methods* 14 (4): 417–19.

Penkner, Alexandra, Zsuzsanna Portik-Dobos, Lois Tang, Ralf Schnabel, Maria Novatchkova, Verena Jantsch, and Josef Loidl. 2007. "A Conserved Function for a *Caenorhabditis elegans* Com1/Sae2/CtIP Protein Homolog in Meiotic Recombination." *EMBO Journal* 26 (24): 5071–82.

Pérez-Callejón, Encarna, Antonio Casamayor, Gemma Pujol, Elisabet Clua, Albert Ferrer, and Joaquín Ariño. 1993. “Identification and Molecular Cloning of Two Homologues of Protein Phosphatase X from *Arabidopsis thaliana*.” *Plant Molecular Biology* 23 (6): 1177–85.

Peters, Janny L., Filip Cnudde, and Tom Gerats. 2003. “Forward Genetics and Map-Based Cloning Approaches.” *Trends in Plant Science* 8 (10): 484–91.

Pradillo, Mónica, Javier Varas, Cecilia Oliver, and Juan L. Santos. 2014. “On the Role of AtDMC1, AtRAD51 and Its Paralogs during Arabidopsis Meiosis.” *Frontiers in Plant Science* 5 (February): 1–13.

Puizina, J., Jiri Siroky, Petr Mokros, Dieter Schweizer, and Karel Riha. 2004. “Mre11 Deficiency in Arabidopsis Is Associated with Chromosomal Instability in Somatic Cells and Spo11-Dependent Genome Fragmentation during Meiosis.” *The Plant Cell Online* 16 (8): 1968–78.

Pujol, G., T. I. Baskin, A. Casamayor, N. Cortadellas, A. Ferrer, and J. Ariño. 2000. “The Arabidopsis Thaliana PPX/PP4 Phosphatases: Molecular Cloning and Structural Organization of the Genes and Immunolocalization of the Proteins to Plastids.” *Plant Molecular Biology* 44 (4): 499–511.

Qiao, Huanyu, H. B.D. Prasada Rao, Ye Yang, Jared H. Fong, Jeffrey M. Cloutier, Dekker C. Deacon, Kathryn E. Nagel, et al. 2014. “Antagonistic Roles of Ubiquitin Ligase HEI10 and SUMO Ligase RNF212 Regulate Meiotic Recombination.” *Nature Genetics* 46 (2): 194–99.

Ramesh, Marilee A., Shehre Banoo Malik, and John M. Logsdon. 2005. “A PhylogenomicInventory of MeioticGenes: Evidence for Sex in Giardia and an Early Eukaryotic Origin of Meiosis.” *Current Biology* 15: 185–91.

Ranjha, Lepakshi, Roopesh Anand, and Petr Cejka. 2014. “The Saccharomyces Cerevisiae Mlh1-Mlh3 Heterodimer Is an Endonuclease That Preferentially Binds to Holliday Junctions.” *Journal of Biological Chemistry* 289 (9): 5674–86.

Reynolds, April, Huanyu Qiao, Ye Yang, Jefferson K. Chen, Neil Jackson, Kajal Biswas, J. Kim Holloway, et al. 2013. “RNF212 Is a Dosage-Sensitive Regulator of Crossing-over during Mammalian Meiosis.” *Nature Genetics* 45 (3): 269–78.

Rogacheva, Maria V., Carol M. Manhart, G. Chen, Alba Guarne, Jennifer Surtees, and Eric Alani. 2014. “Mlh1-Mlh3, a Meiotic Crossover and DNA Mismatch Repair Factor,Is a Msh2-Msh3-Stimulated Endonuclease.” *Journal of Biological Chemistry* 289 (9): 5664–73.

Roitinger, Elisabeth, Manuel Hofer, Thomas Kocher, Peter Pichler, Maria Novatchkova, Jianhua Yang, Peter Schlogelhofer, and Karl Mechtler. 2015. “Quantitative Phosphoproteomics of the ATM and ATR Dependent DNA Damage Response in Arabidopsis Thaliana.” *Molecular & Cellular Proteomics* 301: 1–36.

Ross, K. J., P. Fransz, S. J. Armstrong, I. Vizir, B. Mulligan, F. C.H. Franklin, and G. H. Jones. 1997. “Cytological Characterization of Four Meiotic Mutants of Arabidopsis Isolated from T-DNA-Transformed Lines.” *Chromosome Research* 5 (8): 551–59.

Ross, K. J., P. Fransz, and G. H. Jones. 1996. “A Light Microscopic Atlas of Meiosis InArabidopsis Thaliana.” *Chromosome Research* 4 (7): 507–16.

Salomé, P. A., K. Bomblies, J. Fitz, R. A.E. Laitinen, N. Warthmann, L. Yant, and D. Weigel. 2012. “The Recombination Landscape in *Arabidopsis thaliana* F2 populations.” *Heredity* 108 (4): 447–55.

Šamanić, Ivica, Juraj Simunić, Karel Riha, and Jasna Puizina. 2013. “Evidence for Distinct Functions of MRE11 in Arabidopsis Meiosis.” *PLoS One* 8 (10): e78760.

Sanchez-Moran, Eugenio, Juan Luis Santos, Gareth H. Jones, and F. Christopher H Franklin. 2007. “ASY1 Mediates AtDMC1-Dependent Interhomolog Recombination during Meiosis in Arabidopsis.” *Genes and Development*

21 (17): 2220–33.

Sato-Carlton, Aya, Xuan Li, Oliver Crawley, Sarah Testori, Enrique Martinez-Perez, Asako Sugimoto, and Peter M. Carlton. 2014. “Protein Phosphatase 4 Promotes Chromosome Pairing and Synapsis, and Contributes to Maintaining Crossover Competence with Increasing Age.” *PLoS Genetics* 10 (10): e1004638.

Schneeberger, Korbinian. 2009. “SHOREmap : Simultaneous Mapping and Mutation Identification by Deep Sequencing.” *Nature Methods* 6 (8): 550–52.

Schneeberger, Korbinian. 2014. “Using Next-Generation Sequencing to Isolate Mutant Genes from Forward Genetic Screens.” *Nature Reviews Genetics* 15 (10): 662–76.

Schuermann, David, Jean Molinier, Olivier Fritsch, and Barbara Hohn. 2005. “The Dual Nature of Homologous Recombination in Plants.” *Trends in Genetics* 21 (3): 172–81.

Schwacha, Anthony, and Nancy Kleckner. 1997. “Interhomolog Bias during Meiotic Recombination: Meiotic Functions Promote a Highly Differentiated Interhomolog-Only Pathway.” *Cell* 90 (6): 1123–35.

Schwartz, Erin K., and Wolf Dietrich Heyer. 2011. “Processing of Joint Molecule Intermediates by Structure-Selective Endonucleases during Homologous Recombination in Eukaryotes.” *Chromosoma* 120 (2): 109–27.

Séguéla-Arnaud, Mathilde, Wayne Crismani, Cécile Larchevêque, Julien Mazel, Nicole Froger, Sandrine Choinard, Afef Lemhemdi, et al. 2015. “Multiple Mechanisms Limit Meiotic Crossovers: TOP3α and Two BLM Homologs Antagonize Crossovers in Parallel to FANCM.” *Proceedings of the National Academy of Sciences* 112 (15): 4713–18.

Serra, Heïdi, Christophe Lambing, Catherine H. Griffin, Stephanie D. Topp, Divyashree C. Nageswaran, Charles J. Underwood, Piotr A. Ziolkowski, et al.

2018. “Massive Crossover Elevation via Combination of HEI10 and Recq4a Recq4b during Arabidopsis Meiosis.” *Proceedings of the National Academy of Sciences* 115(10): 2437-2442.

Shi, Yigong. 2009. “Serine/Threonine Phosphatases: Mechanism through Structure.” *Cell* 139 (3): 468–84.

Shiloh, Y. 2001. “ATM and ATR: Networking Cellular Responses to DNA Damage.” *Current Opinion in Genetics and Development* 11 (1): 71–77.

Shinohara, A, S Gasior, T Ogawa, N Kleckner, and D K Bishop. 1997. “Saccharomyces Cerevisiae RecA Homologues RAD51 and DMC1 Have Both Distinct and Overlapping Roles in Meiotic Recombination.” *Genes Cells* 2 (10): 615–29.

Shinohara, Akira, Hideyuki Ogawa, and Tomoko Ogawa. 1992. “Rad51 Protein Involved in Repair and Recombination in S. Cerevisiae Is a RecA-like Protein.” *Cell* 69 (3): 457–70.

Shinohara, Miki, Steve D. Oh, Neil Hunter, and Akira Shinohara. 2008. “Crossover Assurance and Crossover Interference Are Distinctly Regulated by the ZMM Proteins during Yeast Meiosis.” *Nature Genetics* 40 (3): 299–309.

Smagulova, Fatima, Ivan V. Gregoretti, Kevin Brick, Pavel Khil, R. Daniel Camerini-Otero, and Galina V. Petukhova. 2011. “Genome-Wide Analysis Reveals Novel Molecular Features of Mouse Recombination Hotspots.” *Nature* 472 (7343): 375–78.

Smith, Gerald R., Michael N. Boddy, Paul Shanahan, and Paul Russell. 2003. “Fission Yeast Mus81·Eme1 Holliday Junction Resolvase Is Required for Meiotic Crossing over but Not for Gene Conversion.” *Genetics* 165 (4): 2289–93.

Smyth, D. R., J.L. Bowman, and E.M. Meyerowitz. 1990. “Early Flower Development

in Arabidopsis." *The Plant Cell Online* 2 (8): 755–67.

Snowden, Timothy, Samir Acharya, Charles Butz, Mark Berardini, and Richard Fishel. 2004. "HMSH4-HMSH5 Recognizes Holliday Junctions and forms a Meiosis-Specific Sliding Clamp that embraces Homologous Chromosomes." *Molecular Cell* 15 (3): 437–51.

Sommermeyer, Vérane, Claire Béneut, Emmanuel Chaplais, Maria Elisabetta Serrentino, and Valérie Borde. 2013. "Spp1, a Member of the Set1 Complex, Promotes Meiotic DSB Formation in Promoters by Tethering Histone H3K4 Methylation Sites to Chromosome Axes." *Molecular Cell* 49 (1): 43–54.

Soneson, Charlotte, Michael I. Love, and Mark D. Robinson. 2016. "Differential Analyses for RNA-Seq: Transcript-Level Estimates Improve Gene-Level Inferences." *F1000Research* 4 (2): 1521.

Stacey, Nicola J., Takashi Kuromori, Yoshitaka Azumi, Gethin Roberts, Christian Breuer, Takuji Wada, Anthony Maxwell, Keith Roberts, and Keiko Sugimoto-Shirasu. 2006. "Arabidopsis SPO11-2 Functions with SPO11-1 in Meiotic Recombination." *Plant Journal* 48 (2): 206–16.

Storlazzi, Aurora, Sophie Tesse, Gwenael Ruprich-Robert, Silvana Gargano, Stefanie Pöggeler, Nancy Kleckner, and Denise Zickler. 2008. "Coupling Meiotic Chromosome Axis Integrity to Recombination." *Genes and Development* 22 (6): 796–809.

Stuitje, Antoine R., Elizabeth C. Verbree, Karin H. Van Der Linden, Elzbieta M. Mietkiewska, Jan-Peter Nap, and Tarcies J. A. Kneppers. 2003. "Seed-Expressed Fluorescent Proteins as Versatile Tools for Easy (Co)Transformation and High-Throughput Functional Genomics in Arabidopsis." *Plant Biotechnology Journal* 1 (4): 301–9.

Sturtevant, A.H. 1913. "The Linear Arrangement of Six Sex-Linked Factors in Drosophila, as Shown by Their Mode of Association." *Journal of Experimental*

Zoology 14: 43–59.

Su, Chuanbin, Ziwei Li, Jinping Cheng, Lei Li, Songxiao Zhong, Li Liu, Yun Zheng, and Binglian Zheng. 2017. “The Protein Phosphatase 4 and SMEK1 Complex Dephosphorylates HYL1 to Promote MiRNA Biogenesis by Antagonizing the MAPK Cascade in Arabidopsis.” *Developmental Cell* 41 (5): 527–539.

Sumiyoshi, Eisuke, Asako Sugimoto, and Masayuki Yamamoto. 2002. “Protein Phosphatase 4 Is Required for Centrosome Maturation in Mitosis and Sperm Meiosis in C. Elegans.” *Journal of Cell Science* 115 (7): 1403–10.

Svendsen, Jennifer M., Agata Smogorzewska, Mathew E. Sowa, Brenda C. O’Connell, Steven P. Gygi, Stephen J. Elledge, and J. Wade Harper. 2009. “Mammalian BTBD12/SLX4 Assembles A Holliday Junction Resolvase and Is Required for DNA Repair.” *Cell* 138 (1): 63–77.

Symington, Lorraine S, Anna H Bizard, Ian D Hickson, Christian Bernd Schiller, Florian Ulrich Seifert, and Christian Linke-winnebeck. 2014. “End Resection at Double-Strand Breaks : Mechanism and Regulation End Resection at Double-Strand Breaks : Mechanism and Regulation.” *Cold Spring Harb Perspect Biol* 6: a016436.

Tanaka, Tomoyuki U. 2005. “Chromosome Bi-Orientation on the Mitotic Spindle.” *Philosophical Transactions of the Royal Society B: Biological Sciences* 360 (1455): 581–89.

Tang, Shangming, Michelle Ka Yan Wu, Ruoxi Zhang, and Neil Hunter. 2015. “Pervasive and Essential Roles of the Top3-Rmi1 Decatenase Orchestrate Recombination and Facilitate Chromosome Segregation in Meiosis.” *Molecular Cell* 57 (4): 607–21.

Thacker, Drew, Neeman Mohibullah, Xuan Zhu, and Scott Keeney. 2014. “Homologue Engagement Controls Meiotic DNA Break Number and Distribution.” *Nature* 510 (7504): 241–46.

Uanschou, Clemens, Tanja Siwiec, Andrea Pedrosa-Harand, Claudia Kerzendorfer, Eugenio Sanchez-Moran, Maria Novatchkova, Svetlana Akimcheva, Alexander Woglar, Franz Klein, and Peter Schlögelhofer. 2007. “A Novel Plant Gene Essential for Meiosis Is Related to the Human CtIP and the Yeast COM1/SAE2 Gene.” *EMBO Journal* 26 (24): 5061–70.

Uhlmann, Frank, and Kim Nasmyth. 1998. “Cohesion between Sister Chromatids Must Be Established during DNA Replication.” *Current Biology* 8 (20): 1095–1102.

Uhrig, R. Glen, Anne Marie Labandera, and Greg B. Moorhead. 2013. “Arabidopsis PPP Family of Serine/Threonine Protein Phosphatases: Many Targets but Few Engines.” *Trends in Plant Science* 18 (9): 505–13.

Underwood, Charles J, Kyuha Choi, Christophe Lambing, Xiaohui Zhao, Heïdi Serra, Filipe Borges, Joe Simorowski, et al. 2018. “Epigenetic Activation of Meiotic Recombination Near *Arabidopsis thaliana* centromeres via Loss of H3K9me2 and Non-CG DNA Methylation.” *Genome Research*, 1–13.

Vignard, Julien, Tanja Siwiec, Liudmila Chelysheva, Nathalie Vrielynck, Florine Gonord, Susan J. Armstrong, Peter Schlögelhofer, and Raphael Mercier. 2007. “The Interplay of RecA-Related Proteins and the MND1-HOP2 Complex during Meiosis in Arabidopsis Thaliana.” *PLoS Genetics* 3 (10): 1894–1906.

Villeneuve, a M, and K J Hillers. 2001. “Whence Meiosis?” *Cell* 106 (6): 647–50.

Vrielynck, Nathalie, A. Chambon, D. Vezon, L. Pereira, L. Chelysheva, A. De Muyt, C. Mézard, C. Mayer, and M. Grelon. 2016. “A DNA Topoisomerase VI – like Complex Initiates Meiotic Recombination.” *Science (New York, NY)* 351 (6276): 939–44.

Walker, James, Hongbo Gao, Jingyi Zhang, Billy Aldridge, Martin Vickers, and James D Higgins. 2018. “Sexual-Lineage-Specific DNA Methylation Regulates

Meiosis in Arabidopsis." *Nature Genetics* 50: 130–37.

Wang, Shunxin, Terry Hassold, Patricia Hunt, Martin A. White, Denise Zickler, Nancy Kleckner, and Liangran Zhang. 2017. "Inefficient Crossover Maturation Underlies Elevated Aneuploidy in Human Female Meiosis." *Cell* 168 (6): 977–989.

Wang, Shunxin, Denise Zickler, Nancy Kleckner, and Liangran Zhang. 2015. "Meiotic Crossover Patterns: Obligatory Crossover, Interference and Homeostasis in a Single Process." *Cell Cycle* 14 (3): 305–14.

Wang, Yi Hong. 2008. "How Effective Is T-DNA Insertional Mutagenesis in Arabidopsis?" *Journal of Biochemical Technology* 1 (1): 11–20.

Wang, Yingxiang, and Gregory P. Copenhaver. 2018. "Meiotic Recombination: Mixing It Up in Plants." *Annual Review of Plant Biology* 69 (1): 577-609.

Watanabe, Yoshinori. 2012. "Geometry and Force behind Kinetochore Orientation: Lessons from Meiosis." *Nature Reviews Molecular Cell Biology* 13 (6): 370–82.

Watanebe, Y, and P Nurse. 1999. "Cohesin Rec8 Is Requires for Reductional Chromosome Segregation Al Meiosis." *Nature* 400 (6743): 461–64.

Waterworth, Wanda M., Cagla Altun, Susan J. Armstrong, Nicola Roberts, Philip J. Dean, Kim Young, Clifford F. Weil, Clifford M. Bray, and Christopher E. West. 2007. "NBS1 Is Involved in DNA Repair and Plays a Synergistic Role with ATM in Mediating Meiotic Homologous Recombination in Plants." *Plant Journal* 52 (1): 41–52.

Weigel, D., and J. Glazebrook. 2006. "EMS Mutagenesis of Arabidopsis Seed." *Cold Spring Harbor Protocols* 2006 (5).

Wijnker, Erik, Geo Velikkakam James, Jia Ding, Frank Becker, Jonas R. Klasen, Vimal Rawat, Beth A. Rowan, et al. 2013. "The Genomic Landscape of Meiotic

Crossovers and Gene Conversions in *Arabidopsis thaliana*." *ELife* 2: e01426.

Wu, Gang, Gabrielle Rossidivito, Tieqiang Hu, Yosef Berlyand, and R. Scott Poethig. 2015. "Traffic Lines: New Tools for Genetic Analysis in *Arabidopsis thaliana*." *Genetics* 200 (1): 35–45.

Yelina, Nataliya E., Kyuha Choi, Liudmila Chelysheva, Malcolm Macaulay, Bastiaan de Snoo, Erik Wijnker, Nigel Miller, et al. 2012. "Epigenetic Remodeling of Meiotic Crossover Frequency in *Arabidopsis thaliana* DNA Methyltransferase Mutants." *PLoS Genetics* 8 (8): e1002844.

Yelina, Nataliya E., Christophe Lambing, Thomas J. Hardcastle, Xiaohui Zhao, Bruno Santos, and Ian R. Henderson. 2015. "DNA Methylation Epigenetically Silences Crossover Hot Spots and Controls Chromosomal Domains of Meiotic Recombination in Arabidopsis." *Genes and Development* 29 (20): 2183–2202.

Yelina, Nataliya E., Piotr A. Ziolkowski, Nigel Miller, Xiaohui Zhao, Krystyna A. Kelly, Daniela F. Muñoz, David J. Mann, Gregory P. Copenhaver, and Ian R. Henderson. 2013. "High-Throughput Analysis of Meiotic Crossover Frequency and Interference via Flow Cytometry of Fluorescent Pollen in *Arabidopsis thaliana*." *Nature Protocols* 8 (11): 2119–34.

Yin, Y., and S. Smolikove. 2013. "Impaired Resection of Meiotic Double-Strand Breaks Channels Repair to Nonhomologous End Joining in Caenorhabditis Elegans." *Molecular and Cellular Biology* 33 (14): 2732–47.

Yokoo, Rayka, Karl A. Zawadzki, Kentaro Nabeshima, Melanie Drake, Swathi Arur, and Anne M. Villeneuve. 2012. "COSA-1 Reveals Robust Homeostasis and Separable Licensing and Reinforcement Steps Governing Meiotic Crossovers." *Cell* 149 (1): 75–87.

Zakharyevich, Kseniya, Yunmei Ma, Shangming Tang, Yi-Hwa Patty Hwang, Serge Boiteux, and Neil Hunter. 2010. "Temporally and Biochemically Distinct Activities of Exo1 during Meiosis: Double-Strand-Break Resection and Resolution of Double-Holliday Junctions." *Mol Cell* 40 (6): 1001–15.

Zakharyevich, Kseniya, Shangming Tang, Yunmei Ma, and Neil Hunter. 2012. “Delineation of Joint Molecule Resolution Pathways in Meiosis Identifies a Crossover-Specific Resolvase.” *Cell* 149 (2): 334–47.

Zamariola, Linda, Choon Lin Tiang, Nico De Storme, Wojtek Pawlowski, and Danny Geelen. 2014a. “Chromosome Segregation in Plant Meiosis.” *Frontiers in Plant Science* 5: 279.

Zamariola, Linda, Nico De Storme, Katrijn Vannerum, Klaas Vandepoele, Susan J. Armstrong, F. Christopher H. Franklin, and Danny Geelen. 2014b. “SHUGOSHINs and PATRONUS Protect Meiotic Centromere Cohesion in *Arabidopsis thaliana*.” *Plant Journal* 77 (5): 782–94.

Zhang, Cheng, Yao Song, Zhi Hao Cheng, Ying Xiang Wang, Jun Zhu, Hong Ma, Ling Xu, and Zhong Nan Yang. 2012. “The *Arabidopsis thaliana* DSB Formation (AtDFO) Gene Is Required for Meiotic Double-Strand Break Formation.” *Plant Journal* 72 (2): 271–81.

Zhang, Liangran, Keun P Kim, Nancy E Kleckner, and Aurora Storlazzi. 2011. “Meiotic Double-Strand Breaks Occur Once per Pair of (Sister) Chromatids and, via Mec1/ATR and Tel1/ATM, Once per Quartet of Chromatids.” *Proceedings of the National Academy of Sciences* 108 (50): 20036–41.

Zhang, Liangran, Zhangyi Liang, John Hutchinson, and Nancy Kleckner. 2014a. “Crossover Patterning by the Beam-Film Model: Analysis and Implications.” *PLoS Genetics* 10 (1): e1004042.

Zhang, Liangran, Shunxin Wang, Shen Yin, Soogil Hong, Keun P. Kim, and Nancy Kleckner. 2014b. “Topoisomerase II Mediates Meiotic Crossover Interference.” *Nature* 511 (7511): 551–56.

Zhang, Xiuren, Rossana Henriques, Shih Shun Lin, Qi Wen Niu, and Nam Hai Chua. 2006. “Agrobacterium-Mediated Transformation of *Arabidopsis thaliana* Using

the Floral Dip Method." *Nature Protocols* 1 (2): 641–46.

Zickler, D., and N. Kleckner. 1999. "Meiotic Chromosomes: Integrating Structure and Function." *Annual Review of Genetics* 33 (1): 603–754.

Zickler, Denise, and Nancy Kleckner. 2015. "Recombination, Pairing, and Synapsis of Homologs during Meiosis." *Cold Spring Harbor Perspectives in Biology* 7(6): a016626.

Ziolkowski, Piotr A., Luke E. Berchowitz, Christophe Lambing, Nataliya E. Yelina, Xiaohui Zhao, Krystyna A. Kelly, Kyuha Choi, et al. 2015. "Juxtaposition of Heterozygous and Homozygous Regions Causes Reciprocal Crossover Remodelling via Interference during Arabidopsis Meiosis." *ELife* 4: e03708.

Ziolkowski, Piotr A., and Ian R. Henderson. 2016. "Interconnections between Meiotic Recombination and Sequence Polymorphism in Plant Genomes." *New Phytologist* 213 (3): 1022–29.

Ziolkowski, Piotr A., Charles J. Underwood, Christophe Lambing, Marina Martinez-Garcia, Emma J. Lawrence, Liliana Ziolkowska, Catherine Griffin, et al. 2017. "Natural Variation and Dosage of the HEI10 Meiotic E3 Ligase Control Arabidopsis Crossover Recombination." *Genes and Development* 31 (3): 306–17.

Zuryn, Steven, Stéphanie Le Gras, Karine Jamet, and Sophie Jarriault. 2010. "A Strategy for Direct Mapping and Identification of Mutations by Whole-Genome Sequencing." *Genetics* 186 (1): 427–30.

Zuryn, Steven, and Sophie Jarriault. 2013. "Deep Sequencing Strategies for Mapping and Identifying Mutations from Genetic Screens." *Worm* 2 (3): e25081.

Appendix

1. Preparation of Reagents

All buffers and solutions were prepared with MilliQ or ddH_2O water. Chemical ingredients were supplied by Sigma-Aldrich and ThermoFisher Scientific.

1.1. DNA extraction for genotyping

Extraction Buffer:

Tris-HCl pH 7.5 - 200 mM

NaCl - 250 mM

EDTA - 25 mM

For Extraction buffer with SDS: 1% SDS

To make 1 L:

1M Tris-HCl pH 7.5 - 200 ml

NaCl - 14.61 g dissolved in MilliQ H_2O

0.5M EDTA - 50 ml

10% SDS - 100 ml

1.2. Nuclear DNA isolation for sequencing library

Nuclear Isolation Buffer:

To make 500 ml:

1M HEPES pH 8.0 - 30 ml

2M Sucrose - 250 ml

1M KCl - 2.5 ml

1M $MgCl_2$ - 2.5 ml

0.5M EDTA - 5 ml

10% Triton X-100 - 30 ml

1.3. High quality DNA extraction using CTAB

CTAB buffer

Adapted from Cold Spring Harbour protocols

To make 10 ml

CTAB (10% in H_2O)	- 3 ml
5M NaCl	- 2.8 ml
0.5M EDTA pH 8.0	- 0.4 ml
1M Tris-HCl	- 1 ml
PVP	- 0.3 g
H_2O	- made up to 10 ml

1.4. Agarose gel electrophoresis buffer

10X TBE

Adapted from Cold Spring Harbour protocols

To make 1L

1M Tris base	- 121.1 g
1M Boric acid	- 61.8 g
0.02M EDTA (Disodium salt)	- 7.4 g

Dissolved in MilliQ H_2O and 1X TBE was diluted from the 10X stock stored at room temperature.

1.5. Pollen sorting buffer

10 mM $CaCl_2$

1 mM KCl

2 mM MES

5% w/v sucrose

To make 1L

1M $CaCl_2$	- 10 ml
1M KCl	- 1 ml
Sucrose	- 50 g
MES	- 0.4 g

Adjusted pH to 6.5 with NaOH and added 10% Triton X-100 before use.

1.6. Cytology

Fixative solution (3:1)

Ethanol (v/v) - 75%

Glacial acetic acid - 25%

Citrate buffer

Citric acid - 44.5 mM

Tris-Sodium citrate - 55.5 mM

To make 10 mL

0.1 M Tris-Sodium citrate - 445 μl (Solution I)

0.1 M citric acid - 555 μl (Solution II)

1 ml of Solution I +II was added to 9 ml of MilliQ water.

Stock digestion medium

Cellulase (Sigma-Aldrich) - 100 mg

Pectolysase (Sigma-Aldrich) - 100 mg

Citrate buffer - 10 ml

Enzyme mix for DAPI-stained acid chromosome spreads

Stock digestion medium - 333 μl

Citrate buffer - 667 μl

DAPI Counterstaining solution

DAPI (Sigma-Aldrich) (1 mg/ml in MilliQ H_2O) - 10 μl

Vectashield mounting medium (Vector) - 1 ml

EM digestion mix for Lipsol chromosome spreads

Cytohelicase - 0.1 g

Sucrose - 0.375 g

PVP - 0.25 g

Adjusted to 25 ml with MilliQ H_2O and filter-sterilized using a 0.2 μm filter.

1% Lipsol

1ml of lipsol (detergent) in 100 ml of MilliQ H_2O.

4% Paraformaldehyde

100 ml of ddH_2O was boiled for 3-4 min in a microwave and 3-4 drops of 1M NaOH was added to the boiled H_2O under fume hood. Then, 4 g of paraformaldehyde (Sigma-Aldrich) was added, immediately closed with a lid and gave a stir. The contents were left still for 15 min to dissolve. Finally, the pH was adjusted to 8.0 with 1M HCl and stored at 4°C up to a month.

1X PBST

1 tablet of PBS (Sigma-Aldrich) in 100 ml of MilliQ H_2O = 1X PBS

0.1% Triton X-100

1% EM block

BSA - 0.1 g

PBST - 10 ml

Filter-sterilized through a 0.2 μm filter.

Alexander's stain solution

Ethanol	- 10 ml
Malachite green (1 % in 95 % Ethanol)	- 1 ml
Fuchsin acid (1 % in MilliQ H_2O)	- 5 ml
Orange G (1 % in MilliQ H_2O)	- 0.5 ml
Phenol	- 5 g
Glacial acetic acid	- 2 ml
Chloral hydrate	- 5 g
Glycerol	- 25 ml
MilliQ H_2O	- 50 ml

2. Vector systems

Table S1. List of vectors used during the study.

Vector	Resistance gene	Size	Purpose
pGEM-T Easy	Kanamycin	3015 bp	Cloning for sanger sequencing
pGREEN0029	Kanamycin	4632 bp	Cloning for Agrobacterium-mediated transformation in Arabidopsis

3. Growth media

All media was prepared with MilliQ water and autoclaved at 15 psi at 121°C for 20 minutes.

3.1. Bacterial media

Adapted from Cold Spring Harbour protocols

LB

To make 1L

Tryptone - 10 g

Yeast extract - 5 g

NaCl - 10 g

Agar - 20 g (for solid medium only)

Adjusted pH to 7.0 and made up the volume to 1L.

Antibiotics stocks

All antibiotics were supplied by Sigma-Aldrich.

For *E.coli* culture

100 mg/ml Kanamycin - 1g

Made up to 10 ml of MilliQ H_2O and filter-sterilized through 0.2 μm filter.

Added 25 μl of 100mg/ml Kanamycin in 50 ml LB broth for growing *E.coli* (DH5α strain) carrying pGEM-T Easy or pGREEN0029 plasmids.

For Agrobacterium culture

10 mg/ml Rifamycin - 0.1 g

100 mg/ml Kanamycin - 1 g

5 mg/ml Tetracycline - 0.05 g

25 mg/ml Gentamycin - 0.25 g

Made up to 10 ml of MilliQ H_2O and filter-sterilized through 0.2 μm filter.

Added 250 μl of 10 mg/ml Rifamycin + 25 μl of 100mg/ml Kanamycin + 50 μl of 5 mg/ml Tetracycline + 50 μl of 25 mg/ml Gentamycin in 50 ml LB broth for growing Agrobacterium (GV3101 strain) carrying pGREEN0029 vector + pSoup (helper plasmid).

SOC medium

Adapted from Cold Spring Harbour protocols

Tryptone - 20 g

Yeast extract - 5 g

NaCl - 0.5 g

MilliQ H_2O - 950 ml

Adjusted pH to 7.0 with 1M NaOH and autoclaved. Then, 20 ml of 1M glucose solution was filter-sterilized using 0.2 μm filter and added to the above contents. Finally, the solution was made up to 1L.

3.2. Plant media

½ MS media (no sucrose)

Murashige and Skoog (Sigma-Aldrich) - 2.2 g

1% Agar - 10.0 g

Made up to 1L with MilliQ H_2O. Adjusted pH to 5.8 with 1M KOH and autoclaved.

Added 500 μl of 100 mg/ml Kanamycin to 1L of ½ MS media (no sucrose) with Agar for the selection of transformants.

4. T-DNA insertion lines

Table S2. List of T-DNA insertion lines used during the study. Wild type (WT) and T-DNA primer pairs distinguished between homozygotes, heterozygotes and wild type individuals for the T-DNA insertion in the gene sequence of interest. In the absence of inserted T-DNA, the WT primer pair was amplified. T-DNA primer pair includes the left border primer (LBP) of the inserted T-DNA and the right primer (RP)

from the gene sequence of interest. In the presence of T-DNA, this primer pair was amplified and was also sequenced to confirm the T-DNA location in the gene of interest.

Line	Gene ID	Allele	WT primer pair	T-DNA primer pair	PCR amplicon size
Atppx-1	At4g26720	GK-651B07	ppx1-F, ppx1-R	ppx1-F, GABI_LB	WT ~750 bp T-DNA ~500 bp
Atppx-2	At5g55260	GK-488H09	ppx2-F, ppx2-R	ppx2-R, GABI_LB	WT ~600 bp T-DNA ~400 bp
Atpp4r2	At5g17070	SALK_093051	pp4r2-F, pp4r2-R	pp4r2-R, LBb1.3	WT ~800 bp T-DNA ~400 bp
Atzip4-2	At5g48390	SALK_068052	zip4-2-F, zip4-2-R	zip4-2-F, LBb1.3	WT ~680 bp T-DNA ~800 bp

5. Primers

Table S3. List of primers for T-DNA genotyping. I used all three primers (F, R and LB) in a single PCR reaction and amplified at an annealing temperature 55°C for 30 seconds.

Primer	Nucleotide sequence (5' to 3')	T_m (°C)
ppx1-F	CCATTTGATACAACATTACGAATCC	63.9
ppx1-R	CTTAAGAACACGACTGAA	50.7
GABI_LB	ATAATAACGCTGCGGACATCTACATTTT	67.5
ppx2-F	ATTTTGTTGACCGAGGTTTTTATT	62.4
ppx2-R	TGATCTGCCACAAGATATGTATGA	63.1
pp4r2-F	TGAAAAACCTTCTCTTTGGGG	64.0
pp4r2-R	TGTTCAACAGATCCTTTTGGC	63.9
LBb1.3	ATTTTGCCGATTTCGGAAC	63.6
zip4-2-F	TTGCTACCTTGGGCTCTCTC	63.4
zip4-2-R	ATTCTGTTCTCGCTTTCCAG	61.0

Table S4. List of dCAPS primers for genotyping. The primer pairs differentiated between WT and mutant lines caused by a single nucleotide change. The amplified PCR products were digested with a restriction enzyme and the cleaved products were recognized on a 3.5 % agarose gel.

Primer	Nucleotide sequence (5' to 3')	T_m (°C)	PCR T_m (°C)	Enzyme	Product size
hcr1-F	CATGAAAGCAGGCAAATCACACGG	73.0	63.0	FokI	WT ~145 bp, mutant ~112 bp
hcr1-R	GAGCCATATTTACGCAAACACTC	63.4			
lcr1-taf4b-F	GATGATGCTTTAGTGACGGTTAGTC	63.7			WT ~114 bp mutant ~147 bp
lcr1-taf4b-R	TTCTGCAGTTTCATATACCGAGGAT	65.5			
lcr1-fan1-F	ATACTCCGGTATTAATCTTTTGCCC	64.7			WT ~ 105 bp mutant ~138 bp
lcr1-fan1-R	AGAGAATTTACTCGGGTCATCGGAT	67.5			
fancm-F	ACAATATATGTTTCGTGCAGGTAAGACATTGGAAG	72.3		MboII	WT ~215 bp, mutant ~180 bp
fancm-R	CACCAATAGATGTTGCGACAAT	63.6			
QRT-F	GATGATGGTAATGTTTATGTTTGAGG	63.1	55.0	AatII	WT ~ 600 bp, mutant ~300 and 400 bp (two bands)
QRT-R	CAAACACGGTTTATGTCTTAAATC	60.2			

Table S5. List of primers for cloning genomic *AtPPX-1*, sequencing and genotyping. The recognition sequences (in bold) of restriction enzymes PstI (CTGCAG) and SmaI (CCCGGG) that form the multiple cloning sites (MCS) of pGREEN0029 vector were added to the primer pair for PCR amplification and cloning of *PPX-1* genomic fragment.

Primer	Nucleotide sequence (5' to 3')	T_m (°C)	PCR T_m (°C)	Purpose
PPX1-F	AAAA**CTGCAG**GCTGTTATCAACCTGACCCTTAGC	76.1	60	Cloning *HCR1/PPX-1* genomic DNA (~4.4 kb)
PPX1-R	TCC**CCCGGG**GTCCTAATGCTTCCCTGTGAATTC	82.9		
PPX1-mid-F1	GCTGTTATCAACCTGACCCTTAGC	65.7	n/a	Sanger sequencing of *HCR1/PPX-1* genomic DNA. Each mid primer sequenced ~500 bp.
PPX1-mid-R1	GCAAGTACAACAGTCCCCACTCT	65.4		
PPX1-mid-F2	ATGTATGTATTAGGATCGCAGGC	62.8		
PPX1-mid-R2	GTATGAGGTTTCGATGGAGCTTCT	65.4		
PPX1-mid-F3	GTGATTATGATTCTCCAGACGCC	65.6		
PPX1-mid-R3	GTCCTTTTAGAGTCTTGAAGTTTG	59.1		
PPX1-mid-F4	CCAAGATCGTTGATGTTGCTAATG	66.2		
PPX1-mid-R4	CTGTCGAATGTATTAAGCTCGT	59.9		
PPX1-mid-F5	AGCTAATTCTCTCTCCTTGGGAAG	63.9		
PPX1-mid-R5	CATAGAACTGCCCATGGATGTC	65.4		
PPX1-mid-F6	TCCATTGGGATAGTTATGTGGT	61.8		
PPX1-mid-F7	GACTTGTCTTTGGAATATTCCGAC	63.6		
PPX1-mid-F8	ACTCCTATTTCACTTATGCTCCAG	61.4		
pGreen-kan-NosT-F	ATCGCCTTCTTGACGAGTT	61.4	55	Selection of transformants. Amplified ~600 bp of the *HCR1*/*PPX-1* transgene.
pGreen-kan-NosT-R	CGATCCCCGGAATTAGAT	61.3		
pGreen-PPX1-LB-F	CCATGCTTTGACTTGTGTATGT	61.5		
pGreen-PPX1-LB-R	CTGACGTATGTGCTTAGCTCAT	60.9		
pGreen-PPX1-RB-F	AGCTCGGAATTAACCCTCACT	62.8		
pGreen-PPX1-RB-R	CTTCAATTCTAGAGCTTGACG	58.4		
FANCM-1F	CTAAGGGTTTCTTCCAAAGAACG	63.7		
FANCM-1R	CAGTAAGAGCCAGTATTCTCAGCT	61.8		
FANCM-2F	GTGTTTGGACTTTTAAGTATCTTTC	58.0		

FANCM-2R	GACTGGCCTTTCAATGTCTTACC	64.7	n/a	Sanger sequencing of *FANCM* genomic DNA.
FANCM-3F	TGAGTTTATTGGTCAAAGTTCAGG	63.0		
FANCM-3R	ACCATGATTGATGCAAGAACACTC	66.1		
FANCM-4F	CTAGAGTAACCACTACGAGAACAGG	61.1		
FANCM-4R	GCACTGTACTTCAATAGGATATAC	55.3		
FANCM-3F-1	CAATCAAGCAATTCGTTCCACGTG	71.1		
FANCM-4F-1	GTGGTATACATCTGCGTTAGATCA	61.7		
FANCM-2R-1	CACCTTGGATGGCAATGTCTG	67.6		
FANCM-2R-2	CTGGAAAGCTGGAGTCTCAGTG	65.3		

Table S6. List of primers for RT-PCR. The primer pairs were amplified at an annealing temperature 58°C, 30 seconds, 26-28 cycles for RT-PCR reactions. *GAPC*, the housekeeping gene was used as control.

Primer	Nucleotide sequence (5' to 3')	T_m (°C)	cDNA ID from NCBI	WT Amplicon size
ppx1-F3	AGCAGGCAAATCACACAGGT	64.7	NM_18806	~122 bp
ppx1-R3	TCCACAACAGCTGAAAGACTCA	64.9		
ppx2-F3	CCGGCAGATTACGCAGGTAT	65.9	NM_124908	~187 bp
ppx2-R3	AGCCCTGATCTGGTCTAGAGT	60.9		
pp4r2-F5	CGACCACGAGTGAGAGTGAG	63.9	NM_001343480	~102 bp
pp4r2-R5	ACGTTGTAGGCAACCGTGAA	65.4		
GAPC-RTF1	CGAGAAAGCTGCTACCTACGAT	63.5	NM_111283	~200 bp
GAPC-RTR1	GTTGTCGTACCATGACACCAAT	63.5		

6. SHOREmap script

FastQC check

A FastQC report was obtained, determined the Phred score (+33 or +64) using Illumina encoding and trimmed the adaptor sequences.

/applications/fastqc/fastqc_v0.11.5/fastqc hcr1.reads1.fq

Trim Adaptors

export PATH=/applications/trim_galore/v0_4_1/:/applications/cutadapt/cutadapt-1.3/bin/:$PATH
/applications/trim_galore/v0_4_1/trim_galore --paired hcr1.reads1.fq hcr1.reads2.fq -a GTCCGC --phred64

SHORE and SHOREmap

1. shore import -v fastq --sample-name=WT420_1 -e shore -a genomic -Qsanger -x hcr1.reads1_val_1.fq.gz -x hcr1. reads2_ val_2.fq.gz -o hcr1/flowcell --rplot

2. shore mapflowcell -f hcr1/flowcell -i /data/public_data/arabidopsis/TAIR_10/TAIR10_chr_all.fa.shore -n 10% -g 7% --cores=24 --rplot

3. shore correct4pe -l hcr1/flowcell/1/sample_hcr1/ -x 300

4. shore merge -m hcr1/flowcell -o hcr1/alignment -p

5. shore consensus -n hcr1 -f /data/public_data/arabidopsis/TAIR_10/TAIR10_chr_all.fa.shore -o hcr1/consensus -m hcr1/ alignment/map.list.xz -a /home/dcn23/hcr1/scoring_matrix_het.txt -g 5 -v -r

6. unxz hcr1/consensus/ConsensusAnalysis/supplementary_data/consensus_summary.txt.xz

7. SHOREmap extract --chrsizes chrSizes.txt --folder SHOREmap_analysis/ --marker hcr1/consensus/ConsensusAnalysis/ quality_variant.txt --consen hcr1/consensus/ConsensusAnalysis/supplementary_data/consensus_summary.txt -verbose

8. gzip hcr1/consensus/ConsensusAnalysis/supplementary_data/consensus_summary.txt

9. SHOREmap backcross --chrsizes chrSizes.txt --marker hcr1/consensus/ConsensusAnalysis/quality_variant.txt --consen SHOREmap_analysis/extracted_consensus_0.txt --folder SHOREmap_analysis -plot-bc --marker-score 40 --marker-freq 0.0 --min-coverage 10 --max-coverage 500 --bg home/meiosis/dcn23/wt-420/WT420_1/consensus/ConsensusAnalysis/quality_variant.txt --bg-cov 1 --bg-freq 0.0 --bg-score 1 -non-EMS --cluster 1 --marker-hit 1 -verbose

10. SHOREmap annotate --chrsizes chrSizes.txt --folder SHOREmap_analysis/ann/ --snp SHOREmap_analysis/SHOREmap_marker.bg_corrected_mh1.0000_ic10_ac500_q40_f0.0_EMS --chrom 1 --start 1000000 --end 28000000 --genome indexs/TAIR10_chr_all.fas.shore --gff ../hcr1/TAIR10_GFF3_genes.gff

11. SHOREmap annotate --chrsizes chrSizes.txt --folder SHOREmap_analysis/ann/ --snp SHOREmap_analysis/SHOREmap_marker.bg_corrected_mh1.0000_ic10_ac500_q40_f0.0_EMS --chrom 2 --start 1000000 --end 18000000 --genome indexs/TAIR10_chr_all.fas.shore --gff ../hcr1/TAIR10_GFF3_genes.gff

12. SHOREmap annotate --chrsizes chrSizes.txt --folder SHOREmap_analysis/ann/ --snp SHOREmap_analysis/SHOREmap_marker.bg_corrected_mh1.0000_ic10_ac500_q40_f0.0_EMS --chrom 3 --start 1000000 --end 22000000 --genome indexs/TAIR10_chr_all.fas.shore --gff ../hcr1/TAIR10_GFF3_genes.gff

13. SHOREmap annotate --chrsizes chrSizes.txt --folder SHOREmap_analysis/ann/ --snp SHOREmap_analysis/SHOREmap_marker.bg_corrected_mh1.0000_ic10_ac500_q40_f0.0_EMS --chrom 4 --start 1000000 --end 18000000 --genome indexs/TAIR10_chr_all.fas.shore --gff ../hcr1/TAIR10_GFF3_genes.gff

14. SHOREmap annotate --chrsizes chrSizes.txt --folder SHOREmap_analysis/ann/ --snp SHOREmap_analysis/SHOREmap_marker.bg_corrected_mh1.0000_ic10_ac500_q40_f0.0_EMS --chrom 5 --start 1000000 --end 26000000 --genome indexs/TAIR10_chr_all.fas.shore --gff ../hcr1/TAIR10_GFF3_genes.gff

7. Supplemental Figures

Figure S1. *FANCM* (At1g35530) nucleotide sequence with identified EMS mutation. The point mutation at genomic position 13092874 bp and exon 15 led to the change in nucleotide G (in green) to A as indicated in the sequence obtained from the TAIR database (https://www.arabidopsis.org). Gene with 5'UTR (in red), start and stop codon (in blue), intron (in violet) and exon (in yellow) are shown.

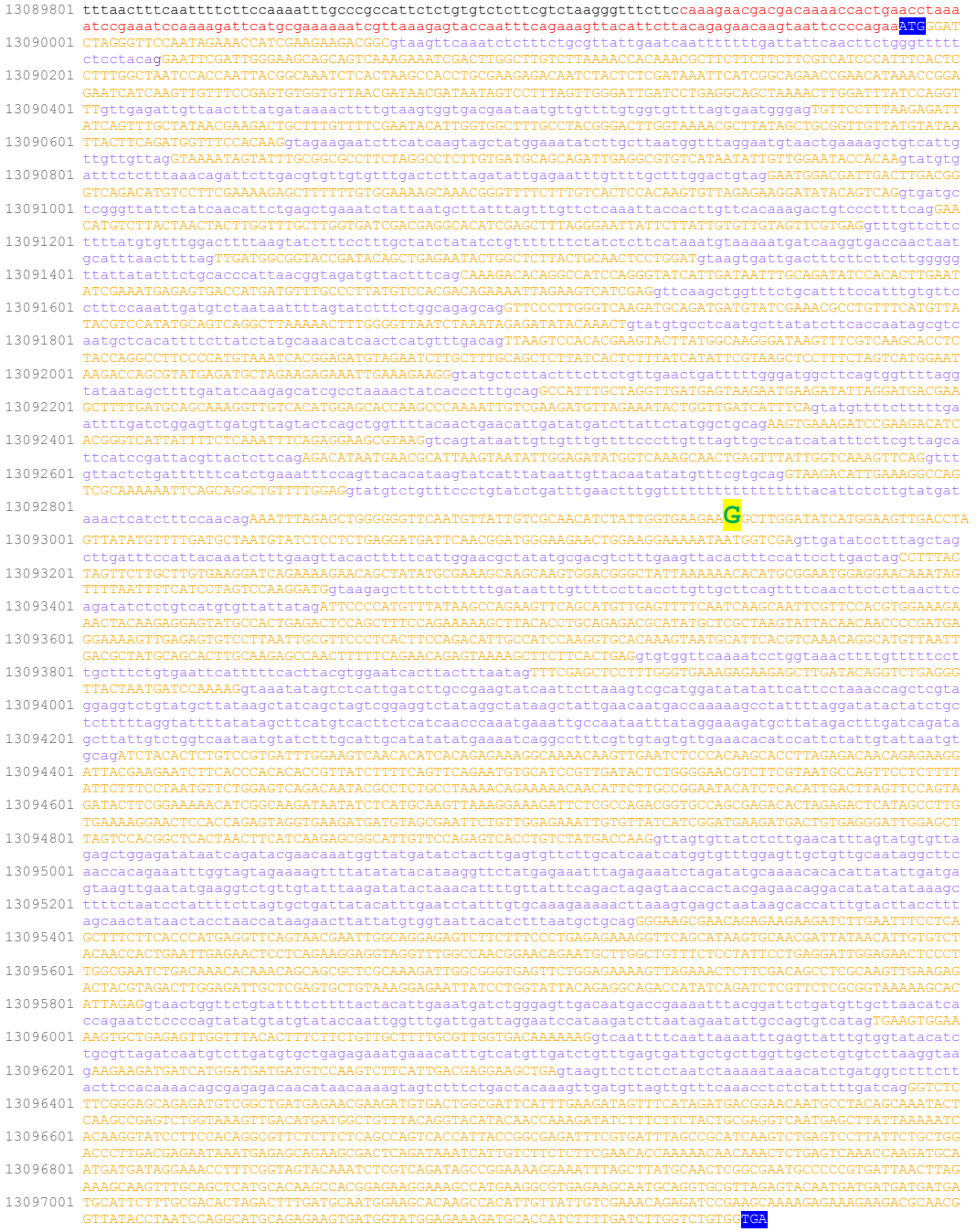

Figure S2. T-DNA nucleotide sequencing of *PPX-1*, *PPX-2* and *PP4R2* genes. Nucleotide sequence from GenBank accessions for *PPX-1* (NM_118806; 2457 bp), *PPX-2* (NM_124908; 2411 bp) and *PP4R2* (NM_121713; 2927 bp) were used for identifying T-DNA position at bp resolution. Nucleotide sequence from the gene (in yellow), T-DNA sequence (in red) and ATG/CAT start codon (in blue) are shown.

> *Atppx-1 or hcr1-2* (GK_651B07)

ATTTTCTTCAGATTTATTGATTAATAAGCTCATAATTCCGAAACCCAGATCGAGAAGTAAGGTAAA
GTAAGAACTTACAGTGACAGGGGCATCAACTCTCTGAACATTACTCTCTTCAACAAGAATTTCCAT
GGCTTTGAGGCAAAGAGCCTTCACCTCCGATTCGCTCAATGGTTCGCATCGCTTAAGCTGCCCT
ATTTGCCGATCTAGGTCTGACATTTTTACCTCTCCTCTCCTCTTCTTCCTCCTTCTATTACTCTTCA
GCCACCGGAAACGATCCTTAATCTGATGAATAAGAAGGAATCAACCAACCCTCGCCAAAAAGAAT
CTGATATTCTCCAAGAAATTGTAAATGGCTTCATGTCCGGGAAATCTACATGGATCAGCAATGAG
TATGATGGTCAATATGGAGAAAAAGAAAGAGTAATTACCAATTTTTTTTCAATTCAAAAATGTAGAT
GTCCGCGGGGTTTATTTATAA

T-DNA insertion position: between 211 and 212 bp position in the 5' prime UTR.

> *Atppx-2* (GK_488H09)

CCTTATGATTGTATTATCACTGTCTCAACCTGGTCTAGAGTCATAATAGCTGGAGAGAGACCTCC
ATGAACACAAAATATCTTGTTCTCGACAAGAGCTGAAAGACTTAGACAAATAAAAGATAGGAAGTT
TCCATTACATTAACCGAAATAATATCTACTCGGAACTCCAAAACAAAAGCAGAAAAAGGGTGTATA
CCTCAAGTAGTCAAAGATATCTGTGCAGTATCTCCAAACATTTACAGAGCCATATTTACGCAGACA
CTCATCATAAAATCCATATATTCAATTGTAAATGGCTTCATGTCCGGGAAATCTACATGGATCAGC
AATGAGTATGATGGTCAATATGGAGAAAAAGAAAGAGTAATTACCAATTTTTTTTCAATTCAAAAAT
GTAGATGTCCGCACGGGTTATTATAACAA

T-DNA insertion position: between 1138 and 1139 bp position at 3' prime end of intron 3.

> *Atpp4r2* (SALK_093051)

AACTCGCTCTTGCATTAGAAAAGGTACGAATTTGAAACTCTTACCTCTGTAACTTTGTACTTGATG
TACACATTTCTTCATTGATTTTGTGGAATATATGCAGAATCTGTTGGTTACTTCTATGTTAGCCATC
AGTACAGAGCCACAATCACAAACCACTGAGGATCCAAACACAGCAACCTCAGAGACAATAACATC
TGCTGCAAGTTGCGATCCAAATGTAATTGAGTCAATGGGAGGCGATAAGGATGAGATAATGACA
GAGGTAGAAGAAGCAGATGTTGATGACGCAATGACTGTTGACATGGAAACAATCGATGAACCAT
CAGAGACAATGACGACCACGAGTGAGAGTGAGACTCTAAGCGAAAACAGTTGAGTTTCTTTTCAC
CAGTGAGACGCTTAGACAACTTAATAACACATTGCGGACGTTTTTAATGTACTGGGGTGGTTTTT
CTTTTCACCAGTGAGACGGGCAACAGCTGATTGCCCTTCACCGCCTGGCCCTGAGAGAGTTGCA
GCAAGCGGTCCACGCTGGTTTGCCCCAGCAGGCGAAAATCCTGTTTGATGGTGGTTCCGTTGG
GTAAAAAAATAAT

T-DNA insertion position: between 2557 and 2558 bp position at 3'prime end of exon 7.

8. Supplemental Tables

Table S7. *420* genetic distance (cM) of wild type Non-EMS treated Col *420 RG/++*. This external control was grown along with M_2 isolates and M_3 progenies under the same growth conditions. Mean CO frequency (cM) and Standard deviation (SD) were calculated. Wild type is abbreviated as WT in all the tables.

Control	Green	Red	Both	None	Total	None/Total	CO rate (cM)	G/non G	R/non R	G/T	R/T	G/R
WT-1	223	238	1576	374	2411	0.19	21.41	2.94	3.04	0.09	0.10	0.94
WT-2	249	249	1745	540	2783	0.18	19.87	2.53	2.53	0.09	0.09	1.00
WT-3	247	245	1762	518	2772	0.18	19.69	2.63	2.62	0.09	0.09	1.01
WT-4	215	280	1795	567	2857	0.17	19.16	2.37	2.65	0.08	0.10	0.77
WT-5	185	182	1272	299	1938	0.19	21.18	3.03	3.00	0.10	0.09	1.02
WT-6	208	189	1545	374	2316	0.17	18.93	3.11	2.98	0.09	0.08	1.10
WT-7	197	182	1432	294	2105	0.18	20.01	3.42	3.29	0.09	0.09	1.08
WT-8	211	178	1288	292	1969	0.20	22.23	3.19	2.91	0.11	0.09	1.19
WT-9	180	184	1468	277	2109	0.17	19.08	3.57	3.61	0.09	0.09	0.98
WT-10	204	202	1525	335	2266	0.18	19.90	3.22	3.20	0.09	0.09	1.01
WT-11	195	225	1473	326	2219	0.19	21.17	3.03	3.26	0.09	0.10	0.87
WT-12	208	206	1455	377	2246	0.18	20.54	2.85	2.84	0.09	0.09	1.01
WT-13	182	179	1496	369	2226	0.16	17.80	3.06	3.04	0.08	0.08	1.02
WT-14	146	164	1017	255	1582	0.20	22.02	2.78	2.95	0.09	0.10	0.89
WT-15	180	215	1404	331	2130	0.19	20.68	2.90	3.17	0.08	0.10	0.84
WT-16	207	194	1474	360	2235	0.18	19.93	3.03	2.94	0.09	0.09	1.07
WT-17	218	229	1468	359	2274	0.20	22.10	2.87	2.94	0.10	0.10	0.95
WT-18	65	70	530	125	790	0.17	18.87	3.05	3.16	0.08	0.09	0.93
WT-19	157	175	1166	289	1787	0.19	20.73	2.85	3.01	0.09	0.10	0.90
WT-20	192	186	1378	335	2091	0.18	20.10	3.01	2.97	0.09	0.09	1.03
WT-21	225	216	1501	344	2286	0.19	21.63	3.08	3.02	0.10	0.09	1.04
WT-22	190	180	1253	295	1918	0.19	21.63	3.04	2.95	0.10	0.09	1.06
WT-23	175	241	1349	330	2095	0.20	22.36	2.67	3.15	0.08	0.12	0.73
WT-24	204	208	1485	395	2292	0.18	19.97	2.80	2.83	0.09	0.09	0.98
WT-25	209	235	1473	275	2192	0.20	22.87	3.30	3.53	0.10	0.11	0.89
WT-26	207	207	1453	352	2219	0.19	20.83	2.97	2.97	0.09	0.09	1.00
WT-27	216	223	1304	292	2035	0.22	24.60	2.95	3.01	0.11	0.11	0.97
WT-28	228	239	1559	356	2382	0.20	22.03	3.00	3.08	0.10	0.10	0.95
WT-29	191	190	1290	300	1971	0.19	21.68	3.02	3.01	0.10	0.10	1.01
WT-30	207	237	1471	355	2270	0.20	21.97	2.83	3.04	0.09	0.10	0.87
WT-31	236	216	1398	331	2181	0.21	23.48	2.99	2.85	0.11	0.10	1.09
WT-32	187	188	1408	341	2124	0.18	19.57	3.02	3.02	0.09	0.09	0.99
WT-33	209	207	1494	343	2253	0.18	20.58	3.10	3.08	0.09	0.09	1.01
WT-34	181	201	1478	354	2214	0.17	19.07	2.99	3.14	0.08	0.09	0.90
WT-35	97	106	693	184	1080	0.19	21.00	2.72	2.84	0.09	0.10	0.92
WT-36	267	257	1693	426	2643	0.20	22.32	2.87	2.81	0.10	0.10	1.04
WT-37	250	229	1709	402	2590	0.18	20.62	3.10	2.97	0.10	0.09	1.09
WT-38	153	148	1007	247	1555	0.19	21.71	2.94	2.89	0.10	0.10	1.03
WT-39	239	256	1695	385	2575	0.19	21.54	3.02	3.13	0.09	0.10	0.93
						Mean	20.89					
						SD	1.40					

Table S8. *420* genetic distance (cM) of scorable individuals from 14 M_2 pools. Scoring data tables of M_2 population from which 29 putative mutants were isolated (*high crossover rate* mutant or *hcr* - orange; *low crossover rate* mutant or *lcr* - blue). Non-scorable individuals were removed from the list.

1) Pool #1

M_2 individuals	Green	Red	Both	None	Total	None/Total	CO rate (cM)	G/non G	R/non R	G/T	R/T	G/R
1a-1	221	205	1490	377	2293	0.19	20.73	2.94	2.83	0.10	0.09	1.08
1a-2	255	229	1655	405	2544	0.19	21.29	3.01	2.85	0.10	0.09	1.11
1a-3	190	167	1601	241	2199	0.16	17.82	4.39	4.10	0.09	0.08	1.14
1a-4	221	223	1268	269	1981	0.22	25.72	3.03	3.04	0.11	0.11	0.99
1a-5	236	217	1602	403	2458	0.18	20.54	2.96	2.85	0.10	0.09	1.09
1a-6	272	231	1056	917	2476	0.20	22.95	1.16	1.08	0.11	0.09	1.18
1a-7	227	221	1567	343	2358	0.19	21.26	3.18	3.14	0.10	0.09	1.03
1a-8	259	257	1670	388	2574	0.20	22.60	2.99	2.98	0.10	0.10	1.01
1a-9	222	221	1682	399	2524	0.18	19.44	3.07	3.06	0.09	0.09	1.00
1a-10	228	214	1291	286	2019	0.22	25.02	3.04	2.93	0.11	0.11	1.07
1a-11	216	197	1190	307	1910	0.22	24.66	2.79	2.65	0.11	0.10	1.10
1a-12	246	226	1492	382	2346	0.20	22.69	2.86	2.74	0.10	0.10	1.09
1a-13	222	247	1630	380	2479	0.19	21.16	2.95	3.12	0.09	0.10	0.90
1a-14	233	252	1652	404	2541	0.19	21.37	2.87	2.99	0.09	0.10	0.92
1a-15	206	244	1521	368	2339	0.19	21.56	2.82	3.07	0.09	0.10	0.84
1a-16	224	217	1460	388	2289	0.19	21.60	2.78	2.74	0.10	0.09	1.03
1a-17	246	244	1664	389	2543	0.19	21.60	3.02	3.00	0.10	0.10	1.01
1a-18	208	214	1482	316	2220	0.19	21.27	3.19	3.24	0.09	0.10	0.97
1a-19	237	253	1752	462	2704	0.18	20.15	2.78	2.87	0.09	0.09	0.94
1a-20	218	211	1656	402	2487	0.17	19.07	3.06	3.01	0.09	0.08	1.03
1a-21	241	296	1406	311	2254	0.24	27.65	2.71	3.08	0.11	0.13	0.81
1a-22	275	242	1635	391	2543	0.20	22.97	3.02	2.82	0.11	0.10	1.14
1a-23	205	189	1113	254	1761	0.22	25.67	2.98	2.84	0.12	0.11	1.08
1a-24	252	260	1755	404	2671	0.19	21.47	3.02	3.07	0.09	0.10	0.97
1a-25	251	246	1582	365	2444	0.20	22.97	3.00	2.97	0.10	0.10	1.02
1a-26	258	247	1694	421	2620	0.19	21.61	2.92	2.86	0.10	0.09	1.04
1a-27	241	228	1581	380	2430	0.19	21.64	3.00	2.91	0.10	0.09	1.06
1a-28	146	166	1056	250	1618	0.19	21.62	2.89	3.09	0.09	0.10	0.88
1a-29	259	264	1660	388	2571	0.20	22.98	2.94	2.97	0.10	0.10	0.98
1a-30	248	243	1735	440	2666	0.18	20.52	2.90	2.88	0.09	0.09	1.02
1a-31	258	273	1695	391	2617	0.20	22.92	2.94	3.03	0.10	0.10	0.95
1a-32	222	229	1629	359	2439	0.18	20.62	3.15	3.20	0.09	0.09	0.97
1a-33	262	260	1627	388	2537	0.21	23.29	2.92	2.90	0.10	0.10	1.01
1a-34	116	122	868	211	1317	0.18	20.09	2.95	3.03	0.09	0.09	0.95
1a-35	201	269	1536	348	2354	0.20	22.50	2.82	3.29	0.09	0.11	0.75
1a-36	184	190	1205	386	1965	0.19	21.30	2.41	2.45	0.09	0.10	0.97
1a-37	241	265	1626	448	2580	0.20	22.04	2.62	2.74	0.09	0.10	0.91
1a-38	282	278	1741	380	2681	0.21	23.69	3.07	3.05	0.11	0.10	1.01
1a-39	235	240	1653	354	2482	0.19	21.44	3.18	3.21	0.09	0.10	0.98
1a-40	267	252	1673	412	2604	0.20	22.45	2.92	2.84	0.10	0.10	1.06
1a-41	203	289	1727	392	2611	0.19	21.06	2.83	3.39	0.08	0.11	0.70
1a-42	223	267	1593	346	2429	0.20	22.76	2.96	3.27	0.09	0.11	0.84
1a-43	156	133	1096	286	1671	0.17	19.12	2.99	2.78	0.09	0.08	1.17
1b-1	193	168	1201	321	1883	0.19	21.48	2.85	2.66	0.10	0.09	1.15
1b-2	178	191	1307	354	2030	0.18	20.22	2.72	2.82	0.09	0.09	0.93
1b-3	14	14	111	32	171	0.16	17.99	2.72	2.72	0.08	0.08	1.00
1b-4	195	159	1137	276	1767	0.20	22.58	3.06	2.75	0.11	0.09	1.23
1b-5	159	149	1061	256	1625	0.19	21.20	3.01	2.92	0.10	0.09	1.07
1b-6	161	166	1116	286	1729	0.19	21.15	2.83	2.87	0.09	0.10	0.97
1b-7	147	138	1044	278	1607	0.18	19.67	2.86	2.78	0.09	0.09	1.07
1b-8	169	160	1059	267	1655	0.20	22.38	2.88	2.80	0.10	0.10	1.06
1b-9	185	194	1265	335	1979	0.19	21.45	2.74	2.81	0.09	0.10	0.95

1b-10	146	132	920	269	1467	0.19	21.20	2.66	2.53	0.10	0.09	1.11
1b-11	166	169	1194	318	1847	0.18	20.17	2.79	2.82	0.09	0.09	0.98
1b-12	191	183	1274	322	1970	0.19	21.24	2.90	2.84	0.10	0.09	1.04
1b-13	156	170	1003	270	1599	0.20	23.04	2.63	2.75	0.10	0.11	0.92
1b-15	201	224	1422	343	2190	0.19	21.78	2.86	3.03	0.09	0.10	0.90
1b-16	180	176	1375	285	2016	0.18	19.57	3.37	3.34	0.09	0.09	1.02
1b-17	166	184	1225	341	1916	0.18	20.33	2.65	2.78	0.09	0.10	0.90
1b-18	218	177	1459	303	2157	0.18	20.39	3.49	3.14	0.10	0.08	1.23
1b-19	225	195	1328	309	2057	0.20	23.08	3.08	2.85	0.11	0.09	1.15
1b-20	199	169	1309	370	2047	0.18	19.97	2.80	2.60	0.10	0.08	1.18
1b-22	177	173	1170	328	1848	0.19	21.18	2.69	2.66	0.10	0.09	1.02
1b-23	243	182	1420	414	2259	0.19	21.02	2.79	2.44	0.11	0.08	1.34
1b-24	198	141	1207	333	1879	0.18	20.05	2.96	2.54	0.11	0.08	1.40
1b-25	189	202	1386	412	2189	0.18	19.83	2.57	2.64	0.09	0.09	0.94
1b-26	186	174	1245	350	1955	0.18	20.52	2.73	2.65	0.10	0.09	1.07
1b-27	166	163	1162	350	1841	0.18	19.84	2.59	2.57	0.09	0.09	1.02
1b-28	153	137	1016	267	1573	0.18	20.55	2.89	2.75	0.10	0.09	1.12
1b-29	184	158	1250	312	1904	0.18	19.95	3.05	2.84	0.10	0.08	1.16
1b-30	175	166	1242	321	1904	0.18	19.89	2.91	2.84	0.09	0.09	1.05
1b-31	158	179	1206	338	1881	0.18	19.90	2.64	2.79	0.08	0.10	0.88
1b-32	211	222	1270	300	2003	0.22	24.66	2.84	2.92	0.11	0.11	0.95
1b-33	189	171	1247	310	1917	0.19	20.98	2.99	2.84	0.10	0.09	1.11
1b-34	207	199	1410	387	2203	0.18	20.54	2.76	2.71	0.09	0.09	1.04
1b-35	216	195	1406	335	2152	0.19	21.39	3.06	2.91	0.10	0.09	1.11
1b-36	186	201	1278	297	1962	0.20	22.19	2.94	3.06	0.09	0.10	0.93
1b-37	136	169	1132	285	1722	0.18	19.64	2.79	3.09	0.08	0.10	0.80
1b-38	203	208	1348	343	2102	0.20	21.97	2.81	2.85	0.10	0.10	0.98
1b-39	153	252	1327	410	2142	0.19	21.14	2.24	2.80	0.07	0.12	0.61
1b-40	227	230	1307	334	2098	0.22	24.88	2.72	2.74	0.11	0.11	0.99
1b-41	158	130	998	278	1564	0.18	20.52	2.83	2.59	0.10	0.08	1.22
1b-42	167	184	1335	316	2002	0.18	19.42	3.00	3.14	0.08	0.09	0.91
1b-43	221	236	1289	313	2059	0.22	25.43	2.75	2.86	0.11	0.11	0.94
1b-44	168	154	1265	333	1920	0.17	18.48	2.94	2.83	0.09	0.08	1.09

2) Pool #3

M_2 individuals	Green	Red	Both	None	Total	None/Total	CO rate (cM)	G/non G	R/non R	G/T	R/T	G/R
3a-1	128	155	991	219	1493	0.19	21.20	2.99	3.30	0.09	0.10	0.83
3a-2	119	117	976	249	1461	0.16	17.72	2.99	2.97	0.08	0.08	1.02
3a-3	143	165	1091	244	1643	0.19	20.94	3.02	3.25	0.09	0.10	0.87
3a-4	139	125	1085	308	1657	0.16	17.46	2.83	2.71	0.08	0.08	1.11
3a-5	169	151	1143	261	1724	0.19	20.70	3.18	3.01	0.10	0.09	1.12
3a-6	159	139	1114	291	1703	0.17	19.38	2.96	2.78	0.09	0.08	1.14
3a-7	185	139	1126	256	1706	0.19	21.25	3.32	2.87	0.11	0.08	1.33
3a-8	152	173	945	216	1486	0.22	24.99	2.82	3.04	0.10	0.12	0.88
3a-9	203	218	875	193	1489	0.28	34.08	2.62	2.76	0.14	0.15	0.93
3a-10	111	111	821	208	1251	0.18	19.68	2.92	2.92	0.09	0.09	1.00
3a-11	137	149	992	293	1571	0.18	20.26	2.55	2.65	0.09	0.09	0.92
3a-12	120	125	811	191	1247	0.20	22.09	2.95	3.01	0.10	0.10	0.96
3a-14	137	150	1096	273	1656	0.17	19.17	2.91	3.04	0.08	0.09	0.91
3a-15	156	139	1095	256	1646	0.18	19.90	3.17	3.00	0.09	0.08	1.12
3a-16	146	128	1035	258	1567	0.17	19.36	3.06	2.88	0.09	0.08	1.14
3a-17	137	142	980	250	1509	0.18	20.61	2.85	2.90	0.09	0.09	0.96
3a-18	169	142	945	246	1502	0.21	23.46	2.87	2.62	0.11	0.09	1.19
3a-19	73	71	446	130	720	0.20	22.54	2.58	2.55	0.10	0.10	1.03
3a-20	141	127	1027	232	1527	0.18	19.44	3.25	3.09	0.09	0.08	1.11
3a-21	130	144	1043	245	1562	0.18	19.43	3.02	3.17	0.08	0.09	0.90
3a-22	127	151	1097	233	1608	0.17	19.12	3.19	3.47	0.08	0.09	0.84
3a-23	145	170	1000	260	1575	0.20	22.54	2.66	2.89	0.09	0.11	0.85
3a-24	131	153	1024	232	1540	0.18	20.55	3.00	3.24	0.09	0.10	0.86
3a-25	180	148	1147	282	1757	0.19	20.84	3.09	2.80	0.10	0.08	1.22
3a-26	132	142	1017	251	1542	0.18	19.71	2.92	3.03	0.09	0.09	0.93
3a-27	157	142	1178	288	1765	0.17	18.69	3.10	2.97	0.09	0.08	1.11
3a-28	106	94	768	182	1150	0.17	19.24	3.17	2.99	0.09	0.08	1.13
3a-29	100	116	748	189	1153	0.19	20.92	2.78	2.99	0.09	0.10	0.86
3a-30	155	165	1153	271	1744	0.18	20.44	3.00	3.09	0.09	0.09	0.94
3a-31	118	102	797	200	1217	0.18	20.10	3.03	2.83	0.10	0.08	1.16
3a-32	147	150	1250	320	1867	0.16	17.43	2.97	3.00	0.08	0.08	0.98
3a-33	138	146	1119	281	1684	0.17	18.59	2.94	3.02	0.08	0.09	0.95
3a-34	201	192	1129	261	1783	0.22	25.22	2.94	2.86	0.11	0.11	1.05
3a-35	181	191	1027	229	1628	0.23	26.31	2.88	2.97	0.11	0.12	0.95
3a-36	152	174	1090	271	1687	0.19	21.67	2.79	2.99	0.09	0.10	0.87
3a-37	133	118	958	223	1432	0.18	19.41	3.20	3.02	0.09	0.08	1.13
3b-1	186	200	1222	298	1906	0.20	22.87	2.83	2.94	0.10	0.10	0.93
3b-2	268	222	1708	365	2563	0.19	21.41	3.37	3.05	0.10	0.09	1.21
3b-3	233	235	1557	354	2379	0.20	22.12	3.04	3.05	0.10	0.10	0.99
3b-4	276	182	1643	354	2455	0.19	20.82	3.58	2.90	0.11	0.07	1.52
3b-5	216	219	1600	433	2468	0.18	19.53	2.79	2.80	0.09	0.09	0.99
3b-6	198	213	1414	429	2254	0.18	20.29	2.51	2.59	0.09	0.09	0.93
3b-7	184	223	1491	369	2267	0.18	19.94	2.83	3.10	0.08	0.10	0.83
3b-8	207	276	1687	426	2596	0.19	20.76	2.70	3.10	0.08	0.11	0.75
3b-9	251	257	1611	369	2488	0.20	23.08	2.97	3.01	0.10	0.10	0.98
3b-11	212	244	1394	334	2184	0.21	23.68	2.78	3.00	0.10	0.11	0.87
3b-12	213	245	1641	422	2521	0.18	20.21	2.78	2.97	0.08	0.10	0.87
3b-13	232	242	1623	450	2547	0.19	20.77	2.68	2.73	0.09	0.10	0.96
3b-14	239	175	1385	326	2125	0.19	21.87	3.24	2.76	0.11	0.08	1.37
3b-16	267	196	1499	446	2408	0.19	21.55	2.75	2.38	0.11	0.08	1.36
3b-18	201	162	1318	372	2053	0.18	19.60	2.84	2.58	0.10	0.08	1.24
3b-20	246	234	1620	446	2546	0.19	21.07	2.74	2.68	0.10	0.09	1.05

3b-21	237	212	1507	421	2377	0.19	21.12	2.76	2.61	0.10	0.09	1.12
3b-22	283	252	1641	384	2560	0.21	23.71	3.03	2.84	0.11	0.10	1.12
3b-24	202	260	1613	379	2454	0.19	21.04	2.84	3.22	0.08	0.11	0.78
3b-25	234	254	1580	374	2442	0.20	22.52	2.89	3.02	0.10	0.10	0.92
3b-26	283	247	1721	617	2868	0.18	20.60	2.32	2.19	0.10	0.09	1.15
3b-27	240	240	1689	448	2617	0.18	20.43	2.80	2.80	0.09	0.09	1.00
3b-30	283	246	1677	473	2679	0.20	22.21	2.73	2.54	0.11	0.09	1.15
3b-31	286	244	1753	396	2679	0.20	22.26	3.19	2.93	0.11	0.09	1.17
3b-32	566	566	1177	17	2326	0.49	83.67	2.99	2.99	0.24	0.24	1.00
3b-33	259	276	1587	383	2505	0.21	24.31	2.80	2.90	0.10	0.11	0.94
3b-34	235	188	1496	329	2248	0.19	21.03	3.35	2.99	0.10	0.08	1.25
3b-35	242	264	1565	358	2429	0.21	23.62	2.91	3.05	0.10	0.11	0.92
3b-36	249	182	1526	311	2268	0.19	21.26	3.60	3.05	0.11	0.08	1.37
3b-37	113	92	742	215	1162	0.18	19.55	2.79	2.54	0.10	0.08	1.23
3b-38	206	186	1414	427	2233	0.18	19.45	2.64	2.53	0.09	0.08	1.11
3b-39	237	214	1505	436	2392	0.19	21.08	2.68	2.55	0.10	0.09	1.11
3c-1	165	204	1291	323	1983	0.19	20.76	2.76	3.06	0.08	0.10	0.81
3c-2	191	161	1352	351	2055	0.17	18.92	3.01	2.79	0.09	0.08	1.19
3c-3	157	145	1191	314	1807	0.17	18.41	2.94	2.84	0.09	0.08	1.08
3c-4	196	179	1418	360	2153	0.17	19.28	2.99	2.87	0.09	0.08	1.09
3c-5	163	200	1440	365	2168	0.17	18.44	2.84	3.11	0.08	0.09	0.82
3c-6	188	193	1503	373	2257	0.17	18.61	2.99	3.02	0.08	0.09	0.97
3c-7	211	207	1534	392	2344	0.18	19.79	2.91	2.89	0.09	0.09	1.02
3c-9	244	248	1471	314	2277	0.22	24.64	3.05	3.08	0.11	0.11	0.98
3c-10	162	178	1074	250	1664	0.20	23.10	2.89	3.04	0.10	0.11	0.91
3c-11	214	212	1596	412	2434	0.18	19.38	2.90	2.89	0.09	0.09	1.01
3c-12	228	246	1488	351	2313	0.20	23.18	2.87	2.99	0.10	0.11	0.93
3c-13	197	196	1387	343	2123	0.19	20.64	2.94	2.93	0.09	0.09	1.01
3c-14	254	225	1597	447	2523	0.19	21.24	2.75	2.60	0.10	0.09	1.13
3c-15	230	206	1622	427	2485	0.18	19.43	2.93	2.78	0.09	0.08	1.12
3c-16	219	236	1591	349	2395	0.19	21.26	3.09	3.22	0.09	0.10	0.93
3c-17	215	198	1570	417	2400	0.17	19.02	2.90	2.80	0.09	0.08	1.09
3c-18	241	166	1544	403	2354	0.17	19.12	3.14	2.66	0.10	0.07	1.45
3c-19	67	65	332	98	562	0.23	27.18	2.45	2.41	0.12	0.12	1.03
3c-20	225	245	1397	321	2188	0.21	24.48	2.87	3.01	0.10	0.11	0.92
3c-22	248	197	1610	419	2474	0.18	19.98	3.02	2.71	0.10	0.08	1.26
3c-23	263	213	1465	355	2296	0.21	23.49	3.04	2.72	0.11	0.09	1.23
3c-24	657	621	1365	18	2661	0.48	80.14	3.16	2.94	0.25	0.23	1.06
3c-25	545	438	1227	36	2246	0.44	64.69	3.74	2.87	0.24	0.20	1.24
3c-26	256	240	1603	374	2473	0.20	22.61	3.03	2.93	0.10	0.10	1.07
3c-27	228	251	1622	408	2509	0.19	21.38	2.81	2.94	0.09	0.10	0.91
3c-28	196	263	1647	417	2523	0.18	20.24	2.71	3.12	0.08	0.10	0.75
3c-29	237	233	1485	339	2294	0.20	23.17	3.01	2.98	0.10	0.10	1.02
3c-30	214	252	1596	406	2468	0.19	21.11	2.75	2.98	0.09	0.10	0.85
3c-31	195	205	1405	341	2146	0.19	20.80	2.93	3.00	0.09	0.10	0.95
3c-32	218	232	1572	430	2452	0.18	20.44	2.70	2.78	0.09	0.09	0.94
3c-33	226	181	1353	346	2106	0.19	21.67	3.00	2.68	0.11	0.09	1.25
3c-34	246	208	1695	452	2601	0.17	19.32	2.94	2.73	0.09	0.08	1.18
3c-35	197	225	1721	397	2540	0.17	18.29	3.08	3.28	0.08	0.09	0.88
3c-36	173	192	1037	259	1661	0.22	25.13	2.68	2.84	0.10	0.12	0.90
3c-37	239	226	1514	363	2342	0.20	22.35	2.98	2.89	0.10	0.10	1.06
3c-38	186	183	1420	321	2110	0.17	19.36	3.19	3.16	0.09	0.09	1.02
3c-39	229	208	1730	452	2619	0.17	18.37	2.97	2.85	0.09	0.08	1.10

3) Pool #5

M_2 individuals	Green	Red	Both	None	Total	None/Total	CO rate (cM)	G/non G	R/non R	G/T	R/T	G/R
5a-1	182	172	1310	322	1986	0.18	19.78	3.02	2.94	0.09	0.09	1.06
5a-2	148	180	1133	306	1767	0.19	20.71	2.64	2.89	0.08	0.10	0.82
5a-3	179	171	1176	309	1835	0.19	21.35	2.82	2.76	0.10	0.09	1.05
5a-4	217	166	1364	357	2104	0.18	20.25	3.02	2.67	0.10	0.08	1.31
5a-5	31	22	291	87	431	0.12	13.16	2.95	2.65	0.07	0.05	1.41
5a-6	164	207	1321	358	2050	0.18	20.12	2.63	2.93	0.08	0.10	0.79
5a-7	194	181	1457	385	2217	0.17	18.65	2.92	2.83	0.09	0.08	1.07
5a-8	152	126	1150	319	1747	0.16	17.43	2.93	2.71	0.09	0.07	1.21
5a-9	148	143	1338	335	1964	0.15	16.12	3.11	3.07	0.08	0.07	1.03
5a-10	197	203	1452	401	2253	0.18	19.69	2.73	2.77	0.09	0.09	0.97
5a-11	195	189	1475	372	2231	0.17	19.02	2.98	2.93	0.09	0.08	1.03
5a-12	202	239	1542	396	2379	0.19	20.67	2.75	2.98	0.08	0.10	0.85
5a-13	222	213	1521	412	2368	0.18	20.46	2.79	2.74	0.09	0.09	1.04
5a-14	228	208	1443	431	2310	0.19	21.10	2.62	2.51	0.10	0.09	1.10
5a-15	236	231	1376	386	2229	0.21	23.78	2.61	2.58	0.11	0.10	1.02
5a-16	206	226	1469	391	2292	0.19	21.07	2.71	2.84	0.09	0.10	0.91
5a-17	243	197	1634	369	2443	0.18	20.01	3.32	2.99	0.10	0.08	1.23
5a-18	212	228	1394	349	2183	0.20	22.74	2.78	2.89	0.10	0.10	0.93
5a-20	167	193	1250	319	1929	0.19	20.83	2.77	2.97	0.09	0.10	0.87
5a-21	146	127	1140	290	1703	0.16	17.57	3.08	2.91	0.09	0.07	1.15
5a-22	199	200	1256	323	1978	0.20	22.76	2.78	2.79	0.10	0.10	1.00
5a-23	58	64	1200	356	1678	0.07	7.56	3.00	3.05	0.03	0.04	0.91
5a-24	207	192	1452	373	2224	0.18	19.93	2.94	2.83	0.09	0.09	1.08
5a-25	198	179	1411	348	2136	0.18	19.56	3.05	2.91	0.09	0.08	1.11
5a-26	238	155	1392	320	2105	0.19	20.84	3.43	2.77	0.11	0.07	1.54
5a-27	230	177	1378	419	2204	0.18	20.59	2.70	2.40	0.10	0.08	1.30
5a-28	59	55	445	118	677	0.17	18.56	2.91	2.82	0.09	0.08	1.07
5a-29	179	187	1257	329	1952	0.19	20.94	2.78	2.84	0.09	0.10	0.96
5a-30	206	197	1328	347	2078	0.19	21.76	2.82	2.76	0.10	0.09	1.05
5a-31	185	160	1390	373	2108	0.16	17.98	2.95	2.78	0.09	0.08	1.16
5a-32	211	212	1441	359	2223	0.19	21.30	2.89	2.90	0.09	0.10	1.00
5a-34	228	194	1529	402	2353	0.18	19.92	2.95	2.73	0.10	0.08	1.18
5b-2	179	205	1156	276	1816	0.21	24.03	2.78	2.99	0.10	0.11	0.87
5b-3	163	174	1116	267	1720	0.20	22.02	2.90	3.00	0.09	0.10	0.94
5b-4	194	194	1182	297	1867	0.21	23.56	2.80	2.80	0.10	0.10	1.00
5b-5	192	142	1169	284	1787	0.19	20.87	3.19	2.75	0.11	0.08	1.35
5b-6	208	171	1448	391	2218	0.17	18.87	2.95	2.70	0.09	0.08	1.22
5b-8	183	214	1545	384	2326	0.17	18.84	2.89	3.10	0.08	0.09	0.86
5b-9	506	542	1059	18	2125	0.49	88.32	2.79	3.06	0.24	0.26	0.93
5b-10	155	141	1012	248	1556	0.19	21.29	3.00	2.86	0.10	0.09	1.10
5b-11	213	228	1404	358	2203	0.20	22.56	2.76	2.86	0.10	0.10	0.93
5b-12	182	241	1308	304	2035	0.21	23.56	2.73	3.19	0.09	0.12	0.76
5b-13	241	220	1416	346	2223	0.21	23.50	2.93	2.79	0.11	0.10	1.10
5b-14	163	168	1569	413	2313	0.14	15.51	2.98	3.02	0.07	0.07	0.97
5b-15	182	185	1486	399	2252	0.16	17.90	2.86	2.88	0.08	0.08	0.98
5b-16	176	186	1491	405	2258	0.16	17.58	2.82	2.89	0.08	0.08	0.95
5b-17	49	63	494	137	743	0.15	16.42	2.72	2.99	0.07	0.08	0.78
5b-18	214	201	1539	388	2342	0.18	19.65	2.98	2.89	0.09	0.09	1.06
5b-19	96	85	772	206	1159	0.16	17.07	2.98	2.84	0.08	0.07	1.13
5b-20	586	527	1190	44	2347	0.47	77.29	3.11	2.73	0.25	0.22	1.11
5b-21	219	175	1500	407	2301	0.17	18.91	2.95	2.68	0.10	0.08	1.25
5b-22	161	153	1283	306	1903	0.17	18.15	3.15	3.07	0.08	0.08	1.05

5b-23	222	227	1484	416	2349	0.19	21.41	2.65	2.68	0.09	0.10	0.98
5b-24	181	177	1398	359	2115	0.17	18.67	2.95	2.92	0.09	0.08	1.02
5b-25	180	188	1264	299	1931	0.19	21.33	2.97	3.03	0.09	0.10	0.96
5b-26	185	168	1234	287	1874	0.19	21.05	3.12	2.97	0.10	0.09	1.10
5b-27	155	155	1042	276	1628	0.19	21.31	2.78	2.78	0.10	0.10	1.00
5b-28	207	199	1298	294	1998	0.20	22.95	3.05	2.99	0.10	0.10	1.04
5b-29	190	185	1232	276	1883	0.20	22.43	3.08	3.04	0.10	0.10	1.03
5b-30	175	201	1463	369	2208	0.17	18.80	2.87	3.06	0.08	0.09	0.87
5b-31	206	207	1596	383	2392	0.17	19.09	3.05	3.06	0.09	0.09	1.00
5b-32	84	96	838	233	1251	0.14	15.61	2.80	2.95	0.07	0.08	0.88
5c-1	172	273	1353	354	2152	0.21	23.42	2.43	3.09	0.08	0.13	0.63
5c-2	224	234	1585	349	2392	0.19	21.45	3.10	3.17	0.09	0.10	0.96
5c-3	256	218	1659	420	2553	0.19	20.71	3.00	2.78	0.10	0.09	1.17
5c-4	240	232	1626	362	2460	0.19	21.50	3.14	3.09	0.10	0.09	1.03
5c-5	276	248	1507	466	2497	0.21	23.82	2.50	2.37	0.11	0.10	1.11
5c-6	230	226	1459	343	2258	0.20	22.79	2.97	2.94	0.10	0.10	1.02
5c-7	311	97	1463	240	2111	0.19	21.68	5.26	2.83	0.15	0.05	3.21
5c-8	213	233	1542	409	2397	0.19	20.76	2.73	2.85	0.09	0.10	0.91
5c-9	140	167	1261	233	1801	0.17	18.82	3.50	3.83	0.08	0.09	0.84
5c-10	188	148	1429	193	1958	0.17	18.96	4.74	4.14	0.10	0.08	1.27
5c-11	236	229	1525	345	2335	0.20	22.43	3.07	3.02	0.10	0.10	1.03
5c-12	225	239	1585	375	2424	0.19	21.44	2.95	3.04	0.09	0.10	0.94
5c-13	216	254	1617	383	2470	0.19	21.30	2.88	3.12	0.09	0.10	0.85
5c-14	251	207	1585	410	2453	0.19	20.84	2.98	2.71	0.10	0.08	1.21
5c-15	206	287	1500	413	2406	0.20	23.18	2.44	2.89	0.09	0.12	0.72
5c-16	267	275	1639	415	2596	0.21	23.68	2.76	2.81	0.10	0.11	0.97
5c-17	84	349	1746	249	2428	0.18	19.79	3.06	6.29	0.03	0.14	0.24
5c-18	218	239	1476	357	2290	0.20	22.48	2.84	2.98	0.10	0.10	0.91
5c-19	45	266	1571	155	2037	0.15	16.65	3.84	9.19	0.02	0.13	0.17
5c-20	237	254	1663	438	2592	0.19	21.19	2.75	2.84	0.09	0.10	0.93
5c-21	192	210	1455	343	2200	0.18	20.34	2.98	3.11	0.09	0.10	0.91
5c-22	206	208	1529	388	2331	0.18	19.70	2.91	2.92	0.09	0.09	0.99
5c-23	211	294	1639	492	2636	0.19	21.46	2.35	2.75	0.08	0.11	0.72
5c-24	226	223	1518	371	2338	0.19	21.52	2.94	2.92	0.10	0.10	1.01
5c-25	188	251	1529	377	2345	0.19	20.91	2.73	3.15	0.08	0.11	0.75
5c-26	216	293	1533	351	2393	0.21	24.20	2.72	3.22	0.09	0.12	0.74

4) Pool #6

M_2 individuals	Green	Red	Both	None	Total	None/Total	CO rate (cM)	G/non G	R/non R	G/T	R/T	G/R
6a-1	169	190	1209	383	1951	0.18	20.50	2.40	2.53	0.09	0.10	0.89
6a-2	220	200	1670	414	2504	0.17	18.48	3.08	2.95	0.09	0.08	1.10
6a-3	207	252	1541	480	2480	0.19	20.64	2.39	2.61	0.08	0.10	0.82
6a-4	202	235	1638	369	2444	0.18	19.85	3.05	3.28	0.08	0.10	0.86
6a-5	232	221	1473	371	2297	0.20	22.18	2.88	2.81	0.10	0.10	1.05
6a-6	336	159	1555	558	2608	0.19	21.23	2.64	1.92	0.13	0.06	2.11
6a-7	240	318	600	30	1188	0.47	75.38	2.41	3.40	0.20	0.27	0.75
6a-8	203	232	1389	349	2173	0.20	22.56	2.74	2.94	0.09	0.11	0.88
6a-9	194	282	1499	423	2398	0.20	22.35	2.40	2.89	0.08	0.12	0.69
6a-10	232	261	1494	403	2390	0.21	23.35	2.60	2.76	0.10	0.11	0.89
6a-11	231	192	1579	398	2400	0.18	19.53	3.07	2.82	0.10	0.08	1.20
6a-12	207	217	1562	395	2381	0.18	19.76	2.89	2.96	0.09	0.09	0.95
6a-13	220	199	1526	467	2412	0.17	19.22	2.62	2.51	0.09	0.08	1.11
6a-14	237	226	1342	456	2261	0.20	23.16	2.32	2.26	0.10	0.10	1.05
6a-15	193	275	1647	377	2492	0.19	20.98	2.82	3.37	0.08	0.11	0.70
6a-16	165	168	1164	293	1790	0.19	20.76	2.88	2.91	0.09	0.09	0.98
6a-17	236	243	1623	398	2500	0.19	21.46	2.90	2.94	0.09	0.10	0.97
6a-18	221	261	1665	400	2547	0.19	21.16	2.85	3.10	0.09	0.10	0.85
6a-19	250	240	1407	396	2293	0.21	24.33	2.61	2.55	0.11	0.10	1.04
6a-20	231	246	1606	418	2501	0.19	21.35	2.77	2.85	0.09	0.10	0.94
6a-21	259	209	1634	437	2539	0.18	20.54	2.93	2.65	0.10	0.08	1.24
6a-22	559	609	1156	82	2406	0.49	82.94	2.48	2.75	0.23	0.25	0.92
6a-23	208	217	1746	464	2635	0.16	17.69	2.87	2.92	0.08	0.08	0.96
6a-24	536	573	1125	47	2281	0.49	83.38	2.68	2.91	0.23	0.25	0.94
6a-25	151	137	1043	274	1605	0.18	19.93	2.91	2.78	0.09	0.09	1.10
6a-26	140	236	1096	321	1793	0.21	23.80	2.22	2.89	0.08	0.13	0.59
6b-1	83	278	1672	123	2156	0.17	18.45	4.38	9.47	0.04	0.13	0.30
6b-2	297	212	1445	262	2216	0.23	26.47	3.68	2.96	0.13	0.10	1.40
6b-3	239	197	1470	380	2286	0.19	21.35	2.96	2.69	0.10	0.09	1.21
6b-4	229	160	1612	386	2387	0.16	17.90	3.37	2.88	0.10	0.07	1.43
6b-5	254	227	1378	329	2188	0.22	25.14	2.94	2.75	0.12	0.10	1.12
6b-6	247	201	1393	356	2197	0.20	23.05	2.94	2.64	0.11	0.09	1.23
6b-7	228	196	1542	359	2325	0.18	20.30	3.19	2.96	0.10	0.08	1.16
6b-8	232	194	1504	383	2313	0.18	20.52	3.01	2.76	0.10	0.08	1.20
6b-9	187	186	1394	289	2056	0.18	20.18	3.33	3.32	0.09	0.09	1.01
6b-10	248	247	1428	335	2258	0.22	25.06	2.88	2.87	0.11	0.11	1.00
6b-11	219	231	1462	345	2257	0.20	22.46	2.92	3.00	0.10	0.10	0.95
6b-12	227	227	1568	374	2396	0.19	21.19	2.99	2.99	0.09	0.09	1.00
6b-13	77	65	478	155	775	0.18	20.40	2.52	2.34	0.10	0.08	1.18
6b-14	220	236	1380	305	2141	0.21	24.24	2.96	3.08	0.10	0.11	0.93
6b-15	197	194	1358	396	2145	0.18	20.29	2.64	2.62	0.09	0.09	1.02
6b-16	176	203	1425	363	2167	0.17	19.36	2.83	3.02	0.08	0.09	0.87
6b-17	182	206	1290	303	1981	0.20	22.01	2.89	3.08	0.09	0.10	0.88
6b-18	238	262	1548	340	2388	0.21	23.76	2.97	3.13	0.10	0.11	0.91
6b-19	177	213	1523	394	2307	0.17	18.64	2.80	3.04	0.08	0.09	0.83
6b-20	187	183	1185	280	1835	0.20	22.75	2.96	2.93	0.10	0.10	1.02
6b-21	216	258	1534	356	2364	0.20	22.61	2.85	3.13	0.09	0.11	0.84
6b-22	225	213	1501	344	2283	0.19	21.50	3.10	3.01	0.10	0.09	1.06
6b-23	259	231	1556	383	2429	0.20	22.76	2.96	2.78	0.11	0.10	1.12
6b-24	181	167	1150	255	1753	0.20	22.35	3.15	3.02	0.10	0.10	1.08
6b-25	30	38	218	61	347	0.20	22.02	2.51	2.81	0.09	0.11	0.79
6b-26	216	213	1612	372	2413	0.18	19.72	3.12	3.10	0.09	0.09	1.01

6b-27	257	262	1646	389	2554	0.20	22.96	2.92	2.95	0.10	0.10	0.98
6b-28	258	269	1583	354	2464	0.21	24.35	2.96	3.03	0.10	0.11	0.96
6b-29	255	236	1622	402	2515	0.20	21.93	2.94	2.83	0.10	0.09	1.08
6b-30	268	264	1604	357	2493	0.21	24.29	3.01	2.99	0.11	0.11	1.02
6b-31	234	221	1536	353	2344	0.19	21.78	3.08	2.99	0.10	0.09	1.06
6b-32	182	168	1239	294	1883	0.19	20.74	3.08	2.96	0.10	0.09	1.08
6b-33	210	256	1498	356	2320	0.20	22.65	2.79	3.10	0.09	0.11	0.82
6b-34	242	239	1506	339	2326	0.21	23.42	3.02	3.00	0.10	0.10	1.01
6b-35	228	241	1388	334	2191	0.21	24.38	2.81	2.90	0.10	0.11	0.95
6b-36	134	134	753	167	1188	0.23	25.92	2.95	2.95	0.11	0.11	1.00
6b-37	122	135	954	224	1435	0.18	19.89	3.00	3.15	0.09	0.09	0.90
6b-38	196	205	1531	366	2298	0.17	19.32	3.02	3.09	0.09	0.09	0.96
6c-1	564	386	1480	101	2531	0.38	50.07	4.20	2.81	0.22	0.15	1.46
6c-2	217	311	1728	501	2757	0.19	21.45	2.40	2.84	0.08	0.11	0.70
6c-3	246	261	1731	475	2713	0.19	20.86	2.69	2.76	0.09	0.10	0.94
6c-4	252	277	1753	503	2785	0.19	21.25	2.57	2.69	0.09	0.10	0.91
6c-5	239	387	1590	515	2731	0.23	26.41	2.03	2.62	0.09	0.14	0.62
6c-6	256	274	1872	443	2845	0.19	20.79	2.97	3.07	0.09	0.10	0.93
6c-7	330	262	1698	338	2628	0.23	25.87	3.38	2.93	0.13	0.10	1.26
6c-8	218	282	1739	447	2686	0.19	20.77	2.68	3.04	0.08	0.10	0.77
6c-9	245	377	1670	525	2817	0.22	25.27	2.12	2.66	0.09	0.13	0.65
6c-10	282	321	1791	518	2912	0.21	23.46	2.47	2.64	0.10	0.11	0.88
6c-11	232	273	1730	431	2666	0.19	21.19	2.79	3.02	0.09	0.10	0.85
6c-12	236	261	1674	422	2593	0.19	21.47	2.80	2.94	0.09	0.10	0.90
6c-13	269	385	1638	499	2791	0.23	27.11	2.16	2.63	0.10	0.14	0.70
6c-14	246	247	1769	468	2730	0.18	20.07	2.82	2.82	0.09	0.09	1.00
6c-15	257	302	1803	509	2871	0.19	21.86	2.54	2.75	0.09	0.11	0.85
6c-16	242	293	1663	470	2668	0.20	22.61	2.50	2.75	0.09	0.11	0.83
6c-18	240	261	1705	451	2657	0.19	21.08	2.73	2.85	0.09	0.10	0.92
6c-19	37	129	387	101	654	0.25	29.83	1.84	3.74	0.06	0.20	0.29
6c-20	233	566	1372	486	2657	0.30	36.87	1.53	2.70	0.09	0.21	0.41
6c-21	274	287	1795	487	2843	0.20	22.20	2.67	2.74	0.10	0.10	0.95
6c-22	246	250	1778	419	2693	0.18	20.52	3.03	3.05	0.09	0.09	0.98
6c-23	11	259	352	54	676	0.40	55.15	1.16	9.40	0.02	0.38	0.04
6c-24	262	306	1709	512	2789	0.20	23.01	2.41	2.60	0.09	0.11	0.86
6c-25	239	257	1826	445	2767	0.18	19.91	2.94	3.05	0.09	0.09	0.93
6c-26	236	265	1856	413	2770	0.18	20.11	3.09	3.27	0.09	0.10	0.89
6c-27	223	232	1845	508	2808	0.16	17.79	2.79	2.84	0.08	0.08	0.96
6c-29	245	315	1688	445	2693	0.21	23.57	2.54	2.90	0.09	0.12	0.78
6c-30	242	398	1627	497	2764	0.23	26.73	2.09	2.74	0.09	0.14	0.61
6c-31	154	263	1143	367	1927	0.22	24.69	2.06	2.70	0.08	0.14	0.59
6d-1	216	196	1434	358	2204	0.19	20.87	2.98	2.84	0.10	0.09	1.10
6d-2	188	195	1160	264	1807	0.21	24.10	2.94	3.00	0.10	0.11	0.96
6d-3	229	234	1479	332	2274	0.20	23.01	3.02	3.05	0.10	0.10	0.98
6d-4	215	206	1281	286	1988	0.21	24.08	3.04	2.97	0.11	0.10	1.04
6d-5	272	228	1593	386	2479	0.20	22.76	3.04	2.77	0.11	0.09	1.19
6d-6	247	237	1506	377	2367	0.20	23.12	2.86	2.79	0.10	0.10	1.04
6d-7	219	216	1563	368	2366	0.18	20.48	3.05	3.03	0.09	0.09	1.01
6d-8	213	209	1579	414	2415	0.17	19.35	2.88	2.85	0.09	0.09	1.02
6d-9	218	210	869	168	1465	0.29	35.53	2.88	2.80	0.15	0.14	1.04
6d-10	227	209	1498	397	2331	0.19	20.89	2.85	2.74	0.10	0.09	1.09
6d-11	254	247	1565	392	2458	0.20	23.04	2.85	2.80	0.10	0.10	1.03
6d-13	258	246	1506	344	2354	0.21	24.38	2.99	2.91	0.11	0.10	1.05

6d-14	169	163	1087	260	1679	0.20	22.25	2.97	2.91	0.10	0.10	1.04
6d-15	236	200	1624	412	2472	0.18	19.55	3.04	2.81	0.10	0.08	1.18
6d-16	218	172	1483	390	2263	0.17	19.05	3.03	2.72	0.10	0.08	1.27
6d-17	97	94	628	150	969	0.20	22.17	2.97	2.92	0.10	0.10	1.03
6d-18	198	234	1378	298	2108	0.20	23.18	2.96	3.25	0.09	0.11	0.85
6d-19	231	214	1614	412	2471	0.18	20.01	2.95	2.84	0.09	0.09	1.08
6d-20	265	236	1603	361	2465	0.20	22.96	3.13	2.94	0.11	0.10	1.12
6d-21	146	142	1179	294	1761	0.16	17.97	3.04	3.00	0.08	0.08	1.03
6d-22	220	219	1497	454	2390	0.18	20.46	2.55	2.55	0.09	0.09	1.00
6d-23	250	241	1539	355	2385	0.21	23.30	3.00	2.94	0.10	0.10	1.04
6d-24	243	212	1415	336	2206	0.21	23.35	3.03	2.81	0.11	0.10	1.15
6d-25	105	91	617	136	949	0.21	23.39	3.18	2.94	0.11	0.10	1.15
6d-26	239	256	1537	347	2379	0.21	23.59	2.95	3.06	0.10	0.11	0.93
6d-27	219	212	1628	384	2443	0.18	19.55	3.10	3.05	0.09	0.09	1.03
6d-28	244	183	1349	319	2095	0.20	23.03	3.17	2.72	0.12	0.09	1.33
6d-29	234	241	1560	344	2379	0.20	22.50	3.07	3.12	0.10	0.10	0.97
6d-30	242	224	1567	360	2393	0.19	21.86	3.10	2.98	0.10	0.09	1.08
6d-31	246	240	1490	347	2323	0.21	23.74	2.96	2.92	0.11	0.10	1.03
6d-32	138	110	783	189	1220	0.20	22.96	3.08	2.73	0.11	0.09	1.25
6d-33	256	212	1456	352	2276	0.21	23.27	3.04	2.74	0.11	0.09	1.21
6d-34	216	214	1488	383	2301	0.19	20.86	2.85	2.84	0.09	0.09	1.01
6d-35	244	234	1333	291	2102	0.23	26.16	3.00	2.93	0.12	0.11	1.04
6d-36	263	249	1472	339	2323	0.22	25.22	2.95	2.86	0.11	0.11	1.06
6d-37	163	157	957	252	1529	0.21	23.75	2.74	2.68	0.11	0.10	1.04

5) Pool #7

M_2 individuals	Green	Red	Both	None	Total	None/Total	CO rate (cM)	G/non G	R/non R	G/T	R/T	G/R
7a-1	183	162	1222	283	1850	0.19	20.81	3.16	2.97	0.10	0.09	1.13
7a-2	214	193	1313	348	2068	0.20	22.13	2.82	2.68	0.10	0.09	1.11
7a-3	172	171	1300	288	1931	0.18	19.70	3.21	3.20	0.09	0.09	1.01
7a-4	201	167	1101	259	1728	0.21	24.23	3.06	2.76	0.12	0.10	1.20
7a-5	178	189	1262	335	1964	0.19	20.86	2.75	2.83	0.09	0.10	0.94
7a-7	473	557	1062	21	2113	0.49	84.16	2.66	3.28	0.22	0.26	0.85
7a-8	216	223	1544	352	2335	0.19	21.01	3.06	3.11	0.09	0.10	0.97
7a-9	208	178	1364	318	2068	0.19	20.84	3.17	2.93	0.10	0.09	1.17
7a-10	216	194	1372	318	2100	0.20	21.93	3.10	2.93	0.10	0.09	1.11
7a-11	216	199	1344	345	2104	0.20	22.19	2.87	2.75	0.10	0.09	1.09
7a-12	244	260	1482	328	2314	0.22	24.87	2.94	3.05	0.11	0.11	0.94
7a-14	234	218	1486	292	2230	0.20	22.89	3.37	3.24	0.10	0.10	1.07
7a-15	247	222	1573	394	2436	0.19	21.58	2.95	2.80	0.10	0.09	1.11
7a-16	238	193	1536	290	2257	0.19	21.38	3.67	3.27	0.11	0.09	1.23
7a-17	182	221	1382	330	2115	0.19	21.33	2.84	3.13	0.09	0.10	0.82
7a-18	94	97	848	222	1261	0.15	16.51	2.95	2.99	0.07	0.08	0.97
7a-19	264	206	1506	320	2296	0.20	23.15	3.37	2.93	0.11	0.09	1.28
7a-20	246	228	1582	377	2433	0.19	21.87	3.02	2.91	0.10	0.09	1.08
7a-21	261	181	1457	401	2300	0.19	21.54	2.95	2.47	0.11	0.08	1.44
7a-22	267	242	1484	322	2315	0.22	25.15	3.10	2.93	0.12	0.10	1.10
7a-23	243	197	1433	369	2242	0.20	22.06	2.96	2.66	0.11	0.09	1.23
7a-24	225	232	1528	340	2325	0.20	22.10	3.06	3.12	0.10	0.10	0.97
7a-25	240	221	1632	374	2467	0.19	20.86	3.15	3.02	0.10	0.09	1.09

7a-26	226	207	1410	342	2185	0.20	22.30	2.98	2.85	0.10	0.09	1.09
7a-27	224	207	1514	392	2337	0.18	20.55	2.90	2.79	0.10	0.09	1.08
7a-28	268	176	1420	347	2211	0.20	22.65	3.23	2.60	0.12	0.08	1.52
7a-29	522	421	946	91	1980	0.48	78.21	2.87	2.23	0.26	0.21	1.24
7a-30	238	159	1401	304	2102	0.19	21.12	3.54	2.88	0.11	0.08	1.50
7a-31	123	134	983	233	1473	0.17	19.31	3.01	3.14	0.08	0.09	0.92
7a-32	220	154	1328	306	2008	0.19	20.79	3.37	2.82	0.11	0.08	1.43
7a-33	244	249	1605	374	2472	0.20	22.47	2.97	3.00	0.10	0.10	0.98
7a-34	276	167	1609	350	2402	0.18	20.56	3.65	2.84	0.11	0.07	1.65
7a-35	209	199	1486	389	2283	0.18	19.84	2.88	2.82	0.09	0.09	1.05
7a-36	238	224	1434	372	2268	0.20	23.02	2.81	2.72	0.10	0.10	1.06
7a-37	216	167	1292	324	1999	0.19	21.46	3.07	2.70	0.11	0.08	1.29
7a-38	289	255	1546	352	2442	0.22	25.54	3.02	2.81	0.12	0.10	1.13
7b-1	274	185	1621	387	2467	0.19	20.76	3.31	2.73	0.11	0.07	1.48
7b-2	100	122	1750	79	2051	0.11	11.48	9.20	10.46	0.05	0.06	0.82
7b-3	218	222	1660	421	2521	0.17	19.32	2.92	2.95	0.09	0.09	0.98
7b-4	234	234	1690	404	2562	0.18	20.33	3.02	3.02	0.09	0.09	1.00
7b-5	223	239	1678	378	2518	0.18	20.44	3.08	3.19	0.09	0.09	0.93
7b-6	42	224	1801	145	2212	0.12	12.85	4.99	10.83	0.02	0.10	0.19
7b-7	237	247	1667	394	2545	0.19	21.28	2.97	3.03	0.09	0.10	0.96
7b-8	262	269	1638	374	2543	0.21	23.69	2.95	3.00	0.10	0.11	0.97
7b-9	100	102	986	255	1443	0.14	15.15	3.04	3.06	0.07	0.07	0.98
7b-10	282	215	1681	425	2603	0.19	21.38	3.07	2.68	0.11	0.08	1.31
7b-11	6	22	1070	103	1201	0.02	2.36	8.61	10.02	0.00	0.02	0.27
7b-13	287	247	1675	423	2632	0.20	22.91	2.93	2.71	0.11	0.09	1.16
7b-14	283	225	1586	406	2500	0.20	22.95	2.96	2.63	0.11	0.09	1.26
7b-16	250	220	1746	408	2624	0.18	19.89	3.18	2.99	0.10	0.08	1.14
7b-17	224	223	1784	449	2680	0.17	18.37	2.99	2.98	0.08	0.08	1.00
7b-18	199	212	1470	360	2241	0.18	20.43	2.92	3.01	0.09	0.09	0.94
7b-19	245	256	1662	393	2556	0.20	22.03	2.94	3.01	0.10	0.10	0.96
7b-20	242	234	1639	370	2485	0.19	21.46	3.11	3.06	0.10	0.09	1.03
7b-21	188	193	1626	411	2418	0.16	17.24	3.00	3.04	0.08	0.08	0.97
7b-22	257	274	1695	425	2651	0.20	22.58	2.79	2.89	0.10	0.10	0.94
7b-23	234	233	1632	388	2487	0.19	20.98	3.00	3.00	0.09	0.09	1.00
7b-24	253	232	1474	359	2318	0.21	23.74	2.92	2.79	0.11	0.10	1.09
7b-25	207	193	1338	329	2067	0.19	21.71	2.96	2.86	0.10	0.09	1.07
7b-26	232	217	1510	416	2375	0.19	21.14	2.75	2.67	0.10	0.09	1.07
7b-27	235	248	1519	386	2388	0.20	22.83	2.77	2.85	0.10	0.10	0.95
7b-28	226	243	1525	375	2369	0.20	22.28	2.83	2.94	0.10	0.10	0.93
7b-29	216	205	1538	376	2335	0.18	20.04	3.02	2.94	0.09	0.09	1.05
7b-30	215	221	1621	400	2457	0.18	19.68	2.96	3.00	0.09	0.09	0.97
7b-31	228	246	1558	378	2410	0.20	22.11	2.86	2.98	0.09	0.10	0.93
7b-33	202	216	1363	362	2143	0.20	21.90	2.71	2.80	0.09	0.10	0.94
7b-34	60	85	484	182	811	0.18	19.85	2.04	2.35	0.07	0.10	0.71
7b-35	213	205	1532	427	2377	0.18	19.48	2.76	2.71	0.09	0.09	1.04
7b-36	225	216	1405	373	2219	0.20	22.38	2.77	2.71	0.10	0.10	1.04
7b-37	214	212	1637	390	2453	0.17	19.21	3.07	3.06	0.09	0.09	1.01
7b-38	216	230	1662	396	2504	0.18	19.76	3.00	3.09	0.09	0.09	0.94
7b-39	220	223	1553	395	2391	0.19	20.66	2.87	2.89	0.09	0.09	0.99
7c-1	252	186	1537	371	2346	0.19	20.84	3.21	2.77	0.11	0.08	1.35
7c-2	209	205	1230	305	1949	0.21	24.16	2.82	2.79	0.11	0.11	1.02
7c-3	249	242	1745	411	2647	0.19	20.69	3.05	3.01	0.09	0.09	1.03
7c-4	250	269	1538	379	2436	0.21	24.24	2.76	2.87	0.10	0.11	0.93
7c-5	228	210	1601	385	2424	0.18	20.09	3.07	2.95	0.09	0.09	1.09
7c-7	13	38	439	46	536	0.10	10.02	5.38	8.08	0.02	0.07	0.34
7c-8	166	160	1017	229	1572	0.21	23.50	3.04	2.98	0.11	0.10	1.04

7c-9	203	202	1611	393	2409	0.17	18.53	3.05	3.04	0.08	0.08	1.00
7c-10	198	189	1578	311	2276	0.17	18.76	3.55	3.47	0.09	0.08	1.05
7c-11	240	221	1619	394	2474	0.19	20.80	3.02	2.90	0.10	0.09	1.09
7c-12	234	238	1517	401	2390	0.20	22.22	2.74	2.76	0.10	0.10	0.98
7c-13	224	240	1586	360	2410	0.19	21.58	3.02	3.13	0.09	0.10	0.93
7c-14	220	213	1665	430	2528	0.17	18.92	2.93	2.89	0.09	0.08	1.03
7c-15	239	208	1630	391	2468	0.18	20.14	3.12	2.92	0.10	0.08	1.15
7c-16	127	150	907	272	1456	0.19	21.29	2.45	2.65	0.09	0.10	0.85
7c-19	165	164	1381	341	2051	0.16	17.59	3.06	3.05	0.08	0.08	1.01
7c-20	232	186	1548	476	2442	0.17	18.90	2.69	2.45	0.10	0.08	1.25
7c-21	205	252	1588	392	2437	0.19	20.95	2.78	3.08	0.08	0.10	0.81
7c-22	239	218	1722	435	2614	0.17	19.36	3.00	2.88	0.09	0.08	1.10
7c-23	275	228	1664	395	2562	0.20	22.07	3.11	2.82	0.11	0.09	1.21
7c-24	223	224	1456	375	2278	0.20	22.05	2.80	2.81	0.10	0.10	1.00
7c-25	281	214	1656	401	2552	0.19	21.77	3.15	2.74	0.11	0.08	1.31
7c-26	260	228	1659	400	2547	0.19	21.46	3.06	2.86	0.10	0.09	1.14
7c-27	242	260	1739	402	2643	0.19	21.25	2.99	3.10	0.09	0.10	0.93
7c-28	249	203	1563	335	2350	0.19	21.56	3.37	3.02	0.11	0.09	1.23
7c-29	191	186	1297	306	1980	0.19	21.31	3.02	2.98	0.10	0.09	1.03
7c-30	218	263	1754	420	2655	0.18	20.15	2.89	3.16	0.08	0.10	0.83
7c-31	264	256	1707	431	2658	0.20	21.98	2.87	2.82	0.10	0.10	1.03
7c-32	230	226	1595	373	2424	0.19	21.02	3.05	3.02	0.09	0.09	1.02
7c-33	224	231	1553	397	2405	0.19	21.16	2.83	2.87	0.09	0.10	0.97
7c-34	154	611	1351	15	2131	0.36	46.89	2.40	11.61	0.07	0.29	0.25
7c-35	263	268	1584	359	2474	0.21	24.45	2.95	2.98	0.11	0.11	0.98
7c-36	593	532	1247	59	2431	0.46	72.71	3.11	2.73	0.24	0.22	1.11
7c-37	224	237	1613	402	2476	0.19	20.78	2.87	2.96	0.09	0.10	0.95
7c-38	244	219	1718	485	2666	0.17	19.21	2.79	2.66	0.09	0.08	1.11
7c-39	139	126	921	223	1409	0.19	21.02	3.04	2.89	0.10	0.09	1.10
7c-40	48	34	294	73	449	0.18	20.33	3.20	2.71	0.11	0.08	1.41
7c-41	221	251	1464	353	2289	0.21	23.35	2.79	2.99	0.10	0.11	0.88
7c-42	248	227	1698	357	2530	0.19	20.97	3.33	3.18	0.10	0.09	1.09
7c-43	283	252	1695	430	2660	0.20	22.69	2.90	2.73	0.11	0.09	1.12
7c-44	271	267	1598	370	2506	0.21	24.46	2.93	2.91	0.11	0.11	1.01
7c-45	216	230	1346	343	2135	0.21	23.70	2.73	2.82	0.10	0.11	0.94
7c-46	224	212	1383	344	2163	0.20	22.74	2.89	2.81	0.10	0.10	1.06
7c-47	239	234	1538	368	2379	0.20	22.39	2.95	2.92	0.10	0.10	1.02
7c-48	242	212	1503	389	2346	0.19	21.71	2.90	2.72	0.10	0.09	1.14
7c-49	219	214	1459	349	2241	0.19	21.67	2.98	2.95	0.10	0.10	1.02
7c-50	252	260	1505	369	2386	0.21	24.45	2.79	2.84	0.11	0.11	0.97

6) Pool #8

M_2 individuals	Green	Red	Both	None	Total	None/Total	CO rate (cM)	G/non G	R/non R	G/T	R/T	G/R
8a-1	236	205	1364	325	2130	0.21	23.45	3.02	2.80	0.11	0.10	1.15
8a-2	313	189	1032	558	2092	0.24	27.88	1.80	1.40	0.15	0.09	1.66
8a-3	216	225	1448	320	2209	0.20	22.49	3.05	3.12	0.10	0.10	0.96
8a-4	201	213	1553	343	2310	0.18	19.90	3.15	3.25	0.09	0.09	0.94
8a-5	193	179	1123	276	1771	0.21	23.85	2.89	2.78	0.11	0.10	1.08
8a-6	193	211	1296	357	2057	0.20	22.08	2.62	2.74	0.09	0.10	0.91
8a-7	522	526	1055	54	2157	0.49	83.18	2.72	2.74	0.24	0.24	0.99
8a-8	249	234	1595	375	2453	0.20	22.14	3.03	2.93	0.10	0.10	1.06
8a-9	253	284	1506	442	2485	0.22	24.65	2.42	2.58	0.10	0.11	0.89
8a-10	355	218	1096	776	2445	0.23	27.11	1.46	1.16	0.15	0.09	1.63
8a-11	209	177	1329	369	2084	0.19	20.66	2.82	2.61	0.10	0.08	1.18
8a-12	215	189	1270	394	2068	0.20	21.94	2.55	2.40	0.10	0.09	1.14
8a-13	177	222	1371	320	2090	0.19	21.38	2.86	3.21	0.08	0.11	0.80
8a-14	169	135	1087	309	1700	0.18	19.85	2.83	2.56	0.10	0.08	1.25
8a-15	207	156	1247	318	1928	0.19	21.04	3.07	2.67	0.11	0.08	1.33
8a-16	251	269	1524	437	2481	0.21	23.79	2.51	2.61	0.10	0.11	0.93
8a-17	203	237	1664	414	2518	0.17	19.35	2.87	3.08	0.08	0.09	0.86
8a-18	209	314	1387	435	2345	0.22	25.57	2.13	2.64	0.09	0.13	0.67
8a-19	538	590	1247	50	2425	0.47	73.60	2.79	3.12	0.22	0.24	0.91
8a-20	473	553	955	158	2139	0.48	79.83	2.01	2.39	0.22	0.26	0.86
8a-21	233	240	1664	384	2521	0.19	20.96	3.04	3.09	0.09	0.10	0.97
8a-22	238	231	1597	402	2468	0.19	21.26	2.90	2.86	0.10	0.09	1.03
8a-23	290	284	1340	263	2177	0.26	31.25	2.98	2.94	0.13	0.13	1.02
8a-24	236	259	1728	459	2682	0.18	20.57	2.74	2.86	0.09	0.10	0.91
8a-25	219	247	1693	447	2606	0.18	19.85	2.76	2.91	0.08	0.09	0.89
8a-26	273	216	1004	670	2163	0.23	25.98	1.44	1.29	0.13	0.10	1.26
8a-27	353	256	1289	572	2470	0.25	28.80	1.98	1.67	0.14	0.10	1.38
8a-28	200	246	1431	401	2278	0.20	22.00	2.52	2.79	0.09	0.11	0.81
8a-29	268	209	1567	428	2472	0.19	21.64	2.88	2.55	0.11	0.08	1.28
8a-30	133	257	1480	421	2291	0.17	18.79	2.38	3.14	0.06	0.11	0.52
8a-31	223	203	1512	424	2362	0.18	20.04	2.77	2.65	0.09	0.09	1.10
8a-32	283	265	1679	465	2692	0.20	23.00	2.69	2.60	0.11	0.10	1.07
8a-33	252	209	981	482	1924	0.24	27.83	1.78	1.62	0.13	0.11	1.21
8a-34	256	309	1586	450	2601	0.22	24.80	2.43	2.68	0.10	0.12	0.83
8b-1	213	225	1376	337	2151	0.20	23.01	2.83	2.91	0.10	0.10	0.95
8b-2	208	290	1497	405	2400	0.21	23.51	2.45	2.92	0.09	0.12	0.72
8b-3	204	173	1225	316	1918	0.20	22.10	2.92	2.69	0.11	0.09	1.18
8b-4	251	236	1584	383	2454	0.20	22.34	2.96	2.87	0.10	0.10	1.06
8b-5	305	200	1600	333	2438	0.21	23.47	3.57	2.82	0.13	0.08	1.53
8b-6	178	172	1623	445	2418	0.14	15.71	2.92	2.88	0.07	0.07	1.03
8b-7	199	223	1441	424	2287	0.18	20.57	2.53	2.67	0.09	0.10	0.89
8b-8	211	192	1332	326	2061	0.20	21.97	2.98	2.84	0.10	0.09	1.10
8b-9	203	271	1638	452	2564	0.18	20.61	2.55	2.91	0.08	0.11	0.75
8b-10	519	595	1142	27	2283	0.49	84.48	2.67	3.18	0.23	0.26	0.87
8b-11	241	257	1480	455	2433	0.20	23.15	2.42	2.50	0.10	0.11	0.94
8b-12	265	292	1488	413	2458	0.23	26.06	2.49	2.63	0.11	0.12	0.91
8b-13	214	137	1117	261	1729	0.20	22.93	3.34	2.64	0.12	0.08	1.56
8b-14	226	235	1540	344	2345	0.20	22.10	3.05	3.11	0.10	0.10	0.96
8b-15	173	192	1185	332	1882	0.19	21.76	2.59	2.73	0.09	0.10	0.90
8b-16	178	231	1232	299	1940	0.21	23.95	2.66	3.07	0.09	0.12	0.77
8b-17	224	239	1542	396	2401	0.19	21.62	2.78	2.87	0.09	0.10	0.94
8b-18	241	243	1671	419	2574	0.19	21.01	2.89	2.90	0.09	0.09	0.99
8b-19	280	296	1635	450	2661	0.22	24.70	2.57	2.65	0.11	0.11	0.95
8b-20	240	301	1591	408	2540	0.21	24.24	2.58	2.92	0.09	0.12	0.80
8b-21	255	245	1572	387	2459	0.20	22.97	2.89	2.83	0.10	0.10	1.04

8b-22	245	254	1672	372	2543	0.20	22.05	3.06	3.12	0.10	0.10	0.96
8b-23	1	1	190	58	250	0.01	0.80	3.24	3.24	0.00	0.00	1.00
8b-24	240	258	1518	417	2433	0.20	23.15	2.60	2.70	0.10	0.11	0.93
8b-25	280	297	1647	446	2670	0.22	24.65	2.59	2.68	0.10	0.11	0.94
8b-26	219	260	1698	420	2597	0.18	20.56	2.82	3.06	0.08	0.10	0.84
8b-27	34	714	1477	174	2399	0.31	38.65	1.70	10.53	0.01	0.30	0.05
8b-28	132	1	498	25	656	0.20	22.90	24.23	3.18	0.20	0.00	132.00
8b-29	243	274	1601	427	2545	0.20	22.95	2.63	2.80	0.10	0.11	0.89
8b-30	230	230	1581	358	2399	0.19	21.48	3.08	3.08	0.10	0.10	1.00
8b-31	218	286	1421	431	2356	0.21	24.36	2.29	2.63	0.09	0.12	0.76
8b-32	210	218	1560	390	2378	0.18	20.00	2.91	2.96	0.09	0.09	0.96
8b-33	317	279	1072	294	1962	0.30	37.35	2.42	2.21	0.16	0.14	1.14
8b-36	269	254	1654	381	2558	0.20	23.12	3.03	2.94	0.11	0.10	1.06
8b-37	610	613	1257	44	2524	0.48	82.42	2.84	2.86	0.24	0.24	1.00
8b-38	260	242	1714	437	2653	0.19	21.16	2.91	2.81	0.10	0.09	1.07
8b-39	671	686	1389	31	2777	0.49	84.94	2.87	2.96	0.24	0.25	0.98
8b-40	19	22	150	43	234	0.18	19.40	2.60	2.77	0.08	0.09	0.86
8c-2	254	246	1013	191	1704	0.29	35.72	2.90	2.83	0.15	0.14	1.03
8c-3	187	197	1213	340	1937	0.20	22.31	2.61	2.68	0.10	0.10	0.95
8c-4	223	181	1397	321	2122	0.19	21.31	3.23	2.90	0.11	0.09	1.23
8c-5	174	151	1188	250	1763	0.18	20.54	3.40	3.16	0.10	0.09	1.15
8c-6	211	219	1323	365	2118	0.20	22.93	2.63	2.68	0.10	0.10	0.96
8c-7	222	181	1458	379	2240	0.18	19.99	3.00	2.73	0.10	0.08	1.23
8c-8	233	206	1396	311	2146	0.20	23.13	3.15	2.94	0.11	0.10	1.13
8c-9	201	177	1388	339	2105	0.18	19.95	3.08	2.90	0.10	0.08	1.14
8c-10	163	173	1228	284	1848	0.18	20.23	3.04	3.13	0.09	0.09	0.94
8c-11	218	221	1348	326	2113	0.21	23.55	2.86	2.88	0.10	0.10	0.99
8c-12	44	38	357	92	531	0.15	16.86	3.08	2.90	0.08	0.07	1.16
8c-13	150	137	955	198	1440	0.20	22.45	3.30	3.14	0.10	0.10	1.09
8c-14	202	197	1177	284	1860	0.21	24.44	2.87	2.83	0.11	0.11	1.03
8c-15	206	170	1283	369	2028	0.19	20.68	2.76	2.53	0.10	0.08	1.21
8c-16	224	197	1394	393	2208	0.19	21.35	2.74	2.58	0.10	0.09	1.14
8c-17	204	223	1422	359	2208	0.19	21.69	2.79	2.92	0.09	0.10	0.91
8c-18	169	229	1550	322	2270	0.18	19.42	3.12	3.62	0.07	0.10	0.74
8c-19	214	189	1460	399	2262	0.18	19.77	2.85	2.69	0.09	0.08	1.13
8c-20	136	166	1348	358	2008	0.15	16.38	2.83	3.06	0.07	0.08	0.82
8c-21	247	233	1454	342	2276	0.21	23.96	2.96	2.86	0.11	0.10	1.06
8c-22	250	219	1494	365	2328	0.20	22.73	2.99	2.79	0.11	0.09	1.14
8c-23	218	208	1525	325	2276	0.19	20.90	3.27	3.19	0.10	0.09	1.05
8c-24	259	238	1527	389	2413	0.21	23.31	2.85	2.72	0.11	0.10	1.09
8c-25	216	253	1492	361	2322	0.20	22.80	2.78	3.02	0.09	0.11	0.85
8c-26	208	206	1373	360	2147	0.19	21.62	2.79	2.78	0.10	0.10	1.01
8c-27	209	222	1409	337	2177	0.20	22.28	2.89	2.99	0.10	0.10	0.94
8c-28	208	212	1303	308	2031	0.21	23.42	2.91	2.94	0.10	0.10	0.98
8c-29	271	228	1464	398	2361	0.21	24.02	2.77	2.53	0.11	0.10	1.19
8c-30	238	242	1557	395	2432	0.20	22.20	2.82	2.84	0.10	0.10	0.98
8c-31	217	202	1501	343	2263	0.19	20.65	3.15	3.04	0.10	0.09	1.07
8c-32	168	143	1095	304	1710	0.18	20.23	2.83	2.62	0.10	0.08	1.17
8c-33	207	179	1278	291	1955	0.20	22.21	3.16	2.93	0.11	0.09	1.16
8c-34	202	201	1376	309	2088	0.19	21.64	3.09	3.09	0.10	0.10	1.00
8c-35	191	176	1358	343	2068	0.18	19.68	2.98	2.87	0.09	0.09	1.09
8c-36	241	229	1503	373	2346	0.20	22.58	2.90	2.82	0.10	0.10	1.05
8c-37	99	104	667	155	1025	0.20	22.29	2.96	3.04	0.10	0.10	0.95
8c-38	194	182	1212	353	1941	0.19	21.73	2.63	2.55	0.10	0.09	1.07
8c-39	172	190	1158	254	1774	0.20	23.07	3.00	3.16	0.10	0.11	0.91
8c-41	151	134	913	247	1445	0.20	22.18	2.79	2.63	0.10	0.09	1.13
8c-43	238	242	1557	395	2432	0.20	22.20	2.82	2.84	0.10	0.10	0.98

7) Pool #11

M_2 individuals	Green	Red	Both	None	Total	None/Total	CO rate (cM)	G/non G	R/non R	G/T	R/T	G/R
11a-1	223	228	1526	344	2321	0.19	21.81	3.06	3.09	0.10	0.10	0.98
11a-2	230	184	1252	348	2014	0.21	23.26	2.79	2.48	0.11	0.09	1.25
11a-3	165	194	1356	322	2037	0.18	19.53	2.95	3.18	0.08	0.10	0.85
11a-4	157	235	1302	315	2009	0.20	21.91	2.65	3.26	0.08	0.12	0.67
11a-5	141	134	769	184	1228	0.22	25.70	2.86	2.78	0.11	0.11	1.05
11a-6	138	141	1038	220	1537	0.18	20.19	3.26	3.29	0.09	0.09	0.98
11a-7	132	163	965	198	1458	0.20	22.84	3.04	3.42	0.09	0.11	0.81
11a-8	138	193	1003	215	1549	0.21	24.33	2.80	3.39	0.09	0.12	0.72
11a-9	168	204	1096	269	1737	0.21	24.39	2.67	2.97	0.10	0.12	0.82
11a-10	138	212	1072	209	1631	0.21	24.45	2.87	3.70	0.08	0.13	0.65
11a-11	184	213	1258	318	1973	0.20	22.70	2.72	2.93	0.09	0.11	0.86
11a-12	249	222	1410	283	2164	0.22	24.85	3.29	3.07	0.12	0.10	1.12
11a-13	210	271	1350	349	2180	0.22	25.25	2.52	2.90	0.10	0.12	0.77
11a-14	241	272	1342	402	2257	0.23	26.15	2.35	2.51	0.11	0.12	0.89
11a-15	135	163	997	222	1517	0.20	22.08	2.94	3.25	0.09	0.11	0.83
11a-16	187	260	1181	300	1928	0.23	26.77	2.44	2.96	0.10	0.13	0.72
11a-17	146	244	998	241	1629	0.24	27.81	2.36	3.21	0.09	0.15	0.60
11a-18	391	188	1156	43	1778	0.33	40.95	6.70	3.10	0.22	0.11	2.08
11a-19	214	225	1484	390	2313	0.19	21.23	2.76	2.83	0.09	0.10	0.95
11a-20	201	185	1258	336	1980	0.19	21.89	2.80	2.69	0.10	0.09	1.09
11a-21	225	234	1555	368	2382	0.19	21.60	2.96	3.02	0.09	0.10	0.96
11a-22	194	254	1472	359	2279	0.20	22.10	2.72	3.12	0.09	0.11	0.76
11a-23	164	219	1096	269	1748	0.22	25.05	2.58	3.04	0.09	0.13	0.75
11a-24	66	38	425	61	590	0.18	19.54	4.96	3.65	0.11	0.06	1.74
11a-25	5	23	141	27	196	0.14	15.48	2.92	5.13	0.03	0.12	0.22
11a-26	228	196	1399	333	2156	0.20	22.11	3.08	2.84	0.11	0.09	1.16
11a-27	140	157	1053	229	1579	0.19	21.02	3.09	3.28	0.09	0.10	0.89
11a-28	227	185	1345	329	2086	0.20	22.22	3.06	2.75	0.11	0.09	1.23
11a-29	179	201	1413	321	2114	0.18	19.97	3.05	3.23	0.08	0.10	0.89
11a-30	137	163	1016	271	1587	0.19	21.14	2.66	2.89	0.09	0.10	0.84
11b-1	196	202	1370	320	2088	0.19	21.34	3.00	3.05	0.09	0.10	0.97
11b-2	250	291	1409	377	2327	0.23	26.85	2.48	2.71	0.11	0.13	0.86
11b-3	183	259	1063	292	1797	0.25	28.72	2.26	2.78	0.10	0.14	0.71
11b-4	29	41	390	31	491	0.14	15.45	5.82	7.18	0.06	0.08	0.71
11b-5	177	298	1300	343	2118	0.22	25.74	2.30	3.07	0.08	0.14	0.59
11b-6	207	301	1360	360	2228	0.23	26.24	2.37	2.93	0.09	0.14	0.69
11b-7	233	330	1511	421	2495	0.23	25.93	2.32	2.81	0.09	0.13	0.71
11b-8	181	204	1292	312	1989	0.19	21.71	2.85	3.03	0.09	0.10	0.89
11b-9	219	174	1341	310	2044	0.19	21.55	3.22	2.86	0.11	0.09	1.26
11b-10	229	217	1502	363	2311	0.19	21.64	2.98	2.90	0.10	0.09	1.06
11b-11	201	162	1197	279	1839	0.20	22.20	3.17	2.83	0.11	0.09	1.24
11b-12	203	212	1364	339	2118	0.20	22.02	2.84	2.91	0.10	0.10	0.96
11b-13	204	144	443	16	807	0.43	62.91	4.04	2.67	0.25	0.18	1.42
11b-14	151	179	1131	282	1743	0.19	21.17	2.78	3.03	0.09	0.10	0.84
11b-15	188	209	1278	291	1966	0.20	22.79	2.93	3.10	0.10	0.11	0.90
11b-16	118	197	984	196	1495	0.21	23.93	2.80	3.76	0.08	0.13	0.60
11b-17	204	249	1404	372	2229	0.20	22.96	2.59	2.87	0.09	0.11	0.82
11b-18	189	224	1271	349	2033	0.20	22.95	2.55	2.78	0.09	0.11	0.84
11b-19	88	175	1064	199	1526	0.17	19.05	3.08	4.32	0.06	0.11	0.50
11b-20	218	220	1501	381	2320	0.19	21.11	2.86	2.87	0.09	0.09	0.99
11b-21	141	156	1129	247	1673	0.18	19.69	3.15	3.31	0.08	0.09	0.90
11b-22	200	257	1699	438	2594	0.18	19.52	2.73	3.07	0.08	0.10	0.78

11b-23	186	243	1347	303	2079	0.21	23.36	2.81	3.25	0.09	0.12	0.77
11b-24	186	273	1473	311	2243	0.20	23.14	2.84	3.51	0.08	0.12	0.68
11b-25	181	256	1196	281	1914	0.23	26.29	2.56	3.14	0.09	0.13	0.71
11b-26	198	276	1522	310	2306	0.21	23.26	2.94	3.54	0.09	0.12	0.72
11b-27	112	122	797	143	1174	0.20	22.45	3.43	3.60	0.10	0.10	0.92
11b-28	195	214	1262	315	1986	0.21	23.31	2.75	2.89	0.10	0.11	0.91
11b-29	174	146	1196	209	1725	0.19	20.69	3.86	3.50	0.10	0.08	1.19
11b-30	163	200	1270	297	1930	0.19	21.02	2.88	3.20	0.08	0.10	0.82
11b-31	78	122	729	160	1089	0.18	20.46	2.86	3.58	0.07	0.11	0.64
11c-1	175	242	1384	337	2138	0.20	21.90	2.69	3.18	0.08	0.11	0.72
11c-2	186	176	1281	314	1957	0.18	20.62	2.99	2.91	0.10	0.09	1.06
11c-3	209	204	1384	316	2113	0.20	21.96	3.06	3.02	0.10	0.10	1.02
11c-4	273	273	1140	199	1885	0.29	35.14	2.99	2.99	0.14	0.14	1.00
11c-5	178	183	1326	295	1982	0.18	20.27	3.15	3.19	0.09	0.09	0.97
11c-6	247	217	1511	379	2354	0.20	22.17	2.95	2.76	0.10	0.09	1.14
11c-7	227	210	1603	418	2458	0.18	19.72	2.91	2.81	0.09	0.09	1.08
11c-8	225	218	1693	437	2573	0.17	19.03	2.93	2.89	0.09	0.08	1.03
11c-9	477	521	1375	142	2515	0.40	54.57	2.79	3.06	0.19	0.21	0.92
11c-10	225	190	1504	407	2326	0.18	19.80	2.90	2.68	0.10	0.08	1.18
11c-11	203	243	1549	357	2352	0.19	21.21	2.92	3.20	0.09	0.10	0.84
11c-12	206	241	1575	381	2403	0.19	20.76	2.86	3.09	0.09	0.10	0.85
11c-13	222	245	1640	363	2470	0.19	21.14	3.06	3.22	0.09	0.10	0.91
11c-14	254	240	1658	395	2547	0.19	21.76	3.01	2.92	0.10	0.09	1.06
11c-15	196	207	1203	386	1992	0.20	22.84	2.36	2.42	0.10	0.10	0.95
11c-16	166	180	1200	326	1872	0.18	20.61	2.70	2.80	0.09	0.10	0.92
11c-17	174	189	1181	299	1843	0.20	22.15	2.78	2.90	0.09	0.10	0.92
11c-18	219	228	1660	429	2536	0.18	19.53	2.86	2.91	0.09	0.09	0.96
11c-19	635	631	1277	18	2561	0.49	89.36	2.95	2.92	0.25	0.25	1.01
11c-20	242	242	1796	414	2694	0.18	19.96	3.11	3.11	0.09	0.09	1.00
11c-21	208	239	1364	311	2122	0.21	23.93	2.86	3.09	0.10	0.11	0.87
11c-22	248	215	1607	410	2480	0.19	20.84	2.97	2.77	0.10	0.09	1.15
11c-23	216	209	1279	286	1990	0.21	24.31	3.02	2.96	0.11	0.11	1.03
11c-24	236	224	1654	391	2505	0.18	20.46	3.07	3.00	0.09	0.09	1.05
11c-25	159	189	1267	286	1901	0.18	20.38	3.00	3.27	0.08	0.10	0.84
11c-26	253	249	1517	372	2391	0.21	23.84	2.85	2.83	0.11	0.10	1.02
11c-28	163	158	1110	263	1694	0.19	21.20	3.02	2.98	0.10	0.09	1.03

8) Pool #14

M_2 individuals	Green	Red	Both	None	Total	None/Total	CO rate (cM)	G/non G	R/non R	G/T	R/T	G/R
14a-1	166	154	1018	250	1588	0.20	22.74	2.93	2.82	0.10	0.10	1.08
14a-3	141	216	1192	287	1836	0.19	21.83	2.65	3.29	0.08	0.12	0.65
14a-4	228	226	1486	407	2347	0.19	21.70	2.71	2.70	0.10	0.10	1.01
14a-5	157	206	1279	277	1919	0.19	21.15	2.97	3.42	0.08	0.11	0.76
14a-6	208	228	1402	301	2139	0.20	23.04	3.04	3.20	0.10	0.11	0.91
14a-7	161	169	1223	259	1812	0.18	20.27	3.23	3.31	0.09	0.09	0.95
14a-8	264	250	1350	274	2138	0.24	27.95	3.08	2.97	0.12	0.12	1.06
14a-9	211	193	1392	316	2112	0.19	21.42	3.15	3.01	0.10	0.09	1.09
14a-10	205	191	1219	278	1893	0.21	23.74	3.04	2.92	0.11	0.10	1.07
14a-11	2	126	370	38	536	0.24	27.72	2.27	12.40	0.00	0.24	0.02
14a-12	198	226	1159	283	1866	0.23	26.14	2.67	2.88	0.11	0.12	0.88
14a-13	220	225	1439	333	2217	0.20	22.63	2.97	3.01	0.10	0.10	0.98
14a-14	224	225	1356	291	2096	0.21	24.40	3.06	3.07	0.11	0.11	1.00
14a-15	214	187	1348	292	2041	0.20	22.09	3.26	3.03	0.10	0.09	1.14
14a-16	197	228	1470	381	2276	0.19	20.85	2.74	2.94	0.09	0.10	0.86
14a-17	184	199	1150	286	1819	0.21	23.92	2.75	2.87	0.10	0.11	0.92
14a-18	114	149	824	181	1268	0.21	23.50	2.84	3.30	0.09	0.12	0.77
14a-19	141	135	859	212	1347	0.20	23.18	2.88	2.82	0.10	0.10	1.04
14a-20	5	79	247	26	357	0.24	27.24	2.40	10.52	0.01	0.22	0.06
14a-21	93	75	518	75	761	0.22	25.27	4.07	3.53	0.12	0.10	1.24
14a-22	67	85	492	95	739	0.21	23.28	3.11	3.56	0.09	0.12	0.79
14a-23	142	199	1074	251	1666	0.20	23.15	2.70	3.24	0.09	0.12	0.71
14a-24	90	124	710	137	1061	0.20	22.76	3.07	3.67	0.08	0.12	0.73
14a-25	87	104	687	108	986	0.19	21.73	3.65	4.06	0.09	0.11	0.84
14b-1	139	148	1216	255	1758	0.16	17.93	3.36	3.46	0.08	0.08	0.94
14b-2	225	225	1344	334	2128	0.21	24.04	2.81	2.81	0.11	0.11	1.00
14b-3	211	239	1413	347	2210	0.20	23.01	2.77	2.96	0.10	0.11	0.88
14b-4	53	61	458	42	614	0.19	20.71	4.96	5.46	0.09	0.10	0.87
14b-5	197	224	1205	322	1948	0.22	24.65	2.57	2.75	0.10	0.11	0.88
14b-6	225	257	1421	366	2269	0.21	24.16	2.64	2.84	0.10	0.11	0.88
14b-7	162	198	1383	299	2042	0.18	19.54	3.11	3.43	0.08	0.10	0.82
14b-8	211	225	1454	334	2224	0.20	22.03	2.98	3.08	0.09	0.10	0.94
14b-9	141	174	938	238	1491	0.21	24.01	2.62	2.93	0.09	0.12	0.81
14b-10	239	187	1359	305	2090	0.20	23.04	3.25	2.84	0.11	0.09	1.28
14b-11	225	208	1485	365	2283	0.19	21.22	2.98	2.87	0.10	0.09	1.08
14b-12	210	193	1487	346	2236	0.18	20.03	3.15	3.02	0.09	0.09	1.09
14b-13	244	216	1501	359	2320	0.20	22.32	3.03	2.85	0.11	0.09	1.13
14b-14	142	209	1209	287	1847	0.19	21.26	2.72	3.31	0.08	0.11	0.68
14b-15	216	213	1392	354	2175	0.20	22.19	2.84	2.82	0.10	0.10	1.01
14b-16	15	3	213	13	244	0.07	7.67	14.25	7.71	0.06	0.01	5.00
14b-17	224	238	1330	355	2147	0.22	24.53	2.62	2.71	0.10	0.11	0.94
14b-18	198	162	1263	299	1922	0.19	20.92	3.17	2.87	0.10	0.08	1.22
14b-19	116	15	642	23	796	0.16	18.09	19.95	4.73	0.15	0.02	7.73

9) Pool #15

M_2 individuals	Green	Red	Both	None	Total	None/Total	CO rate (cM)	G/non G	R/non R	G/T	R/T	G/R
15a-1	177	161	1410	355	2103	0.16	17.63	3.08	2.95	0.08	0.08	1.10
15a-2	229	205	1620	422	2476	0.18	19.41	2.95	2.80	0.09	0.08	1.12
15a-3	143	131	1164	292	1730	0.16	17.34	3.09	2.98	0.08	0.08	1.09
15a-4	146	120	1004	281	1551	0.17	18.94	2.87	2.63	0.09	0.08	1.22
15a-5	177	180	1455	345	2157	0.17	18.21	3.11	3.13	0.08	0.08	0.98
15a-6	195	212	1374	312	2093	0.19	21.83	2.99	3.13	0.09	0.10	0.92
15a-7	243	236	1705	416	2600	0.18	20.53	2.99	2.95	0.09	0.09	1.03
15a-8	233	176	1365	364	2138	0.19	21.43	2.96	2.58	0.11	0.08	1.32
15a-9	193	189	1193	316	1891	0.20	22.80	2.74	2.72	0.10	0.10	1.02
15a-10	207	147	1362	393	2109	0.17	18.50	2.91	2.52	0.10	0.07	1.41
15a-11	146	154	960	271	1531	0.20	22.02	2.60	2.67	0.10	0.10	0.95
15a-12	178	171	1392	394	2135	0.16	17.96	2.78	2.73	0.08	0.08	1.04
15a-13	189	209	1507	370	2275	0.17	19.37	2.93	3.07	0.08	0.09	0.90
15a-14	198	224	1428	400	2250	0.19	20.95	2.61	2.76	0.09	0.10	0.88
15a-15	196	251	1486	387	2320	0.19	21.60	2.64	2.98	0.08	0.11	0.78
15a-16	197	234	1343	310	2084	0.21	23.43	2.83	3.11	0.09	0.11	0.84
15a-17	211	223	1475	395	2304	0.19	21.05	2.73	2.80	0.09	0.10	0.95
15a-18	262	230	1491	390	2373	0.21	23.49	2.83	2.64	0.11	0.10	1.14
15a-19	152	134	1187	319	1792	0.16	17.49	2.96	2.80	0.08	0.07	1.13
15a-22	202	206	1495	420	2323	0.18	19.46	2.71	2.73	0.09	0.09	0.98
15a-23	36	29	1329	470	1864	0.03	3.55	2.74	2.68	0.02	0.02	1.24

10) Pool #16

M_2 individuals	Green	Red	Both	None	Total	None/Total	CO rate (cM)	G/non G	R/non R	G/T	R/T	G/R
16a-1	188	244	1448	358	2238	0.19	21.65	2.72	3.10	0.08	0.11	0.77
16a-2	242	291	1648	427	2608	0.20	23.11	2.63	2.90	0.09	0.11	0.83
16a-3	167	153	1142	267	1729	0.19	20.64	3.12	2.98	0.10	0.09	1.09
16a-4	184	237	1438	294	2153	0.20	21.97	3.05	3.50	0.09	0.11	0.78
16a-5	221	340	1415	475	2451	0.23	26.36	2.01	2.52	0.09	0.14	0.65
16a-6	193	165	1301	341	2000	0.18	19.88	2.95	2.75	0.10	0.08	1.17
16a-7	168	160	1085	237	1650	0.20	22.38	3.16	3.07	0.10	0.10	1.05
16a-8	174	161	1163	253	1751	0.19	21.43	3.23	3.10	0.10	0.09	1.08
16a-9	112	169	907	151	1339	0.21	23.82	3.18	4.09	0.08	0.13	0.66
16a-10	206	215	1080	231	1732	0.24	28.32	2.88	2.96	0.12	0.12	0.96
16a-11	195	204	1322	304	2025	0.20	22.16	2.99	3.06	0.10	0.10	0.96
16a-12	153	175	1060	199	1587	0.21	23.41	3.24	3.51	0.10	0.11	0.87
16a-13	139	83	979	185	1386	0.16	17.56	4.17	3.28	0.10	0.06	1.67
16a-14	210	319	1580	392	2501	0.21	24.04	2.52	3.15	0.08	0.13	0.66
16a-15	57	61	494	69	681	0.17	19.16	4.24	4.40	0.08	0.09	0.93
16a-16	226	264	1583	426	2499	0.20	22.04	2.62	2.83	0.09	0.11	0.86
16a-17	130	169	1045	212	1556	0.19	21.53	3.08	3.55	0.08	0.11	0.77
16a-18	195	257	1468	332	2252	0.20	22.63	2.82	3.27	0.09	0.11	0.76
16a-19	16	85	624	42	767	0.13	14.17	5.04	12.22	0.02	0.11	0.19
16a-20	99	79	627	123	928	0.19	21.49	3.59	3.18	0.11	0.09	1.25
16a-21	194	225	1519	338	2276	0.18	20.51	3.04	3.28	0.09	0.10	0.86
16a-22	110	92	795	110	1107	0.18	20.31	4.48	4.03	0.10	0.08	1.20
16a-23	46	16	158	40	260	0.24	27.68	3.64	2.02	0.18	0.06	2.88
16a-24	205	199	1185	279	1868	0.22	24.67	2.91	2.86	0.11	0.11	1.03

11) Pool #581

M_2 individuals	Green	Red	Both	None	Total	None/Total	CO rate (cM)	G/non G	R/non R	G/T	R/T	G/R
581a-1	238	250	1732	442	2662	0.18	20.42	2.85	2.91	0.09	0.09	0.95
581a-2	253	385	1691	509	2838	0.22	25.81	2.17	2.72	0.09	0.14	0.66
581a-3	243	288	1792	457	2780	0.19	21.39	2.73	2.97	0.09	0.10	0.84
581a-4	243	287	1780	472	2782	0.19	21.32	2.67	2.89	0.09	0.10	0.85
581a-5	281	229	1666	379	2555	0.20	22.49	3.20	2.87	0.11	0.09	1.23
581a-6	37	55	232	75	399	0.23	26.59	2.07	2.56	0.09	0.14	0.67
581a-7	207	153	1401	322	2083	0.17	19.11	3.39	2.94	0.10	0.07	1.35
581a-8	212	130	894	280	1516	0.23	25.92	2.70	2.08	0.14	0.09	1.63
581a-9	240	277	1692	410	2619	0.20	22.21	2.81	3.03	0.09	0.11	0.87
581a-10	215	236	1171	272	1894	0.24	27.63	2.73	2.89	0.11	0.12	0.91
581a-11	202	177	1589	346	2314	0.16	18.00	3.42	3.22	0.09	0.08	1.14
581a-12	187	197	1474	398	2256	0.17	18.79	2.79	2.86	0.08	0.09	0.95
581a-13	207	230	1400	376	2213	0.20	22.21	2.65	2.80	0.09	0.10	0.90
581a-14	238	228	1720	408	2594	0.18	19.96	3.08	3.02	0.09	0.09	1.04
581a-15	302	265	1772	377	2716	0.21	23.68	3.23	3.00	0.11	0.10	1.14
581a-16	40	34	313	71	458	0.16	17.73	3.36	3.13	0.09	0.07	1.18
581a-17	229	286	1757	474	2746	0.19	20.95	2.61	2.91	0.08	0.10	0.80
581a-18	220	264	1800	438	2722	0.18	19.73	2.88	3.14	0.08	0.10	0.83
581a-19	251	267	1739	435	2692	0.19	21.57	2.83	2.92	0.09	0.10	0.94
581a-20	217	316	1633	395	2561	0.21	23.60	2.60	3.18	0.08	0.12	0.69
581a-21	244	241	1664	406	2555	0.19	21.24	2.95	2.93	0.10	0.09	1.01
581a-22	213	266	1772	499	2750	0.17	19.28	2.59	2.86	0.08	0.10	0.80
581a-23	98	74	510	154	836	0.21	23.29	2.67	2.32	0.12	0.09	1.32
581a-24	239	305	1631	473	2648	0.21	23.25	2.40	2.72	0.09	0.12	0.78
581a-25	207	392	1567	450	2616	0.23	26.38	2.11	2.98	0.08	0.15	0.53
581a-26	255	410	1582	460	2707	0.25	28.68	2.11	2.79	0.09	0.15	0.62
581a-27	225	373	1620	472	2690	0.22	25.48	2.18	2.86	0.08	0.14	0.60
581a-28	213	403	1773	485	2874	0.21	24.41	2.24	3.12	0.07	0.14	0.53
581a-29	107	435	1193	954	2689	0.20	22.74	0.94	1.53	0.04	0.16	0.25
581a-30	578	731	1328	70	2707	0.48	81.87	2.38	3.18	0.21	0.27	0.79
581a-31	229	308	1585	484	2606	0.21	23.33	2.29	2.65	0.09	0.12	0.74
581a-32	295	261	1738	447	2741	0.20	22.91	2.87	2.69	0.11	0.10	1.13
581a-33	236	280	1502	374	2392	0.22	24.60	2.66	2.92	0.10	0.12	0.84
581a-34	214	397	1716	513	2840	0.22	24.52	2.12	2.91	0.08	0.14	0.54
581a-35	213	264	1615	426	2518	0.19	21.19	2.65	2.94	0.08	0.10	0.81
581a-36	221	322	1410	476	2429	0.22	25.64	2.04	2.48	0.09	0.13	0.69
581a-37	341	489	1308	650	2788	0.30	36.39	1.45	1.81	0.12	0.18	0.70
581a-38	213	238	1549	365	2365	0.19	21.35	2.92	3.09	0.09	0.10	0.89
581a-39	181	175	923	192	1471	0.24	28.17	3.01	2.94	0.12	0.12	1.03
581a-40	253	266	1197	516	2232	0.23	26.86	1.85	1.90	0.11	0.12	0.95
581a-41	261	231	1588	422	2502	0.20	22.11	2.83	2.66	0.10	0.09	1.13
581a-42	261	205	1654	432	2552	0.18	20.33	3.01	2.68	0.10	0.08	1.27
581a-43	364	425	886	18	1693	0.47	73.94	2.82	3.43	0.22	0.25	0.86
581a-44	222	225	1539	408	2394	0.19	20.84	2.78	2.80	0.09	0.09	0.99
581a-45	22	600	99	778	1499	0.41	58.76	0.09	0.87	0.01	0.40	0.04
581b-1	221	230	1624	427	2502	0.18	20.03	2.81	2.86	0.09	0.09	0.96
581b-2	599	672	1323	23	2617	0.49	83.07	2.77	3.21	0.23	0.26	0.89
581b-3	237	227	1562	390	2416	0.19	21.52	2.92	2.85	0.10	0.09	1.04
581b-4	240	294	1805	483	2822	0.19	21.16	2.63	2.90	0.09	0.10	0.82
581b-5	191	125	26	1878	2220	0.14	15.42	0.11	0.07	0.09	0.06	1.53
581b-6	142	166	1031	264	1603	0.19	21.53	2.73	2.95	0.09	0.10	0.86
581b-7	207	278	1733	428	2646	0.18	20.41	2.75	3.17	0.08	0.11	0.74

581b-8	214	190	1634	336	2374	0.17	18.78	3.51	3.32	0.09	0.08	1.13
581b-9	243	261	1757	413	2674	0.19	21.07	2.97	3.08	0.09	0.10	0.93
581b-10	215	327	1318	428	2288	0.24	27.46	2.03	2.56	0.09	0.14	0.66
581b-11	508	582	1107	20	2217	0.49	87.08	2.68	3.20	0.23	0.26	0.87
581b-12	216	272	1718	421	2627	0.19	20.72	2.79	3.12	0.08	0.10	0.79
581b-13	215	273	1400	369	2257	0.22	24.66	2.52	2.86	0.10	0.12	0.79
581b-14	249	212	1342	240	2043	0.23	25.93	3.52	3.18	0.12	0.10	1.17
581b-15	149	112	964	246	1471	0.18	19.68	3.11	2.72	0.10	0.08	1.33
581b-17	114	432	1873	243	2662	0.21	23.20	2.94	6.46	0.04	0.16	0.26
581b-18	250	180	1520	314	2264	0.19	21.25	3.58	3.01	0.11	0.08	1.39
581b-19	208	205	1536	395	2344	0.18	19.53	2.91	2.89	0.09	0.09	1.01
581b-20	239	319	1715	468	2741	0.20	23.00	2.48	2.88	0.09	0.12	0.75
581b-21	241	316	1837	462	2856	0.20	21.90	2.67	3.06	0.08	0.11	0.76
581b-22	202	226	1610	419	2457	0.17	19.28	2.81	2.96	0.08	0.09	0.89
581b-23	221	286	1703	499	2709	0.19	20.90	2.45	2.76	0.08	0.11	0.77
581b-24	207	282	1775	456	2720	0.18	19.97	2.69	3.10	0.08	0.10	0.73
581b-25	310	328	1236	535	2409	0.26	31.42	1.79	1.85	0.13	0.14	0.95
581b-26	441	196	1239	57	1933	0.33	41.61	6.64	2.88	0.23	0.10	2.25
581b-27	338	252	1437	571	2598	0.23	26.12	2.16	1.86	0.13	0.10	1.34
581b-28	258	251	1501	438	2448	0.21	23.57	2.55	2.52	0.11	0.10	1.03
581b-29	113	85	671	168	1037	0.19	21.38	3.10	2.69	0.11	0.08	1.33
581b-30	235	294	1572	465	2566	0.21	23.34	2.38	2.67	0.09	0.11	0.80
581b-31	159	399	877	627	2062	0.27	32.27	1.01	1.62	0.08	0.19	0.40
581b-32	220	341	1718	522	2801	0.20	22.58	2.25	2.77	0.08	0.12	0.65
581b-34	122	321	795	443	1681	0.26	31.23	1.20	1.98	0.07	0.19	0.38
581b-35	194	503	1591	545	2833	0.25	28.73	1.70	2.83	0.07	0.18	0.39
581b-36	230	249	1591	510	2580	0.19	20.71	2.40	2.49	0.09	0.10	0.92
581b-37	304	298	1305	517	2424	0.25	29.06	1.97	1.95	0.13	0.12	1.02
581b-38	161	182	1194	291	1828	0.19	20.96	2.86	3.04	0.09	0.10	0.88
581b-40	199	231	1515	369	2314	0.19	20.73	2.86	3.07	0.09	0.10	0.86
581b-41	100	614	561	862	2137	0.33	42.40	0.45	1.22	0.05	0.29	0.16
581b-42	216	223	1410	339	2188	0.20	22.62	2.89	2.94	0.10	0.10	0.97
581b-43	236	213	1469	315	2233	0.20	22.68	3.23	3.05	0.11	0.10	1.11
581b-44	114	389	1576	222	2301	0.22	24.98	2.77	5.85	0.05	0.17	0.29
581b-45	229	222	1592	376	2419	0.19	20.81	3.05	3.00	0.09	0.09	1.03

12) Pool #586

M_2 individuals	Green	Red	Both	None	Total	None/Total	CO rate (cM)	G/non G	R/non R	G/T	R/T	G/R
586a-3	120	197	964	230	1511	0.21	23.82	2.54	3.32	0.08	0.13	0.61
586a-4	244	355	1626	442	2667	0.22	25.78	2.35	2.89	0.09	0.13	0.69
586a-5	117	245	1327	241	1930	0.19	20.95	2.97	4.39	0.06	0.13	0.48
586a-6	243	274	1811	429	2757	0.19	20.95	2.92	3.10	0.09	0.10	0.89
586a-7	157	203	1308	272	1940	0.19	20.70	3.08	3.52	0.08	0.10	0.77
586a-8	93	127	710	151	1081	0.20	23.00	2.89	3.43	0.09	0.12	0.73
586a-9	186	227	1158	398	1969	0.21	23.81	2.15	2.37	0.09	0.12	0.82
586a-10	620	292	1942	54	2908	0.31	38.95	7.40	3.31	0.21	0.10	2.12
586a-11	163	101	1617	68	1949	0.14	14.61	10.53	7.44	0.08	0.05	1.61
586a-12	139	233	1327	267	1966	0.19	21.16	2.93	3.84	0.07	0.12	0.60
586a-13	182	186	1741	415	2524	0.15	15.83	3.20	3.23	0.07	0.07	0.98
586a-14	227	244	1561	359	2391	0.20	22.15	2.97	3.08	0.09	0.10	0.93
586a-15	7	89	258	29	383	0.25	29.38	2.25	9.64	0.02	0.23	0.08
586a-16	222	246	1781	405	2654	0.18	19.54	3.08	3.23	0.08	0.09	0.90
586a-17	46	3	398	13	460	0.11	11.29	27.75	6.80	0.10	0.01	15.33
586a-18	244	374	1731	462	2811	0.22	25.15	2.36	2.98	0.09	0.13	0.65
586a-19	210	250	1860	415	2735	0.17	18.54	3.11	3.38	0.08	0.09	0.84
586a-20	196	292	1476	422	2386	0.20	23.13	2.34	2.86	0.08	0.12	0.67
586a-21	312	133	1224	383	2052	0.22	24.75	2.98	1.95	0.15	0.06	2.35
586a-22	209	247	1543	445	2444	0.19	20.83	2.53	2.74	0.09	0.10	0.85
586a-23	241	231	1834	438	2744	0.17	19.01	3.10	3.04	0.09	0.08	1.04
586a-24	202	368	1471	451	2492	0.23	26.34	2.04	2.82	0.08	0.15	0.55
586a-25	210	270	1333	341	2154	0.22	25.55	2.53	2.91	0.10	0.13	0.78
586a-26	99	271	1008	214	1592	0.23	26.84	2.28	4.09	0.06	0.17	0.37
586a-27	160	250	1320	268	1998	0.21	23.22	2.86	3.67	0.08	0.13	0.64
586a-28	248	217	1708	437	2610	0.18	19.77	2.99	2.81	0.10	0.08	1.14
586a-29	123	195	1213	263	1794	0.18	19.66	2.92	3.65	0.07	0.11	0.63
586a-30	195	324	1994	405	2918	0.18	19.73	3.00	3.86	0.07	0.11	0.60
586a-31	237	361	1748	443	2789	0.21	24.42	2.47	3.10	0.08	0.13	0.66
586a-32	213	272	1860	380	2725	0.18	19.75	3.18	3.60	0.08	0.10	0.78
586a-33	151	159	1161	297	1768	0.18	19.42	2.88	2.95	0.09	0.09	0.95
586b-1	55	27	496	31	609	0.13	14.52	9.50	6.08	0.09	0.04	2.04
586b-2	231	286	1766	432	2715	0.19	21.31	2.78	3.10	0.09	0.11	0.81
586b-3	156	207	1087	275	1725	0.21	23.90	2.58	3.00	0.09	0.12	0.75
586b-4	165	221	1344	318	2048	0.19	21.07	2.80	3.24	0.08	0.11	0.75
586b-5	21	33	286	42	382	0.14	15.31	4.09	5.06	0.05	0.09	0.64
586b-6	209	274	1616	358	2457	0.20	22.10	2.89	3.33	0.09	0.11	0.76
586b-7	233	397	1536	433	2599	0.24	28.22	2.13	2.90	0.09	0.15	0.59
586b-8	267	326	1795	476	2864	0.21	23.46	2.57	2.85	0.09	0.11	0.82
586b-9	254	301	1709	442	2706	0.21	23.20	2.64	2.89	0.09	0.11	0.84
586b-10	241	258	1756	406	2661	0.19	20.95	3.01	3.11	0.09	0.10	0.93
586b-11	239	278	1528	400	2445	0.21	24.03	2.61	2.83	0.10	0.11	0.86
586b-12	213	366	1550	416	2545	0.23	26.18	2.25	3.05	0.08	0.14	0.58
586b-13	23	290	1910	151	2374	0.13	14.19	4.38	12.64	0.01	0.12	0.08
586b-14	270	238	1358	310	2176	0.23	26.99	2.97	2.75	0.12	0.11	1.13
586b-15	256	296	1732	410	2694	0.20	23.18	2.82	3.05	0.10	0.11	0.86
586b-16	247	300	1744	368	2659	0.21	23.28	2.98	3.32	0.09	0.11	0.82
586b-17	217	235	1571	328	2351	0.19	21.55	3.18	3.31	0.09	0.10	0.92
586b-18	296	189	1321	422	2228	0.22	24.86	2.65	2.10	0.13	0.08	1.57

586b-19	214	275	1476	383	2348	0.21	23.61	2.57	2.93	0.09	0.12	0.78
586b-20	275	343	1842	413	2873	0.22	24.52	2.80	3.18	0.10	0.12	0.80
586b-21	221	169	1130	281	1801	0.22	24.71	3.00	2.59	0.12	0.09	1.31
586b-22	139	189	1157	234	1719	0.19	21.36	3.06	3.61	0.08	0.11	0.74
586b-23	274	218	1472	365	2329	0.21	24.01	2.99	2.64	0.12	0.09	1.26
586b-24	210	277	1354	441	2282	0.21	24.29	2.18	2.51	0.09	0.12	0.76
586b-25	231	214	1325	344	2114	0.21	23.91	2.79	2.68	0.11	0.10	1.08
586b-26	69	8	525	10	612	0.13	13.49	33.00	6.75	0.11	0.01	8.63
586b-27	150	108	1098	156	1512	0.17	18.84	4.73	3.94	0.10	0.07	1.39
586b-28	241	312	1651	348	2552	0.22	24.73	2.87	3.33	0.09	0.12	0.77
586b-29	260	306	1597	446	2609	0.22	24.76	2.47	2.70	0.10	0.12	0.85
586b-30	161	117	1154	181	1613	0.17	19.05	4.41	3.72	0.10	0.07	1.38
586b-31	555	555	1104	20	2234	0.50	92.08	2.89	2.89	0.25	0.25	1.00
586b-32	174	231	1398	345	2148	0.19	21.08	2.73	3.14	0.08	0.11	0.75
586b-33	96	75	901	106	1178	0.15	15.76	5.51	4.83	0.08	0.06	1.28
586b-35	36	595	256	955	1842	0.34	43.89	0.19	0.86	0.02	0.32	0.06
586b-36	10	631	105	990	1736	0.37	48.86	0.07	0.74	0.01	0.36	0.02

13) Pool #593

M2 individuals	Green	Red	Both	None	Total	None/Total	CO rate (cM)	G/non G	R/non R	G/T	R/T	G/R
593a-1	179	178	1190	350	1897	0.19	21.03	2.59	2.59	0.09	0.09	1.01
593a-2	191	177	1356	408	2132	0.17	19.08	2.64	2.56	0.09	0.08	1.08
593a-3	174	162	1505	367	2208	0.15	16.59	3.17	3.08	0.08	0.07	1.07
593a-4	192	196	1581	411	2380	0.16	17.91	2.92	2.95	0.08	0.08	0.98
593a-5	153	148	1332	354	1987	0.15	16.51	2.96	2.92	0.08	0.07	1.03
593a-6	96	96	784	253	1229	0.16	17.08	2.52	2.52	0.08	0.08	1.00
593a-7	212	184	1643	383	2422	0.16	17.96	3.27	3.07	0.09	0.08	1.15
593a-8	240	195	1771	463	2669	0.16	17.90	3.06	2.80	0.09	0.07	1.23
593a-9	177	182	1834	499	2692	0.13	14.37	2.95	2.98	0.07	0.07	0.97
593a-10	240	240	1755	463	2698	0.18	19.74	2.84	2.84	0.09	0.09	1.00
593a-11	205	194	1543	395	2337	0.17	18.85	2.97	2.90	0.09	0.08	1.06
593a-12	218	232	1682	486	2618	0.17	18.99	2.65	2.72	0.08	0.09	0.94
593a-13	189	183	1516	357	2245	0.17	18.23	3.16	3.11	0.08	0.08	1.03
593a-14	211	202	1683	465	2561	0.16	17.69	2.84	2.79	0.08	0.08	1.04
593a-15	150	184	1276	319	1929	0.17	19.15	2.83	3.11	0.08	0.10	0.82
593a-16	30	53	211	53	347	0.24	27.78	2.27	3.18	0.09	0.15	0.57
593a-17	435	440	975	77	1927	0.45	69.69	2.73	2.76	0.23	0.23	0.99
593a-18	140	134	1132	279	1685	0.16	17.86	3.08	3.02	0.08	0.08	1.04
593a-19	210	186	1623	475	2494	0.16	17.39	2.77	2.64	0.08	0.07	1.13
593a-20	150	159	1301	309	1919	0.16	17.66	3.10	3.18	0.08	0.08	0.94
593a-21	168	157	1379	351	2055	0.16	17.31	3.05	2.96	0.08	0.08	1.07
593a-22	94	81	650	186	1011	0.17	19.14	2.79	2.61	0.09	0.08	1.16
593a-23	182	199	1604	391	2376	0.16	17.58	3.03	3.15	0.08	0.08	0.91
593a-24	178	198	1438	376	2190	0.17	18.97	2.82	2.95	0.08	0.09	0.90
593a-25	135	150	1126	273	1684	0.17	18.67	2.98	3.13	0.08	0.09	0.90
593a-26	182	183	1681	436	2482	0.15	15.98	3.01	3.02	0.07	0.07	0.99
593a-27	211	228	1562	407	2408	0.18	20.29	2.79	2.90	0.09	0.09	0.93
593a-28	187	157	1385	333	2062	0.17	18.37	3.21	2.97	0.09	0.08	1.19
593a-29	567	598	1238	27	2430	0.48	79.71	2.89	3.09	0.23	0.25	0.95
593a-30	251	223	1558	393	2425	0.20	21.96	2.94	2.77	0.10	0.09	1.13
593a-31	189	184	1507	346	2226	0.17	18.46	3.20	3.16	0.08	0.08	1.03
593a-32	114	83	720	148	1065	0.18	20.62	3.61	3.06	0.11	0.08	1.37

593a-33	71	73	659	161	964	0.15	16.26	3.12	3.16	0.07	0.08	0.97
593a-34	218	178	1622	378	2396	0.17	18.18	3.31	3.02	0.09	0.07	1.22
593a-35	143	126	722	284	1275	0.21	23.97	2.11	1.99	0.11	0.10	1.13
593a-36	30	38	287	69	424	0.16	17.58	2.96	3.28	0.07	0.09	0.79
593a-37	156	172	1318	320	1966	0.17	18.37	3.00	3.13	0.08	0.09	0.91
593a-38	272	234	1819	420	2745	0.18	20.54	3.20	2.97	0.10	0.09	1.16
593a-39	204	220	1643	391	2458	0.17	19.07	3.02	3.13	0.08	0.09	0.93
593a-40	150	180	1340	328	1998	0.17	18.17	2.93	3.18	0.08	0.09	0.83
593a-41	175	168	1321	319	1983	0.17	19.13	3.07	3.01	0.09	0.08	1.04
593a-42	100	143	1021	244	1508	0.16	17.68	2.90	3.38	0.07	0.09	0.70
593a-43	196	208	1593	403	2400	0.17	18.55	2.93	3.01	0.08	0.09	0.94
593a-44	223	217	1612	348	2400	0.18	20.42	3.25	3.20	0.09	0.09	1.03
593a-45	153	162	1154	270	1739	0.18	20.14	3.03	3.11	0.09	0.09	0.94
593a-46	182	183	1344	328	2037	0.18	19.90	2.99	2.99	0.09	0.09	0.99
593a-47	176	206	1543	392	2317	0.16	18.13	2.87	3.08	0.08	0.09	0.85
593a-48	231	205	1531	372	2339	0.19	20.80	3.05	2.88	0.10	0.09	1.13
593b-1	531	555	1174	64	2324	0.47	74.43	2.75	2.91	0.23	0.24	0.96
593b-2	202	227	1636	349	2414	0.18	19.71	3.19	3.38	0.08	0.09	0.89
593b-3	182	167	1545	353	2247	0.16	16.97	3.32	3.20	0.08	0.07	1.09
593b-4	79	87	578	138	882	0.19	21.03	2.92	3.06	0.09	0.10	0.91
593b-5	223	191	1560	372	2346	0.18	19.56	3.17	2.94	0.10	0.08	1.17
593b-6	194	161	1390	343	2088	0.17	18.76	3.14	2.89	0.09	0.08	1.20
593b-7	60	64	509	118	751	0.17	18.16	3.13	3.22	0.08	0.09	0.94
593b-8	226	199	1467	338	2230	0.19	21.33	3.15	2.95	0.10	0.09	1.14
593b-9	246	213	1777	414	2650	0.17	19.16	3.23	3.02	0.09	0.08	1.15
593b-10	186	199	1291	303	1979	0.19	21.84	2.94	3.05	0.09	0.10	0.93
593b-11	139	122	1010	219	1490	0.18	19.40	3.37	3.16	0.09	0.08	1.14
593b-12	157	205	1276	303	1941	0.19	20.82	2.82	3.22	0.08	0.11	0.77
593b-13	183	169	1493	390	2235	0.16	17.23	3.00	2.90	0.08	0.08	1.08
593b-14	46	1	626	8	681	0.07	7.16	74.67	11.61	0.07	0.00	46.00
593b-15	266	219	1786	383	2654	0.18	20.34	3.41	3.09	0.10	0.08	1.21
593b-16	209	185	1604	370	2368	0.17	18.32	3.27	3.09	0.09	0.08	1.13
593b-17	235	277	1797	436	2745	0.19	20.82	2.85	3.09	0.09	0.10	0.85
593b-18	131	172	910	246	1459	0.21	23.54	2.49	2.87	0.09	0.12	0.76
593b-19	81	90	620	165	956	0.18	19.86	2.75	2.89	0.08	0.09	0.90
593b-20	254	195	1629	398	2476	0.18	20.17	3.18	2.80	0.10	0.08	1.30
593b-21	197	239	1695	400	2531	0.17	19.04	2.96	3.24	0.08	0.09	0.82
593b-22	217	154	1237	313	1921	0.19	21.66	3.11	2.62	0.11	0.08	1.41
593b-23	189	188	1467	219	2063	0.18	20.34	4.07	4.06	0.09	0.09	1.01
593b-24	301	234	1746	394	2675	0.20	22.54	3.26	2.85	0.11	0.09	1.29
593b-25	149	101	859	221	1330	0.19	21.00	3.13	2.59	0.11	0.08	1.48
593b-26	220	160	1420	332	2132	0.18	19.78	3.33	2.86	0.10	0.08	1.38
593b-27	289	217	1817	391	2714	0.19	20.81	3.46	2.99	0.11	0.08	1.33
593b-28	67	152	774	172	1165	0.19	21.00	2.60	3.87	0.06	0.13	0.44
593b-29	287	187	1767	330	2571	0.18	20.55	3.97	3.17	0.11	0.07	1.53
593b-30	246	213	1703	437	2599	0.18	19.58	3.00	2.81	0.09	0.08	1.15
593b-31	226	198	1700	421	2545	0.17	18.34	3.11	2.93	0.09	0.08	1.14
593b-32	252	242	1672	420	2586	0.19	21.39	2.91	2.85	0.10	0.09	1.04
593b-33	94	102	781	198	1175	0.17	18.37	2.92	3.02	0.08	0.09	0.92
593b-34	54	72	559	90	775	0.16	17.85	3.78	4.38	0.07	0.09	0.75
593b-35	233	116	1316	270	1935	0.18	20.05	4.01	2.85	0.12	0.06	2.01
593b-36	205	157	1379	301	2042	0.18	19.66	3.46	3.04	0.10	0.08	1.31

14) Pool #598

M_2 individuals	Green	Red	Both	None	Total	None/Total	CO rate (cM)	G/non G	R/non R	G/T	R/T	G/R
598a-1	203	245	1467	412	2327	0.19	21.58	2.54	2.78	0.09	0.11	0.83
598a-2	202	165	1293	357	2017	0.18	20.24	2.86	2.61	0.10	0.08	1.22
598a-3	42	119	345	29	535	0.30	36.90	2.61	6.54	0.08	0.22	0.35
598a-4	198	226	1447	357	2228	0.19	21.30	2.82	3.01	0.09	0.10	0.88
598a-5	208	206	1653	399	2466	0.17	18.50	3.08	3.06	0.08	0.08	1.01
598a-6	187	208	1618	394	2407	0.16	18.04	3.00	3.14	0.08	0.09	0.90
598a-7	230	199	1545	398	2372	0.18	20.11	2.97	2.78	0.10	0.08	1.16
598a-8	209	195	1498	431	2333	0.17	19.15	2.73	2.65	0.09	0.08	1.07
598a-9	213	198	1672	425	2508	0.16	18.01	3.03	2.93	0.08	0.08	1.08
598a-10	205	199	1603	396	2403	0.17	18.53	3.04	3.00	0.09	0.08	1.03
598a-11	196	198	1498	346	2238	0.18	19.51	3.11	3.13	0.09	0.09	0.99
598a-12	454	483	984	19	1940	0.48	81.56	2.86	3.10	0.23	0.25	0.94
598a-13	264	240	1546	331	2381	0.21	24.06	3.17	3.00	0.11	0.10	1.10
598a-14	226	221	1618	353	2418	0.18	20.61	3.21	3.18	0.09	0.09	1.02
598a-15	231	238	1658	442	2569	0.18	20.32	2.78	2.82	0.09	0.09	0.97
598a-16	150	151	1222	295	1818	0.17	18.22	3.08	3.09	0.08	0.08	0.99
598a-17	204	246	1705	444	2599	0.17	19.15	2.77	3.01	0.08	0.09	0.83
598a-18	119	121	1085	274	1599	0.15	16.35	3.05	3.07	0.07	0.08	0.98
598a-19	237	222	1594	427	2480	0.19	20.64	2.82	2.73	0.10	0.09	1.07
598a-20	244	223	1854	436	2757	0.17	18.68	3.18	3.05	0.09	0.08	1.09
598a-21	264	230	1771	692	2957	0.17	18.40	2.21	2.09	0.09	0.08	1.15
598a-22	307	279	1682	550	2818	0.21	23.57	2.40	2.29	0.11	0.10	1.10
598a-23	312	369	1381	459	2521	0.27	32.20	2.04	2.27	0.12	0.15	0.85
598a-24	31	34	228	58	351	0.19	20.65	2.82	2.94	0.09	0.10	0.91
598a-25	220	218	1851	494	2783	0.16	17.22	2.91	2.90	0.08	0.08	1.01
598a-26	229	277	1746	493	2745	0.18	20.54	2.56	2.80	0.08	0.10	0.83
598a-27	282	287	1550	698	2817	0.20	22.80	1.86	1.87	0.10	0.10	0.98
598a-28	218	220	1820	662	2920	0.15	16.33	2.31	2.32	0.07	0.08	0.99
598a-29	69	84	574	150	877	0.17	19.31	2.75	3.00	0.08	0.10	0.82
598a-30	214	229	1703	447	2593	0.17	18.86	2.84	2.92	0.08	0.09	0.93
598a-31	242	257	1803	519	2821	0.18	19.61	2.64	2.71	0.09	0.09	0.94
598a-32	221	244	1777	504	2746	0.17	18.68	2.67	2.79	0.08	0.09	0.91
598a-33	191	203	1415	339	2148	0.18	20.43	2.96	3.05	0.09	0.09	0.94
598a-34	178	213	1485	363	2239	0.17	19.33	2.89	3.14	0.08	0.10	0.84
598a-35	229	267	1782	699	2977	0.17	18.34	2.08	2.21	0.08	0.09	0.86
598a-36	139	165	921	280	1505	0.20	22.80	2.38	2.59	0.09	0.11	0.84
598a-37	271	250	1612	887	3020	0.17	19.07	1.66	1.61	0.09	0.08	1.08
598a-38	535	492	1098	58	2183	0.47	75.69	2.97	2.68	0.25	0.23	1.09
598a-39	159	136	1095	284	1674	0.18	19.53	2.99	2.78	0.09	0.08	1.17
598a-40	208	228	1654	473	2563	0.17	18.77	2.66	2.76	0.08	0.09	0.91
598a-41	245	262	1667	420	2594	0.20	21.96	2.80	2.90	0.09	0.10	0.94
598a-42	242	259	1727	753	2981	0.17	18.52	1.95	2.00	0.08	0.09	0.93
598a-43	215	263	1793	434	2705	0.18	19.59	2.88	3.17	0.08	0.10	0.82
598a-44	254	256	1663	723	2896	0.18	19.51	1.96	1.96	0.09	0.09	0.99
598a-45	231	265	1681	395	2572	0.19	21.62	2.90	3.11	0.09	0.10	0.87
598a-46	187	185	1491	387	2250	0.17	18.19	2.93	2.92	0.08	0.08	1.01
598a-47	301	268	1823	296	2688	0.21	24.06	3.77	3.50	0.11	0.10	1.12
598a-48	98	454	1138	433	2123	0.26	30.72	1.39	3.00	0.05	0.21	0.22
598a-49	101	78	532	128	839	0.21	24.28	3.07	2.66	0.12	0.09	1.29
598a-50	192	249	1696	371	2508	0.18	19.48	3.05	3.45	0.08	0.10	0.77
598a-51	236	260	1775	532	2803	0.18	19.62	2.54	2.65	0.08	0.09	0.91
598a-52	205	255	1805	625	2890	0.16	17.44	2.28	2.48	0.07	0.09	0.80

598b-1	87	124	819	203	1233	0.17	18.90	2.77	3.25	0.07	0.10	0.70
598b-2	118	117	997	204	1436	0.16	17.98	3.47	3.46	0.08	0.08	1.01
598b-3	228	168	903	385	1684	0.24	27.22	2.05	1.75	0.14	0.10	1.36
598b-4	149	160	1295	381	1985	0.16	17.01	2.67	2.75	0.08	0.08	0.93
598b-5	125	110	1066	288	1589	0.15	16.08	2.99	2.85	0.08	0.07	1.14
598b-6	152	145	1226	261	1784	0.17	18.33	3.39	3.32	0.09	0.08	1.05
598b-7	153	151	1377	348	2029	0.15	16.31	3.07	3.05	0.08	0.07	1.01
598b-8	40	472	1190	107	1809	0.28	34.13	2.12	11.31	0.02	0.26	0.08
598b-9	136	138	1066	294	1634	0.17	18.48	2.78	2.80	0.08	0.08	0.99
598b-10	161	158	1366	339	2024	0.16	17.25	3.07	3.05	0.08	0.08	1.02
598b-11	86	102	758	203	1149	0.16	17.98	2.77	2.98	0.07	0.09	0.84
598b-12	238	178	1307	515	2238	0.19	20.74	2.23	1.97	0.11	0.08	1.34
598b-13	163	405	791	565	1924	0.30	36.00	0.98	1.64	0.08	0.21	0.40
598b-14	161	157	1322	371	2011	0.16	17.31	2.81	2.78	0.08	0.08	1.03
598b-15	167	437	973	371	1948	0.31	38.37	1.41	2.62	0.09	0.22	0.38
598b-16	132	115	1049	242	1538	0.16	17.61	3.31	3.11	0.09	0.07	1.15
598b-17	210	200	1544	331	2285	0.18	19.93	3.30	3.22	0.09	0.09	1.05
598b-18	171	178	1486	385	2220	0.16	17.20	2.94	2.99	0.08	0.08	0.96
598b-19	201	185	1549	365	2300	0.17	18.49	3.18	3.06	0.09	0.08	1.09
598b-20	165	161	1266	322	1914	0.17	18.80	2.96	2.93	0.09	0.08	1.02
598b-21	202	184	1443	355	2184	0.18	19.59	3.05	2.92	0.09	0.08	1.10
598b-22	209	208	1473	375	2265	0.18	20.51	2.89	2.88	0.09	0.09	1.00
598b-23	143	137	1139	331	1750	0.16	17.54	2.74	2.69	0.08	0.08	1.04
598b-24	450	426	951	25	1852	0.47	76.76	3.11	2.90	0.24	0.23	1.06
598b-25	154	153	1273	304	1884	0.16	17.90	3.12	3.11	0.08	0.08	1.01
598b-26	50	64	383	137	634	0.18	19.98	2.15	2.39	0.08	0.10	0.78
598b-27	160	164	1272	322	1918	0.17	18.63	2.95	2.98	0.08	0.09	0.98
598b-28	189	156	1391	360	2096	0.16	18.10	3.06	2.82	0.09	0.07	1.21
598b-29	84	95	677	142	998	0.18	19.92	3.21	3.42	0.08	0.10	0.88
598b-30	147	151	905	223	1426	0.21	23.71	2.81	2.85	0.10	0.11	0.97
598b-31	17	18	113	27	175	0.20	22.54	2.89	2.98	0.10	0.10	0.94
598b-32	10	10	69	18	107	0.19	20.87	2.82	2.82	0.09	0.09	1.00
598b-33	25	34	164	44	267	0.22	25.30	2.42	2.87	0.09	0.13	0.74
598b-34	0	31	90	7	128	0.24	28.19	2.37	17.29	0.00	0.24	0.00
598b-35	115	102	889	202	1308	0.17	18.26	3.30	3.13	0.09	0.08	1.13
598b-36	125	106	711	166	1108	0.21	23.64	3.07	2.81	0.11	0.10	1.18
598b-37	119	118	860	187	1284	0.18	20.57	3.21	3.20	0.09	0.09	1.01
598b-38	88	101	698	170	1057	0.18	19.85	2.90	3.10	0.08	0.10	0.87
598b-39	153	161	811	238	1363	0.23	26.57	2.42	2.49	0.11	0.12	0.95
598b-40	127	120	785	184	1216	0.20	22.94	3.00	2.91	0.10	0.10	1.06
598b-41	123	108	925	255	1411	0.16	17.99	2.89	2.73	0.09	0.08	1.14
598b-42	79	87	779	139	1084	0.15	16.71	3.80	3.97	0.07	0.08	0.91
598b-43	108	94	672	154	1028	0.20	22.09	3.15	2.92	0.11	0.09	1.15
598b-44	93	96	758	187	1134	0.17	18.35	3.01	3.05	0.08	0.08	0.97

Table S9. *420* recombination rate (cM) of wild type-like Col background in the EMS population. Mean CO frequency (cM) and standard deviation (SD) were calculated.

M_2 WT-like	Green	Red	Both	None	Total	None/Total	CO rate (cM)	G/non G	R/non R	G/T	R/T	G/R
593a-6	96	96	784	253	1229	0.16	17.08	2.52	2.52	0.08	0.08	1.00
598b-10	161	158	1366	339	2024	0.16	17.25	3.07	3.05	0.08	0.08	1.02
598b-16	132	115	1049	242	1538	0.16	17.61	3.31	3.11	0.09	0.07	1.15
593a-7	212	184	1643	383	2422	0.16	17.96	3.27	3.07	0.09	0.08	1.15
4b-12	190	224	1681	419	2514	0.16	18.11	2.91	3.13	0.08	0.09	0.85
17a-19	251	177	1687	458	2573	0.17	18.31	3.05	2.63	0.10	0.07	1.42
593a-28	187	157	1385	333	2062	0.17	18.37	3.21	2.97	0.09	0.08	1.19
3c-2	191	161	1352	351	2055	0.17	18.92	3.01	2.79	0.09	0.08	1.19
5a-11	195	189	1475	372	2231	0.17	19.02	2.98	2.93	0.09	0.08	1.03
6d-16	218	172	1483	390	2263	0.17	19.05	3.03	2.72	0.10	0.08	1.27
593a-22	94	81	650	186	1011	0.17	19.14	2.79	2.61	0.09	0.08	1.16
7c-38	244	219	1718	485	2666	0.17	19.21	2.79	2.66	0.09	0.08	1.11
591a-13	238	250	1850	469	2807	0.17	19.24	2.90	2.97	0.08	0.09	0.95
14b-7	162	198	1383	299	2042	0.18	19.54	3.11	3.43	0.08	0.10	0.82
6d-15	236	200	1624	412	2472	0.18	19.55	3.04	2.81	0.10	0.08	1.18
590a-24	185	180	1302	384	2051	0.18	19.75	2.64	2.60	0.09	0.09	1.03
596a-21	213	199	1548	352	2312	0.18	19.78	3.20	3.09	0.09	0.09	1.07
11c-10	225	190	1504	407	2326	0.18	19.80	2.90	2.68	0.10	0.08	1.18
16a-6	193	165	1301	341	2000	0.18	19.88	2.95	2.75	0.10	0.08	1.17
598b-17	210	200	1544	331	2285	0.18	19.93	3.30	3.22	0.09	0.09	1.05
596a-20	159	168	1185	306	1818	0.18	19.98	2.84	2.91	0.09	0.09	0.95
587a-1	222	225	1646	379	2472	0.18	20.10	3.09	3.11	0.09	0.09	0.99
591a-14	234	282	1829	508	2853	0.18	20.11	2.61	2.85	0.08	0.10	0.83
19a-1	35	30	238	52	355	0.18	20.39	3.33	3.08	0.10	0.08	1.17
15a-7	243	236	1705	416	2600	0.18	20.53	2.99	2.95	0.09	0.09	1.03
592a-37	193	189	1321	365	2068	0.18	20.59	2.73	2.71	0.09	0.09	1.02
13a-1	208	215	1484	376	2283	0.19	20.66	2.86	2.91	0.09	0.09	0.97
5a-12	202	239	1542	396	2379	0.19	20.67	2.75	2.98	0.08	0.10	0.85
586a-7	157	203	1308	272	1940	0.19	20.70	3.08	3.52	0.08	0.10	0.77
1a-1	221	205	1490	377	2293	0.19	20.73	2.94	2.83	0.10	0.09	1.08
588b-22	251	207	1643	364	2465	0.19	20.73	3.32	3.01	0.10	0.08	1.21
3c-1	165	204	1291	323	1983	0.19	20.76	2.76	3.06	0.08	0.10	0.81
7c-37	224	237	1613	402	2476	0.19	20.78	2.87	2.96	0.09	0.10	0.95
582a-33	196	187	1318	356	2057	0.19	20.78	2.79	2.73	0.10	0.09	1.05
586a-6	243	274	1811	429	2757	0.19	20.95	2.92	3.10	0.09	0.10	0.89
21a-24	245	215	1626	365	2451	0.19	20.97	3.23	3.02	0.10	0.09	1.14
594a-33	79	103	647	140	969	0.19	20.98	2.99	3.42	0.08	0.11	0.77
10c-33	173	165	1148	306	1792	0.19	21.08	2.80	2.74	0.10	0.09	1.05
13a-2	196	217	1364	401	2178	0.19	21.21	2.52	2.65	0.09	0.10	0.90
11c-11	203	243	1549	357	2352	0.19	21.21	2.92	3.20	0.09	0.10	0.84
1a-2	255	229	1655	405	2544	0.19	21.29	3.01	2.85	0.10	0.09	1.11
2b-43	239	249	1678	393	2559	0.19	21.35	2.99	3.05	0.09	0.10	0.96
581b-29	113	85	671	168	1037	0.19	21.38	3.10	2.69	0.11	0.08	1.33
17a-18	245	243	1632	433	2553	0.19	21.41	2.78	2.77	0.10	0.10	1.01
15a-8	233	176	1365	364	2138	0.19	21.43	2.96	2.58	0.11	0.08	1.32
590a-23	134	130	912	196	1372	0.19	21.57	3.21	3.16	0.10	0.09	1.03
574a-11	235	202	1432	392	2261	0.19	21.68	2.81	2.61	0.10	0.09	1.16

587a-2	244	223	1564	385	2416	0.19	21.68	2.97	2.84	0.10	0.09	1.09
22a-10	194	174	1229	303	1900	0.19	21.73	2.98	2.82	0.10	0.09	1.11
8b-15	173	192	1185	332	1882	0.19	21.76	2.59	2.73	0.09	0.10	0.90
20b-1	208	258	1498	415	2379	0.20	22.01	2.53	2.82	0.09	0.11	0.81
574a-12	204	184	1257	335	1980	0.20	22.02	2.82	2.67	0.10	0.09	1.11
18a-12	110	105	718	164	1097	0.20	22.02	3.08	3.00	0.10	0.10	1.05
12d-19	207	221	1401	343	2172	0.20	22.16	2.85	2.95	0.10	0.10	0.94
10c-34	129	94	744	163	1130	0.20	22.20	3.40	2.87	0.11	0.08	1.37
23a-31	164	196	1173	282	1815	0.20	22.33	2.80	3.07	0.09	0.11	0.84
12d-18	263	267	1705	433	2668	0.20	22.37	2.81	2.83	0.10	0.10	0.99
16a-7	168	160	1085	237	1650	0.20	22.38	3.16	3.07	0.10	0.10	1.05
4b-14	225	192	1332	346	2095	0.20	22.42	2.89	2.67	0.11	0.09	1.17
9a-1	159	233	1238	335	1965	0.20	22.47	2.46	2.98	0.08	0.12	0.68
20b-2	249	252	1639	350	2490	0.20	22.70	3.14	3.16	0.10	0.10	0.99
4b-13	210	232	1426	325	2193	0.20	22.74	2.94	3.10	0.10	0.11	0.91
21a-27	115	123	762	175	1175	0.20	22.87	2.94	3.05	0.10	0.10	0.93
592b-1	232	223	1372	369	2196	0.21	23.47	2.71	2.65	0.11	0.10	1.04
581b-28	258	251	1501	438	2448	0.21	23.57	2.55	2.52	0.11	0.10	1.03
588b-23	273	337	1837	485	2932	0.21	23.59	2.57	2.87	0.09	0.11	0.81
2b-42	273	254	1613	391	2531	0.21	23.61	2.92	2.81	0.11	0.10	1.07
597b-2	164	154	987	220	1525	0.21	23.65	3.08	2.97	0.11	0.10	1.06
22a-11	242	218	1383	356	2199	0.21	23.74	2.83	2.68	0.11	0.10	1.11
582a-32	254	290	1635	402	2581	0.21	23.94	2.73	2.93	0.10	0.11	0.88
8b-16	178	231	1232	299	1940	0.21	23.95	2.66	3.07	0.09	0.12	0.77
14b-6	225	257	1421	366	2269	0.21	24.16	2.64	2.84	0.10	0.11	0.88
19a-2	77	81	474	106	738	0.21	24.38	2.95	3.03	0.10	0.11	0.95
597b-3	114	155	772	208	1249	0.22	24.55	2.44	2.88	0.09	0.12	0.74
						Mean	21.08					
						SD	1.77					

Table S10. *420* crossover rate (cM) of confirmed *hcr* M_2 mutants in their M_3 progenies. Mean CO frequency (cM) and standard deviation (SD) were calculated. Poor segregation ratio in *hcr2* progenies (in yellow).

hcr	M_3 progeny	Green	Red	Both	None	Total	CO rate (cM)	G/non G	R/non R	G/R	Mean cM	SD
fancm	**11c-4 M_2**	**273**	**273**	**1140**	**199**	**1885**	**35.14**	**2.99**	**2.99**	**1.00**	34.22	2.87
	11c-4-1	290	284	1340	263	2177	31.25	2.98	2.94	1.02		
	11c-4-2	216	234	991	190	1631	33.05	2.85	3.02	0.92		
	11c-4-3	239	250	1076	187	1752	33.53	3.01	3.11	0.96		
	11c-4-4	260	255	1134	163	1812	34.31	3.33	3.28	1.02		
	11c-4-5	292	321	1150	192	1955	38.94	2.81	3.04	0.91		
hcr1	**3a-35 M_2**	**181**	**191**	**1027**	**229**	**1628**	**26.31**	**2.88**	**2.97**	**0.95**	26.51	1.75
	3a-35-1	232	191	1136	258	1817	26.90	3.05	2.71	1.21		
	3a-35-2	208	204	1195	245	1852	25.50	3.12	3.09	1.02		
	3a-35-3	183	211	1172	244	1810	24.86	2.98	3.24	0.87		
	3a-35-4	242	208	1133	242	1825	28.81	3.06	2.77	1.16		
hcr2	**8c-2 M_2**	**254**	**246**	**1013**	**191**	**1704**	**35.72**	**2.90**	**2.83**	**1.03**	40.54	3.08
	8c-2-1	149	211	616	128	1104	41.02	2.26	2.99	0.71		
	8c-2-2	291	226	833	211	1561	41.90	2.57	2.11	1.29		
	8c-2-3	255	224	728	181	1388	44.34	2.43	2.18	1.14		
	8c-2-4	209	294	821	266	1590	39.40	1.84	2.35	0.71		
	8c-2-5	210	186	739	205	1340	36.05	2.43	2.23	1.13		
hcr3	**8a-23 M_2**	**290**	**284**	**1340**	**263**	**2177**	**31.25**	**2.98**	**2.94**	**1.02**	32.87	2.43
	8a-23-1	258	265	1281	230	2034	30.30	3.11	3.17	0.97		
	8a-23-2	281	293	1268	229	2071	33.24	2.97	3.06	0.96		
	8a-23-3	253	257	1168	269	1947	31.00	2.70	2.73	0.98		
	8a-23-4	322	310	1306	202	2140	36.02	3.18	3.08	1.04		
	8a-23-5	288	258	1270	241	2057	31.51	3.12	2.89	1.12		
	8a-23-6	278	282	1374	274	2208	29.80	2.97	3.00	0.99		
	8a-23-7	299	265	1244	229	2037	33.20	3.12	2.86	1.13		
	8a-23-8	214	215	927	157	1513	34.20	3.07	3.08	1.00		
	8a-23-9	311	311	1241	218	2081	36.58	2.93	2.93	1.00		
hcr4	**581a-39 M_2**	**181**	**175**	**923**	**192**	**1471**	**28.17**	**3.01**	**2.94**	**1.03**	25.03	0.55
	581a-39-1	295	294	1711	352	2652	25.45	3.11	3.10	1.00		
	581a-39-2	277	321	1653	488	2739	24.94	2.39	2.58	0.86		
	581a-39-3	251	326	1664	357	2598	25.45	2.80	3.27	0.77		
	581a-39-4	299	293	1697	486	2775	24.28	2.56	2.54	1.02		

Table S11. *420* crossover rate (cM) of confirmed *lcr* M_2 mutants in their M_3 progenies. Mean CO frequency (cM) and standard deviation (SD) were calculated. Poor segregation ratio in *lcr2*, *lcr3* and *lcr4* progenies (in yellow).

lcr	M_3 progeny	Green	Red	Both	None	Total	CO rate (cM)	G/non G	R/non R	G/R	Mean cM	SD
	593a-9 M_2	**177**	**182**	**1834**	**499**	**2692**	**14.37**	**2.95**	**2.98**	**0.97**		
	593a-9-1	27	32	318	85	462	13.71	2.95	3.13	0.84		
	593a-9-2	176	187	1584	400	2347	16.89	3.00	3.07	0.94		
	593a-9-3	191	193	1631	422	2437	17.24	2.96	2.98	0.99		
	593a-9-4	157	155	1477	373	2162	15.66	3.09	3.08	1.01		
	593a-9-5	155	185	1613	433	2386	15.44	2.86	3.06	0.84		
	593a-9-6	169	183	1550	411	2313	16.60	2.89	2.99	0.92		
	593a-9-7	127	144	1217	328	1816	16.24	2.85	2.99	0.88		
lcr1	593a-9-8	181	179	1497	429	2286	17.23	2.76	2.75	1.01	16.08	1.10
	593a-9-9	161	166	1618	410	2355	15.01	3.09	3.12	0.97		
	593a-9-10	140	142	1213	330	1825	16.88	2.87	2.88	0.99		
	593a-9-11	158	172	1543	464	2337	15.29	2.67	2.76	0.92		
	593a-9-12	95	109	811	247	1262	17.74	2.54	2.69	0.87		
	593a-9-13	198	177	1659	382	2416	16.96	3.32	3.17	1.12		
	593a-9-14	182	166	1537	445	2330	16.26	2.81	2.72	1.10		
	593a-9-15	150	159	1491	392	2192	15.26	2.98	3.04	0.94		
	593a-9-16	154	171	1568	479	2372	14.80	2.65	2.75	0.90		
	5a-9 M_2	**148**	**143**	**1338**	**335**	**1964**	**16.12**	**3.11**	**3.07**	**1.03**		
	5a-9-1	80	113	1130	209	1532	13.51	3.76	4.30	0.71		
	5a-9-2	69	84	1410	93	1656	9.71	8.36	9.22	0.82		
lcr2	5a-9-3	87	167	1478	134	1866	14.69	5.20	7.44	0.52	12.52	1.67
	5a-9-4	67	148	1568	92	1875	12.21	6.81	10.79	0.45		
	5a-9-5	60	134	1397	110	1701	12.14	5.97	9.01	0.45		
	5a-9-6	94	130	1468	170	1862	12.86	5.21	6.05	0.72		
	5a-23 M_2	**58**	**64**	**1200**	**356**	**1678**	**7.56**	**3.00**	**3.05**	**0.91**		
lcr3	5a-23-1	48	29	1437	312	1826	4.31	4.35	4.07	1.66	5.06	1.08
	5a-23-2	51	28	1391	296	1766	4.58	4.45	4.09	1.82		
	5a-23-3	59	36	1212	252	1559	6.29	4.41	4.01	1.64		
	15a-23 M_2	**36**	**29**	**1329**	**470**	**1864**	**3.55**	**2.74**	**2.68**	**1.24**		
	15a-23-1	2	2	1364	439	1807	0.22	3.10	3.10	1.00		
lcr4	15a-23-2	2	3	1212	395	1612	0.31	3.05	3.06	0.67	0.25	0.20
	15a-23-3	9	0	1402	471	1882	0.48	3.00	2.92	0.00		
	15a-23-4	0	0	1619	529	2148	0.00	3.06	3.06	0.00		

Table S12. *420* crossover rate (cM) of M_3 progenies of remaining M_2 mutants. Mean CO rate (cM) and standard deviation (SD) were calculated. Poor segregation ratio in 8c-20 progenies (in yellow).

M_2 isolates	M_3 progeny	Green	Red	Both	None	Total	CO rate (cM)	G/non G	R/non R	G/R	Mean cM	SD
1a-21	**1a-21 M_2**	**193**	**343**	**1359**	**359**	**2254**	**27.65**	**2.71**	**3.08**	**0.81**	18.64	1.60
	1a-21-1	153	147	1286	279	1865	17.64	3.38	3.32	1.04		
	1a-21-2	180	159	1404	324	2067	18.03	3.28	3.10	1.13		
	1a-21-3	167	194	1290	335	1986	20.22	2.75	2.96	0.86		
	1a-21-4	198	183	1361	333	2075	20.45	3.02	2.91	1.08		
	1a-21-5	145	146	1278	314	1883	16.88	3.09	3.10	0.99		
1b-43	**1b-43 M_2**	**221**	**236**	**1289**	**313**	**2059**	**25.43**	**2.75**	**2.86**	**0.94**	23.13	0.78
	1b-43-1	193	205	1237	272	1907	23.67	3.00	3.10	0.94		
	1b-43-2	178	170	1165	263	1776	22.02	3.10	3.03	1.05		
	1b-43-3	198	216	1255	290	1959	24.02	2.87	3.01	0.92		
	1b-43-4	165	169	1069	229	1632	23.14	3.10	3.14	0.98		
	1b-43-5	178	160	1097	238	1673	22.80	3.20	3.02	1.11		
6d-9	**6d-9 M_2**	**218**	**210**	**869**	**168**	**1465**	**35.53**	**2.88**	**2.80**	**1.04**	23.70	1.68
	6d-9-1	168	165	1043	198	1574	24.05	3.34	3.30	1.02		
	6d-9-2	168	177	1171	297	1813	21.30	2.82	2.90	0.95		
	6d-9-3	198	166	1067	222	1653	25.19	3.26	2.94	1.19		
	6d-9-4	188	165	1082	222	1657	24.24	3.28	3.04	1.14		
6d-35	**6d-35 M_2**	**244**	**234**	**1333**	**291**	**2102**	**26.16**	**3.00**	**2.93**	**1.04**	17.82	4.50
	6d-35-1	73	48	909	248	1278	9.96	3.32	2.98	1.52		
	6d-35-2	230	177	1384	342	2133	21.36	3.11	2.73	1.30		
	6d-35-3	159	202	1353	318	2032	19.71	2.91	3.26	0.79		
	6d-35-4	168	191	1386	325	2070	19.18	3.01	3.20	0.88		
	6d-35-5	166	173	1350	292	1981	18.90	3.26	3.33	0.96		
7a-38	**7a-38 M_2**	**289**	**255**	**1546**	**352**	**2442**	**25.54**	**3.02**	**2.81**	**1.13**	19.05	1.29
	7a-38-1	155	165	1133	289	1742	20.46	2.84	2.92	0.94		
	7a-38-2	154	166	1202	321	1843	19.21	2.78	2.88	0.93		
	7a-38-3	157	140	1253	326	1876	17.33	3.03	2.88	1.12		
	7a-38-4	154	166	1202	321	1843	19.21	2.78	2.88	0.93		
14a-8	**14a-8 M_2**	**264**	**250**	**1350**	**274**	**2138**	**27.95**	**3.08**	**2.97**	**1.06**	23.86	1.36
	14a-8-1	245	239	1534	369	2387	22.90	2.93	2.89	1.03		
	14a-8-2	277	244	1546	329	2396	24.83	3.18	2.95	1.14		
16a-10	**16a-10 M_2**	**206**	**215**	**1080**	**231**	**1732**	**28.32**	**2.88**	**2.96**	**0.96**	22.76	1.55
	16a-10-1	178	187	1103	271	1739	23.83	2.80	2.87	0.95		
	16a-10-2	232	239	1474	329	2274	23.47	3.00	3.05	0.97		
	16a-10-3	187	225	1425	357	2194	20.98	2.77	3.03	0.83		
586b-14	**586b-14 M_2**	**270**	**238**	**1358**	**310**	**2176**	**26.99**	**2.97**	**2.75**	**1.13**	21.90	2.02
	586b-14-1	220	239	1552	392	2403	21.39	2.81	2.93	0.92		
	586b-14-2	221	200	1408	364	2193	21.51	2.89	2.75	1.11		
	586b-14-3	210	222	1247	272	1951	25.36	2.95	3.05	0.95		
	586b-14-4	245	249	1686	422	2602	21.24	2.88	2.90	0.98		
	586b-14-5	222	243	1710	408	2583	20.00	2.97	3.10	0.91		

7b-9	**7b-9 M2**	**100**	**102**	**986**	**255**	**1443**	**15.15**	**3.04**	**3.06**	**0.98**	20.03	1.83
	7b-9-1	171	194	1296	305	1966	20.71	2.94	3.13	0.88		
	7b-9-2	203	151	1281	318	1953	20.16	3.16	2.75	1.34		
	7b-9-3	160	151	1333	310	1954	17.44	3.24	3.16	1.06		
	7b-9-4	180	170	1116	291	1757	22.44	2.81	2.73	1.06		
	7b-9-5	149	132	1024	298	1603	19.41	2.73	2.59	1.13		
8c-20	**8c-20 M2**	**136**	**166**	**1348**	**358**	**2008**	**16.38**	**2.83**	**3.06**	**0.82**	23.73	4.03
	8c-20-1	302	154	856	548	1860	28.61	1.65	1.19	1.96		
	8c-20-2	76	123	715	161	1075	20.64	2.79	3.54	0.62		
	8c-20-3	82	136	772	210	1200	20.21	2.47	3.11	0.60		
	8c-20-4	244	169	863	583	1859	25.46	1.47	1.25	1.44		
593a-26	**593a-26 M2**	**182**	**183**	**1681**	**436**	**2482**	**15.98**	**3.01**	**3.02**	**0.99**	18.15	1.53
	593a-26-1	188	181	1635	396	2400	16.78	3.16	3.11	1.04		
	593a-26-2	131	151	1106	368	1756	17.61	2.38	2.52	0.87		
	593a-26-3	140	133	1027	258	1558	19.41	2.98	2.91	1.05		
	593a-26-4	36	35	308	89	468	16.54	2.77	2.74	1.03		
	593a-26-5	184	172	1388	401	2145	18.26	2.74	2.67	1.07		
	593a-26-6	94	99	875	226	1294	16.23	2.98	3.04	0.95		
	593a-26-7	178	203	1254	405	2040	20.85	2.36	2.50	0.88		
	593a-26-8	195	207	1530	371	2303	19.32	2.98	3.07	0.94		
	593a-26-9	105	88	765	199	1157	18.37	3.03	2.81	1.19		
598a-18	**598a-18 M2**	**119**	**121**	**1085**	**274**	**1599**	**16.35**	**3.05**	**3.07**	**0.98**	17.61	1.23
	598a-18-1	123	115	965	255	1458	17.93	2.94	2.86	1.07		
	598a-18-2	131	135	1082	284	1632	17.90	2.89	2.93	0.97		
	598a-18-3	142	126	1333	366	1967	14.71	3.00	2.87	1.13		
	598a-18-4	164	131	1108	329	1732	18.80	2.77	2.51	1.25		
	598a-18-5	103	128	976	264	1471	17.18	2.75	3.01	0.80		
	598a-18-6	56	71	532	143	802	17.34	2.75	3.03	0.79		
	598a-18-7	155	131	1112	334	1732	18.16	2.72	2.54	1.18		
	598a-18-8	78	98	719	186	1081	17.88	2.81	3.09	0.80		
	598a-18-9	111	82	839	203	1235	17.09	3.33	2.93	1.35		
	598a-18-10	162	136	1115	272	1685	19.61	3.13	2.88	1.19		
	598a-18-11	111	104	920	241	1376	17.08	2.99	2.91	1.07		

Table S13. *420* crossover frequency (cM) of *hcr1* BC_1F_2 population. A subset of 66 individuals from ~600 total with 'high' (in orange), 'mid' (in yellow) and 'low' (in green) recombination rates. 'High' individuals showed *hcr1* phenotype (~26-32 cM), 'mid' showed intermediate phenotypes (~23-25 cM) and 'low' displayed wild type level of recombination (~18-22 cM).

BC_1F_2 progeny	Green	Red	Both	None	Total	CO rate (cM)	G/non G	R/non R	G/R
hcr1 F_2 (1) 37	311	296	1412	263	2282	31.59	3.08	2.98	1.05
hcr1 F_2 (1) 43	180	213	976	185	1554	29.70	2.90	3.26	0.85
hcr1 F_2 (1) 63	266	253	1294	272	2085	29.14	2.97	2.88	1.05
hcr1 F_2 (1) 17	248	263	1293	292	2096	28.42	2.78	2.88	0.94
hcr1 F_2 (1) 23	270	290	1466	276	2302	28.34	3.07	3.22	0.93
hcr1 F_2 (1) 30	272	298	1475	300	2345	28.32	2.92	3.10	0.91
hcr1 F_2 (1) 9	245	279	1362	271	2157	28.30	2.92	3.18	0.88
hcr1 F_2 (1) 41	157	190	916	201	1464	27.48	2.74	3.09	0.83
hcr1 F_2 (1) 5	250	286	1445	286	2267	27.40	2.96	3.23	0.87
hcr1 F_2 (1) 29	256	256	1364	293	2169	27.34	2.95	2.95	1.00
hcr1 F_2 (1) 60	250	270	1387	307	2214	27.18	2.84	2.97	0.93
hcr1 F_2 (1) 38	272	237	1376	322	2207	26.60	2.95	2.72	1.15
hcr1 F_2 (1) 32	266	273	1464	336	2339	26.58	2.84	2.89	0.97
hcr1 F_2 (1) 46	263	263	1444	319	2289	26.49	2.93	2.93	1.00
hcr1 F_2 (1) 12	258	265	1427	340	2290	26.30	2.79	2.83	0.97
hcr1 F_2 (1) 44	278	257	1487	331	2353	26.16	3.00	2.86	1.08
hcr1 F_2 (1) 26	245	233	1344	282	2104	26.13	3.09	2.99	1.05
hcr1 F_2 (1) 28	217	241	1278	301	2037	25.82	2.76	2.93	0.90
hcr1 F_2 (1) 39	260	255	1467	309	2291	25.81	3.06	3.03	1.02
hcr1 F_2 (1) 15	258	277	1526	332	2393	25.65	2.93	3.06	0.93
hcr1 F_2 (1) 22	243	284	1503	332	2362	25.58	2.83	3.11	0.86
hcr1 F_2 (1) 8	242	260	1418	331	2251	25.57	2.81	2.93	0.93
hcr1 F_2 (1) 24	266	250	1465	340	2321	25.48	2.93	2.83	1.06
hcr1 F_2 (1) 7	135	137	764	195	1231	25.30	2.71	2.73	0.99
hcr1 F_2 (1) 61	219	263	1397	308	2187	25.22	2.83	3.15	0.83
hcr1 F_2 (1) 40	271	214	1387	334	2206	25.15	3.03	2.65	1.27
hcr1 F_2 (1) 57	257	250	1490	318	2315	25.03	3.08	3.03	1.03
hcr1 F_2 (1) 25	252	246	1469	322	2289	24.84	3.03	2.99	1.02
hcr1 F_2 (1) 18	272	234	1491	330	2327	24.83	3.13	2.87	1.16
hcr1 F_2 (1) 53	213	262	1439	304	2218	24.39	2.92	3.29	0.81
hcr1 F_2 (1) 10	235	272	1515	352	2374	24.31	2.80	3.04	0.86
hcr1 F_2 (1) 14	259	233	1456	356	2304	24.31	2.91	2.75	1.11
hcr1 F_2 (1) 58	249	204	1368	303	2124	24.27	3.19	2.85	1.22
hcr1 F_2 (1) 67	234	273	1542	335	2384	24.19	2.92	3.19	0.86
hcr1 F_2 (1) 3	229	221	1322	344	2116	24.19	2.75	2.69	1.04
hcr1 F_2 (1) 65	212	224	1309	306	2051	24.18	2.87	2.96	0.95
hcr1 F_2 (1) 54	261	222	1460	331	2274	24.16	3.11	2.84	1.18
hcr1 F_2 (1) 19	244	237	1466	320	2267	24.13	3.07	3.02	1.03
hcr1 F_2 (1) 4	204	219	1286	290	1999	24.05	2.93	3.05	0.93

hcr1 F_2 (1) 45	251	261	1555	353	2420	24.05	2.94	3.01	0.96
hcr1 F_2 (1) 55	246	259	1498	386	2389	24.02	2.70	2.78	0.95
hcr1 F_2 (1) 34	199	191	1231	229	1850	23.95	3.40	3.32	1.04
hcr1 F_2 (1) 35	256	254	1561	357	2428	23.85	2.97	2.96	1.01
hcr1 F_2 (1) 64	233	241	1472	312	2258	23.83	3.08	3.14	0.97
hcr1 F_2 (1) 52	224	200	1326	271	2021	23.82	3.29	3.08	1.12
hcr1 F_2 (1) 33	238	274	1546	389	2447	23.74	2.69	2.90	0.87
hcr1 F_2 (1) 48	269	235	1551	363	2418	23.64	3.04	2.83	1.14
hcr1 F_2 (1) 42	263	241	1551	378	2433	23.47	2.93	2.80	1.09
hcr1 F_2 (1) 16	235	201	1370	308	2114	23.35	3.15	2.89	1.17
hcr1 F_2 (1) 13	196	199	1261	266	1922	23.26	3.13	3.16	0.98
hcr1 F_2 (1) 11	243	260	1597	352	2452	23.21	3.01	3.12	0.93
hcr1 F_2 (1) 51	224	209	1394	300	2127	23.00	3.18	3.06	1.07
hcr1 F_2 (1) 47	239	227	1505	353	2324	22.61	3.01	2.93	1.05
hcr1 F_2 (1) 59	202	244	1433	352	2231	22.53	2.74	3.03	0.83
hcr1 F_2 (1) 49	241	238	1585	368	2432	22.15	3.01	2.99	1.01
hcr1 F_2 (1) 21	203	232	1473	323	2231	21.89	3.02	3.24	0.88
hcr1 F_2 (1) 66	209	253	1506	412	2380	21.78	2.58	2.83	0.83
hcr1 F_2 (1) 20	248	228	1632	357	2465	21.66	3.21	3.07	1.09
hcr1 F_2 (1) 62	126	131	860	214	1331	21.65	2.86	2.91	0.96
hcr1 F_2 (1) 36	240	221	1564	370	2395	21.58	3.05	2.93	1.09
hcr1 F_2 (1) 50	153	177	1096	293	1719	21.51	2.66	2.85	0.86
hcr1 F_2 (1) 56	214	228	1519	350	2311	21.42	3.00	3.10	0.94
hcr1 F_2 (1) 31	224	226	1611	341	2402	20.92	3.24	3.25	0.99
hcr1 F_2 (1) 2	225	210	1535	355	2325	20.89	3.12	3.01	1.07
hcr1 F_2 (1) 1	220	200	1473	371	2264	20.69	2.96	2.83	1.10
hcr1 F_2 (1) 6	180	186	1421	346	2133	18.96	3.01	3.06	0.97

Table S14. *420* crossover frequency (cM) of *lcr1* BC_1F_2 population. A subset of 69 individuals from ~300 total with 'low' (in green), 'mid' (in yellow) and 'high' (in orange) crossover rates. 'low' individuals with *lcr1* phenotype (~13-15 cM), 'mid' lines with intermediate phenotypes (~16-17cM) and 'high' individuals with wild type recombination rate (~18-22 cM).

BC_1F_2 progeny	Green	Red	Both	None	Total	CO rate (cM)	G/non G	R/non R	G/R
lcr1 F_2 (2)-6	34	30	341	111	516	13.29	2.66	2.56	1.13
lcr1 F_2 (2)-3	110	104	1201	291	1706	13.45	3.32	3.25	1.06
lcr1 F_2 (2)-11	86	99	977	287	1449	13.71	2.75	2.88	0.87
lcr1 F_2 (2)-42	125	124	1326	350	1925	13.90	3.06	3.05	1.01
lcr1 F_2 (2)-37	57	77	677	218	1029	14.00	2.49	2.74	0.74
lcr1 F_2 (2)-12	76	69	723	218	1086	14.39	2.78	2.69	1.10
lcr1 F_2 (2)-69	103	104	1075	268	1550	14.39	3.17	3.18	0.99
lcr1 F_2 (2)-49	129	126	1290	352	1897	14.49	2.97	2.94	1.02
lcr1 F_2 (2)-8	129	121	1287	317	1854	14.54	3.23	3.16	1.07
lcr1 F_2 (2)-44	67	72	705	183	1027	14.60	3.03	3.11	0.93
lcr1 F_2 (2)-21	120	114	1214	277	1725	14.64	3.41	3.35	1.05
lcr1 F_2 (2)-31	108	103	1052	291	1554	14.65	2.94	2.89	1.05
lcr1 F_2 (2)-30	153	135	1407	389	2084	14.93	2.98	2.85	1.13
lcr1 F_2 (2)-48	100	100	935	304	1439	15.03	2.56	2.56	1.00
lcr1 F_2 (2)-29	125	151	1311	397	1984	15.04	2.62	2.80	0.83
lcr1 F_2 (2)-68	139	145	1375	363	2022	15.20	2.98	3.03	0.96
lcr1 F_2 (2)-9	91	88	845	250	1274	15.21	2.77	2.74	1.03
lcr1 F_2 (2)-60	34	30	282	93	439	15.83	2.57	2.46	1.13
lcr1 F_2 (2)-47	116	105	991	274	1486	16.18	2.92	2.81	1.10
lcr1 F_2 (2)-1	135	147	1248	364	1894	16.20	2.71	2.80	0.92
lcr1 F_2 (2)-7	108	113	994	261	1476	16.30	2.95	3.00	0.96
lcr1 F_2 (2)-35	137	140	1185	370	1832	16.48	2.59	2.61	0.98
lcr1 F_2 (2)-27	126	131	1143	298	1698	16.50	2.96	3.00	0.96
lcr1 F_2 (2)-66	114	123	1061	251	1549	16.69	3.14	3.24	0.93
lcr1 F_2 (2)-59	136	127	1196	253	1712	16.77	3.51	3.40	1.07
lcr1 F_2 (2)-57	103	145	1048	313	1609	16.83	2.51	2.87	0.71
lcr1 F_2 (2)-43	105	107	944	209	1365	16.97	3.32	3.35	0.98
lcr1 F_2 (2)-33	119	131	1090	269	1609	16.98	3.02	3.15	0.91
lcr1 F_2 (2)-2	55	61	485	136	737	17.22	2.74	2.86	0.90
lcr1 F_2 (2)-54	124	133	1105	270	1632	17.23	3.05	3.14	0.93
lcr1 F_2 (2)-10	129	131	1113	270	1643	17.33	3.10	3.12	0.98
lcr1 F_2 (2)-5	149	138	1199	319	1805	17.42	2.95	2.86	1.08
lcr1 F_2 (2)-22	122	118	994	273	1507	17.45	2.85	2.82	1.03
lcr1 F_2 (2)-52	110	111	915	250	1386	17.47	2.84	2.85	0.99
lcr1 F_2 (2)-16	136	160	1249	310	1855	17.49	2.95	3.16	0.85
lcr1 F_2 (2)-36	125	142	1058	344	1669	17.53	2.43	2.56	0.88
lcr1 F_2 (2)-56	132	105	988	255	1480	17.55	3.11	2.82	1.26

lcr1 F_2 (2)-32	160	129	1171	337	1797	17.64	2.86	2.62	1.24
lcr1 F_2 (2)-18	100	81	733	210	1124	17.66	2.86	2.63	1.23
lcr1 F_2 (2)-15	141	118	1043	304	1606	17.69	2.81	2.61	1.19
lcr1 F_2 (2)-26	138	121	1059	282	1600	17.77	2.97	2.81	1.14
lcr1 F_2 (2)-39	101	70	689	195	1055	17.79	2.98	2.56	1.44
lcr1 F_2 (2)-23	159	139	1211	327	1836	17.82	2.94	2.78	1.14
lcr1 F_2 (2)-63	136	104	961	277	1478	17.83	2.88	2.58	1.31
lcr1 F_2 (2)-14	175	112	1176	303	1766	17.84	3.26	2.69	1.56
lcr1 F_2 (2)-53	147	102	1059	224	1532	17.85	3.70	3.13	1.44
lcr1 F_2 (2)-51	133	116	1020	262	1531	17.86	3.05	2.88	1.15
lcr1 F_2 (2)-38	139	119	1024	301	1583	17.90	2.77	2.60	1.17
lcr1 F_2 (2)-46	156	125	1094	339	1714	18.02	2.69	2.46	1.25
lcr1 F_2 (2)-70	41	48	360	93	542	18.05	2.84	3.04	0.85
lcr1 F_2 (2)-13	96	86	699	227	1108	18.06	2.54	2.43	1.12
lcr1 F_2 (2)-17	154	145	1184	319	1802	18.26	2.88	2.81	1.06
lcr1 F_2 (2)-62	158	134	1166	298	1756	18.30	3.06	2.85	1.18
lcr1 F_2 (2)-50	153	138	1174	282	1747	18.34	3.16	3.02	1.11
lcr1 F_2 (2)-58	146	109	1026	238	1519	18.50	3.38	2.96	1.34
lcr1 F_2 (2)-4	115	145	989	288	1537	18.66	2.55	2.81	0.79
lcr1 F_2 (2)-24	146	131	1080	272	1629	18.76	3.04	2.90	1.11
lcr1 F_2 (2)-41	117	126	968	218	1429	18.77	3.15	3.27	0.93
lcr1 F_2 (2)-71	104	138	902	278	1422	18.78	2.42	2.72	0.75
lcr1 F_2 (2)-64	168	180	1317	377	2042	18.81	2.67	2.75	0.93
lcr1 F_2 (2)-28	142	130	1045	273	1590	18.89	2.95	2.83	1.09
lcr1 F_2 (2)-65	146	106	976	216	1444	19.32	3.48	2.99	1.38
lcr1 F_2 (2)-45	187	151	1248	311	1897	19.77	3.11	2.81	1.24
lcr1 F_2 (2)-19	151	113	959	256	1479	19.81	3.01	2.63	1.34
lcr1 F_2 (2)-67	156	176	1209	315	1856	19.86	2.78	2.94	0.89
lcr1 F_2 (2)-61	171	122	986	278	1557	21.03	2.89	2.47	1.40
lcr1 F_2 (2)-25	124	106	771	219	1220	21.07	2.75	2.56	1.17
lcr1 F_2 (2)-34	189	150	1141	317	1797	21.09	2.85	2.55	1.26
lcr1 F_2 (2)-55	121	148	882	240	1391	21.69	2.59	2.85	0.82

Table S15. *420* crossover frequency (cM) of *hcr2* BC_1F_2 population. A subset of 55 individuals from ~500 total with 'high' (in orange), 'mid' (in yellow) and 'low' (in green) recombination rates. 'High' individuals with *hcr2* phenotype (~38-47 cM), 'mid' in with intermediate phenotypes (~24-32 cM) and 'low' individuals with wild type phenotype (~18-22 cM).

BC_1F_2 progeny	Green	Red	Both	None	Total	CO rate (cM)	G/non G	R/non R	G/R
hcr2 F_2 (8)-14	358	299	923	253	1833	46.79	2.32	2.00	1.20
hcr2 F_2 (8)-20	387	324	1044	262	2017	45.69	2.44	2.11	1.19
hcr2 F_2 (8)-42	316	275	920	200	1711	44.40	2.60	2.32	1.15
hcr2 F_2 (8)-4	349	310	990	278	1927	43.78	2.28	2.07	1.13
hcr2 F_2 (8)-23	406	295	1069	280	2050	43.78	2.57	1.99	1.38
hcr2 F_2 (8)-35	349	283	977	244	1853	43.62	2.52	2.12	1.23
hcr2 F_2 (8)-28	364	292	1005	278	1939	43.14	2.40	2.02	1.25
hcr2 F_2 (8)-27	346	308	1006	286	1946	42.74	2.28	2.08	1.12
hcr2 F_2 (8)-45	342	306	1024	268	1940	42.38	2.38	2.18	1.12
hcr2 F_2 (8)-2	326	298	965	300	1889	41.75	2.16	2.02	1.09
hcr2 F_2 (8)-32	352	241	965	251	1809	41.32	2.68	2.00	1.46
hcr2 F_2 (8)-39	372	277	1066	283	1998	40.81	2.57	2.05	1.34
hcr2 F_2 (8)-48	342	273	1027	277	1919	40.08	2.49	2.10	1.25
hcr2 F_2 (8)-36	338	286	1056	283	1963	39.65	2.45	2.16	1.18
hcr2 F_2 (8)-16	351	272	1087	262	1972	39.32	2.69	2.22	1.29
hcr2 F_2 (8)-44	98	97	351	72	618	39.26	2.66	2.64	1.01
hcr2 F_2 (8)-6	342	279	1062	287	1970	39.21	2.48	2.13	1.23
hcr2 F_2 (8)-37	312	213	931	467	1923	32.62	1.83	1.47	1.46
hcr2 F_2 (8)-56	280	239	996	409	1924	32.14	1.97	1.79	1.17
hcr2 F_2 (8)-22	256	252	1019	385	1912	31.54	2.00	1.98	1.02
hcr2 F_2 (8)-12	238	272	1045	378	1933	31.27	1.97	2.14	0.88
hcr2 F_2 (8)-31	198	234	889	365	1686	30.18	1.81	1.99	0.85
hcr2 F_2 (8)-33	233	238	1040	348	1859	29.77	2.17	2.20	0.98
hcr2 F_2 (8)-30	246	218	1025	343	1832	29.75	2.27	2.11	1.13
hcr2 F_2 (8)-13	237	247	1062	370	1916	29.66	2.11	2.16	0.96
hcr2 F_2 (8)-41	282	261	1241	388	2172	29.29	2.35	2.24	1.08
hcr2 F_2 (8)-40	246	235	1080	370	1931	29.16	2.19	2.13	1.05
hcr2 F_2 (8)-1	236	245	1069	386	1936	29.07	2.07	2.11	0.96
hcr2 F_2 (8)-51	249	199	1041	322	1811	28.92	2.48	2.17	1.25
hcr2 F_2 (8)-15	189	221	916	339	1665	28.76	1.97	2.15	0.86
hcr2 F_2 (8)-43	248	221	1115	323	1907	28.72	2.51	2.34	1.12
hcr2 F_2 (8)-55	219	219	985	378	1801	28.33	2.02	2.02	1.00
hcr2 F_2 (8)-26	255	233	1147	377	2012	28.24	2.30	2.18	1.09
hcr2 F_2 (8)-24	233	247	1074	427	1981	28.21	1.94	2.00	0.94
hcr2 F_2 (8)-18	244	252	1137	415	2048	28.19	2.07	2.11	0.97
hcr2 F_2 (8)-53	221	242	1041	409	1913	28.17	1.94	2.04	0.91
hcr2 F_2 (8)-7	233	237	1037	437	1944	28.13	1.88	1.90	0.98
hcr2 F_2 (8)-10	202	232	1021	352	1807	27.91	2.09	2.26	0.87
hcr2 F_2 (8)-25	250	278	1297	379	2204	27.83	2.35	2.50	0.90

hcr2 F_2 (8)-52	227	199	1019	334	1779	27.81	2.34	2.17	1.14
hcr2 F_2 (8)-57	227	233	1117	368	1945	27.41	2.24	2.27	0.97
hcr2 F_2 (8)-11	258	221	1102	448	2029	27.35	2.03	1.87	1.17
hcr2 F_2 (8)-21	237	209	1120	400	1966	26.09	2.23	2.09	1.13
hcr2 F_2 (8)-3	257	175	1061	416	1909	26.01	2.23	1.84	1.47
hcr2 F_2 (8)-47	219	173	1010	331	1733	26.00	2.44	2.15	1.27
hcr2 F_2 (8)-29	187	208	1031	328	1754	25.86	2.27	2.41	0.90
hcr2 F_2 (8)-19	196	249	1166	370	1981	25.79	2.20	2.50	0.79
hcr2 F_2 (8)-50	205	221	1099	383	1908	25.61	2.16	2.24	0.93
hcr2 F_2 (8)-9	172	272	1213	346	2003	25.39	2.24	2.87	0.63
hcr2 F_2 (8)-49	215	213	1093	420	1941	25.23	2.07	2.06	1.01
hcr2 F_2 (8)-46	195	183	985	368	1731	24.95	2.14	2.07	1.07
hcr2 F_2 (8)-8	188	231	1136	381	1936	24.69	2.16	2.40	0.81
hcr2 F_2 (8)-54	193	185	1037	334	1749	24.65	2.37	2.32	1.04
hcr2 F_2 (8)-34	219	184	1121	393	1917	23.87	2.32	2.13	1.19
hcr2 F_2 (8)-38	193	200	1628	410	2431	17.74	2.99	3.03	0.97

Table S16. *420* crossover rate (cM) of 64 *hcr1* BC_1F_2 individuals used for DNA library construction. Selected 'high' recombination individuals are shown in the range of ~27-32 cM.

BC_1F_2 progeny	Green	Red	Both	None	Total	CO rate (cM)	G/non G	R/non R	G/R
hcr1 F_2 (8) 58	155	148	669	135	1107	32.73	2.91	2.82	1.05
hcr1 F_2 (7) 55	337	370	835	34	1576	32.06	2.90	3.25	0.91
hcr1 F_2 (1) 37	311	296	1412	263	2282	31.59	3.08	2.98	1.05
hcr1 F_2 (6) 5	285	265	1258	278	2086	31.25	2.84	2.71	1.08
hcr1 F_2 (2) 26	288	277	1308	301	2174	30.70	2.76	2.69	1.04
hcr1 F_2 (3) 47	325	347	1544	370	2586	30.70	2.61	2.72	0.94
hcr1 F_2 (8) 62	215	212	1035	191	1653	30.48	3.10	3.07	1.01
hcr1 F_2 (7) 52	177	189	868	183	1417	30.47	2.81	2.94	0.94
hcr1 F_2 (3) 54	348	299	1547	318	2512	30.37	3.07	2.77	1.16
hcr1 F_2 (7) 12	321	325	1524	344	2514	30.28	2.76	2.78	0.99
hcr1 F_2 (7) 48	306	303	1468	295	2372	30.25	2.97	2.95	1.01
hcr1 F_2 (8) 49	298	251	1333	257	2139	30.24	3.21	2.85	1.19
hcr1 F_2 (8) 42	146	172	767	155	1240	30.21	2.79	3.12	0.85
hcr1 F_2 (5) 40	313	315	1504	318	2450	30.19	2.87	2.88	0.99
hcr1 F_2 (2) 65	162	159	750	191	1262	29.91	2.61	2.58	1.02
hcr1 F_2 (6) 63	274	262	1281	293	2110	29.86	2.80	2.72	1.05
hcr1 F_2 (6) 22	236	236	1165	223	1860	29.82	3.05	3.05	1.00
hcr1 F_2 (1) 43	180	213	976	185	1554	29.70	2.90	3.26	0.85
hcr1 F_2 (2) 61	223	213	1093	203	1732	29.53	3.16	3.07	1.05
hcr1 F_2 (7) 27	217	246	1135	243	1841	29.50	2.76	3.00	0.88
hcr1 F_2 (8) 12	311	303	1511	324	2449	29.39	2.91	2.86	1.03
hcr1 F_2 (8) 50	203	207	1007	220	1637	29.35	2.83	2.87	0.98
hcr1 F_2 (4) 29	244	268	1257	279	2048	29.29	2.74	2.92	0.91
hcr1 F_2 (3) 59	324	298	1554	316	2492	29.23	3.06	2.89	1.09
hcr1 F_2 (1) 63	266	253	1294	272	2085	29.14	2.97	2.88	1.05
hcr1 F_2 (7) 56	154	172	822	166	1314	29.02	2.89	3.11	0.90
hcr1 F_2 (4) 62	544	554	1263	37	2398	29.02	3.06	3.13	0.98
hcr1 F_2 (2) 18	307	306	1518	340	2471	29.02	2.83	2.82	1.00
hcr1 F_2 (3) 41	293	288	1448	321	2350	28.90	2.86	2.83	1.02
hcr1 F_2 (8) 44	278	298	1445	309	2330	28.90	2.84	2.97	0.93
hcr1 F_2 (4) 27	274	297	1431	308	2310	28.89	2.82	2.97	0.92
hcr1 F_2 (2) 3	276	295	1427	314	2312	28.86	2.80	2.92	0.94
hcr1 F_2 (5) 15	294	278	1395	354	2321	28.79	2.67	2.58	1.06
hcr1 F_2 (7) 40	274	268	1338	320	2200	28.78	2.74	2.70	1.02
hcr1 F_2 (7) 20	276	296	1429	322	2323	28.76	2.76	2.88	0.93
hcr1 F_2 (8) 47	133	119	648	124	1024	28.74	3.21	2.98	1.12
hcr1 F_2 (5) 8	220	210	1096	223	1749	28.71	3.04	2.95	1.05
hcr1 F_2 (6) 18	194	228	1058	238	1718	28.67	2.69	2.98	0.85
hcr1 F_2 (6) 27	292	291	1469	322	2374	28.67	2.87	2.87	1.00

hcr1 F_2 (3) 20	147	146	754	147	1194	28.64	3.08	3.06	1.01
hcr1 F_2 (5) 59	300	284	1426	375	2385	28.57	2.62	2.53	1.06
hcr1 F_2 (6) 14	302	265	1428	323	2318	28.53	2.94	2.71	1.14
hcr1 F_2 (6) 12	295	310	1539	331	2475	28.51	2.86	2.95	0.95
hcr1 F_2 (4) 20	141	152	731	175	1199	28.50	2.67	2.79	0.93
hcr1 F_2 (1) 17	248	263	1293	292	2096	28.42	2.78	2.88	0.94
hcr1 F_2 (1) 23	270	290	1466	276	2302	28.34	3.07	3.22	0.93
hcr1 F_2 (1) 30	272	298	1475	300	2345	28.32	2.92	3.10	0.91
hcr1 F_2 (6) 66	297	309	1573	315	2494	28.30	3.00	3.08	0.96
hcr1 F_2 (1) 9	245	279	1362	271	2157	28.30	2.92	3.18	0.88
hcr1 F_2 (2) 5	224	238	1187	254	1903	28.27	2.87	2.98	0.94
hcr1 F_2 (2) 23	265	306	1469	323	2363	28.12	2.76	3.02	0.87
hcr1 F_2 (3) 4	283	322	1565	337	2507	28.07	2.80	3.04	0.88
hcr1 F_2 (2) 2	186	168	934	180	1468	28.05	3.22	3.01	1.11
hcr1 F_2 (4) 31	211	188	1050	208	1657	28.00	3.18	2.95	1.12
hcr1 F_2 (4) 50	274	274	1422	307	2277	27.98	2.92	2.92	1.00
hcr1 F_2 (4) 59	276	281	1430	330	2317	27.94	2.79	2.82	0.98
hcr1 F_2 (3) 49	290	310	1555	346	2501	27.88	2.81	2.93	0.94
hcr1 F_2 (4) 9	164	166	879	170	1379	27.79	3.10	3.13	0.99
hcr1 F_2 (3) 6	298	288	1555	312	2453	27.74	3.09	3.02	1.03
hcr1 F_2 (5) 62	300	282	1532	323	2437	27.73	3.03	2.91	1.06
hcr1 F_2 (1) 41	157	190	916	201	1464	27.48	2.74	3.09	0.83
hcr1 F_2 (5) 51	270	267	1411	318	2266	27.47	2.87	2.85	1.01
hcr1 F_2 (5) 67	314	282	1569	365	2530	27.28	2.91	2.73	1.11
hcr1 F_2 (5) 6	263	296	1507	311	2377	27.22	2.92	3.14	0.89

Table S17. *420* crossover rate (cM) of 87 *hcr2* BC_1F_2 individuals used for DNA library construction. Selected 'high' individuals from the total population (~400) are shown in the range of ~38-47 cM.

BC_1F_2 progeny	Green	Red	Both	None	Total	CO rate (cM)	G/non G	R/non R	G/R
hcr2 F_2 (6)-47	385	364	988	321	2058	47.84	2.00	1.92	1.06
hcr2 F_2 (3)-44	352	264	856	222	1694	47.78	2.49	1.95	1.33
hcr2 F_2 (6)-50	365	382	961	363	2071	47.22	1.78	1.84	0.96
hcr2 F_2 (8)-14	358	299	923	253	1833	46.79	2.32	2.00	1.20
hcr2 F_2 (6)-44	426	358	1090	321	2195	46.55	2.23	1.94	1.19
hcr2 F_2 (1)-43	346	251	830	248	1675	46.41	2.36	1.82	1.38
hcr2 F_2 (8)-20	387	324	1044	262	2017	45.69	2.44	2.11	1.19
hcr2 F_2 (5)-43	421	346	1144	288	2199	45.01	2.47	2.10	1.22
hcr2 F_2 (8)-42	316	275	920	200	1711	44.40	2.60	2.32	1.15
hcr2 F_2 (6)-28	382	355	1071	327	2135	44.36	2.13	2.01	1.08
hcr2 F_2 (3)-24	339	268	908	249	1764	44.16	2.41	2.00	1.26
hcr2 F_2 (7)-48	345	296	981	244	1866	44.06	2.46	2.17	1.17
hcr2 F_2 (7)-45	342	287	939	264	1832	44.03	2.32	2.02	1.19
hcr2 F_2 (2)-26	384	344	1093	300	2121	44.01	2.29	2.10	1.12
hcr2 F_2 (6)-2	315	253	844	244	1656	43.96	2.31	1.96	1.25
hcr2 F_2 (1)-45	361	248	891	276	1776	43.95	2.39	1.79	1.46
hcr2 F_2 (4)-48	327	257	870	250	1704	43.91	2.36	1.95	1.27
hcr2 F_2 (4)-2	337	301	957	267	1862	43.90	2.28	2.08	1.12
hcr2 F_2 (7)-14	352	249	911	244	1756	43.83	2.56	1.95	1.41
hcr2 F_2 (8)-4	349	310	990	278	1927	43.78	2.28	2.07	1.13
hcr2 F_2 (8)-23	406	295	1069	280	2050	43.78	2.57	1.99	1.38
hcr2 F_2 (5)-25	379	347	1107	291	2124	43.75	2.33	2.17	1.09
hcr2 F_2 (4)-11	286	287	867	237	1677	43.73	2.20	2.21	1.00
hcr2 F_2 (8)-35	349	283	977	244	1853	43.62	2.52	2.12	1.23
hcr2 F_2 (1)-17	300	266	853	244	1663	43.49	2.26	2.06	1.13
hcr2 F_2 (6)-13	385	346	1099	323	2153	43.35	2.22	2.04	1.11
hcr2 F_2 (4)-24	267	241	779	213	1500	43.20	2.30	2.13	1.11
hcr2 F_2 (3)-43	211	172	585	163	1131	43.19	2.38	2.02	1.23
hcr2 F_2 (8)-28	364	292	1005	278	1939	43.14	2.40	2.02	1.25
hcr2 F_2 (7)-11	365	278	997	267	1907	42.93	2.50	2.02	1.31
hcr2 F_2 (7)-32	359	315	1042	286	2002	42.84	2.33	2.10	1.14
hcr2 F_2 (7)-15	342	344	1093	260	2039	42.81	2.38	2.39	0.99
hcr2 F_2 (1)-11	339	264	936	255	1794	42.75	2.46	2.02	1.28
hcr2 F_2 (8)-27	346	308	1006	286	1946	42.74	2.28	2.08	1.12
hcr2 F_2 (5)-8	385	324	1091	312	2112	42.68	2.32	2.03	1.19
hcr2 F_2 (3)-26	316	296	958	255	1825	42.61	2.31	2.20	1.07
hcr2 F_2 (7)-20	367	291	1071	238	1967	42.47	2.72	2.25	1.26
hcr2 F_2 (4)-26	321	289	958	256	1824	42.46	2.35	2.16	1.11
hcr2 F_2 (4)-4	356	299	1023	281	1959	42.44	2.38	2.08	1.19

hcr2 F_2 (8)-45	342	306	1024	268	1940	42.38	2.38	2.18	1.12
hcr2 F_2 (3)-15	289	232	812	230	1563	42.26	2.38	2.01	1.25
hcr2 F_2 (4)-50	326	280	978	234	1818	42.26	2.54	2.25	1.16
hcr2 F_2 (7)-40	347	276	982	268	1873	42.14	2.44	2.05	1.26
hcr2 F_2 (7)-42	353	300	1031	284	1968	42.00	2.37	2.09	1.18
hcr2 F_2 (5)-23	332	311	997	302	1942	41.88	2.17	2.06	1.07
hcr2 F_2 (2)-13	405	310	1126	320	2161	41.84	2.43	1.98	1.31
hcr2 F_2 (7)-13	316	242	902	227	1687	41.82	2.60	2.11	1.31
hcr2 F_2 (5)-17	354	328	1089	292	2063	41.79	2.33	2.19	1.08
hcr2 F_2 (8)-2	326	298	965	300	1889	41.75	2.16	2.02	1.09
hcr2 F_2 (3)-3	288	232	836	219	1575	41.72	2.49	2.11	1.24
hcr2 F_2 (2)-17	167	148	525	115	955	41.66	2.63	2.39	1.13
hcr2 F_2 (6)-10	364	264	997	282	1907	41.57	2.49	1.95	1.38
hcr2 F_2 (6)-45	332	323	1061	277	1993	41.46	2.32	2.27	1.03
hcr2 F_2 (1)-40	259	203	714	230	1406	41.45	2.25	1.88	1.28
hcr2 F_2 (8)-32	352	241	965	251	1809	41.32	2.68	2.00	1.46
hcr2 F_2 (2)-21	346	290	1019	290	1945	41.18	2.35	2.06	1.19
hcr2 F_2 (4)-28	257	280	857	256	1650	40.92	2.08	2.22	0.92
hcr2 F_2 (8)-39	372	277	1066	283	1998	40.81	2.57	2.05	1.34
hcr2 F_2 (7)-23	290	274	916	258	1738	40.76	2.27	2.17	1.06
hcr2 F_2 (5)-20	338	300	1078	254	1970	40.65	2.56	2.33	1.13
hcr2 F_2 (5)-5	366	294	1074	310	2044	40.48	2.38	2.02	1.24
hcr2 F_2 (2)-16	347	287	1043	287	1964	40.47	2.42	2.10	1.21
hcr2 F_2 (6)-24	395	350	1231	312	2308	40.47	2.38	2.17	1.13
hcr2 F_2 (1)-9	337	252	976	260	1825	40.46	2.56	2.06	1.34
hcr2 F_2 (7)-37	313	317	1050	275	1955	40.38	2.30	2.32	0.99
hcr2 F_2 (4)-12	330	268	974	284	1856	40.37	2.36	2.02	1.23
hcr2 F_2 (6)-32	395	299	1129	333	2156	40.32	2.41	1.96	1.32
hcr2 F_2 (5)-31	362	274	1025	319	1980	40.20	2.34	1.91	1.32
hcr2 F_2 (6)-22	343	319	1174	271	2127	40.11	2.49	2.46	1.01
hcr2 F_2 (8)-48	342	273	1027	277	1919	40.08	2.49	2.10	1.25
hcr2 F_2 (4)-19	323	272	971	292	1858	40.04	2.29	2.02	1.19
hcr2 F_2 (5)-51	387	334	1240	293	2254	39.98	2.59	2.31	1.16
hcr2 F_2 (5)-35	357	308	1077	340	2082	39.90	2.21	1.99	1.16
hcr2 F_2 (5)-34	345	282	1047	294	1968	39.77	2.42	2.08	1.22
hcr2 F_2 (4)-43	271	214	800	238	1523	39.74	2.37	1.99	1.27
hcr2 F_2 (5)-45	373	324	1166	327	2190	39.71	2.36	2.13	1.15
hcr2 F_2 (3)-7	275	219	808	252	1554	39.65	2.30	1.95	1.26
hcr2 F_2 (8)-36	338	286	1056	283	1963	39.65	2.45	2.16	1.18
hcr2 F_2 (7)-36	293	286	980	263	1822	39.63	2.32	2.28	1.02

hcr2 F_2 (4)-7	85	92	293	89	559	39.44	2.09	2.21	0.92
hcr2 F_2 (8)-16	351	272	1087	262	1972	39.32	2.69	2.22	1.29
hcr2 F_2 (8)-44	98	97	351	72	618	39.26	2.66	2.64	1.01
hcr2 F_2 (8)-6	342	279	1062	287	1970	39.21	2.48	2.13	1.23
hcr2 F_2 (4)-10	279	279	941	273	1772	39.16	2.21	2.21	1.00
hcr2 F_2 (3)-10	261	211	826	202	1500	39.12	2.63	2.24	1.24
hcr2 F_2 (4)-41	289	234	919	236	1678	38.63	2.57	2.20	1.24
hcr2 F_2 (6)-18	327	282	1064	304	1977	38.04	2.37	2.13	1.16

Table S18. *420* crossover rate (cM) of 27 *lcr1* BC_1F_2 individuals used for DNA library construction. Selected 'low' individuals from the total population (~300) are shown in the range of ~13-15 cM.

BC_1F_2 progeny	Green	Red	Both	None	Total	CO rate (cM)	G/non G	R/non R	G/R
lcr1 F_2 (2)-11	86	99	977	287	1449	13.71	2.75	2.88	0.87
lcr1 F_2 (2)-12	76	69	723	218	1086	14.39	2.78	2.69	1.10
lcr1 F_2 (2)-21	120	114	1214	277	1725	14.64	3.41	3.35	1.05
lcr1 F_2 (2)-3	110	104	1201	291	1706	13.45	3.32	3.25	1.06
lcr1 F_2 (2)-31	108	103	1052	291	1554	14.65	2.94	2.89	1.05
lcr1 F_2 (2)-37	57	77	677	218	1029	14.00	2.49	2.74	0.74
lcr1 F_2 (2)-42	125	124	1326	350	1925	13.90	3.06	3.05	1.01
lcr1 F_2 (2)-44	67	72	705	183	1027	14.60	3.03	3.11	0.93
lcr1 F_2 (2)-49	129	126	1290	352	1897	14.49	2.97	2.94	1.02
lcr1 F_2 (2)-6	34	30	341	111	516	13.29	2.66	2.56	1.13
lcr1 F_2 (2)-69	103	104	1075	268	1550	14.39	3.17	3.18	0.99
lcr1 F_2 (2)-8	129	121	1287	317	1854	14.54	3.23	3.16	1.07
lcr1 F_2 (3)-17	51	47	504	151	753	13.99	2.80	2.73	1.09
lcr1 F_2 (3)-25	107	135	1338	284	1864	13.96	3.45	3.77	0.79
lcr1 F_2 (3)-53	101	110	1188	296	1695	13.34	3.17	3.27	0.92
lcr1 F_2 (3)-66	92	87	898	231	1308	14.78	3.11	3.05	1.06
lcr1 F_2 (3)-77	142	157	1519	380	2198	14.68	3.09	3.21	0.90
lcr1 F_2 (4)-13	113	110	1200	307	1730	13.85	3.15	3.12	1.03
lcr1 F_2 (4)-16	35	42	404	106	587	14.11	2.97	3.16	0.83
lcr1 F_2 (4)-26	167	168	1764	439	2538	14.21	3.18	3.19	0.99
lcr1 F_2 (4)-77	84	80	868	206	1238	14.26	3.33	3.27	1.05
lcr1 F_2 (1)-25	121	120	1267	390	1898	13.63	2.72	2.71	1.01
lcr1 F_2 (1)-27	171	176	1711	528	2586	14.46	2.67	2.70	0.97
lcr1 F_2 (1)-29	157	156	1664	391	2368	14.23	3.33	3.32	1.01
lcr1 F_2 (1)-34	43	51	536	131	761	13.23	3.18	3.37	0.84
lcr1 F_2 (1)-35	159	166	1672	473	2470	14.16	2.87	2.91	0.96
lcr1 F_2 (1)-37	99	76	881	248	1304	14.47	3.02	2.76	1.30

Table S19. List of EMS-SNPs and its corresponding nucleotide/amino acid (aa) transitions plotted in *hcr1* SHOREmap. A splice site mutation change of a single nucleotide C>T with 0.98 allele frequency located at 13471378 bp genomic position in chromosome 4 (in orange).

Chromosome	Position (bp)	Reference allele	Mutant allele	Support	Frequency	Quality score	Type	Sequence feature	Gene ID	Type of Change	Reference aa	Mutation-induced aa
1	3493292	G	A	62	0.46	40	NEWSNP	CDS	AT1G10580.1	Nonsyn	P	L
1	8849288	C	T	34	0.41	40	NEWSNP	intergenic				
1	11371412	C	T	14	0.42	40	NEWSNP	intronic/noncoding	AT1G31750.1			
1	12255550	C	T	41	0.49	40	NEWSNP	intergenic				
1	12592042	C	T	42	0.68	40	NEWSNP	CDS	AT1G34440.1	Syn	Q	Q
1	14592362	C	T	68	0.38	40	NEWSNP	intergenic				
1	15931420	G	A	37	0.41	40	NEWSNP	CDS	AT1G42470.1	Nonsyn	A	T
1	16026725	G	A	32	0.39	40	NEWSNP	intergenic				
1	20697206	C	T	35	0.41	40	NEWSNP	intergenic				
1	20820201	G	A	19	0.47	40	NEWSNP	intergenic				
1	21529618	C	T	23	0.56	40	NEWSNP	intergenic				
1	24478713	C	T	52	0.48	40	NEWSNP	intronic/noncoding	AT1G65810.1			
1	24478713	C	T	52	0.48	40	NEWSNP	intronic/noncoding	AT1G65810.2			
2	2561293	C	T	75	0.45	40	NEWSNP	intergenic				
2	2646255	C	T	63	0.53	40	NEWSNP	intergenic				
2	2680417	G	A	42	0.38	40	NEWSNP	intergenic				
2	4489446	C	T	70	0.55	40	NEWSNP	intergenic				
2	6851201	C	T	52	0.50	40	NEWSNP	CDS	AT2G15730.1	Syn	N	N
2	9351668	C	T	48	0.50	40	NEWSNP	intronic/noncoding	AT2G21940.1			
2	9351668	C	T	48	0.50	40	NEWSNP	intronic/noncoding	AT2G21940.2			
2	9351668	C	T	48	0.50	40	NEWSNP	intronic/noncoding	AT2G21940.3			
2	9351668	C	T	48	0.50	40	NEWSNP	intronic/noncoding	AT2G21940.4			
2	9351668	C	T	48	0.50	40	NEWSNP	intronic/noncoding	AT2G21940.5			
2	17189098	C	T	21	0.36	40	NEWSNP	intergenic				
3	2350190	G	A	28	0.58	40	NEWSNP	intergenic				
3	2968465	C	T	62	0.50	40	NEWSNP	CDS	AT3G09670.1	Nonsyn	T	I
3	2968465	C	T	62	0.50	40	NEWSNP	CDS	AT3G09670.2	Nonsyn	T	I
3	4426808	G	A	65	0.45	40	NEWSNP	CDS	AT3G13560.1	Nonsyn	A	V
3	4426808	G	A	65	0.45	40	NEWSNP	CDS	AT3G13560.2	Nonsyn	A	V
3	4426808	G	A	65	0.45	40	NEWSNP	CDS	AT3G13560.3	Nonsyn	A	V
3	8598244	G	A	37	0.51	40	NEWSNP	intergenic				
3	8901306	G	A	20	0.49	40	NEWSNP	CDS	AT3G24480.1	Nonsyn	P	S
3	12217216	C	T	72	0.51	40	NEWSNP	intergenic				
3	13801565	C	T	14	0.47	40	NEWSNP	intergenic				

4	3565927	C	T	95	0.71	40	NEWSNP	intergenic				
4	4397378	G	A	83	0.65	40	NEWSNP	intergenic				
4	4455632	C	T	67	0.61	40	NEWSNP	intergenic				
4	6786832	G	A	62	0.77	40	NEWSNP	intergenic				
4	12032472	C	T	88	0.96	40	NEWSNP	intronic/noncoding	AT4G22960.1			
4	13471378	C	T	119	0.98	40	NEWSNP	splice_site_change	AT4G26720.1			
4	15277823	C	T	56	0.86	40	NEWSNP	intergenic				
4	15484080	G	A	101	0.89	40	NEWSNP	intronic/noncoding	AT4G32010.1			
5	1999606	G	A	67	0.56	40	NEWSNP	CDS	AT5G06540.1	Nonsyn	L	F
5	4004534	G	A	97	0.51	40	NEWSNP	intronic/noncoding	AT5G12370.1			
5	4004534	G	A	97	0.51	40	NEWSNP	intronic/noncoding	AT5G12370.2			
5	4004534	G	A	97	0.51	40	NEWSNP	intronic/noncoding	AT5G12370.3			
5	4046904	C	T	58	0.42	40	NEWSNP	CDS	AT5G12470.1	Syn	A	A
5	5153800	G	A	35	0.45	40	NEWSNP	five_prime_UTR	AT5G15800.1			
5	5153800	G	A	35	0.45	40	NEWSNP	five_prime_UTR	AT5G15800.2			
5	10075739	G	A	40	0.43	40	NEWSNP	intergenic				
5	10214637	G	A	36	0.47	40	NEWSNP	intergenic				
5	10336128	G	A	56	0.43	40	NEWSNP	intergenic				
5	10459490	G	A	10	0.48	40	NEWSNP	intergenic				
5	10994278	C	T	34	0.43	40	NEWSNP	intergenic				
5	12769404	G	A	57	0.43	40	NEWSNP	intergenic				
5	13299008	C	T	44	0.55	40	NEWSNP	intergenic				
5	13313698	C	T	29	0.43	40	NEWSNP	intergenic				
5	13664914	C	T	62	0.48	40	NEWSNP	CDS	AT5G35430.1	Nonsyn	R	W
5	17848364	C	T	28	0.36	40	NEWSNP	CDS	AT5G44310.1	Syn	K	K
5	17848364	C	T	28	0.36	40	NEWSNP	CDS	AT5G44310.2	Syn	K	K
5	17848369	C	T	33	0.45	40	NEWSNP	CDS	AT5G44310.1	Nonsyn	V	M
5	17848369	C	T	33	0.45	40	NEWSNP	CDS	AT5G44310.2	Nonsyn	V	M
5	18666017	G	A	27	0.47	40	NEWSNP	intergenic				
5	21318563	G	A	135	0.48	40	NEWSNP	CDS	AT5G52530.1	Nonsyn	V	M
5	21318563	G	A	135	0.48	40	NEWSNP	CDS	AT5G52530.2	Nonsyn	V	M
5	21318563	G	A	135	0.48	40	NEWSNP	CDS	AT5G52530.3	Nonsyn	V	M
5	22166578	C	T	30	0.43	40	NEWSNP	intergenic				
5	25962334	C	T	73	0.51	40	NEWSNP	CDS	AT5G64980.1	Nonsyn	G	E

Table S20. List of EMS-SNPs and its corresponding nucleotide/amino acid transitions plotted in *hcr2* SHOREmap. Based on allele frequency (>80%) and functional relevance, a non-synonymous change of a single nucleotide from G to A in the coding region (CDS) located at 11231903 bp in chromosome 4 (in orange).

Chromosome	Position	Reference allele	Mutant allele	Support	Frequency	Quality score	Type	Sequence feature	Gene ID	Type of Change	Reference aa	Mutation-induced aa
1	1031530	C	T	22	0.43	40	NEWSNP	three_prime_UTR	AT1G04010.1			
1	2892436	C	T	40	0.50	40	NEWSNP	CDS	AT1G09000.1	Nonsyn	P	S
1	3318260	G	A	32	0.42	40	NEWSNP	CDS	AT1G10130.1	Syn	G	G
1	3493292	G	A	55	0.47	40	NEWSNP	CDS	AT1G10580.1	Nonsyn	P	L
1	4227606	G	A	45	0.41	40	NEWSNP	CDS	AT1G12420.1	Nonsyn	A	V
1	4972879	C	T	28	0.41	40	NEWSNP	CDS	AT1G14530.1	Syn	L	L
1	4972879	C	T	28	0.41	40	NEWSNP	CDS	AT1G14530.2	Syn	L	L
1	5472453	C	T	31	0.39	40	NEWSNP	intronic/noncoding	AT1G15930.1			
1	5472453	C	T	31	0.39	40	NEWSNP	intronic/noncoding	AT1G15930.2			
1	5481316	C	T	12	0.36	40	NEWSNP	intronic/noncoding	AT1G15950.1			
1	5481316	C	T	12	0.36	40	NEWSNP	intronic/noncoding	AT1G15950.2			
1	6005658	C	T	30	0.39	40	NEWSNP	CDS	AT1G17470.1	Nonsyn	P	S
1	6005658	C	T	30	0.39	40	NEWSNP	CDS	AT1G17470.2	Nonsyn	P	S
1	6846162	C	T	22	0.38	40	NEWSNP	intergenic				
1	8669892	C	T	28	0.37	40	NEWSNP	intronic/noncoding	AT1G24460.1			
1	8669892	C	T	28	0.37	40	NEWSNP	intronic/noncoding	AT1G24460.2			
1	10383572	C	T	17	0.49	40	NEWSNP	intergenic				
1	10962603	C	T	26	0.39	40	NEWSNP	intronic/noncoding	AT1G30825.1			
1	10989207	C	T	31	0.48	40	NEWSNP	CDS	AT1G30860.1	Nonsyn	D	N
1	11729488	C	T	27	0.43	40	NEWSNP	intergenic				
1	15061362	C	T	55	0.52	40	NEWSNP	intergenic				
1	15925613	C	T	17	0.52	40	NEWSNP	intergenic				
1	16716347	C	T	42	0.51	40	NEWSNP	three_prime_UTR	AT1G44020.1			
1	17261817	C	T	48	0.62	40	NEWSNP	intergenic				
1	18629738	C	T	20	0.36	40	NEWSNP	CDS	AT1G50300.1	Nonsyn	G	D
1	19450673	C	T	26	0.41	40	NEWSNP	intergenic				
1	21524149	G	A	13	0.52	40	NEWSNP	intergenic				
1	23280529	C	T	30	0.64	40	NEWSNP	intergenic				
1	24173119	C	T	43	0.49	40	NEWSNP	intronic/noncoding	AT1G65070.1			
1	24173119	C	T	43	0.49	40	NEWSNP	CDS	AT1G65070.2	Syn	K	K
1	27192559	C	T	16	0.37	40	NEWSNP	intergenic				
1	27317714	C	T	25	0.46	40	NEWSNP	intergenic				
1	27352157	C	T	43	0.46	40	NEWSNP	CDS	AT1G72650.1	Nonsyn	S	F
1	27352157	C	T	43	0.46	40	NEWSNP	CDS	AT1G72650.2	Nonsyn	S	F
2	2414053	G	A	40	0.63	40	NEWSNP	intergenic				
2	2426364	G	A	42	0.54	40	NEWSNP	CDS	AT2G06200.1	Nonsyn	E	K
2	2646255	C	T	53	0.56	40	NEWSNP	intergenic				
2	2680417	G	A	44	0.40	40	NEWSNP	intergenic				
2	2773331	G	A	49	0.54	40	NEWSNP	intergenic				

2	2988024	G	A	24	0.60	40	NEWSNP	splice_site_change	AT2G07190.1			
2	3082719	G	A	69	0.59	40	NEWSNP	intergenic				
2	3637495	G	A	44	0.50	40	NEWSNP	intergenic				
2	3756150	G	A	44	0.85	40	NEWSNP	intergenic				
2	3799792	G	A	23	0.68	40	NEWSNP	intergenic				
2	4400393	C	T	56	0.59	40	NEWSNP	intergenic				
2	4489446	C	T	61	0.60	40	NEWSNP	intergenic				
2	4505198	G	A	47	0.41	40	NEWSNP	intergenic				
2	5464826	G	A	30	0.47	40	NEWSNP	intergenic				
2	5732638	G	A	15	0.54	40	NEWSNP	intergenic				
2	6329810	C	T	23	0.40	40	NEWSNP	intergenic				
2	6550072	G	A	46	0.48	40	NEWSNP	intergenic				
2	6963454	C	T	35	0.46	40	NEWSNP	intergenic				
2	7915022	G	A	52	0.55	40	NEWSNP	CDS	AT2G18190.1	Nonsyn	A	V
2	10583637	G	A	24	0.60	40	NEWSNP	CDS	AT2G24850.1	Nonsyn	P	L
2	11096892	G	A	11	0.48	40	NEWSNP	intergenic				
2	11312320	G	A	30	0.48	40	NEWSNP	CDS	AT2G26590.1	Syn	D	D
2	11312320	G	A	30	0.48	40	NEWSNP	CDS	AT2G26590.2	Syn	D	D
2	11312320	G	A	30	0.48	40	NEWSNP	CDS	AT2G26590.3	Syn	D	D
2	11649451	G	A	29	0.55	40	NEWSNP	CDS	AT2G27229.1	Nonsyn	R	K
2	12114302	G	A	29	0.49	40	NEWSNP	intergenic				
2	13417156	C	T	24	0.38	40	NEWSNP	CDS	AT2G31510.1	Syn	L	L
2	15319340	C	T	60	0.54	40	NEWSNP	CDS	AT2G36500.1	Nonsyn	L	F
2	15534145	G	A	17	0.44	40	NEWSNP	intergenic				
2	15605181	G	A	51	0.49	40	NEWSNP	CDS	AT2G37150.1	Nonsyn	T	I
2	15605181	G	A	51	0.49	40	NEWSNP	CDS	AT2G37150.2	Nonsyn	T	I
2	15605181	G	A	51	0.49	40	NEWSNP	CDS	AT2G37150.3	Nonsyn	T	I
2	16140093	G	A	26	0.48	40	NEWSNP	CDS	AT2G38580.1	Nonsyn	E	K
2	16174290	G	A	26	0.65	40	NEWSNP	intronic/noncoding	AT2G38680.1			
2	16355346	G	A	34	0.39	40	NEWSNP	three_prime_UTR	AT2G39190.1			
2	16355346	G	A	34	0.39	40	NEWSNP	CDS	AT2G39190.2	Syn	G	G
2	17221038	G	A	12	0.52	40	NEWSNP	intergenic				
2	17682792	G	A	31	0.46	40	NEWSNP	intronic/noncoding	AT2G42470.1			
3	1611832	C	T	23	0.40	40	NEWSNP	CDS	AT3G05545.1	Nonsyn	S	F
3	3504948	C	T	22	0.35	40	NEWSNP	CDS	AT3G11180.1	Syn	Y	Y
3	3504948	C	T	22	0.35	40	NEWSNP	CDS	AT3G11180.2	Syn	Y	Y
3	5651178	G	A	24	0.44	40	NEWSNP	intergenic				
3	5957417	C	T	51	0.43	40	NEWSNP	CDS	AT3G17410.1	Syn	L	L
3	8901306	G	A	11	0.52	40	NEWSNP	CDS	AT3G24480.1	Nonsyn	P	S
3	9644950	C	T	35	0.38	40	NEWSNP	CDS	AT3G26320.1	Nonsyn	W	*
3	10129789	C	T	44	0.46	40	NEWSNP	CDS	AT3G27360.1	Syn	R	R

3	10129789	C	T	44	0.46	40	NEWSNP	three_prime_UTR	AT3G27380.1			
3	10129789	C	T	44	0.46	40	NEWSNP	three_prime_UTR	AT3G27380.2			
3	12397197	G	A	42	0.35	40	NEWSNP	intergenic				
3	13403049	G	A	14	0.50	40	NEWSNP	intergenic				
3	13555948	C	T	39	0.49	40	NEWSNP	intergenic				
3	14347712	C	T	19	0.36	40	NEWSNP	intergenic				
3	15848416	C	T	32	0.40	40	NEWSNP	intergenic				
3	17971822	C	T	21	0.39	40	NEWSNP	intergenic				
4	1967265	G	A	62	0.71	40	NEWSNP	intergenic				
4	2508965	G	A	14	0.41	40	NEWSNP	intergenic				
4	3437643	G	A	64	0.77	40	NEWSNP	intergenic				
4	3580503	G	A	68	0.83	40	NEWSNP	intergenic				
4	3646746	C	T	53	0.78	40	NEWSNP	intergenic				
4	4856197	G	A	79	0.74	40	NEWSNP	intergenic				
4	5487407	G	A	45	0.74	40	NEWSNP	intergenic				
4	6700268	C	T	14	0.35	40	NEWSNP	intergenic				
4	8987414	G	A	69	0.97	40	NEWSNP	intronic/noncoding	AT4G15802.1			
4	9742963	G	A	71	0.95	40	NEWSNP	CDS	AT4G17470.1	Nonsyn	Q	*
4	9742963	G	A	71	0.95	40	NEWSNP	CDS	AT4G17470.2	Nonsyn	Q	*
4	9742963	G	A	71	0.95	40	NEWSNP	CDS	AT4G17470.3	Nonsyn	Q	*
4	10632917	C	T	17	0.40	40	NEWSNP	intergenic				
4	11231903	G	A	53	0.88	40	NEWSNP	CDS	AT4G21030.1	Nonsyn	D	N
4	13747409	G	A	70	0.75	40	NEWSNP	CDS	AT4G27510.1	Nonsyn	S	F
4	13747409	G	A	70	0.75	40	NEWSNP	CDS	AT4G27510.2	Nonsyn	S	F
4	14718117	G	A	77	0.73	40	NEWSNP	CDS	AT4G30100.1	Nonsyn	G	D
5	2876441	C	T	31	0.44	40	NEWSNP	intronic/noncoding	AT5G09250.1			
5	2876441	C	T	31	0.44	40	NEWSNP	intronic/noncoding	AT5G09250.2			
5	3372488	C	T	49	0.58	40	NEWSNP	intergenic				
5	3585603	C	T	41	0.59	40	NEWSNP	intronic/noncoding	AT5G11240.1			
5	4004534	G	A	73	0.45	40	NEWSNP	intronic/noncoding	AT5G12370.1			
5	4004534	G	A	73	0.45	40	NEWSNP	intronic/noncoding	AT5G12370.2			
5	4004534	G	A	73	0.45	40	NEWSNP	intronic/noncoding	AT5G12370.3			
5	4020078	C	T	30	0.60	40	NEWSNP	intronic/noncoding	AT5G12400.1			
5	5116642	C	T	36	0.59	40	NEWSNP	CDS	AT5G15700.1	Nonsyn	E	K
5	5116642	C	T	36	0.59	40	NEWSNP	CDS	AT5G15700.2	Nonsyn	E	K
5	5526181	C	T	47	0.54	40	NEWSNP	CDS	AT5G16800.1	Nonsyn	E	K
5	5526181	C	T	47	0.54	40	NEWSNP	CDS	AT5G16800.2	Nonsyn	E	K
5	5526181	C	T	47	0.54	40	NEWSNP	CDS	AT5G16800.3	Nonsyn	E	K
5	6509610	C	T	50	0.62	40	NEWSNP	CDS	AT5G19330.1	Nonsyn	V	I
5	6509610	C	T	50	0.62	40	NEWSNP	CDS	AT5G19330.2	Nonsyn	V	I
5	7481761	C	T	48	0.53	40	NEWSNP	CDS	AT5G22540.1	Nonsyn	D	N

5	9013739	C	T	24	0.67	40	NEWSNP	intergenic				
5	9013798	C	T	18	0.62	40	NEWSNP	intergenic				
5	9644532	G	A	12	0.60	40	NEWSNP	intergenic				
5	10816741	C	T	42	0.49	40	NEWSNP	intergenic				
5	10877866	C	T	36	0.61	40	NEWSNP	CDS	AT5G28850.1	Nonsyn	G	E
5	10877866	C	T	36	0.61	40	NEWSNP	CDS	AT5G28850.2	Nonsyn	G	E
5	14030275	C	T	31	0.58	40	NEWSNP	CDS	AT5G35910.1	Nonsyn	E	K
5	14132164	C	T	45	0.65	40	NEWSNP	CDS	AT5G35980.1	Nonsyn	P	S
5	14132164	C	T	45	0.65	40	NEWSNP	CDS	AT5G35980.2	Nonsyn	P	S
5	14900735	C	T	25	0.56	40	NEWSNP	intergenic				
5	15809558	G	A	26	0.60	40	NEWSNP	intergenic				
5	16710225	C	T	30	0.44	40	NEWSNP	intergenic				
5	17593307	C	T	57	0.58	40	NEWSNP	CDS	AT5G43790.1	Nonsyn	A	T
5	21318563	G	A	88	0.49	40	NEWSNP	CDS	AT5G52530.1	Nonsyn	V	M
5	21318563	G	A	88	0.49	40	NEWSNP	CDS	AT5G52530.2	Nonsyn	V	M
5	21318563	G	A	88	0.49	40	NEWSNP	CDS	AT5G52530.3	Nonsyn	V	M
5	22646827	C	T	31	0.61	40	NEWSNP	intronic/noncoding	AT5G55920.1			
5	24420186	C	T	40	0.62	40	NEWSNP	CDS	AT5G60720.1	Nonsyn	D	N
5	25894245	C	T	33	0.46	40	NEWSNP	CDS	AT5G64760.1	Nonsyn	E	K
5	25894245	C	T	33	0.46	40	NEWSNP	CDS	AT5G64760.2	Nonsyn	E	K

Table S21. List of EMS-SNPs and its corresponding nucleotide/amino acid transitions plotted in *hcr3* SHOREmap. Based on allele frequency (>80%) and functional relevance, two putative candidate (in orange) with a C>T transition located in chromosome 3.

Chromosome	Position	Reference allele	Mutant allele	Support	Frequency	Quality score	Type	Sequence feature	Gene ID	Type of Change	Reference aa	Mutation-induced aa
1	1715165	G	A	25	0.36	40	NEWSNP	intronic/noncoding	AT1G05710.1			
1	1715165	G	A	25	0.36	40	NEWSNP	five_prime_UTR	AT1G05710.2			
1	1715165	G	A	25	0.36	40	NEWSNP	five_prime_UTR	AT1G05710.3			
1	1715165	G	A	25	0.36	40	NEWSNP	intronic/noncoding	AT1G05710.4			
1	1715165	G	A	25	0.36	40	NEWSNP	five_prime_UTR	AT1G05710.5			
1	2978694	G	A	42	0.41	40	NEWSNP	CDS	AT1G09220.1	Nonsyn	T	I
1	5262646	G	A	21	0.37	40	NEWSNP	CDS	AT1G15290.1	Nonsyn	S	F
1	5891548	G	A	32	0.39	40	NEWSNP	CDS	AT1G17230.1	Nonsyn	W	*
1	8139801	G	A	44	0.60	40	NEWSNP	CDS	AT1G22990.1	Nonsyn	G	D
1	8546722	C	T	12	0.80	40	NEWSNP	intergenic				
1	8901082	G	A	23	0.66	40	NEWSNP	intronic/noncoding	AT1G25375.1			
1	9066458	G	A	49	0.70	40	NEWSNP	intergenic				
1	10810088	G	A	47	0.80	40	NEWSNP	intergenic				
1	10858556	G	A	62	0.65	40	NEWSNP	CDS	AT1G30630.1	Nonsyn	S	F
1	11036840	G	A	58	0.60	40	NEWSNP	CDS	AT1G30950.1	Nonsyn	A	T
1	12523908	G	A	48	0.71	40	NEWSNP	CDS	AT1G34320.1	Nonsyn	M	I
1	13430063	G	A	52	0.70	40	NEWSNP	intergenic				
1	17990845	G	A	61	0.67	40	NEWSNP	CDS	AT1G48650.1	Syn	V	V
1	17990845	G	A	61	0.67	40	NEWSNP	CDS	AT1G48650.2	Syn	V	V
1	19738947	G	A	64	0.65	40	NEWSNP	CDS	AT1G52980.1	Syn	R	R
1	21236808	G	A	64	0.48	40	NEWSNP	intergenic				
1	21344061	G	A	61	0.70	40	NEWSNP	CDS	AT1G57620.1	Nonsyn	D	N
1	22077267	G	A	18	0.67	40	NEWSNP	intergenic				
1	22107957	G	A	40	0.71	40	NEWSNP	intergenic				
1	22443262	G	A	32	0.56	40	NEWSNP	intergenic				
1	23464857	G	A	39	0.51	40	NEWSNP	CDS	AT1G63250.1	Syn	R	R
1	24995511	G	A	52	0.64	40	NEWSNP	CDS	AT1G66970.1	Syn	A	A
1	24995511	G	A	52	0.64	40	NEWSNP	CDS	AT1G66970.2	Syn	A	A
1	25325329	G	A	57	0.65	40	NEWSNP	CDS	AT1G67570.1	Syn	Q	Q
1	25510038	G	A	60	0.61	40	NEWSNP	CDS	AT1G68050.1	Nonsyn	A	T
1	26691315	G	A	30	0.60	40	NEWSNP	intergenic				
1	27660648	G	A	46	0.60	40	NEWSNP	CDS	AT1G73590.1	Nonsyn	E	K
1	27923699	G	A	34	0.58	40	NEWSNP	CDS	AT1G74260.1	Nonsyn	A	V
2	2561293	C	T	57	0.50	40	NEWSNP	intergenic				
2	2680378	C	T	15	0.54	40	NEWSNP	intergenic				
2	2680392	G	A	25	0.71	40	NEWSNP	intergenic				
2	2692810	G	A	68	0.77	40	NEWSNP	intergenic				

2	3085929	G	A	52	0.38	40	NEWSNP	intergenic				
2	3971674	C	T	84	0.43	40	NEWSNP	intergenic				
2	4031113	C	T	45	0.45	40	NEWSNP	intergenic				
2	4267991	G	A	35	0.42	40	NEWSNP	intergenic				
2	5358405	G	A	27	0.39	40	NEWSNP	intergenic				
2	6119201	G	A	37	0.35	40	NEWSNP	intergenic				
2	9921883	G	A	20	0.38	40	NEWSNP	intergenic				
2	11996269	G	A	30	0.45	40	NEWSNP	intergenic				
2	15053126	G	A	59	0.53	40	NEWSNP	CDS	AT2G35830.1	Nonsyn	G	E
2	15053126	G	A	59	0.53	40	NEWSNP	CDS	AT2G35830.2	Nonsyn	G	E
2	15064315	G	A	32	0.39	40	NEWSNP	intronic/noncoding	AT2G35880.1			
2	15773814	C	T	12	0.50	40	NEWSNP	intergenic				
3	1686022	G	A	43	0.47	40	NEWSNP	CDS	AT3G05710.1	Syn	Q	Q
3	1686022	G	A	43	0.47	40	NEWSNP	CDS	AT3G05710.2	Syn	Q	Q
3	2274704	G	A	28	0.42	40	NEWSNP	CDS	AT3G07160.1	Nonsyn	R	C
3	2366094	G	A	36	0.35	40	NEWSNP	CDS	AT3G07390.1	Nonsyn	D	N
3	4740011	C	T	18	0.38	40	NEWSNP	intergenic				
3	5007786	G	A	27	0.49	40	NEWSNP	intergenic				
3	5278141	C	T	66	0.47	40	NEWSNP	intergenic				
3	5278151	C	T	68	0.48	40	NEWSNP	intergenic				
3	6245083	G	A	12	0.63	40	NEWSNP	intergenic				
3	6365033	G	A	35	0.61	40	NEWSNP	CDS	AT3G18520.1	Syn	E	E
3	6365033	G	A	35	0.61	40	NEWSNP	CDS	AT3G18520.2	Syn	E	E
3	6367032	C	T	32	0.52	40	NEWSNP	intergenic				
3	7074539	G	A	34	0.46	40	NEWSNP	three_prime_UTR	AT3G20280.1			
3	7074539	G	A	34	0.46	40	NEWSNP	three_prime_UTR	AT3G20280.2			
3	7371101	G	A	46	0.52	40	NEWSNP	intergenic				
3	7776825	G	A	20	0.50	40	NEWSNP	intergenic				
3	8823030	G	A	42	0.55	40	NEWSNP	three_prime_UTR	AT3G24320.1			
3	9136568	G	A	45	0.78	40	NEWSNP	intergenic				
3	9219249	G	A	32	0.52	40	NEWSNP	CDS	AT3G25420.1	Nonsyn	V	M
3	9576024	G	A	32	0.53	40	NEWSNP	intergenic				
3	9824616	G	A	40	0.63	40	NEWSNP	CDS	AT3G26730.1	Nonsyn	D	N
3	10308569	G	A	32	0.63	40	NEWSNP	intronic/noncoding	AT3G27810.1			
3	10430601	C	T	74	0.77	40	NEWSNP	intronic/noncoding	AT3G28030.1			
3	10806663	C	T	18	0.51	40	NEWSNP	CDS	AT3G28780.1	Nonsyn	G	D
3	10841264	C	T	25	0.61	40	NEWSNP	intergenic				
3	11342052	C	T	40	0.60	40	NEWSNP	intergenic				
3	11927788	C	T	40	0.71	40	NEWSNP	intergenic				
3	12186126	C	T	54	0.77	40	NEWSNP	intergenic				
3	12356208	C	T	62	0.71	40	NEWSNP	intergenic				
3	12558149	C	T	40	0.80	40	NEWSNP	intergenic				

3	13217165	C	T	12	0.80	40	NEWSNP	intergenic				
3	13586890	C	T	59	0.53	40	NEWSNP	intergenic				
3	14038424	C	T	84	0.73	40	NEWSNP	CDS	AT3G33494.1	Nonsyn	T	I
3	14212042	C	T	74	0.53	40	NEWSNP	intergenic				
3	14253363	C	T	60	0.66	40	NEWSNP	CDS	AT3G42060.1	Nonsyn	R	Q
3	14313747	C	T	37	0.40	40	NEWSNP	intergenic				
3	14338945	G	A	55	0.42	40	NEWSNP	intergenic				
3	14707560	C	T	78	0.77	40	NEWSNP	intergenic				
3	15389713	C	T	53	0.76	40	NEWSNP	intergenic				
3	15413497	C	T	62	0.81	40	NEWSNP	intergenic				
3	15870106	C	T	70	0.79	40	NEWSNP	CDS	AT3G44110.1	Nonsyn	G	R
3	15870106	C	T	70	0.79	40	NEWSNP	CDS	AT3G44110.2	Nonsyn	G	R
3	15963367	C	T	69	0.70	40	NEWSNP	intergenic				
3	16628886	C	T	68	0.79	40	NEWSNP	CDS	AT3G45310.1	Nonsyn	G	R
3	16628886	C	T	68	0.79	40	NEWSNP	CDS	AT3G45310.2	Nonsyn	G	R
3	16731099	C	T	73	0.89	40	NEWSNP	splice_site_change	AT3G45580.1			
3	17059899	C	T	55	0.92	40	NEWSNP	intergenic				
3	17188662	C	T	27	0.79	40	NEWSNP	intergenic				
3	17889210	C	T	55	0.68	40	NEWSNP	CDS	AT3G48310.1	Nonsyn	P	S
3	19150980	C	T	49	0.56	40	NEWSNP	CDS	AT3G51630.1	Nonsyn	P	S
3	19150980	C	T	49	0.56	40	NEWSNP	CDS	AT3G51630.2	Nonsyn	P	S
3	19150980	C	T	49	0.56	40	NEWSNP	three_prime_UTR	AT3G51632.1			
3	19261979	C	T	33	0.61	40	NEWSNP	intergenic				
3	21488672	C	T	28	0.39	40	NEWSNP	five_prime_UTR	AT3G58040.1			
4	1808162	C	T	30	0.39	40	NEWSNP	intergenic				
4	3646746	C	T	63	0.69	40	NEWSNP	intergenic				
4	8292658	C	T	36	0.51	40	NEWSNP	intergenic				
4	9018165	C	T	34	0.54	40	NEWSNP	CDS	AT4G15890.1	Nonsyn	S	F
4	10306495	C	T	37	0.41	40	NEWSNP	CDS	AT4G18750.1	Nonsyn	A	V
4	11937855	C	T	44	0.46	40	NEWSNP	CDS	AT4G22720.1	Nonsyn	P	L
4	11937855	C	T	44	0.46	40	NEWSNP	CDS	AT4G22720.2	Nonsyn	P	L
4	12631244	C	T	46	0.46	40	NEWSNP	intronic/noncoding	AT4G24430.1			
4	12860499	C	T	38	0.50	40	NEWSNP	intergenic				
4	13313800	C	T	31	0.63	40	NEWSNP	three_prime_UTR	AT4G26310.1			
4	13313800	C	T	31	0.63	40	NEWSNP	three_prime_UTR	AT4G26310.2			
4	13863665	C	T	40	0.62	40	NEWSNP	CDS	AT4G27830.1	Nonsyn	G	R
4	14459105	G	A	45	0.45	40	NEWSNP	intronic/noncoding	AT4G29380.1			
4	15173243	G	A	36	0.41	40	NEWSNP	CDS	AT4G31230.1	Nonsyn	A	V
4	17002451	G	A	13	0.36	40	NEWSNP	intergenic				
4	17523302	G	A	19	0.39	40	NEWSNP	intergenic				
4	17997230	G	A	37	0.64	40	NEWSNP	intergenic				

5	2485066	C	T	24	0.42	40	NEWSNP	CDS	AT5G07790.1	Syn	S	S
5	2485066	C	T	24	0.42	40	NEWSNP	CDS	AT5G07790.2	Syn	S	S
5	3822835	C	T	41	0.48	40	NEWSNP	CDS	AT5G11860.1	Nonsyn	E	K
5	3822835	C	T	41	0.48	40	NEWSNP	CDS	AT5G11860.2	Nonsyn	E	K
5	3822835	C	T	41	0.48	40	NEWSNP	CDS	AT5G11860.3	Nonsyn	E	K
5	3822835	C	T	41	0.48	40	NEWSNP	CDS	AT5G11860.4	Nonsyn	E	K
5	4046904	C	T	26	0.45	40	NEWSNP	CDS	AT5G12470.1	Syn	A	A
5	4799471	C	T	38	0.40	40	NEWSNP	intergenic				
5	4818792	C	T	28	0.50	40	NEWSNP	intronic/noncoding	AT5G14890.1			
5	4938265	C	T	55	0.49	40	NEWSNP	CDS	AT5G15210.1	Nonsyn	R	H
5	5220120	C	T	33	0.40	40	NEWSNP	intergenic				
5	5466520	C	T	25	0.46	40	NEWSNP	CDS	AT5G16660.1	Nonsyn	G	E
5	5466520	C	T	25	0.46	40	NEWSNP	CDS	AT5G16660.2	Nonsyn	G	E
5	5507815	C	T	54	0.54	40	NEWSNP	CDS	AT5G16750.1	Nonsyn	V	I
5	7481761	C	T	35	0.42	40	NEWSNP	CDS	AT5G22540.1	Nonsyn	D	N
5	9644532	G	A	36	0.61	40	NEWSNP	intergenic				
5	10075739	G	A	22	0.37	40	NEWSNP	intergenic				
5	10549485	C	T	33	0.43	40	NEWSNP	intergenic				
5	11101169	C	T	36	0.45	40	NEWSNP	intergenic				
5	11751001	C	T	33	0.50	40	NEWSNP	intergenic				
5	12211325	C	T	23	0.36	40	NEWSNP	intergenic				
5	12615190	C	T	57	0.38	40	NEWSNP	intergenic				
5	12921698	C	T	32	0.36	40	NEWSNP	intergenic				
5	12921754	C	T	32	0.38	40	NEWSNP	intergenic				
5	12922246	C	T	44	0.36	40	NEWSNP	intergenic				
5	13313698	C	T	22	0.41	40	NEWSNP	intergenic				
5	13376471	C	T	38	0.45	40	NEWSNP	intergenic				
5	13406790	C	T	22	0.67	40	NEWSNP	intergenic				
5	13435108	C	T	34	0.52	40	NEWSNP	CDS	AT5G35190.1	Nonsyn	P	S
5	13664914	C	T	42	0.51	40	NEWSNP	CDS	AT5G35430.1	Nonsyn	R	W
5	14037849	C	T	28	0.55	40	NEWSNP	intergenic				
5	15710498	C	T	29	0.60	40	NEWSNP	intergenic				
5	16834305	C	T	42	0.48	40	NEWSNP	CDS	AT5G42120.1	Nonsyn	G	R
5	17848369	C	T	15	0.39	40	NEWSNP	CDS	AT5G44310.1	Nonsyn	V	M
5	17848369	C	T	15	0.39	40	NEWSNP	CDS	AT5G44310.2	Nonsyn	V	M
5	18597443	C	T	11	0.42	40	NEWSNP	intronic/noncoding	AT5G45840.1			
5	18597443	C	T	11	0.42	40	NEWSNP	five_prime_UTR	AT5G45840.2			
5	18666017	G	A	31	0.42	40	NEWSNP	intergenic				
5	18723488	C	T	28	0.38	40	NEWSNP	CDS	AT5G46190.1	Nonsyn	E	K
5	18763360	G	A	30	0.41	40	NEWSNP	intergenic				
5	21318563	G	A	70	0.45	40	NEWSNP	CDS	AT5G52530.1	Nonsyn	V	M
5	21318563	G	A	70	0.45	40	NEWSNP	CDS	AT5G52530.2	Nonsyn	V	M
5	21318563	G	A	70	0.45	40	NEWSNP	CDS	AT5G52530.3	Nonsyn	V	M
5	22060290	C	T	27	0.71	40	NEWSNP	intronic/noncoding	AT5G54310.1			
5	22450101	C	T	36	0.50	40	NEWSNP	intronic/noncoding	AT5G55390.1			
5	22450101	C	T	36	0.50	40	NEWSNP	intronic/noncoding	AT5G55390.2			
5	23023085	C	T	43	0.51	40	NEWSNP	CDS	AT5G56910.1	Syn	S	S

Table S22. List of EMS-SNPs and its corresponding nucleotide/amino acid transitions plotted in *lcr1* SHOREmap. Based on functional relevance and allele frequency (>80%), two non-synonymous candidate mutations with G>A and C>T transitions respectively were identified in chromosome 1.

Chromosome	Position	Reference allele	Mutant allele	Support	Frequency	Quality score	Type	Sequence feature	Gene ID	Type of Change	Reference aa	Mutation-induced aa
1	1307285	C	T	23	0.85	40	NEWSNP	intronic/noncoding	AT1G04680.1			
1	2098022	C	T	13	0.54	40	NEWSNP	CDS	AT1G06840.1	Nonsyn	W	*
1	3318260	G	A	17	0.74	40	NEWSNP	CDS	AT1G10130.1	Syn	G	G
1	3445800	C	T	14	0.74	40	NEWSNP	intergenic				
1	3493292	G	A	15	0.75	40	NEWSNP	CDS	AT1G10580.1	Nonsyn	P	L
1	3861358	C	T	16	0.62	40	NEWSNP	intergenic				
1	4123885	C	T	21	0.72	40	NEWSNP	intronic/noncoding	AT1G12140.1			
1	4123885	C	T	21	0.72	40	NEWSNP	intronic/noncoding	AT1G12140.2			
1	4123885	C	T	21	0.72	40	NEWSNP	CDS	AT1G12150.1	Nonsyn	R	H
1	4415430	G	A	11	0.73	40	NEWSNP	intergenic				
1	4472326	C	T	12	0.71	40	NEWSNP	CDS	AT1G13120.1	Nonsyn	D	N
1	4524507	C	T	20	0.8	40	NEWSNP	intergenic				
1	4895071	C	T	16	0.73	40	NEWSNP	intergenic				
1	5449652	C	T	12	0.92	40	NEWSNP	CDS	AT1G15830.1	Syn	V	V
1	6147166	G	A	11	0.61	40	NEWSNP	intronic/noncoding	AT1G17850.1			
1	6147166	G	A	11	0.61	40	NEWSNP	intronic/noncoding	AT1G17850.2			
1	7011610	G	A	16	0.94	40	NEWSNP	CDS	AT1G20230.1	Nonsyn	E	K
1	7625587	G	A	15	0.75	40	NEWSNP	intronic/noncoding	AT1G21710.1			
1	7965536	G	A	11	0.79	40	NEWSNP	CDS	AT1G22540.1	Nonsyn	A	T
1	8370216	G	A	16	0.8	40	NEWSNP	intronic/noncoding	AT1G23640.1			
1	8537525	G	A	13	0.76	40	NEWSNP	intergenic				
1	9646825	G	A	21	0.84	40	NEWSNP	CDS	AT1G27720.1	Nonsyn	Q	*
1	9729104	G	A	12	0.67	40	NEWSNP	CDS	AT1G27920.1	Syn	R	R
1	9729104	G	A	12	0.67	40	NEWSNP	intronic/noncoding	AT1G27921.1			
1	9729104	G	A	12	0.67	40	NEWSNP	intronic/noncoding	AT1G27921.2			
1	10897737	G	A	26	0.93	40	NEWSNP	intergenic				
1	12375577	G	A	17	0.68	40	NEWSNP	intronic/noncoding	AT1G34040.1			
1	13068988	C	T	15	0.79	40	NEWSNP	intergenic				
1	13068989	G	A	15	0.79	40	NEWSNP	intergenic				
1	13227934	G	A	21	0.81	40	NEWSNP	CDS	AT1G35730.1	Syn	C	C
1	13248487	G	A	21	0.72	40	NEWSNP	intergenic				
1	13605382	G	A	16	0.84	40	NEWSNP	intergenic				
1	15425228	G	A	10	0.83	40	NEWSNP	intergenic				
1	15588568	G	A	20	0.77	40	NEWSNP	intergenic				
1	15590498	G	A	13	0.68	40	NEWSNP	intergenic				

1	15827057	G	A	12	0.86	40	NEWSNP	intergenic				
1	15876925	G	A	18	0.86	40	NEWSNP	intergenic				
1	17414041	G	A	14	0.82	40	NEWSNP	intergenic				
1	17868922	C	T	14	0.78	40	NEWSNP	CDS	AT1G48360.1	Nonsyn	S	F
1	17868922	C	T	14	0.78	40	NEWSNP	CDS	AT1G48360.2	Nonsyn	S	F
1	17868922	C	T	14	0.78	40	NEWSNP	CDS	AT1G48360.3	Nonsyn	S	F
1	17930341	G	A	16	0.76	40	NEWSNP	intergenic				
1	19383116	G	A	18	0.82	40	NEWSNP	intergenic				
1	20333168	G	A	11	0.69	40	NEWSNP	intergenic				
1	20647468	G	A	16	0.64	40	NEWSNP	intronic/noncoding	AT1G55325.1			
1	20647468	G	A	16	0.64	40	NEWSNP	CDS	AT1G55325.2	Nonsyn	G	R
1	22011979	G	A	15	0.62	40	NEWSNP	intronic/noncoding	AT1G59820.1			
1	23011472	G	A	17	0.65	40	NEWSNP	CDS	AT1G62290.1	Nonsyn	A	V
1	23011472	G	A	17	0.65	40	NEWSNP	CDS	AT1G62290.2	Nonsyn	A	V
1	23671773	G	A	12	0.63	40	NEWSNP	CDS	AT1G63810.1	Nonsyn	A	V
1	24434049	G	A	18	0.62	40	NEWSNP	intergenic				
1	25234981	G	A	16	0.67	40	NEWSNP	intergenic				
1	25478050	G	A	17	0.77	40	NEWSNP	CDS	AT1G67940.1	Syn	P	P
1	25528150	G	A	13	0.62	40	NEWSNP	intergenic				
1	26744870	G	A	14	0.78	40	NEWSNP	CDS	AT1G70940.1	Nonsyn	A	T
1	26990652	G	A	14	0.64	40	NEWSNP	three_prime_UTR	AT1G71770.1			
1	26990652	G	A	14	0.64	40	NEWSNP	three_prime_UTR	AT1G71770.2			
2	1856630	C	T	12	1	40	NEWSNP	intergenic				
2	2861864	C	T	13	0.57	40	NEWSNP	intergenic				
2	2862298	C	T	10	0.48	40	NEWSNP	intergenic				
2	4222894	C	T	13	0.45	40	NEWSNP	intergenic				
2	5364361	C	T	16	0.47	40	NEWSNP	intergenic				
2	6851201	C	T	17	0.68	40	NEWSNP	CDS	AT2G15730.1	Syn	N	N
2	7958253	C	T	10	0.56	40	NEWSNP	intergenic				
2	9014769	C	T	10	0.48	40	NEWSNP	five_prime_UTR	AT2G20990.1			
2	9014769	C	T	10	0.48	40	NEWSNP	five_prime_UTR	AT2G20990.2			
2	9014769	C	T	10	0.48	40	NEWSNP	five_prime_UTR	AT2G20990.3			
2	9937059	C	T	11	0.42	40	NEWSNP	intergenic				
2	14062840	C	T	11	0.46	40	NEWSNP	CDS	AT2G33175.1	Nonsyn	E	K
3	2233154	C	T	12	0.6	40	NEWSNP	CDS	AT3G07060.1	Nonsyn	S	F
3	2330070	C	T	14	0.58	40	NEWSNP	intergenic				
3	2968465	C	T	10	0.45	40	NEWSNP	CDS	AT3G09670.1	Nonsyn	T	I
3	2968465	C	T	10	0.45	40	NEWSNP	CDS	AT3G09670.2	Nonsyn	T	I
3	4075037	C	T	11	0.55	40	NEWSNP	intronic/noncoding	AT3G12820.1			
3	6612924	C	T	11	0.41	40	NEWSNP	CDS	AT3G19130.1	Nonsyn	E	K
3	11534744	C	T	10	0.71	40	NEWSNP	intergenic				
3	12493631	C	T	16	0.57	40	NEWSNP	intergenic				
3	14476372	G	A	10	0.37	40	NEWSNP	intergenic				
3	14577752	C	T	12	0.5	40	NEWSNP	intergenic				

3	15085986	C	T	14	0.67	40	NEWSNP	intergenic				
3	15393248	C	T	16	0.7	40	NEWSNP	CDS	AT3G43470.1	Nonsyn	E	K
3	16117983	G	A	13	0.65	40	NEWSNP	intronic/noncoding	AT3G44530.1			
3	16117983	G	A	13	0.65	40	NEWSNP	intronic/noncoding	AT3G44530.2			
3	16665613	G	A	12	0.44	40	NEWSNP	CDS	AT3G45440.1	Syn	D	D
3	18398827	G	A	16	0.76	40	NEWSNP	intronic/noncoding	AT3G49630.1			
3	18916808	G	A	11	0.5	40	NEWSNP	CDS	AT3G50890.1	Nonsyn	S	N
3	19501341	G	A	10	0.56	40	NEWSNP	CDS	AT3G52570.1	Nonsyn	G	D
3	20316980	G	A	11	0.55	40	NEWSNP	intergenic				
3	20571491	G	A	15	0.75	40	NEWSNP	intronic/noncoding	AT3G55485.1			
3	21783346	G	A	21	0.72	40	NEWSNP	intronic/noncoding	AT3G58940.1			
4	1176421	G	A	11	0.69	40	NEWSNP	CDS	AT4G02670.1	Syn	D	D
4	1326835	G	A	16	0.64	40	NEWSNP	CDS	AT4G03000.1	Syn	K	K
4	1326835	G	A	16	0.64	40	NEWSNP	CDS	AT4G03000.2	Syn	K	K
4	1560407	G	A	15	0.62	40	NEWSNP	intergenic				
4	1707287	G	A	17	0.74	40	NEWSNP	intergenic				
4	2059069	C	T	13	0.38	40	NEWSNP	intergenic				
4	2357503	G	A	11	0.69	40	NEWSNP	intergenic				
4	4647966	C	T	13	0.68	40	NEWSNP	intergenic				
4	4981148	C	T	13	0.72	40	NEWSNP	intergenic				
4	5335880	C	T	13	0.68	40	NEWSNP	intergenic				
4	5556956	C	T	15	0.71	40	NEWSNP	intergenic				
4	6937223	C	T	10	0.53	40	NEWSNP	intergenic				
4	10400884	C	T	10	0.56	40	NEWSNP	intergenic				
4	10583067	C	T	10	0.37	40	NEWSNP	splice_site_change	AT4G19410.1			
4	10583067	C	T	10	0.37	40	NEWSNP	splice_site_change	AT4G19410.2			
4	11139288	C	T	10	0.59	40	NEWSNP	intergenic				
4	11885955	C	T	14	0.67	40	NEWSNP	intergenic				
4	12570983	G	A	14	0.64	40	NEWSNP	intergenic				
4	12666382	G	A	15	0.62	40	NEWSNP	intronic/noncoding	AT4G24520.1			
4	12666382	G	A	15	0.62	40	NEWSNP	intronic/noncoding	AT4G24520.2			
4	14399081	G	A	12	0.67	40	NEWSNP	CDS	AT4G29200.1	Nonsyn	S	L
4	15883031	G	A	14	0.56	40	NEWSNP	CDS	AT4G32910.1	Nonsyn	R	K
4	16707075	G	A	17	0.74	40	NEWSNP	intergenic				
4	17599751	G	A	12	0.57	40	NEWSNP	intergenic				
5	1385615	G	A	12	0.43	40	NEWSNP	CDS	AT5G04780.1	Nonsyn	G	E
5	2229860	G	A	11	0.61	40	NEWSNP	intronic/noncoding	AT5G07180.1			
5	3428598	G	A	11	0.65	40	NEWSNP	intergenic				
5	4177870	G	A	11	0.65	40	NEWSNP	intronic/noncoding	AT5G13160.1			
5	4443247	G	A	12	0.5	40	NEWSNP	CDS	AT5G13760.1	Syn	L	L
5	4502847	G	A	11	0.61	40	NEWSNP	CDS	AT5G13960.1	Nonsyn	G	S
5	4846647	G	A	11	0.55	40	NEWSNP	intergenic				

5	4864616	G	A	11	0.55	40	NEWSNP	CDS	AT5G15020.1	Nonsyn	T	I
5	4864616	G	A	11	0.55	40	NEWSNP	CDS	AT5G15020.2	Nonsyn	T	I
5	5427758	G	A	13	0.76	40	NEWSNP	intergenic				
5	5712129	G	A	13	0.57	40	NEWSNP	intronic/noncoding	AT5G17330.1			
5	6798237	G	A	13	0.68	40	NEWSNP	CDS	AT5G20130.1	Syn	K	K
5	8117604	G	A	12	0.6	40	NEWSNP	CDS	AT5G24020.1	Nonsyn	A	T
5	8306018	G	A	14	0.7	40	NEWSNP	CDS	AT5G24350.1	Nonsyn	G	S
5	8306018	G	A	14	0.7	40	NEWSNP	CDS	AT5G24350.2	Nonsyn	G	S
5	8362267	G	A	14	0.61	40	NEWSNP	intergenic				
5	9447936	G	A	12	0.46	40	NEWSNP	CDS	AT5G26850.1	Nonsyn	A	T
5	9447936	G	A	12	0.46	40	NEWSNP	CDS	AT5G26850.2	Nonsyn	A	T
5	9447936	G	A	12	0.46	40	NEWSNP	CDS	AT5G26850.3	Nonsyn	A	T
5	9447936	G	A	12	0.46	40	NEWSNP	CDS	AT5G26850.4	Nonsyn	A	T
5	10455266	G	A	15	0.68	40	NEWSNP	intergenic				
5	11173592	G	A	11	0.42	40	NEWSNP	intergenic				
5	11201062	G	A	10	0.56	40	NEWSNP	intergenic				
5	11403291	G	A	11	0.58	40	NEWSNP	intergenic				
5	11657492	G	A	13	0.62	40	NEWSNP	intergenic				
5	12574480	G	A	11	0.52	40	NEWSNP	intergenic				
5	12711013	G	A	11	0.58	40	NEWSNP	intergenic				
5	14646014	G	A	10	0.67	40	NEWSNP	intergenic				
5	15743276	G	A	13	0.65	40	NEWSNP	CDS	AT5G39320.1	Nonsyn	G	E
5	15966341	G	A	12	0.75	40	NEWSNP	CDS	AT5G39865.1	Nonsyn	T	I
5	16941137	G	A	13	0.52	40	NEWSNP	CDS	AT5G42370.1	Nonsyn	Q	*
5	16941137	G	A	13	0.52	40	NEWSNP	CDS	AT5G42370.2	Nonsyn	Q	*
5	17780314	G	A	15	0.62	40	NEWSNP	intergenic				
5	18512401	C	T	10	0.43	40	NEWSNP	intergenic				
5	19113047	G	A	10	0.56	40	NEWSNP	intergenic				
5	19360376	G	A	13	0.65	40	NEWSNP	intergenic				
5	20112802	G	A	10	0.5	40	NEWSNP	intronic/noncoding	AT5G49570.1			
5	21318563	G	A	10	0.4	40	NEWSNP	CDS	AT5G52530.1	Nonsyn	V	M
5	21318563	G	A	10	0.4	40	NEWSNP	CDS	AT5G52530.2	Nonsyn	V	M
5	21318563	G	A	10	0.4	40	NEWSNP	CDS	AT5G52530.3	Nonsyn	V	M
5	22931089	G	A	15	0.54	40	NEWSNP	CDS	AT5G56650.1	Nonsyn	V	I
5	23847018	G	A	16	0.67	40	NEWSNP	CDS	AT5G59070.1	Nonsyn	A	T
5	24135802	G	A	13	0.48	40	NEWSNP	CDS	AT5G59930.1	Nonsyn	R	K

Table S23. *420* crossover frequency (cM) of *hcr1-1* BC_2F_2 progeny and their corresponding genotype. A population of 50 individuals with genotypes, including *hcr1-1/hcr1-1*, *hcr1-1/+* and wild type Col. Mean CO rate (cM) and standard deviation (SD) were calculated.

Genotype	Green	Red	Both	None	Total	CO rate (cM)	G/non G	R/non R	G/R	Mean	SD
hcr1-1/hcr1-1	214	243	1472	286	2215	23.36	3.19	3.43	0.88		
hcr1-1/hcr1-1	230	189	1173	261	1853	25.99	3.12	2.77	1.22		
hcr1-1/hcr1-1	189	167	1097	281	1734	23.23	2.87	2.69	1.13		
hcr1-1/hcr1-1	207	201	1072	248	1728	27.35	2.85	2.80	1.03		
hcr1-1/hcr1-1	167	138	862	169	1336	26.28	3.35	2.98	1.21		
hcr1-1/hcr1-1	204	229	1248	269	1950	25.44	2.92	3.12	0.89	25.27	1.78
hcr1-1/hcr1-1	188	161	972	263	1584	25.21	2.74	2.51	1.17		
hcr1-1/hcr1-1	182	174	1095	242	1693	23.88	3.07	2.99	1.05		
hcr1-1/hcr1-1	205	165	920	190	1480	29.29	3.17	2.75	1.24		
hcr1-1/hcr1-1	178	177	1116	229	1700	23.69	3.19	3.18	1.01		
hcr1-1/hcr1-1	185	148	983	223	1539	24.68	3.15	2.77	1.25		
hcr1-1/hcr1-1	193	184	1118	238	1733	24.84	3.11	3.02	1.05		
hcr1-1/+	204	182	1424	349	2159	19.85	3.07	2.90	1.12		
hcr1-1/+	130	155	1091	239	1615	19.56	3.10	3.38	0.84		
hcr1-1/+	184	182	1357	333	2056	19.75	2.99	2.98	1.01		
hcr1-1/+	228	196	1313	357	2094	22.86	2.79	2.58	1.16		
hcr1-1/+	181	150	993	209	1533	24.62	3.27	2.93	1.21		
hcr1-1/+	158	122	825	204	1309	24.36	3.02	2.62	1.30		
hcr1-1/+	199	162	1120	248	1729	23.68	3.22	2.87	1.23		
hcr1-1/+	123	131	1009	222	1485	18.89	3.21	3.30	0.94		
hcr1-1/+	160	160	1006	229	1555	23.29	3.00	3.00	1.00		
hcr1-1/+	133	121	758	166	1178	24.58	3.10	2.94	1.10		
hcr1-1/+	185	152	1059	256	1652	23.06	3.05	2.75	1.22		
hcr1-1/+	171	204	1339	316	2030	20.59	2.90	3.17	0.84	21.42	1.89
hcr1-1/+	183	159	1392	326	2060	18.27	3.25	3.05	1.15		
hcr1-1/+	173	166	1193	310	1842	20.51	2.87	2.81	1.04		
hcr1-1/+	154	122	983	249	1508	20.38	3.06	2.74	1.26		
hcr1-1/+	136	112	862	214	1324	20.92	3.06	2.78	1.21		
hcr1-1/+	125	119	856	188	1288	21.19	3.20	3.12	1.05		
hcr1-1/+	156	190	1156	257	1759	22.12	2.94	3.26	0.82		
hcr1-1/+	187	166	1366	301	2020	19.35	3.33	3.14	1.13		
hcr1-1/+	149	158	1015	235	1557	22.18	2.96	3.05	0.94		
hcr1-1/+	177	183	1315	305	1980	20.23	3.06	3.11	0.97		
hcr1-1/+	195	177	1342	323	2037	20.33	3.07	2.93	1.10		
hcr1-1/+	182	162	1143	260	1747	22.14	3.14	2.95	1.12		
WT	147	106	903	212	1368	20.62	3.30	2.81	1.39		
WT	155	132	1148	254	1689	18.75	3.38	3.13	1.17		
WT	198	176	1451	372	2197	18.79	3.01	2.85	1.13		
WT	176	157	1257	265	1855	19.94	3.40	3.21	1.12		
WT	190	155	1290	301	1936	19.78	3.25	2.94	1.23		
WT	152	137	1032	236	1557	20.70	3.17	3.01	1.11		
WT	148	156	1166	285	1755	19.16	2.98	3.05	0.95		
WT	147	156	1172	299	1774	18.86	2.90	2.98	0.94	19.16	1.03
WT	162	136	1029	288	1615	20.57	2.81	2.59	1.19		
WT	141	145	1073	253	1612	19.68	3.05	3.09	0.97		
WT	140	140	1185	279	1744	17.60	3.16	3.16	1.00		
WT	178	154	1390	358	2080	17.49	3.06	2.88	1.16		
WT	172	156	1294	352	1974	18.29	2.89	2.77	1.10		
WT	189	153	1349	321	2012	18.76	3.24	2.95	1.24		
WT	186	175	1429	364	2154	18.46	3.00	2.92	1.06		

Table S24. *420* genetic distance (cM) of T_1 *HCR1* complementing and control lines. T_1 *HCR1* complementing lines are *hcr1-1*/*hcr1-1* genotype introduced with *HCR1* transgene. Wild type Col *420 RG/++* and *hcr1-1/hcr1-1 420 RG/++* introduced with empty vector are control T_1 lines. Untransformed wild type Col and *hcr1-1/hcr1-1* with segregating *420* are additional controls. Mean CO rate (cM) and standard deviation (SD) as calculated.

Genotype	Transgene	Green	Red	Both	None	Total	CO rate (cM)	G/non G	R/non R	G/R	Mean	SD
WT	Empty	131	107	859	202	1299	20.40	3.20	2.90	1.22	19.88	2.15
WT	Empty	182	222	1186	280	1870	24.64	2.73	3.05	0.82		
WT	Empty	130	102	881	222	1335	19.23	3.12	2.79	1.27		
WT	Empty	78	66	476	119	739	21.88	2.99	2.75	1.18		
WT	Empty	127	158	1120	296	1701	18.46	2.75	3.02	0.80		
WT	Empty	167	118	990	236	1511	21.08	3.27	2.75	1.42		
WT	Empty	146	110	986	253	1495	18.91	3.12	2.75	1.33		
WT	Empty	53	62	457	101	673	18.87	3.13	3.37	0.85		
WT	Empty	88	94	731	173	1086	18.46	3.07	3.16	0.94		
WT	Empty	108	129	921	221	1379	18.99	2.94	3.19	0.84		
WT	Empty	234	194	1245	391	2064	23.50	2.53	2.30	1.21		
WT	Empty	191	219	1805	604	2819	15.79	2.43	2.55	0.87		
WT	Empty	227	254	1655	462	2598	20.65	2.63	2.77	0.89		
WT	Empty	187	174	1549	393	2303	17.14	3.06	2.97	1.07		
WT	Empty	267	200	1564	396	2427	21.57	3.07	2.66	1.34		
WT	Empty	204	170	1440	413	2227	18.51	2.82	2.61	1.20		
WT	Empty	250	221	1688	439	2598	20.16	2.94	2.77	1.13		
WT	Empty	229	223	1685	426	2563	19.55	2.95	2.91	1.03		
hcr1-1/hcr1-1	Empty	213	188	1131	225	1757	26.27	3.25	3.01	1.13	24.06	2.15
hcr1-1/hcr1-1	Empty	173	195	1171	245	1784	23.36	3.05	3.27	0.89		
hcr1-1/hcr1-1	Empty	142	135	699	180	1156	27.84	2.67	2.59	1.05		
hcr1-1/hcr1-1	Empty	213	218	1183	234	1848	26.96	3.09	3.13	0.98		
hcr1-1/hcr1-1	Empty	141	92	678	157	1068	24.92	3.29	2.58	1.53		
hcr1-1/hcr1-1	Empty	148	94	787	175	1204	22.67	3.48	2.73	1.57		
hcr1-1/hcr1-1	Empty	204	164	1123	226	1717	24.41	3.40	2.99	1.24		
hcr1-1/hcr1-1	Empty	146	149	985	228	1508	21.98	3.00	3.03	0.98		
hcr1-1/hcr1-1	Empty	175	187	1143	259	1764	23.22	2.96	3.06	0.94		
hcr1-1/hcr1-1	Empty	119	140	983	211	1453	19.78	3.14	3.40	0.85		
hcr1-1/hcr1-1	Empty	162	142	963	200	1467	23.48	3.29	3.05	1.14		
hcr1-1/hcr1-1	Empty	106	107	741	165	1119	21.30	3.11	3.13	0.99		
hcr1-1/hcr1-1	Empty	72	80	461	93	706	24.54	3.08	3.28	0.90		
hcr1-1/hcr1-1	Empty	157	187	1002	237	1583	24.81	2.73	3.02	0.84		
hcr1-1/hcr1-1	Empty	169	168	949	239	1525	25.30	2.75	2.74	1.01		
hcr1-1/hcr1-1	*HCR1*	157	185	1178	284	1804	21.21	2.85	3.09	0.85	19.40	0.96
hcr1-1/hcr1-1	*HCR1*	144	112	969	187	1412	20.16	3.72	3.27	1.29		
hcr1-1/hcr1-1	*HCR1*	159	181	1329	327	1996	18.80	2.93	3.11	0.88		
hcr1-1/hcr1-1	*HCR1*	171	181	1318	295	1965	19.89	3.13	3.22	0.94		
hcr1-1/hcr1-1	*HCR1*	172	230	1612	415	2429	18.21	2.77	3.14	0.75		
hcr1-1/hcr1-1	*HCR1*	210	205	1567	410	2392	19.19	2.89	2.86	1.02		
hcr1-1/hcr1-1	*HCR1*	243	205	1715	462	2625	18.84	2.94	2.72	1.19		
hcr1-1/hcr1-1	*HCR1*	142	137	1064	287	1630	18.90	2.84	2.80	1.04		

WT	None	215	174	1427	379	2195	19.65	2.97	2.70	1.24		
WT	None	131	121	1120	267	1639	16.78	3.22	3.12	1.08		
WT	None	151	147	1168	308	1774	18.51	2.90	2.86	1.03		
WT	None	122	122	1064	241	1549	17.24	3.27	3.27	1.00		
WT	None	180	182	1453	350	2165	18.42	3.07	3.08	0.99		
WT	None	199	191	1503	357	2250	19.17	3.11	3.05	1.04	18.74	1.09
WT	None	170	216	1560	362	2308	18.42	2.99	3.34	0.79		
WT	None	200	185	1404	324	2113	20.28	3.15	3.03	1.08		
WT	None	196	180	1388	350	2114	19.73	2.99	2.87	1.09		
WT	None	195	159	1328	310	1992	19.71	3.25	2.94	1.23		
WT	None	177	197	1508	377	2259	18.21	2.94	3.08	0.90		
hcr1-1/hcr1-1	None	175	145	922	183	1425	25.78	3.34	2.98	1.21		
hcr1-1/hcr1-1	None	188	202	1158	269	1817	24.45	2.86	2.98	0.93		
hcr1-1/hcr1-1	None	190	201	1204	237	1832	24.29	3.18	3.29	0.95		
hcr1-1/hcr1-1	None	144	136	778	145	1203	26.89	3.28	3.16	1.06		
hcr1-1/hcr1-1	None	263	258	1361	264	2146	28.28	3.11	3.07	1.02		
hcr1-1/hcr1-1	None	236	234	1462	267	2199	24.33	3.39	3.37	1.01	25.66	1.33
hcr1-1/hcr1-1	None	232	240	1419	305	2196	24.49	3.03	3.09	0.97		
hcr1-1/hcr1-1	None	286	238	1443	306	2273	26.59	3.18	2.84	1.20		
hcr1-1/hcr1-1	None	252	246	1397	282	2177	26.35	3.12	3.08	1.02		
hcr1-1/hcr1-1	None	208	239	1328	333	2108	24.11	2.69	2.90	0.87		
hcr1-1/hcr1-1	None	253	238	1394	306	2191	25.72	3.03	2.92	1.06		
hcr1-1/hcr1-1	None	286	238	1443	306	2273	26.59	3.18	2.84	1.20		

Table S25. Allelism test crosses between the *hcr1-1* and *hcr1-2* mutations. A cross between EMS allele *hcr1-1 420 RG/*++ and T-DNA allele *hcr1-2* produced F_1 (*hcr1-1/hcr1-2*). Wild type Col, *hcr1-1* and *hcr1-2* control lines with segregating *420* are shown. Mean CO rate (cM) and standard deviation (SD) as calculated.

F_1 progeny	Green	Red	Both	None	Total	CO rate (cM)	G/non G	R/non R	G/R	Mean	SD
WT	175	173	1314	295	1957	19.73	3.18	3.16	1.01	19.87	1.45
WT	158	152	1208	310	1828	18.71	2.96	2.91	1.04		
WT	178	147	1230	317	1872	19.21	3.03	2.78	1.21		
WT	180	169	1323	317	1989	19.44	3.09	3.00	1.07		
WT	181	166	1392	311	2050	18.67	3.30	3.17	1.09		
WT	154	167	1264	342	1927	18.34	2.79	2.89	0.92		
WT	200	160	1406	334	2100	18.94	3.25	2.93	1.25		
WT	148	169	1258	274	1849	18.94	3.17	3.38	0.88		
WT	222	175	1196	333	1926	23.34	2.79	2.47	1.27		
WT	154	151	1137	293	1735	19.48	2.91	2.88	1.02		
WT	162	186	1205	284	1837	21.19	2.91	3.12	0.87		
WT	162	156	1168	294	1780	19.83	2.96	2.90	1.04		
WT	160	159	1048	259	1626	22.05	2.89	2.88	1.01		
WT	198	154	1230	345	1927	20.33	2.86	2.55	1.29		
WT	191	151	1107	296	1745	22.02	2.90	2.58	1.26		
WT	127	106	972	231	1436	17.81	3.26	3.01	1.20		
WT	172	179	1379	325	2055	18.86	3.08	3.13	0.96		
WT	184	166	1282	292	1924	20.24	3.20	3.04	1.11		
WT	167	159	1265	328	1919	18.74	2.94	2.88	1.05		
WT	188	196	1304	317	2005	21.45	2.91	2.97	0.96		
hcr1-1/hcr1-1	145	129	930	166	1370	22.54	3.64	3.41	1.12	25.01	2.15
hcr1-1/hcr1-1	169	183	965	186	1503	27.09	3.07	3.23	0.92		
hcr1-1/hcr1-1	184	175	1108	243	1710	23.83	3.09	3.00	1.05		
hcr1-1/hcr1-1	195	176	1090	232	1693	25.05	3.15	2.96	1.11		
hcr1-1/hcr1-1	204	155	1042	205	1606	25.64	3.46	2.93	1.32		
hcr1-1/hcr1-1	155	176	1118	228	1677	22.20	3.15	3.38	0.88		
hcr1-1/hcr1-1	150	143	1001	218	1512	21.74	3.19	3.11	1.05		
hcr1-1/hcr1-1	185	198	1216	236	1835	23.67	3.23	3.36	0.93		
hcr1-1/hcr1-1	191	153	996	195	1535	25.72	3.41	2.98	1.25		
hcr1-1/hcr1-1	210	209	1102	216	1737	28.06	3.09	3.08	1.00		
hcr1-1/hcr1-1	155	117	724	194	1190	26.32	2.83	2.41	1.32		
hcr1-1/hcr1-1	207	176	1110	226	1719	25.54	3.28	2.97	1.18		
hcr1-1/hcr1-1	201	157	922	190	1470	28.38	3.24	2.76	1.28		
hcr1-1/hcr1-1	179	184	1156	246	1765	23.28	3.10	3.15	0.97		
hcr1-1/hcr1-1	144	171	1146	239	1700	20.66	3.15	3.44	0.84		
hcr1-1/hcr1-1	180	218	1179	286	1863	24.32	2.70	3.00	0.83		
hcr1-1/hcr1-1	165	141	881	164	1351	26.04	3.43	3.11	1.17		
hcr1-1/hcr1-1	143	132	774	128	1177	27.01	3.53	3.34	1.08		
hcr1-1/hcr1-1	172	182	981	208	1543	26.44	2.96	3.06	0.95		
hcr1-1/hcr1-1	133	157	801	162	1253	26.71	2.93	3.25	0.85		

hcr1-2/hcr1-2	180	147	1042	247	1616	22.84	3.10	2.78	1.22		
hcr1-2/hcr1-2	115	124	816	205	1260	21.22	2.83	2.94	0.93		
hcr1-2/hcr1-2	183	192	1127	265	1767	24.13	2.87	2.94	0.95		
hcr1-2/hcr1-2	173	138	1050	247	1608	21.69	3.18	2.83	1.25		
hcr1-2/hcr1-2	111	150	843	195	1299	22.66	2.77	3.25	0.74		
hcr1-2/hcr1-2	186	167	1107	238	1698	23.57	3.19	3.00	1.11		
hcr1-2/hcr1-2	139	144	882	206	1371	23.37	2.92	2.97	0.97		
hcr1-2/hcr1-2	148	164	928	219	1459	24.35	2.81	2.98	0.90		
hcr1-2/hcr1-2	175	170	1055	274	1674	23.33	2.77	2.73	1.03		
hcr1-2/hcr1-2	166	176	1053	208	1603	24.28	3.17	3.29	0.94	22.98	1.50
hcr1-2/hcr1-2	75	78	500	121	774	22.24	2.89	2.95	0.96		
hcr1-2/hcr1-2	204	167	1093	267	1731	24.41	2.99	2.68	1.22		
hcr1-2/hcr1-2	126	82	729	160	1097	21.21	3.53	2.84	1.54		
hcr1-2/hcr1-2	168	156	1111	252	1687	21.52	3.13	3.02	1.08		
hcr1-2/hcr1-2	171	212	1035	271	1689	26.08	2.50	2.82	0.81		
hcr1-2/hcr1-2	184	140	1155	273	1752	20.62	3.24	2.83	1.31		
hcr1-2/hcr1-2	206	208	1209	254	1877	25.24	3.06	3.08	0.99		
hcr1-2/hcr1-2	135	134	915	205	1389	21.73	3.10	3.09	1.01		
hcr1-2/hcr1-2	191	166	1187	265	1809	22.20	3.20	2.97	1.15		
hcr1-1/hcr1-2 F_1	227	195	1153	256	1831	26.58	3.06	2.79	1.16		
hcr1-1/hcr1-2 F_1	256	172	1175	256	1859	26.55	3.34	2.63	1.49		
hcr1-1/hcr1-2 F_1	194	171	1139	273	1777	23.24	3.00	2.81	1.13		
hcr1-1/hcr1-2 F_1	225	221	1192	316	1954	26.28	2.64	2.61	1.02		
hcr1-1/hcr1-2 F_1	163	192	961	246	1562	26.15	2.57	2.82	0.85		
hcr1-1/hcr1-2 F_1	204	185	1174	221	1784	24.91	3.39	3.20	1.10		
hcr1-1/hcr1-2 F_1	203	164	1191	250	1808	22.93	3.37	2.99	1.24		
hcr1-1/hcr1-2 F_1	159	148	1040	200	1547	22.34	3.45	3.31	1.07		
hcr1-1/hcr1-2 F_1	232	155	1158	243	1788	24.69	3.49	2.76	1.50		
hcr1-1/hcr1-2 F_1	175	160	1181	287	1803	20.73	3.03	2.90	1.09		
hcr1-1/hcr1-2 F_1	188	149	1177	239	1753	21.55	3.52	3.11	1.26	24.17	1.71
hcr1-1/hcr1-2 F_1	141	192	995	237	1565	24.21	2.65	3.14	0.73		
hcr1-1/hcr1-2 F_1	187	174	1038	218	1617	25.60	3.13	2.99	1.07		
hcr1-1/hcr1-2 F_1	126	109	738	182	1155	22.99	2.97	2.75	1.16		
hcr1-1/hcr1-2 F_1	177	212	1154	262	1805	24.57	2.81	3.11	0.83		
hcr1-1/hcr1-2 F_1	203	185	1314	273	1975	22.08	3.31	3.15	1.10		
hcr1-1/hcr1-2 F_1	216	174	1188	234	1812	24.53	3.44	3.03	1.24		
hcr1-1/hcr1-2 F_1	185	162	1070	269	1686	23.29	2.91	2.71	1.14		
hcr1-1/hcr1-2 F_1	229	232	1332	298	2091	25.23	2.95	2.97	0.99		
hcr1-1/hcr1-2 F_1	228	202	1241	300	1971	24.92	2.93	2.73	1.13		

Table S26. *420* crossover rate (cM) measured in *hcr1-2* F_2 progeny. A cross between T-DNA allele *hcr1-2* with *420 RG/++* produced F_1. An F_2 population segregated into wild type Col, *ppx-1* and *ppx1/+* genotypes. Mean CO rate (cM) and standard deviation (SD) were calculated.

Genotype	Green	Red	Both	None	Total	CO rate (cM)	G/non G	R/non R	G/R	Mean	SD
hcr1-2/hcr1-2	238	259	1525	376	2398	23.48	2.78	2.91	0.92	24.04	1.09
hcr1-2/hcr1-2	312	258	1620	400	2590	25.18	2.94	2.64	1.21		
hcr1-2/hcr1-2	193	173	1203	285	1854	22.21	3.05	2.88	1.12		
hcr1-2/hcr1-2	309	267	1619	365	2560	25.84	3.05	2.80	1.16		
hcr1-2/hcr1-2	308	240	1728	334	2610	23.84	3.55	3.07	1.28		
hcr1-2/hcr1-2	263	228	1488	370	2349	23.71	2.93	2.71	1.15		
hcr1-2/hcr1-2	267	277	1643	374	2561	24.16	2.93	3.00	0.96		
hcr1-2/hcr1-2	276	179	1426	281	2162	23.90	3.70	2.88	1.54		
hcr1-2/+	230	228	1810	410	2678	18.89	3.20	3.18	1.01	20.24	1.49
hcr1-2/+	252	240	1697	430	2619	20.99	2.91	2.84	1.05		
hcr1-2/+	221	197	1675	413	2506	18.37	3.11	2.95	1.12		
hcr1-2/+	203	126	1247	277	1853	19.69	3.60	2.86	1.61		
hcr1-2/+	206	233	1632	381	2452	19.88	2.99	3.18	0.88		
hcr1-2/+	242	230	1513	399	2384	22.28	2.79	2.72	1.05		
hcr1-2/+	247	224	1755	434	2660	19.63	3.04	2.91	1.10		
hcr1-2/+	222	202	1594	382	2400	19.58	3.11	2.97	1.10		
hcr1-2/+	259	231	1722	435	2647	20.64	2.97	2.81	1.12		
hcr1-2/+	224	235	1713	405	2577	19.76	3.03	3.10	0.95		
hcr1-2/+	156	185	1368	320	2029	18.52	3.02	3.26	0.84		
hcr1-2/+	264	235	1594	433	2526	22.22	2.78	2.62	1.12		
hcr1-2/+	210	192	1397	363	2162	20.75	2.90	2.77	1.09		
hcr1-2/+	264	226	1575	336	2401	23.07	3.27	3.00	1.17		
hcr1-2/+	217	263	1668	395	2543	21.10	2.86	3.16	0.83		
hcr1-2/+	291	231	1657	384	2563	23.02	3.17	2.80	1.26		
hcr1-2/+	226	261	1672	399	2558	21.31	2.88	3.09	0.87		
hcr1-2/+	173	180	1342	338	2033	19.21	2.92	2.98	0.96		
hcr1-2/+	238	254	1742	394	2628	20.91	3.06	3.16	0.94		
hcr1-2/+	185	159	1408	299	2051	18.48	3.48	3.24	1.16		
hcr1-2/+	99	65	743	189	1096	16.29	3.31	2.81	1.52		
hcr1-2/+	241	240	1707	410	2598	20.65	3.00	2.99	1.00		
hcr1-2/+	246	205	1680	435	2566	19.47	3.01	2.77	1.20		
hcr1-2/+	252	246	1677	414	2589	21.56	2.92	2.89	1.02		
hcr1-2/+	247	240	1771	405	2663	20.36	3.13	3.08	1.03		
hcr1-2/+	244	208	1610	381	2443	20.63	3.15	2.91	1.17		
hcr1-2/+	240	211	1663	432	2546	19.64	2.96	2.79	1.14		
hcr1-2/+	224	249	1759	403	2635	19.94	3.04	3.20	0.90		
WT	240	201	1544	382	2367	20.79	3.06	2.81	1.19	18.58	1.82
WT	199	193	1703	443	2538	16.87	2.99	2.95	1.03		
WT	252	199	1795	521	2767	17.90	2.84	2.58	1.27		
WT	241	233	1707	411	2592	20.36	3.02	2.98	1.03		
WT	218	205	1723	452	2598	17.88	2.95	2.88	1.06		
WT	194	119	1337	332	1982	17.29	3.39	2.77	1.63		
WT	195	203	1854	432	2684	16.13	3.23	3.28	0.96		
WT	172	107	955	237	1471	21.22	3.28	2.60	1.61		
WT	238	196	1683	433	2550	18.78	3.05	2.80	1.21		

Table S27. *420* genetic distance (cM) measured in *ppx-2* F_2 progeny. A cross between *ppx-2* T-DNA line with *420 RG/++* generated F_1. Segregation of genotypes into wild type Col, *ppx-2* and *ppx-2/+* was observed in the F_2. Mean CO rate (cM) and standard deviation (SD) were calculated.

Genotype	Green	Red	Both	None	Total	CO rate (cM)	G/non G	R/non R	G/R	Mean	SD
ppx-2/ppx-2	176	178	1399	308	2061	18.98	3.24	3.26	0.99		
ppx-2/ppx-2	190	157	1276	315	1938	19.88	3.11	2.84	1.21		
ppx-2/ppx-2	165	162	1231	284	1842	19.69	3.13	3.10	1.02		
ppx-2/ppx-2	148	159	1126	289	1722	19.79	2.84	2.94	0.93	19.40	0.68
ppx-2/ppx-2	66	64	495	108	733	19.67	3.26	3.21	1.03		
ppx-2/ppx-2	136	132	1096	270	1634	18.03	3.06	3.02	1.03		
ppx-2/ppx-2	167	160	1225	281	1833	19.80	3.16	3.09	1.04		
ppx-2/+	154	174	1260	275	1863	19.51	3.15	3.34	0.89		
ppx-2/+	167	180	1320	330	1997	19.22	2.92	3.02	0.93		
ppx-2/+	140	153	1173	269	1735	18.62	3.11	3.24	0.92		
ppx-2/+	167	151	1205	266	1789	19.72	3.29	3.13	1.11		
ppx-2/+	124	114	905	207	1350	19.54	3.21	3.08	1.09		
ppx-2/+	163	194	1382	306	2045	19.32	3.09	3.36	0.84		
ppx-2/+	191	156	1348	336	2031	18.86	3.13	2.85	1.22		
ppx-2/+	151	149	1209	310	1819	18.14	2.96	2.95	1.01		
ppx-2/+	155	185	1358	372	2070	18.06	2.72	2.93	0.84		
ppx-2/+	161	148	1311	300	1920	17.65	3.29	3.16	1.09		
ppx-2/+	182	144	1347	342	2015	17.75	3.15	2.85	1.26		
ppx-2/+	123	123	921	230	1397	19.51	2.96	2.96	1.00		
ppx-2/+	93	111	770	172	1146	19.75	3.05	3.32	0.84		
ppx-2/+	165	162	1123	302	1752	20.83	2.78	2.75	1.02		
ppx-2/+	139	105	733	189	1166	23.75	2.97	2.55	1.32	19.53	1.44
ppx-2/+	87	113	693	169	1062	21.05	2.77	3.15	0.77		
ppx-2/+	147	112	975	229	1463	19.63	3.29	2.89	1.31		
ppx-2/+	151	151	1137	241	1680	19.97	3.29	3.29	1.00		
ppx-2/+	178	153	1212	278	1821	20.22	3.23	2.99	1.16		
ppx-2/+	191	153	1213	281	1838	20.90	3.24	2.89	1.25		
ppx-2/+	173	174	1251	340	1938	19.88	2.77	2.78	0.99		
ppx-2/+	161	138	1116	253	1668	19.91	3.27	3.03	1.17		
ppx-2/+	161	158	1112	242	1673	21.35	3.18	3.15	1.02		
ppx-2/+	77	75	651	148	951	17.52	3.26	3.23	1.03		
ppx-2/+	65	56	557	141	819	16.06	3.16	2.98	1.16		
ppx-2/+	192	184	1371	308	2055	20.37	3.18	3.11	1.04		
ppx-2/+	114	111	832	208	1265	19.73	2.97	2.93	1.03		
ppx-2/+	179	173	1344	331	2027	19.21	3.02	2.97	1.03		
ppx-2/+	189	174	1312	306	1981	20.41	3.13	3.00	1.09		
WT	122	104	1000	247	1473	16.74	3.20	2.99	1.17		
WT	124	100	763	198	1185	21.14	2.98	2.68	1.24		
WT	188	197	1318	305	2008	21.48	3.00	3.07	0.95		
WT	149	126	1070	230	1575	19.33	3.42	3.16	1.18		
WT	147	136	1096	263	1642	19.05	3.12	3.00	1.08		
WT	175	131	1051	276	1633	20.93	3.01	2.62	1.34		
WT	81	86	575	140	882	21.18	2.90	2.99	0.94		
WT	64	56	498	106	724	18.24	3.47	3.26	1.14	19.89	1.66
WT	171	151	1254	305	1881	18.91	3.13	2.95	1.13		
WT	160	172	1081	267	1680	22.23	2.83	2.93	0.93		
WT	135	146	1032	261	1574	19.82	2.87	2.97	0.92		
WT	137	154	1095	240	1626	19.87	3.13	3.31	0.89		
WT	157	106	957	194	1414	20.75	3.71	3.03	1.48		
WT	207	163	1250	297	1917	21.64	3.17	2.80	1.27		
WT	149	175	1394	354	2072	17.10	2.92	3.12	0.85		

Table S28. *420* crossover frequency (cM) measured in *pp4r2* F_2 progeny. A cross between *pp4r2* T-DNA line with *420 RG/++* generated F_1. Segregation of genotypes into wild type Col, *pp4r2* and *pp4r2/+*. Mean CO rate (cM) and standard deviation (SD) were calculated.

Genotype	Green	Red	Both	None	Total	CO rate (cM)	G/non G	R/non R	G/R	Mean	SD
pp4r2/pp4r2	162	152	969	204	1487	24.00	3.18	3.06	1.07		
pp4r2/pp4r2	230	179	1372	318	2099	21.88	3.22	2.83	1.28		
pp4r2/pp4r2	128	143	608	130	1009	31.97	2.70	2.91	0.90		
pp4r2/pp4r2	219	198	1252	293	1962	24.18	3.00	2.83	1.11		
pp4r2/pp4r2	190	165	1055	227	1637	24.75	3.18	2.93	1.15		
pp4r2/pp4r2	131	140	841	177	1289	23.87	3.07	3.19	0.94		
pp4r2/pp4r2	101	84	567	120	872	24.13	3.27	2.95	1.20	24.30	3.52
pp4r2/pp4r2	86	87	601	145	919	21.04	2.96	2.98	0.99		
pp4r2/pp4r2	171	166	1063	207	1607	23.80	3.31	3.25	1.03		
pp4r2/pp4r2	215	177	913	177	1482	31.37	3.19	2.78	1.21		
pp4r2/pp4r2	156	169	1146	273	1744	20.80	2.95	3.07	0.92		
pp4r2/pp4r2	220	191	1289	355	2055	22.54	2.76	2.57	1.15		
pp4r2/pp4r2	119	101	754	166	1140	21.64	3.27	3.00	1.18		
pp4r2/+	168	161	1199	329	1857	19.65	2.79	2.74	1.04		
pp4r2/+	73	70	528	129	800	19.84	3.02	2.96	1.04		
pp4r2/+	205	180	1338	299	2022	21.31	3.22	3.01	1.14		
pp4r2/+	137	135	1198	289	1759	16.89	3.15	3.13	1.01		
pp4r2/+	162	150	1339	308	1959	17.45	3.28	3.17	1.08		
pp4r2/+	172	150	994	245	1561	23.36	2.95	2.74	1.15		
pp4r2/+	123	107	749	177	1156	22.41	3.07	2.85	1.15		
pp4r2/+	214	186	1488	335	2223	19.99	3.27	3.05	1.15		
pp4r2/+	187	154	1203	289	1833	20.76	3.14	2.85	1.21		
pp4r2/+	97	80	646	160	983	20.01	3.10	2.82	1.21		
pp4r2/+	210	181	1279	273	1943	22.70	3.28	3.02	1.16		
pp4r2/+	167	137	1198	287	1789	18.75	3.22	2.94	1.22	20.55	2.65
pp4r2/+	177	195	1411	335	2118	19.46	3.00	3.14	0.91		
pp4r2/+	143	148	742	163	1196	28.35	2.85	2.91	0.97		
pp4r2/+	189	148	1369	321	2027	18.30	3.32	2.97	1.28		
pp4r2/+	115	141	839	177	1272	22.70	3.00	3.36	0.82		
pp4r2/+	80	54	512	140	786	18.82	3.05	2.57	1.48		
pp4r2/+	152	126	1203	274	1755	17.34	3.39	3.12	1.21		
pp4r2/+	93	111	614	137	955	24.32	2.85	3.15	0.84		
pp4r2/+	141	129	1052	246	1568	19.03	3.18	3.05	1.09		
pp4r2/+	159	120	996	218	1493	20.86	3.42	2.96	1.33		
pp4r2/+	176	170	1314	284	1944	19.75	3.28	3.23	1.04		
WT	88	80	499	135	802	23.77	2.73	2.60	1.10		
WT	112	134	766	182	1194	23.32	2.78	3.06	0.84		
WT	100	86	704	172	1062	19.39	3.12	2.90	1.16		
WT	79	76	627	186	968	17.55	2.69	2.65	1.04		
WT	98	83	892	184	1257	15.62	3.71	3.46	1.18	20.46	2.96
WT	173	178	1303	304	1958	19.91	3.06	3.10	0.97		
WT	177	163	1369	311	2020	18.55	3.26	3.14	1.09		
WT	99	121	689	147	1056	23.62	2.94	3.29	0.82		
WT	115	120	785	161	1181	22.41	3.20	3.28	0.96		

Table S29. Pollen viability scored using Alexander staining in wild type Col-0, *hcr1-1*, *hcr1-2*, *ppx-2* and *pp4r2*. Pollen viability from 6 plants per genotype was assessed by Alexander staining of ~1,000 pollen grains from mature open flowers, where viable pollen stain purple, whereas inviable pollen stain green. To test for significant differences between wild type and *hcr1-1*, *hcr1-2* (*ppx-1*), *ppx-2* and *pp4r2* mutants pairwise t-tests were performed with correction for multiple testing indicated by *P*-values (*P* > 0.05=non-significant; n.d.= not defined).

Genotype	Plant	Viable	Inviable	Total	% Viable	% Inviable	*P*
WT	1	1180	7	1187	99.41	0.59	
WT	2	1130	6	1136	99.47	0.53	
WT	3	1204	6	1210	99.50	0.50	
WT	4	1002	6	1008	99.40	0.60	n.d.
WT	5	1191	56	1247	95.51	4.49	
WT	6	1121	0	1121	100.00	0.00	
hcr1-1	1	1109	0	1109	100.00	0.00	
hcr1-1	2	1152	0	1152	100.00	0.00	
hcr1-1	3	1288	1	1289	99.92	0.08	
hcr1-1	4	1147	6	1153	99.48	0.52	0.18
hcr1-1	5	1153	9	1162	99.23	0.77	
hcr1-1	6	1068	0	1068	100.00	0.00	
hcr1-2	1	1092	2	1094	99.82	0.18	
hcr1-2	2	1081	4	1085	99.63	0.37	
hcr1-2	3	1012	4	1016	99.61	0.39	
hcr1-2	4	1348	0	1348	100.00	0.00	0.26
hcr1-2	5	1407	1	1408	99.93	0.07	
hcr1-2	6	1093	3	1096	99.73	0.27	
ppx-2	1	1085	0	1085	100.00	0.00	
ppx-2	2	1106	11	1117	99.02	0.98	
ppx-2	3	955	0	955	100.00	0.00	
ppx-2	4	1336	0	1336	100.00	0.00	0.32
ppx-2	5	1194	0	1194	100.00	0.00	
ppx-2	6	1015	7	1022	99.32	0.68	
pp4r2	1	1068	0	1068	100.00	0.00	
pp4r2	2	1067	5	1072	99.53	0.47	
pp4r2	3	1022	0	1022	100.00	0.00	
pp4r2	4	1141	0	1141	100.00	0.00	0.196
pp4r2	5	1258	0	1258	100.00	0.00	
pp4r2	6	1023	0	1023	100.00	0.00	

Table S30. Seed set per silique scored in wild type Col-0, *hcr1-1*, *hcr1-2*, *ppx-2* and *pp4r2*. The number of seeds per silique scored in 5 plants per genotype. From each plant, 5 siliques were selected. Mean seed set per plant per genotype is calculated as shown. To test for significance between wild type and *hcr1-1*, *hcr1-2* (*ppx-1*), *ppx-2* and *pp4r2* mutants, pairwise t-tests were performed with correction for multiple testing indicated by *P*-values (*P* > 0.05=non-significant).

Genotype	Plant	Seeds per silique					Mean	*P*
		1	2	3	4	5		
WT	1	63	52	56	62	65	59.60	
WT	2	53	57	58	61	61	58.00	
WT	3	55	52	58	51	60	55.20	
WT	4	52	63	61	52	54	56.40	
WT	5	61	62	50	54	56	56.60	n.d
hcr1-1	1	58	60	54	60	60	58.40	
hcr1-1	2	61	55	60	65	64	61.00	
hcr1-1	3	58	57	67	58	58	59.60	
hcr1-1	4	68	70	53	68	65	64.80	
hcr1-1	5	64	63	58	56	62	60.60	0.07
hcr1-2	1	71	70	71	72	65	69.80	
hcr1-2	2	69	55	65	61	61	62.20	
hcr1-2	3	56	62	62	63	67	62.00	
hcr1-2	4	60	62	73	63	63	64.20	
hcr1-2	5	57	64	62	55	56	58.80	0.01
ppx-2	1	59	60	58	55	54	57.20	
ppx-2	2	58	52	58	62	56	57.20	
ppx-2	3	60	59	57	54	58	57.60	
ppx-2	4	63	60	64	62	56	61.00	
ppx-2	5	53	50	57	55	51	53.20	0.96
pp4r2	1	62	52	65	58	53	58.00	
pp4r2	2	52	62	48	63	50	55.00	
pp4r2	3	53	55	67	64	67	61.20	
pp4r2	4	55	59	62	58	50	56.80	
pp4r2	5	60	64	60	61	60	61.00	0.51

Table S31. Quantification of MLH1 foci at diakinesis in wild type Col-0 and *hcr1*. Mean MLH1 foci per cell and on DAPI dense regions were calculated from the total number of cells (n) at diakinesis in wild type and *hcr1* (EMS allele). A Mann-Whitney Wilcoxon test was performed to test the significant differences in MLH1 foci number between wild type and *hcr1* (P <0.05= significant).

	Total MLH1 foci in wild type	MLH1 foci on DAPI dense regions in wild type	Total MLH1 foci in *hcr1*	MLH1 foci on DAPI dense regions in *hcr1*
	12	2	14	2
	11	2	10	1
	12	1	14	1
	9	2	11	3
	10	1	13	2
	9	2	12	2
	10	1	13	3
	9	0	12	2
	11	4	14	2
	11	2	12	1
	9	3	12	2
	12	1	14	2
	11	2	10	1
	12	3	12	2
	8	0	15	2
	10	2	12	4
	9	1	9	0
	11	3	13	1
	12	1	11	1
	12	4	12	2
	10	1	11	4
	10	1	9	1
	11	1	11	1
	9	2	14	2
	10	0	11	2
	11	2	12	0
	9	2	9	0
	13	4	12	1
	10	3	10	2
	9	2	14	2
	9	1	12	3
	11	0	13	2
	10	1	10	1
	9	1	12	2
	10	2	13	1
	9	1	11	1
	10	3	14	2
	10	2	14	2
	8	1	9	1
	11	2	14	2
	10	1	11	0
	10	0	12	0
	12	1	11	1
	11	4	11	1
	13	1	12	1
	12	1	14	1
	12	3	14	2
	12	2	15	1
	11	3	13	2
	10	2	13	2
	9	2		
Mean	10.4 (n=51)	1.7 (n=51)	12.1 (n=50)	1.6 (n=50)
SD	1.3	1.1	1.6	0.9
P	n.d.	n.d.	5.26×10^{-7}	0.53

Table S32. Genetic distance (cM) measured in wild type Col and *hcr1* using Columbia traffic lines (CTLs). Mean CO rate (cM) and standard deviation (SD) were calculated.

CTL	Genotype	Green	Red	Both	None	Total	CO rate (cM)	G/non G	R/non R	G/R	Mean	SD
1.17	WT	225	214	1492	324	2255	21.86	3.19	3.11	1.05		
1.17	WT	213	241	1527	355	2336	21.81	2.92	3.11	0.88		
1.17	WT	257	230	1520	328	2335	23.65	3.18	2.99	1.12	22.83	1.73
1.17	WT	269	254	1499	330	2352	25.48	3.03	2.93	1.06		
1.17	WT	211	202	1407	346	2166	21.35	2.95	2.89	1.04		
1.17	*hcr1*	96	107	456	72	731	33.32	3.08	3.35	0.90		
1.17	*hcr1*	299	319	1338	291	2247	32.92	2.68	2.81	0.94		
1.17	*hcr1*	221	230	1188	230	1869	28.07	3.06	3.14	0.96	32.23	3.09
1.17	*hcr1*	242	295	1056	181	1774	37.18	2.73	3.19	0.82		
1.17	*hcr1*	171	152	783	152	1258	30.25	3.14	2.89	1.13		
1.17	*hcr1*	323	301	1488	233	2345	31.60	3.39	3.22	1.07		
3.15	WT	68	76	488	117	749	21.55	2.88	3.05	0.89		
3.15	WT	217	196	1113	250	1776	26.86	2.98	2.80	1.11		
3.15	WT	268	283	1646	381	2578	24.33	2.88	2.97	0.95		
3.15	WT	167	193	1235	259	1854	21.79	3.10	3.35	0.87		
3.15	WT	204	152	1175	235	1766	22.75	3.56	3.02	1.34	23.46	2.15
3.15	WT	182	204	1023	264	1673	26.61	2.57	2.75	0.89		
3.15	WT	146	170	1002	215	1533	23.34	2.98	3.25	0.86		
3.15	WT	102	97	661	114	974	23.10	3.62	3.51	1.05		
3.15	WT	169	175	1051	224	1619	24.17	3.06	3.12	0.97		
3.15	WT	158	144	1129	242	1673	20.06	3.33	3.18	1.10		
3.15	*hcr1*	221	191	936	181	1529	32.10	3.11	2.80	1.16		
3.15	*hcr1*	174	207	968	180	1529	29.17	2.95	3.32	0.84		
3.15	*hcr1*	221	216	1175	219	1831	27.70	3.21	3.16	1.02		
3.15	*hcr1*	224	243	1258	227	1952	27.78	3.15	3.33	0.92		
3.15	*hcr1*	121	119	639	132	1011	27.53	3.03	3.00	1.02		
3.15	*hcr1*	234	246	1154	220	1854	30.56	2.98	3.08	0.95	29.29	1.60
3.15	*hcr1*	246	253	1225	215	1939	30.34	3.14	3.21	0.97		
3.15	*hcr1*	90	136	588	109	923	28.57	2.77	3.64	0.66		
3.15	*hcr1*	50	49	256	51	406	28.42	3.06	3.02	1.02		
3.15	*hcr1*	151	161	857	146	1315	27.51	3.28	3.43	0.94		
3.15	*hcr1*	203	223	1030	187	1643	30.61	3.01	3.21	0.91		
3.15	*hcr1*	253	239	1154	224	1870	31.17	3.04	2.92	1.06		
5.11	WT	298	245	1518	408	2469	25.16	2.78	2.50	1.22		
5.11	WT	192	272	1719	407	2590	19.89	2.81	3.32	0.71		
5.11	WT	287	235	1539	417	2478	23.93	2.80	2.52	1.22		
5.11	WT	238	180	1346	342	2106	22.34	3.03	2.63	1.32		
5.11	WT	221	258	1409	363	2251	24.21	2.62	2.85	0.86	22.22	1.80
5.11	WT	175	170	1099	270	1714	22.71	2.90	2.85	1.03		
5.11	WT	232	198	1489	343	2262	21.27	3.18	2.93	1.17		
5.11	WT	163	113	924	273	1473	20.93	2.82	2.38	1.44		
5.11	WT	204	180	1427	332	2143	19.90	3.19	3.00	1.13		
5.11	WT	258	189	1456	397	2300	21.81	2.92	2.51	1.37		

5.11	*hcr1*	240	204	1375	405	2224	22.49	2.65	2.45	1.18		
5.11	*hcr1*	244	204	1587	411	2446	20.40	2.98	2.73	1.20		
5.11	*hcr1*	228	213	1383	302	2126	23.51	3.13	3.01	1.07		
5.11	*hcr1*	206	265	1602	325	2398	22.08	3.06	3.52	0.78		
5.11	*hcr1*	157	147	980	257	1541	22.19	2.81	2.72	1.07	21.95	1.02
5.11	*hcr1*	205	193	1454	323	2175	20.37	3.22	3.12	1.06		
5.11	*hcr1*	236	223	1439	387	2285	22.65	2.75	2.67	1.06		
5.11	*hcr1*	232	234	1556	345	2367	22.14	3.09	3.10	0.99		
5.11	*hcr1*	256	188	1481	367	2292	21.73	3.13	2.68	1.36		
5.14	WT	97	75	1299	503	1974	9.13	2.42	2.29	1.29		
5.14	WT	112	82	1208	523	1925	10.64	2.18	2.03	1.37		
5.14	WT	64	91	1236	529	1920	8.43	2.10	2.24	0.70		
5.14	WT	91	74	1267	536	1968	8.77	2.23	2.14	1.23		
5.14	WT	65	49	902	355	1371	8.69	2.39	2.26	1.33		
5.14	WT	80	80	1229	464	1853	9.04	2.41	2.41	1.00		
5.14	WT	77	51	920	340	1388	9.69	2.55	2.33	1.51	9.73	1.84
5.14	WT	122	128	1138	386	1774	15.26	2.45	2.49	0.95		
5.14	WT	82	72	1164	479	1797	8.97	2.26	2.20	1.14		
5.14	WT	84	103	1346	501	2034	9.66	2.37	2.48	0.82		
5.14	WT	85	90	1338	574	2087	8.77	2.14	2.17	0.94		
5.14	WT	69	99	1141	510	1819	9.71	1.99	2.14	0.70		
5.14	*hcr1*	91	84	1147	470	1792	10.30	2.23	2.19	1.08		
5.14	*hcr1*	88	101	1127	432	1748	11.47	2.28	2.36	0.87		
5.14	*hcr1*	82	94	1099	480	1755	10.59	2.06	2.12	0.87		
5.14	*hcr1*	94	82	1167	498	1841	10.07	2.17	2.11	1.15		
5.14	*hcr1*	104	110	1284	510	2008	11.30	2.24	2.27	0.95		
5.14	*hcr1*	104	108	1335	492	2039	11.00	2.40	2.42	0.96		
5.14	*hcr1*	120	110	1330	511	2071	11.80	2.33	2.28	1.09		
5.14	*hcr1*	122	119	1186	468	1895	13.65	2.23	2.21	1.03	11.64	1.66
5.14	*hcr1*	111	129	1112	470	1822	14.18	2.04	2.14	0.86		
5.14	*hcr1*	102	93	1161	486	1842	11.22	2.18	2.13	1.10		
5.14	*hcr1*	85	66	1318	550	2019	7.78	2.28	2.18	1.29		
5.14	*hcr1*	114	112	1243	464	1933	12.47	2.36	2.34	1.02		
5.14	*hcr1*	101	109	1172	453	1835	12.19	2.27	2.31	0.93		
5.14	*hcr1*	113	111	1136	498	1858	12.89	2.05	2.04	1.02		
5.14	*hcr1*	95	102	970	375	1542	13.72	2.23	2.28	0.93		

Table S33. *420* genetic distance (cM) measured in wild type Col, *hcr1*, *fancm*, *hcr1 fancm*, *fancm zip4* and *hcr1 fancm zip4* mutants. A cross between *hcr1 420 RG/++* (EMS allele) and *fancm zip4* double mutant generated homozygous double and triple mutants. Mean CO rate (cM) and standard deviation (SD) were calculated.

Genotype	Green	Red	Both	None	Total	CO rate (cM)	G/non G	R/non R	G/R	Mean	SD
WT	196	176	1463	367	2202	18.63	3.06	2.91	1.11	19.01	1.20
WT	160	174	1457	363	2154	16.94	3.01	3.12	0.92		
WT	184	190	1536	369	2279	18.04	3.08	3.12	0.97		
WT	164	169	1320	313	1966	18.68	3.08	3.12	0.97		
WT	223	190	1435	344	2192	21.06	3.10	2.87	1.17		
WT	178	190	1443	249	2060	19.83	3.69	3.82	0.94		
WT	193	151	1384	317	2045	18.54	3.37	3.01	1.28		
WT	145	146	1067	263	1621	19.94	2.96	2.97	0.99		
WT	191	165	1344	333	2033	19.39	3.08	2.88	1.16		
hcr1	219	167	1120	266	1772	24.88	3.09	2.65	1.31	24.48	0.87
hcr1	188	176	1016	241	1621	25.78	2.89	2.78	1.07		
hcr1	164	133	897	204	1398	24.16	3.15	2.80	1.23		
hcr1	201	202	1306	271	1980	23.00	3.19	3.19	1.00		
hcr1	255	202	1332	287	2076	25.18	3.25	2.83	1.26		
hcr1	189	155	1036	224	1604	24.43	3.23	2.88	1.22		
hcr1	186	190	1143	279	1798	23.73	2.83	2.87	0.98		
hcr1	164	194	1046	251	1655	24.68	2.72	2.99	0.85		
fancm	174	155	710	146	1185	33.31	2.94	2.70	1.12	34.52	1.92
fancm	173	152	738	156	1219	31.68	2.96	2.71	1.14		
fancm	206	209	800	165	1380	36.87	2.69	2.72	0.99		
fancm	218	190	830	152	1390	35.74	3.06	2.76	1.15		
fancm	134	150	537	135	956	36.29	2.35	2.55	0.89		
fancm	212	215	961	179	1567	32.55	2.98	3.01	0.99		
fancm	319	277	1218	213	2027	35.82	3.14	2.81	1.15		
fancm	224	250	979	232	1685	33.86	2.50	2.70	0.90		
hcr1 fancm	189	183	672	109	1153	40.44	2.95	2.87	1.03	40.32	1.56
hcr1 fancm	232	209	814	121	1376	40.08	3.17	2.90	1.11		
hcr1 fancm	276	270	1048	161	1755	38.54	3.07	3.02	1.02		
hcr1 fancm	246	250	932	131	1559	39.69	3.09	3.14	0.98		
hcr1 fancm	263	269	892	138	1562	43.54	2.84	2.90	0.98		
hcr1 fancm	309	257	1077	156	1799	39.11	3.36	2.87	1.20		
hcr1 fancm	316	297	1141	172	1926	39.71	3.11	2.95	1.06		
hcr1 fancm	267	245	897	149	1558	41.46	2.95	2.75	1.09		

fancm zip4	269	290	1187	227	1973	34.17	2.82	2.98	0.93		
fancm zip4	252	295	1131	187	1865	35.70	2.87	3.25	0.85		
fancm zip4	354	301	1274	246	2175	36.94	2.98	2.63	1.18		
fancm zip4	278	327	1316	202	2123	34.42	3.01	3.42	0.85		
fancm zip4	160	148	688	110	1106	33.44	3.29	3.10	1.08		
fancm zip4	200	172	708	116	1196	38.52	3.15	2.78	1.16	35.00	1.77
fancm zip4	264	216	1061	179	1720	33.53	3.35	2.88	1.22		
fancm zip4	272	327	1247	208	2054	35.44	2.84	3.28	0.83		
fancm zip4	298	293	1269	262	2122	33.44	2.82	2.79	1.02		
fancm zip4	336	329	1334	232	2231	36.45	2.98	2.93	1.02		
fancm zip4	256	251	1143	193	1843	32.93	3.15	3.10	1.02		
hcr1 fancm zip4	260	282	1074	184	1800	36.93	2.86	3.05	0.92		
hcr1 fancm zip4	232	273	959	145	1609	38.99	2.85	3.27	0.85		
hcr1 fancm zip4	306	292	1201	169	1968	37.37	3.27	3.14	1.05		
hcr1 fancm zip4	250	252	1105	142	1749	34.73	3.44	3.46	0.99		
hcr1 fancm zip4	258	237	987	179	1661	36.44	2.99	2.80	1.09		
hcr1 fancm zip4	251	251	1026	150	1678	36.62	3.18	3.18	1.00		
hcr1 fancm zip4	308	288	1176	225	1997	36.51	2.89	2.75	1.07		
hcr1 fancm zip4	339	312	1230	218	2099	38.38	2.96	2.77	1.09	37.47	1.79
hcr1 fancm zip4	260	293	1003	166	1722	40.19	2.75	3.04	0.89		
hcr1 fancm zip4	290	357	1245	217	2109	37.84	2.67	3.16	0.81		
hcr1 fancm zip4	322	308	1274	210	2114	36.44	3.08	2.97	1.05		
hcr1 fancm zip4	300	332	1235	209	2076	37.46	2.84	3.08	0.90		
hcr1 fancm zip4	381	351	1297	189	2218	41.70	3.11	2.89	1.09		
hcr1 fancm zip4	278	268	1074	184	1804	37.18	2.99	2.90	1.04		
hcr1 fancm zip4	322	291	1271	223	2107	35.34	3.10	2.87	1.11		

Table S34. Pollen viability scored using Alexander staining in *zip4* and *hcr1 zip4* double mutants. Pollen viability from 6 plants per genotype was assessed by Alexander staining from mature open flowers, where viable pollen stain purple, whereas inviable pollen stained green. To test for significant differences between *zip4* and *hcr1 zip4* double mutants, pairwise t-test was performed with correction for multiple testing indicated by a *P*-value (*P* > 0.05=non-significant).

Genotype	Plant	Viable	Inviable	Total	% Viable	% Inviable	*P*
zip4	1	119	102	221	53.85	46.15	
zip4	2	402	339	741	54.25	45.75	
zip4	3	76	83	159	47.80	52.20	
zip4	4	161	140	301	53.49	46.51	n.d.
zip4	5	356	238	594	59.93	40.07	
zip4	6	112	163	275	40.73	59.27	
hcr1 zip4	1	499	553	1052	47.43	52.57	
hcr1 zip4	2	544	650	1194	45.56	54.44	
hcr1 zip4	3	623	421	1044	59.67	40.33	
hcr1 zip4	4	240	397	637	37.68	62.32	0.37
hcr1 zip4	5	265	318	583	45.45	54.55	
hcr1 zip4	6	390	432	822	47.45	52.55	

Table S35. Count data of three colour *l3bc* FTL flow cytometry in wild type Col compared with *hcr1*. Counts of Eight possible fluorescent pollen classes from replicates of wild type and *hcr1* samples are listed. For example, BYR shows blue (B), yellow (Y) and red (R) fluorescence, whereas Byr shows only blue fluorescence. Calculations were followed as previously described (Ziolkowski et al. 2015).

Genotype	Replicate	BYR	byr	bYr	ByR	BYr	byR	bYR	Byr	Total
WT	1	4615	10185	15	23	304	305	1033	885	17365
WT	2	3884	6760	17	17	237	217	573	868	12573
WT	3	5048	10095	24	13	305	325	1155	1054	18019
WT	4	4749	10816	31	19	318	344	918	1148	18343
WT	5	6313	14697	26	22	447	454	1261	1553	24773
WT	6	7215	18163	30	53	530	571	1401	2065	30028
WT	7	6987	15691	31	27	530	529	1649	1939	27383
Total		38811	86407	174	174	2671	2745	7990	9512	148484
hcr1	1	4208	8359	42	25	385	407	1232	1329	15987
hcr1	2	5433	8960	49	42	488	488	1408	1366	18234
hcr1	3	6453	15641	66	39	640	648	2064	2088	27639
hcr1	4	4095	8457	35	19	376	386	1136	1215	15719
hcr1	5	4719	9717	28	28	428	417	1259	1444	18040
hcr1	6	4567	10560	35	32	392	426	1259	1487	18758
Total		29475	61694	255	185	2709	2772	8358	8929	114377

Table S36. Measurement of *I3b* and *I3c* genetic distances (cM) and crossover coincidence. The *I3b* and *I3c* genetic distances for wild type Col and *hcr1* were calculated using the formula, where the N values correspond to total pollen counts as shown in Table S35. N_{total} = (N_{bYr}+N_{ByR}+N_{bYR}+N_{Byr}+N_{BYr}+N_{byR}+N_{BYR}+N_{byr}). *I3b* cM= (N_{bYr} + N_{ByR} + N_{bYR} + N_{Byr}) / N_{total}. *I3c* cM = (N_{bYr} + N_{ByR} + N_{BYr} + N_{byR}) / N_{total}. For example, N_{BYR} is the number of pollen that were all fluorescent, whereas N_{byr} is the number of pollen that were all non-fluorescent. Crossover interference was calculated using the formulas: Observed DCOs = (N_{bYr} + N_{ByR}). Expected DCOs = (I3b cM / 100) x (I3c cM / 100) x N_{total}. Coefficient of Coincidence = Observed DCOs / Expected DCOs. Interference = 1-CoC. Calculations and statistical tests were followed as previously described (Ziolkowski et al. 2015; Serra et al. 2018). A generalised linear model (GLM) was performed to test for significant differences between wild type and *hcr1* genetic distances indicated by *P*-values ($P < 0.05$ = significant). Pearson's χ^2 test with Yates' continuity correction was used to test for significant differences between wild type Col and *hcr1* interference indicated by a *P*-value ($P > 0.05$=non-significant).

Genotype	Replicate	*I3b* (cM)	*I3c* (cM)	Expected DCOs	Observed DCOs	CoC	1-CoC
WT	1	11.26	3.73	72.88	38	0.52	0.48
WT	2	11.73	3.88	57.25	34	0.59	0.41
WT	3	12.46	3.70	83.14	37	0.45	0.55
WT	4	11.54	3.88	82.13	50	0.61	0.39
WT	5	11.55	3.83	109.64	48	0.44	0.56
WT	6	11.82	3.94	139.94	83	0.59	0.41
WT	7	13.31	4.08	148.73	58	0.39	0.61
Mean		11.95	3.86	99.10	49.71	0.51	0.49
SD		0.71	0.13				
P		n.d.	n.d.				n.d.
hcr1	1	16.44	5.37	141.21	67	0.47	0.53
hcr1	2	15.71	5.85	167.65	91	0.54	0.46
hcr1	3	15.40	5.04	214.55	105	0.49	0.51
hcr1	4	15.30	5.19	124.85	54	0.43	0.57
hcr1	5	15.29	4.99	137.80	56	0.41	0.59
hcr1	6	15.00	4.72	132.72	67	0.50	0.50
Mean		15.52	5.19	153.13	73.33	0.48	0.52
SD		0.50	0.39				
P		6.63×10^{-4}	2.71×10^{-3}				0.92

Table S37. Meiotic axis-associated RAD51 foci quantification at leptotene in wild type Col-0 and *hcr1*. Nuclei were immunostained for the axis protein ASY1 to determine the meiotic stage and RAD51 foci were scored at leptotene stage. Mean RAD51 foci per cell and standard deviation (SD) was calculated as shown. A Mann-Whitney-Wilcoxon test was performed to test for significant differences in RAD51 foci number between wild type and *hcr1* indicated by a *P*-value ($P > 0.05$ = non-significant).

	Wild type	***hcr1***
	193	133
	140	134
	153	194
	139	156
	167	134
	164	137
	155	134
	129	159
	177	131
	129	113
	136	144
	143	145
	142	181
	149	134
Mean	151 (n=14)	145 (n=14)
SD	18.5	21.4
P	n.d.	0.32

Table S38. *420* genetic distance (cM) measured in *hcr2* BC_2F_2 progenies. A population of 55 individuals were scored and sorted according to 'high' (in orange; ~29-39 cM) and 'low' (in green; ~15-23 cM) recombination rates.

BC_2F_2 progeny	Green	Red	Both	None	Total	CO rate (cM)	G/non G	R/non R	G/R
hcr2 F_2- 1	288	250	1153	262	1953	32.99	2.81	2.55	1.15
hcr2 F_2- 4	294	253	1183	197	1927	34.25	3.28	2.92	1.16
hcr2 F_2- 5	265	275	1166	217	1923	33.79	2.91	2.99	0.96
hcr2 F_2- 9	245	235	979	197	1656	35.17	2.83	2.75	1.04
hcr2 F_2- 10	212	182	865	142	1401	33.85	3.32	2.96	1.16
hcr2 F_2- 15	196	210	997	180	1583	30.21	3.06	3.21	0.93
hcr2 F_2- 23	203	197	1026	194	1620	28.85	3.14	3.08	1.03
hcr2 F_2- 26	223	195	805	140	1363	37.82	3.07	2.75	1.14
hcr2 F_2- 27	197	215	754	149	1315	38.89	2.61	2.80	0.92
hcr2 F_2- 28	187	189	738	153	1267	36.24	2.70	2.73	0.99
hcr2 F_2- 29	160	174	681	130	1145	35.46	2.77	2.95	0.92
hcr2 F_2- 33	219	195	860	141	1415	35.59	3.21	2.93	1.12
hcr2 F_2- 49	192	204	880	154	1430	33.21	2.99	3.13	0.94
hcr2 F_2- 55	269	243	1178	183	1873	32.67	3.40	3.14	1.11
hcr2 F_2- 2	167	188	1419	374	2148	18.18	2.82	2.97	0.89
hcr2 F_2- 3	125	131	1019	283	1558	18.06	2.76	2.82	0.95
hcr2 F_2- 6	140	156	1463	385	2144	14.92	2.96	3.08	0.90
hcr2 F_2- 7	168	138	1211	368	1885	17.82	2.73	2.52	1.22
hcr2 F_2- 8	109	122	900	246	1377	18.48	2.74	2.88	0.89
hcr2 F_2- 11	155	160	1374	358	2047	16.80	2.95	2.99	0.97
hcr2 F_2- 12	186	154	1352	367	2059	18.16	2.95	2.72	1.21
hcr2 F_2- 13	133	108	945	237	1423	18.68	3.12	2.85	1.23
hcr2 F_2- 14	120	133	960	222	1435	19.54	3.04	3.20	0.90
hcr2 F_2- 16	133	127	1110	272	1642	17.34	3.12	3.05	1.05
hcr2 F_2- 17	143	144	1125	309	1721	18.36	2.80	2.81	0.99
hcr2 F_2- 18	125	126	930	278	1459	19.01	2.61	2.62	0.99
hcr2 F_2- 19	179	159	1332	354	2024	18.39	2.95	2.80	1.13
hcr2 F_2- 20	155	102	1269	292	1818	15.31	3.61	3.07	1.52
hcr2 F_2- 21	162	159	1109	269	1699	21.12	2.97	2.94	1.02
hcr2 F_2- 22	188	197	1325	294	2004	21.53	3.08	3.16	0.95
hcr2 F_2- 24	130	125	952	211	1418	19.98	3.22	3.16	1.04
hcr2 F_2- 25	100	87	626	170	983	21.29	2.82	2.64	1.15
hcr2 F_2- 30	121	111	1117	283	1632	15.40	3.14	3.04	1.09
hcr2 F_2- 31	109	105	658	190	1062	22.74	2.60	2.55	1.04
hcr2 F_2- 32	155	139	1229	284	1807	17.87	3.27	3.12	1.12
hcr2 F_2- 34	123	126	1126	294	1669	16.24	2.97	3.00	0.98
hcr2 F_2- 35	139	131	1067	243	1580	18.87	3.22	3.14	1.06
hcr2 F_2- 36	128	144	1248	321	1841	16.07	2.96	3.10	0.89
hcr2 F_2- 37	70	52	539	154	815	16.30	2.96	2.64	1.35

hcr2 F_2- 38	167	143	1252	305	1867	18.27	3.17	2.96	1.17
hcr2 F_2- 39	140	146	1095	272	1653	19.13	2.95	3.01	0.96
hcr2 F_2- 40	150	154	1235	267	1806	18.55	3.29	3.33	0.97
hcr2 F_2- 41	151	101	972	258	1482	18.76	3.13	2.62	1.50
hcr2 F_2- 42	147	144	905	225	1421	23.16	2.85	2.82	1.02
hcr2 F_2- 43	128	109	1086	271	1594	16.18	3.19	2.99	1.17
hcr2 F_2- 44	145	113	1089	273	1620	17.45	3.20	2.88	1.28
hcr2 F_2- 45	162	97	1006	243	1508	18.98	3.44	2.72	1.67
hcr2 F_2- 46	186	160	1233	320	1899	20.28	2.96	2.75	1.16
hcr2 F_2- 47	150	131	1323	378	1982	15.36	2.89	2.75	1.15
hcr2 F_2- 48	98	93	800	192	1183	17.71	3.15	3.08	1.05
hcr2 F_2- 50	133	151	1163	298	1745	17.87	2.89	3.05	0.88
hcr2 F_2- 51	134	144	1104	281	1663	18.41	2.91	3.01	0.93
hcr2 F_2- 52	157	72	847	184	1260	20.22	3.92	2.70	2.18
hcr2 F_2- 53	109	108	895	202	1314	18.16	3.24	3.23	1.01
hcr2 F_2- 54	176	149	1202	292	1819	19.83	3.12	2.89	1.18

Table S39. Quantification of MLH1 foci at diakinesis in wild type Col-0, *hcr2* and *hcr3*. Mean MLH1 foci per cell and standard deviation (SD) was calculated from the total number of cells (n) at diakinesis in wild type, *hcr2* and *hcr3*. A Mann-Whitney Wilcoxon test was performed to test the significant differences in MLH1 foci number between WT, *hcr2* and *hcr3* indicated by *P*-values ($P < 0.05$ = significant).

	Wild type	***hcr2***	***hcr3***
	10	13	15
	10	11	15
	10	14	18
	11	13	13
	12	10	17
	13	13	17
	11	10	15
	13	13	17
	11	11	14
	10	12	15
	8	10	16
	12	13	16
	9	13	14
	12	13	16
	11	11	12
	9	10	22
	12	10	13
	11	12	16
	9	14	18
	14	13	18
	10	11	19
	7	12	17
	9		14
	13		11
			12
			16
			16
			16
Mean	10.7 (n=24)	11.9 (n=22)	15.6 (n=28)
SD	1.7	1.4	2.3
P	n.d.	0.018	1.592×10^{-8}

Table S40. *420* genetic distance (cM) measured in *lcr1* BC_1F_2 population. The individuals were genotyped for *taf4b* and *fan1* mutations and the *420* phenotypes for wild type Col, *lcr1/+*, *lcr1-taf4b/lcr1-taf4b*, *fan1/fan1* are shown. *taf4b-1/taf4b-1* line from Emma was used as external control. Mean CO rate (cM) and standard deviation (SD) were calculated.

Genotype	Green	Red	Both	None	Total	CO rate (cM)	G/non G	R/non R	G/R	Mean	SD
WT	153	182	1224	365	1924	19.27	2.52	2.71	0.84		
WT	167	210	1492	350	2219	18.75	2.96	3.29	0.80		
WT	174	168	1154	324	1820	21.00	2.70	2.65	1.04		
WT	188	241	1513	374	2316	20.66	2.77	3.12	0.78		
WT	208	200	1570	394	2372	19.01	2.99	2.94	1.04	19.16	1.24
WT	204	219	1706	428	2557	18.20	2.95	3.05	0.93		
WT	104	117	907	261	1389	17.43	2.67	2.81	0.89		
WT	206	196	1644	416	2462	17.94	3.02	2.96	1.05		
WT	206	215	1514	379	2314	20.24	2.90	2.96	0.96		
lcr1/+	161	180	1314	343	1998	18.84	2.82	2.96	0.89		
lcr1/+	175	163	1346	355	2039	18.24	2.94	2.85	1.07		
lcr1/+	113	102	894	244	1353	17.41	2.91	2.79	1.11		
lcr1/+	141	126	1306	368	1941	14.86	2.93	2.81	1.12		
lcr1/+	167	132	1305	332	1936	16.87	3.17	2.88	1.27		
lcr1/+	144	149	1415	381	2089	15.18	2.94	2.98	0.97	17.39	1.48
lcr1/+	160	176	1406	350	2092	17.61	2.98	3.10	0.91		
lcr1/+	201	185	1702	444	2532	16.63	3.03	2.93	1.09		
lcr1/+	199	200	1618	465	2482	17.63	2.73	2.74	1.00		
lcr1/+	244	223	1695	440	2602	19.93	2.92	2.80	1.09		
lcr1/+	192	168	1449	384	2193	18.04	2.97	2.81	1.14		
taf4b-1/taf4b-1	188	166	1584	410	2348	16.43	3.08	2.93	1.13		
taf4b-1/taf4b-1	129	168	1534	419	2250	14.21	2.83	3.11	0.77		
taf4b-1/taf4b-1	138	161	1551	447	2297	14.00	2.78	2.93	0.86		
taf4b-1/taf4b-1	156	165	1585	462	2368	14.63	2.78	2.83	0.95		
taf4b-1/taf4b-1	162	127	1457	410	2156	14.45	3.01	2.77	1.28	14.32	0.98
taf4b-1/taf4b-1	142	131	1536	437	2246	13.00	2.95	2.88	1.08		
taf4b-1/taf4b-1	126	161	1532	405	2224	13.87	2.93	3.19	0.78		
taf4b-1/taf4b-1	158	126	1445	452	2181	14.00	2.77	2.58	1.25		
lcr1-taf4b/lcr1-taf4b	153	178	1682	410	2423	14.75	3.12	3.30	0.86		
lcr1-taf4b/lcr1-taf4b	167	169	1432	405	2173	16.89	2.79	2.80	0.99		
lcr1-taf4b/lcr1-taf4b	79	78	722	217	1096	15.53	2.72	2.70	1.01		
lcr1-taf4b/lcr1-taf4b	152	163	1440	371	2126	16.12	2.98	3.07	0.93	16.13	0.94
lcr1-taf4b/lcr1-taf4b	153	170	1420	366	2109	16.71	2.93	3.06	0.90		
lcr1-taf4b/lcr1-taf4b	187	198	1599	436	2420	17.43	2.82	2.88	0.94		
lcr1-taf4b/lcr1-taf4b	77	97	783	262	1219	15.47	2.40	2.60	0.79		
fan1/fan1	139	150	1034	284	1607	19.98	2.70	2.80	0.93		
fan1/fan1	235	196	1504	360	2295	20.98	3.13	2.86	1.20		
fan1/fan1	181	188	1318	369	2056	19.93	2.69	2.74	0.96		
fan1/fan1	210	181	1444	403	2238	19.34	2.83	2.65	1.16		
fan1/fan1	209	189	1573	362	2333	18.83	3.23	3.09	1.11		
fan1/fan1	163	127	1401	397	2088	15.02	2.98	2.73	1.28		
fan1/fan1	164	184	1553	359	2260	16.81	3.16	3.32	0.89		
fan1/fan1	80	63	619	181	943	16.53	2.86	2.61	1.27	18.11	1.82
fan1/fan1	226	180	1450	355	2211	20.45	3.13	2.81	1.26		
fan1/fan1	192	211	1531	419	2353	18.92	2.73	2.85	0.91		
fan1/fan1	199	151	1397	404	2151	17.87	2.88	2.57	1.32		
fan1/fan1	124	100	1010	316	1550	15.68	2.73	2.52	1.24		
fan1/fan1	176	181	1499	384	2240	17.46	2.96	3.00	0.97		
fan1/fan1	203	174	1608	442	2427	16.97	2.94	2.76	1.17		
fan1/fan1	140	140	1204	329	1813	16.87	2.87	2.87	1.00		

Table S41. Allelism test crosses between the *lcr1* and *taf4b-1* mutations. A cross between EMS allele *lcr1/lcr1 420 RG/++* and *taf4b-1/taf4b-1* produced F_1 (*lcr1/taf4b-1*). Wild type Col, *taf4b-1/+*, *lcr1/lcr1* and *taf4b-1/taf4b-1* are control lines with segregating *420* are shown. Mean CO rate (cM) and standard deviation (SD) were calculated.

Genotype	Green	Red	Both	None	Total	CO rate (cM)	G/non G	R/non R	G/R	Mean	SD
WT	211	220	1819	446	2696	17.52	3.05	3.10	0.96		
WT	224	203	1729	471	2627	17.85	2.90	2.78	1.10		
WT	215	218	1646	450	2529	18.91	2.79	2.80	0.99		
WT	219	228	1658	490	2595	19.04	2.61	2.66	0.96		
WT	209	188	1648	453	2498	17.41	2.90	2.77	1.11		
WT	190	183	1591	406	2370	17.22	3.02	2.98	1.04	18.33	1.14
WT	239	189	1643	388	2459	19.26	3.26	2.92	1.26		
WT	128	101	976	273	1478	16.93	2.95	2.69	1.27		
WT	190	206	1465	370	2231	19.69	2.87	2.98	0.92		
WT	145	136	1160	319	1760	17.50	2.87	2.79	1.07		
WT	242	202	1588	402	2434	20.30	3.03	2.78	1.20		
taf4b-1/+	196	185	1751	488	2620	15.79	2.89	2.83	1.06		
taf4b-1/+	187	202	1830	456	2675	15.79	3.07	3.16	0.93		
taf4b-1/+	163	178	1523	418	2282	16.27	2.83	2.93	0.92		
taf4b-1/+	169	208	1680	431	2488	16.52	2.89	3.15	0.81		
taf4b-1/+	191	200	1686	468	2545	16.77	2.81	2.86	0.96		
taf4b-1/+	201	202	1778	436	2617	16.81	3.10	3.11	1.00	16.77	0.69
taf4b-1/+	201	207	1762	439	2609	17.10	3.04	3.08	0.97		
taf4b-1/+	214	186	1657	443	2500	17.54	2.97	2.81	1.15		
taf4b-1/+	212	182	1686	415	2495	17.29	3.18	2.98	1.16		
taf4b-1/+	218	206	1721	471	2616	17.79	2.86	2.80	1.06		
taf4b-1/taf4b-1	188	166	1584	410	2348	16.43	3.08	2.93	1.13		
taf4b-1/taf4b-1	129	168	1534	419	2250	14.21	2.83	3.11	0.77		
taf4b-1/taf4b-1	138	161	1551	447	2297	14.00	2.78	2.93	0.86		
taf4b-1/taf4b-1	156	165	1585	462	2368	14.63	2.78	2.83	0.95		
taf4b-1/taf4b-1	162	127	1457	410	2156	14.45	3.01	2.77	1.28	14.32	0.98
taf4b-1/taf4b-1	142	131	1536	437	2246	13.00	2.95	2.88	1.08		
taf4b-1/taf4b-1	126	161	1532	405	2224	13.87	2.93	3.19	0.78		
taf4b-1/taf4b-1	158	126	1445	452	2181	14.00	2.77	2.58	1.25		
lcr1lcr1	153	178	1682	410	2423	14.75	3.12	3.30	0.86		
lcr1lcr1	167	169	1432	405	2173	16.89	2.79	2.80	0.99		
lcr1lcr1	79	78	722	217	1096	15.53	2.72	2.70	1.01		
lcr1lcr1	152	163	1440	371	2126	16.12	2.98	3.07	0.93	16.13	0.94
lcr1lcr1	153	170	1420	366	2109	16.71	2.93	3.06	0.90		
lcr1lcr1	187	198	1599	436	2420	17.43	2.82	2.88	0.94		
lcr1lcr1	77	97	783	262	1219	15.47	2.40	2.60	0.79		
lcr1/taf4b-1	143	152	1809	473	2577	12.19	3.12	3.18	0.94		
lcr1/taf4b-1	145	132	1647	465	2389	12.36	3.00	2.92	1.10		
lcr1/taf4b-1	149	147	1630	509	2435	13.00	2.71	2.70	1.01		
lcr1/taf4b-1	151	132	1614	424	2321	13.04	3.17	3.04	1.14		
lcr1/taf4b-1	133	154	1642	420	2349	13.07	3.09	3.25	0.86	13.11	0.66
lcr1/taf4b-1	171	164	1857	523	2715	13.21	2.95	2.91	1.04		
lcr1/taf4b-1	171	173	1780	541	2665	13.87	2.73	2.74	0.99		
lcr1/taf4b-1	168	129	1535	433	2265	14.11	3.03	2.77	1.30		

9. Publications and Presentations

9.1. Publication

Serra, Heïdi, Christophe Lambing, Catherine H. Griffin, Stephanie D. Topp, **Divyashree C. Nageswaran**, Charles J. Underwood, Piotr A. Ziolkowski, et al. 2018. "Massive Crossover Elevation via Combination of HEI10 and Recq4a Recq4b during Arabidopsis Meiosis." *Proceedings of the National Academy of Sciences* 115(10): 2437-2442.

9.2. Presentations

2015 – 1st Annual Marie Curie ITN (COMREC network) meeting, El Escorial, Madrid, Spain. Oral presentation on "A forward genetic screen for factors that control meiotic recombination in *Arabidopsis thaliana*."

2015 – 1st year PhD talk on "A forward genetic screen for factors that control meiotic recombination in *Arabidopsis thaliana"* at Department of Plant Sciences, Cambridge.

2015- SESVanderhave (Sugarbeet breeding company), Tienen, Belgium. A short talk on "A forward genetic screen for factors that control meiotic recombination in *Arabidopsis thaliana*."

2015 - EMBO Meiosis Meeting, Oxford University, UK. Poster presentation on "A forward genetic screen for factors that control meiotic recombination in *Arabidopsis thaliana*."

2016- British Meiosis Meeting, Newcastle University, UK. Presented a poster on "A forward genetic screen to identify factors that control meiotic crossover frequency in *Arabidopsis thaliana*."

2016- 2nd Annual Marie Curie ITN (COMREC network) meeting, IPK, Quedlinburg, Germany. Talk on "A forward genetic screen for factors that control meiotic recombination in *Arabidopsis thaliana*."

2016- ERA-CAPS meeting on DNA repair, University of Vienna, Austria. Oral presentation on "A forward genetic screen to identify factors that control meiotic crossover frequency in *Arabidopsis thaliana*."

2016- 2nd year PhD poster on "A forward genetic screen to identify factors that control meiotic crossover frequency in *Arabidopsis thaliana*" at Department of Plant Sciences, Cambridge, UK.

2017 – 3rd Annual Marie Curie ITN (COMREC network) meeting, NIAB, Cambridge, UK. Talk on “A forward genetic screen for factors that control meiotic recombination in *Arabidopsis thaliana*.”

2017- British Meiosis Meeting, Newcastle University, UK. Oral presentation on “A forward genetic screen to identify factors that control meiotic recombination in *Arabidopsis thaliana.*”

2017 – 3rd year PhD talk on “A forward genetic screen for factors that control meiotic recombination in *Arabidopsis thaliana”* at Department of Plant Sciences, Cambridge.

2017- Spanish Meiosis Meeting, Madrid, Spain. Oral presentation on “A forward genetic screen to identify factors that control meiotic recombination in *Arabidopsis thaliana*.”.

Massive crossover elevation via combination of *HEI10* and *recq4a recq4b* during *Arabidopsis* meiosis

Heïdi Serra[a], Christophe Lambing[a], Catherine H. Griffin[a], Stephanie D. Topp[a], Divyashree C. Nageswaran[a], Charles J. Underwood[a,1], Piotr A. Ziolkowski[a,2], Mathilde Séguéla-Arnaud[b], Joiselle B. Fernandes[b,c], Raphaël Mercier[b], and Ian R. Henderson[a,3]

[a]Department of Plant Sciences, University of Cambridge, CB2 3EA Cambridge, United Kingdom; [b]Institute Jean-Pierre Bourgin (IJPB), Institut National de la Recherche Agronomique, AgroParisTech, CNRS, Université Paris-Saclay, 78000 Versailles, France; and [c]Université Paris-Sud, Université Paris-Saclay, 91405 Orsay, France

Edited by R. Scott Hawley, Stowers Institute for Medical Research, Kansas City, MO, and approved January 26, 2018 (received for review July 24, 2017)

During meiosis, homologous chromosomes undergo reciprocal crossovers, which generate genetic diversity and underpin classical crop improvement. Meiotic recombination initiates from DNA double-strand breaks (DSBs), which are processed into single-stranded DNA that can invade a homologous chromosome. The resulting joint molecules can ultimately be resolved as crossovers. In *Arabidopsis*, competing pathways balance the repair of ∼100–200 meiotic DSBs into ∼10 crossovers per meiosis, with the excess DSBs repaired as noncrossovers. To bias DSB repair toward crossovers, we simultaneously increased dosage of the procrossover E3 ligase gene *HEI10* and introduced mutations in the anticrossovers helicase genes *RECQ4A* and *RECQ4B*. As *HEI10* and *recq4a recq4b* increase interfering and noninterfering crossover pathways, respectively, they combine additively to yield a massive meiotic recombination increase. Interestingly, we also show that increased *HEI10* dosage increases crossover coincidence, which indicates an effect on interference. We also show that patterns of interhomolog polymorphism and heterochromatin drive recombination increases distally towards the subtelomeres in both *HEI10* and *recq4a recq4b* backgrounds, while the centromeres remain crossover suppressed. These results provide a genetic framework for engineering meiotic recombination landscapes in plant genomes.

meiosis | crossover | recombination | HEI10 | RECQ4

Meiosis is a conserved cell division required for eukaryotic sexual reproduction, during which a single round of DNA replication is coupled to two rounds of chromosome segregation, generating haploid gametes (1). Homologous chromosomes pair and recombine during prophase of the first meiotic division, which can result in reciprocal exchange, termed crossover (1). Crossovers have a major effect on sequence variation in populations and create genetic diversity. Meiotic recombination is also an important tool used during crop breeding to combine beneficial variants. However, crossover numbers are typically low, for example, approximately one to two per chromosome per meiosis, and can show restricted chromosomal distributions, which limits crop improvement. For example, recombination is suppressed in large regions surrounding the centromeres of many crop species (2). In this work we sought to use our understanding of meiotic recombination pathways to genetically engineer highly elevated crossover levels in *Arabidopsis*.

Meiotic recombination initiates from DNA double-strand breaks (DSBs), induced by SPO11 transesterases, which act in topoisomerase VI-like complexes (1) (*SI Appendix*, Fig. S1*A*). During catalysis, SPO11 becomes covalently bound to target site DNA (3). In budding yeast, SPO11 is then liberated by endonucleolytic cleavage by the MRX (Mre11–Rad50–Xrs2) complex and Sae2/COM1 (4–6). Simultaneously, exonucleases (Mre11 and Exo1) generate 3′-overhanging single-stranded DNA (ssDNA), hundreds to thousands of nucleotides in length (7, 8). Resected ssDNA is bound by RAD51 and DMC1 RecA-like proteins, which promote invasion of a homologous chromosome and the formation of a displacement loop (D loop) (9) (*SI Appendix*, Fig. S1*A*). Stabilization of the D loop can occur by template-driven DNA synthesis from the invading 3′ end (10) (*SI Appendix*, Fig. S1*A*). Strand invasion intermediates may then progress to second-end capture and formation of a double Holliday junction (dHJ), which can be resolved as a crossover or noncrossover, or undergo dissolution (1, 10) (*SI Appendix*, Fig. S1*A*).

The conserved ZMM pathway acts to promote formation of ∼85% of crossovers in plants, which are known as class I (1, 10) (*SI Appendix*, Fig. S1*A*). Mutations in ZMM genes severely reduce *Arabidopsis* crossover frequency, causing univalent chromosome segregation at anaphase I, aneuploid gametes, and infertility (1). Importantly, ZMM-dependent crossovers show interference, where double crossover (DCO) events are spaced out more widely than expected by chance (11, 12). The ZMM pathway in plants includes the MSH4/MSH5 MutS-related heterodimer, MER3 DNA helicase, SHORTAGE OF CROSSOVERS1 (SHOC1) XPF nuclease, PARTING DANCERS (PTD), ZIP4/SPO22, HEI10 E3 ligase, and

Significance

The majority of eukaryotes reproduce sexually, creating genetic variation within populations. Sexual reproduction requires gamete production via meiotic cell division. During meiosis, homologous chromosomes pair and undergo exchange, called crossover. Crossover is vital for crop breeding and remains a major tool to combine useful traits. Despite the importance of crossovers for breeding, their levels are typically low, with one to two forming per chromosome, irrespective of physical chromosome size. Here we genetically engineer superrecombining *Arabidopsis*, via boosting the major procrossover pathway (using additional copies of the *HEI10* E3-ligase gene), and simultaneously removing a major anti-recombination pathway (using mutations in *RECQ4A* and *RECQ4B* helicase genes). This strategy has the potential to drive massive crossover elevations in crop genomes and accelerate breeding.

Author contributions: H.S., C.L., C.H.G., D.C.N., R.M., and I.R.H. designed research; H.S., C.L., C.H.G., S.D.T., and D.C.N. performed research; C.J.U., P.A.Z., M.S.-A., and J.B.F. contributed new reagents/analytic tools; H.S., C.L., C.H.G., S.D.T., D.C.N., and I.R.H. analyzed data; and H.S., C.L., C.H.G., R.M., and I.R.H. wrote the paper.

Conflict of interest statement: The use of HEI10 to increase meiotic recombination is claimed in UK patent application number GB1620641.9 filed December 5, 2016, by the University of Cambridge. Patents were deposited by Institut National de la Recherche Agronomique on the use of RECQ4 to manipulate meiotic recombination in plants (EP3149027).

This article is a PNAS Direct Submission.

Data deposition: FastQ sequencing data have been deposited in the ArrayExpress database, https://www.ebi.ac.uk/arrayexpress/ (accession no. E-MTAB-5949).

[1]Present address: Vegetable Crop Research, KeyGene, 6708 PW Wageningen, The Netherlands.

[2]Present address: Department of Genome Biology, Adam Mickiewicz University in Poznan, 61-614 Poznan, Poland.

[3]To whom correspondence should be addressed. Email: irh25@cam.ac.uk.

This article contains supporting information online at www.pnas.org/lookup/suppl/doi:10.1073/pnas.1713071115/-/DCSupplemental.

the MLH1/MLH3 MutL-related heterodimer (1, 10) (*SI Appendix*, Fig. S1*A*). Within the ZMM pathway, the *HEI10* E3 ligase gene shows dosage sensitivity, with additional copies being sufficient to increase crossovers throughout euchromatin (13). Approximately 15% of crossovers in plants do not show interference and are known as class II, which form by a different MUS81-dependent pathway (1).

From cytological measurement of *Arabidopsis* DSB-associated foci (e.g., γH2A.X, RAD51, and DMC1) along meiotic chromosomes, it is estimated that between 100 and 200 breaks initiate per nucleus (14–16). However, only ∼10 crossovers typically form throughout the genome (17–20), indicating that anticrossovers pathways prevent maturation of the majority of initiation events into crossovers (1). Indeed, genetic analysis has identified at least three distinct anticrossovers pathways in *Arabidopsis*: (*i*) the FANCM DNA helicase and MHF1 and MHF2 cofactors (21–23), (*ii*) the AAA-ATPase FIDGETIN-LIKE1 (24), and (*iii*) the RTR complex of RECQ4A, RECQ4B DNA helicases, TOPOISOMERASE3α, and RMI1 (25–29) (*SI Appendix*, Fig. S1*A*). For example, *recq4a recq4b* mutants show highly elevated noninterfering crossovers when assayed in specific intervals (26) (*SI Appendix*, Fig. S1*A*). This is thought to primarily result from a failure to dissolve interhomolog strand invasion events, which are alternatively repaired by the noninterfering crossover pathway(s) (21, 24, 26). As combining mutations between these pathways, for example *fancm figl1*, led to additive crossover increases, they reflect parallel mechanisms (24). Hence, during meiosis, competing pathways act on SPO11-dependent DSBs to balance crossover and noncrossover repair outcomes (*SI Appendix*, Fig. S1*A*).

In this work, we explore the functional relationship between ZMM procrossover and RECQ4 anticrossovers meiotic recombination pathways. Using a combination of increased *HEI10* dosage and *recq4a recq4b* mutations, we observe a massive, additive increase in crossover frequency throughout the chromosome arms. Surprisingly, we observe that increased *HEI10* dosage (hereafter referred to as *HEI10*) causes increased crossover coincidence, indicating an effect on interference. We show that *HEI10* and *recq4a recq4b* crossover increases are biased toward regions of low interhomolog divergence that are distal from centromeric heterochromatin. Hence, both genetic and epigenetic information likely constrain the activity of meiotic recombination pathways.

Combination of *HEI10* and *recq4a recq4b* Massively Elevates Crossover Frequency

Crossover increases in *HEI10* and *recq4a recq4b* represent mechanistically distinct effects via class I and class II crossover repair pathways (*SI Appendix*, Fig. S1*A*). We therefore sought to test whether combining these genetic backgrounds would cause further increases in crossover frequency. We previously showed that transgenic line "*C2*," which carries additional *HEI10* copies, shows an approximately two-fold increase in crossovers genome-wide, compared with wild type (13) (*SI Appendix*, Table S1). We crossed *HEI10* line *C2* to *recq4a recq4b* double mutants, in the Col genetic background (13, 26, 28) (*SI Appendix*, Fig. S1*B*). A previous genetic screen isolated an EMS allele of *recq4a* in Ler (26). As Ler carries a natural premature stop codon in *recq4b* (26), this provides a *recq4a recq4b* double mutant in Ler (*SI Appendix*, Fig. S1*B*). These lines were crossed and F_1 progeny identified that were heterozygous for Col/Ler polymorphisms, *recq4a recq4b* homozygous, and with or without additional *HEI10* copies (*SI Appendix*, Fig. S1*B*). These F_1 plants were then used to generate Col/Ler F_2 for crossover analysis (*SI Appendix*, Fig. S1*B*).

During crossing, we maintained the *420* FTL crossover reporter within our lines, which allows measurement of genetic distance in a ∼5.1-Mb subtelomeric region on chromosome 3 (30, 31) (Fig. 1*A* and *SI Appendix*, Fig. S1*B* and Table S2). This showed that *HEI10*, *recq4a recq4b*, and *HEI10 recq4a recq4b* all significantly increase *420* crossover frequency in Col/Ler hybrid backgrounds, by 2.7, 3.3, and 3.7-fold, respectively (χ^2 test, $P = 2.73 \times 10^{-175}$, $P = 4.92 \times 10^{-212}$ and $P = 2.80 \times 10^{-226}$) (Fig. 1*A* and *SI Appendix*, Table S2). However, it is notable that *420* genetic distance reached 47 cM in *HEI10 recq4a recq4b*, which is close to the maximum

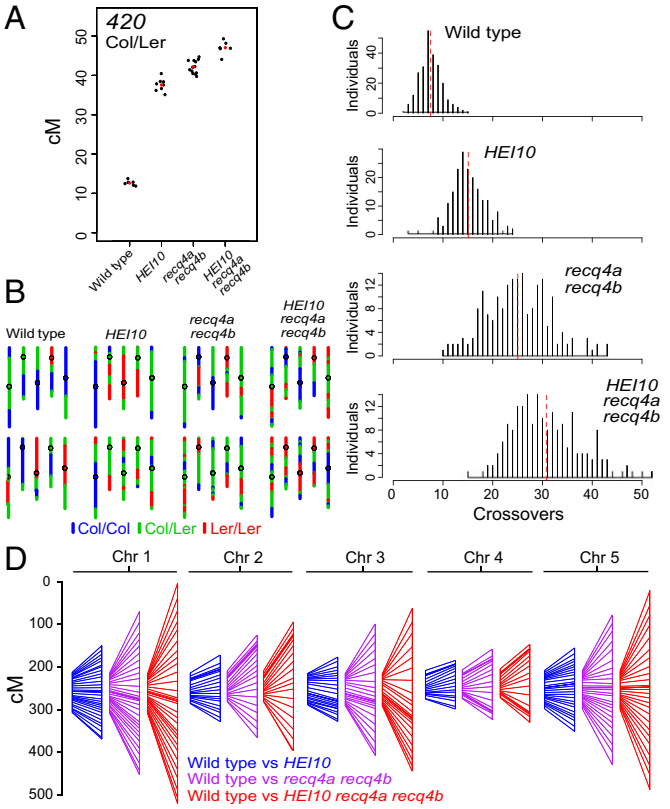

Fig. 1. Combination of *HEI10* and *recq4a recq4b* massively increases meiotic crossover frequency. (*A*) The *420* genetic distance (in centimorgans) was measured during breeding of the *HEI10* and *recq4a recq4b* populations. All samples were Col/Ler heterozygous. Replicate measurements are shown as black dots and mean values as red dots. The *HEI10* data were previously reported (13). (*B*) Chromosomal genotypes are shown for two representative individuals from the wild type, *HEI10*, *recq4a recq4b*, and *HEI10 recq4a recq4b* F_2 populations. The five *Arabidopsis* chromosomes are depicted and color coded according to Col/Col (blue), Col/Ler (green), or Ler/Ler (red) genotypes. Centromere positions are indicated by black circles. (*C*) Histograms showing the frequency of F_2 individuals containing different crossover numbers in each population, with the mean value indicated by the horizontal dotted red lines. (*D*) Genetic maps (in centimorgans) shown for each chromosome for *HEI10* (blue), *recq4a recq4b* (magenta), and *HEI10 recq4a recq4b* (red). Each map is shown alongside the wild-type map (*Left*), and markers between the maps are connected.

observable recombination frequency for linked markers (50 cM) (Fig. 1*A* and *SI Appendix*, Table S2). Therefore, we next sought to use genotyping by sequencing (GBS) to generate genome-wide, high-resolution maps of crossovers in these backgrounds.

We sequenced genomic DNA from between 191 and 245 Col/Ler F_2 progeny derived from wild type, *recq4a recq4b*, and *HEI10 recq4a recq4b* F_1 parents, and compared them with a previously described *HEI10* F_2 population (13) (*SI Appendix*, Figs. S1–S6 and Tables S1 and S3). We observed that *recq4a recq4b* caused 3.3-fold more crossovers genome-wide (25 crossovers/F_2 individual, 95% confidence interval ±0.93), compared with wild type (7.5 crossovers/F_2, 95% confidence interval ±0.28), which is greater than the twofold increase previously seen in *HEI10* (15.1 crossovers/F_2, 95% confidence interval ±0.49) (13) (Fig. 1 *B–D* and *SI Appendix*, Table S1). If the *HEI10* and *recq4a recq4b* crossover increases combined in a purely additive manner, then we would expect to see wild-type crossovers plus the sum of the *HEI10* and *recq4a recq4b* crossover differentials in *HEI10 recq4a recq4b*, equivalent to 7.5 + 7.6 + 17.4 = 32.5 crossovers/F_2. Indeed, this was similar to the observed value for *HEI10 recq4a recq4b* of 30.8 crossovers/F_2 (95% confidence interval ±0.93) (Fig. 1 *B–D* and *SI Appendix*, Table S1). For all populations, the physically largest chromosomes

had the longest genetic maps (Fig. 1*D* and *SI Appendix*, Fig. S7). Together these data show that crossover elevations caused by increased *HEI10* dosage and loss of the *RECQ4A RECQ4B* anticrossovers helicases combine in an additive manner, consistent with class I and class II crossover pathways being independent in *Arabidopsis*.

To assess whether elevated crossover frequency caused by *HEI10* and *recq4a recq4b* were associated with changes to fertility, we performed Alexander staining of pollen and scored the proportion of viable and inviable grains. Compared with wild type, *HEI10 recq4a recq4b* showed significantly higher pollen inviability ($P = 6.3 \times 10^{-4}$), whereas *HEI10* and *recq4a recq4b* were not significantly different (pairwise *t* tests were performed with correction for multiple testing) (*SI Appendix*, Fig. S8*A* and Table S4). We also measured seed set and observed that average seed number per silique in *HEI10* ($P = 1.4 \times 10^{-4}$), *recq4a recq4b* ($P = 3.7 \times 10^{-5}$), and *HEI10 recq4a recq4b* ($P = 1.8 \times 10^{-8}$) were significantly reduced compared with wild type (*SI Appendix*, Fig. S8*B* and Table S5), with the greatest reduction in *HEI10 recq4a recq4b*. Although elevated levels of meiotic crossover associate with significant reductions in fertility in these backgrounds, appreciable seed set is still observed compared with wild type in *HEI10* (94% of wild type), *recq4a recq4b* (95%), and *HEI10 recq4a recq4b* (71%) (*SI Appendix*, Fig. S8*B* and Table S5).

To investigate whether the increased crossovers observed in *HEI10*, *recq4a recq4b*, and *HEI10 recq4a recq4b* arise from additional DSBs, or at the expense of other types of repair, we measured meiotic DSB levels by immunostaining for RAD51 (a RecA homolog that mediates strand invasion) and ASY1 (a HORMA domain protein which forms part of the meiotic chromosome axis). Quantification of axis-associated RAD51 foci at leptotene, zygotene, and pachytene stages showed no significant differences between wild type and *HEI10*, *recq4a recq4b*, or *HEI10 recq4a recq4b* (*SI Appendix*, Fig. S9 and Tables S6–S8). This indicates that recombination changes in *HEI10* and *recq4a recq4b* do not feedback to cause a significant change to DSB foci during *Arabidopsis* meiosis.

Crossover Coincidence Increases in *HEI10* and *recq4a recq4b*

Underdispersion of crossover numbers per meiosis occurs due to the action of crossover interference (1, 10, 32), causing an excess of values close to the mean. Consistently, we observe that the distribution of crossovers per wild-type F_2 individual is significantly non-Poisson (goodness-of-fit test for Poisson distribution, $P = 0.012$) (Fig. 2*A*). Observed frequencies are plotted as bars (gray) originating from the fitted frequencies (red line), such that gray bars lying above or below zero on the *y* axis represent deviation from the Poisson expectation (Fig. 2*A*). Crossover distributions per individual in *HEI10*, *recq4a recq4b*, and *HEI10 recq4a recq4b* were also significantly non-Poisson (*HEI10* $P = 4.23 \times 10^{-3}$, *recq4a recq4b* $P = 1.85 \times 10^{-5}$ and *HEI10 recq4a recq4b* $P = 0.0174$). However, the high recombination populations also showed significantly greater variation in crossover numbers compared with wild type (Brown–Levene test, *HEI10* $P = 1.08 \times 10^{-6}$, *recq4a recq4b* $P \leq 2.2 \times 10^{-16}$, *HEI10 recq4a recq4b* $P \leq 2.2 \times 10^{-16}$) (Fig. 2*A* and *SI Appendix*, Table S1). We therefore sought to examine the distributions of crossovers within the GBS data in more detail, with respect to interevent spacing.

The analysis of F_2 individuals resulting from two independent meioses does not allow us to distinguish between genuine (*cis*) DCOs, which occurred in a single meiosis, or apparent (*trans*) DCOs, which are the result of a single crossover from two different meioses, which combined to form a given F_2 individual (Fig. 2*B*). However, we adopted a hypothesis testing approach to ask whether observed crossover distances differed significantly from those expected from a Poisson distribution. We considered each F_2 individual separately, identified chromosomes with two or more crossovers, and calculated the distance between them. For each individual and chromosome, the same number of randomly chosen positions was used to generate a matched set of distances (Fig. 2*B*). Consistent with the action of interference, wild-type distances were significantly greater than the corresponding random distances (mean = 8.72 Mb vs. 6.91 Mb, Mann–Whitney Wilcoxon test $P = 1.39 \times 10^{-11}$). In *HEI10* the distances were substantially reduced compared with wild type, but were still significantly greater than random (mean = 6.06 Mb vs. 5.15 Mb, Mann–Whitney Wilcoxon test $P = 3.88 \times 10^{-12}$) (Fig. 2*B*). However, in both *recq4a recq4b* (mean = 3.84 Mb vs. 3.45 Mb, Mann–Whitney Wilcoxon test $P = 0.08$) and *HEI10 recq4a recq4b* (mean = 3.30 Mb vs. 3.09 Mb, Mann–Whitney Wilcoxon test $P = 0.257$) populations, the observed distances were not significantly different from random (Fig. 2*B*). This is expected as increased class II crossovers caused by *recq4a recq4b* are randomly distributed (26). We also observed that the differential between observed and randomly generated distances was less in *HEI10* (1.176×), compared with wild type (1.262×). Therefore, we sought to further investigate crossover interference in *HEI10* compared with wild type.

To measure crossover interference in wild type and *HEI10* we used three-color FTL analysis, with the adjacent *I3b* and *I3c* intervals. *I3bc* allows measurement of crossover frequency in a subtelomeric region of chromosome 3 (31, 33) (*I3bc* is located within the *420* FTL interval described earlier) (Figs. 1*A* and 2*C*). We used flow cytometry to measure inheritance of pollen fluorescence in wild type and *HEI10* and calculate *I3b* and *I3c* genetic distances (Fig. 2*C* and *SI Appendix*, Tables S9 and S10). Both *I3b* and *I3c* showed a significant increase in crossover frequency in *HEI10*, consistent with our previous *420* measurements (χ^2 test both $P \leq 2.2 \times 10^{-16}$) (Figs. 1*A* and 2*C* and *SI Appendix*, Tables S9 and S10). *I3b* and *I3c* genetic distances were used to estimate the number of DCO pollen expected in the absence of interference, using the

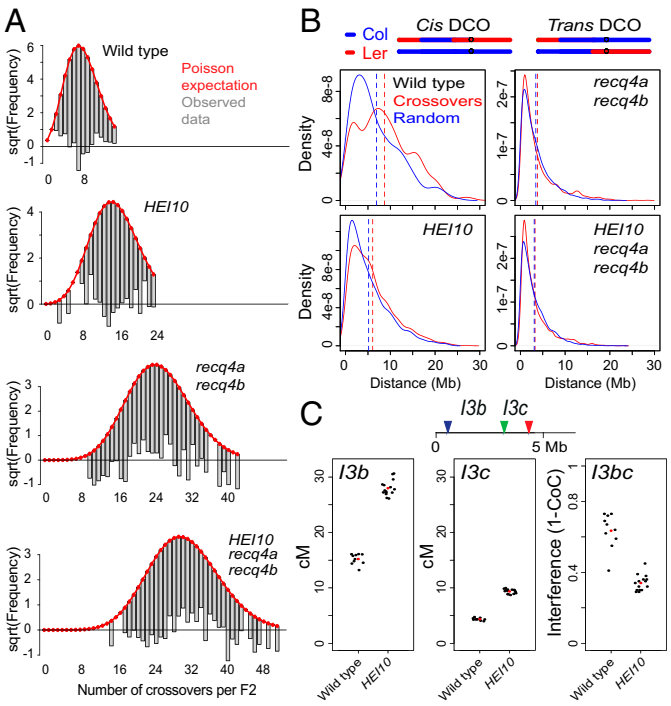

Fig. 2. Decreased crossover interference in *HEI10* and *recq4a recq4b*. (*A*) Plots of the square root of the frequency of total crossovers per F_2 individual in wild type, *HEI10*, *recq4a recq4b*, and *HEI10 recq4a recq4b* populations, generated using the R package goodfit. The expected Poisson distribution is plotted in red, with the observed data below. Deviation from the Poisson expectation is shown by the gray bars (observed data) falling either above or below the zero value on the *y* axis. (*B*) The *Upper* diagram illustrates genuine (*cis*) versus apparent (*trans*) double crossovers detected in F_2 genotyping data. Kernel density estimates are plotted for observed distances between crossovers (red) and the same number of randomly chosen distances (blue), for the indicated genotypes. The vertical dotted lines indicate mean values. (*C*) *I3b* and *I3c* genetic distances in wild type and *HEI10*, and crossover interference (1 – CoC) between the *I3b* and *I3c* intervals. Replicate measurements are shown by black dots and mean values by red dots.

formula: expected DCOs = (*I3b* cM/100) × (*I3c* cM/100) × total pollen number. The ratio of "observed DCOs" to "expected DCOs" gives the coefficient of coincidence (CoC), and interference is calculated as 1 – CoC, such that zero indicates an absence of interference (31, 33) (Fig. 2*C* and *SI Appendix*, Tables S9 and S10). *I3bc* interference (1 – CoC) significantly decreased from 0.64 in wild type to 0.34 in *HEI10* (χ^2 test $P \leq 2.2 \times 10^{-16}$) (Fig. 2*C* and *SI Appendix*, Tables S9 and S10). These experiments reveal that although *HEI10* functions in the interfering ZMM pathway, higher *HEI10* dosage causes increased crossover coincidence compared with wild type, although not to the degree observed in *recq4a recq4b* (25) (Fig. 2*B*).

Crossover, Interhomolog Divergence, and DNA Methylation Landscapes

We next sought to analyze crossover distributions along the chromosomes and relate these patterns to other aspects of genome organization (Fig. 3). On average, 7.5 crossovers were observed per wild-type F_2 individual, 5.6 of which occurred in the chromosome arms and 1.9 in the pericentromeric heterochromatin (*SI Appendix*, Fig. S10 and Table S11). In *HEI10*, *recq4a recq4b*, and *HEI10 recq4a recq4b*, crossovers in the arms increased 2.3, 4.1, and 5-fold, respectively (5.6, 12.9, 23, and 28 crossovers), whereas the pericentromere increases of 1.1, 1.1, and 1.5-fold, respectively (1.9, 2.1, 2.0, and 2.7 crossovers), were considerably lower (*SI Appendix*, Fig. S10 and Table S11). Consistent with previous observations (13, 34), we observed that despite massive crossover increases throughout the chromosome arms, *HEI10*, *recq4a recq4b*, and *HEI10 recq4a recq4b* maintain suppression of recombination within the centromeric regions (Fig. 3). We also observed that a subtelomeric region on the long arm of chromosome 4 showed suppression of crossovers, specifically in the *recq4a recq4b* and *HEI10 recq4a recq4b* populations (Fig. 3). This may reflect a lineage-specific sequence rearrangement, such as an inversion, shared among the *recq4a recq4b* backgrounds.

We hypothesized that genetic and epigenetic factors could contribute to the observed telomeric bias in crossover increases. Therefore, we compared recombination to patterns of Col/Ler interhomolog divergence (35) (i.e., heterozygosity) and DNA cytosine methylation (36). Within the chromosome arms, we observed that wild-type crossovers showed a positive relationship with divergence (all values were calculated in 300-kb adjacent windows, Pearson's $r = 0.564$ $P < 2.2 \times 10^{-16}$), which is reminiscent of correlations previously observed between historical recombination and sequence diversity (31) (Figs. 3 and 4). In contrast, opposite negative correlations were seen between *HEI10* ($r = -0.640$ $P < 2.2 \times 10^{-16}$), *recq4a recq4b* ($r = -0.805$ $P < 2.2 \times 10^{-16}$) and *HEI10 recq4a recq4b* ($r = -0.810$ $P < 2.2 \times 10^{-16}$) crossovers and Col/Ler SNP divergence (Figs. 3 and 4). This indicates that the crossover elevations seen in *HEI10 recq4a recq4b* are biased toward the least polymorphic regions of the chromosomes. Hence, while the class II repair pathway that is active in *recq4a recq4b* is not completely inhibited by heterozygosity, it shows a preference for regions of lower interhomolog divergence.

To further investigate the relationship between crossovers and structural genetic variation, we compared crossovers with a set of 47 Col/Ler inversions (35), which have a mean length of 33.8 kb and comprise 1.59 Mb in total. For each genotype, we counted overlap of crossovers with the inversions and compared inversion overlap with a matched set of randomly chosen intervals with the same widths. In total, we observed that 8 of 15,425 crossovers overlapped the inversions, which was significantly fewer than the 189 overlaps observed for random (χ^2 test $P < 2.2 \times 10^{-16}$). This is consistent with Col/Ler inversions potently inhibiting crossovers (35). We also note that zero crossovers overlapped the 1.17 Mb heterochromatic knob inversion on chromosome 4 (37). The densely DNA methylated centromeric regions were strongly

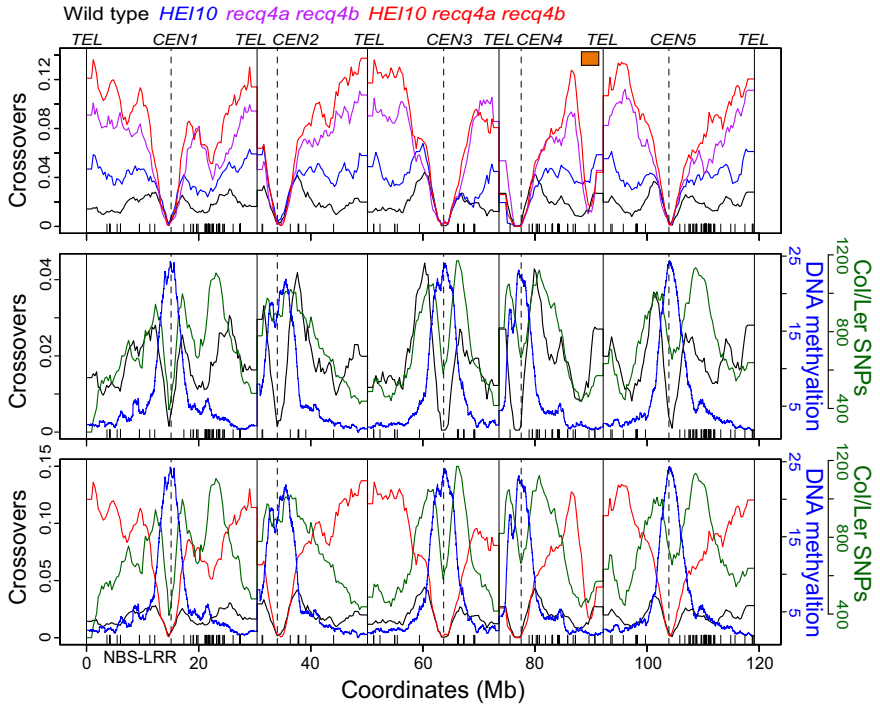

Fig. 3. Genomic landscapes of crossover frequency, interhomolog divergence, and DNA methylation. (*Upper*) Plots of crossover frequency (crossovers per 300 kb, normalized by the number of F_2 individuals analyzed) measured in wild type (black), *HEI10* (blue) (13), *recq4a recq4b* (purple), and *HEI10 recq4a recq4b* (red). The five chromosomes are plotted on a continuous *x* axis, with the positions of telomeres (*TEL*) and centromeres (*CEN*) indicated by vertical lines. The position of NBS-LRR resistance gene homologs are indicated by the *x* axis ticks. The putative location of an inversion in the *recq4a recq4b*-derived populations is also indicated by the *Inset* orange rectangle. (*Middle*) As for *Upper*, but showing wild-type crossover frequency (black) plotted against Col/Ler SNPs (SNPs/300 kb, green) (35) and DNA methylation (% per 10 kb, blue) (36). (*Lower*) As for *Middle*, but showing both wild-type (black) and *HEI10 recq4a recq4b* (red) crossover frequency using a greater *y* axis range.

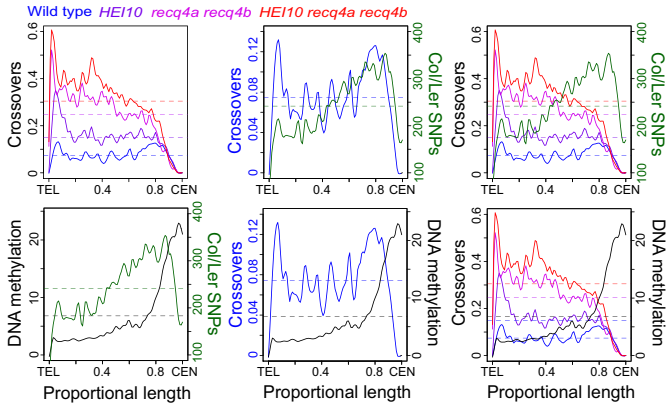

Fig. 4. Crossover frequency, interhomolog divergence, and DNA methylation along telomere–centromere chromosome axes. Analysis of crossover frequency in wild type (blue), *HEI10* (purple), *recq4a recq4b* (magenta), *HEI10 recq4a recq4b* (red), Col/Ler SNPs (green) (35), and DNA methylation (black) (36), analyzed along the proportional length of all chromosome arms, orientated from telomeres (*TEL*) to centromeres (*CEN*).

crossover suppressed in all populations, consistent with heterochromatin inhibiting meiotic recombination (36) (Figs. 3 and 4). Crossovers were negatively correlated with DNA methylation in all populations, but most strongly in the high recombination backgrounds (wild type $r = -0.233$ $P = 2.13 \times 10^{-6}$, *HEI10* $r = -0.740$ $P \leq 2.2 \times 10^{-16}$, *recq4a recq4b* $r = -0.828$ $P \leq 2.2 \times 10^{-16}$, and *HEI10 recq4a recq4b* $r = -0.810$ $P \leq 2.2 \times 10^{-16}$). Therefore, although combination of *HEI10* and *recq4a recq4b* causes a massive crossover increase, the localization of recombination appears to be constrained by both interhomolog sequence divergence and chromatin.

Discussion

We show that elevating the ZMM crossover pathway, via increased dosage of the *HEI10* meiotic E3 ligase gene, while simultaneously increasing the activity of noninterfering repair, via mutation of *RECQ4A* and *RECQ4B* antirecombination helicase genes, is sufficient to cause a massive increase in *Arabidopsis* meiotic crossovers. This is consistent with class I and class II acting as independent crossover repair pathways in *Arabidopsis*. HEI10 is a highly conserved ubiquitin/SUMO E3 ligase with unknown targets during *Arabidopsis* meiosis, which may include other ZMM factors (1, 10, 38). In plants, HEI10 associates with paired homologous chromosomes throughout meiotic prophase, showing gradual restriction to a small number of foci that correspond to crossover locations (39, 40). We propose that HEI10 acts to quantitatively promote ZMM pathway crossover repair at recombination sites via SUMO or ubiquitin transfer. Unexpectedly, we show that increased *HEI10* dosage causes higher crossover coincidence and therefore a decrease in genetic interference. Crossover interference has been modeled as a mechanical force, thought to be transmitted via the meiotic chromosome axis and/or synaptonemal complex (SC) (41). Therefore, HEI10 may modify recombination factors at repair foci and decrease their sensitivity to the interference signal, thereby increasing the likelihood of ZMM-dependent crossover designation. Alternatively HEI10 may alter transmission of the interference signal per se, for example, if components of the axis or SC are SUMO/ubiquitin targets.

The RECQ4 helicases have biochemically characterized activities in (*i*) disassembly of D loops and (*ii*) decatenation of dHJs (42–45), and thus can promote noncrossover outcomes at multiple recombination steps poststrand invasion. In the *recq4a recq4b* mutant, it is likely that unrepaired joint molecules persist, which are instead repaired as noninterfering class II crossovers (26). We show that combination of genetic backgrounds that increase class I and class II crossovers is sufficient to cause a massive and additive recombination increase from 7.5 to 31 crossovers per *Arabidopsis* F_2 individual. However, given that ~100–200 DSB foci have been cytogenetically observed in *Arabidopsis*, there likely remains the capacity for further crossover increases (14–16). As the *Arabidopsis* anticrossovers pathways do not show complete redundancy (21, 24, 26, 46), combination of mutations in the *FANCM*, *RECQ4A-RECQ4B*, and *FIGL1* pathways can cause further crossover increases (34). Furthermore, the *Arabidopsis* MSH2 MutS homolog acts to suppress crossovers specifically when homologous chromosomes are polymorphic (47), and therefore introduction of *msh2* mutations may further increase recombination in hybrids. The use of *msh2* is attractive, as it may reduce the bias against crossovers observed in divergent regions in *HEI10 recq4a recq4b*.

It is notable that the effects of *HEI10* and *recq4a recq4b* are most potent at increasing crossovers in euchromatin. Therefore, in crop species with large heterochromatic regions, these strategies may increase recombination most strongly in subtelomeric euchromatin (2). Interestingly, in maize, <3% of the genome has been identified as nucleosome depleted, recombination active, and contributing to the majority of heritable variation (48), meaning that increased crossovers in these regions would likely influence inheritance of key traits. To unlock recombination in the pericentromeric regions, modification of epigenetic information may be required. However, as plant heterochromatin is maintained by multiple interacting systems of epigenetic marks, including DNA methylation, H3K9me2, H3K27me1, and H2A.W (49), these varying modifications may have differentiated functions in control of meiotic recombination (36, 50, 51). Importantly, the balance of heterochromatic systems is also known to vary between species. For example, islands of CHH DNA methylation occur adjacent to active genes in maize, which are not evident in *Arabidopsis* (52). In conclusion, advanced tailoring of genetic backgrounds may further bias meiotic DSB repair to crossover fates, which has the potential to accelerate crop breeding and improvement.

Materials and Methods

Plant Materials. *Arabidopsis* lines used in this study were the Col *HEI10* line *C2* (13), Col *recq4a-4* (N419423) (28), Col *recq4b-2* (N511130) (28), and Ler *recq4a* line (W387*) (26). Genotyping of *recq4a-4* was performed by PCR amplification using recq4a-F and recq4-wt-R oligonucleotides for wild type and recq4a-F and recq4-mut-R for *recq4a-4*. Genotyping of *recq4b-2* was carried out by PCR amplification using recq4b-wt-F and R oligonucleotides for wild type and recq4b-mut-F and R oligonucleotides for *recq4b-2*. Genotyping of *recq4a* mutation in Ler was performed by PCR amplification using recq4a-Ler-F and R oligonucleotides and subsequent digestion of the PCR products by ScrFI restriction enzyme, which yields ~160 bp products for wild type and ~180 bp products for *recq4a*. The presence of *HEI10* transgene was tested by PCR amplification using HEI10-F and HEI10-R oligonucleotides. Oligonucleotide sequences are provided in *SI Appendix*, Table S12.

Measurement of Crossover Frequency Using Fluorescent Tagged Lines. The *420* genetic distance was measured using microscopic analysis of seed fluorescence, as described (30, 31). *I3bc* genetic distances and coefficient of coincidence were measured using fluorescent pollen and flow cytometry, as described (31). Statistical analysis of FTL crossover frequency and interference measurements were performed as described (13, 31).

Immunocytological Analysis. Chromosome spreads of *Arabidopsis* pollen mother cells and immunostaining of ASY1 and RAD51 were prepared as described (53). Individual cells were acquired as Z stacks of 10 optical sections of 0.2 μM each. The maximum intensity projection for each cell was rendered using ImageJ, and RAD51 foci associated with the meiotic chromosome axis were counted manually. The following antibodies were used: α-ASY1 (53) (rat, 1:300 dilution) and α-RAD51 (54) (rabbit, 1:300 dilution). Microscopy was conducted using a DeltaVision Personal DV microscope (Applied Precision/GE Healthcare) equipped with a CDD Coolsnap HQ2 camera (Photometrics). Image capture was performed using SoftWoRx software version 5.5 (Applied Precision/GE Healthcare).

Genotyping by Sequencing. Ler genomic DNA was sequenced and reads were aligned to the TAIR10 genome assembly using Bowtie2. Variant sites were called using SAMtools and BCFtools. Sites were filtered to remove those with qualities <100 and >2.5× mean coverage and repeat masked (15). A set of 481,252 SNPs (mean spacing = 248 bp) were selected for analysis using the TIGER pipeline (36, 55). DNA was extracted from F_2 plants and used to generate GBS libraries, and crossovers were identified between "complete" SNP positions.

Across all datasets, crossovers were resolved to a mean distance of 1,409 bp. FastQ sequencing data files are available from ArrayExpress accession E-MTAB-5949.

To generate genetic maps, GBS genotypes from each library were used to call "marker" genotypes at 1-Mb intervals. These genotypes were used with the R package Rqtl to generate genetic maps using the Haldane mapping function. The R package goodfit was used to compare observed crossover numbers per individual to the Poisson expectation. For analysis of crossover locations, we used a genetic definition of the centromeres as the contiguous regions surrounding the centromeric assembly gaps that show an absence of crossovers in wild type (56). We defined the surrounding regions with higher than average DNA methylation as the pericentromeres (36). The chromosome arms were defined as the remainder of the genome. The *HEI10* line *C2* contains a translocation between chromosomes 3 (~159,900 bp) and 4 (~20,780,000) associated with the *HEI10* transgene, which results in false crossover calls at these locations. For this reason, 74 crossovers at these positions were masked from further analysis.

ACKNOWLEDGMENTS. We thank Gregory Copenhaver (University of North Carolina, Chapel Hill) for *I3bc*, Avraham Levy (Weizmann Institute) for *420*, Chris Franklin (University of Birmingham) for ASY1 and RAD51 antibodies, and the Gurdon Institute Imaging Facility for access to microscopes. This work was supported by grants from the Biotechnology and Biological Sciences Research Council (BBSRC) (BB/L006847/1), BBSRC-Meiogenix IPA (BB/N007557/1), European Research Area Network for Coodinating Action in Plant Sciences/BBSRC "DeCOP" (BB/M004937/1), Marie-Curie "COMREC" network FP7 ITN-606956, European Research Council (SynthHotspot CoG), the Gatsby Charitable Foundation (GAT2962), a Royal Society University Research Fellowship, and the Bettencourt Schueller Foundation.

1. Mercier R, Mézard C, Jenczewski E, Macaisne N, Grelon M (2015) The molecular biology of meiosis in plants. *Annu Rev Plant Biol* 66:297–327.
2. Higgins JD, Osman K, Jones GH, Franklin FCH (2014) Factors underlying restricted crossover localization in barley meiosis. *Annu Rev Genet* 48:29–47.
3. Keeney S, Kleckner N (1995) Covalent protein-DNA complexes at the 5′ strand termini of meiosis-specific double-strand breaks in yeast. *Proc Natl Acad Sci USA* 92:11274–11278.
4. Neale MJ, Pan J, Keeney S (2005) Endonucleolytic processing of covalent protein-linked DNA double-strand breaks. *Nature* 436:1053–1057.
5. Cannavo E, Cejka P (2014) Sae2 promotes dsDNA endonuclease activity within Mre11-Rad50-Xrs2 to resect DNA breaks. *Nature* 514:122–125.
6. Garcia V, Phelps SEL, Gray S, Neale MJ (2011) Bidirectional resection of DNA double-strand breaks by Mre11 and Exo1. *Nature* 479:241–244.
7. Zakharyevich K, et al. (2010) Temporally and biochemically distinct activities of Exo1 during meiosis: Double-strand break resection and resolution of double Holliday junctions. *Mol Cell* 40:1001–1015.
8. Mimitou EP, Yamada S, Keeney S (2017) A global view of meiotic double-strand break end resection. *Science* 355:40–45.
9. Brown MS, Bishop DK (2014) DNA strand exchange and RecA homologs in meiosis. *Cold Spring Harb Perspect Biol* 7:a016659.
10. Hunter N (2015) Meiotic recombination: The essence of heredity. *Cold Spring Harb Perspect Biol* 7:a016618.
11. Copenhaver GP, Housworth EA, Stahl FW (2002) Crossover interference in Arabidopsis. *Genetics* 160:1631–1639.
12. Mercier R, et al. (2005) Two meiotic crossover classes cohabit in Arabidopsis: One is dependent on MER3,whereas the other one is not. *Curr Biol* 15:692–701.
13. Ziolkowski PA, et al. (2017) Natural variation and dosage of the HEI10 meiotic E3 ligase control *Arabidopsis* crossover recombination. *Genes Dev* 31:306–317.
14. Chelysheva L, et al. (2010) An easy protocol for studying chromatin and recombination protein dynamics during Arabidopsis thaliana meiosis: Immunodetection of cohesins, histones and MLH1. *Cytogenet Genome Res* 129:143–153.
15. Choi K, et al. (2013) Arabidopsis meiotic crossover hot spots overlap with H2A.Z nucleosomes at gene promoters. *Nat Genet* 45:1327–1336.
16. Ferdous M, et al. (2012) Inter-homolog crossing-over and synapsis in Arabidopsis meiosis are dependent on the chromosome axis protein AtASY3. *PLoS Genet* 8: e1002507.
17. Wijnker E, et al. (2013) The genomic landscape of meiotic crossovers and gene conversions in Arabidopsis thaliana. *eLife* 2:e01426.
18. Copenhaver GP, Browne WE, Preuss D (1998) Assaying genome-wide recombination and centromere functions with Arabidopsis tetrads. *Proc Natl Acad Sci USA* 95: 247–252.
19. Salomé PA, et al. (2012) The recombination landscape in Arabidopsis thaliana F2 populations. *Heredity (Edinb)* 108:447–455.
20. Giraut L, et al. (2011) Genome-wide crossover distribution in Arabidopsis thaliana meiosis reveals sex-specific patterns along chromosomes. *PLoS Genet* 7:e1002354.
21. Crismani W, et al. (2012) FANCM limits meiotic crossovers. *Science* 336:1588–1590.
22. Girard C, et al. (2014) FANCM-associated proteins MHF1 and MHF2, but not the other Fanconi anemia factors, limit meiotic crossovers. *Nucleic Acids Res* 42:9087–9095.
23. Knoll A, et al. (2012) The Fanconi anemia ortholog FANCM ensures ordered homologous recombination in both somatic and meiotic cells in Arabidopsis. *Plant Cell* 24: 1448–1464.
24. Girard C, et al. (2015) AAA-ATPase FIDGETIN-LIKE 1 and helicase FANCM antagonize meiotic crossovers by distinct mechanisms. *PLoS Genet* 11:e1005369, and erratum (2015) 11:e1005448.
25. Séguéla-Arnaud M, et al. (2016) RMI1 and TOP3α limit meiotic CO formation through their C-terminal domains. *Nucleic Acids Res* 287:gkw1210.
26. Séguéla-Arnaud M, et al. (2015) Multiple mechanisms limit meiotic crossovers: TOP3α and two BLM homologs antagonize crossovers in parallel to FANCM. *Proc Natl Acad Sci USA* 112:4713–4718.
27. Bonnet S, Knoll A, Hartung F, Puchta H (2013) Different functions for the domains of the Arabidopsis thaliana RMI1 protein in DNA cross-link repair, somatic and meiotic recombination. *Nucleic Acids Res* 41:9349–9360.
28. Hartung F, Suer S, Puchta H (2007) Two closely related RecQ helicases have antagonistic roles in homologous recombination and DNA repair in Arabidopsis thaliana. *Proc Natl Acad Sci USA* 104:18836–18841.
29. Higgins JD, Ferdous M, Osman K, Franklin FCH (2011) The RecQ helicase AtRECQ4A is required to remove inter-chromosomal telomeric connections that arise during meiotic recombination in Arabidopsis. *Plant J* 65:492–502.
30. Melamed-Bessudo C, Yehuda E, Stuitje AR, Levy AA (2005) A new seed-based assay for meiotic recombination in Arabidopsis thaliana. *Plant J* 43:458–466.
31. Ziolkowski PA, et al. (2015) Juxtaposition of heterozygous and homozygous regions causes reciprocal crossover remodelling via interference during Arabidopsis meiosis. *eLife* 4:e03708.
32. Jones GH, Franklin FCH (2006) Meiotic crossing-over: Obligation and interference. *Cell* 126:246–248.
33. Berchowitz LE, Copenhaver GP (2008) Fluorescent Arabidopsis tetrads: A visual assay for quickly developing large crossover and crossover interference data sets. *Nat Protoc* 3:41–50.
34. Fernandes JB, Séguéla-Arnaud M, Larchevêque C, Lloyd AH, Mercier R (2017) Unleashing meiotic crossovers in hybrid plants. *Proc Natl Acad Sci USA*, 10.1073/pnas.1713078114.
35. Zapata L, et al. (2016) Chromosome-level assembly of *Arabidopsis thaliana* Ler reveals the extent of translocation and inversion polymorphisms. *Proc Natl Acad Sci USA* 113: E4052–E4060.
36. Yelina NE, et al. (2015) DNA methylation epigenetically silences crossover hot spots and controls chromosomal domains of meiotic recombination in Arabidopsis. *Genes Dev* 29:2183–2202.
37. Fransz PF, et al. (2000) Integrated cytogenetic map of chromosome arm 4S of A. thaliana: Structural organization of heterochromatic knob and centromere region. *Cell* 100:367–376.
38. Gray S, Cohen PE (2016) Control of meiotic crossovers: From double-strand break formation to designation. *Annu Rev Genet* 50:175–210.
39. Chelysheva L, et al. (2012) The Arabidopsis HEI10 is a new ZMM protein related to Zip3. *PLoS Genet* 8:e1002799.
40. Wang K, et al. (2012) The role of rice HEI10 in the formation of meiotic crossovers. *PLoS Genet* 8:e1002809.
41. Kleckner N, et al. (2004) A mechanical basis for chromosome function. *Proc Natl Acad Sci USA* 101:12592–12597.
42. Bachrati CZ, Borts RH, Hickson ID (2006) Mobile D-loops are a preferred substrate for the Bloom's syndrome helicase. *Nucleic Acids Res* 34:2269–2279.
43. Cejka P, Plank JL, Bachrati CZ, Hickson ID, Kowalczykowski SC (2010) Rmi1 stimulates decatenation of double Holliday junctions during dissolution by Sgs1-Top3. *Nat Struct Mol Biol* 17:1377–1382.
44. Wu L, Hickson ID (2003) The Bloom's syndrome helicase suppresses crossing over during homologous recombination. *Nature* 426:870–874.
45. Hatkevich T, Sekelsky J (2017) Bloom syndrome helicase in meiosis: Pro-crossover functions of an anti-crossover protein. *BioEssays* 39:1700073.
46. Choi K, et al. (2016) Recombination rate heterogeneity within Arabidopsis disease resistance genes. *PLoS Genet* 12:e1006179.
47. Emmanuel E, Yehuda E, Melamed-Bessudo C, Avivi-Ragolsky N, Levy AA (2006) The role of AtMSH2 in homologous recombination in Arabidopsis thaliana. *EMBO Rep* 7: 100–105.
48. Rodgers-Melnick E, Vera DL, Bass HW, Buckler ES (2016) Open chromatin reveals the functional maize genome. *Proc Natl Acad Sci USA* 113:E3177–E3184.
49. Law JA, Jacobsen SE (2010) Establishing, maintaining and modifying DNA methylation patterns in plants and animals. *Nat Rev Genet* 11:204–220.
50. Choi K, et al. (2017) Nucleosomes and DNA methylation shape meiotic DSB frequency in Arabidopsis transposons and gene regulatory regions. bioRxiv:10.1101/160911.
51. Underwood CJ, et al. (2017) Epigenetic activation of meiotic recombination in Arabidopsis centromeres via loss of H3K9me2 and non-CG DNA methylation. bioRxiv: 10.1101/160929.
52. Li Q, et al. (2015) RNA-directed DNA methylation enforces boundaries between heterochromatin and euchromatin in the maize genome. *Proc Natl Acad Sci USA* 112: 14728–14733.
53. Armstrong SJ, Caryl AP, Jones GH, Franklin FCH (2002) Asy1, a protein required for meiotic chromosome synapsis, localizes to axis-associated chromatin in Arabidopsis and Brassica. *J Cell Sci* 115:3645–3655.
54. Sanchez-Moran E, Santos J-L, Jones GH, Franklin FCH (2007) ASY1 mediates AtDMC1-dependent interhomolog recombination during meiosis in Arabidopsis. *Genes Dev* 21: 2220–2233.
55. Rowan BA, Patel V, Weigel D, Schneeberger K (2015) Rapid and inexpensive whole-genome genotyping-by-sequencing for crossover localization and fine-scale genetic mapping. *G3 (Bethesda)* 5:385–398.
56. Copenhaver GP, et al. (1999) Genetic definition and sequence analysis of Arabidopsis centromeres. *Science* 286:2468–2474.